



# Water Droplet Impingement on Simulated Glaze, Mixed, and Rime Ice Accretions

*Michael Papadakis, Arief Rachman, See-Cheuk Wong, and Hsiung-Wei Yeong  
Wichita State University, Wichita, Kansas*

*Kuohsing E. Hung and Giao T. Vu  
The Boeing Company, Wichita, Kansas*

*Colin S. Bidwell  
Glenn Research Center, Cleveland, Ohio*

## The NASA STI Program Office . . . in Profile

Since its founding, NASA has been dedicated to the advancement of aeronautics and space science. The NASA Scientific and Technical Information (STI) Program Office plays a key part in helping NASA maintain this important role.

The NASA STI Program Office is operated by Langley Research Center, the Lead Center for NASA's scientific and technical information. The NASA STI Program Office provides access to the NASA STI Database, the largest collection of aeronautical and space science STI in the world. The Program Office is also NASA's institutional mechanism for disseminating the results of its research and development activities. These results are published by NASA in the NASA STI Report Series, which includes the following report types:

- **TECHNICAL PUBLICATION.** Reports of completed research or a major significant phase of research that present the results of NASA programs and include extensive data or theoretical analysis. Includes compilations of significant scientific and technical data and information deemed to be of continuing reference value. NASA's counterpart of peer-reviewed formal professional papers but has less stringent limitations on manuscript length and extent of graphic presentations.
- **TECHNICAL MEMORANDUM.** Scientific and technical findings that are preliminary or of specialized interest, e.g., quick release reports, working papers, and bibliographies that contain minimal annotation. Does not contain extensive analysis.
- **CONTRACTOR REPORT.** Scientific and technical findings by NASA-sponsored contractors and grantees.

- **CONFERENCE PUBLICATION.** Collected papers from scientific and technical conferences, symposia, seminars, or other meetings sponsored or cosponsored by NASA.
- **SPECIAL PUBLICATION.** Scientific, technical, or historical information from NASA programs, projects, and missions, often concerned with subjects having substantial public interest.
- **TECHNICAL TRANSLATION.** English-language translations of foreign scientific and technical material pertinent to NASA's mission.

Specialized services that complement the STI Program Office's diverse offerings include creating custom thesauri, building customized databases, organizing and publishing research results . . . even providing videos.

For more information about the NASA STI Program Office, see the following:

- Access the NASA STI Program Home Page at <http://www.sti.nasa.gov>
- E-mail your question via the Internet to [help@sti.nasa.gov](mailto:help@sti.nasa.gov)
- Fax your question to the NASA Access Help Desk at 301-621-0134
- Telephone the NASA Access Help Desk at 301-621-0390
- Write to:  
NASA Access Help Desk  
NASA Center for AeroSpace Information  
7115 Standard Drive  
Hanover, MD 21076



# Water Droplet Impingement on Simulated Glaze, Mixed, and Rime Ice Accretions

*Michael Papadakis, Arief Rachman, See-Cheuk Wong, and Hsiung-Wei Yeong*  
Wichita State University, Wichita, Kansas

*Kuohsing E. Hung and Giao T. Vu*  
The Boeing Company, Wichita, Kansas

*Colin S. Bidwell*  
Glenn Research Center, Cleveland, Ohio

National Aeronautics and  
Space Administration

Glenn Research Center

## Acknowledgments

Funding for this work was provided by the Federal Aviation Administration (FAA) and NASA Glenn Research Center (NASA Glenn). The authors would like to thank the following FAA and NASA senior personnel for their encouragement and support: Manny Rios and Jim Riley, project managers; Eugene Hill, national icing research specialist, Federal Aviation Administration; and Tom Bond, Chief, Icing Branch, NASA Glenn. Thanks are also due to Robert F. Ide, Dave Sheldon, Tim Bencic, John R. Oldenburg, Charlie Andracchio, and the IRT personnel of NASA Glenn for their extensive support with the impingement tests. Finally, the support provided by The Boeing Company and the extensive contributions of Art Porter, Emily Smythe, Norma Campos, Duc Pham, and Dennis Regnier, Wichita State University, to this program are acknowledged.

Available from

NASA Center for Aerospace Information  
7115 Standard Drive  
Hanover, MD 21076

National Technical Information Service  
5285 Port Royal Road  
Springfield, VA 22100

Available electronically at <http://gltrs.grc.nasa.gov>

## Contents

|   |    |
|---|----|
| Abstract.....   | 1  |
| Executive Summary .....                                     | 2  |
| List of Abbreviations and Symbols .....                     | 3  |
| 1.0 Introduction .....                                      | 5  |
| 2.0 Background .....  | 6  |
| 3.0 Droplet Trajectory and Impingement Parameters .....     | 9  |
| 3.1 Droplet Trajectory.....                                 | 9  |
| 3.2 Impingement Parameters .....                            | 10 |
| 3.2.1 Liquid Water Content ( <i>LWC</i> ) .....             | 10 |
| 3.2.2 Cloud Droplet Distribution .....                      | 10 |
| 3.2.3 Median Volumetric Diameter ( <i>MVD</i> ).....        | 10 |
| 3.2.4 Local Impingement Efficiency.....                     | 11 |
| 3.2.5 Total Impingement Efficiency.....                     | 11 |
| 3.2.6 Impingement Limits .....                              | 12 |
| 3.2.7 Summary of Droplet Impingement Parameters .....       | 12 |
| 3.3 Large Droplet Impingement Issues .....                  | 12 |
| 3.3.1 Large Droplet Deformation and Breakup.....            | 12 |
| 3.3.2 Large Droplet Splashing and Re-impingement .....      | 13 |
| 4.0 Experimental Setup.....                                 | 14 |
| 4.1 Wind Tunnel Facility.....                               | 14 |
| 4.2 Test Models.....  | 15 |
| 4.2.1 MS(1)-317 Airfoil.....                                | 15 |
| 4.2.2 NACA 23012 Airfoil .....                              | 15 |
| 4.2.3 LEWICE Ice Shapes for NACA 23012 Airfoil .....        | 15 |
| 4.2.4 Installation of LEWICE Ice Shapes on NACA 23012 ..... | 16 |
| 4.3 Dye Tracer Method .....                                 | 17 |
| 4.4 Spray System.....                                       | 17 |
| 4.5 Spray System Data Acquisition and Control .....         | 19 |
| 4.6 Cloud Uniformity.....                                   | 20 |
| 4.7 MVD and LWC Measurement .....                           | 21 |
| 4.8 Reference Collector Mechanism .....                     | 21 |
| 4.9 Test Matrix .....                                       | 22 |
| 4.10 Pressure Measurements .....                            | 23 |
| 4.11 Impingement Test Procedure .....                       | 23 |
| 5.0 Data Reduction Methods .....                            | 24 |
| 5.1 Colorimetric Analysis.....                              | 24 |
| 5.2 Reflectance Spectroscopy .....                          | 25 |
| 5.2.1 Reflectance Calibration Curve.....                    | 25 |
| 5.2.2 Laser Reflectometer .....                             | 25 |
| 5.2.3 Charge-Coupled Device (CCD) Reflectometer .....       | 26 |
| 6.0 LEWICE-2D Impingement Analysis Method .....             | 28 |
| 7.0 Results and Discussion.....                             | 29 |
| 7.1 Discussion of Experimental Errors .....                 | 29 |
| 7.1.1 Experimental Method .....                             | 30 |
| 7.1.2 Data Reduction Method.....                            | 31 |
| 7.2 Pressure Distributions .....                            | 32 |
| 7.3 Impingement Results .....                               | 32 |
| 7.3.1 Test Repeatability.....                               | 32 |
| 7.3.2 Experimental and LEWICE Impingement Data .....        | 33 |

|  |     |
|--|-----|
| 7.3.3 Effect of Geometry .....   | 36  |
| 7.3.4 Effect of MVD .....  | 38  |
| 7.4 Droplet Trajectories.....  | 38  |
| 8.0 Summary and Conclusions .....  | 39  |
| Appendix A—Model Geometry and Pressure Port Coordinates .....  | 179 |
| Appendix B—Run Log for 2003 Impingement Tests.....   | 225 |
| Appendix C—Summary of Experimental and LEWICE Impingement Data—All Test Geometries and MVDs.....             | 237 |
| Appendix D—Droplet Trajectories .....  | 249 |
| Appendix E—Analysis Impingement Data Computed with a Modified LEWICE Code Using the Monte-Carlo Method ..... | 259 |
| References.....  | 294 |

# Water Droplet Impingement on Simulated Glaze, Mixed and Rime Ice Accretions

Michael Papadakis, Arief Rachman, See-Cheuk Wong, and Hsiung-Wei Yeong

Wichita State University

Wichita, Kansas 67260

Kuohsing E. Hung and Giao T. Vu

The Boeing Company

Wichita, Kansas 67277

Colin S. Bidwell

National Aeronautics and Space Administration

Glenn Research Center

Cleveland, Ohio 44135

## Abstract

Water droplet impingement data were obtained at the NASA Glenn Icing Research Tunnel (IRT) for a 36-in. chord NACA 23012 airfoil and ten simulated ice shapes using a dye-tracer method. The simulated ice shapes were defined with the NASA Glenn LEWICE 2.2 ice accretion code and included one rime, four mixed and five glaze ice shapes. The impingement experiments were performed with spray clouds having median volumetric diameters of 20, 52, 111, 154, and 236  $\mu\text{m}$ . Flow conditions included angle of attack of 2.5°, total air temperature in the range of 40 to 77 °F and airspeed of 175 mph corresponding to a Reynolds number of approximately 1.6 million per foot. Each test case was repeated three to four times to evaluate the repeatability of the test conditions and of the experimental setup. Test repeatability was established by computing the maximum difference of the peak and total impingement efficiencies of individual test results from the average of all repeated tests at a given condition. The maximum variation of the peak impingement efficiency,  $\bar{\beta}_{\max}$ , from the average was less than 10 percent for 52 out of the 56 cases tested while the maximum variation of the total impingement efficiency from the average was less than 10 percent for 55 out of the 56 cases presented. The experimental data showed that in general, the peak efficiencies and impingement limits for the clean and iced cases increased as the MVD was increased. The impingement curves of the glaze and mixed ice shapes exhibited multiple peaks in the region between the horns. In many cases, peaks in the impingement curves were also observed downstream of the horns. For the large MVD cases, the majority of the ice shapes tested had considerable impingement downstream of the horns along the airfoil upper and lower surfaces.

Analysis impingement data were computed with a modified version of the NASA Glenn LEWICE 1.6 code (this code can use droplet distributions with more than 10 droplet sizes; a Monte-Carlo method is also available for impingement computations) and were compared with the experimental results. For the 20  $\mu\text{m}$  MVD and the clean airfoil, the LEWICE results and the experimental data were in good agreement. For the iced configurations, however, the predicted impingement efficiency for the 20  $\mu\text{m}$  MVD was higher than that obtained experimentally. The percentage difference in total impingement efficiency between the LEWICE 1.6 result and experimental data for the 20  $\mu\text{m}$  MVD clean airfoil configuration was -6.8 percent whereas the percentage difference for the 20  $\mu\text{m}$  MVD iced configurations ranged from -0.9 to 48 percent. For the large MVD cases of 52, 111, 154, and 236  $\mu\text{m}$ , the LEWICE impingement data for the clean and iced configurations exhibited considerably higher local and total impingement

efficiencies and larger impingement limits than the experimental results. The percentage difference in total impingement efficiency for the larger MVD cases ranged from 49 to 70 percent for the clean configuration and 33 to 145 percent for the iced configurations. This discrepancy was attributed to droplet splashing experienced by the large droplets during impingement.

## Executive Summary

Aircraft flying through clouds below 26,000 ft at subsonic speeds can experience ice formation on critical aerodynamic surfaces. This situation can lead to deterioration of aircraft aerodynamic performance and handling qualities. Typically, ice accretion results from small (5 to 50 $\mu\text{m}$ ) supercooled droplets (droplets cooled below freezing) which can freeze upon impact with the aircraft surface. Recently, however, ice accretions resulting from supercooled large droplets (SLD) have become a safety concern.

Ice accretion and droplet trajectory computer codes, such as the NASA Glenn LEWICE code, can provide cost-effective information for the design and certification of ice protection systems. In addition, these codes are often used to predict ice shapes on critical aerodynamic surfaces for icing conditions within the appendix C icing envelope in FAR part 25. These ice shapes are then examined to select those that have the potential of causing large performance losses for further evaluation and testing.

The computation of ice shapes with ice accretion codes is usually performed incrementally by building small layers of ice until the required ice shape is obtained. During each ice accretion increment, a new flowfield is computed by the ice accretion code. This is followed by droplet trajectory and impingement calculations for the new ice shape and an ice accretion analysis. It is important that during each ice accretion step, the impingement characteristics of the iced airfoil are computed accurately, since the prediction of the next layer of ice relies heavily on the computed impingement data.

Current droplet trajectory and ice accretion codes have been extensively tested for the FAR part 25, appendix C icing conditions and, in general, have demonstrated good agreement with experimental impingement data. Computation of large droplet impingement (droplets outside the FAR part 25, app. C certification envelope) characteristics, however, may require additional improvements to the existing numerical models to include large droplet impingement dynamics phenomena such as droplet splashing and breakup that have been observed in recent experimental impingement studies with large droplets.

The main goal of the research effort described in this report was the development of an extensive impingement database for a range of simulated LEWICE ice shapes to validate ice accretion codes. Impingement experiments were conducted in the NASA Glenn Icing Research Tunnel with an airfoil section representative of general aviation and commuter aircraft and with five glaze, four mixed, and one rime ice shapes. Impingement data were obtained for median volumetric diameters of 20, 52, 111, 154, and 236  $\mu\text{m}$  and airspeed of 175 mph. Comparison of the experimental impingement data with LEWICE-2D analysis data showed that, in general, agreement between analysis and experiment was good for the 20  $\mu\text{m}$  case. However, for the large droplet cases the impingement efficiencies predicted by LEWICE were considerably greater than the experimental results for both the clean and iced airfoil cases. The observed differences between experiment and analysis for the large droplet cases were attributed to droplet splashing, differences between the analysis and experimental flowfields, particularly for the 22.5- and 45-min ice shapes, and, in some cases, to droplet breakup downstream of the ice shape horns.

## List of Abbreviations and Symbols

|            |   |
|------------|---|
| AOA        | Angle of Attack   |
| CCD        | Charge-Coupled Device   |
| DAQ        | Data Acquisition  |
| DIO        | Digital Input Output  |
| FAA        | Federal Aviation Administration   |
| FS         | Full-Scale  |
| FSSP       | Forward Scattering Spectrometer Probe   |
| IRT        | Icing Research Tunnel   |
| LE         | Leading Edge  |
| LWC        | Liquid Water Content  |
| MVD        | Median Volumetric Diameter  |
| OAP        | Optical Array Probe   |
| RCM        | Reference Collector Mechanism   |
| PC         | Personal Computer   |
| SLD        | Supercooled Large Droplets  |
| SSR        | Solid State Relay   |
| TE         | Trailing Edge   |
| WSU        | Wichita State University  |
| $A_f$      | Frontal area of a body projected parallel to freestream velocity direction                      |
| $A_\infty$ | Area perpendicular to freestream direction, defined by the tangent trajectories                 |
| $c$        | Model chord length  |
| $C_D$      | Droplet drag coefficient  |
| $C_f$      | Nozzle flow coefficient   |
| $D, d$     | Droplet diameter  |
| $D_{\max}$ | Maximum droplet diameter in clouds of non-uniform droplet size                                  |
| $D_{\min}$ | Minimum droplet diameter in clouds of non-uniform droplet size                                  |
| $D_{MVD}$  | Droplet diameter based on MVD   |
| $\bar{E}$  | Total impingement efficiency in clouds of non-uniform droplet size                              |
| $g$        | Acceleration due to gravity   |
| Highlight  | Reference point on test geometry for measuring impingement efficiency                           |
| $K$        | Droplet inertia parameter, $\rho_{droplet} \cdot V_\infty \cdot MVD^2 / (18 \cdot \mu \cdot c)$ |
| $K_{IP}$   | Impact parameter  |
| $K_0$      | Modified droplet inertia parameter, $K \cdot \lambda / \lambda_s$                               |
| $L$        | Characteristic dimension of a body  |
| $M$        | Mach number of airflow relative to droplet  |

|                   |  |
|-------------------|--|
| $M_\infty$        | Freestream Mach number of airflow  |
| $R_{\max}$        | Repeatability based on maximum local impingement efficiency  |
| $R_{\text{AREA}}$ | Repeatability based on total impingement efficiency  |
| $Re_c$            | Reynolds number based on chord length  |
| $Re_v$            | Reynolds number of airflow relative to droplet   |
| $Re_{MVD}$        | Reynolds number based on MVD and freestream speed  |
| $R_n$             | Normalized reflectance   |
| $S$               | Surface distance from highlight  |
| $\bar{\beta}_1$   | Absolute maximum local impingement efficiency observed at the leading edge region of the clean or iced models            |
| $\bar{\beta}_2$   | Minimum local impingement efficiency observed between the upper and lower horns of the glaze and mixed ice shapes tested |
| $S_u$             | Surface distance from highlight to impingement limit on upper surface  |
| $S_l$             | Surface distance from highlight to impingement limit on lower surface  |
| $t$               | Time; Airfoil thickness  |
| $U_i$             | Initial droplet velocity   |
| $V$               | Potential flow velocity dimensionless with $V_\infty$  |
| $V_i$             | Initial potential flow velocity  |
| $V_\infty$        | Freestream airspeed  |
| $w$               | Water flow rate from WSU spray nozzles   |
| $x, y$            | Cartesian coordinates  |
| $x_l$             | Chordwise distance corresponding to the impingement limit on the lower surface   |
| $x_u$             | Chordwise distance corresponding to the impingement limit on the upper surface   |
| $\alpha$          | Angle of attack  |
| $\bar{\beta}$     | Local impingement efficiency   |
| $\Delta P$        | $P_{\text{water}} - P_{\text{air}}$  |
| $\delta_{ij}$     | Kronecker delta  |
| $\phi$            | Independent impingement parameter, $(Re_{MVD})^2 / K$  |
| $\lambda$         | True range of droplet as projectile injected into still air  |
| $\lambda_s$       | Range of droplet as projectile following Stokes' law   |
| $\mu$             | Absolute air viscosity   |
| $\rho$            | Air density  |
| $\rho_w$          | Density of water   |

## 1.0 Introduction

Aircraft flying at subsonic speeds through clouds below 8000 m (approximately 26,000 ft) can be subject to ice formation on critical aerodynamic surfaces. This situation can lead to deterioration of aircraft aerodynamic performance and handling qualities. Typically, ice accretion has resulted from small super-cooled (cooled below freezing) droplets freezing upon impact with the aircraft surface. These droplets are usually 5 to 50  $\mu\text{m}$  in diameter. Recently, however, ice accretions resulting from super-cooled large droplets (SLD) have become a safety concern. The impact of SLD ice accretions on aircraft safety is under evaluation by the Federal Aviation Administration (FAA) and the Joint Aviation Authorities (JAA). FAA/JAA rulemaking is under development to ensure safe flight in large supercooled droplet (SLD) icing conditions.

Ice accretion and droplet trajectory computer codes such as the NASA Glenn LEWICE code, can provide information for the design and certification of ice protection systems. In addition, ice accretion codes are often used by aircraft manufacturers to predict ice shapes on critical aerodynamic surfaces for a range of icing conditions within the appendix C icing envelope in FAR part 25. These ice shapes are then examined to select those that have the potential of causing considerable losses in performance for further evaluation and testing.

The computation of ice shapes with ice accretion codes is usually performed incrementally by building small layers of ice until the required ice shape is obtained. For example, a 22-min glaze ice accretion might be constructed using 2-min time increments. During each ice accretion increment, a new flowfield is computed by the ice accretion code. This is followed by droplet trajectory and droplet impingement calculations for the new ice shape and an ice accretion analysis. It is important that during each ice accretion step, the computer code provides an accurate prediction of the impingement characteristics of the iced airfoil since the prediction of the next layer of ice relies heavily on the computed impingement data.

Current droplet trajectory and ice accretion codes have been extensively tested for cloud conditions within the FAR part 25, appendix C icing envelope and, in general, have demonstrated good agreement with experimental impingement data. Application of these codes to compute large droplet impingement (droplets outside the current icing certification envelope), however, may require additional improvements to the existing numerical models to include physical phenomena related to large droplet impingement dynamics such as droplet splashing and breakup (refs. 1 to 3) that have been observed in recent experimental impingement studies with large droplets (refs. 4 and 5). The impact of these phenomena on the simulation of the impingement characteristics of aerodynamic surfaces can be considerable, as demonstrated in references 6 and 7. Large droplet experimental and LEWICE impingement data presented in references 6 and 7 for two-dimensional airfoil sections exhibited considerable differences in the magnitude and extent of the local impingement efficiency. The main reason for the observed discrepancy between experiment and analysis was attributed to large droplet splashing effects. More impingement data are needed for clean and iced wing geometries and for a range of large median volumetric diameters in order to support the development and validation of trajectory and ice accretion codes.

This report presents experiments conducted to provide the first extensive impingement database on progressively larger glaze, mixed and rime ice shapes for SLD as well as FAR part 25, appendix C icing conditions. The ice shapes tested were defined with the LEWICE ice accretion code for a NACA 23012 airfoil using FAR part 25, appendix C icing conditions. In the following sections, the experimental and data reduction methods used to generate the impingement data are discussed and the results obtained are compared with impingement predictions obtained with the NASA Glenn LEWICE code.

## 2.0 Background

The first extensive water droplet impingement database was developed by NACA in the 1950's. A dye-tracer technique was developed for measuring local impingement efficiency on aircraft aerodynamic surfaces (ref. 8). In this technique, water containing a small amount of water-soluble dye was injected in the form of droplets through a system of spray nozzles into the airstream ahead of the body. The surface of the body was covered with blotter material upon which the dyed water impinged and was absorbed. At the point of impact and droplet absorption, a permanent dye deposit (dye trace) was obtained. The impingement limits were obtained directly from the rearmost dye trace on the absorbent material.

Data analysis consisted of removing the dyed blotter strips from the body and punching out small segments of the blotter material for the determination of local impingement characteristics. The dye was dissolved out of each segment in a known quantity of water. The weight of dye in this solution was determined by the amount of light in a proper wavelength that was transmitted through the solution using a calibrated colorimeter, a process known as colorimetric analysis. The weight of water that impinged at any surface location per unit time was determined from the weight of dye collected per unit area, and from knowledge of the original concentration of the dye in the water droplets.

The liquid water content in the cloud was determined using an aspirating device (refs. 8 and 9). This device consisted essentially of a tube, which sucked in the approaching air and cloud droplets at the freestream velocity (inlet velocity ratio 1) so that both the air streamlines and droplets entered the tube along straight-line paths. The dyed droplets were deposited on a filter mounted within the tube, leaving a dye trace that could be analyzed using colorimetric analysis. The droplet size distribution was determined by comparing experimental local impingement rates on cylinders of different sizes with theoretical predictions of droplet trajectories and impingement points using a differential analyzer.

Between 1955 and 1958 NACA personnel developed a water droplet impingement database for a wide range of cylinders, airfoils sections, bodies of revolution and a supersonic inlet (refs. 8 to 12). For most test configurations, the NACA method was sufficiently accurate. The error in evaluating maximum local impingement efficiency varied from 10 to 25 percent (refs. 8 and 9). The major limitations of the NACA method included reduced spatial resolution and a laborious and time-consuming process for reducing the experimental data. In addition, the uncertainty in measuring the LWC and MVD values of the spray clouds used in the impingement tests was considerable.

In 1984, a research program was initiated to further expand and update the experimental water droplet impingement database. This program was sponsored by the NASA Glenn Research Center in Cleveland, Ohio and the FAA Technical Center in Atlantic City, New Jersey. The work was performed by researchers at Wichita State University and Boeing. During this research program, an experimental method similar to the one used in the early 1950's by NACA researchers was developed for measuring local impingement efficiency (ref. 13). A new method for extracting the impingement data from the blotter strips was also developed. In this method, the amount of dye on a blotter strip obtained in a given time interval was converted into local impingement efficiency distribution using a laser reflectance spectroscopy method. Numerous tests showed that the new data reduction method was significantly more efficient than the method of colorimetric analysis used in the 1950's by NACA personnel.

To generate the required spray clouds for the impingement tests, a 12-nozzle spray system was fabricated. This system was designed to have a very fast on/off response because the spray duration had to be very short (approximately 2 to 4 sec) to avoid saturation of the blotter paper. In order to achieve accuracy in using the reflectance method, dye penetration into the blotter paper had to be kept to a minimum.

The first series of impingement tests were conducted in September of 1985 in the NASA IRT for a period of four weeks. The geometries tested included a 4-in. cylinder, a NACA 65<sub>2</sub>-015, an MS(1)-0317 supercritical airfoil, three simulated ice shapes, an axisymmetric engine inlet model and a Boeing 737-300 engine inlet model. The second and final series of impingement tests were performed in the IRT facility during April of 1989 and lasted for approximately four weeks. Models tested during this phase of the research program included two simulated ice shapes, a Natural Laminar Flow airfoil section NLF(1)-0414F, an infinite span 30° swept MS(1)-0317 wing, a finite span 30° swept NACA 0012 wing, and a Boeing 737-300 engine inlet model. The experimental impingement data obtained during the 1985 and 1989 impingement tests can be found in references 13 and 14. In summary, the water droplet impingement research program conducted between 1984 and 1993 was successful and considerably expanded the impingement database.

A peer review of NASA Glenn icing research activities conducted in 1994 indicated that additional water droplet impingement data were needed. Large droplet impingement data were also requested in response to a recent commuter aircraft icing related accident which had raised the question of the effect of ice accretion due to Supercooled Large Droplets (SLD) on aircraft performance and handling characteristics (refs. 15 and 16).

To address the needs of the icing community, the Icing Technology Branch at NASA Glenn Research Center awarded a research grant to Wichita State University (WSU) in 1995 to begin work on modernizing and expanding the water droplet impingement database. WSU and NASA conducted an industry survey in November of 1995 to identify geometries and conditions to be considered for the next series of water droplet impingement tests.

In December of 1996, NASA awarded a second grant to WSU to improve the experimental method developed during the 1984 to 1993 research program and to develop a more efficient reflectance method utilizing a CCD camera to extract the impingement data from the blotter strips. In addition, extensive impingement tests were planned in the NASA Glenn Icing Research Tunnel with a range of two-dimensional airfoils, finite wings, and a turboprop S-duct engine inlet.

The first series of the IRT impingement tests were conducted during the period of July 25 to September 7, 1997. The second series of impingement tests were conducted from January 31 to March 1, 1999. A total of 11 wind tunnel models were tested during these two IRT entries. Test models included six two-dimensional airfoils, a two-dimensional high-lift system, three swept horizontal tails and an engine inlet S-duct. Tests were performed for a range of angles of attack and for median volumetric diameters of 11, 11.5, 21, 92, and 94  $\mu\text{m}$ . The 92 to 94 MVD case was selected to provide preliminary SLD impingement data for assessing the performance of trajectory computer codes for large droplet conditions. Comparison of the experimental impingement data with analysis data obtained with the NASA Glenn LEWICE-2D and LEWICE-3D computer codes demonstrated good agreement for the 11-, 11.5-, and 21- $\mu\text{m}$  cases. However, for the 92- and 94- $\mu\text{m}$  cases the analysis produced considerably higher overall impingement than the experiment for nine out of the eleven models tested and for all angles of attack. Details of the 1997 and 1999 impingement research effort are provided in reference 17. The discrepancy between analysis and experiment for the large MVD conditions was attributed to droplet splashing and droplet breakup effects, which are not currently modeled in the LEWICE code. It was determined that additional experimental work was needed to elucidate SLD impingement physics and to provide a more extensive SLD impingement database for trajectory code development and validation.

Recent developments in aviation rulemaking addressing aircraft operations in SLD conditions which are outside the current icing certification envelopes have heightened the need for additional large droplet impingement research. Specifically, the impact of SLD ice accretions

on aircraft safety is under evaluation by the Federal Aviation Administration (FAA) and the Joint Aviation Authorities (JAA). FAA/JAA rulemaking is under development to ensure safe flight in large supercooled droplet icing conditions. In support of the rulemaking, NASA has provided a "roadmap" describing the technology required for implementing the proposed SLD rulemaking, including: a) Atmospheric environment definition, b) Instrumentation, test methods, test facilities, and computer codes required to provide means-of-compliance with the proposed rule.

Current droplet trajectory and ice accretion computer codes are not validated for SLD conditions. To address the need for validated analysis tools for simulating SLD impingement on aircraft surfaces the Federal Aviation Administration awarded a grant to Wichita State University (WSU) in the fall of 2000 to document large droplet impingement dynamics using advanced imaging methods, apply the dye tracer method developed at WSU to obtain large droplet impingement data for a range of airfoils, and investigate the use of this method for measuring impingement on airfoils with simulated ice shapes. To address the program goals, Wichita State University refined the experimental methodology for measuring large droplet impingement and made extensive updates to the hardware and software of the laser and charge-coupled device (CCD) reflectometers used for the reduction of the raw impingement data. In June of 2001, experiments were conducted with a 21-in. chord NACA 0012 airfoil section in the Goodrich Icing Wind Tunnel facility using advanced flow visualization techniques to document basic large droplet impingement splashing for the first time. In September and October of 2001, extensive impingement tests were conducted at the National Aeronautics and Space Administration (NASA) Glenn Icing Research Tunnel (IRT) facility. Impingement data were obtained for a range of airfoil sections including three 36-in. chord airfoils (MS(1)-0317, GLC-305, and NACA 652-415), as well as a 57-in. chord Twin Otter horizontal tail section and a 22.5- and 45-min LEWICE glaze ice shape for the Twin Otter tail section. Data were obtained for median volumetric diameters of 11, 21, 79, 137, and 168  $\mu\text{m}$ . The experimental impingement data were compared with analysis data obtained with the LEWICE-2D computer code. The comparisons performed demonstrated that for the large droplet cases the LEWICE total collection efficiencies were considerably greater than the experimental values for both the clean and iced airfoil cases. Details of the 2000 to 2002 impingement program are provided in reference 6.

During the 2000 to 2002 impingement program, it was demonstrated that the improvements and modifications made to the experimental methodology produced highly repeatable experimental impingement data for airfoils with simulated ice shapes. Thereafter, in the fall of 2002 the Federal Aviation Administration awarded a grant to WSU to obtain small and large droplet impingement data on a NACA 23012 airfoil with a series of progressively larger LEWICE ice shapes. The impingement data were needed to expand the validation scope and database for the NASA Glenn LEWICE ice accretion code. The computation of ice shapes with LEWICE is usually performed incrementally by building small layers of ice until the required ice shape is obtained. During each ice accretion increment, a new flowfield is computed by the ice accretion code. This is followed by droplet trajectory and droplet impingement calculations for the new ice shape and an ice accretion analysis. It is important that during each ice accretion step, the computer code provides an accurate prediction of the impingement characteristics of the iced airfoil since the prediction of the next layer of ice relies heavily on the computed impingement data. Impingement tests were performed in March and April of 2003 with ten simulated LEWICE ice shapes that included five glaze, four mixed and one rime cases. The new water droplet impingement program was a collaborative effort between the FAA, NASA, WSU and the Boeing Company. This report provides details of the methods used and results obtained during the 2002 to 2004 water droplet impingement research effort.

## 3.0 Droplet Trajectory and Impingement Parameters

In this section, impingement parameters that are commonly used in the presentation of theoretical and experimental data are discussed. They constitute the governing non-dimensional form of the droplet trajectory equations. Also discussed is their relevance to conditions with icing clouds of uniform and non-uniform droplet size distributions from small to large super-cooled droplets.

### 3.1 Droplet Trajectory

The forces acting on a small spherical droplet moving in the steady flow of air include droplet drag, weight, and buoyancy. The predominant force exerted on a droplet is the fluid dynamic drag resulting from the relative (slip) velocity of air with respect to the droplet. The development of the droplet trajectory equations is based on a simplified approach taken by researchers as early as the 1940's. In this approach, the quasi-steady motion of small spherical droplets moving in the steady flow of air is considered and it is assumed that the motion of droplets does not disturb the airflow. Since the physical phenomena involved in the process of ice accretion are very complex, these assumptions are necessary and are commonly used in analytical tools for modeling ice accretions. The main assumptions used in the derivation of the small particle trajectory equations are summarized below:

1. Single phase (air) flow about the body; i.e., flowfield is not disturbed by the presence of droplets
2. Quasi-steady-state approximation: at each instant and position, the steady state drag and other forces act on the particle
3. The drag coefficient for stationary sphere applies
4. Particles are assumed to be solid and spherical in shape
5. Particles do not rotate and have no lift and no moment
6. All drops which strike the airfoil deposit on the surface. Droplets do not splash/breakup during the impingement process
7. Droplets do not interact with other droplets
8. Compressible or incompressible potential flowfield of the gas phase about the body
9. Viscous flow effects such as thick boundary layer formation and flow separation are not considered.

The droplet trajectory equation is given below.

$$\frac{dU_i}{dt} = \frac{C_D(\text{Re}_V) \cdot \text{Re}_V \cdot (V_i - U_i)}{24K} - \frac{(1-\sigma) \cdot g \cdot L \cdot \delta_{i2}}{V_\infty^2} \quad (3.1)$$

where

$K = \rho_p V_\infty d^2 / 18\mu L$ , inertia parameter of droplet

$d$  = Droplet diameter

$\mu$  = Absolute air viscosity

$V_\infty$  = Freestream speed

$t$  = Time, dimensionless with  $L/V_\infty$

$\sigma$  =  $\rho/\rho_p$ , density ratio of air to particle

$L$  = Characteristic dimension of body

$\text{Re}_V$  = Reynolds number of airflow relative to droplet

$U_i$  =  $i^{th}$  directional component of particle velocity, dimensionless with  $V_\infty$

$V_i$  =  $i^{th}$  directional component of air velocity, dimensionless with  $V_\infty$

### 3.2 Impingement Parameters

Spray cloud characteristics and droplet impingement parameters for clouds with a range of drop sizes are discussed below.

#### 3.2.1 Liquid Water Content (LWC)

Generally expressed in grams of water per cubic meter of cloud, the liquid water content (*LWC*) of a cloud is defined as the amount of water contained in a given volume of cloud. *LWC<sub>max</sub>* values for icing clouds according to the FAR part 25, appendix C icing envelopes are presented in reference 18. In icing tunnels, the cloud *LWC* is controlled by the water and/or air pressures of the spray system used to create the spray clouds.

#### 3.2.2 Cloud Droplet Distribution

The distribution of droplets in a cloud can be expressed in various forms (ref. 13). Briefly, the following four types of distributions are most commonly used:

1. Number density of droplets versus droplet diameter.
2. Percent of liquid water content versus droplet diameter.
3. Percent of liquid water content versus droplet diameter normalized to median volumetric diameter.
4. Percent cumulative liquid water content versus droplet diameter normalized to median volumetric diameter.

A distribution which has been employed in various analytical studies is the Langmuir "D". This distribution and other similar ones were established by Langmuir (ref. 19) from natural-icing cloud measurements made on Mt. Washington. The rate of deposition of ice on slowly rotating cylinders exposed to supercooled clouds blowing over the summit was correlated with that of theoretical calculations. A dimensionless Langmuir "D" distribution is shown in figure 1.

#### 3.2.3 Median Volumetric Diameter (MVD)

The Median Volumetric Diameter (*MVD*) of a droplet distribution is defined as the droplet diameter for which half the total liquid water content is contained in droplets larger than the median and half in droplets smaller than the median. Given a droplet distribution, the *MVD* can be calculated as follows:

1. For a continuous distribution, if  $n(D)$  is the number of particles per unit sampling volume having diameters between  $D$  and  $D+dD$  (volumes between  $V$  and  $V+dV$ ) then  $D_{MVD}$  can be calculated from

$$\frac{\frac{\pi}{2} \rho_\infty \int_{D_{min}}^{D_{MVD}} n(x) x^2 dx}{\frac{\pi}{2} \rho_\infty \int_{D_{min}}^{D_{max}} n(x) x^2 dx} = 0.5 \quad (3.2)$$

2. For a discrete distribution, if the particle number density is given in  $N$  discrete groups such that  $n_i(D_i)$  is the number of the particles in group  $i$  having diameters between  $D$  and  $D+dD$  then, eq. (3.1) can be written as

$$\frac{\frac{\pi}{6} \rho_{\omega} \sum_{i=1}^K n_i(D_i) D_i^3}{\frac{\pi}{6} \rho_{\omega} \sum_{i=1}^N n_i(D_i) D_i^3} = 0.5 \quad (3.3)$$

where

$D_K$  = the diameter of group  $K$ , is equal to the MVD ( $D_{MVD}$ )  
 $\rho_{\omega}$  = density of water,  $kg/m^3$

### 3.2.4 Local Impingement Efficiency

Considering a body in a cloud with uniform droplet size distribution, the local impingement efficiency  $\bar{\beta}$  for any point on the body surface is defined as the local droplet flux rate at the body surface normalized to the freestream flux rate. Referring to figure 2a,  $\beta$  is defined as the ratio of that infinitesimal area  $dA_{\infty}$  to the corresponding impingement area on the body surface  $dA_s$ . This definition follows from the continuity of droplet mass flow.

For a continuous non-uniform cloud distribution, the impingement efficiency is given by the following expression

$$\bar{\beta} = \frac{1}{\omega_t} \int_0^{\omega_t} \beta d\omega \quad (3.4)$$

where  $\beta$  is a function of drop size and therefore can be expressed as a function of  $\omega$ , the liquid content for a given drop size.

For a discrete cloud distribution,  $\bar{\beta}$  is defined as the weighted average of the local impingement efficiency values due to each droplet group in the cloud. Let  $\omega_t$  be the liquid water content of the cloud,  $\Delta\omega_i$  be the partial liquid water content contained in the droplets of size ( $d_i$ ) in the group ( $i$ ) of the distribution, and  $N$  be the total number of discrete size droplet groups available. For a body exposed to a cloud with such a droplet distribution, the local impingement efficiency due to a single droplet group of size  $d_i$  is  $\beta_i$ , where  $\beta$  is defined in figure 2a. The local impingement efficiency due to all  $N$  groups in the distribution over an infinitesimal area of the body is given by the following expression

$$\bar{\beta} = \frac{1}{\omega_t} \sum_{i=1}^N \beta_i \Delta\omega_i \quad (3.5)$$

### 3.2.5 Total Impingement Efficiency

The total impingement efficiency of a three dimensional body exposed to a cloud of droplet distribution is defined as

$$\bar{E} = \frac{1}{A_f} \int \bar{\beta} dA_s \quad (3.6)$$

where

$A_f$  is the projected frontal area of the body  
 $dA_s$  is an infinitesimal impingement area on the surface of the body

In order to integrate eq. (3.6),  $\bar{\beta}$  must be known as a function of surface location. Such a function can be defined from experimental or analytical results.

### 3.2.6 Impingement Limits

Droplets which start out at freestream position  $y_\infty$  (fig. 2b) with respect to a reference line that passes through the highlight (most forward point at  $\alpha=0^\circ$ ) of a body downstream will impinge at some locations on that body. As these initial freestream droplet positions increase in distance from the reference line they will impinge farther back along the surface of the body until a maximum distance  $y_{\infty,\max}$  is obtained. This limiting trajectory is defined as the tangent trajectory to the body at point P (fig. 2b). Any droplets starting at a freestream location farther from the reference line than  $y_{\infty,\max}$  will miss the body entirely. The distance ( $S_m$ ) measured along the body surface from the highlight of the body to point P is called the limit of impingement. This distance is usually expressed in dimensionless form by dividing  $S_m$  by the characteristic length ( $L$ ) of the body.

For two-dimensional flow, there are two impingement limits, an upper and lower (for external flow, e.g., airfoil section) or an outer and inner (for partly internal flow, e.g., engine inlet). For three-dimensional flow, the limits of impingement may vary spanwise along the surface of a finite wing or circumferentially along the surface of an engine inlet. For a droplet distribution that varies from  $D_{\min}$  to  $D_{\max}$ , the impingement limits can be established for each droplet size. The maximum impingement limits are defined by the impingement limits of the largest droplet diameter in the distribution.

### 3.2.7 Summary of Droplet Impingement Parameters

Table 1 provides a list of definitions and expressions for key non-dimensional parameters that relate to droplet impingement and trajectory. They include droplet inertia parameter,  $K$ ; droplet modified inertia parameter,  $K_0$ ; Reynolds number based on MVD,  $Re_{MVD}$ ; true droplet range,  $\lambda$ ; and independent impingement parameter,  $\phi$ , which represents the deviation of the droplet drag force from Stoke's law. They are defined in such way that the droplet diameter,  $d$ , has been eliminated from the formulations. These non-dimensional impingement parameters are also useful in linking the impingement data presented in this report with early experimental and numerical studies of airfoil water impingement characteristics (refs. 8 and 9). In some of these early studies, the impingement characteristics of bodies were sometimes presented in terms of non-dimensional impingement parameters such as  $K$  and  $\phi$ . Note that the definitions in table 1 are based on the reference length, typically the airfoil chord for two-dimensional sections.

## 3.3 Large Droplet Impingement Issues

The mathematical models for droplet trajectory and impingement analysis have been shown to be accurate for icing conditions within the intermittent and continuous maximum icing envelopes defined in the FAR part 25, appendix C (refs. 6 and 17). For large droplet impingement, however, the current numerical models do not account for large droplet impingement phenomena such as droplet splashing and droplet breakup (refs. 5 and 6). In addition, large droplet distortion due to pressure gradients can result in considerable more drag force than that predicted by the current models which assume spherical droplets.

### 3.3.1 Large Droplet Deformation and Breakup

As a droplet moves closer to a surface, it is subjected to non-uniform pressure forces which cause the droplet to deform. The droplet is held together by surface tension. However, if the

pressure force is large enough, the droplet cannot sustain its surface integrity and begins to break up.

The drag change due to droplet deformation was studied by Wright and Potapczuk (ref. 20). Wright compared calculations of impingement efficiency using LEWICE with two different drag models. The first model was a standard drag model used in LEWICE while an alternative model was devised by increasing the drag coefficient by 15 percent at all Reynolds number. Wright concluded that the effect of droplet deformation on impingement efficiency is negligible as long as breakup does not occur. The latter drag model was based on experimental results by Beard and Pruppacher (ref. 21) which showed that drag of a deformed/non-spherical droplet was at most 15 percent higher than that of a sphere.

A variety of independent variables have been used to correlate droplet breakup properties such as Weber, Bond, and Rabin numbers, (refs. 4 and 22). These parameters are defined as follows:

$$\text{Weber Number, } \text{We} = \frac{\rho V_r^2 D}{\sigma_d} \quad (3.7)$$

$$\text{Bond Number, } \text{Bo} = \frac{\rho_d D^2}{\sigma_d} \left( \frac{dV_r}{dt} \right) \quad (3.8)$$

$$\text{Rabin Number, } \text{Ra} = \frac{\text{We}}{\sqrt{\text{Re}_v}} \quad (3.9)$$

with,

$$\text{Reynolds Number, } \text{Re}_v = \frac{\rho V_r D}{\mu} \quad (3.10)$$

Pilch (ref. 22) stated that there is a critical Weber number ( $\text{We}_c$ ) below which droplet breakup does not occur. The critical Weber number has been investigated experimentally for fluids with different surface tension and viscosity values. A useful empirical correlation for the critical Weber number is given by Pilch as:

$$\text{We}_c = 12 \cdot (1 + 1.077 \cdot \text{Oh}^{1.6}) \quad (3.11)$$

where,

Ohnesorge number,  $\text{Oh}$ , is given as:

$$\text{Oh} = \frac{\mu_d}{\sqrt{\rho_d D \sigma_d}} \quad (\text{Oh} \approx 0.01 \text{ for water (ref. 4)}) \quad (3.12)$$

The critical Weber number was found to be approximately 12 when the Ohnesorge number is small ( $\text{Oh} < 0.1$ ).

### 3.3.2 Large Droplet Splashing and Re-impingement

When water droplets impinge on a surface, they may either (i) spread out on the surface without splashing and create a thin film of water, (ii) splash on impact and create secondary droplets, or (iii) "bounce" off without breakup at very shallow impact angles (refs. 3 and 4). Droplet splashing is a function of droplet kinetic energy and contact angle (refs. 3 and 6), thus it depends heavily on the droplet mass and velocity profiles.

Splashing test conducted in 2001 (ref. 6) provided insight into the relation between droplet mass and velocity with splashing intensity. Splashing images were obtained using a 512 by 512 pixel CCD PI-MAX intensified camera from Princeton Instruments, which is capable of collecting 16-bit images at a readout rate of 1 million pixels per second with 100-milliwatt red laser sheet illumination. Although it was not possible to obtain quantitative results from these images, the experiments showed that splashing phenomena are indeed related to droplet size and the impact velocity. The intensity of droplet splashing increased as the spray cloud MVD was increased for fixed airspeed and it also increased as the airspeed was increased for fixed spray cloud MVD.

The impact parameter,  $K_{IP}$ , (ref. 3) has been used to define threshold conditions for incipient splash. The  $K_{IP}$  parameter is defined as follows:

$$K_{IP} = \text{Oh} \cdot \text{Re}^{1.25} \quad (3.13)$$

Research by Mundo (ref. 3) has shown that a value of  $K_{IP}$  exceeding 57.7 leads to incipient splashing whereas  $K_{IP}$  less than 57.7 leads to complete deposition of the droplet. Tan (ref. 4) showed that on a 21-in. chord NACA0012 airfoil with a relative droplet-air velocity of 100 m/s and droplet diameter of 100  $\mu\text{m}$ , splashing occurred over a significant part of the surface.

When splashing occurred, secondary droplets were ejected from the impingement point. Rutkowsky et al. (ref. 23) observed that for droplet velocities below a threshold value, these secondary droplets re-impinged on the surface. When the velocity of the splashed droplet, however, exceeded the threshold value, they were carried by the external flow past the trailing edge of an airfoil and did not re-impinge. This threshold velocity was referred to as the escape velocity. Even though splashed droplets with velocity below the threshold value were shown to re-impinge on the airfoil surface, locating the point of droplet re-impingement was not a simple matter. The numerical study conducted by Rutkowsky et al. demonstrated that splashed droplets did not necessarily re-impinge close to the initial impingement location. As a result, droplet splashing and re-impingement can result in redistribution of the impinging water mass in ways not currently accounted for by state-of-the-art ice accretion codes.

## 4.0 Experimental Setup

### 4.1 Wind Tunnel Facility

The 2003 water droplet impingement tests were conducted in the NASA Glenn Icing Research Tunnel (IRT). The IRT has a 6- by 9-ft test section that measures 20-ft long and can attain a maximum speed of 390 mph when it is empty. A plan view of the IRT circuit is shown in figure 3. The IRT is a closed-looped refrigerated facility with a test section total temperature controllable from  $-20$  to  $33$  °F. The operational static pressure at the tunnel test section is near or below the atmospheric value. Test models are typically installed on the tunnel turntable using a floor mounting plate as shown in figure 4. A view of the test section is provided in figure 5. Two sets of nozzles (the standard and MOD-1 types) are utilized in the IRT spray system, which consists of 10 spray bars with 54 nozzle locations per bar. The basic IRT nozzle design is shown in figure 6. Only 251 nozzles are currently being used to generate the required icing clouds. Two mechanical vent doors located upstream of the heat exchanger can be open and shut remotely to allow air to vent in and out of the facility. The IRT spray system is capable of simulating icing clouds with MVDs in the range of 14 to 40  $\mu\text{m}$ , and Liquid Water Content (LWC) of 0.3 to 3 g/m<sup>3</sup> as shown in figures 7 and 8. In addition, a limited range of large droplet clouds with MVDs in the range 70 to 270  $\mu\text{m}$  can be produced in this facility. Further details regarding the IRT facility are provided in reference 24.

## 4.2 Test Models

Details of the test models used in the 2003 impingement experiments and their related instrumentation are given below.

### 4.2.1 MS(1)–317 Airfoil

The MS(1)–317 airfoil is representative of modern medium speed airfoils. It was designed in the mid 1970's for general aviation aircraft (ref. 25). This two-dimensional airfoil was constructed out of Fiberglass skin, which was epoxied to an aluminum spar and aluminum ribs. The interior of the airfoil model was filled with foam. An aluminum plate was installed at each end of the model for mounting in the IRT test section. The model had a nominal span of 72 in. and a chord of 36 in. and it was mounted vertically in the test section. The maximum thickness for this airfoil was 6.12 in. ( $t_{max}/c = 0.17$ ) and was located at 37.5 percent chord. The center of rotation of the airfoil was at 42 percent chord. A total of 47 static pressure taps were available for this airfoil. These taps were distributed in the chordwise direction 35.5 in. above the tunnel floor. The MS(1)–317 airfoil section and model installation details are given in figures 9a to c. Impingement data for this airfoil were obtained during the 1985, 1997, 1999, and 2001 IRT tests performed by WSU and Boeing. This airfoil was used during the 2003 IRT impingement to verify the repeatability of the experimental setup.

### 4.2.2 NACA 23012 Airfoil

The NACA 23012 airfoil is representative of general aviation and commuter aircraft wing sections. The two-dimensional wind tunnel model was designed and fabricated at WSU. It was constructed out of aluminum with a 72-in. span and 36-in. chord. The maximum thickness for this airfoil was 4.32 in. ( $t_{max/c} = 0.12$ ) and was located at approximately 30 percent chord. The center of rotation of the airfoil was at 50 percent chord. The airfoil was instrumented with 65 pressure taps at a spanwise location 30 in. above the tunnel floor—40 taps on the suction surface, 23 on the pressure surface, plus 2 pressure ports located at the leading and trailing edges of the airfoil. The NACA 23012 airfoil section and model installation details are given in figures 10a to c.

The two airfoil sections, MS–317 and NACA 23012, are shown in figure 21.

### 4.2.3 LEWICE Ice Shapes for NACA 23012 Airfoil

The simulated ice shapes for the 36-in. airfoil were determined using the NASA Glenn LEWICE 2.2 computer code (ref. 26) with the following icing conditions:

- $V_\infty = 175$  mph
- AOA =  $2.5^\circ$
- MVD =  $20 \mu\text{m}$
- LWC =  $0.5 \text{ g/m}^3$
- Pressure altitude: 1,800 ft selected to approximate the static pressure (approximately 13.75 psi;  $13.75 \times 6,895 = 94,806 \text{ Pa}$ ) in the IRT test section for a test speed of 175 mph. In the actual tests, the freestream static pressure ranged from 13.73 to 13.87 with an average value 13.80 which is close to 13.75 used in the icing analysis

The ice shapes tested for the 2003 impingement test are listed below:

#### ***Glaze Icing Conditions***

1. ***5-min Glaze***: 5 min glaze ice accretion, 1.25 min time step, model installation details are given in figure 11a to c

2. *10-min Glaze*: 10 min glaze ice accretion, 1.25 min time step, model installation details are given in figure 12a to c
3. *15-min Glaze*: 15 min glaze ice accretion, 1.25 min time step, model installation details are given in figure 13a to c
4. *22.5-min Glaze*: 22.5 min glaze ice accretion, 1.25 min time step, model installation details are given in figure 14a to c
5. *45-min Glaze*: 45 min glaze ice accretion, 2.5 min time step, model installation details are given in figure 15a to c

### ***Mixed Icing Conditions***

6. *7.5-min Mixed*: 7.5 min mixed ice accretion, 1.25 min time step, model installation details are given in figure 16a to c
7. *15-min Mixed*: 15 min mixed ice accretion, 1.25 min time step, model installation details are given in figure 17a to c
8. *22.5-min Mixed*: 22.5 min mixed ice accretion, 1.25 min time step, model installation details are given in figures 18a to c
9. *45-min Mixed*: 45 min mixed ice accretion, 2.5 min time step, model installation details are given in figure 19a to c

### ***Rime Icing Condition***

10. *45-min Rime*: 45 min rime ice accretion, 2.5 min time step, model installation details are given in figure 20a to c

All glaze ice shapes were computed using a total temperature at 267.9 K (approx.  $-5^{\circ}\text{C}$ ). All mixed ice shapes were obtained at 264 K (approx.  $-9^{\circ}\text{C}$ ), whereas the 45-min rime ice shape was obtained at 252.3 K (approx.  $-21^{\circ}\text{C}$ ). The LEWICE input Files for the above ice shapes are provided in appendix A.

The glaze, mixed and rime ice shapes tested are presented in figures 21 to 23.

#### **4.2.4 Installation of LEWICE Ice Shapes on NACA 23012**

To ensure repeatable and precise installation of the LEWICE ice shapes to the wing leading edge, the airfoil was designed with a removable leading edge as shown in figure 24a. The removable leading edge extended 1.5 in. on the pressure surface (4.167 percent chord) and 0.8 in. on the suction surface (2.22 percent chord) over the entire span of the wing model. All the LEWICE ice shapes were constructed out of aluminum and were designed so that the removable portion of the wing leading edge was part of each ice shape as shown in figure 23. For ice shapes with long ice limits, however, this method of ice shape installation resulted in a small step between the wing surface and the ice shape trailing edge as shown in figure 24b. To maintain a smooth transition between the ice shape and the wing surface over the spanwise region where the impingement data were to be collected, 6-in. span inserts (plugs) were fabricated that extended to the ice limits in the chordwise direction as shown in figure 24b. Each ice shape was designed with two inserts; one for the upper surface and one for the lower surface. On the suction (upper) surface the inserts extended from 2.22 percent chord to 6.5 percent chord, while along the lower surface the inserts extended from 4.167 percent chord to 15 percent chord. In the spanwise direction, the inserts extended from 33 to 39 in. above the tunnel floor. Photos of the slots on wing surface for the ice shape inserts are provided in figure 24c to d. Note that all pressure taps on the airfoil were placed at 30 in. above the tunnel floor so

the installation of the ice shape inserts did not affect the number of active ports. However, approximately ten pressure ports near the airfoil leading edge were eliminated when an ice shape was installed. Active pressure ports for the clean wing and for each ice shape configuration are provided in appendix A.

#### **4.3 Dye Tracer Method**

The dye-tracer technique was initially developed by NACA (ref. 8) and was subsequently modified by Papadakis et al. (refs. 13 and 14). In the modified method, distilled water containing a known concentration of blue dye (0.3 g of FD&C Blue No.1 dye per liter of water) is injected into the air stream of the IRT in the form of a droplet spray cloud through a specially designed 16-nozzle spray system. The test models are covered with thin strips of blotter paper (James River Paper Company Verigood 100 lb Blotting Paper) in areas of interest and are exposed to the spray cloud for certain lengths of time. The amount of dye-mass per unit area of blotter strip obtained in a given time interval is measured using reflectance spectroscopy. The water impingement characteristics of a test model are obtained by converting the dye color density distribution on each strip into water impingement density using specially developed calibration curves.

#### **4.4 Spray System**

The impingement tests were conducted with an automated 16-nozzle spray system, which was developed at WSU and was capable of producing consistent and repeatable short duration sprays (as short as 0.75 seconds). The short spray duration was needed to avoid blotter saturation and dye penetration into the blotter paper. These requirements were dictated by the data extraction method which relies on accurate reflectance measurements from the surface of the dye laden blotter strips. The IRT spray system was not capable of providing short duration sprays and could not be used with the blue dye solution required for the impingement tests. The 16-nozzle system was based on a 12-nozzle system developed previously at WSU. Details of the development and testing of the 12-nozzle spray system can be found in references 13 and 17. The expansion from 12 to 16 nozzles was based on tests conducted by Papadakis et al. (ref. 17), which showed that for large droplet clouds, cloud uniformity over the region of interest was considerably reduced and more nozzles were needed to cover impingement region for the test models selected.

Blue dye solution stored in a 30-gal stainless steel supply tank was supplied under pressure to 16 nozzle assemblies using rubber hoses. Each nozzle assembly consisted of an IRT MOD-1 spray nozzle, nozzle housing, a fast action solenoid valve, an oil-filled pressure gage, a SETRA 206 pressure transducer to monitor water pressure, an adjustable flow valve, a 0.75-in. diameter 3-ft long stainless steel pipe for the atomizing air supply, a support bracket for attaching the nozzle to the IRT spray bars and a range of fittings for connecting the nozzle to the spray system air and water supply lines.

Water pressure for the supply tank was obtained from a 125 psig air line, while a separate 100 psig high volume flow air source (atomizing air manifold) provided air to the nozzle assemblies for atomizing the water. Quick response pressure regulators were used for setting the water and atomizing air pressures. These regulators were continually adjusted using miniature electro-pneumatic transducers to maintain the required pressures. The electro-pneumatic transducers were controlled by feedback loops incorporated into the spray system computer control unit. The activation pressure for the electro-pneumatic transducers was set to 130 psig and was obtained from a low volume high pressure source. This source was independent of the water and atomizing air pressure lines to ensure that fluctuations in the high volume lines did not affect the operation of the electro-pneumatic transducers.

The pressure of the atomizing air was monitored at the supply line regulator with a SETRA 204 transducer. In addition, three SETRA 206 transducers were used to monitor atomizing air pressures at selected nozzles. A SETRA 204 pressure transducer was installed in the water tank to monitor the water pressure. Also, two high-precision analog pressure gauges were installed at the water tank and at the regulator of the atomizing air line to confirm the pressure readings from the electronic transducers. Pressure transducers characteristics are summarized in table 2. Prior to the IRT test entry, the NASA Glenn flow calibration lab tested and calibrated all the pressure transducers used in the WSU spray system.

The NASA Glenn IRT MOD-1 nozzles were selected for the 2003 impingement tests. Details of the specific spray nozzles used can be found in reference 6. These nozzles have a lower flow rate (approximately 1/3) for a given air pressure and delta pressure ( $P_{\text{water}} - P_{\text{air}}$ ) than the standard IRT nozzles so that longer spray times could be achieved without saturating the blotter strips. Longer spray times are desirable because they result in more stable sprays. These nozzles were also capable of producing the large MVD sizes that were needed for the large droplet impingement tests.

Although the impingement tests are conducted at warm temperatures, typically 50 °F, sometimes during testing the tunnel temperature is lowered to near freezing for controlling the humidity levels in the airstream. To ensure that nozzle freeze-out did not occur during impingement tests, the water temperature in the spray system was monitored continually with two thermocouples. A thermocouple was placed inside the housing of spray nozzle no. 9 and the other was placed immediately downstream of the 30-gal supply tank. Nozzle no. 9 was chosen because it was located approximately in the center of the tunnel plenum where the total air temperature was approximately equal to the average of the total freestream temperature. The thermocouples used were the T-Type NPT thermocouples (Omega TC-T-NPT-G-72) and were connected to Omega TX-251 transmitters to amplify the voltage difference before connecting to the spray system computer. Two drum heaters were also wrapped around the supply tank to maintain the dye solution at the desired temperature and prevent the water in the spray system from freezing.

A sensitive flow meter was installed in the main water supply line of the spray system to ensure that the spray system was working properly and that the amount of water sprayed was repeatable. This instrument was capable of measuring volume flow rates in the range 0.02 to 1 gallon per minute with an accuracy of 0.2 percent full scale (FS). The flow meter was calibrated by the NASA Glenn flow calibration lab prior to the start of the tests.

Fast acting solenoid valves were used to turn the spray on and off. During testing, the main air supply solenoid was turned on approximately 30 sec before the spray was initiated to allow the atomizing air pressure to stabilize. Next, the 16 water solenoid valves were activated by the computer system and a spray cloud was produced. The median volumetric diameter (MVD) of the spray cloud was set by varying the spray system air-to-water pressure ratio. The duration of the spray was controlled by the computer hardware.

Sixteen brackets were designed and built for mounting the 16-nozzle spray system to the IRT spray bars. The brackets allowed for a more precise installation of the 16 nozzle assemblies. The complete 16-nozzle spray system is shown in figure 25a and b. The installation of the spray system and the coordinates of each spray nozzle with respect to the IRT spray bars are given in figure 26a and b.

A heavy-duty electronic balance was utilized to monitor the amount of liquid left in the supply tank. A VAISALA humidity sensor was also installed at the inlet of the IRT test section, to record the relative humidity and temperature of the airstream. In previous impingement tests (refs. 6, 13, and 17), the only humidity and temperature readings available were provided by the IRT humidity sensor, which was located on the IRT spray bar in the plenum chamber.

Various components of the spray system—the stainless steel pressure tank for storing the dye solution, the main air and water pressure lines, and the air and water pressure regulators

are shown in figures 27 and 28. A close-up view of one of the WSU nozzle assemblies is provided in figure 29. The schematic of the spray system shown in figure 30 provides a summary of key system components.

The WSU spray system was assembled and tested extensively at WSU before it was transported to NASA Glenn for the water droplet impingement tests. During the impingement tests at the NASA Glenn IRT facility, detailed analyses of recorded spray system parameters were performed. The results showed that the system was capable of maintaining air and water pressures to within  $\pm 1.5$  psi from the required settings as demonstrated in table 3.

During the impingement tests, high-pressure air from the IRT spray bars was used to enhance cloud mixing and to improve the uniformity of LWC in the test section. The IRT spray bars were also used periodically to produce very fine sprays in order to maintain the required relative humidity in the test section. These fine sprays were conducted prior to the start of the impingement tests. Another method used to control the humidity was releasing water steam downstream of the test section.

#### **4.5 Spray System Data Acquisition and Control**

A 900 MHz Pentium III personal computer, equipped with a data acquisition card (DAQ) and a digital I/O (DIO) board was used to monitor and control the performance of the spray system. Data acquisition and system control software was developed to monitor, store and analyze spray system performance parameters. A schematic of the spray system data acquisition and control can be found in figure 31.

The data acquisition card used was a PCI-6071E from National Instruments with 32 input differential channels, and a sampling rate capability of up to 1,200,000 samples per second. The signals from all spray system pressure transducers, thermocouples, humidity sensor, flow meter and tank balance were directed to the PCI-6071 board through a shielded I/O connector block (SCB). All signals from the pressure transducers were transferred to the SCB through shielded cables from two control units which provided the excitation voltage for the SETRA transducers. The signals from the electro-pneumatic transducers used to control the air and water pressures were processed through a Fairchild control box before connecting to the SCB (fig. 32). Thermocouples signals were passed through a SC-2311 signal-conditioning unit from National Instruments which was modified to provide the required excitation voltages. The humidity sensor and the tank balance were equipped with their own power supplies and signal conditioning units. Consequently, they were directly connected to the SCB.

A solenoid valve on the water line of each nozzle assembly enabled the spray to be switched on and off individually from the spray system computer. Another solenoid valve was also installed in the main air supply which provided high pressure air for atomizing water sprays. Seventeen solid-state digital relay (SSR) modules were installed on three backplane boards to activate and deactivate these solenoid valves. The SSR modules were controlled by a high-speed, 32-bit parallel digital I/O ISA interface DIO card, PCI-DIO-32HS, from National Instruments.

The spray system software was developed using LabVIEW, a graphical programming language for data acquisition, analysis and presentation. The LabVIEW software provided a Windows driven menu for controlling and monitoring the performance of the spray system. Any combination of nozzles and transducers could be selected from the window menu. The user could also specify spray time, plot the transducer signals in real time, and store a range of test parameters as well as other information related to each test. Figure 33 shows spray system performance parameters recorded with LabVIEW during a typical spray system test. All test parameters and transducer readings were also written out to a Microsoft Excel file at the end of each test.

Data from the DAQ board were recorded at regular time intervals for the complete spray duration. The sampling rates were varied based on spray time. For the shortest 0.75 sec spray, the sampling interval was 0.005 sec. For the longer sprays (1 to 4 sec), a sampling interval of 0.01 sec was used. This was done to keep the size of the output files to a manageable level while providing sufficient resolution for monitoring the spray system parameters.

#### 4.6 Cloud Uniformity

One of the vital aspects of the experimental method is cloud uniformity for it has a significant effect on test repeatability and accuracy. A spray cloud is characterized by three parameters: droplet size, droplet distribution and LWC. Of the three parameters, LWC uniformity is the most difficult to control. Extensive cloud uniformity tests were conducted to set the locations of the 16 nozzles to provide a 1-ft high by 2-ft wide uniform cloud region centered in the IRT test section. Cloud uniformity was accomplished when LWC variation within the 1- by 2-ft test area, for all spray conditions selected for the impingement tests, was within  $\pm 20$  percent of the average. Note that for the test models, angle of attack and MVD cases used in the 2003 impingement tests the cloud area corresponding to model impingement region was 0.5-ft high by 1-ft wide. For this smaller cloud region, LWC uniformity was within  $\pm 10$  percent of the average.

During the 2003 impingement tests, cloud uniformity was measured using a laser imaging method and a grid/blotter method. In the laser imaging method a laser sheet was established in the test section with its plane normal to the tunnel axis. Light scattered by the droplets crossing the laser sheet was recorded with a CCD camera and was converted through software to LWC intensity. The laser sheet was established with 5-W Argon-Ion laser beam that was transmitted to a collimator through a fiber optic cable. The beam from the collimator was directed to a mirror attached to a rotating galvanometer which reflected the beam to a large (64 cm long) cylindrical lens. As the laser beam scanned the span of the lens a laser sheet was produced across the tunnel test section. The laser sheet setup is shown in figure 34a to e. The location of the laser sheet plane with respect to the IRT test section is shown in figure 35a.

A 14-bit CCD array camera installed outside the tunnel near the second tunnel control room was used to capture the laser sheet images by means of a boroscope. The boroscope was installed through the tunnel sidewall and was placed downstream of the laser sheet as shown in figure 35a and b. Approximately 2 in. of the boroscope was extended into the tunnel and was exposed to the flow. The uniformity tests were conducted with all the lights in the test section and in the secondary control room turned off. In addition, the lights in the main control room were dimmed. It was necessary to eliminate all light sources other than the laser light sheet to ensure that the cloud images recorded by the CCD camera were not affected by unwanted light sources and reflections. With the tunnel set to the required airspeed (175 mph), the spray system was activated for approximately 30 to 50 sec and several CCD images were recorded. In the CCD images, the high light intensity regions corresponded to high LWC region and vice versa. Using camera software, the images were analyzed to determine variations in LWC within the desired uniformity region.

In the second method (grid/blotter) for establishing cloud uniformity, a 6- by 6-ft stainless steel grid with horizontal and vertical grid spacing of 6 in. apart was installed in the test section as shown in figure 36. The plane of the grid was normal to the flow and passed through the center of the turntable. Blotter strips were installed on the grid to cover an area of 2-ft high by 2-ft wide as shown in figure 37. The tunnel was brought up to test speed and the blotters were sprayed. The dye distribution on each blotter was determined using the CCD reflectometer described in chapter 5 of this report. This grid/blotter method was found to be laborious and time consuming.

The majority of the cloud uniformity tests were conducted with the laser sheet method. The grid/blotter method was used at the end of the uniformity tests to verify the results obtained with the laser sheet method. The final spray nozzles locations are given in figure 26.

#### 4.7 MVD and LWC Measurement

Droplet size and distribution measurements for all spray conditions were determined using the NASA Glenn Forward Scattering Spectrometer Probe (FSSP), the 1D Optical Array Cloud Probe (OAP-C) and the 1D Optical Array Precipitation Probe (OAP-P). The OAP-P is also known as the OAP-Y probe due to the geometrical arrangement of the two probe arms containing the mirrors that are used to direct the laser beam. Details of the FSSP and OAP probes can be found in reference 27. The data from these instruments was combined to obtain a single droplet distribution using algorithms customarily employed for this purpose by the IRT droplet-sizing specialists. Pictures of FSSP and OAP installation in the test section are provided in figures 38a and b, and 39a to c. The LWC measurements were conducted using the NASA Glenn heated wire King Probe Model KLWC-5 described in reference 28. The probe operates on the theory that when a heated wire is maintained at a constant temperature, any excess power consumed by the wire impacted by the water is proportional to the mass of the water. The installation of the King Probe in the IRT test section is shown in figure 40a and b.

Two sets of droplet and LWC measurements were conducted during the six-week impingement tests. The first set was performed after the completion of the cloud uniformity tests and the second near the end of the impingement tests. Each series of droplet size, droplet distribution and LWC tests consisted of several repeated measurements of the desired spray cloud conditions. Note that the LWC measurements with the King Probe were used to evaluate spray cloud characteristics and to compare with local LWC measurements conducted with the collector mechanism. The King probe LWC measurements were not used in the reduction of the experimental impingement data.

To determine the effect of cloud unsteadiness on LWC, short and long duration sprays were conducted during the LWC measurements. Traces of LWC as a function of time showed no significant impact of spray duration on the average LWC value. Measured MVD and LWC distributions obtained at the center of the IRT test section are summarized in figures 41 to 45. MVD sizes and corresponding spray system air and water pressure settings are given in table 3.

Relative humidity studies conducted during the 1997 and 1999 impingement tests (refs. 17 and 29) showed that the effect of relative humidity on LWC was considerable, particularly for the 11- $\mu\text{m}$  MVD. Based on the findings of these studies, the 2003 impingement tests were conducted at a relative humidity of  $70 \pm 4$  percent.

#### 4.8 Reference Collector Mechanism

To correct the experimental impingement data for local variations in LWC, a measurement of local LWC was needed at all locations in the IRT test section where the test model blotter strips positioned. A reference collector device was developed at WSU to address this need. (Details of the development of the collector device are provided in ref. 13).

The collector device had six short blades and one long blade. Each blade was 0.2-in. wide and 1-in. in chord as shown in figure 46a. The original cross-section of the blade was triangular as discussed in references 6, 13, and 14. For the 2003 impingement tests Computational Fluid Dynamic analysis was used to redesign the cross section of the collector blade to reduce flow separation and improve local LWC measurements. A rectangular shape section was found to provide the least disturbance to the flowfield because it minimized vortex shedding downstream of the blade leading edge. The length (span) of the collector blades was 4 in. for the short blades and 9 in. for the long blade.

The collector device was tested in the empty IRT test section with its long 9-in. blade horizontal and vertical to provide a detailed map of the local LWC in the proximity of model blotter strip locations. The horizontal extent of local LWC measurements was determined by the distance between the upper and lower ice horns of the largest ice shape tested. This distance was approximately 4.7 in. and required data from the reference collector device to be collected at multiple locations in the test section. Collector tests were performed with the long blade placed vertically at location A, B, C, and D to provide local LWC values for data reduction. The four locations are shown in figure 46b and described below.

1. Location A: the furthest point provided by the lower horn of all ice shapes away from the centerline of the tunnel at the test angle of attack.
2. Location B: the centerline of the tunnel.
3. Location C: the projected location of the leading edge of the clean airfoil at the test angle of attack.
4. Location D: the furthest point provided by the upper horn of all ice shapes away from the centerline of the tunnel at the test angle of attack.

In addition, extensive tests were performed with the collector blade horizontal and placed 37.5 in. above the tunnel floor. With the blade horizontal, local LWC data could be collected over the complete horizontal extent of the impingement region of interest. The problem with placing the blade horizontal is that small vertical fluctuations in the spray cloud could impact the accuracy of the local LWC measurements for sprays which are less than 2 seconds in duration. Local LWC data obtained with the blade horizontal are typically used to provide a more accurate assessment of local LWC variation over the region of impingement compared to the results obtained from uniformity tests. Approximately 168 collector tests were performed to provide the required local LWC measurements for the analysis of the impingement data. On the average, 8 test repeats were performed for each MVD and collector location case.

For the collector tests, blotter strips 0.2 in. wide were placed on the long collector blade so that the plane of each blotter strip was normal to the flow. All collector tests were performed at the same airspeed and cloud conditions as those used for the test models. In addition, the spray duration for the collector tests was identical to that used for the airfoil tests.

The impingement data from the collector strips were analyzed using the data reduction methods described in chapter 5. The collector dye mass per unit area and its impingement efficiency were used to obtain the LWC in the freestream, which was then used to convert the raw impingement data for each test model into impingement efficiency distributions. Table 4 provides computed impingement efficiencies obtained with the LEWICE code for the collector blades for all spray cloud conditions used in the impingement tests. The table shows that the collector blade had high impingement collection efficiency. This is attributed to the small chord and thickness of the collector blades.

For clean, glaze, and mixed ice geometries, the collector dye mass used for normalization of the local impingement data was the average value from locations A, B, C, and D obtained with the collector long blade placed vertically. The collector dye mass selected for the reduction of the rime ice shape data was from location B only. This was done because the horn of this ice shape was very close to location B and its extent in the direction normal to the airfoil chord (i.e., ice thickness) was considerably smaller than the other ice shapes tested.

#### 4.9 Test Matrix

Models and conditions for the 2003 impingement tests are provided in table 5. All tests were conducted at total air temperature of 40 to 77 °F and a relative humidity of 70 ± 4 percent.

#### **4.10 Pressure Measurements**

The two airfoil models used in the 2003 impingement test were equipped with surface pressure ports as discussed in section 4.2. Note that the ten ice shapes tested were not instrumented with pressure taps. However, pressure measurements were made immediately downstream of the ice shapes. The IRT electronically scanned pressure system (ESP) was used to perform the pressure measurements. The ESP system consisted of six 32-port pressure modules with a range of  $\pm 5$  psid. One data port in each module was used for pressure checks. Thus, the total number of ports available for pressure measurements was 186 ports (31 ports per module). The ESP system used a three-point pressure calibration system to all port transducers. The calibration pressures were measured with precision digital quartz transducers. The three-point calibration was performed every 400 cycles (approximately 15 min) to ensure that the error in the measurements did not exceed 0.1 percent of the full-scale (ref. 6).

#### **4.11 Impingement Test Procedure**

To obtain water droplet impingement data for each test model, the following procedures were followed:

1. The spray system air and dyed water pressures were set to generate the desired MVD. Air and water pressure settings for all MVD sizes used in the impingement tests are given in table 3.
2. Blotter strips were attached to the model at the required spanwise location using aluminum tape. The blotter strips were approximately 1.5 in. wide and had two different lengths (24- and 48-in.). The longer strips were used on selected cases and for long duration sprays to study the extent of the impingement limits. For the 2003 impingement test, blotter strip installation fixtures were designed to ensure that the blotter attachment was precise and consistent between tests. The fixtures consisted of ten 0.75-in. thick plastic plates (one for each ice shape), which were cut so as to match the LEWICE ice shape traces as shown in figure 15. In addition, each plastic plate was under-cut to accommodate the thickness of the blotter paper. A table platform was also constructed along with brackets for attaching the table platform to the wing. The platform was used to maintain the blotter installation fixtures horizontal while installing the blotter paper. After the blotter strip was fitted and taped down following the contour of the ice shape, pencil marks were used to mark locations of interest on each ice shape, e.g., the "peaks" and "valleys" between the horns and the location corresponding to the clean wing leading edge. The marks were inscribed on the blotter installation tools to make certain that the pencil markings were consistent.
3. The tunnel was set to the required speed and water steam was injected into the airstream to attain the required level of relative humidity. Once the speed, relative humidity, and the air stream temperature were stable, the spray system was activated for a certain period of time (0.75 to 4.5 sec, based on the MVD as shown in table 3) and a dye trace was obtained on the blotter strips attached to the model.
4. After the spray was completed, the tunnel was set to idle. Each blotter strip was carefully removed from the model and hung in the control room to dry before storage. The model was then wiped clean using alcohol and a new blotter strip was attached for the next test.
5. Each test condition was repeated two to three times (i.e., 3 to 4 tests per MVD and angle of attack) to establish a measure of test repeatability. Blotter strips from the repeated tests were processed immediately after the strips were dried using the CCD system (description of the CCD data reduction system can be found in section 5.2.3) to evaluate

test repeatability before model changes. Note that the data reduction conducted in the IRT was preliminary and was only used to evaluate data repeatability.

Prior to the production impingement tests, test sprays for all MVD cases were carried out with model blotter strips and collector strips to assess dye penetration into the blotter and set the appropriate spray time duration for each MVD case. Dye penetration into blotter strips was evaluated by carefully segmenting the strip and viewing the cross section of each strip under a microscope to determine the level of dye penetration. To ensure that reflectance measurements were not adversely affected by dye penetration, the allowed dye penetration into the blotter strip was limited to less than 30 percent of the blotter thickness.

The collector mechanism was tested several times between model tests to provide local LWC measurements for reducing the model impingement results.

## 5.0 Data Reduction Methods

Two different methods were used to extract the data from the dye-laden blotter strips. The first method, developed by NACA in the 1950's, was based on colorimetric analysis (ref. 8) and the second method, which was found to be significantly more efficient and was able to provide higher resolution impingement data, was based on diffuse reflectance spectroscopy (refs. 13 and 17) developed by WSU and Boeing in the 1980's. Descriptions of the data reduction methods and the systems used for analyzing the 2003 raw impingement data from the blotter strips are presented below.

### 5.1 Colorimetric Analysis

The principle of colorimetric analysis conforms to Beer's law which states that the light absorbance of a solute at a particular wavelength is a function of its concentration in the solution, thus absorbance measurement can be used to measure concentration. To extract the dye amount from a blotter strip, first it was cut into small segments and stored into test tubes. Cutting each blotter segment into smaller pieces was performed in order to speed up the dye dissolving process. A precise amount of de-ionized water was then added to each test tube to fully submerge the pieces of each small blotter strip segment.

After sealing the tubes, the diluted blotter strips were left in a refrigerator for 1 to 2 days to allow dye extraction to occur. The dye used in the impingement test was highly soluble so that no mechanical agitation was required to extract the dye from the blotter paper. A white blotter strip (i.e. blotter strip with no dye on it) was also diluted to observe if the blotter fiber in suspension could affect the concentration reading and whether any correction was needed. The dye solution concentration was then measured using a spectrophotometer. The device used in this analysis was a GENESYS 20 spectrophotometer using a wavelength of 629 nm. This wavelength was used since the maximum absorption of the blue dye selected for the impingement tests occurred at 629.5 nm (ref. 6). Figure 47 depicts the equipment used in the colorimetric analysis.

For the colorimetric analysis to work, a relation between absorption and dye concentration must be established. Carefully prepared dye solutions with known concentrations were measured using the spectrophotometer to provide the relation needed. The relation between concentration and absorption readings from the spectrophotometer was found to be linear.

After the concentration of the diluted blotter strip was determined, it was multiplied by the volume of the de-ionized water added in the dilution process to obtain the dye mass. Due to the fact that the colorimetric analysis is laborious and time consuming, this method was used only with specially prepared dyed blotter strips for the purpose of defining the reflectance calibration curves (described in section 5.2.1). In addition, a few model impingement strips and a collector

strips were reduced using colorimetric analysis to verify the impingement results obtained from the reflectance measurements.

## 5.2 Reflectance Spectroscopy

The principle of the reflectance spectroscopy method is that when a dye-laden blotter strip is illuminated by a light source, the intensity of light scattered from the blotter surface can be used as a measure of the dye mass per unit area of the blotter strip. Regions on the blotter strip corresponding to high impingement rates are darker in color and reflect less light than those corresponding to low impingement rates. Regions with no dye accumulation are white and scatter the maximum amount of light. The relation between dye concentration and reflectance is not linear and is defined from calibration tests. To enhance the sensitivity of the reflectance method, the dye must have a strong absorption at the wavelength of the light source used for illuminating the blotter strips. For improved accuracy, dye penetration normal to the blotter surface should be kept to a minimum since the data reduction method relies on surface reflectance measurements. Tests to define the calibration curves and the two data reduction systems are described below.

### 5.2.1 Reflectance Calibration Curve

The reflectance calibration curve relates normalized reflectance (reflectance of dye-laden blotter paper divided by reflectance of white blotter paper) from the dye-laden blotter strip to dye mass and therefore water impingement on the blotter strip. The curve is a standard against which the reflectance of each blotter strip is compared during the data reduction process.

Blotter strips were placed on a 6- by 6-ft grid installed in the IRT tests section as described in section 4.6 and were sprayed with same dye solution used for the tests models. By varying the time that the strips were exposed to the spray, blotter strips with a range of uniform color densities were obtained, covering the spectrum from very light blue to dark blue color. The strips were measured 24-in. long and 1.5-in. wide.

These blotter strips were stored for analysis at Wichita State University. The calibration strips were scanned using the Laser and CCD reflectometers. The recorded reflectance measurements were then used to identify uniform color density regions on each sample strip. Disks with diameter of 1 in. were then punched out from these uniform color areas. The mass of the blue dye on each disc was extracted using colorimetric analysis described in section 5.1. Subsequently, the dye mass from each blotter disc was divided by the disc area to provide the dye mass per unit area. In addition to the calibration discs, selected collector blotter strips tested were also analyzed using colorimetric analysis and used as calibration points.

The dye mass per unit area and reflectance data obtained from the discs and collector strips were used to define the standard reflectance calibration curves for the Laser and the CCD reflectometer systems. The normalized reflectance calibration curve shown in figure 48 was produced by plotting the normalized reflectance from all blotter calibration samples against the corresponding dye mass per unit area. The calibration results show that the normalized reflectance of the laser data reduction system is very similar to the CCD system, thus only one calibration curve was needed. In this curve, a normalized reflectance value of 1 corresponds to the white blotter paper and indicates zero dye mass.

### 5.2.2 Laser Reflectometer

The first data reduction system used for the analysis of the 2003 impingement data was the laser reflectometer, which was developed and tested extensively during the 1985 and 1993 impingement research programs conducted by WSU and the Boeing Company (refs. 13 and 17). The data reduction system uses a laser beam to illuminate the blotter strip. In brief, the ratio

of the intensity of the reflected light from the blotter paper to the light intensity of the laser beam is a measure of impingement efficiency.

The main components of the laser reflectometer are depicted in figure 49a and b and include: (a) a red He-Ne laser with a wavelength of 632.8 nm, (b) a rotating drum for mounting the blotter strips, (c) a convergent lens for focusing the reflected light from the blotter strip onto a silicon photodetector and (d) an EG&G silicon photodetector for converting the reflected light collected by the lens into a voltage ( $V_1$ ) which was stored for further analysis, and (e) a splitter glass plate and another silicon photodetector for monitoring fluctuations in laser light intensity. The voltage ( $V_2$ ) from the second photodetector was also stored and was used in the data analysis. Note that the maximum absorption of the blue dye selected for the impingement tests occurred at 629.5 nm, which is very close to the wavelength of the laser, thus, ensuring that small changes in dye color density could be resolved by the system.

Voltages from the photodetectors and the rotating drum were monitored and controlled by a PC by means of a data acquisition board. A LabVIEW program was developed during this research program to control the operation of the reflectometer, but also analyze and plot the reflectance data. Details of the laser reflectometer can be found in reference 17.

Converting raw color density distribution from a dye-laden blotter strip into impingement efficiency distribution involved a number of steps. First, the raw reflectance versus surface distance data were extracted by mounting each blotter strip on the drum of the laser reflectometer and scanning the strip along its length as shown in figure 50a. The voltages  $V_1$  and  $V_2$  from the two photodetectors obtained during a scan were stored in computer files and their ratio was used to generate the raw reflectance values as shown in equation 5.1. These values were then normalized by the average raw reflectance of a reference white blotter strip which was scanned before and after each dye-laden blotter strip. The normalization equation is shown in the equation below.

$$R_{raw} = \frac{\text{Laser Intensity After Reflectance}}{\text{Laser Intensity Prior to Reflectance}} = \frac{V_1}{V_2} \quad (5.1)$$

$$R_{normalized} = \frac{R_{Raw} (\text{Dyed blotter strip})}{R_{Raw} (\text{White blotter strip})} \quad (5.2)$$

Typical normalized reflectance values from a blotter strip are plotted in figure 50b. Note that long blotter strips had to be scanned in segments because the reflectometer could only accommodate rectangular strips with a maximum length of 16.5 in. The normalized reflectance data from each segment of the blotter were then combined using a computer program and stored for further analysis. The spatial resolution of the reflectometer was 47 data points per inch.

### 5.2.3 Charge-Coupled Device (CCD) Reflectometer

The second data reduction system made use of a CCD array camera for digitizing the images of the dyed blotter strips, which were then stored in arrays of reflectance intensities for analysis later. The CCD system developed by WSU is shown in figure 51a and b. The system consisted of a Pentium 200 MHz PC, a CCD array camera with 14-bit resolution, a camera electronics unit, a camera PC controller, a 24 mm Nikkor lens, 12 high flux red LED lights, a power supply for the LEDs, a camera stand and a portable dark room for reducing the data.

The lighting system, which was developed by WSU personnel in 2001 (ref. 6), consisted of 12 red high flux Light Emitting Diode (LED) illuminators as shown in the schematic provided in figure 52a. The LEDs were OptoTechnology High Flux LED Illuminators, Shark Series, OTL-

630A-5-10-66-E, with 630 nm wavelength. This wavelength was chosen to match the absorption characteristics of the blue dye so that small changes in dye color density could be better resolved by the system. The LEDs were connected in parallel to a single power supply. A 1 KW potentiometer was connected in series to each LED. With its light intensity adjusted individually, uniform illumination region ensued over a large area. The potentiometers were placed on a single circuit board and were mounted onto an aluminum frame designed for the 12 LEDs. The aluminum frame consisted of two plates with a wide rectangular slot to house the LEDs, and a T-shape bar for structural reinforcement. The rectangular slot allowed adjustment of the LED locations to achieve uniform illumination over the image capture area. Uniform illumination was determined with a sensitive light meter. The aluminum plate holding the LEDs and the potentiometers was mounted on a light steel frame attached to the CCD camera mount as shown in figure 52b.

The data from each dye-laden blotter strip were extracted as follows. Each strip was placed next to a reference scale on a table inside a specially constructed dark room. The highlight mark on the blotter strip was aligned with a fixed mark on the reference scale. The LED lights were set to the required intensity level by adjusting the voltage and amperage of the two power supplies. The camera shutter was activated through the PMIS software and it was kept open for a specified time period, which was determined during the system calibration. A 512 by 512 pixel array image of the blotter strip was obtained and it was stored on disk for later analysis. The camera was capable of resolving nearly 14 bits (or approximately 16,000 level) of intensity values of scattered light from the blotter strip. The blue strip was removed and a white reference strip was placed on the table in the same location. The process was repeated and a 512 by 512 image of the white strip was obtained and stored.

The images were then processed through a Windows-driven software that was written in PV-WAVE command language. The process for generating the reflectance data from these images involved the following steps:

1. Each dyed strip image and the corresponding white strip image were read using the PV-WAVE software developed at WSU. Both images were corrected using reference images to compensate for camera noise and lens distortions, which were obtained and stored during the calibration of the CCD array camera.
2. The images stored were in arrays of reflectance intensities and pixel locations only, thus a relation between real distance and pixel location had to be established. The program allowed users to define a length scale by selecting two points on the blotter strip image. The number of pixels in the horizontal direction and the actual distance between the selected points were used to establish the length scale.
3. Using the computer mouse, a rectangular region was selected on the white strip image. This region was processed by the software to provide an average reflectance value for the white paper.
4. For a dye-laden blotter strip, a region that was large enough to cover the complete extent of dye impingement was selected using the computer mouse as shown in figure 53. Using the highlight on the strips (typically the point on the leading edge of the test geometry corresponding to  $y/c=0$ ), the location of zero distance can be defined.

The software produced an array of reflectance versus surface distance for the dyed strip. These values were processed through a 3-point moving average algorithm and the smoothed values were normalized by the average intensity of a white blotter strip using eq. (5.2). An array of normalized intensity values (i.e., 0 to 1) versus surface distance was obtained for each blotter strip as shown in figure 54 and was stored in a file for further analysis.

A FORTRAN program was developed to extract the impingement efficiency distribution from the stored normalized reflectance data which were generated from either reflectance measurement method. Because impingement tests were repeated a number of times for each

test condition, the program processed the normalized intensity values from several blotter strips into a single array of averaged normalized intensity versus surface distance. This array was then converted into dye mass ( $\mu\text{g}/\text{cm}^2$ ) versus surface distance using the calibration curve shown in figure 48. The impingement efficiency for each data point recorded was then obtained using the following equation.

$$\bar{\beta} = \frac{\text{Local Dye Mass per Unit Area}}{\text{Average Collector Dye Mass per Unit Area}} \times \bar{\beta}_{\text{collector}} \quad (5.3)$$

Collector strips were reduced prior to the model strips since the collector dye mass was required for normalization to define the impingement efficiency of each test model. The values of  $\bar{\beta}_{\text{collector}}$  for all spray cloud conditions used in the impingement tests are given in table 4.

## 6.0 LEWICE-2D Impingement Analysis Method

Analysis results for all test cases presented in this report were obtained by NASA Glenn personnel using the LEWICE-2D code. This code is a panel-based ice accretion code that applies a time-stepping procedure to calculate an ice shape. The potential flowfield in LEWICE (ref. 30) is calculated with the Douglas Hess-Smith 2-D panel code. This potential flowfield is then used to calculate the trajectories of the water droplets and the impingement distribution on the body.

Three versions of LEWICE 2D were used in this work as follows:

- LEWICE 1.6: This version was used by NASA personnel to generate the analytical impingement efficiency data for comparison with the experimental data shown in figures 84 to 94
- LEWICE 1.7: This version of LEWICE was used by WSU personnel to produce the trajectories in figures 111 to 114, and figures D1 to D8 in appendix D. This code was selected because it allows the user to turn off the gravity effect in NAMELIST TRAJ1. With the wing placed vertically in the tunnel, the gravity term was turned off in the trajectory analysis, because the droplet trajectories were computed on a horizontal plane normal to the wing leading edge (i.e., no gravity effect on droplets)
- LEWICE 2.2: This version of LEWICE was used by NASA personnel to generate the simulated ice shapes in figure 22a to c which were tested during the 2003 IRT entry.

Note that all of the LEWICE versions listed above, as well as the most recent version of LEWICE (version 3.0), use the same integration routine and impact equations in the calculation of impingement efficiency. The main differences between the three codes regarding impingement analysis is mainly in the schemes used to discretize the surface of the geometry.

Prior to the impingement analyses, the computed flowfield from the LEWICE code was compared with the measured pressured distributions for each model and angle of attack tested. If the agreement between the experimental and the computed pressure was not favorable, the angle of attack in the computer code was slightly modified until a good match was obtained. This small adjustment in AOA was necessary because the LEWICE code does not account for wind tunnel wall and flow angularity effects. For the cases involving the large 22.5- and 45-min ice shapes it was not possible to match the experimental pressure distributions due to flow separation immediately downstream from the ice shape horns. LEWICE uses a potential flow code which cannot simulate regions with extensive flow separation. For such cases a Navier-Stokes flowfield should be used prior to conducting trajectory analysis with the LEWICE code. This was not attempted in this work.

Next, the impingement characteristics were computed using a 27-point (also referred to as 27-bin) discrete approximations of the experimental droplet distributions measured with the

FSSP, OAP-C and OAP-P during the impingement tests (fig. 55 and table 6). A 10-bin discrete droplet size distribution was also generated for each MVD case for use with the public version of the LEWICE code, which allows up to a maximum of 10 droplet sizes per distribution. The 10-bin droplet size distributions can be found in table 7 and in figure 56.

## 7.0 Results and Discussion

In this section, potential sources of experimental error and the steps taken to minimize or eliminate these errors are discussed. In addition, the experimental water droplet impingement data for the two airfoils and the ten ice shapes tested in 2003 are presented and compared with LEWICE analysis data. All experimental data are averaged data from repeated tests. The analysis impingement data were obtained with the LEWICE computer code using the procedure discussed in chapter 6.

In most cases the impingement data are presented in the form of local impingement efficiency ( $\bar{\beta}$ ) plotted versus surface distance ( $s$ ) in mm. Surface distance is measured from the highlight (a reference point where  $s = 0$  mm) which in all cases corresponds to the location near the leading edge where  $y/c$  is zero. For the clean airfoil the highlight was at the leading edge while for the ice shapes, the highlight was located between the ice horns. Note that negative surface distance corresponds to the upper surface of the airfoil. Geometric parameters, as well as flow and droplet parameters for the airfoils and ice shapes tested are summarized in table 8.

### 7.1 Discussion of Experimental Errors

A discussion of potential sources of error affecting the impingement data can be found in reference 17. In general, the experimental errors can be divided into two groups. The first group involves errors in the experimental method used to obtain the raw impingement data while the second group includes errors related to the data reduction methods. Errors in the experimental method originate from variations in spray system performance, cloud uniformity, cloud unsteadiness, tunnel flow conditions, relative humidity, and inaccuracies in measuring local LWC, cloud median volumetric diameter and cloud droplet distribution. Errors in the data reduction methods arise from variations in blotter paper properties, light illumination intensity, and errors in the normalized reflectance calibration curves and in the data reduction systems. As discussed in reference 17, several improvements have been made to the experimental and data reduction methods since 1996 and these improvements have significantly enhanced the quality of the experimental.

During the impingement experiments, extreme care is taken to monitor all aspects of the experiment and to perform daily checks of all systems used in the experimental and data reduction methods. Experience gained from twenty years of testing has shown that the best indicator of data quality is test repeatability. During production runs each test condition is typically repeated three to four times. In addition, during each IRT entry a considerable number of repeats (as many as 10 to 20) are performed with selected configurations to better assess test repeatability. In addition, prior to the start of the production runs, impingement tests are conducted with a calibration model to verify the experimental setup with results from prior IRT entries. During the 2003 impingement tests, processes were developed to ensure consistency in all aspects of the experimental and data reduction methods as described below. Samples of the variation in the spray system water flow rate for different geometries are presented in figure 57, whereas the time traces in spray system pressures for different MVD conditions are presented in figure 58.

### 7.1.1 Experimental Method

- Extensive tests were performed in a WSU laboratory to calibrate and verify the performance of the spray system two months prior to the impingement tests. During these tests the spray behavior of each of the 16 nozzles was documented and analyzed to determine the on-off response of each nozzle. This was done for all MVD conditions selected for the tests.
- All spray system transducers were calibrated by the NASA Glenn calibration laboratory prior to the IRT entry.
- A process was developed for preparing large quantities (about 30 gal) of dye solution. Accurate gravimetric balances were used to measure precisely the amount of dye and water to be mixed every time a new batch of dye solution was prepared. Solution samples were checked with a spectrophotometer to ensure consistency in dye concentration. Furthermore, each time a new batch of solution was added to the tank, samples of the solution were taken from various parts of the spray system such as the tank, before and after the water filter, and from selected spray nozzles to ensure that the solution was consistent throughout the spray system components.
- Experiments were conducted in a laboratory for the first time to investigate the effect of dye on water surface tension properties as discussed in reference 17. It was found that the dye had no impact on water surface tension. Surface tension plays a significant role in large droplet impingement dynamics as discussed in reference 2.
- Preliminary spray tests were performed in the IRT with all MVD conditions selected for the impingement tests to determine the spray time required for optimum color density and dye penetration into the blotter paper. Blotter strips from these preliminary tests were segmented and examined under a microscope to determine the level of dye penetration. The spray times selected maintained maximum dye penetration to less than 30 percent of the blotter paper thickness for most MVD cases.
- The spray system was tested each day prior to the start of the tests by conducting single nozzle sprays and combination nozzle sprays. During each test, the volume flow from the nozzle(s) was monitored to ensure consistent nozzle performance. Note that a slightly blocked nozzle can affect cloud uniformity and impact the experimental results. The IRT MOD-1 nozzles installed on the WSU spray system were carefully picked to have very similar flow rates.
- To eliminate potential problems with nozzle freeze out during the impingement tests, thermocouples were installed at strategic locations of the spray system to monitor the temperature of the dye solution. Water temperature was maintained above 40 °F using heaters attached to the dye-solution tank of the spray system. Nozzle freeze out can have a significant impact on LWC uniformity.
- Extensive uniformity tests were performed prior to the start of the production runs to ensure uniform LWC distribution in the test section for all MVD conditions as described in section 2.4 of this paper.
- During production runs test sprays were performed prior to the tunnel start and the spray system performance was assessed by examining the time traces stored by the computer system used to control and monitor spray system performance. The test sprays were performed to determine if all nozzles were spraying properly.
- Special tools were developed for installing the blotter strips on the ice shape tested. Experience with impingement tests has shown that data repeatability is considerably affected by how well the blotter conforms to the surface of the geometry. Even if the blotter paper is only slightly raised above the surface of the geometry, the impingement data will be affected. The tools ensured that the paper conformed to the model surface and that the paper installation was identical for each test. A tool was designed for each

ice shape tested using a CNC milling machine. Each tool had several reference markings on it for relating the dye trace on the blotter paper to locations on the surface of the airfoil and ice shape.

- Each impingement test was repeated several times and the blotter strips were analyzed with the CCD reflectometer to verify test repeatability. All data obtained during each day were analyzed during the following morning and the results were used to determine if additional runs were needed for a specific test condition before installing the next ice shape on the airfoil.
- For each test condition one long spray was performed and the dye trace on the blotter paper was used to verify the impingement limits obtained from the short sprays. The verification was done by visual inspection. Blotter strips from the long sprays were saturated with dye and could not be analyzed with the data reduction systems. However, selected strips were analyzed using colorimetric analysis and the results were used to verify the data from the laser and CCD reflectometers.
- Humidity has been shown to have a significant effect on LWC for small and large droplets (refs. 11, 14, and 17). During the 2003 impingement tests the relative humidity in the IRT test section was maintained at  $70\pm4$  percent. Humidity was monitored with humidity sensors installed in the test section and on the IRT spray bars. A process was also developed for setting tunnel humidity for the impingement tests.
- Repeated measurements of spray cloud droplet distribution and LWC properties were performed to document the spray clouds and to assess the repeatability of the spray system air and water pressure settings. Measurements were conducted prior and after the impingement tests to warrant consistencies within the test period.
- Over 160 local LWC measurements were performed in the IRT test section using the collector device. These measurements were taken over a range of model surface locations to evaluate local variations in LWC uniformity and to obtain reference LWC values for data analysis (fig. 59).
- During production runs, impingement data for the test models and collector device were obtained with the same batch of dye to ensure that potential small changes in dye concentration did not affect the impingement data.
- A concern in impingement testing has been dye recirculation in the IRT circuit. Blotter strips were placed at strategic locations upstream of the spray bars and were monitored at regular intervals during the impingement tests. No dye trace was ever found on these blotter strips.
- Pressure data for each test model were obtained at the start and end of the impingement tests to verify flow conditions and evaluate the repeatability of the pressure data.

### 7.1.2 Data Reduction Method

- Blotter paper properties are important to the quality of impingement results as discussed in reference 11. The complex geometries of the ice shapes tested resulted in crease formation on certain locations of the blotter strips. The effect of creasing on reflectance measurements was evaluated during laboratory tests at WSU with the CCD reflectometer and it was found that it did not affect the data reduction.
- New calibration curves were prepared for both data reduction systems to develop the relationship between normalized reflectance and dye mass density. The calibration was conducted using dyed blotter strips that were generated in laboratory tests as well as blotter strips generated during the IRT tests.
- The impingement data from the dye-laden blotter strips were extracted using both the laser and CCD reflectometers and the results from the two systems were compared for consistency.

- During the data reduction process, reference strips were used at regular time intervals to verify the repeatability of the data reduction systems.
- Selected blotter strips were reduced repeatedly over a period of several months to evaluate the repeatability of the data reduction process.
- Blotter strip illumination uniformity during data reduction with the CCD reflectometer was monitored at selected locations with an accurate light meter to verify that the light intensity over the blotter strip was consistent throughout the data reduction process.
- All impingement limits obtained from the impingement curves produced by the data reduction systems were verified by inspecting each blotter strip visually. The visual inspection was conducted independently by two researchers.
- Selected collector strips were analyzed using colorimetric analysis for comparison with the collector dye mass data obtained with the laser and CCD reflectometers. The results were found to be in good agreement.

## 7.2 Pressure Distributions

Experimental pressure data for the MS(1)-0317 at zero angle of attack are compared with analysis results obtained with LEWICE in figure 60 and demonstrate good agreement. Pressure data for the clean and iced NACA 23012 airfoil and for an angle of attack of 2.5° are presented in figures 61 to 71. The pressures provided are for the airfoil surfaces only since the ice shapes were not instrumented with pressure taps. The LEWICE pressure distributions presented were obtained at an angle of attack of 2.1° because this angle resulted in the closest match with the experimental pressure distributions. Note that LEWICE uses a potential flow (panel) method to compute surface pressures which does not model tunnel wall effects and viscous flow effects such as boundary layers and wakes, and regions of flow separation.

Comparison of the experimental and LEWICE pressure distributions were in good agreement for the clean NACA 23012 airfoil and for the 5- and 10-min glaze ice shapes as shown in figures 61 to 63. For the 15- and 22.5-min glaze ice shapes, LEWICE did not match the experimental data over the forward 10 to 20 percent chord as demonstrated in figures 64 and 65. In both cases flow separation in the form of a long leading edge bubble is evident in the experimental pressure distributions. For the 45-min ice shape, the leading edge bubble over the forward 30 to 35 percent chord of the NACA 23012 airfoil downstream of the ice shape upper and lower horns was not predicted by LEWICE as shown in figure 66.

For the NACA 23012 airfoil with the 7.5-, 15-, 22.5-, and 45-min mixed ice shapes tested, the computational and experimental pressure data were in good agreement as shown in figures 67 to 70. The reason for the improved correlation between LEWICE and experiment in the case of the mixed ice accretion is attributed to the more streamlined shape of the mixed ice shape tested.

The experimental and analysis pressure data for the NACA 23012 airfoil with the 45-min rime ice shape exhibited good agreement as shown in figure 71. This was attributed to the streamlined shape of the rime ice.

## 7.3 Impingement Results

### 7.3.1 Test Repeatability

Test repeatability is an important indicator of the quality of the experimental results. Test repeatability is assessed by computing the maximum percent variation,  $R_{max}$ , of repeated tests from the average. For clean airfoils and wings, the maximum variation in the test data is typically observed at the point of maximum impingement efficiency (i.e., the peak of the impingement curve). However, with the simulated ice shapes tested multiple sharp impingement peaks were obtained making it difficult to compute the value of  $R_{max}$ . The absolute maximum local

impingement efficiency observed at the leading edge region of the clean or iced models is denoted by  $\beta_1$ , whereas the minimum local impingement efficiency observed between the upper and lower horns of the glaze and mixed ice shapes tested is denoted by  $\beta_2$ . The  $\beta_1$  and  $\beta_2$  values of the experimental data are tabulated in table 10. To better define test repeatability for the iced configurations, an additional parameter,  $R_{\text{AREA}}$ , was computed by determining the maximum percent difference in the total area under the impingement curve of each repeated test from the average. This difference is representative of the variation in total impingement efficiency.

Data repeatability for the 2003 impingement tests conducted with the NACA 23012 airfoil and the five glaze ice shapes is demonstrated in figures 73 to 82 and in table 9. The maximum variation ( $R_{\text{max}}$ ) in  $\beta_1$  from the average of repeated runs (3 to 4 per test case) was less than 10 percent for 52 out of the 56 cases tested. In addition, the maximum variation in the area under the impingement curve ( $R_{\text{AREA}}$ ), was less than 10 percent for 55 out of the 56 cases tested. These values indicate very good test repeatability. Only, in 4 out of the 56 cases tested  $R_{\text{MAX}}$  was between 10 and 13 percent and in one case the value of  $R_{\text{AREA}}$  was between 10 and 13 percent.

Figure 83 demonstrates the repeatability of the experimental setup by comparing experimental impingement data obtained with the MS(1)-0317 airfoil during five IRT entries spanning the time period 1985 to 2003 (refs. 6, 13, 17, and 29). The results are for MVDs in the range of 19 to 21  $\mu\text{m}$  and show very good agreement in magnitude and overall trend. LEWICE analysis data for an MVD of 20  $\mu\text{m}$  are also provided for comparison and are in very good agreement with the experimental data.

### 7.3.2 Experimental and LEWICE Impingement Data

Comparisons of LEWICE and experimental impingement data are provided in figures 83 to 94 for all configurations tested. The experimental data presented were obtained by averaging results from repeated tests conducted for each geometry and test condition. All experimental data presented were reduced with the CCD reflectometer. Impingement data reduced using the laser reflectometer were practically identical to those obtained with the CCD data reduction system. The main difference between the CCD and laser reflectometer data was in regions between the ice shape horns where creases were present in the blotter paper. The laser reflectometer which relies on point reflectance measurements was more sensitive to the crease formation and the impingement curves obtained from this data reduction were not as smooth in the region between the ice shape horns as those from the CCD system. As discussed in chapter 6 the LEWICE analyses were performed by NASA personnel using 27-bin approximations of the spray cloud droplet distributions measured with the FSSP and OAP probes during the experimental investigation.

**7.3.2.1 NACA 23012 airfoil.**—On the clean NACA 23012 airfoil, good agreement between experiment and analysis was observed for the 20  $\mu\text{m}$  case. For the larger MVDs, however, LEWICE predicted higher total water impingement and greater impingement limits compared to the experimental data. Total impingement efficiency based on the experimental data ranged from 18.7 to 56.2 percent as the MVD was increased from 20 to 236  $\mu\text{m}$  compared with 17.4 to 84 percent for LEWICE.

**7.3.2.2 NACA 23012 airfoil with simulated glaze ice shapes.**—Overall, the trends in the computed and experimental impingement curves were in good agreement for most of the ice shapes tests. However, for the large MVDs of 52, 111, 154, and 236  $\mu\text{m}$  the efficiency and extent of water impingement predicted by LEWICE were considerably greater than those obtained from the experiment. Even for the 20  $\mu\text{m}$  case, the LEWICE impingement efficiencies near the leading edge (region between ice horns) were higher than the experimental values by approximately 0.1 to 0.25 depending on surface location. Although the exact reason for the observed differences is not known, potential contributors include the difference in the

experimental and computed flowfields as shown in figures 62 to 66 and small variations in cloud uniformity within the region of measurement.

Experimental,  $\bar{E}_E$ , and LEWICE,  $\bar{E}_L$ , total impingement efficiencies for the five glaze ice shapes are provided in table 10. Note that in all cases,  $\bar{E}_E$  and  $\bar{E}_L$  increased as MVD increased, albeit at different rates. For the five MVDs tested, the maximum  $\bar{E}_E$  was obtained with the 45-min ice shape while the minimum was obtained with the 10-min glaze ice shape. The results also demonstrate the differences between LEWICE and experimental total impingement efficiencies,  $\Delta\bar{E} = \bar{E}_L - \bar{E}_E$ . For the 20  $\mu\text{m}$  case,  $\Delta\bar{E}$  ranged from -0.002 to 0.05 depending on test configuration. For the large droplet cases (52, 111, 154, and 236  $\mu\text{m}$ ),  $\Delta\bar{E}$  ranged from 0.24 to 0.69 and increased as the ice shape size increased from 5- to 22.5-min glaze ice shape. The observed difference between LEWICE and experiment was mainly due to the impingement region downstream of the ice horns which was considerably overpredicted by LEWICE. For the 45-min ice shape  $\Delta\bar{E}$  was smaller than the rest of the four glaze ice shapes because the horns of this ice shape shielded the airfoil surface downstream of the horns from direct droplet impingement. For this case, LEWICE and experimental impingement data downstream of the horns were in good agreement. For the large MVDs (greater than 20  $\mu\text{m}$ ), the maximum total impingement efficiency computed with LEWICE corresponded to the 22.5-min glaze ice shape, whereas the experimental data showed that maximum total impingement was obtained with the 45-min glaze. The main reason for this difference between experiment and analysis is due to an interpolation method used in LEWICE to compute impingement efficiency between adjacent surface points as discussed in section 7.3.2.5.

**7.3.2.3 NACA 23012 airfoil with simulated mixed ice shapes.**—The trends exhibited by the computational and experimental impingement are as follows:

- The total impingement efficiency and the extent of impingement limits increased as the MVD increased. For the 52, 111, 154, and 236  $\mu\text{m}$  MVD cases, LEWICE significantly over-predicted both the impingement limits and the local impingement efficiencies. For the 20  $\mu\text{m}$  case, LEWICE predicted higher local impingement efficiency over the ice shape region by up to 0.2 depending on surface location.
- Total impingement efficiencies based on experiment ( $\bar{E}_E$ ) and those of LEWICE analysis ( $\bar{E}_L$ ) for all mixed ice shape geometries increased as MVD increased, albeit at different rates.
- For MVD of 20  $\mu\text{m}$ ,  $\Delta\bar{E}$  ranged from -0.002 to 0.05 while for the larger MVDs  $\Delta\bar{E}$  ranged from 0.27 to 0.56. For most of the large MVDs,  $\Delta\bar{E}$  increased as the ice shape size increased.
- Referring to figure 93b to e, the secondary impingement peaks on the upper and lower surfaces (indicated by the symbols A and B respectively) were due to direct impingement by the large droplets. Note that the peaks predicted by LEWICE (A1 and B1) were considerably higher than the experimental peaks (A2 and B2). The main reason for the observed difference is droplet splashing which is not simulated in LEWICE. Another interesting observation is that the experimental impingement peak (B2) on the lower surface occurred downstream of the peak predicted by LEWICE. A possible reason for this difference is droplet breakup downstream of the lower horn which is not simulated in LEWICE. Studies performed at WSU (not presented) with simulated ice shapes featuring large horns have shown that large droplets could breakup downstream of the horns. The trajectories of the droplet fragments (smaller droplets) are affected by the shear flow behind the ice horn and as a result impinge further downstream compared to the impingement location without droplet breakup. In addition, because the airfoil surface slope is lower at the point where the droplet fragments impinge, the incoming water mass is spread over a larger surface area resulting in lower local impingement efficiency.

**7.3.2.4 NACA 23012 airfoil with simulated rime ice shape.**—For the 45-min rime ice shape, the total impingement efficiency increased as the MVD size was increased. LEWICE predictions of the local impingement efficiency and extent of water impingement, however, were considerably greater than the experiment, especially for the larger MVDs. For all MVDs tested, LEWICE over-predicted the total impingement efficiency by 0.06 to 0.36.

**7.3.2.5 Comments on the difference between experimental and LEWICE results.**—For the large MVD cases (52, 111, 154, and 236  $\mu\text{m}$ ) involving the 10-min glaze, 15-min glaze, 22.5-min glaze, 15-min mixed, 22.5-min mixed, and 45-min mixed ice shapes, the LEWICE data corresponding to the region immediately downstream of the horns (region A, fig. 86b) exhibited a gradual decrease in  $\bar{\beta}$  compared to the sharp drop seen in the experimental data. The reason for this difference between experiment and analysis is attributed to a numerical artifact in LEWICE. A detailed explanation is provided below.

The interpolation scheme used in LEWICE to calculate collection efficiency at a surface point can have difficulties for geometries with multiple impingement regions. Multiple impingement regions can occur on complex ice shapes, highly cambered wings, and multi-element wings. The method predicts water impingement in some of these cases where in fact there is no water impingement. The problem is due to the way in which the method calculates collection efficiency and assigns it to a surface point.

Collection efficiency is calculated as the distance between two adjacent impacting particles divided by the distance between these trajectories at the freestream release point. The collection efficiency at any surface point located between the impact points is calculated using the collection efficiency generated from these two particles.

The interpolation problem occurs when the two adjacent impacting particles are not part of the same impact region but of two different impingement regions. In these cases the trajectories are actually the limiting or “tangent” trajectories of two distinct impingement regions. For example, one trajectory represents the aft impingement limit of a forward impingement region and one trajectory represents the forward limit of the aft impingement region. In these cases, the collection efficiency between the two regions should be zero but LEWICE interpolates values linearly between the two regions from the value at the limits of both regions. Solutions to this problem are difficult because it is hard to differentiate between two distinct smaller impingement regions and one larger one. One approach for solving the impingement efficiency interpolation issue in LEWICE is the use of the Monte-Carlo method for computing droplet impingement efficiency. This method is presented in appendix E along with computed impingement curves obtained with a Monte-Carlo trajectory code developed at NASA Glenn. The computed impingement curves show the same sharp drop off behind the ice horns as those from the experimental results. Note that Monte-Carlo computations are very intensive due to the large number of droplets that are needed to accurately compute the impingement characteristics as discussed in appendix E.

One crucial point to note is that although these errors appear large for some cases, they probably do not affect the ice shape generation in LEWICE greatly. This is because the observed errors occur mostly when there is a mismatch between the droplet size used to generate the ice shape and the one used for the comparison to the experimental data. When the collection efficiencies are compared at the same droplet size for both experimental data and for that at which the ice shape was generated the agreement is good. For larger droplet sizes, the error increases mostly in the region aft of the ice shape due to the larger droplets hitting further back on the wing and forming a secondary impingement region.

The falloff in agreement between the experimental and LEWICE collection efficiencies for the case of droplets larger than those used to accrete the ice shape is due to a close coupling between the icing and impingement limits for ice shapes. In general, as the ice shape generation progresses, the impingement limits, which are directly related to droplet size, and the

icing limits converge. This implies that the droplets used to generate the ice shape do not impact aft of the icing limit. For this droplet size, we generally have only a single impingement region with no associated interpolation errors. When the droplet size is increased from this value, the droplets begin to hit aft of the ice shape which results in secondary impingement regions. The formation of these secondary impingement regions causes interpolation errors between the two impingement regions for the reasons described above. This is the reason for the observed discrepancy in the comparison to the experimental data.

Other potential reasons for the discrepancies between the analysis and the experimental impingement data include the following:

- Differences between the actual and the computed flowfield particularly in the region between the horns. Also, flow separation downstream of the horns is not well modeled by potential flow models such as the one used in LEWICE. For the large ice shapes, the pressure data presented indicate considerable differences between the LEWICE and the experimental flowfields.
- Droplet splashing has been observed during large droplet impingement experiments (refs. 6 and 7). The effect of splashing reduces water mass deposited on the surface of the airfoil. LEWICE does not model the effects of large droplet splashing.
- Errors associated with the experimental investigation.

### 7.3.3 Effect of Geometry

In this section, the change in the impingement characteristics as a function of ice shape size is discussed. The ice accretions considered are the five progressively larger (5-min to the 45-min) glaze ice shapes and the four mixed condition cases ranging from the 7.5-min to the 45-min ice shapes. In addition, the differences between the impingement efficiencies of the three types of ice shapes tested are compared.

**7.3.3.1 NACA 23012 airfoil with simulated glaze ice shapes.**—Figure 95 demonstrates the change in water impingement efficiency as the glaze ice shapes become progressively larger in size while the MVD is kept constant. The main observations from the experimental results presented are as follows:

- The extent of the water impingement in the vicinity of the leading edge increased monotonically as the size of the glaze ice shape was increased. For the 5-min glaze ice, the extent of water impingement over the leading edge ranged from approximately –25 mm (upper surface) to 25 mm (lower surface). For the 45-min ice shape the impingement extent was from –80 to 60 mm.
- Multiple local impingement peaks were observed between the ice horns. The magnitude of the peaks decreased near the center of the ice shape ( $s = 0$  mm) and increased near the horn tips as the ice shapes became progressively larger.
- For all MVD cases, the maximum local impingement efficiency of the clean airfoil was greater than the maximum impingement efficiency of the ice shapes tested.
- Secondary impingement peaks were observed over the lower and upper surfaces of the airfoil downstream of the ice horns. These secondary peaks occurred between –30 and –90 mm (upper surface) and 30 and 60 mm (lower surface). The secondary impingement peaks decreased in magnitude and extent as the ice shapes increased in size from 5- to 15-min. For the 22.5 and 45-min ice shapes, no secondary peaks were observed immediately downstream of the horns due to the large horn size.
- For all MVDs tested, the maximum local impingement efficiency of the 45-min ice shape was less than that of the other four ice shapes.

- For all MVD cases, the total water impingement efficiency decreased in the following sequence: clean airfoil, 5-min glaze ice shape, and 10-min glaze ice shape. For the 15-, 22.5-, and 45-min ice accretions the total impingement efficiency increased as the ice shape size was increased, except for the 236  $\mu\text{m}$  case. For all MVD cases, the maximum total impingement efficiency was obtained with the 45-min ice shape while the minimum total impingement efficiency was obtained with the 10-min glaze ice shape.

**7.3.3.2 NACA 23012 airfoil with simulated mixed ice shapes.**—Figure 96 demonstrates the change in impingement efficiency as the mixed ice shape become progressively larger in size while the MVD is kept constant. The key observations from the experimental results presented are as follows:

- The coverage of water impingement in the airfoil leading edge vicinity increased monotonically as the size of the mixed ice shape increased from 7.5- to 22.5-min. For the 7.5-min mixed ice shape, the extent of water impingement over the leading edge ranged from approximately –20 mm (upper surface) to 20 mm (lower surface). For the 22.5-min ice shape, the impingement extent was from –45 to 35 mm. For the 45-min mixed ice shape, the impingement extent increased substantially, from –10 to 90 mm. These limits on both surfaces shifted toward the upper surface: a trend not observed with the smaller ice shapes (7.5 to 22.5 min).
- Multiple local impingement peaks were observed between the ice horns. The magnitude of the peaks decreased near the center of the ice shape ( $s = 0 \text{ mm}$ ) and increased near the horn tips as the ice shapes became progressively larger.
- For most MVDs tested, the maximum local impingement efficiency increased as the ice shape size increased.
- Maximum local impingement efficiency for the clean airfoil was greater than for all mixed ice shape cases and for all MVDs tested (except for the 45-min 52  $\mu\text{m}$  case).
- Secondary impingement peaks were found downstream of the ice shapes between –30 and –80 mm along the airfoil upper surface and from 30 to 300 mm over the lower surface of the airfoil. The extent of the impingement peaks shifted downstream along both upper and lower surfaces as the ice shape size was increased.
- For most of the mixed ice shapes tested the total impingement efficiency increased as the size of the ice accretion increased from 7.5- to 45-min. The 15-min mixed ice shape with MVDs of 52, 111, and 154  $\mu\text{m}$  had higher total impingement efficiency than its larger counterparts.

**7.3.3.3 Comparison between glaze, mixed and rime ice shape.**—Figure 97 summarizes the impingement efficiency obtained with the 45-min rime ice shape for all MVDs tested. From table 10, the trends observed among the three types of ice shapes are as follows:

- Amongst the three 45-min ice accretions, the glaze ice shape had the largest total impingement efficiency. Total impingement efficiency for the 20, 52, 111, and 154  $\mu\text{m}$  MVDs decreased in the following sequence: glaze, mixed, and rime. For the 236  $\mu\text{m}$  case, however, the rime ice shape exhibited higher total collection efficiency than the mixed ice shape.
- For all MVDs tested with the 45-min ice shapes, the glaze ice shape had the lowest maximum local impingement efficiency.
- Multiple peaks within the ice horns were observed in the glaze and mixed ice shape cases while the rime ice shape had a single impingement peak.

- The secondary impingement peaks (downstream of the horns) on the glaze ice shapes shifted downstream from the highlight ( $s = 0$  mm) by similar amount as the ice shape size increased, while for the mixed ice shape the peak on the lower surface shifted significantly more than that on the upper surface.
- The secondary impingement peaks in the glaze ice shapes tended to flatten out as the ice shape increased in size from 5- to 45-min. On the contrary, the secondary peaks in the mixed ice shape impingement curves remained distinctive as the ice shape increased in size from 7.5- to 45-min.

#### 7.3.4 Effect of MVD

The effect of MVD on impingement efficiency for all ice shapes tested is demonstrated in figures 98 to 110 and in table 10. In figures 98 and 99, local impingement efficiency ( $\bar{\beta}$ ) is plotted versus surface distance from the highlight. In figures 100 to 110, impingement efficiency (horizontal axis) is plotted versus  $y/c$  and is related to model geometry to better illustrate the relation between impingement efficiency and body location.

The experimental results demonstrate the following trends.

- In general, local impingement efficiency and extent for the configurations tested increased as the cloud MVD was increased from 20 to 236  $\mu\text{m}$ . Note that for the 45-min glaze ice shape, the impingement limits did not change with MVD because the large horns of this ice shape prevented impingement downstream of the horns for the angle of attack tested. The incremental growth in  $\bar{\beta}$  (difference in  $\bar{\beta}$  between adjacent MVD cases) decreased as the MVD was increased. The most growth in  $\bar{\beta}$  was observed between 20 and 52  $\mu\text{m}$  and between 52 and 111  $\mu\text{m}$ . For most of the larger MVDs, however, the growth in  $\bar{\beta}$  decreased.
- For all glaze geometries tested, the change in total impingement efficiency between the 20 and 52  $\mu\text{m}$  MVD cases defined as  $\Delta\bar{E} = \bar{E}_{52} - \bar{E}_{20}$ , ranged from 0.065 to 0.166 depending on the glaze ice shape. The incremental growth in total impingement efficiency as the MVD was increased from 52 to 111  $\mu\text{m}$  ranged from 0.057 to 0.114. Further increases in MVD from 111 to 154 and then from 154 to 236  $\mu\text{m}$  resulted in total impingement efficiency increments of 0.042 to 0.100 and 0.027 to 0.093 respectively.
- For all mixed ice shape geometries tested, the change in total impingement efficiency between the 20 and 52  $\mu\text{m}$  MVD cases ranged from 0.102 to 0.140 depending on ice shape. The incremental growth in total impingement efficiency as the MVD was increased from 52 to 111  $\mu\text{m}$  ranged from 0.086 to 0.109. Further increases in MVD from 111 to 154 and then from 154 to 236  $\mu\text{m}$  resulted in total impingement efficiency increments of 0.101 to 0.117 and 0.002 to 0.047 respectively.
- For the 45-min rime ice shape tested, the increments in total impingement efficiency as the MVD was increased from 20 to 236  $\mu\text{m}$  were 0.143, 0.101, 0.079, and 0.118.
- The results in figures 98 and 99 indicate multiple impingement peaks between the ice shape horns in the glaze and mixed ice shape cases. In general, these peaks became more prominent as the MVD and the size of the ice were increased.

## 7.4 Droplet Trajectories

Droplet trajectories for selected test cases are depicted in figures 111 to 114 to elucidate the impingement distribution trends observed with the iced configuration tested. The droplet trajectories presented are for the clean NACA 23012 airfoil, the three 45-min ice shapes, and all

five MVDs tested. All trajectories were computed with the LEWICE 1.7 code using a single drop size set equal to the MVD of the experimental droplet distribution.

The droplet trajectories presented in figures 111 to 114 for the 20  $\mu\text{m}$  case demonstrate considerable deflection in the vicinity to the ice shapes. The deflection of the trajectories became progressively smaller as the MVD size increased. At a droplet size of 236  $\mu\text{m}$ , the trajectories calculated for the 45-min mixed case were practically straight.

The experimental and computed impingement distributions presented exhibited several peaks in the region between the ice horns in the glaze and mixed ice shape cases. The trajectory simulations presented can be used to explain how these peaks form. For example, from the trajectory results presented in figure 112e, it is evident that near point "A" on the upper ice horn the impingement efficiency will be relatively high since the surface is nearly normal to the incoming droplets. However, as the droplets hit between locations "A" and "B" the impingement efficiency decreases due to the local slope of the surface. In the region between locations "B" and "C", the impingement efficiency increases and decreases depending on local slope.

The formation of the peaks in the experimental results was due to direct droplet impingement as in the LEWICE case, but also due to potential water re-impingement due to droplet splashing. The version of LEWICE used for the analysis did not have a splashing model so it did not include the deposition due to re-impingement. Additional droplet trajectories are provided in appendix D.

## 8.0 Summary and Conclusions

Extensive wind tunnel tests were conducted at the NASA Glenn Icing Research Tunnel to expand the water droplet impingement database for simulated ice shape configurations and for large droplet (SLD) conditions. Tests were conducted with an MS(1)-0317 airfoil, and with a clean and iced NACA 23012 airfoil. The iced configurations included ten simulated ice shapes that were defined with the NASA Glenn LEWICE 2.2 ice accretion code. The ice accretions tested with the NACA 23012 airfoil included 5-, 10-, 15-, 22.5-, and 45-min glaze ice shapes, 7.5-, 15-, 22.5-, and 45-min mixed ice shapes, and a 45-min rime ice shape. Test conditions included freestream velocity of approximately 175 mph, 2.5° angle of attack and cloud median volumetric diameters of 20, 52, 111, 154, and 236  $\mu\text{m}$ . Each experimental condition was repeated 3 to 4 times to establish a measure of test repeatability. Comparisons of experimental with analysis impingement data obtained with the NASA Glenn LEWICE (modified 27-bin, version 1.6) ice accretion code were performed. Below is a summary of key findings based on the work performed.

### ***Test Repeatability***

1. Repeated droplet distribution measurements showed that the variation in MVD was  $\pm 0.5 \mu\text{m}$  from the average for the 20  $\mu\text{m}$  cloud,  $\pm 2 \mu\text{m}$  for the 52 cloud,  $\pm 5 \mu\text{m}$  for the 111 and 154  $\mu\text{m}$  clouds, and  $\pm 10 \mu\text{m}$  for the 236  $\mu\text{m}$  cloud.
2. For 55 out of the 56 cases presented, the variation in total impingement efficiency of repeated impingement tests (3 to 4 tests) from the average was less than 10 percent. The number of repeats performed per test condition was not sufficient to establish a statistical average. However, the variations recorded were consistent for the 389 impingement tests conducted with the two airfoils, ten ice shapes and the collector device. In addition, impingement data for the MS(1)-0317 airfoil obtained during the 2003 IRT entry were in very good agreement with data obtained for similar test

conditions during five previous IRT entries. Thus, it would be reasonable to conclude that the experimental method used was repeatable.

### **Pressure Data**

3. Comparison of experimental and LEWICE pressure distributions for the clean NACA 23012 airfoil and for most of the ice shapes tested were in good agreement. The main differences in the LEWICE and the experimental pressure distributions were observed in the case of the large glaze ice shapes. In the cases of the 15- and 22.5-min glaze ice shapes, LEWICE did not match the experimental pressure data over the forward 10 to 20 percent chord. For the 45-min ice shape, considerable disagreement between the experimental and the LEWICE pressure distributions were observed for the entire upper and lower surfaces. The observed discrepancy between experiment and analysis was due to the limitations of the potential method used in LEWICE in simulating viscous flowfields with extensive flow separation.

### **Experimental Impingement Data**

4. The impingement data for the clean NACA 23012 airfoil exhibited the following trends:

- Maximum impingement efficiency of 56, 71, 85, 92, and 95 percent for MVDs of 20, 52, 111, 154 and 236  $\mu\text{m}$  respectively. The corresponding values of total impingement efficiency were 19, 30, 42, 51, and 56 percent.
- The upper and lower impingement limits increased considerably as the MVD was increased. For the 236  $\mu\text{m}$  case the upper impingement limit extended to 11.6 percent chord and the lower impingement limit to 40.7 percent chord. Impingement limits locations for the clean NACA 23012 airfoil are depicted in figure 115.
- For the large MVDs of 111, 154, and 236  $\mu\text{m}$ , the growth in maximum and total impingement efficiencies and in the extent of impingement was reduced as the MVD was increased from 111 to 236  $\mu\text{m}$ .

### **Glaze Ice Shapes**

5. The impingement data for the NACA 23012 airfoil with the five glaze ice shapes exhibited the following trends:

- Considerable impingement, characterized by multiple peaks, was observed in the leading edge region between the ice horns. The impingement efficiency was in general greater near the horn tips than in the “cavity” between the horns, particularly for the larger ice shapes.
- Impingement efficiency and extent increased as the MVD was increased. The chordwise locations of the impingement limits are summarized in figures 116 to 120.
- In general, for all MVD cases the total impingement efficiency decreased in the following sequence: clean, 5-min glaze ice shape, 10-min glaze ice shape. For the 15-, 22.5-, and 45-min glaze ice shapes, however, the total impingement efficiency increased as the size of the ice shape was increased. For all MVD cases, the maximum total impingement efficiency was obtained with the 45-min ice shape while the minimum total impingement efficiency was obtained with the 10-min glaze ice shape.
- For the 5-, 10-, and 15-min ice shapes, considerable impingement was observed on the upper and lower airfoil surfaces downstream of the horns for MVDs in the range of 52 to 236  $\mu\text{m}$ . The efficiency and extent of the impingement decreased as the horn size was increased. For the 22.5- and 45-min ice shapes a sharp drop in

impingement downstream of the horns was observed due to the horn shielding effect.

### **Mixed Ice Shapes**

6. The impingement data for the NACA 23012 airfoil with the four mixed ice shapes exhibited the following trends:

- Multiple impingement peaks were observed in the leading edge region between the ice horns. The peak within the cavity area of the larger ice shapes was smaller than the impingement peaks obtained near the tip of the ice horns.
- In general, total impingement efficiency for all mixed ice shapes tested was lower than for the clean airfoil.
- Impingement efficiency and extent increased as the MVD was increased. For each MVD tested, the minimum total impingement efficiency was obtained with the 7.5-min mixed ice shape.
- The upper and lower impingement limits increased as the MVD was increased for all mixed ice shape cases. The upper impingement limits for each MVD were very similar for all ice shapes. The upper impingement limit was in the range of 5 to 8 percent, 7 to 9 percent, 10 to 11 percent, 12 to 13 percent, and 13 to 14 percent of chord for MVDs of 20, 52, 111, 154, and 236  $\mu\text{m}$  respectively. The lower impingement limit was found to be in the range of -4 to 30 percent, -3 to 32 percent, 31 to 36 percent, 39 to 43 percent, and 40 to 47 percent of chord as the MVD was increased from 20 to 236  $\mu\text{m}$ . The negative sign indicates that the impingement limit was on the ice shape upstream of the airfoil leading edge. Impingement limits locations for the NACA 23012 airfoil with the mixed ice shapes are depicted in figures 121 to 124.

### **Rime Ice Shape**

7. The impingement data for the NACA 23012 airfoil with the rime ice shape exhibited the following trends:

- Total impingement efficiency for the 45-min rime ice shape was less than for the clean NACA 23012 airfoil for all MVDs except for the 236  $\mu\text{m}$  case.
- Only a single peak was observed in the vicinity of the airfoil leading edge. The maximum local impingement efficiency for each MVDs tested was also lower than that of the clean NACA 23012 airfoil.
- Maximum impingement efficiency of the 45-min rime ice shape was 52, 68, 74, 83, and 91 percent while total impingement efficiency was 13, 27, 37, 45, and 57 percent for MVDs of 20, 52, 111, 154 and 236  $\mu\text{m}$  respectively.
- As the MVD increased from 20 to 236  $\mu\text{m}$ , for the 45-min rime ice shape, the upper limit ranged from 6 to 13 percent chord while the lower impingement limit ranged from 20 to 40 percent chord. Impingement limits locations for the NACA 23012 airfoil with 45-min rime ice shape are depicted in figure 125.

### **LEWICE vs Experimental Impingement Data**

8. For the 20  $\mu\text{m}$  MVD and the clean airfoil the LEWICE and the experimental data were in good agreement. For the iced configurations, however, the predicted impingement efficiency for the 20  $\mu\text{m}$  MVD was higher than that obtained experimentally. For the large MVD cases of 52, 111, 154, and 236  $\mu\text{m}$ , the LEWICE impingement data exhibited considerably higher local and total impingement efficiencies and greater impingement

limits compared to the experimental results. A possible reason for the observed differences between LEWICE and experiment for the large MVD cases is droplet splashing which is not simulated in the LEWICE code. Another potential reason is the difference between the computed and the experimental flowfields, particularly for the large 22.5- and 45-min glaze ice shapes. Finally, a numerical interpolation scheme used in LEWICE to compute impingement efficiency resulted in unrealistic impingement tails immediately downstream of the large glaze ice shape horns. This further exacerbated the difference between experimental and computed total impingement efficiencies. It was demonstrated that the use of the Monte-Carlo method to compute impingement efficiency in these cases improved the correlation between the experimental and computed results.

#### ***Recommendations for Further Work***

9. Experiments using advanced imaging methods should be conducted to investigate and document large droplet splashing on large glaze ice shapes to determine the effects of splashed droplets on the impingement characteristics of ice accretions. Of interest is the deposition of splashed droplets in the region between the horns and the trajectories of droplets splashing off the horn tips.
10. Based on the pressure data presented, the LEWICE did not match the experimental results particularly for the cases of the 22.5 and 45-min ice shapes. A Navier-Stokes analysis should be performed for the large ice shapes tested and the computed flowfield should be used in place of the LEWICE potential flow solution to perform a new impingement analysis.
11. Incorporate a droplet splash and breakup models in a trajectory code and use the model to compute impingement characteristics for the ice shapes tested. The calibration of this model may require additional impingement data at lower and higher tunnel speeds than the ones available in the 1985 to 2003 impingement database.

TABLE 1.—LIST OF DROPLET TRAJECTORY PARAMETERS.

| Parameter                   | Definition   | Expression  |
|-----------------------------|--|---|
| $Re_{MVD}$                  | Reynolds number based on droplet diameter  | $MVD \cdot V_\infty \cdot \frac{\rho_{air}}{\mu}$ where MVD represents Median Volumetric Diameter, $\rho_{air}$ is the air density and $\mu$ is the absolute air viscosity      |
| $K$                         | Droplet inertia parameter  | $\rho_{droplet} \cdot V_\infty \cdot \frac{MVD^2}{18 \cdot \mu \cdot c}$ where $\rho_{droplet}$ is the droplet (water) density and $c$ is the chord length of the airfoil model |
| $\frac{\lambda}{\lambda_s}$ | Ratio of the true range of droplet as projectile injected into still air to the range of droplet as projectile following Stokes' law | $-0.022466 \cdot x^4 + 0.20109 \cdot x^3 - 0.59067 \cdot x^2 + 0.36072 \cdot x + 0.74544$<br>where $x = \log(Re_{MVD})$ and $6 < Re_{MVD} < 1000$                               |
| $K_0$                       | Droplet modified inertia parameter   | $K \cdot \frac{\lambda}{\lambda_s}$   |
| $\phi$                      | Deviation of the droplet drag force from Stokes' law   | $\frac{(Re_{MVD})^2}{K}$  |

TABLE 2.—SUMMARY OF PRESSURE TRANSDUCER CHARACTERISTICS

| Transducer   | Usage            | Range (psig) | Error           | Thermal Zero Shift Error | Thermal Span Shift Error |
|--------------|------------------|--------------|-----------------|--------------------------|--------------------------|
| 16 SETRA 206 | Water lines      | 0-125        | $\pm 0.13\%$ FS | $\pm 1.0\%$ FS/100 °F    | $\pm 1.5\%$ FS/100 °F    |
| 1 SETRA 204  | Main air line    | 0-100        | $\pm 0.11\%$ FS | $\pm 0.4\%$ FS/100 °F    | $\pm 0.3\%$ FS/100 °F    |
| 1 SETRA 204  | Water tank       | 0-100        | $\pm 0.11\%$ FS | $\pm 0.4\%$ FS/100 °F    | $\pm 0.3\%$ FS/100 °F    |
| 4 SETRA 206  | Nozzle air lines | 0-100        | $\pm 0.13\%$ FS | $\pm 1.0\%$ FS/100 °F    | $\pm 1.5\%$ FS/100 °F    |

Note: All transducers were calibrated at temperature of 50 °F.

TABLE 3.—CLOUD MVD AND CORRESPONDING SPRAY SYSTEM PARAMETERS FROM TEST MEASUREMENTS (2003 IRT TESTS)

| MVD range (μm) | Average air supply pressure at regulator (psig ± psi) | Average tank water pressure (psig ± psi) | Average water pressure at nozzle (psig ± psi) | Average air pressure at nozzle (psig ± psi) | $\Delta P = P_{water} - P_{air}$ at nozzle (psi) | Average volume flow rate 16 nozzles (gpm) | Spray time (sec) |
|----------------|---|--|---|---|--|---|------------------|
| 20 ± 0.5       | 22.1 ± 0.3  | 70.4 ± 1.0                               | 66.2 ± 1.3                                    | 18.2 ± 0.5                                  | 48.0   | 0.276                                     | 1.5              |
| 52 ± 2.0       | 9.9 ± 0.5   | 45.3 ± 1.0                               | 41.9 ± 1.2                                    | 7.6 ± 0.3                                   | 34.3   | 0.167                                     | 1.5              |
| 111 ± 5.0      | 5.8 ± 0.3   | 37.2 ± 0.9                               | 34.2 ± 1.0                                    | 4.3 ± 0.3                                   | 29.9   | 0.104                                     | 1.5              |
| 154 ± 5.0      | 4.8 ± 0.3   | 55.5 ± 1.2                               | 52.0 ± 1.4                                    | 3.5 ± 0.2                                   | 48.5   | 0.105                                     | 1                |
| 236 ± 10.0     | 4.8 ± 0.4   | 70.4 ± 1.1                               | 66.4 ± 1.3                                    | 3.5 ± 0.3                                   | 62.9   | 0.091                                     | 0.75             |

Pressures, flow rates and errors have been calculated from randomly selected tests for each MVD case.

TABLE 4.—COLLECTOR THEORETICAL EFFICIENCY AND KING PROBE LWC MEASUREMENTS FOR 2003 TEST MVDS

| MVD (μm) | Average LWC* (g/m³) | Collector Efficiency (%) |
|----------|---------------------|--------------------------|
| 20       | 0.19                | 89                       |
| 52       | 0.40                | 92                       |
| 111      | 0.73                | 95                       |
| 154      | 1.44                | 97                       |
| 236      | 1.89                | 100                      |

\*The King probe LWC data is not used in the data reduction, it is only used to compare with collector trends.

TABLE 5.—TEST MODELS AND CONDITIONS FOR 2003 IMPINGEMENT TESTS.

| Test model   | Total number of surface pressure taps | Number of active surface pressure taps | Angle of attack ( $\alpha$ ) (degree) | MVD ( $\mu\text{m}$ ) | Avg. air-speed (mph) | Number of runs per MVD | Total number of runs |
|--|---------------------------------------|--|---------------------------------------|-----------------------|----------------------|------------------------|----------------------|
| MS(1)-0317 (c = 36 in)                               | 47                                    | 34                                     | $\alpha=0^\circ$                      | 20, 52, 111, 154, 236 | 175                  | 1 to 4                 | 15                   |
| NACA 23012 (c = 36 in)                               | 65                                    | 61                                     | $\alpha=2.5^\circ$                    | 20, 52, 111, 154, 236 | 175                  | 4                      | 20                   |
| NACA 23012 with 5-min Glaze ice shape (c = 36 in)    | 55                                    | 52                                     | $\alpha=2.5^\circ$                    | 20, 52, 111, 154, 236 | 175                  | 2 to 4                 | 14                   |
| NACA 23012 with 10-min Glaze ice shape (c = 36 in)   | 55                                    | 52                                     | $\alpha=2.5^\circ$                    | 20, 52, 111, 154, 236 | 175                  | 4 to 5                 | 21                   |
| NACA 23012 with 15-min Glaze ice shape (c = 36 in)   | 55                                    | 52                                     | $\alpha=2.5^\circ$                    | 20, 52, 111, 154, 236 | 175                  | 4 to 5                 | 21                   |
| NACA 23012 with 22.5-min Glaze ice shape (c = 36 in) | 55                                    | 52                                     | $\alpha=2.5^\circ$                    | 20, 52, 111, 154, 236 | 175                  | 4 to 5                 | 21                   |
| NACA 23012 with 45-min Glaze ice shape (c = 36 in)   | 55                                    | 52                                     | $\alpha=2.5^\circ$                    | 20, 52, 111, 154, 236 | 175                  | 3 to 5                 | 20                   |
| NACA 23012 with 7.5-min Mixed ice shape (c = 36 in)  | 55                                    | 52                                     | $\alpha=2.5^\circ$                    | 20, 52, 111, 154, 236 | 175                  | 2 to 4                 | 14                   |
| NACA 23012 with 15-min Mixed ice shape (c = 36 in)   | 55                                    | 52                                     | $\alpha=2.5^\circ$                    | 20, 52, 111, 154, 236 | 175                  | 4 to 5                 | 22                   |
| NACA 23012 with 22.5-min Mixed ice shape (c = 36 in) | 55                                    | 52                                     | $\alpha=2.5^\circ$                    | 20, 52, 111, 154, 236 | 175                  | 4                      | 20                   |
| NACA 23012 with 45-min Mixed ice shape (c = 36 in)   | 55                                    | 52                                     | $\alpha=2.5^\circ$                    | 20, 52, 111, 154, 236 | 175                  | 4                      | 20                   |
| NACA 23012 with 45-min Rime ice shape (c = 36 in)    | 55                                    | 52                                     | $\alpha=2.5^\circ$                    | 20, 52, 111, 154, 236 | 175                  | 2 to 3                 | 12                   |
| Collector Mechanism                                  | N/A                                   | N/A                                    | N/A                                   | 20, 52, 111, 154, 236 | 175                  | 33 to 36               | 169                  |
| Uniformity 6- by 6-ft Grid                           | N/A                                   | N/A                                    | N/A                                   | 20, 52, 111, 154, 236 | 175                  | 5 to 6                 | 28                   |
| MVD, LWC measurements                                | N/A                                   | N/A                                    | N/A                                   | 20, 52, 111, 154, 236 | 175                  | 2                      | 10                   |

N/A: Not Applicable

TABLE 6.—27-BIN DROPLET DISTRIBUTIONS.

| Bin Number | %    | Analytical Droplet Size ( $\mu\text{m}$ ) |                        |                         |                         |                         |
|------------|------|---|------------------------|-------------------------|-------------------------|-------------------------|
|            |      | MVD = 20 $\mu\text{m}$                    | MVD = 52 $\mu\text{m}$ | MVD = 111 $\mu\text{m}$ | MVD = 154 $\mu\text{m}$ | MVD = 236 $\mu\text{m}$ |
| 1          | 4.75 | 3.771785                                  | 6.544005               | 10.86511                | 13.63081                | 15.90700                |
| 2          | 4.75 | 8.424081                                  | 15.16583               | 24.51947                | 32.00148                | 45.33918                |
| 3          | 4.75 | 10.07453                                  | 18.61629               | 29.64239                | 47.12857                | 74.84499                |
| 4          | 4.75 | 11.55813                                  | 21.20615               | 34.95594                | 67.20577                | 102.0387                |
| 5          | 4.75 | 12.97915                                  | 23.57229               | 44.73852                | 84.29376                | 122.5518                |
| 6          | 4.75 | 14.30065                                  | 25.88050               | 58.34341                | 98.09358                | 141.6284                |
| 7          | 4.75 | 15.50242                                  | 28.27308               | 70.67189                | 110.1533                | 160.5375                |
| 8          | 4.75 | 16.65027                                  | 30.93579               | 81.29308                | 120.7427                | 178.4472                |
| 9          | 4.75 | 17.67680                                  | 34.45036               | 91.18996                | 131.1980                | 197.6876                |
| 10         | 4.75 | 18.60940                                  | 40.80994               | 100.9387                | 142.4821                | 217.9631                |
| 11         | 4.75 | 19.54230                                  | 51.35849               | 110.5958                | 153.9673                | 240.7987                |
| 12         | 4.75 | 20.50887                                  | 63.07714               | 119.4937                | 164.8876                | 271.0245                |
| 13         | 4.75 | 21.50879                                  | 73.98405               | 128.8270                | 175.5589                | 320.0266                |
| 14         | 4.75 | 22.50936                                  | 85.72330               | 140.1095                | 187.0793                | 393.5336                |
| 15         | 4.75 | 23.58441                                  | 99.79768               | 152.8340                | 199.5778                | 455.5443                |
| 16         | 4.75 | 24.73329                                  | 115.9025               | 165.8621                | 211.8856                | 494.6245                |
| 17         | 4.75 | 25.98042                                  | 138.7903               | 179.3563                | 223.9060                | 534.1075                |
| 18         | 4.75 | 27.47479                                  | 164.9857               | 193.7323                | 240.1437                | 577.9580                |
| 19         | 4.75 | 29.32443                                  | 185.6289               | 207.1929                | 263.9714                | 624.0164                |
| 20         | 4.75 | 31.84920                                  | 202.7462               | 219.6752                | 299.4286                | 670.9214                |
| 21         | 1.00 | 33.81317                                  | 212.4191               | 227.3925                | 327.2080                | 701.1499                |
| 22         | 1.00 | 34.83165                                  | 215.5869               | 230.1392                | 341.6878                | 713.6254                |
| 23         | 1.00 | 36.21635                                  | 219.7380               | 237.7504                | 358.1966                | 728.3444                |
| 24         | 0.50 | 37.46642                                  | 223.6459               | 250.5209                | 375.0911                | 742.1095                |
| 25         | 0.50 | 38.74237                                  | 226.3273               | 264.2335                | 389.0540                | 752.6775                |
| 26         | 0.50 | 40.66698                                  | 229.0086               | 279.5445                | 400.9250                | 763.2454                |
| 27         | 0.50 | 44.36609                                  | 253.9263               | 312.5888                | 425.0598                | 1046.765                |

TABLE 7.—10-BIN DROPLET DISTRIBUTIONS.

| Bin Number | %     | Analytical Droplet Size ( $\mu\text{m}$ ) |                        |                         |                         |                         |
|------------|-------|---|------------------------|-------------------------|-------------------------|-------------------------|
|            |       | MVD = 20 $\mu\text{m}$                    | MVD = 52 $\mu\text{m}$ | MVD = 111 $\mu\text{m}$ | MVD = 154 $\mu\text{m}$ | MVD = 236 $\mu\text{m}$ |
| 1          | 5.00  | 3.850397                                  | 6.693706               | 11.05374                | 13.88450                | 16.25037                |
| 2          | 10.00 | 9.390637                                  | 16.88090               | 27.48959                | 44.44510                | 63.65823                |
| 3          | 20.00 | 13.80175                                  | 25.44875               | 56.48542                | 90.28305                | 135.4827                |
| 4          | 30.00 | 19.60797                                  | 59.17969               | 111.1060                | 154.1635                | 298.5197                |
| 5          | 20.00 | 25.4820                                   | 131.2511               | 170.8107                | 218.3283                | 508.4572                |
| 6          | 10.00 | 30.73474                                  | 192.7506               | 212.7639                | 284.4519                | 645.4684                |
| 7          | 3.00  | 35.19787                                  | 216.5703               | 235.0038                | 343.7168                | 715.8689                |
| 8          | 1.00  | 38.32569                                  | 224.9867               | 257.7010                | 380.2672                | 747.3936                |
| 9          | 0.50  | 40.66701                                  | 229.0087               | 279.5447                | 400.9252                | 763.2455                |
| 10         | 0.50  | 44.36619                                  | 253.9279               | 312.5901                | 425.0601                | 1046.767                |

TABLE 8.—SUMMARY OF MODEL GEOMETRY AND IMPINGEMENT PARAMETERS. ALL DIMENSIONS ARE IN ENGLISH UNITS (in., mph); VALUES INSIDE PARENTHESIS ARE IN SI UNITS (m, m/s)

| Geometry  | Chord<br>(in) | $t_{max}$<br>(in) | x/c<br>$att_{max}$ | $V_\infty$<br>mph | AOA<br>(deg.) | MVD<br>( $\mu\text{m}$ ) | $Re_c$<br>Million | $Re_{MVD}$ | K      | $K_0$ | $\phi$  |
|---|---------------|-------------------|--------------------|-------------------|---------------|--------------------------|-------------------|------------|--------|-------|---------|
| MS(1)-0317  | 36<br>(0.914) | 6.12<br>(0.155)   | 0.376              | 175               | 0             | 20                       | 4.92              | 108        | 0.108  | 0.037 | 107,054 |
|   |               |                   |                    |                   |               | 52                       | 4.91              | 279        | 0.731  | 0.170 | 106,772 |
|   |               |                   |                    |                   |               | 111                      | 4.91              | 596        | 3.329  | 0.542 | 106,613 |
|   |               |                   |                    |                   |               | 154                      | 4.91              | 828        | 6.409  | 0.873 | 106,851 |
|   |               |                   |                    |                   |               | 236                      | 4.92              | 1269       | 15.053 | 1.544 | 106,985 |
| NACA 23012  | 36<br>(0.914) | 4.32<br>(0.110)   | 0.300              | 175               | 2.5           | 20                       | 4.58              | 100        | 0.106  | 0.038 | 94,271  |
|   |               |                   |                    |                   |               | 52                       | 4.58              | 260        | 0.720  | 0.172 | 94,243  |
|   |               |                   |                    |                   |               | 111                      | 4.57              | 554        | 3.278  | 0.553 | 93,795  |
|   |               |                   |                    |                   |               | 154                      | 4.58              | 772        | 6.314  | 0.895 | 94,346  |
|   |               |                   |                    |                   |               | 236                      | 4.59              | 1184       | 14.832 | 1.602 | 94,554  |
| NACA 23012<br>with 5-min<br>Glaze ice<br>shape    | 36<br>(0.914) | 4.32<br>(0.110)   | 0.300              | 175               | 2.5           | 20                       | 4.61              | 101        | 0.106  | 0.038 | 95,313  |
|   |               |                   |                    |                   |               | 52                       | 4.60              | 261        | 0.720  | 0.172 | 94,988  |
|   |               |                   |                    |                   |               | 111                      | 4.60              | 558        | 3.279  | 0.552 | 94,936  |
|   |               |                   |                    |                   |               | 154                      | 4.61              | 776        | 6.315  | 0.892 | 95,413  |
|   |               |                   |                    |                   |               | 236                      | 4.61              | 1190       | 14.831 | 1.596 | 95,488  |
| NACA 23012<br>with 10-min<br>Glaze ice<br>shape   | 36<br>(0.914) | 4.32<br>(0.110)   | 0.300              | 175               | 2.5           | 20                       | 4.56              | 100        | 0.106  | 0.038 | 93,612  |
|   |               |                   |                    |                   |               | 52                       | 4.57              | 260        | 0.719  | 0.172 | 94,043  |
|   |               |                   |                    |                   |               | 111                      | 4.53              | 550        | 3.269  | 0.554 | 92,569  |
|   |               |                   |                    |                   |               | 154                      | 4.56              | 768        | 6.307  | 0.896 | 93,635  |
|   |               |                   |                    |                   |               | 236                      | 4.56              | 1177       | 14.807 | 1.607 | 93,539  |
| NACA 23012<br>with 15-min<br>Glaze ice<br>shape   | 36<br>(0.914) | 4.32<br>(0.110)   | 0.300              | 175               | 2.5           | 20                       | 4.53              | 99         | 0.106  | 0.038 | 92,286  |
|   |               |                   |                    |                   |               | 52                       | 4.53              | 258        | 0.718  | 0.173 | 92,569  |
|   |               |                   |                    |                   |               | 111                      | 4.54              | 551        | 3.271  | 0.554 | 92,703  |
|   |               |                   |                    |                   |               | 154                      | 4.52              | 762        | 6.292  | 0.898 | 92,274  |
|   |               |                   |                    |                   |               | 236                      | 4.52              | 1167       | 14.776 | 1.613 | 92,195  |
| NACA 23012<br>with 22.5-min<br>Glaze ice<br>shape | 36<br>(0.914) | 4.32<br>(0.110)   | 0.300              | 175               | 2.5           | 20                       | 4.54              | 99         | 0.106  | 0.038 | 92,558  |
|   |               |                   |                    |                   |               | 52                       | 4.56              | 259        | 0.720  | 0.173 | 93,289  |
|   |               |                   |                    |                   |               | 111                      | 4.54              | 551        | 3.278  | 0.555 | 92,779  |
|   |               |                   |                    |                   |               | 154                      | 4.55              | 766        | 6.310  | 0.898 | 93,080  |
|   |               |                   |                    |                   |               | 236                      | 4.55              | 1174       | 14.808 | 1.610 | 93,075  |
| NACA 23012<br>with 45-min<br>Glaze ice<br>shape   | 36<br>(0.914) | 4.32<br>(0.110)   | 0.300              | 175               | 2.5           | 20                       | 4.56              | 100        | 0.106  | 0.038 | 93,496  |
|   |               |                   |                    |                   |               | 52                       | 4.56              | 259        | 0.719  | 0.173 | 93,676  |
|   |               |                   |                    |                   |               | 111                      | 4.56              | 554        | 3.275  | 0.553 | 93,688  |
|   |               |                   |                    |                   |               | 154                      | 4.57              | 769        | 6.301  | 0.895 | 93,781  |
|   |               |                   |                    |                   |               | 236                      | 4.57              | 1179       | 14.800 | 1.604 | 93,871  |
| NACA 23012<br>with 7.5-min<br>Mixed ice<br>shape  | 36<br>(0.914) | 4.32<br>(0.110)   | 0.300              | 175               | 2.5           | 20                       | 4.55              | 99         | 0.106  | 0.038 | 92,950  |
|   |               |                   |                    |                   |               | 52                       | 4.54              | 258        | 0.718  | 0.173 | 92,944  |
|   |               |                   |                    |                   |               | 111                      | 4.55              | 552        | 3.274  | 0.554 | 93,050  |
|   |               |                   |                    |                   |               | 154                      | 4.55              | 765        | 6.303  | 0.897 | 92,970  |
|   |               |                   |                    |                   |               | 236                      | 4.55              | 1174       | 14.803 | 1.609 | 93,067  |
| NACA 23012<br>with 15-min<br>Mixed ice<br>shape   | 36<br>(0.914) | 4.32<br>(0.110)   | 0.300              | 175               | 2.5           | 20                       | 4.52              | 99         | 0.106  | 0.038 | 91,965  |
|   |               |                   |                    |                   |               | 52                       | 4.53              | 258        | 0.719  | 0.173 | 92,440  |
|   |               |                   |                    |                   |               | 111                      | 4.54              | 551        | 3.275  | 0.555 | 92,755  |
|   |               |                   |                    |                   |               | 154                      | 4.52              | 761        | 6.298  | 0.900 | 91,909  |
|   |               |                   |                    |                   |               | 236                      | 4.52              | 1166       | 14.790 | 1.616 | 91,846  |
| NACA 23012<br>with 22.5-min<br>Mixed ice<br>shape | 36<br>(0.914) | 4.32<br>(0.110)   | 0.300              | 175               | 2.5           | 20                       | 4.46              | 98         | 0.106  | 0.038 | 89,894  |
|   |               |                   |                    |                   |               | 52                       | 4.47              | 254        | 0.719  | 0.173 | 90,247  |
|   |               |                   |                    |                   |               | 111                      | 4.47              | 543        | 3.265  | 0.557 | 90,287  |
|   |               |                   |                    |                   |               | 154                      | 4.46              | 752        | 6.283  | 0.904 | 89,913  |
|   |               |                   |                    |                   |               | 236                      | 4.46              | 1152       | 14.756 | 1.626 | 89,960  |
| NACA 23012<br>with 45-min<br>Mixed ice<br>shape   | 36<br>(0.914) | 4.32<br>(0.110)   | 0.300              | 175               | 2.5           | 20                       | 4.49              | 98         | 0.106  | 0.038 | 90,951  |
|   |               |                   |                    |                   |               | 52                       | 4.48              | 255        | 0.717  | 0.173 | 90,419  |
|   |               |                   |                    |                   |               | 111                      | 4.47              | 543        | 3.264  | 0.557 | 90,214  |
|   |               |                   |                    |                   |               | 154                      | 4.49              | 756        | 6.288  | 0.902 | 90,799  |
|   |               |                   |                    |                   |               | 236                      | 4.50              | 1161       | 14.774 | 1.619 | 91,280  |
| NACA 23012<br>with 45-min<br>Rime ice<br>shape    | 36<br>(0.914) | 4.32<br>(0.110)   | 0.300              | 175               | 2.5           | 20                       | 4.55              | 100        | 0.106  | 0.038 | 93,158  |
|   |               |                   |                    |                   |               | 52                       | 4.55              | 259        | 0.719  | 0.173 | 93,272  |
|   |               |                   |                    |                   |               | 111                      | 4.56              | 553        | 3.277  | 0.554 | 93,400  |
|   |               |                   |                    |                   |               | 154                      | 4.55              | 767        | 6.306  | 0.897 | 93,174  |
|   |               |                   |                    |                   |               | 236                      | 4.55              | 1175       | 14.811 | 1.609 | 93,184  |

TABLE 9.—SUMMARY OF TEST REPEATABILITY RESULTS

| Test Case                                | AOA<br>deg | MVD<br>20 $\mu\text{m}$ |                  | MVD<br>52 $\mu\text{m}$ |                  | MVD<br>111 $\mu\text{m}$ |                  | MVD<br>154 $\mu\text{m}$ |                  | MVD<br>236 $\mu\text{m}$ |                  |
|--|------------|-------------------------|------------------|-------------------------|------------------|--------------------------|------------------|--------------------------|------------------|--------------------------|------------------|
|  |            | R <sub>AREA</sub>       | R <sub>MAX</sub> | R <sub>AREA</sub>       | R <sub>MAX</sub> | R <sub>AREA</sub>        | R <sub>MAX</sub> | R <sub>AREA</sub>        | R <sub>MAX</sub> | R <sub>AREA</sub>        | R <sub>MAX</sub> |
| MS(1)-0317                               | 0          | 2.1                     | 1.6              | NA                      | NA               | NA                       | NA               | NA                       | NA               | NA                       | NA               |
| NACA 23012                               | 2.5        | 5.6                     | 4.9              | 2.6                     | 1.6              | 7.6                      | 9.4              | 2.2                      | 1.3              | 5.3                      | 4.8              |
| NACA 23012 with 5-min glaze ice shape    | 2.5        | 5.1                     | 2.9              | 1.5                     | 0.2              | 1.9                      | 0.6              | 9.1                      | 11.4             | 1.4                      | 0.4              |
| NACA 23012 with 10-min glaze ice shape   | 2.5        | 1.8                     | 1.2              | 5.1                     | 3.9              | 6.9                      | 6.4              | 1.4                      | 7.2              | 8.6                      | 3.4              |
| NACA 23012 with 15-min Glaze ice shape   | 2.5        | 1.0                     | 1.4              | 2.0                     | 2.2              | 3.4                      | 7.8              | 2.5                      | 7.5              | 7.8                      | 8.8              |
| NACA 23012 with 22.5-min glaze ice shape | 2.5        | 1.4                     | 2.5              | 2.9                     | 2.1              | 5.3                      | 7.1              | 3.6                      | 8.2              | 12.3                     | 12.5             |
| NACA 23012 with 45-min glaze ice shape   | 2.5        | 5.3                     | 12.5             | 2.3                     | 4.1              | 3.2                      | 4.5              | 2.7                      | 2.5              | 0.8                      | 1.3              |
| NACA 23012 with 7.5-min mixed ice shape  | 2.5        | 1.2                     | 0.2              | 0.9                     | 0.4              | 1.1                      | 4.4              | 3.8                      | 6.0              | 2.3                      | 5.0              |
| NACA 23012 with 15-min mixed ice shape   | 2.5        | 3.2                     | 2.5              | 3.2                     | 1.9              | 5.1                      | 6.9              | 8.5                      | 12.4             | 6.6                      | 5.9              |
| NACA 23012 with 22.5-min mixed ice shape | 2.5        | 1.8                     | 2.6              | 0.6                     | 4.8              | 1.1                      | 3.7              | 6.7                      | 7.4              | 7.3                      | 7.8              |
| NACA 23012 with 45-min mixed ice shape   | 2.5        | 3.4                     | 8.4              | 8.2                     | 8.4              | 1.8                      | 2.6              | 3.1                      | 7.8              | 3.8                      | 7.5              |
| NACA 23012 with 45-min rime ice shape    | 2.5        | 3.6                     | 2.1              | 4.1                     | 5.1              | 6.8                      | 8.7              | 3.4                      | 6.5              | 2.1                      | 2.4              |

R<sub>AREA</sub> = % repeatability for the area under the curveR<sub>MAX</sub> = % repeatability of the maximum beta

NA: data not available

TABLE 10.—SUMMARY OF IMPINGEMENT EFFICIENCY DATA FOR 2003 IRT TESTS

| Model   | Test Conditions |     | $\beta_1$ | $S_1$<br>(mm) | $\beta_2$ | $S_2$<br>(mm) | $S_u$<br>(mm) | $S_l$<br>(mm) | $x_u/c$ | $x_l/c$ | $\bar{E}_L$ | $\bar{E}_E$ | $(\bar{E}_L - \bar{E}_E)/\bar{E}_E$<br>(%) |
|---|-----------------|-----|-----------|---------------|-----------|---------------|---------------|---------------|---------|---------|-------------|-------------|--|
|   | AOA             | MVD |           |               |           |               |               |               |         |         |             |             |  |
| <b>MS(1)-0317</b>                               | 0               | 20  | 0.46      | -3            | NA        | NA            | -98           | 80            | 0.0744  | 0.0696  | 0.1868      | 0.1759      | 6.2  |
| <b>NACA 23012</b>                               | 2.5             | 20  | 0.56      | 3             | NA        | NA            | -64           | 145           | 0.0458  | 0.1505  | 0.1738      | 0.1865      | -6.8                                       |
|   |                 | 52  | 0.71      | 3             | NA        | NA            | -84           | 200           | 0.0661  | 0.2104  | 0.5102      | 0.3000      | 70.1                                       |
|   |                 | 111 | 0.85      | 3             | NA        | NA            | -105          | 277           | 0.0882  | 0.2945  | 0.6753      | 0.4150      | 62.7                                       |
|   |                 | 154 | 0.92      | 2             | NA        | NA            | -121          | 340           | 0.1052  | 0.3634  | 0.7643      | 0.5118      | 49.3                                       |
|   |                 | 236 | 0.95      | 2             | NA        | NA            | -131          | 380           | 0.1159  | 0.4072  | 0.8403      | 0.5622      | 49.5                                       |
| <b>NACA 23012 with 5-min glaze ice shape</b>    | 2.5             | 20  | 0.43      | -8            | 0.35      | 10            | -91           | 171           | 0.0679  | 0.1748  | 0.1788      | 0.1805      | -0.9                                       |
|   |                 | 52  | 0.53      | -9            | 0.44      | 11            | -100          | 233           | 0.0773  | 0.2424  | 0.5236      | 0.2823      | 85.5                                       |
|   |                 | 111 | 0.68      | -8            | 0.54      | 11            | -110          | 270           | 0.0879  | 0.2829  | 0.6928      | 0.3961      | 74.9                                       |
|   |                 | 154 | 0.73      | -9            | 0.53      | 9             | -130          | 310           | 0.1092  | 0.3266  | 0.7830      | 0.4963      | 57.8                                       |
|   |                 | 236 | 0.73      | -8            | 0.58      | 9             | -140          | 360           | 0.1200  | 0.3813  | 0.8590      | 0.5228      | 64.3                                       |
| <b>NACA 23012 with 10-min glaze ice shape</b>   | 2.5             | 20  | 0.40      | 13            | 0.33      | 8             | -101          | 205           | 0.0676  | 0.2056  | 0.1902      | 0.1713      | 11.0                                       |
|   |                 | 52  | 0.49      | 14            | 0.42      | 9             | -122          | 250           | 0.0886  | 0.2547  | 0.5539      | 0.2366      | 134.1                                      |
|   |                 | 111 | 0.60      | 14            | 0.48      | 9             | -135          | 329           | 0.1035  | 0.3411  | 0.7400      | 0.3251      | 127.6                                      |
|   |                 | 154 | 0.70      | 13            | 0.48      | 8             | -148          | 357           | 0.1175  | 0.3717  | 0.8320      | 0.4103      | 102.8                                      |
|   |                 | 236 | 0.73      | 14            | 0.55      | 9             | -165          | 367           | 0.1359  | 0.3827  | 0.9168      | 0.4942      | 85.5                                       |
| <b>NACA 23012 with 15-min glaze ice shape</b>   | 2.5             | 20  | 0.45      | -23           | 0.33      | 8             | -121          | 205           | 0.0754  | 0.1960  | 0.2124      | 0.1862      | 14.1                                       |
|   |                 | 52  | 0.59      | -23           | 0.43      | 8             | -125          | 250           | 0.0796  | 0.2451  | 0.6223      | 0.2857      | 117.8                                      |
|   |                 | 111 | 0.67      | 14            | 0.49      | -7            | -142          | 280           | 0.0976  | 0.2779  | 0.8198      | 0.3423      | 139.5                                      |
|   |                 | 154 | 0.85      | 14            | 0.53      | -8            | -162          | 343           | 0.1191  | 0.3468  | 0.9269      | 0.4351      | 113.0                                      |
|   |                 | 236 | 0.92      | 14            | 0.58      | -9            | -170          | 395           | 0.1277  | 0.4036  | 0.1077      | 0.5277      | 92.9                                       |
| <b>NACA 23012 with 22.5-min glaze ice shape</b> | 2.5             | 20  | 0.47      | -35           | 0.28      | -8            | -45           | 38            | -0.0268 | 0.0023  | 0.2515      | 0.2319      | 8.5  |
|   |                 | 52  | 0.59      | -36           | 0.39      | -8            | -45           | 257           | -0.0268 | 0.2348  | 0.7069      | 0.3236      | 118.4                                      |
|   |                 | 111 | 0.71      | 14            | 0.46      | -7            | -45           | 271           | -0.0268 | 0.2501  | 0.9212      | 0.4015      | 129.4                                      |
|   |                 | 154 | 0.80      | 12            | 0.47      | -8            | -210          | 325†          | 0.1411  | 0.3091† | 1.0874      | 0.4436      | 145.1                                      |
|   |                 | 236 | 0.88      | 13            | 0.53      | -8            | -230          | 325†          | 0.1628  | 0.3091† | 1.1840      | 0.4988      | 137.4                                      |
| <b>NACA 23012 with 45-min glaze ice shape</b>   | 2.5             | 20  | 0.33      | -64           | 0.11      | -7            | -83           | 61            | -0.0555 | -0.0102 | 0.3227      | 0.2705      | 19.3                                       |
|   |                 | 52  | 0.46      | -65           | 0.26      | -8            | -83           | 57            | -0.0555 | -0.0144 | 0.6360      | 0.4360      | 45.9                                       |
|   |                 | 111 | 0.53      | -68           | 0.33      | -29           | ‡             | ‡             | ‡       | ‡       | 0.7586      | 0.5239      | 44.8                                       |
|   |                 | 154 | 0.62      | 12            | 0.38      | -30           | ‡             | ‡             | ‡       | ‡       | 0.8097      | 0.6072      | 33.3                                       |
|   |                 | 236 | 0.65      | 13            | 0.41      | -30           | ‡             | ‡             | ‡       | ‡       | 0.8455      | 0.6362      | 32.9                                       |
| <b>NACA 23012 with 7.5-min mixed ice shape</b>  | 2.5             | 20  | 0.47      | -9            | 0.36      | 9             | -85           | 190           | 0.0548  | 0.1890  | 0.1896      | 0.1377      | 37.7                                       |
|   |                 | 52  | 0.60      | 14            | 0.47      | 9             | -98           | 252           | 0.0681  | 0.2566  | 0.5434      | 0.2411      | 125.4                                      |
|   |                 | 111 | 0.66      | -11           | 0.50      | -4            | -130          | 300           | 0.1019  | 0.3091  | 0.7108      | 0.3496      | 103.3                                      |
|   |                 | 154 | 0.79      | 14            | 0.59      | 9             | -152          | 375           | 0.1256  | 0.3911  | 0.8006      | 0.4600      | 74.0                                       |
|   |                 | 236 | 0.79      | 13            | 0.60      | 8             | -155          | 380           | 0.1289  | 0.3966  | 0.8751      | 0.4754      | 84.1                                       |
| <b>NACA 23012 with 15-min mixed ice shape</b>   | 2.5             | 20  | 0.45      | -14           | 0.23      | -6            | -125          | 310           | 0.0814  | 0.3015  | 0.1921      | 0.1563      | 22.9                                       |
|   |                 | 52  | 0.61      | -14           | 0.28      | -6            | -135          | 330           | 0.0919  | 0.3233  | 0.5942      | 0.2963      | 100.5                                      |
|   |                 | 111 | 0.67      | -15           | 0.29      | -8            | -145          | 360           | 0.1026  | 0.3561  | 0.7789      | 0.3854      | 102.1                                      |
|   |                 | 154 | 0.77      | 17            | 0.30      | -8            | -170          | 430           | 0.1295  | 0.4327  | 0.8683      | 0.5024      | 72.8                                       |
|   |                 | 236 | 0.77      | 15            | 0.29      | -8            | -175          | 460           | 0.1349  | 0.4655  | 0.9501      | 0.5040      | 88.5                                       |
| <b>NACA 23012 with 22.5-min mixed ice shape</b> | 2.5             | 20  | 0.51      | -17           | 0.11      | -5            | -110          | 280           | 0.0534  | 0.2523  | 0.1809      | 0.1579      | 14.6                                       |
|   |                 | 52  | 0.61      | -17           | 0.13      | -6            | -140          | 325           | 0.0845  | 0.3015  | 0.6021      | 0.2602      | 131.4                                      |
|   |                 | 111 | 0.68      | -18           | 0.13      | -7            | -160          | 330           | 0.1058  | 0.3069  | 0.7939      | 0.3566      | 122.6                                      |
|   |                 | 154 | 0.76      | 24            | 0.13      | -7            | -175          | 425           | 0.1220  | 0.4108  | 0.8892      | 0.4718      | 88.5                                       |
|   |                 | 236 | 0.81      | 23            | 0.12      | -7            | -185          | 440           | 0.1328  | 0.4272  | 0.9671      | 0.5140      | 88.2                                       |
| <b>NACA 23012 with 45-min mixed ice shape</b>   | 2.5             | 20  | 0.55      | -1            | 0.04      | 27            | -140          | 85            | 0.0698  | -0.0415 | 0.1690      | 0.1713      | -1.3                                       |
|   |                 | 52  | 0.72      | -2            | 0.07      | 25            | -150          | 90            | 0.0804  | -0.0362 | 0.5424      | 0.2874      | 88.7                                       |
|   |                 | 111 | 0.73      | -2            | 0.08      | 23            | -180          | 420           | 0.1123  | 0.3188  | 0.8819      | 0.3731      | 136.4                                      |
|   |                 | 154 | 0.78      | 73            | 0.11      | 22            | -200          | 490           | 0.1340  | 0.3953  | 1.0041      | 0.4737      | 112.0                                      |
|   |                 | 236 | 0.87      | -1            | 0.10      | 22            | -205          | 520           | 0.1394  | 0.4281  | 1.0808      | 0.5208      | 107.5                                      |
| <b>NACA 23012 with 45-min rime ice shape</b>    | 2.5             | 20  | 0.52      | 0             | NA        | NA            | -125          | 263           | 0.0629  | 0.2010  | 0.1855      | 0.1253      | 48.0                                       |
|   |                 | 52  | 0.68      | -4            | NA        | NA            | -144          | 320           | 0.0829  | 0.2633  | 0.5424      | 0.2683      | 102.2                                      |
|   |                 | 111 | 0.74      | -2            | NA        | NA            | -174          | 350           | 0.1149  | 0.2961  | 0.7135      | 0.3697      | 93.0                                       |
|   |                 | 154 | 0.83      | 1             | NA        | NA            | -188          | 390           | 0.1300  | 0.3398  | 0.8041      | 0.4491      | 79.0                                       |
|   |                 | 236 | 0.91      | -1            | NA        | NA            | -191          | 440           | 0.1333  | 0.3945  | 0.8772      | 0.5670      | 54.7                                       |

## Nomenclature for Table 10

1.  $\beta_1$  represents the maximum impingement efficiency.
2.  $S_1$  represents the surface distance from the reference point (the highlight) to the location of the maximum impingement efficiency.
3.  $\beta_2$  represents the minimum impingement efficiency on the front surface of the simulated ice shapes.
4.  $S_2$  represents the surface distance from the reference point (the highlight) to the location of the minimum impingement efficiency on the front surface of the simulated ice shapes.

5.  $S_u$  and  $S_l$  represent the surface distances of impingement limits on the upper and lower surfaces.  $x_u/c$  and  $x_l/c$  represent the stations of the impingement limits on upper and lower surfaces with respect to the chord.
6.  $\bar{E}$  represents the total impingement efficiency, which is defined as  $\bar{E} = \frac{A_p}{A_f}$ , where  $A_f$  represents the projected frontal area of the airfoil ( $A_f = 2.672"$  per unit span).  $\bar{E}_L$  is computational total impingement efficiency using LEWICE 1.6 (modified 27-bin version) and  $\bar{E}_E$  is the experimental total impingement efficiency. A few  $\bar{E}_L$  exceeded 1.0 due to presence of artificial impingement tails.
7. NA Not Available
8. † End of blotter strip (blotter strip was not long enough to define the impingement limit on the lower surface)
9. ‡ Analysis in progress

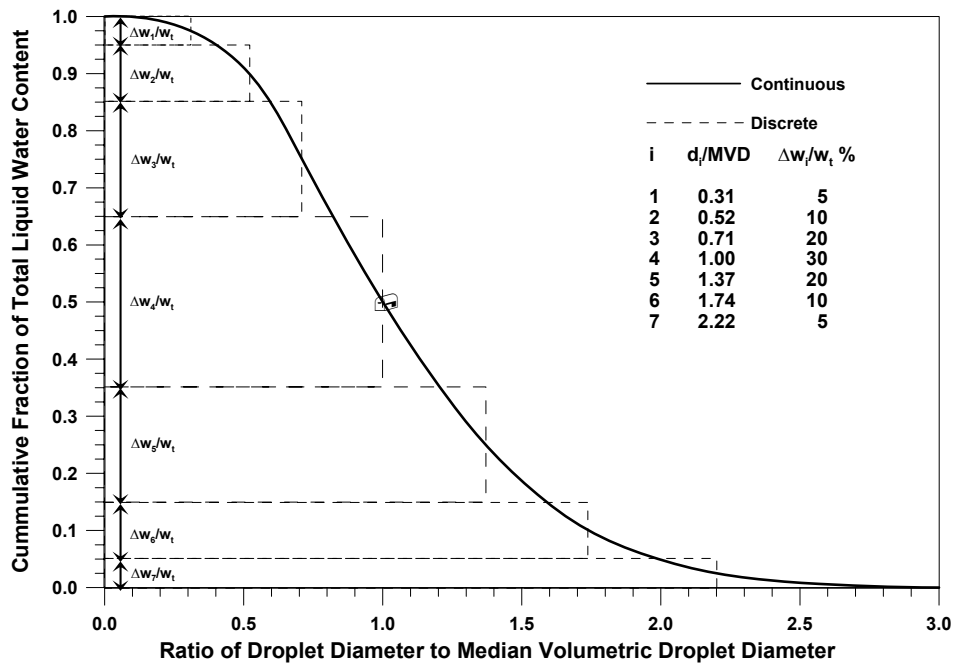


Figure 1.—Langmuir “D” dimensionless distribution of droplet sizes.

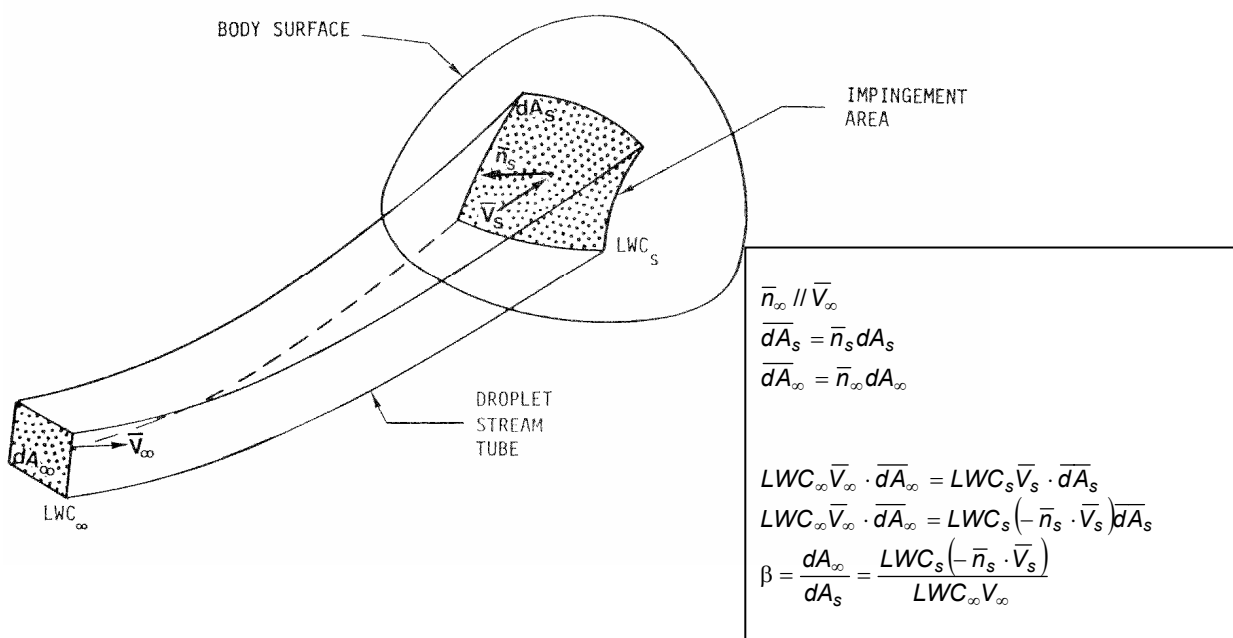


Figure 2a.—Definition of local impingement efficiency for a body in a cloud of uniform droplet size.

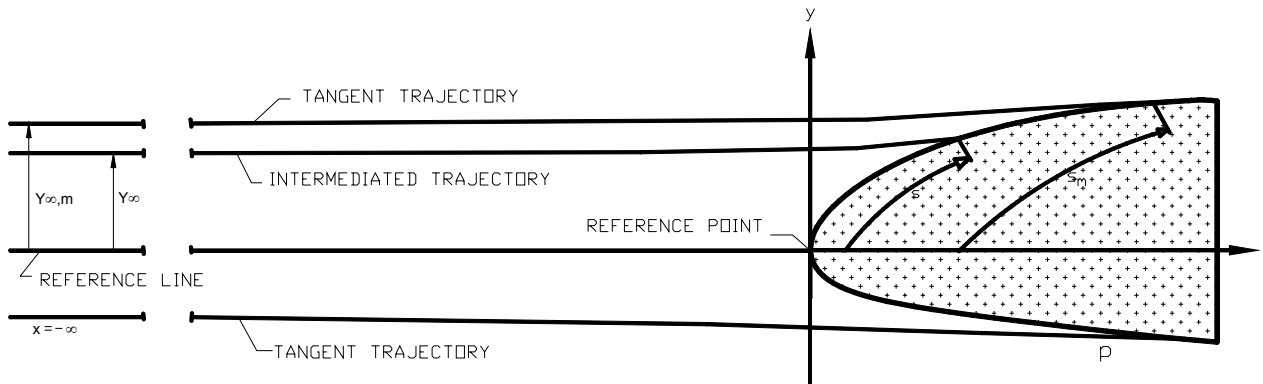


Figure 2b.—Two-dimensional droplet trajectories for a body in a cloud of uniform droplet size.

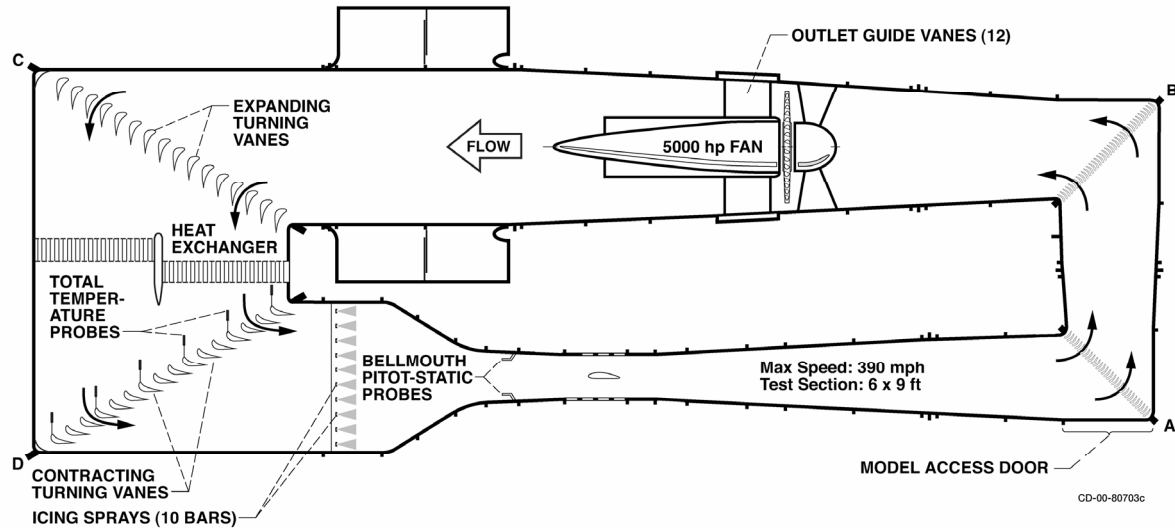


Figure 3.—Plan view of NASA Glenn Icing Research Tunnel (IRT).

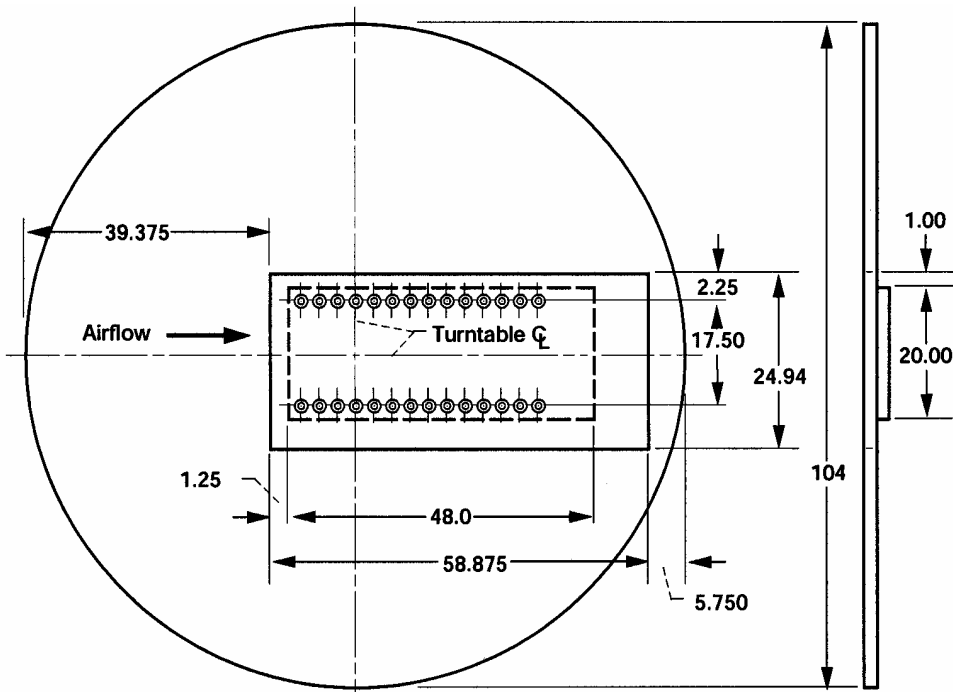


Figure 4.—Icing Research Tunnel turntable and model mounting plate (all dimensions are given in inches).

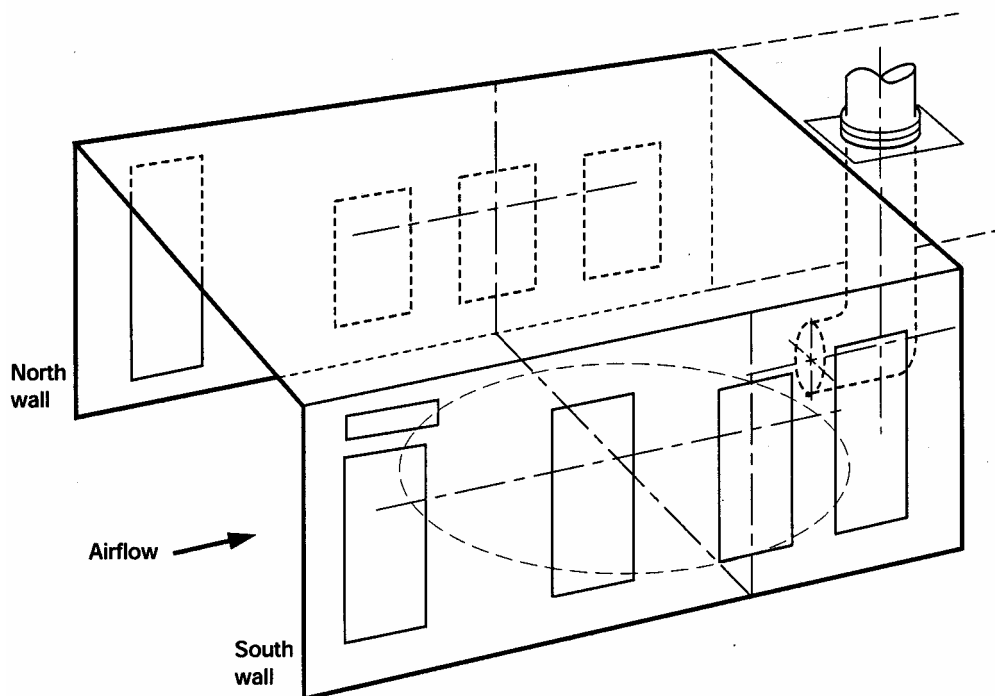


Figure 5.—IRT test section north and south walls showing visual access windows, turntable, and altitude exhaust piping.

Water tube diameter of an IRT nozzle:  
Standard Nozzle – 0.025 in.  
Mod-1 Nozzle – 0.015 in. (used in 2003 impingement tests)

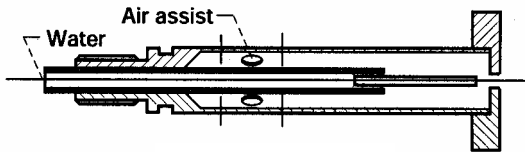


Figure 6.—Schematic of an IRT spray nozzle.

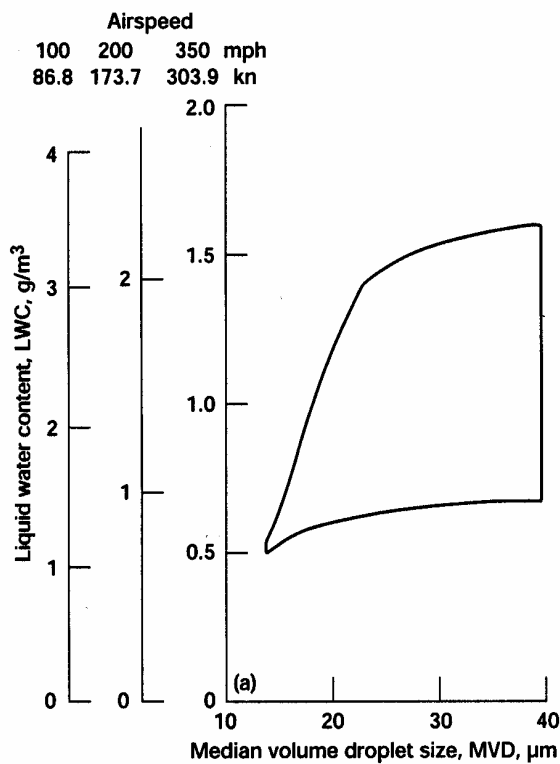


Figure 7.—IRT icing cloud operating envelopes for standard nozzles.

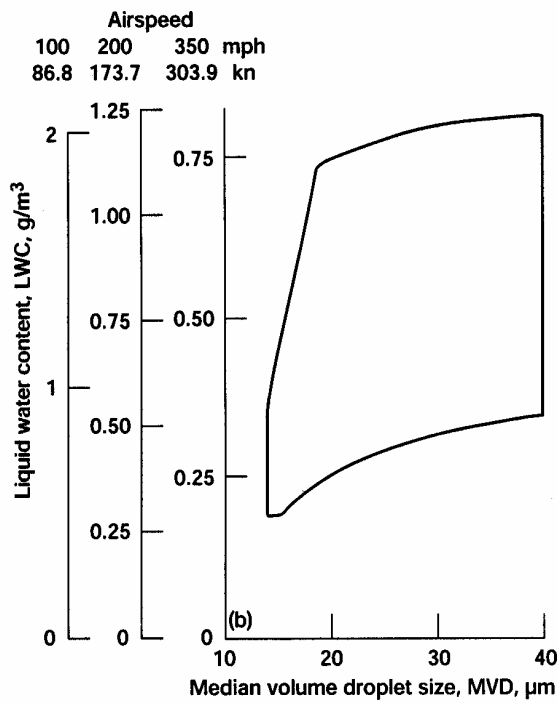


Figure 8.—IRT icing cloud operating envelopes for MOD-1 type nozzles.

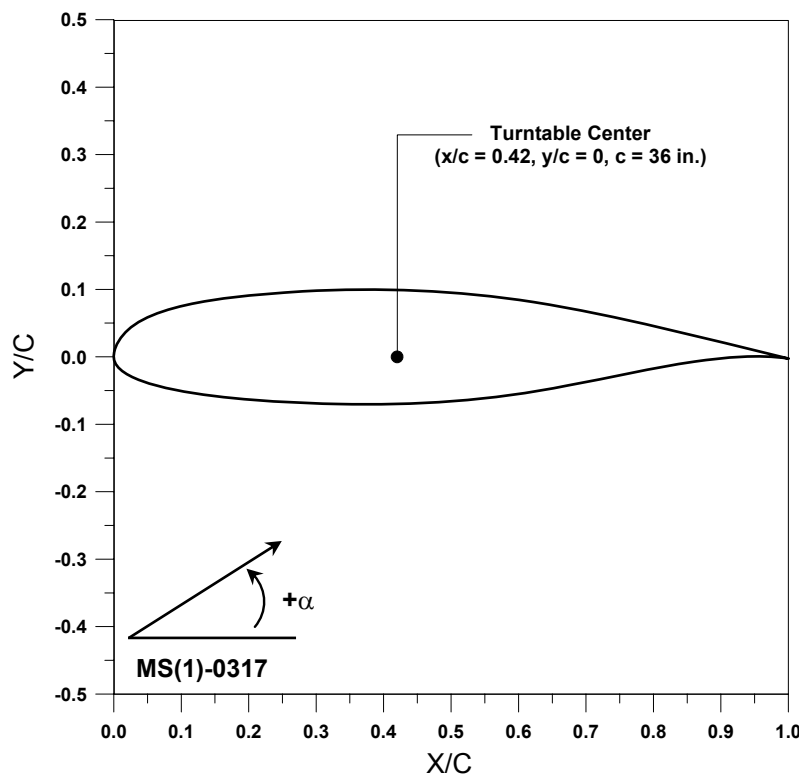


Figure 9a.—MS(1)-0317 airfoil section.

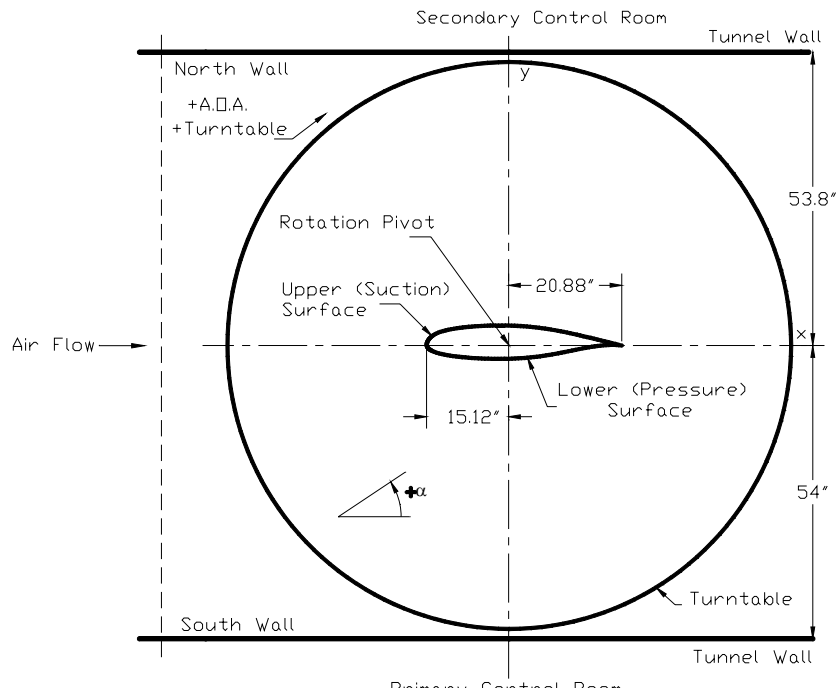


Figure 9b.—MS(1)-0317 airfoil installation in IRT test section (top view).



Figure 9c.—MS(1)-0317 airfoil installed in IRT test section.

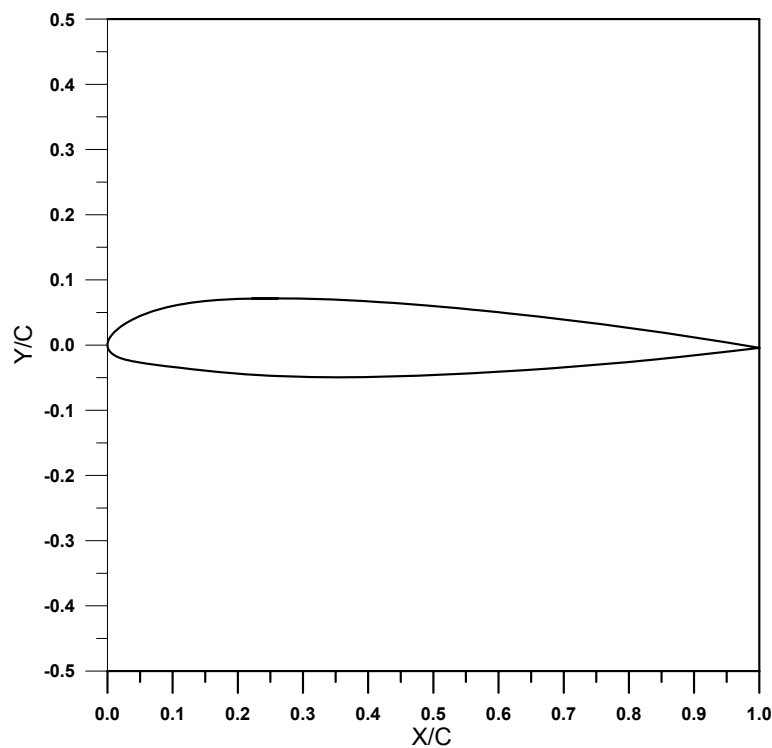


figure 10a.—NACA 23012 airfoil section.

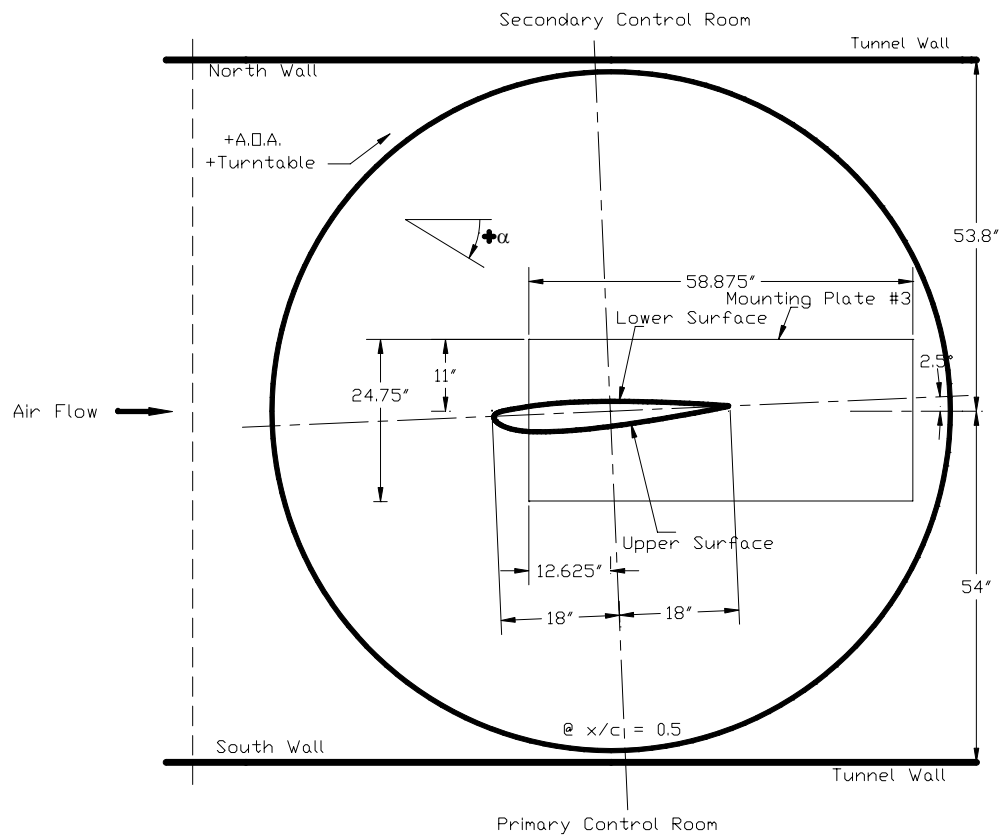
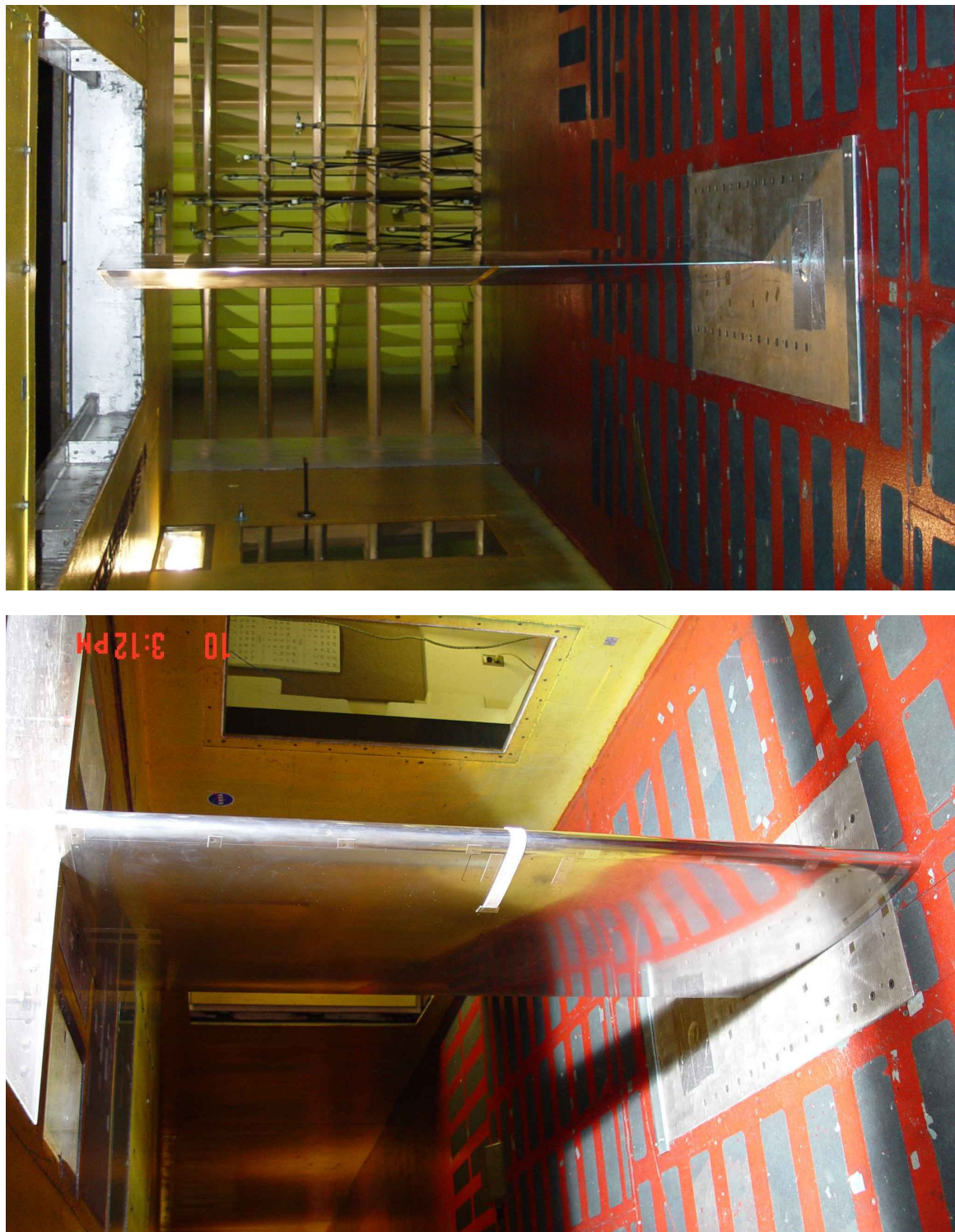


Figure 10b.—NACA 23012 airfoil installation in IRT test section (top view).

Figure 10c.—NACA 23012 airfoil installed in IRT test section.



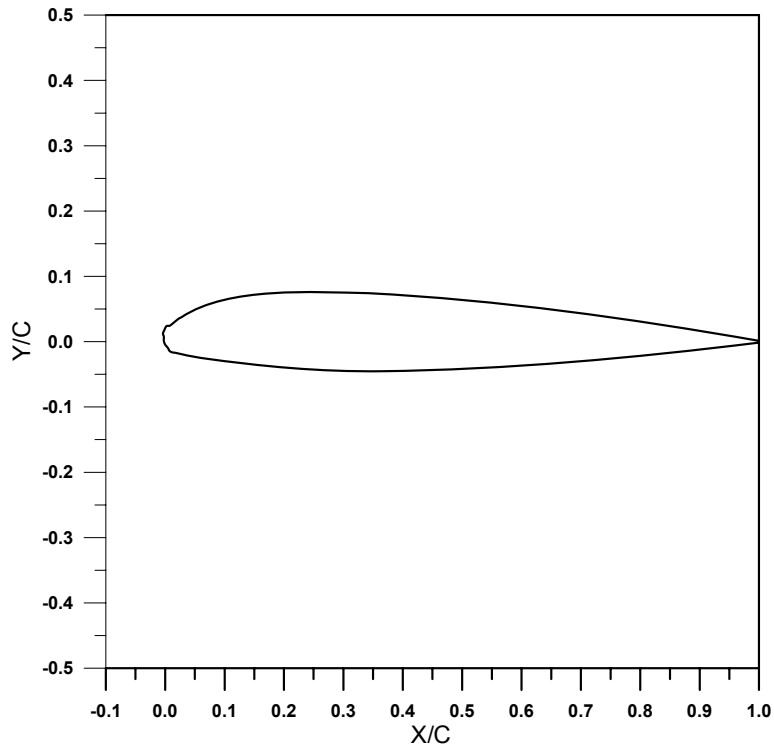


Figure 11a.—NACA 23012 with 5-min glaze ice shape.

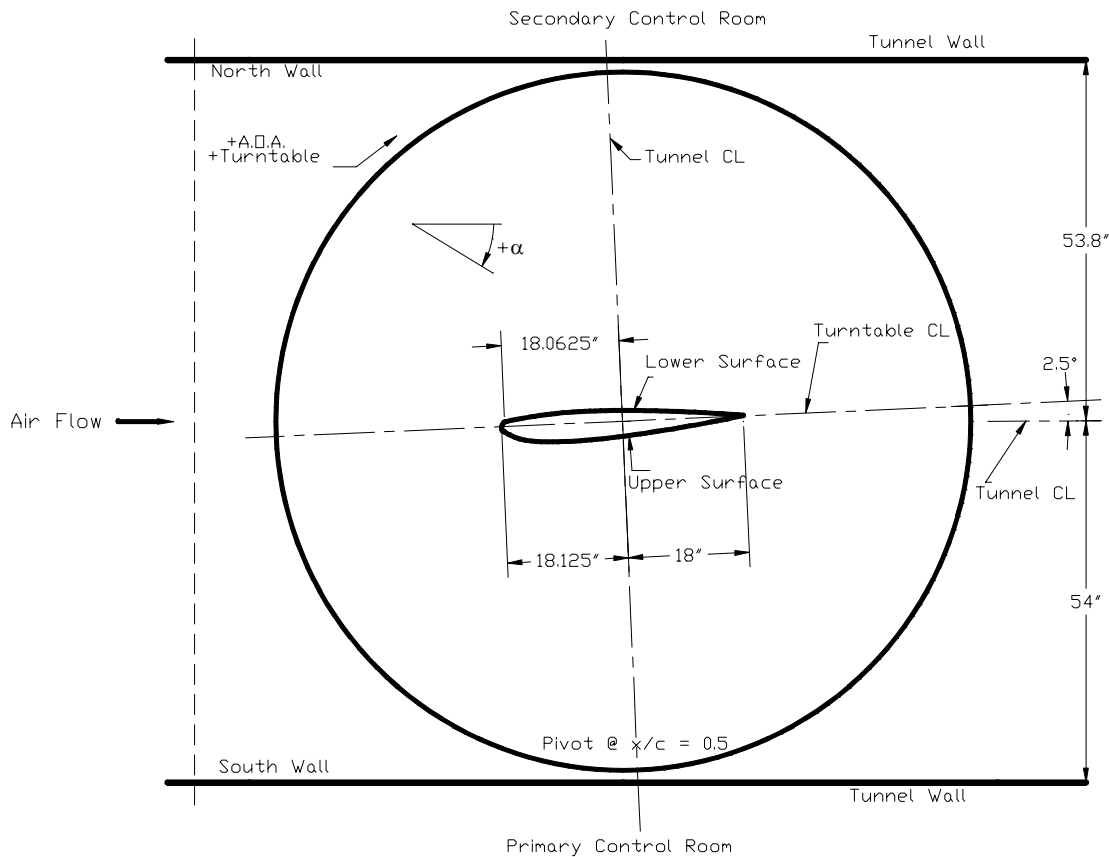


Figure 11b.—NACA 23012 with 5-min glaze ice shape installation in IRT test section (top view).



Figure 11c.—Various views of NACA 23012 with 5-min glaze ice shape installation in IRT test section and blotter strip installation.

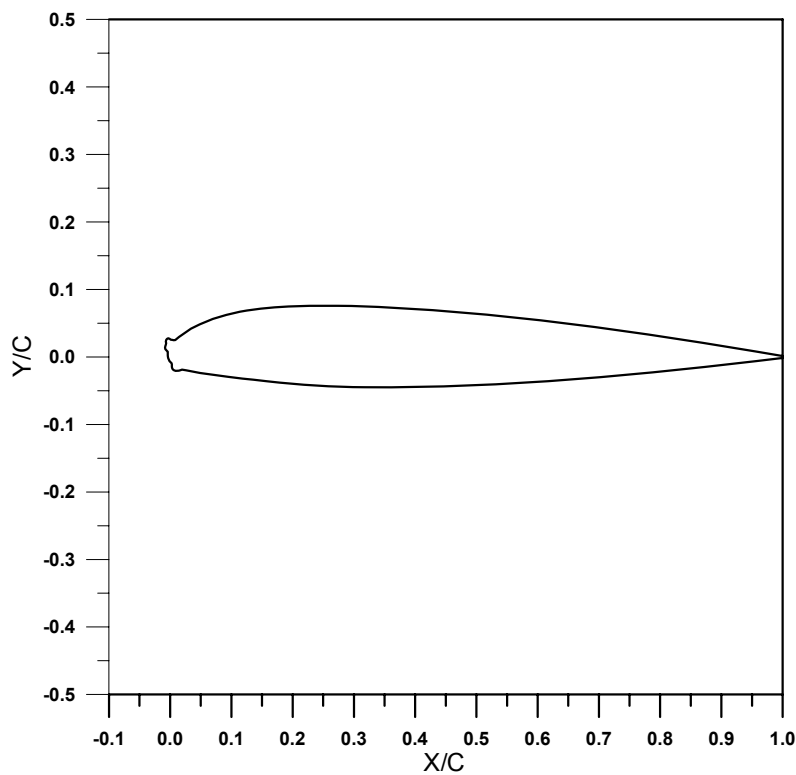


Figure 12a.—NACA 23012 with 10-min glaze ice shape.

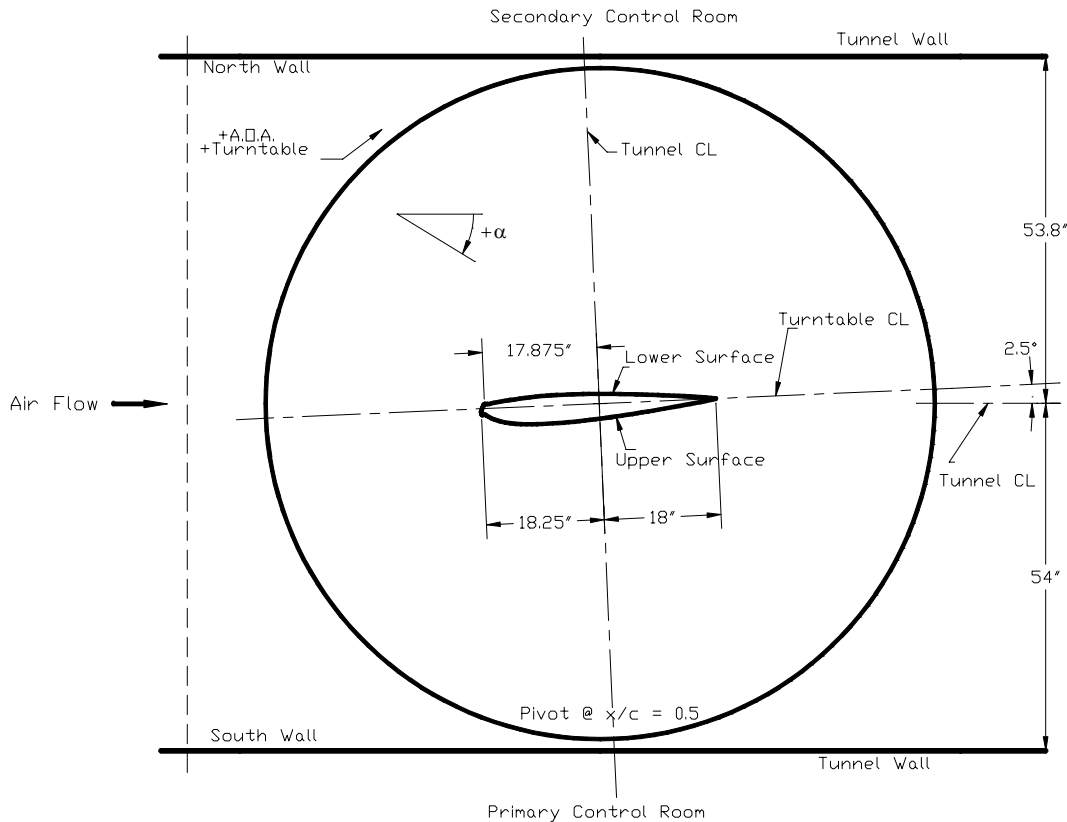


Figure 12b.—Installation of NACA 23012 with 10-min glaze ice shape in IRT test section (top view).

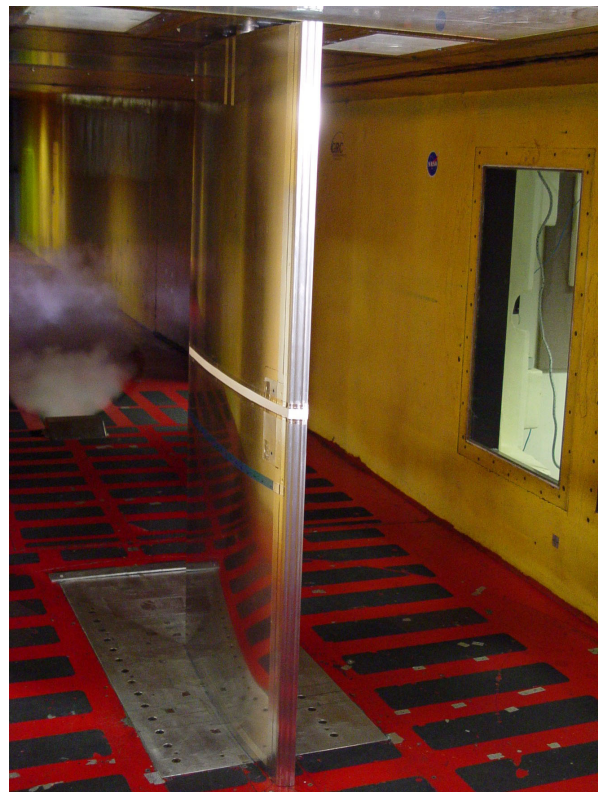
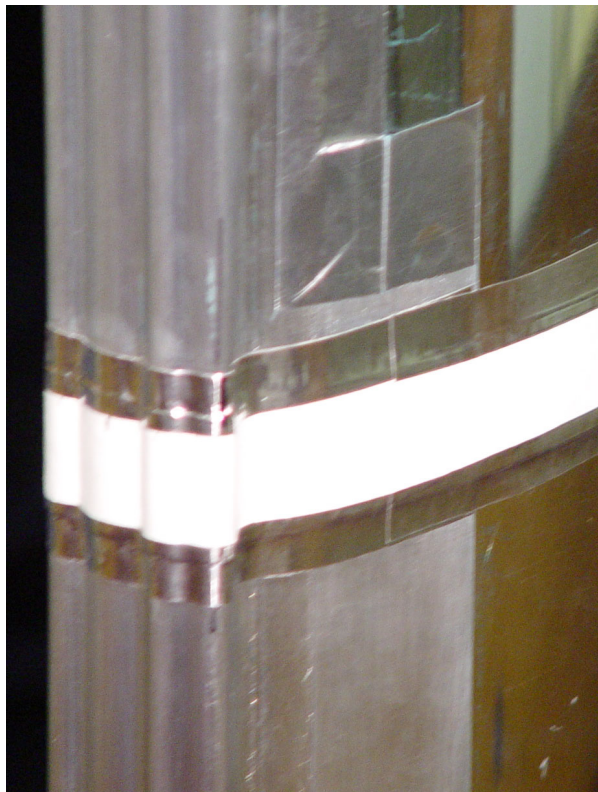


Figure 12c.—Various views of NACA 23012 with 10-min glaze ice shape installation in IRT test section and blotter strip installation.

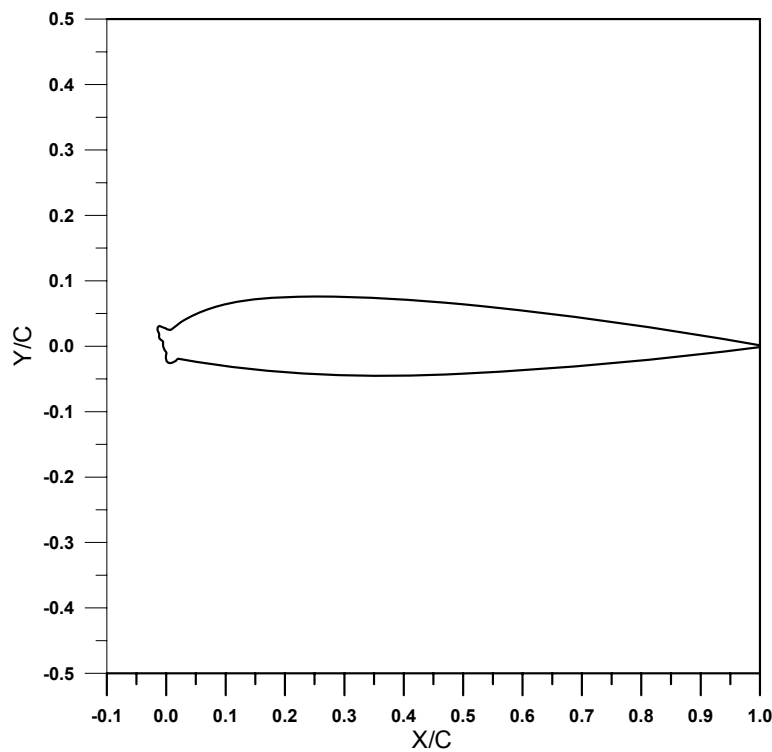


Figure 13a.—NACA 23012 with 15-min glaze ice shape.

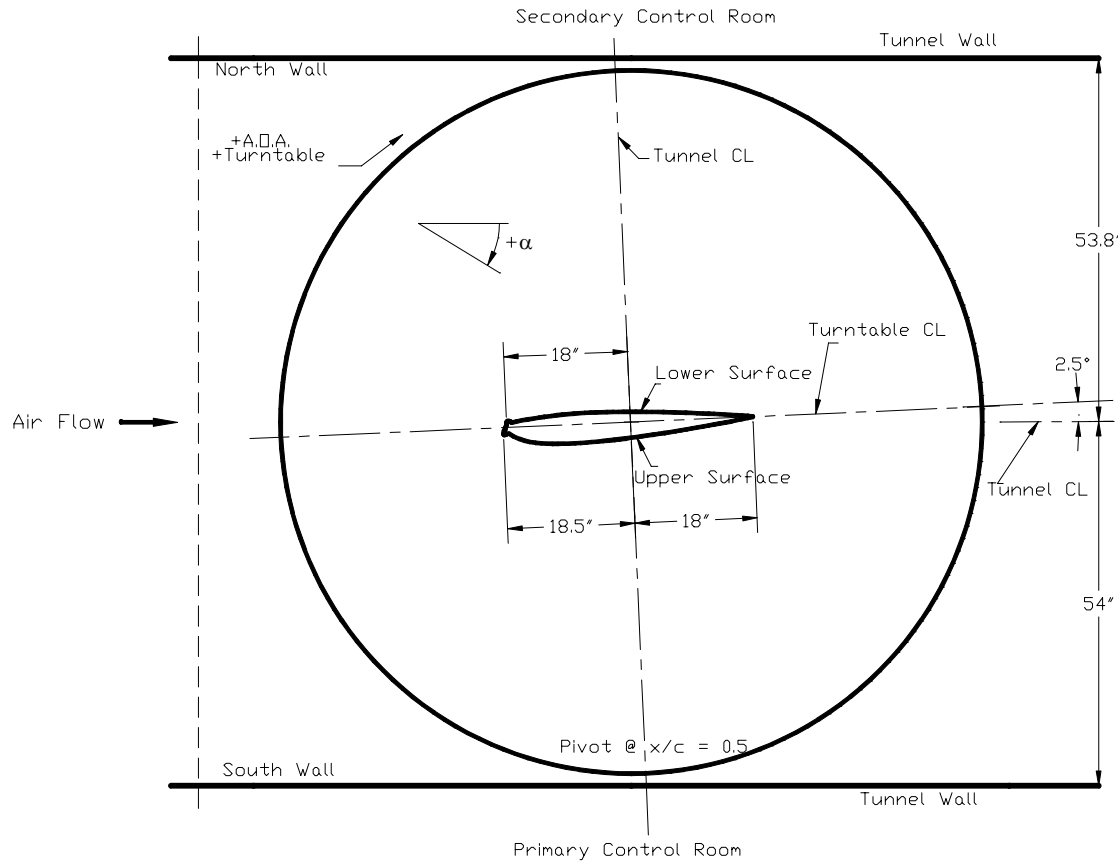


Figure 13b.—NACA 23012 with 15-min glaze ice shape installation in IRT test section (top view).



Figure 13c.—Various views of NACA 23012 with 15-min glaze ice shape installation in IRT test section and blotter strip installation.

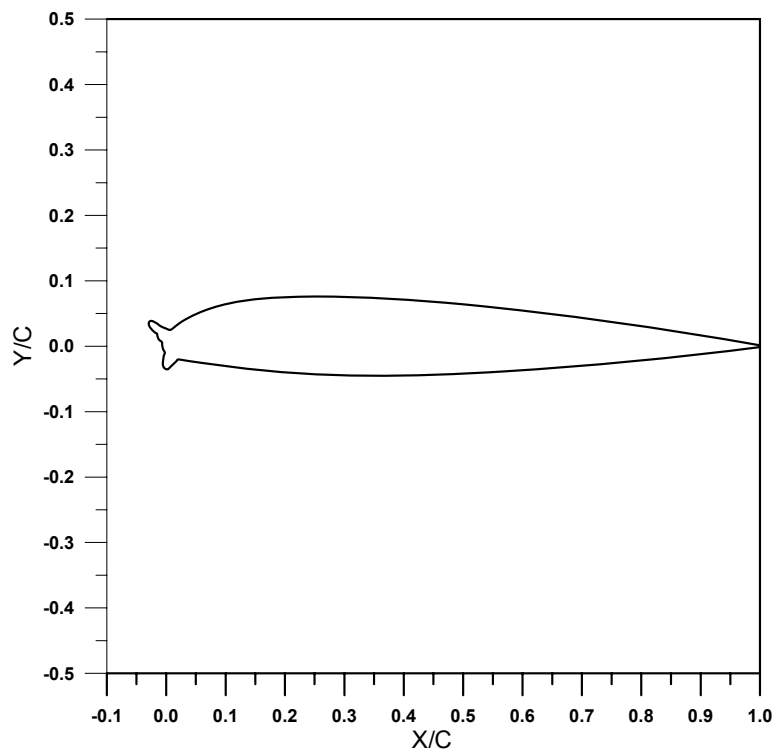


Figure 14a.—NACA 23012 with 22.5-min glaze ice shape.

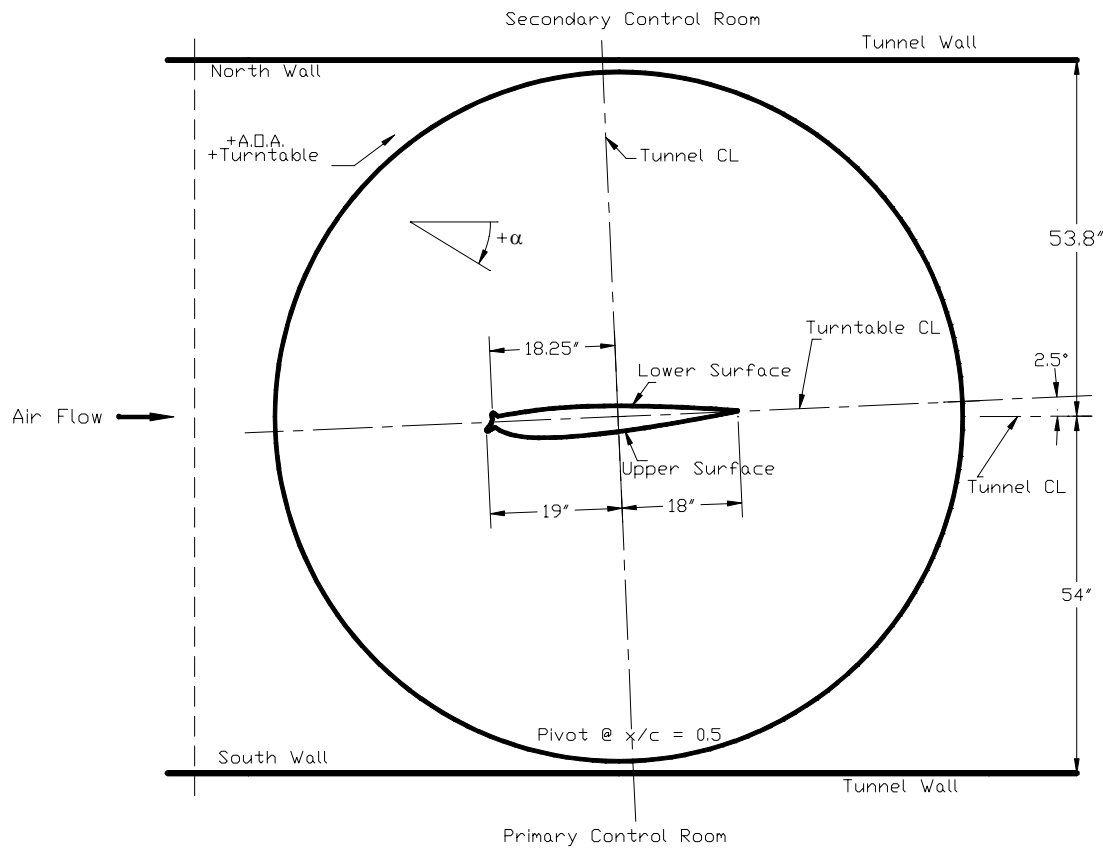


Figure 14b.—NACA 23012 with 22.5-min glaze ice shape installation in IRT test section (top view).

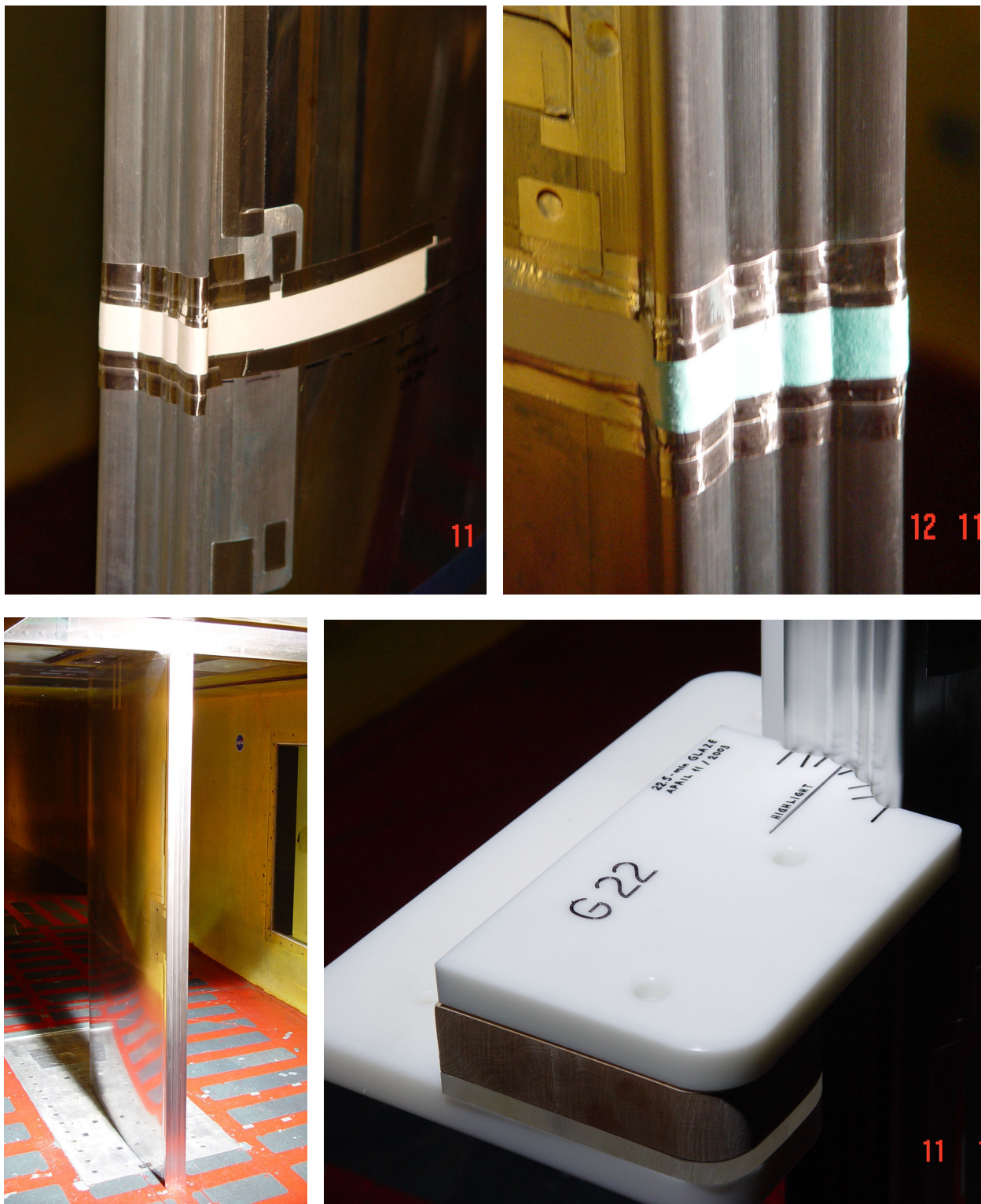


Figure 14c.—Various views of NACA 23012 with 22.5-min glaze ice shape installation in IRT test section and blotter strip installation.

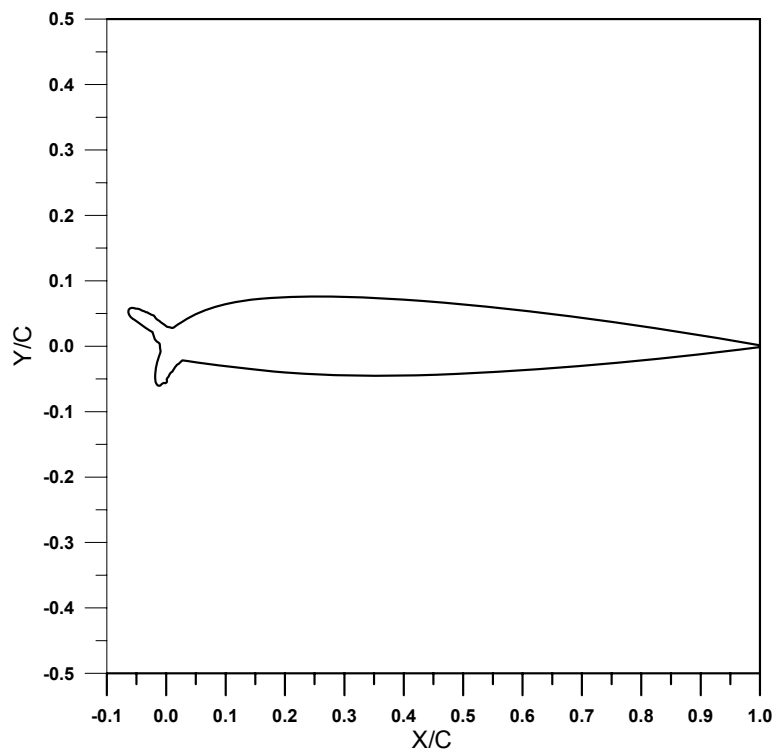


Figure 15a.—NACA 23012 with 45-min glaze ice shape.

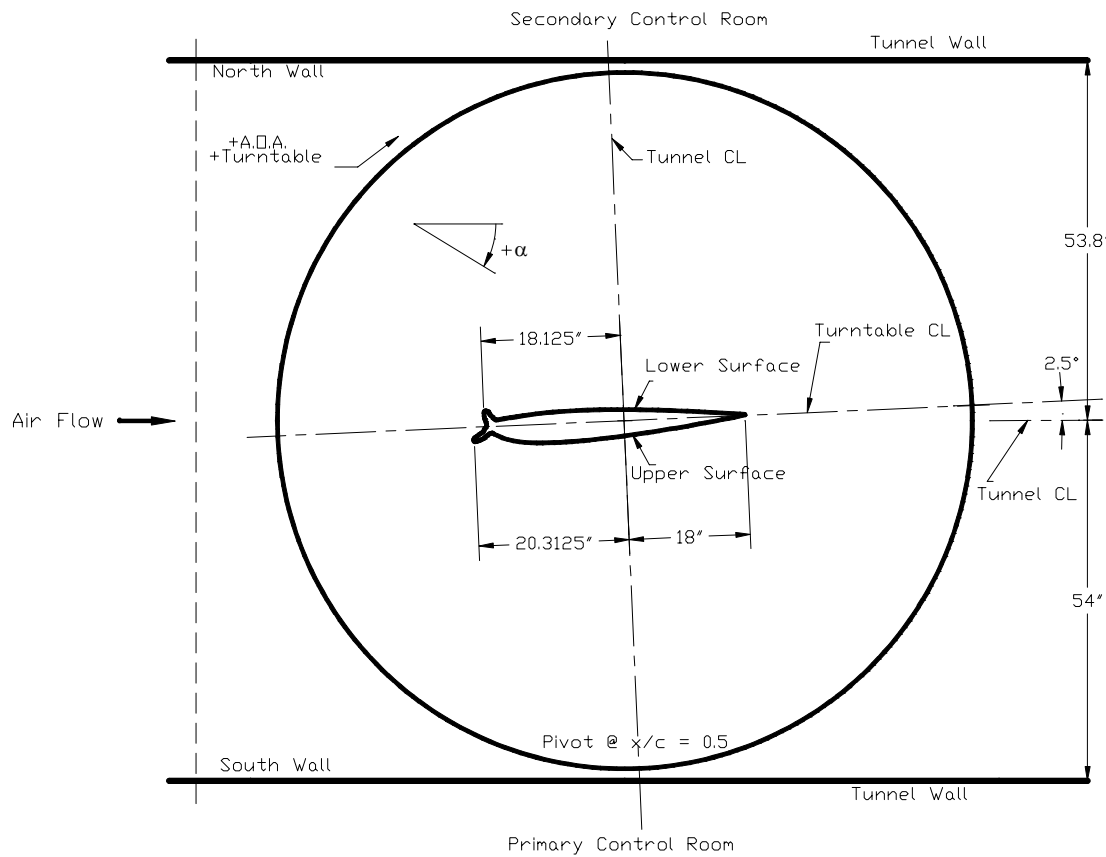


Figure 15b.—NACA 23012 with 45-min glaze ice shape installation in IRT test section (top view).



Figure 15c.—Various views of NACA 23012 with 45-min glaze ice shape installation in IRT test section and blotter strip installation.

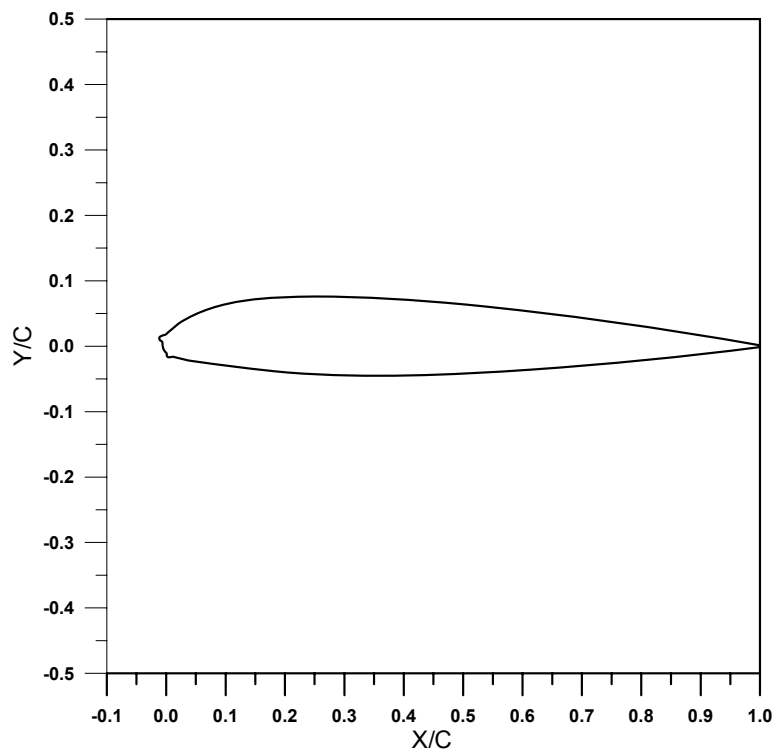


Figure 16a.—NACA 23012 with 7.5-min mixed ice shape.

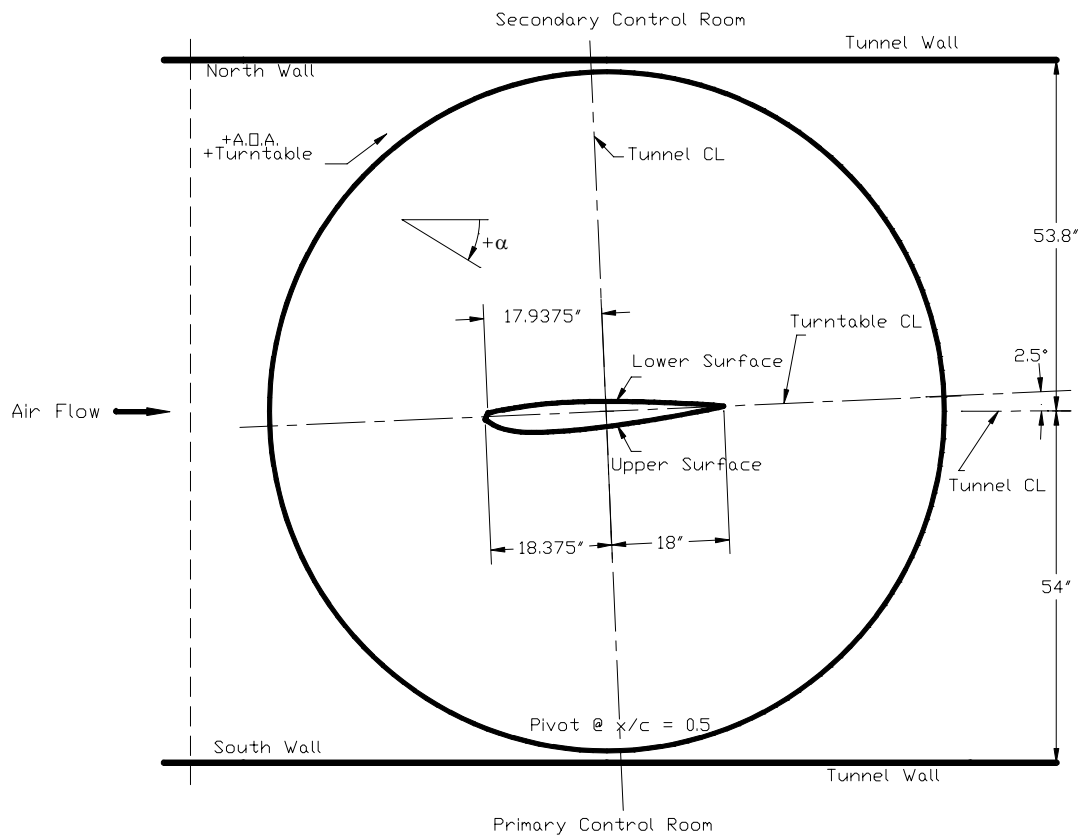


Figure 16b.—NACA 23012 with 7.5-min mixed ice shape installation in IRT test section (top view).



Figure 16c.—Various views of NACA 23012 with 7.5-min mixed ice shape installation in IRT test section and blotter strip installation.

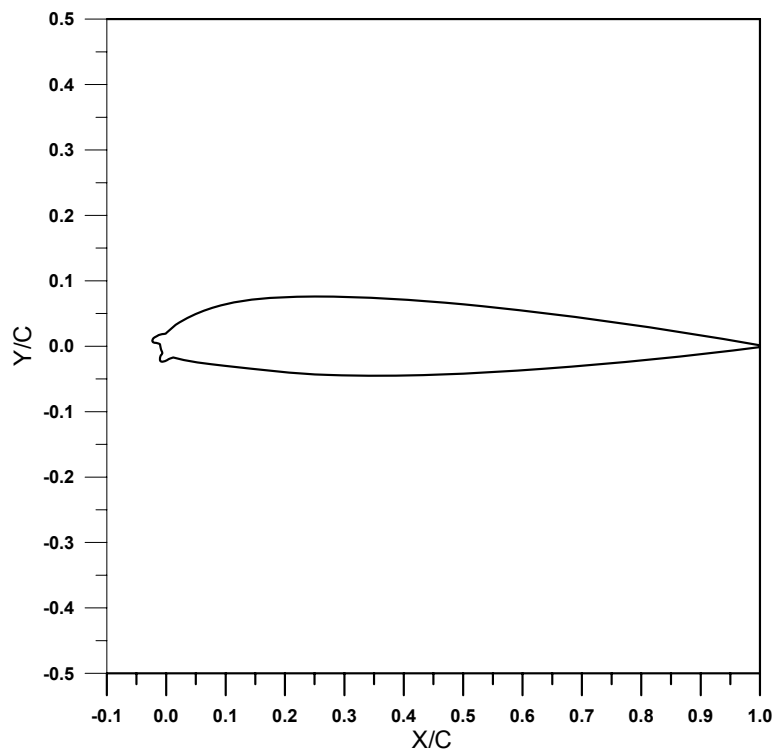


Figure 17a.—NACA 23012 with 15-min mixed ice shape.

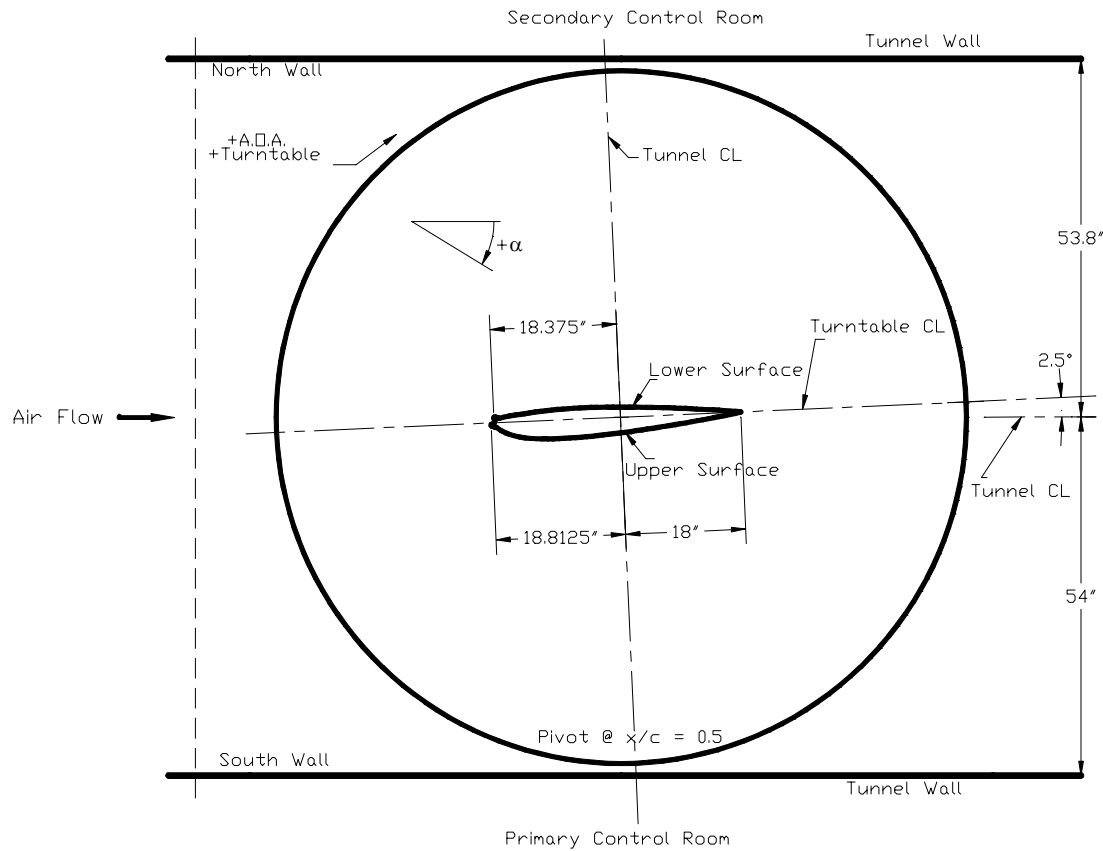


Figure 17b.—NACA 23012 with 15-min mixed ice shape installation in IRT test section (top view).



Figure 17c.—Various views of NACA 23012 with 15-min mixed ice shape installation in IRT test section and blotter strip installation.

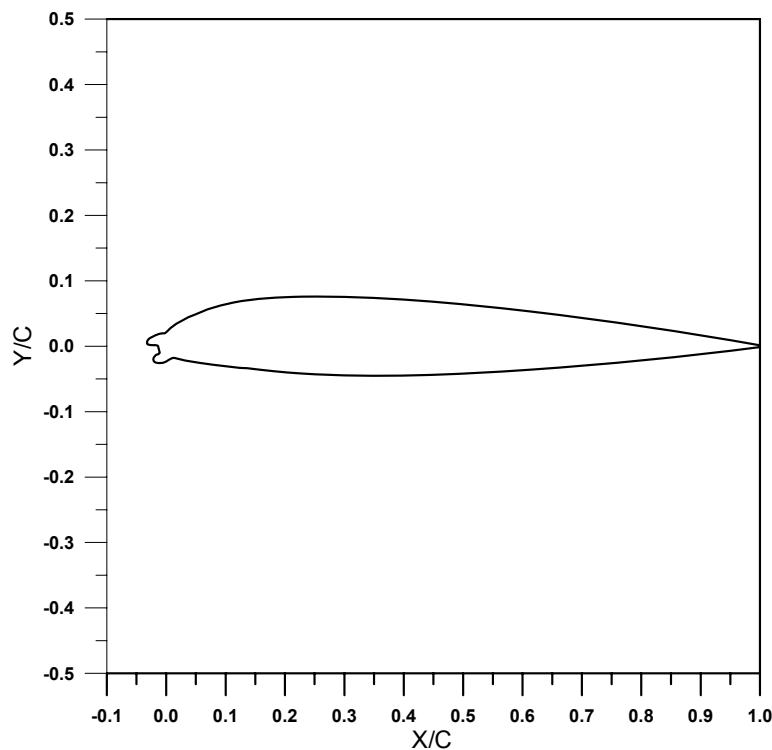


Figure 18a.—NACA 23012 with 22.5-min mixed ice shape.

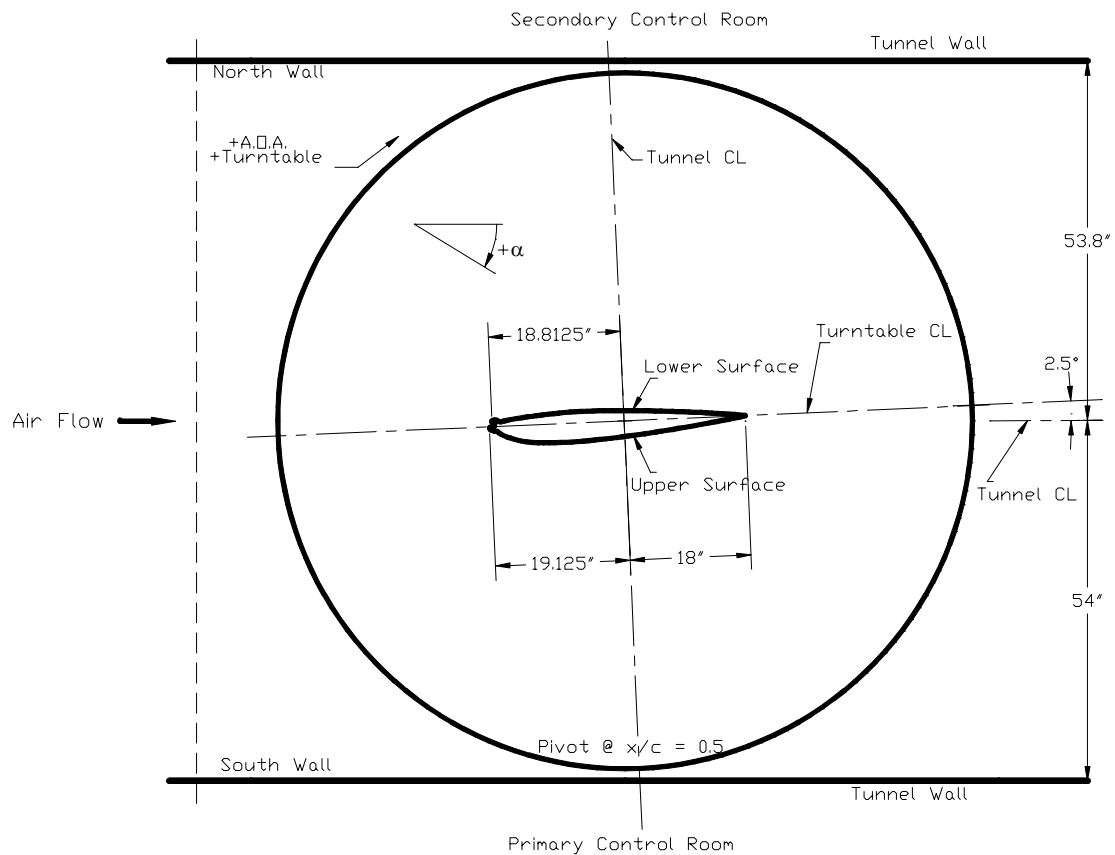


Figure 18b.—NACA 23012 with 22.5-min mixed ice shape installation in IRT test section (top view).

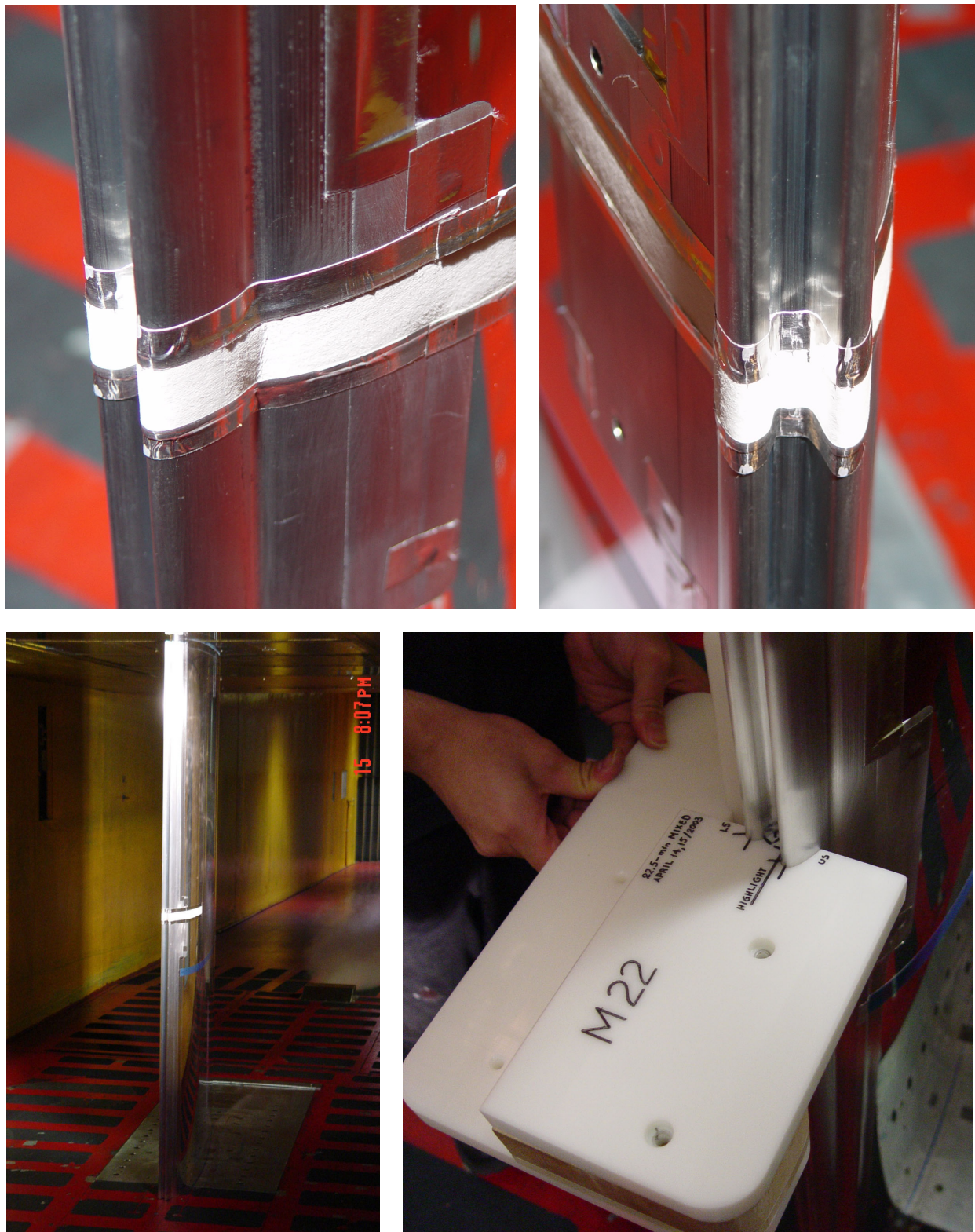


Figure 18c.—Various views of NACA 23012 with 22.5-min mixed ice shape installation in IRT test section and blotter strip installation.

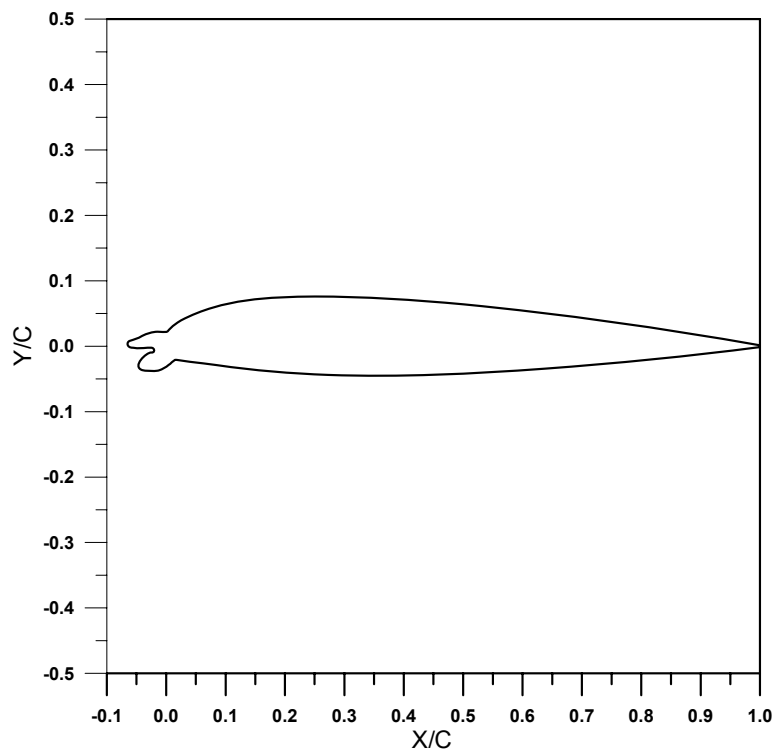


Figure 19a.—NACA 23012 with 45-min mixed ice shape.

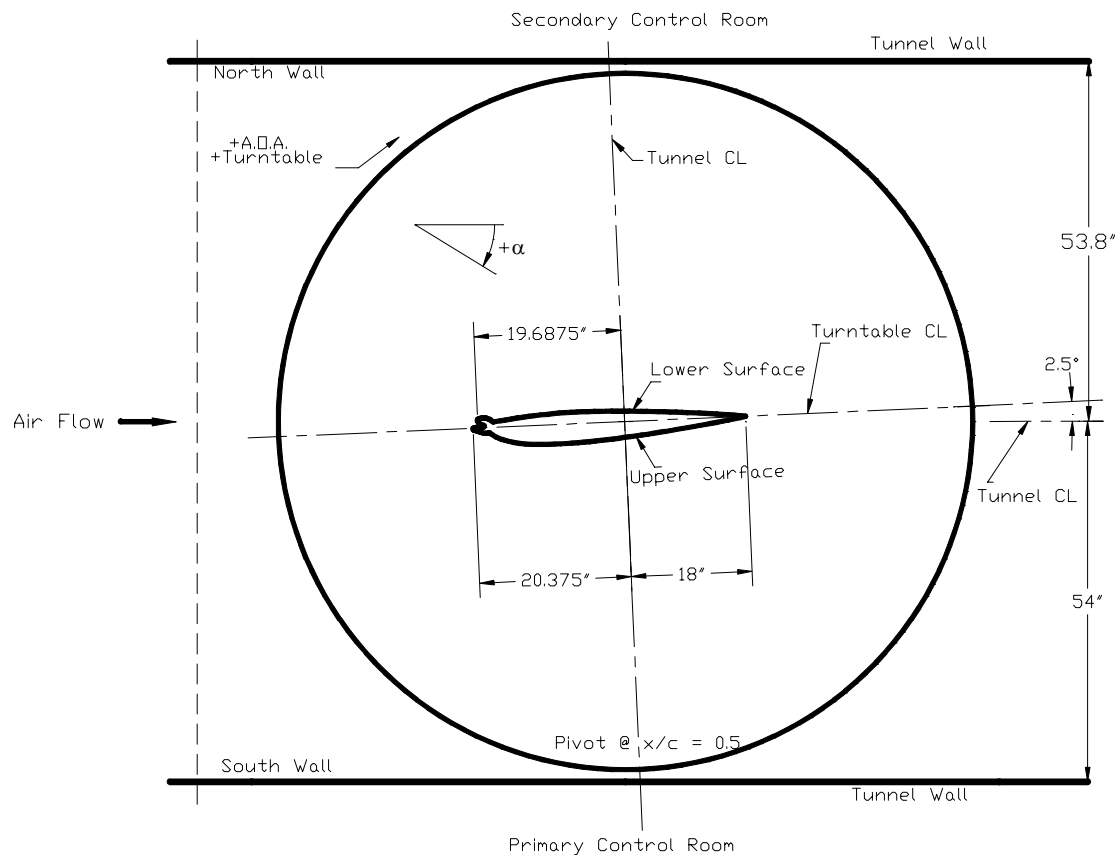


Figure 19b.—NACA 23012 with 45-min mixed ice shape installation in IRT test section (top view).



Figure 19c.—Various views of NACA 23012 with 45-min mixed ice shape installation in IRT test section and blotter strip installation.

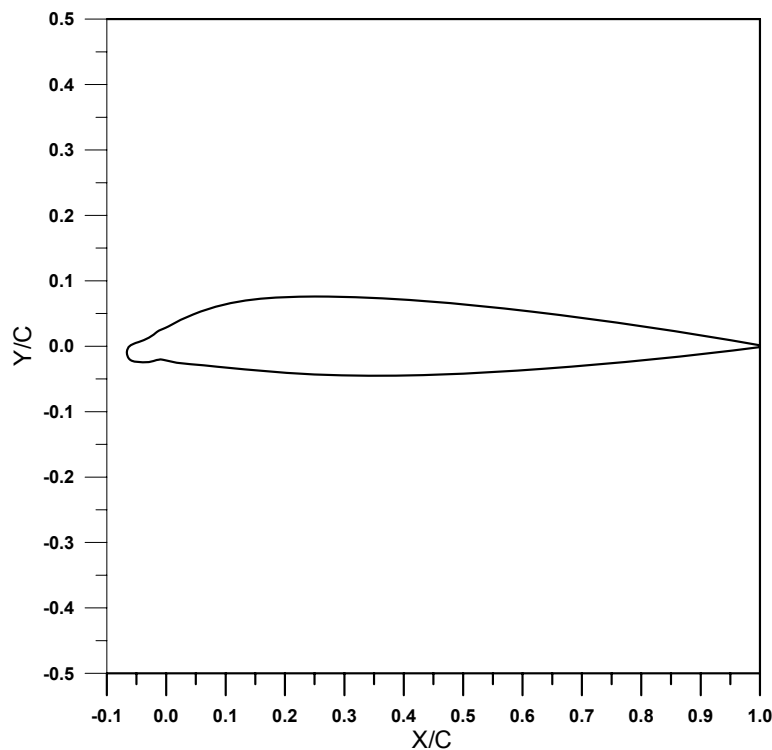


Figure 20a.—NACA 23012 with 45-min rime ice shape.

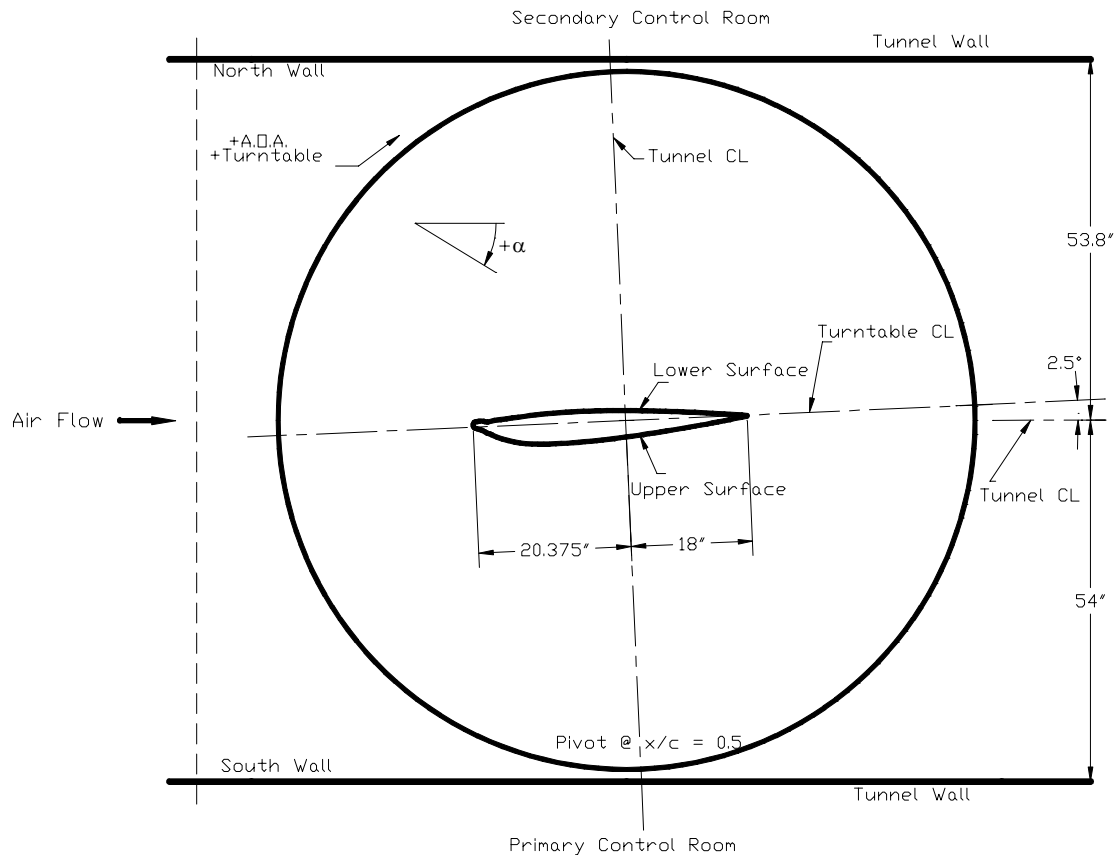


Figure 20b.—NACA 23012 with 45-min rime ice shape installation in IRT test section (top view).



Figure 20c.—Various views of NACA 23012 with 45-min rime ice shape installation in IRT test section and blotter strip installation.

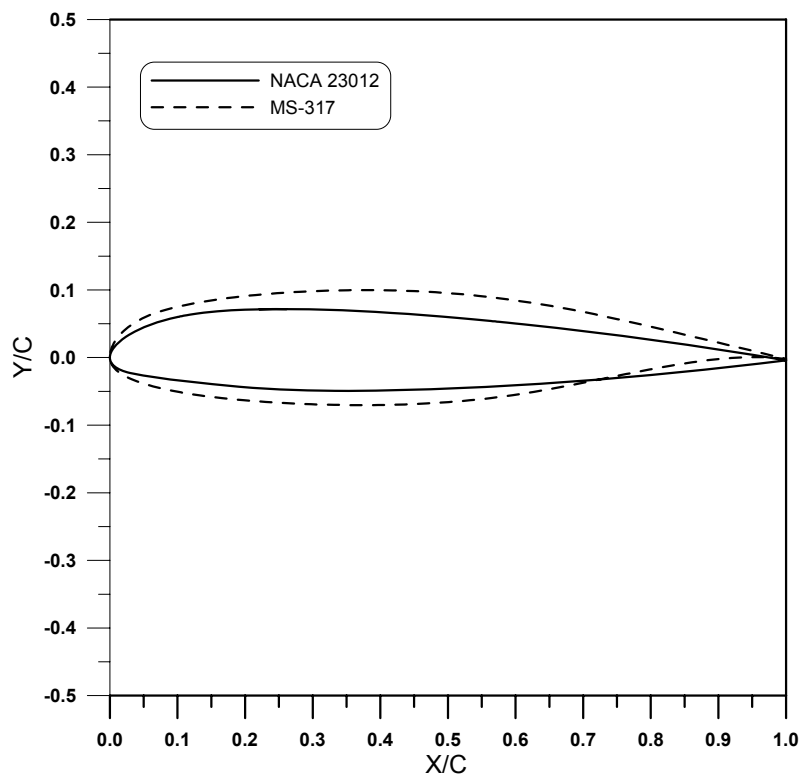


Figure 21.—Comparison of clean airfoil sections.

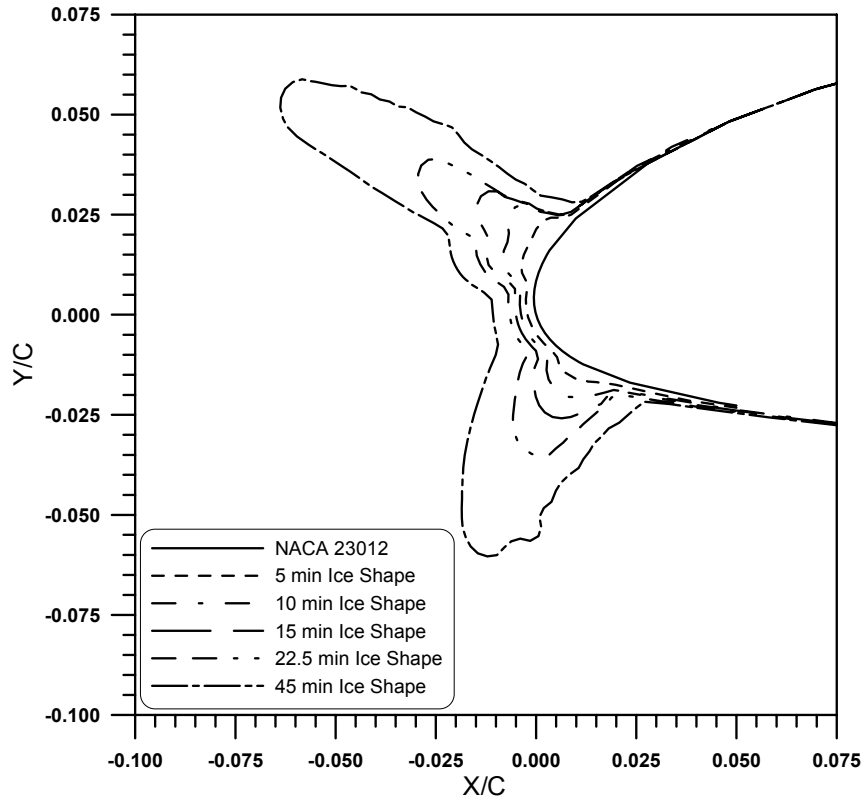


Figure 22a.—Comparison of clean NACA 23012 and glaze ice shape sections.

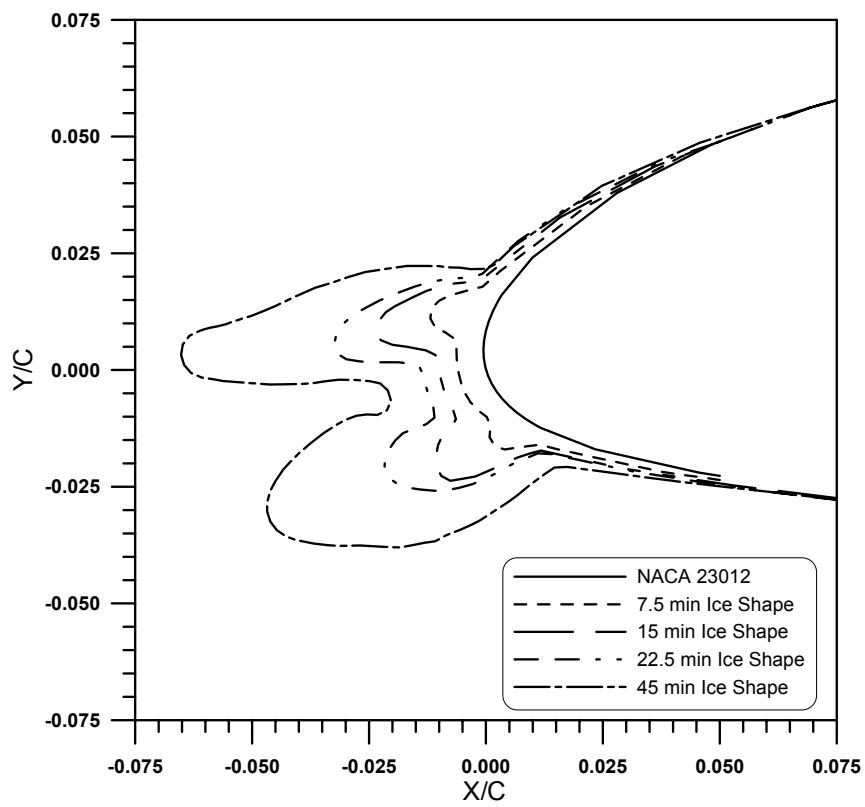


Figure 22b.—Comparison of clean NACA 23012 and mixed ice shape sections.

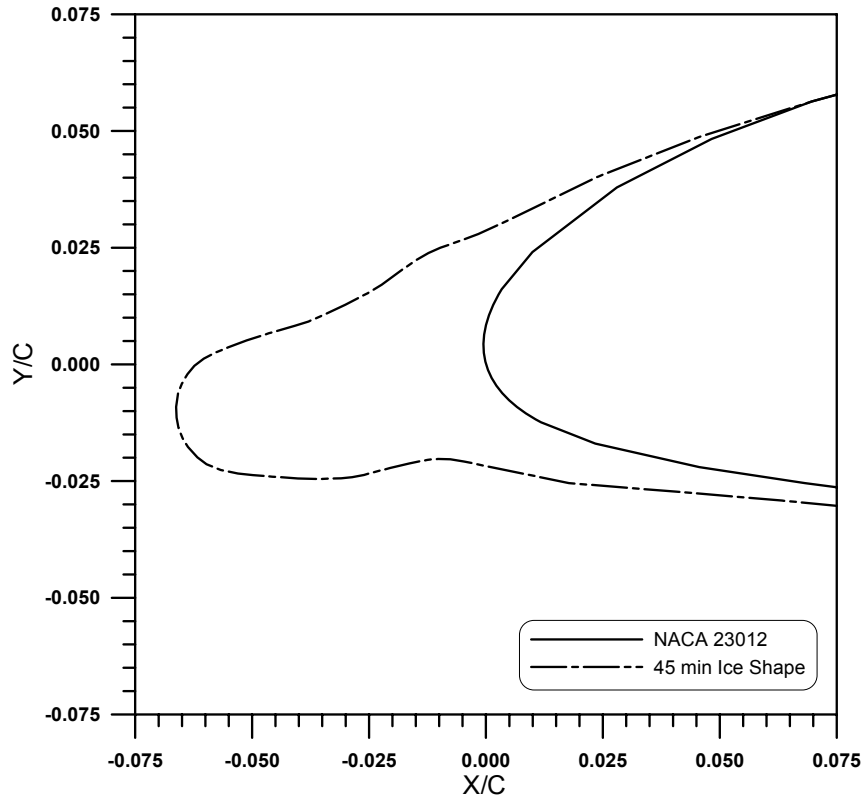


Figure 22c.—Comparison of clean NACA 23012 and rime ice shape sections.

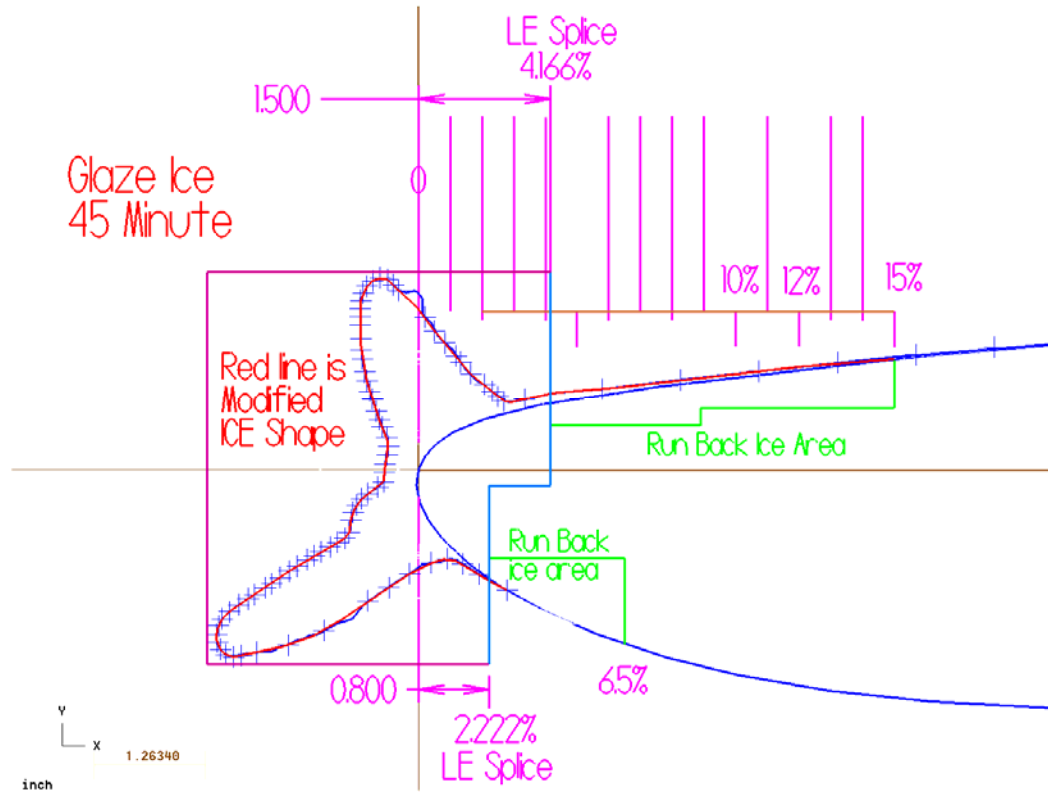


Figure 23a.—Removable wing leading edge and 45-min glaze ice shape.

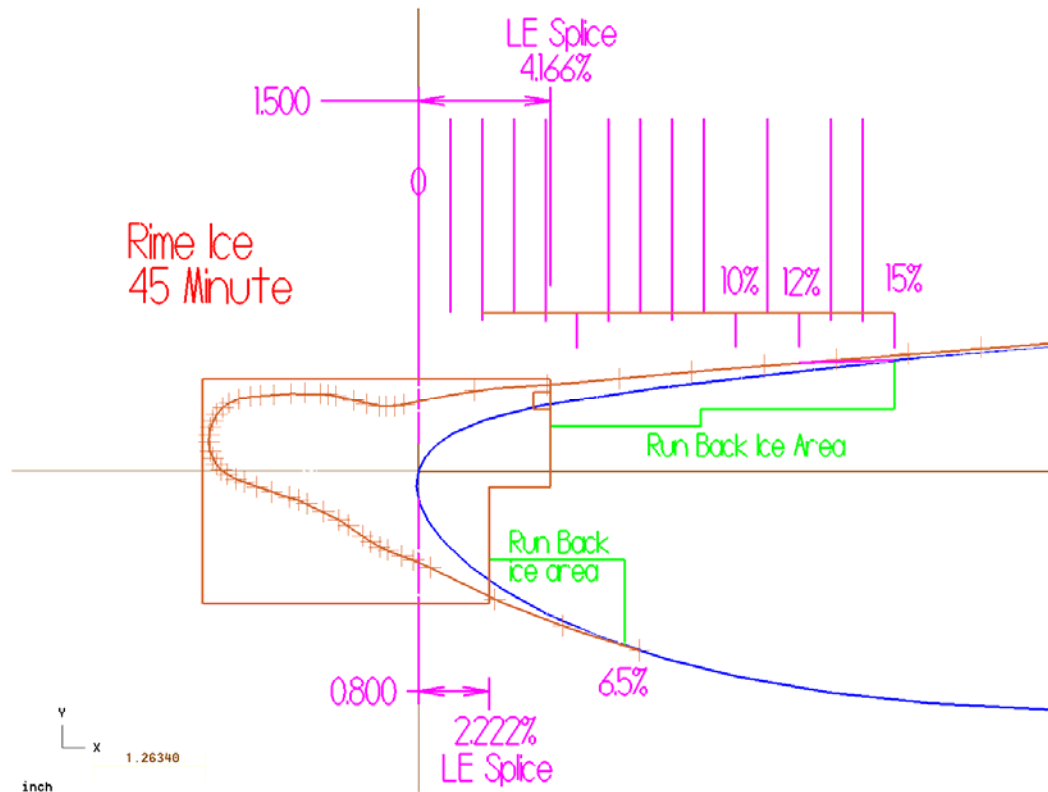


Figure 23b.—Removable wing leading edge and 45-min rime ice shape.



Figure 24a.—NACA 23012 airfoil with the leading edge section removed.

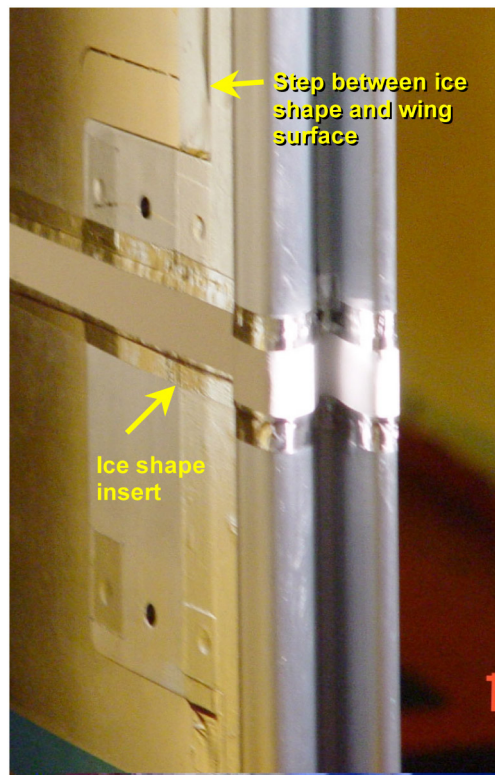


Figure 24b.—Ice shape insert installed on the pressure surface.

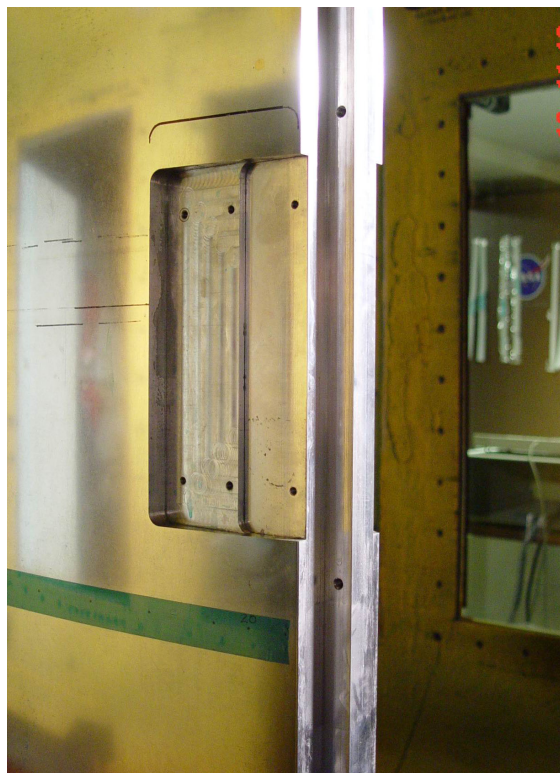


Figure 24c.—Slot for ice shape insert on the pressure surface.



Figure 24d.—Slot for ice shape insert on the suction surface.

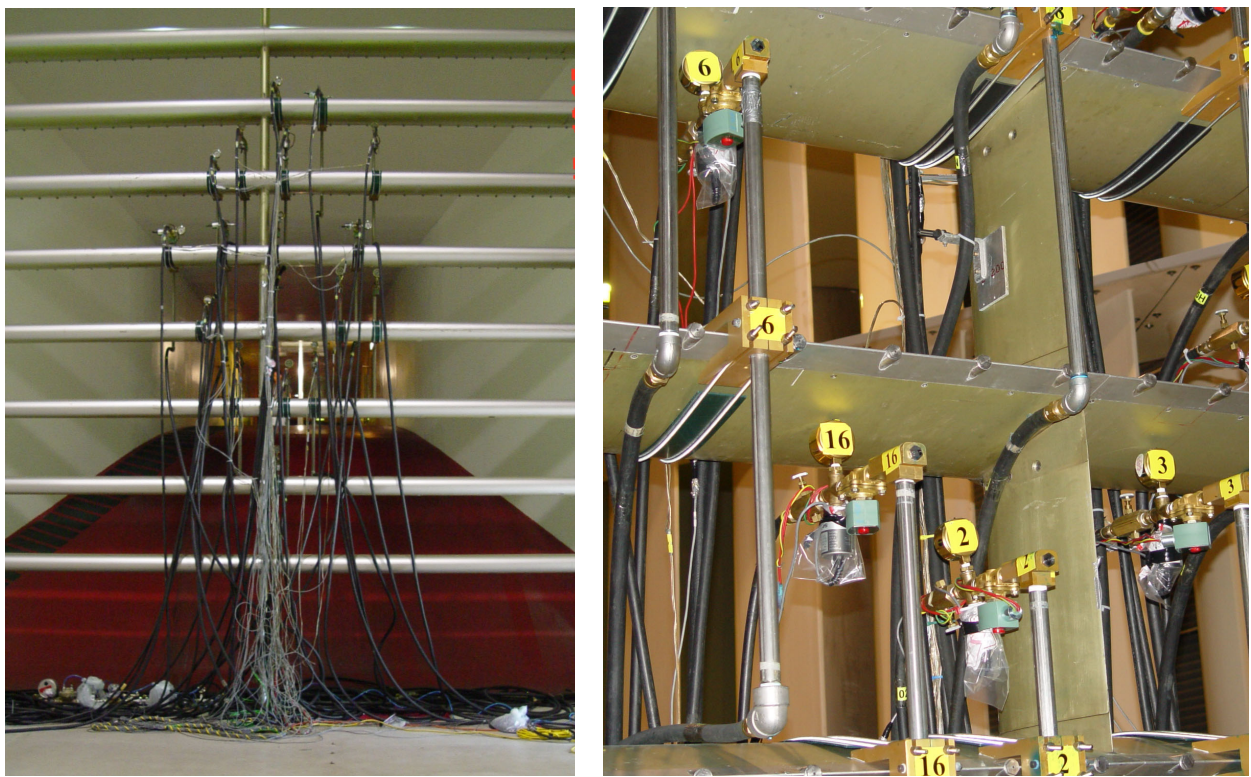


Figure 25a.—WSU spray system installed in IRT plenum chamber.

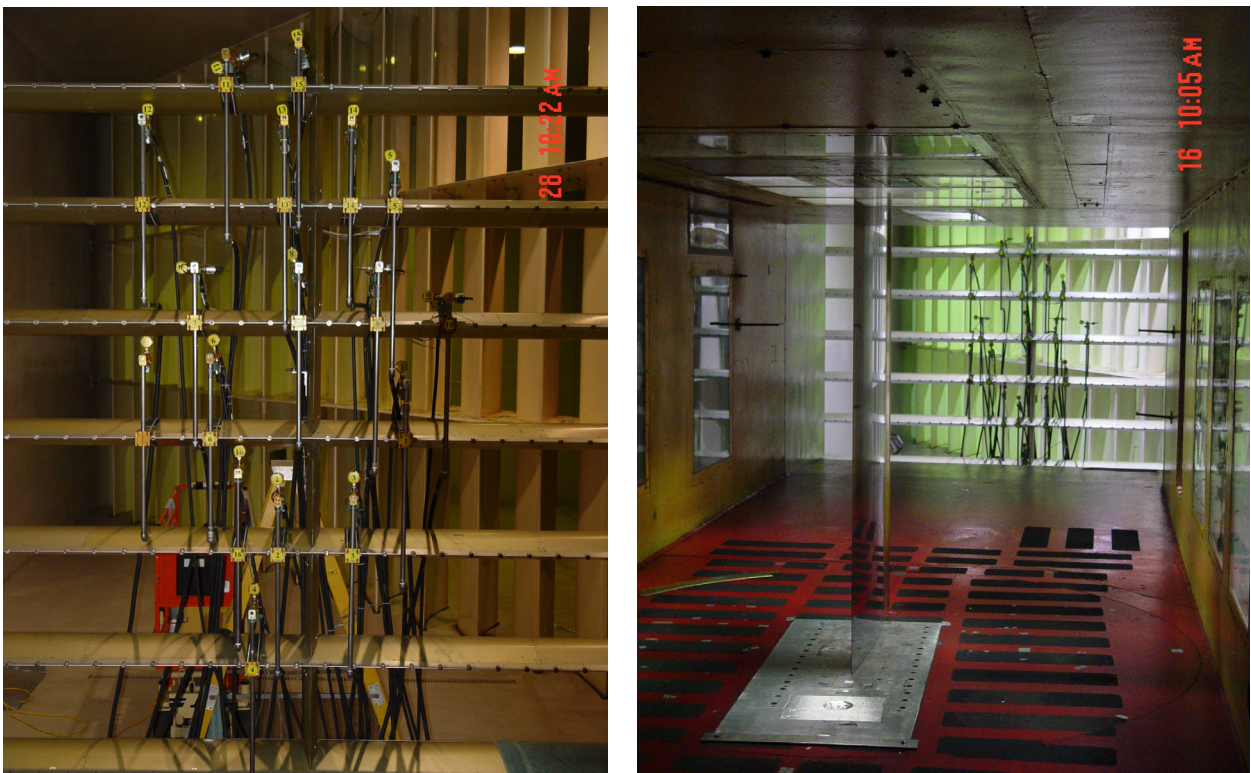


Figure 25b.—Views of WSU spray system installed from IRT test section.

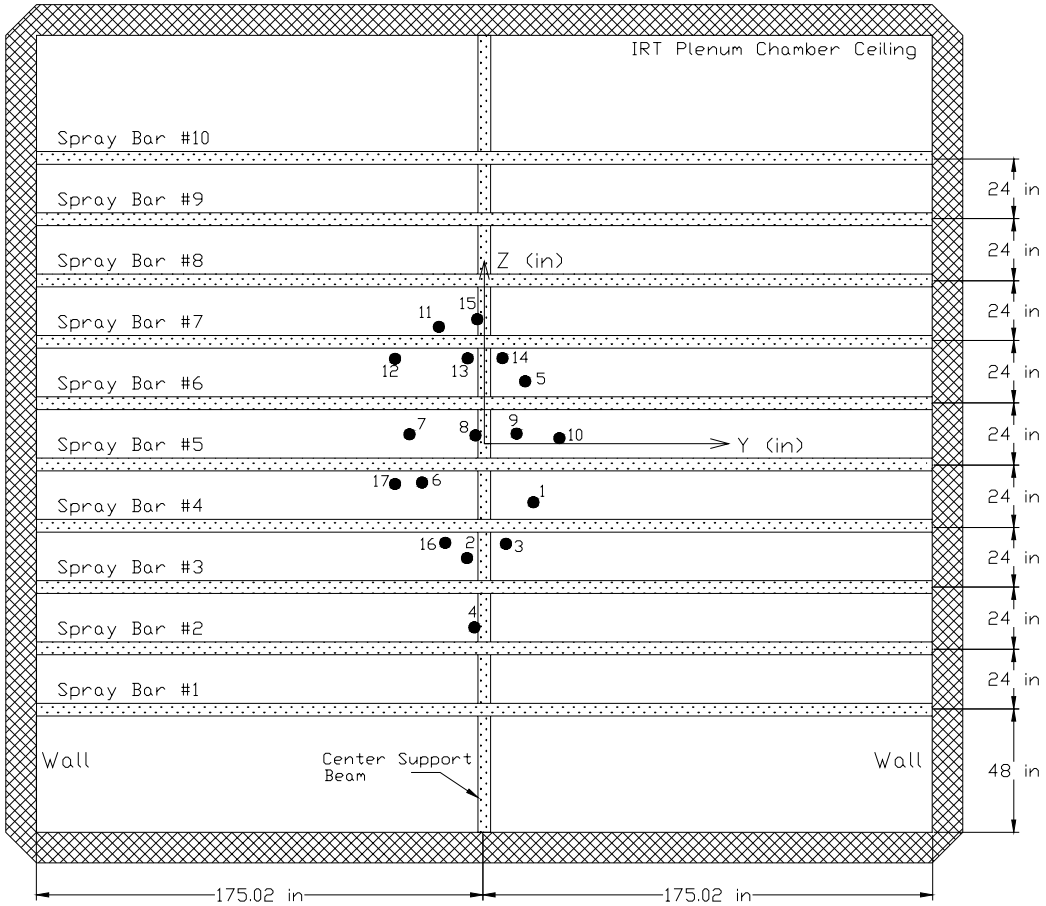


Figure 26a.—Schematic drawing of 2003 WSU spray system (all dimensions in inches).

| WSU nozzle assembly no. | NASA MOD-1 nozzle no. | $C_f$   | Y-Coordinate (in.) | Z-Coordinates (in.) |
|-------------------------|-----------------------|---------|--------------------|---------------------|
| 1                       | M277                  | 0.00400 | +19.000            | +9.000/SP4          |
| 2                       | M264                  | NA      | -7.000             | +11.500/SP3         |
| 3                       | M234                  | 0.00399 | +8.500             | +17.500/SP3         |
| 4                       | M217                  | 0.00398 | -3.750             | +8.750/SP2          |
| 5                       | M308                  | 0.00401 | +16.125            | +8.500/SP6          |
| 6                       | M243                  | 0.00401 | -24.000            | +17.250/SP4         |
| 7                       | M300                  | NA      | -28.875            | +11.750/SP5         |
| 8                       | M233                  | 0.00400 | -3.500             | +11.500/SP5         |
| 9                       | M242                  | 0.00401 | +12.750            | +12.000/SP5         |
| 10                      | M210                  | 0.00406 | +29.500            | +10.250/SP5         |
| 11                      | M249                  | 0.00401 | -18.000            | +6.000/SP7          |
| 12                      | M252                  | 0.00403 | -34.750            | +17.500/SP6         |
| 13                      | M269                  | NA      | -6.500             | +17.500/SP6         |
| 14                      | M291                  | NA      | +7.250             | +17.750/SP6         |
| 15                      | M268                  | NA      | -3.000             | +9.000/SP7          |
| 16                      | M203                  | NA      | -15.125            | +17.250/SP3         |
| 17                      |                       | NA      | -34.75             | +16.500/SP4         |

Figure 26b.—WSU spray system nozzle locations with respect to the IRT spray bars (2003 IRT Entry).

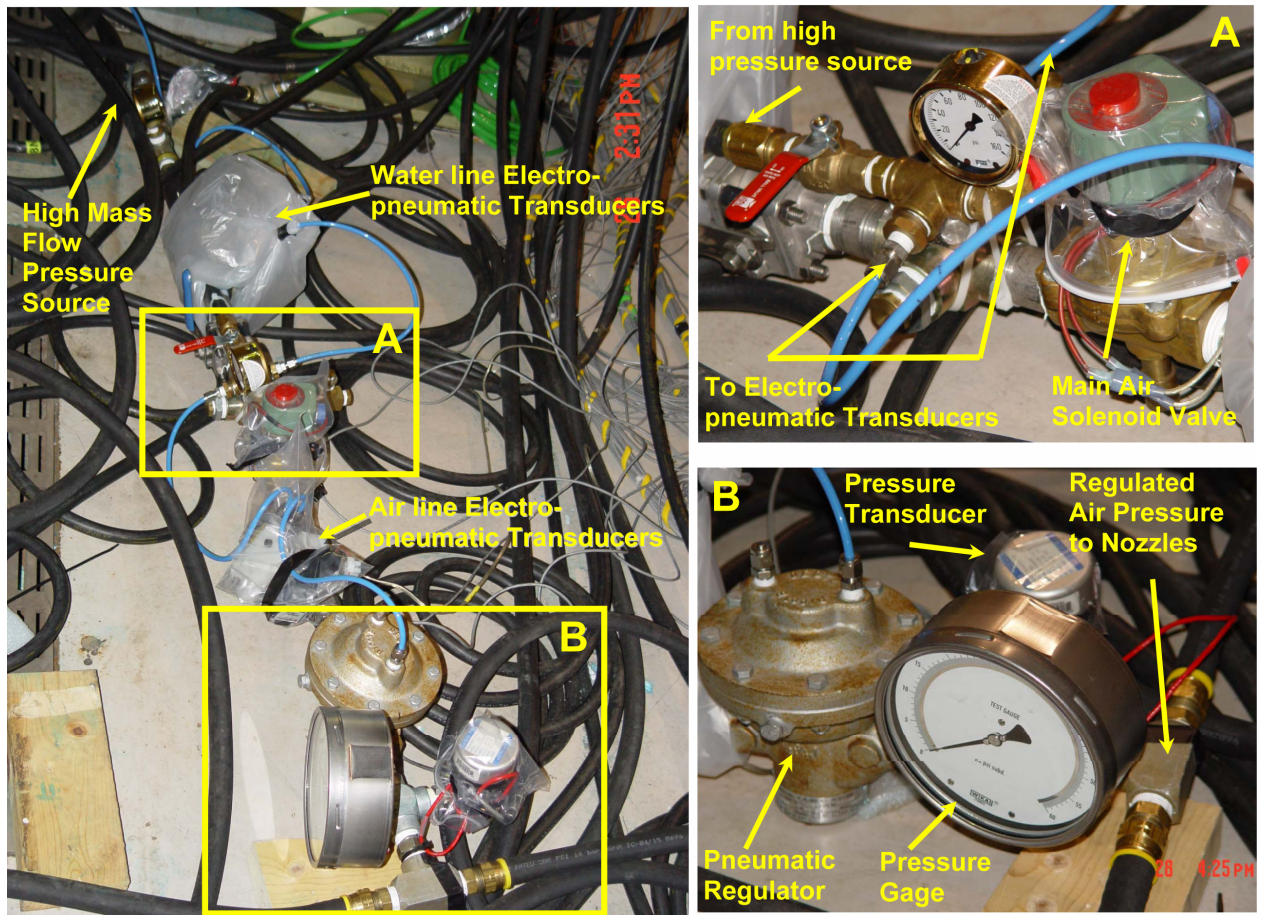


Figure 27.—Main air supply control system for WSU spray nozzles.

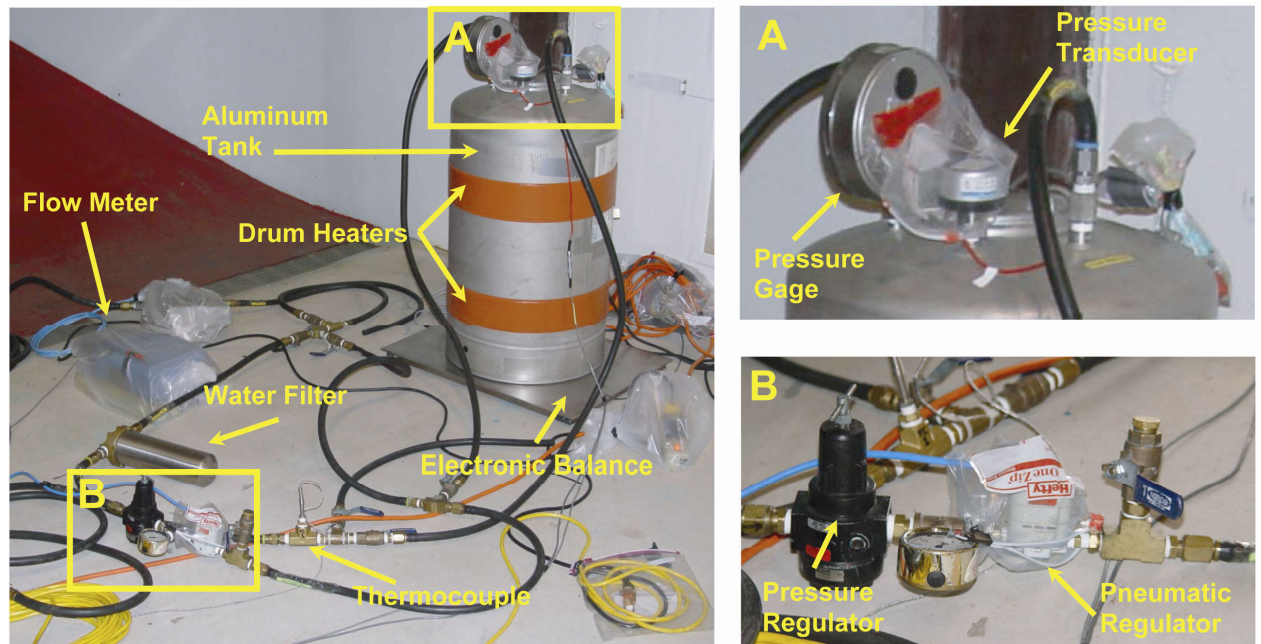


Figure 28.—Water supply tank and the water line system.

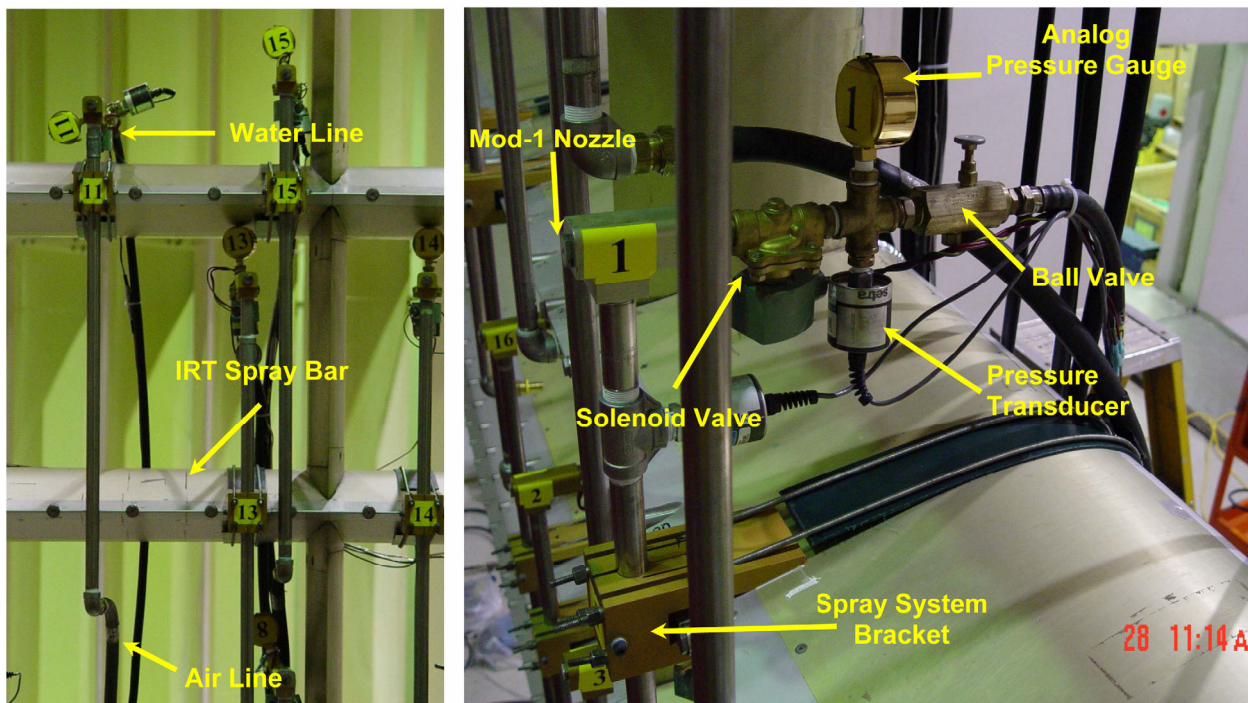


Figure 29.—Components of nozzle assembly.

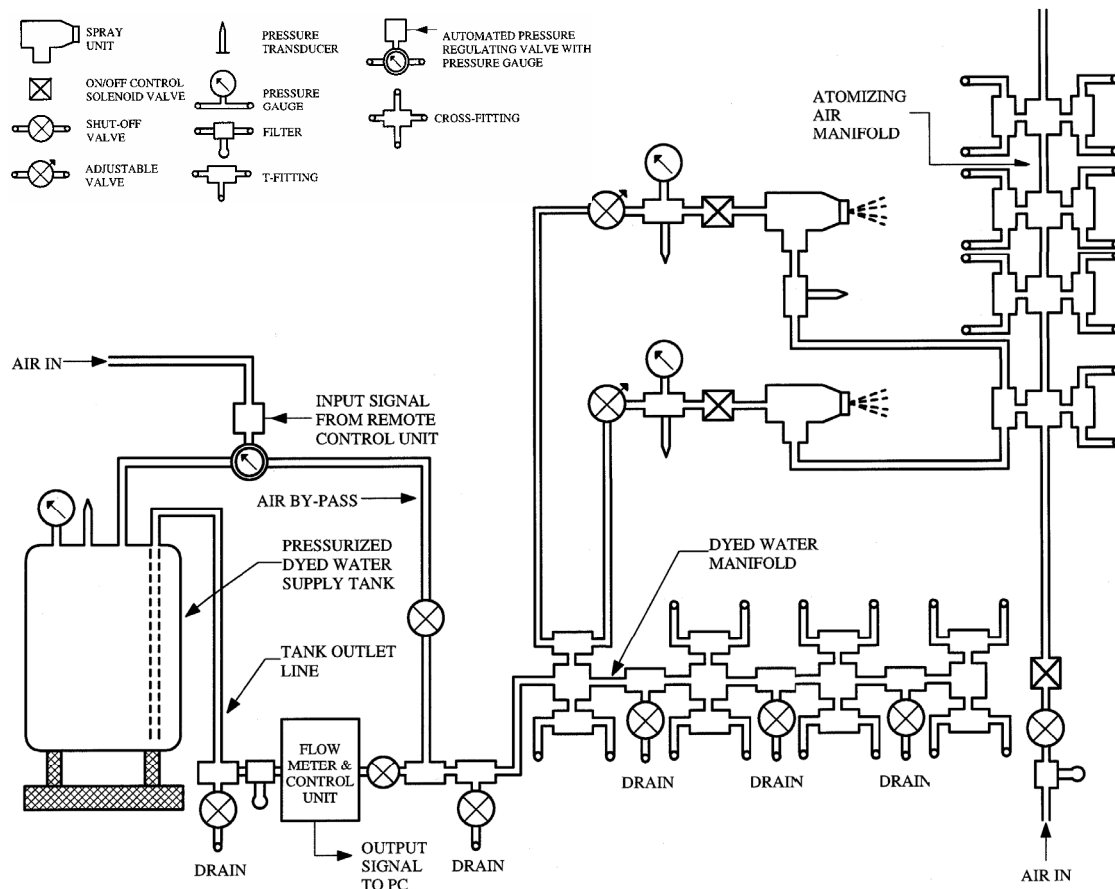


Figure 30.—Schematic of the new WSU 16-nozzle spray system.

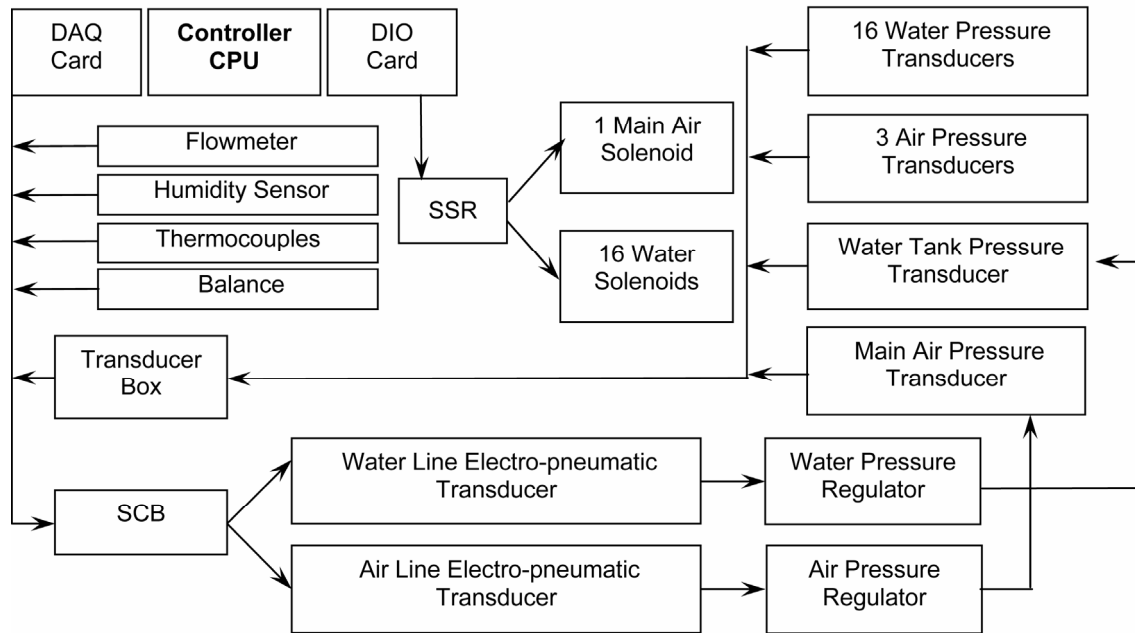


Figure 31.—Schematic of the spray system data acquisition and control.

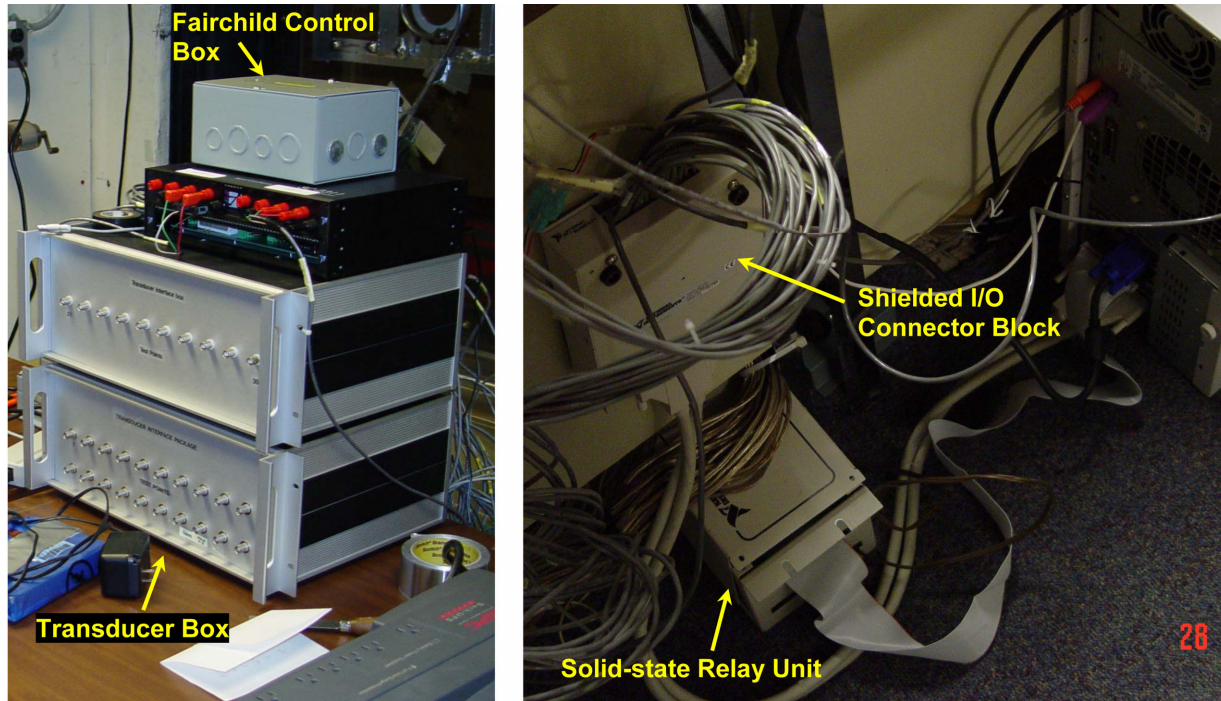


Figure 32.—Main components of the spray system data acquisition and control.

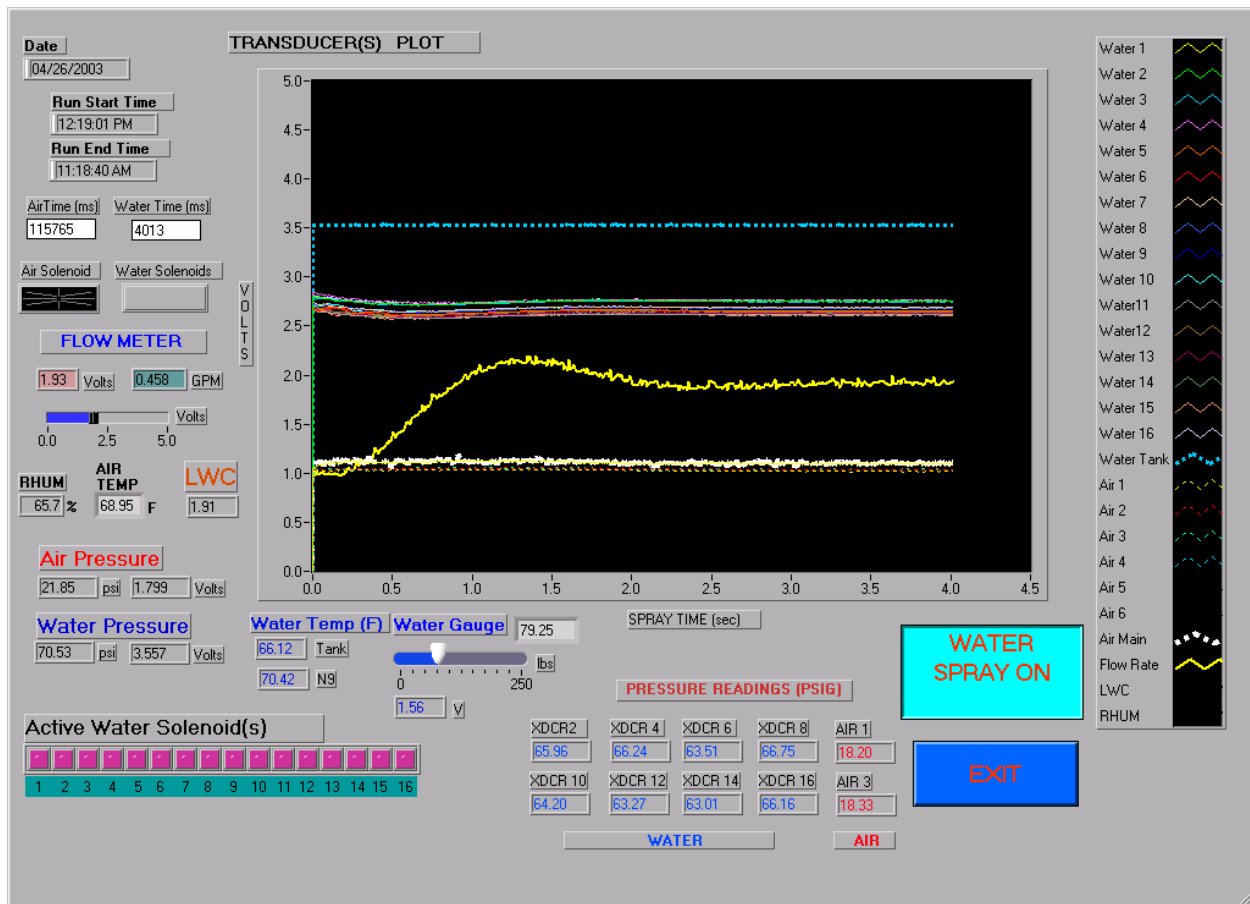


Figure 33.—LabVIEW program used to control and monitor spray system performance (display is not from an actual test run).



Figure 34a.—Argon-Ion laser emission.

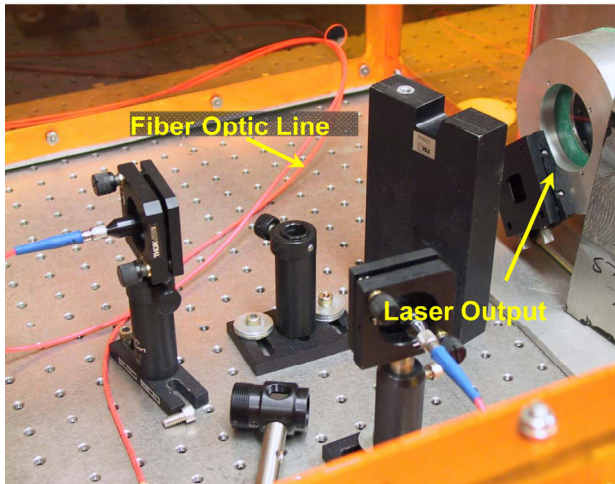


Figure 34b.—Close-up of the laser head setup.

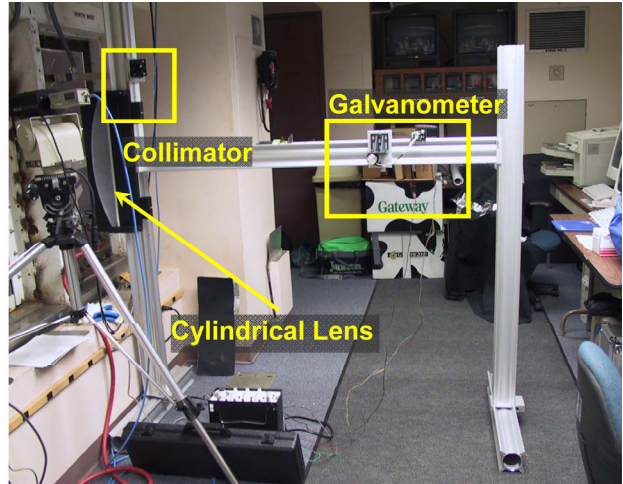


Figure 34c.—Laser Sheet generator setup.

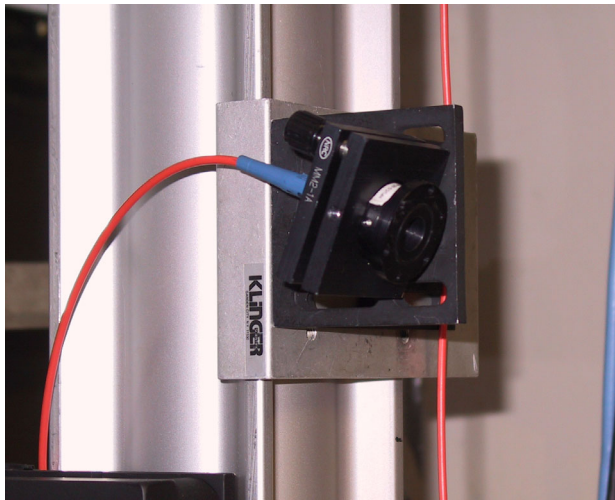


Figure 34d.—Close-up of the Collimator.

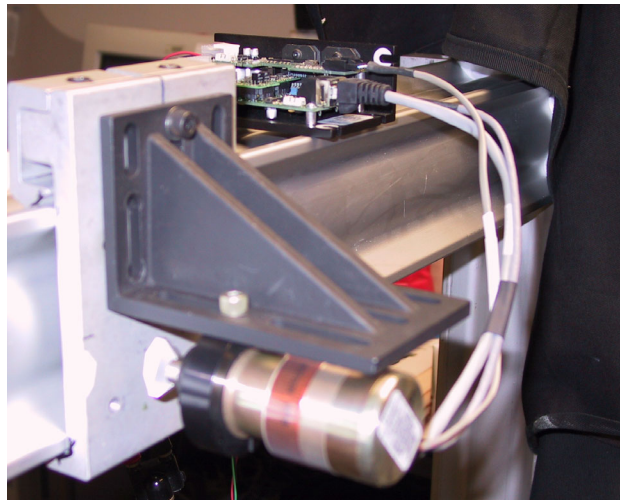


Figure 34e.—Close-up of the Galvanometer.

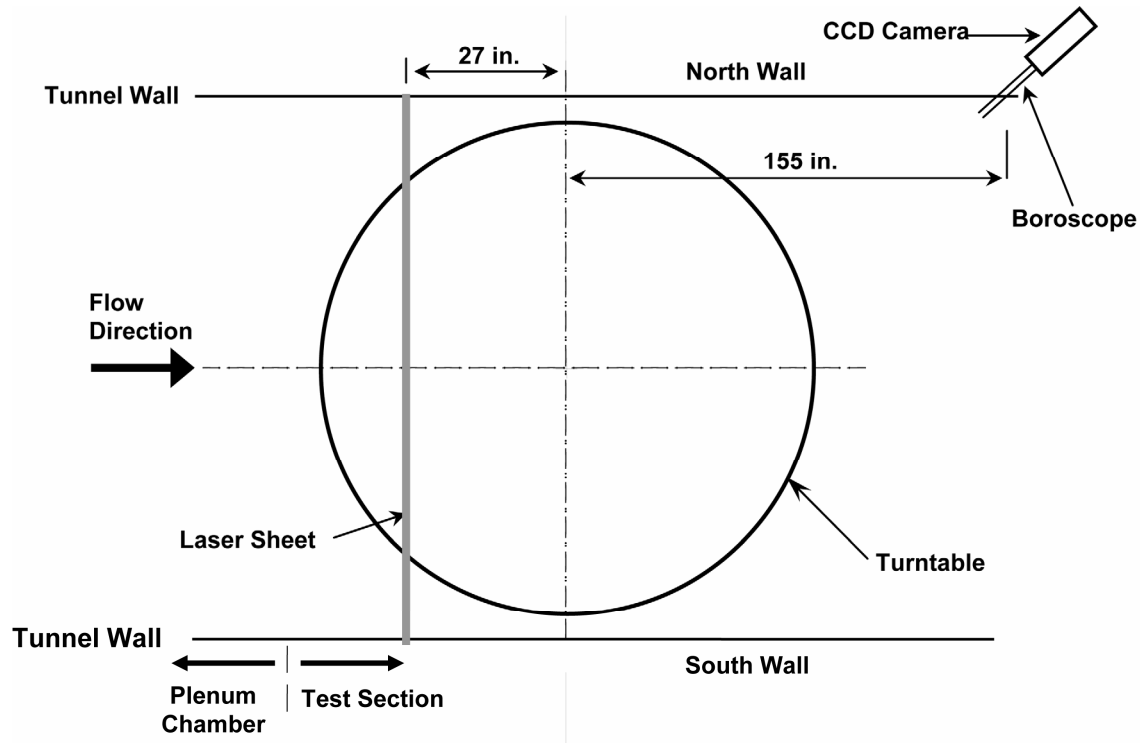


Figure 35a.—Laser sheet and CCD camera axial locations in IRT test section.

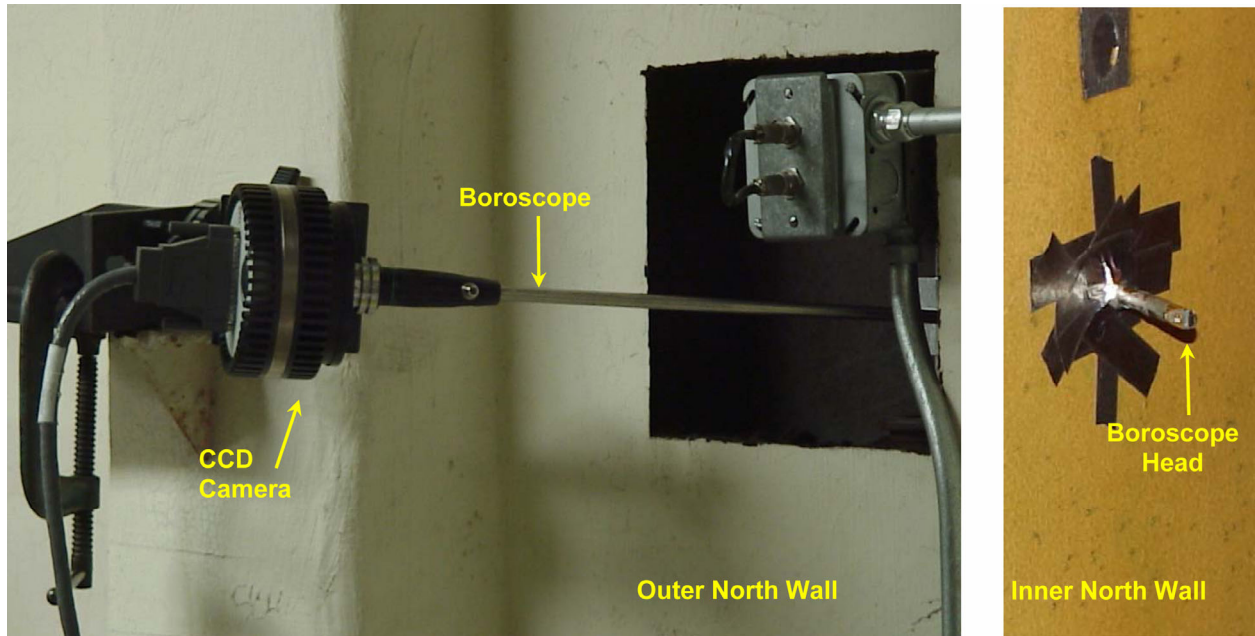


Figure 35b.—CCD camera installation in the IRT.



Figure 36.—6-ft by 6-ft grid installed in the IRT test section.



Figure 37.—Blotter strips attachment on the 6-ft by 6-ft grid.

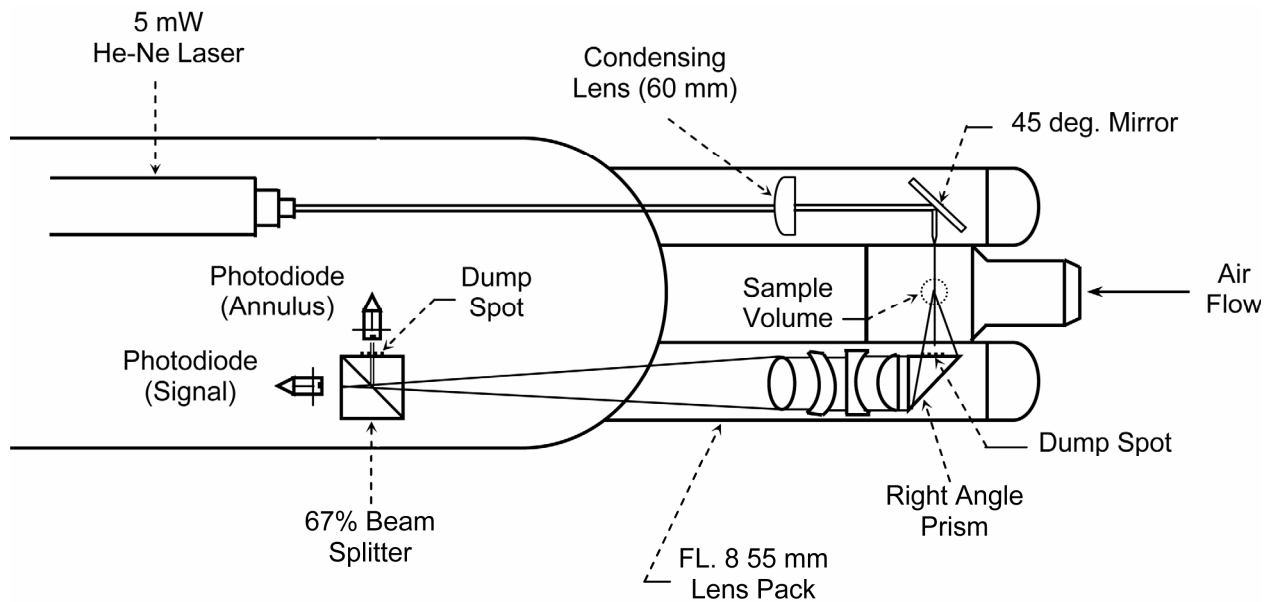


Figure 38a.—Forward Scattering Spectroscopy Probe (FSSP) optical configuration.

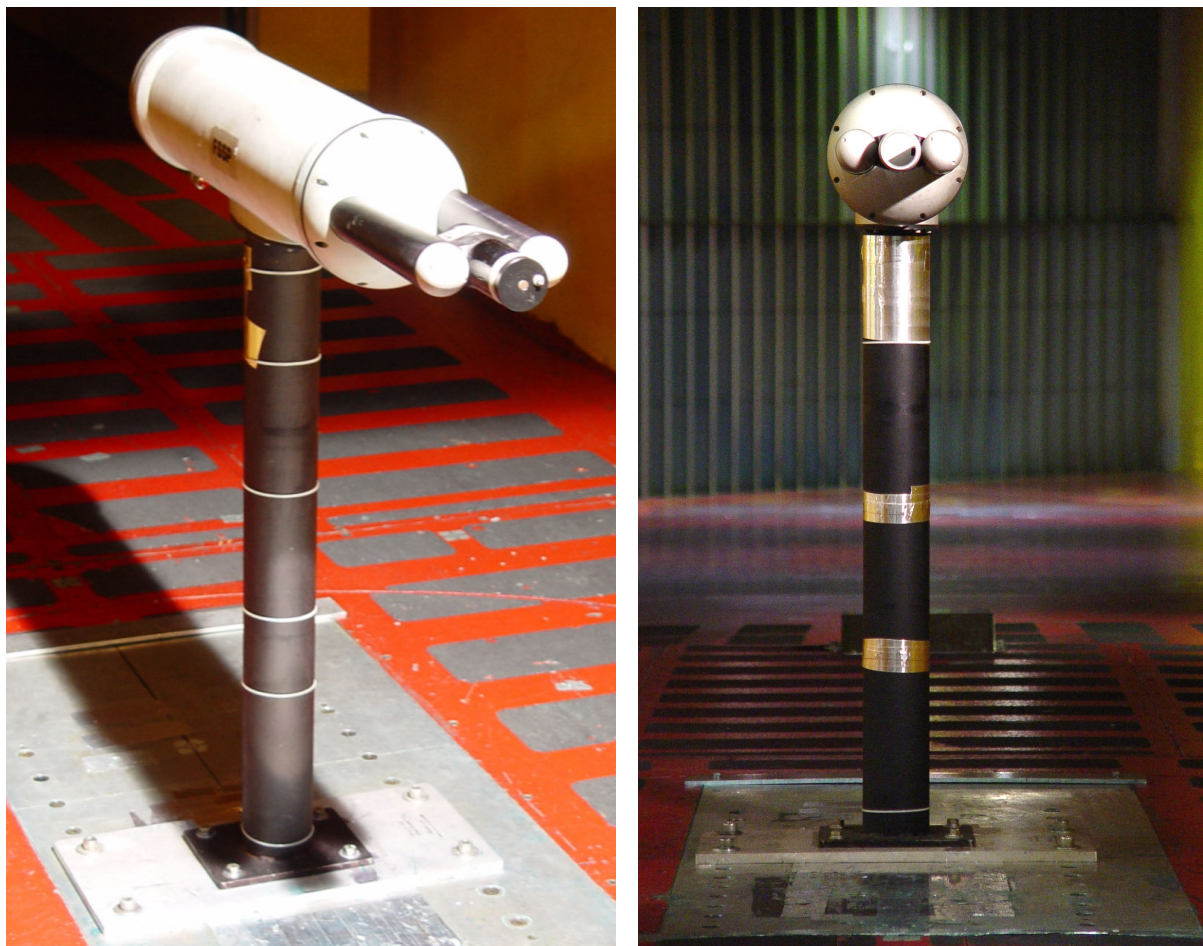


Figure 38b.—FSSP installed in the IRT test section.

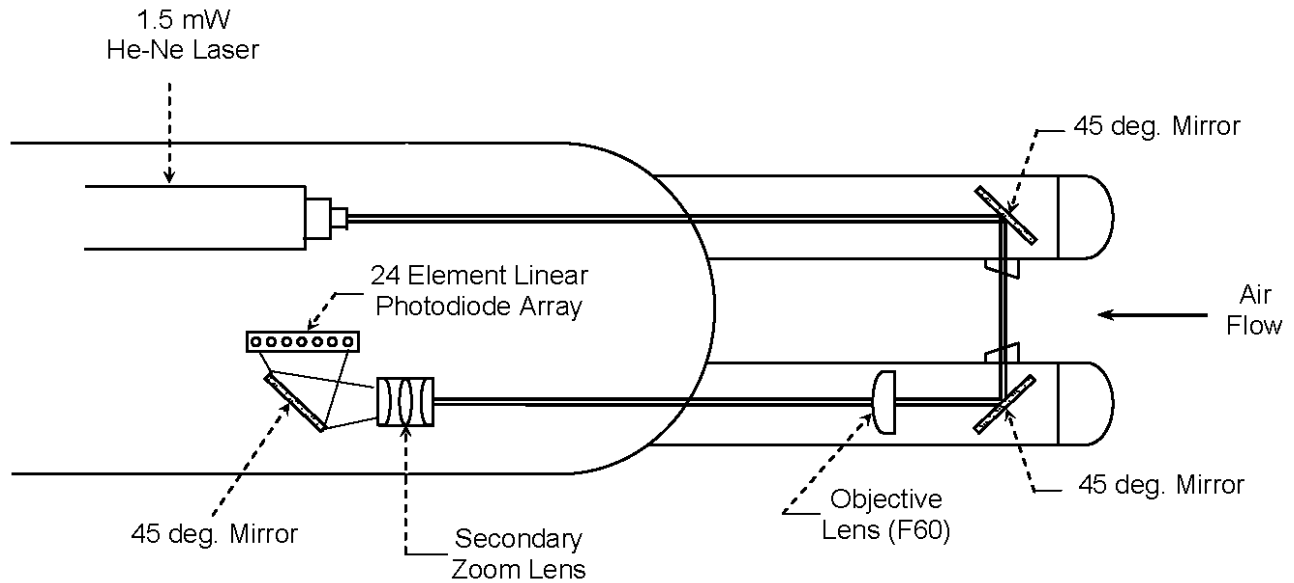


Figure 39a.—Optical Array Probe (OAP) configuration.



Figure 39b.—OAP-C installed  
in the IRT test section.



Figure 39c.—OAP-P installed in the IRT test section.

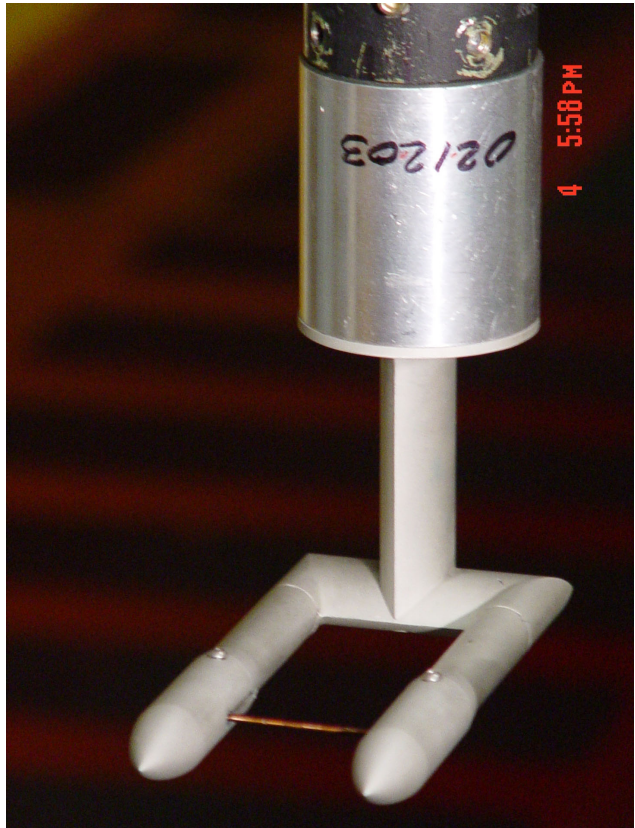


Figure 40a.—King Probe installed  
in the IRT test section.

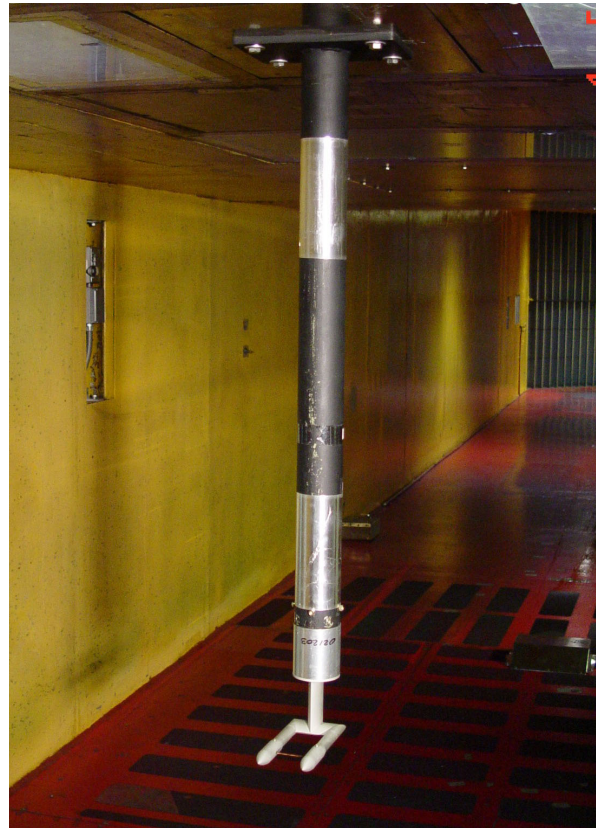


Figure 40b.—King Probe (looking downstream).

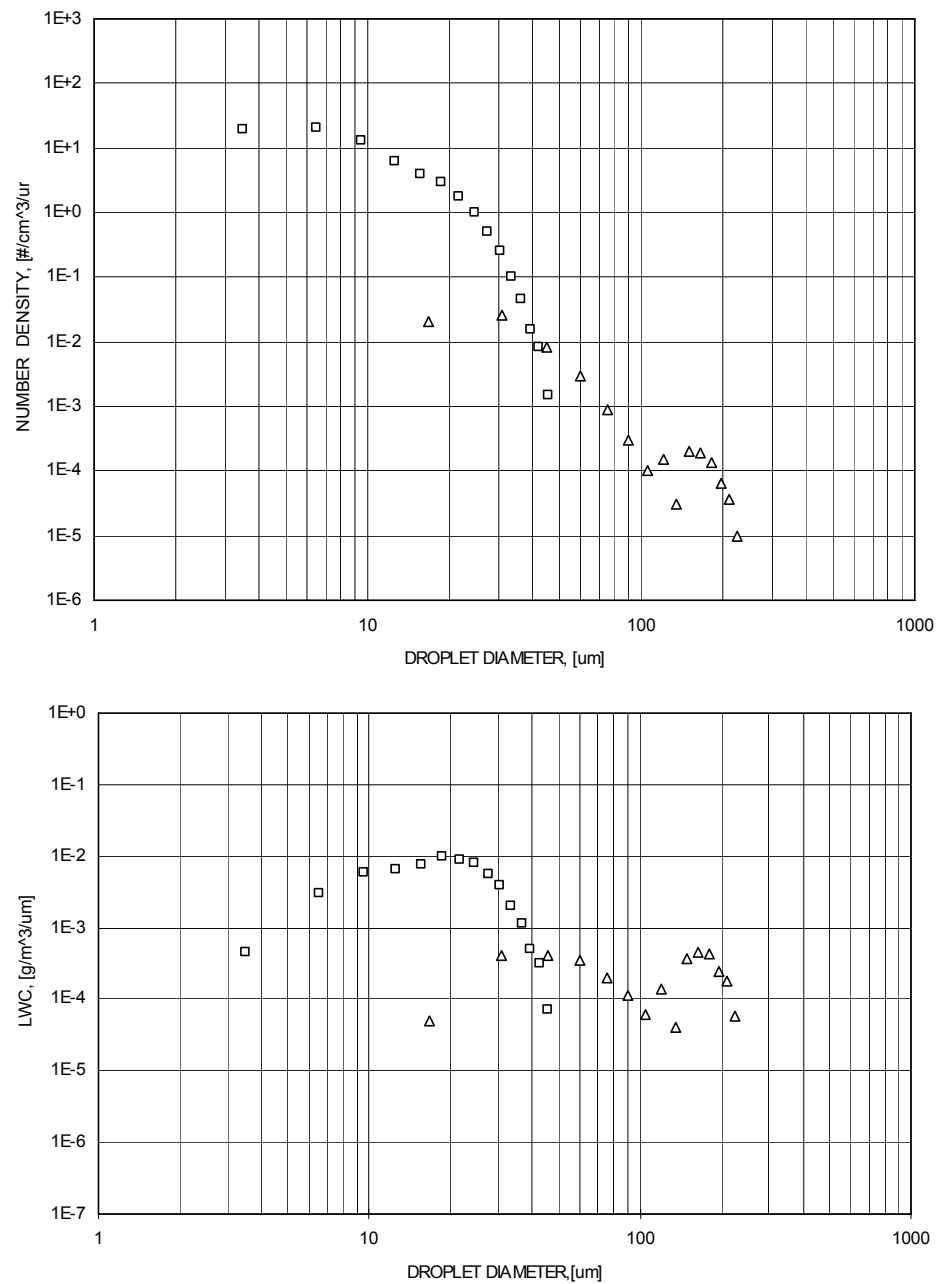


Figure 41.—Measured MVD and LWC distributions for 2003 IRT tests (MVD = 20  $\mu\text{m}$ ).

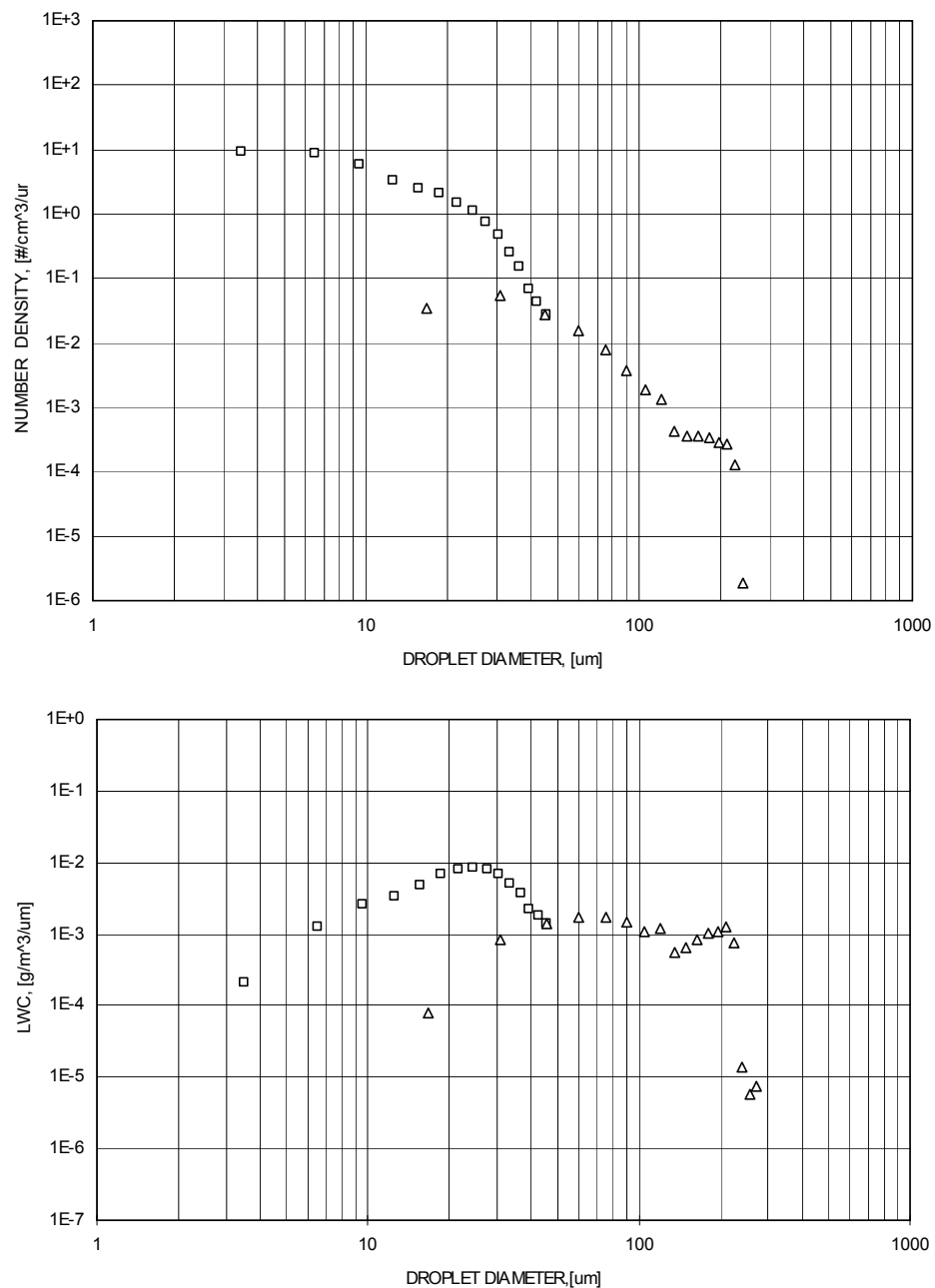


Figure 42.—Measured MVD and LWC distributions for 2003 IRT tests (MVD = 52 μm).

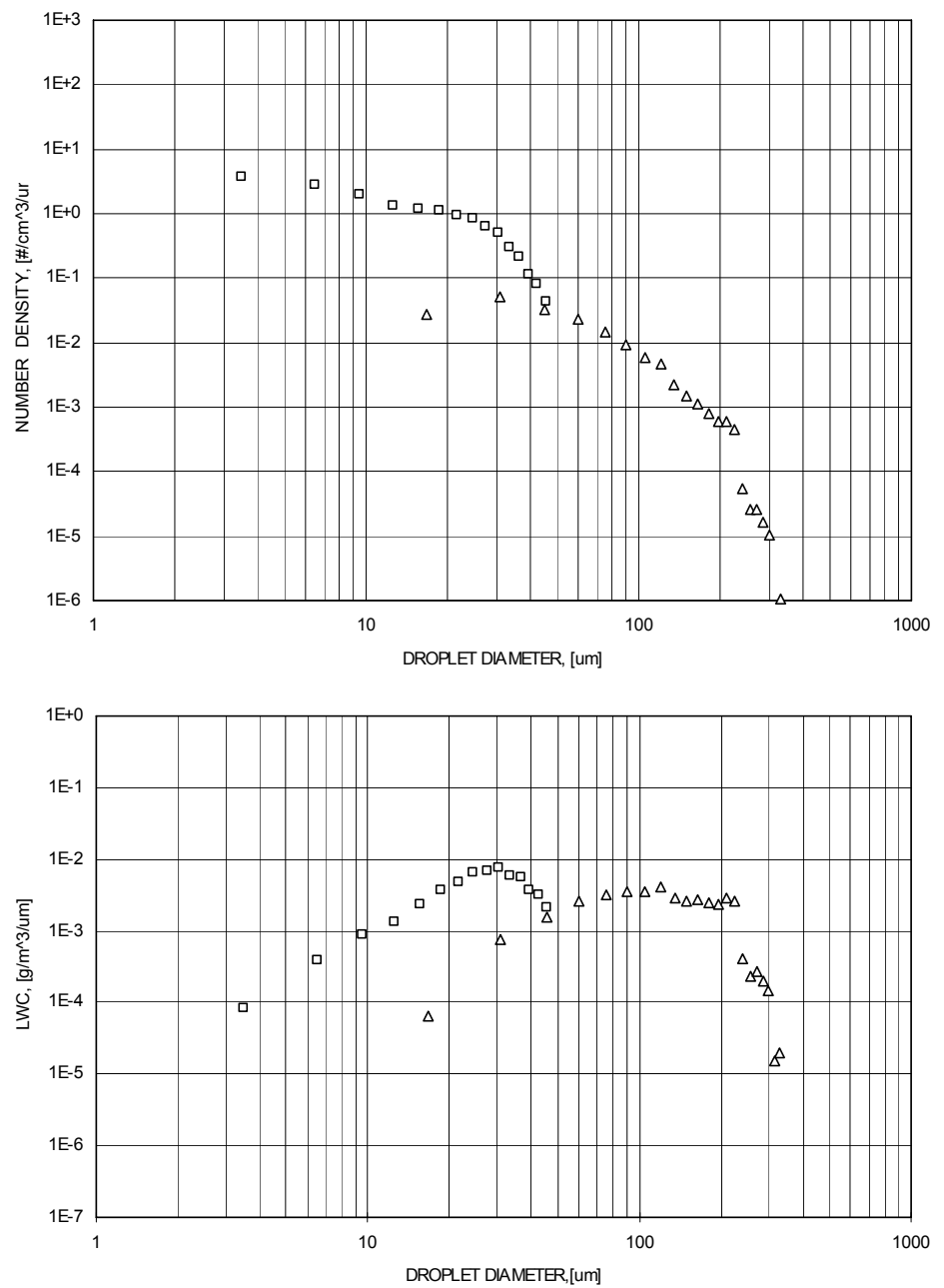


Figure 43.—Measured MVD and LWC distributions  
for 2003 IRT tests (MVD = 111  $\mu\text{m}$ ).

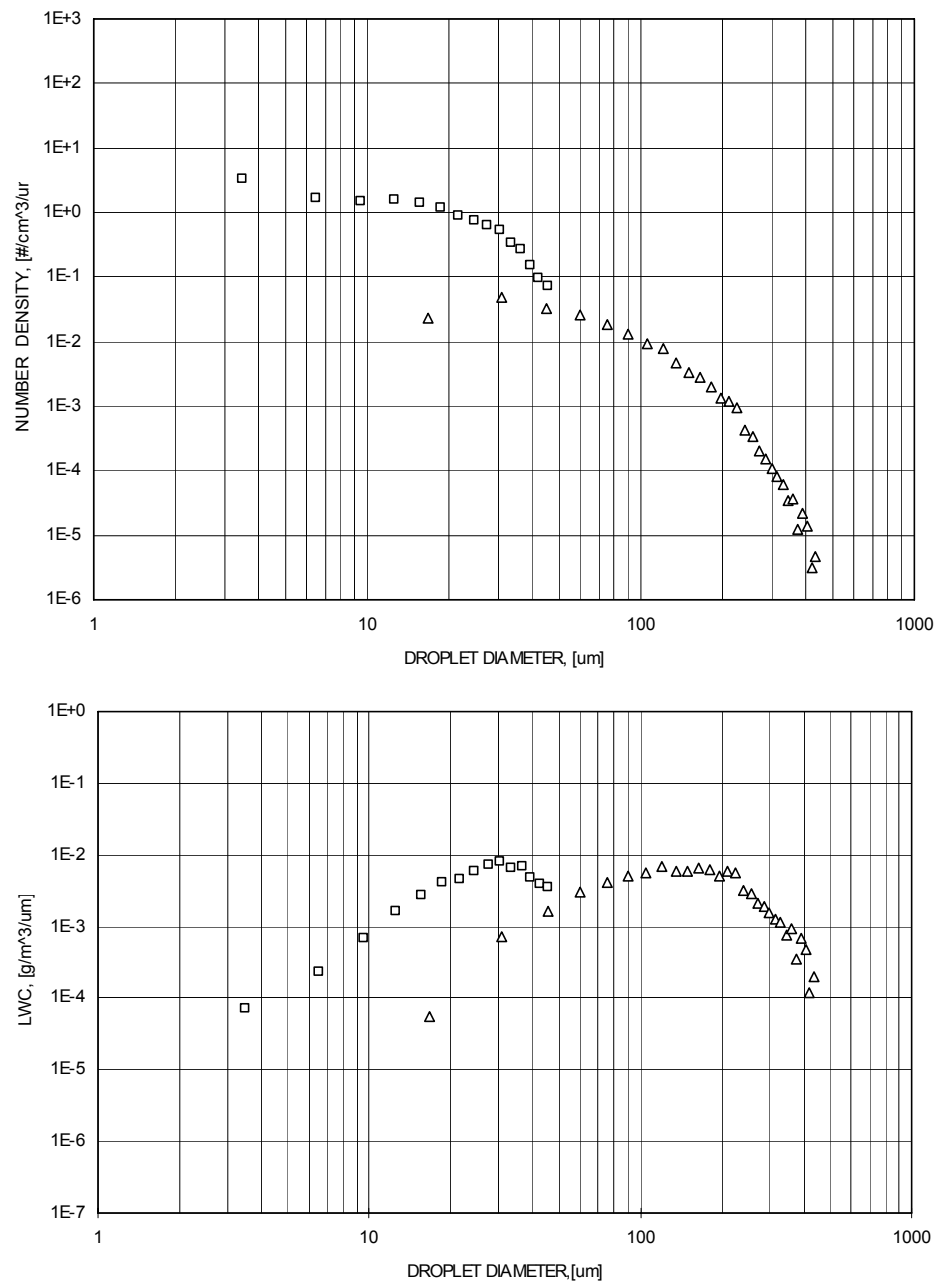


Figure 44.—Measured MVD and LWC distributions for 2003 IRT tests (MVD = 154  $\mu m$ ).

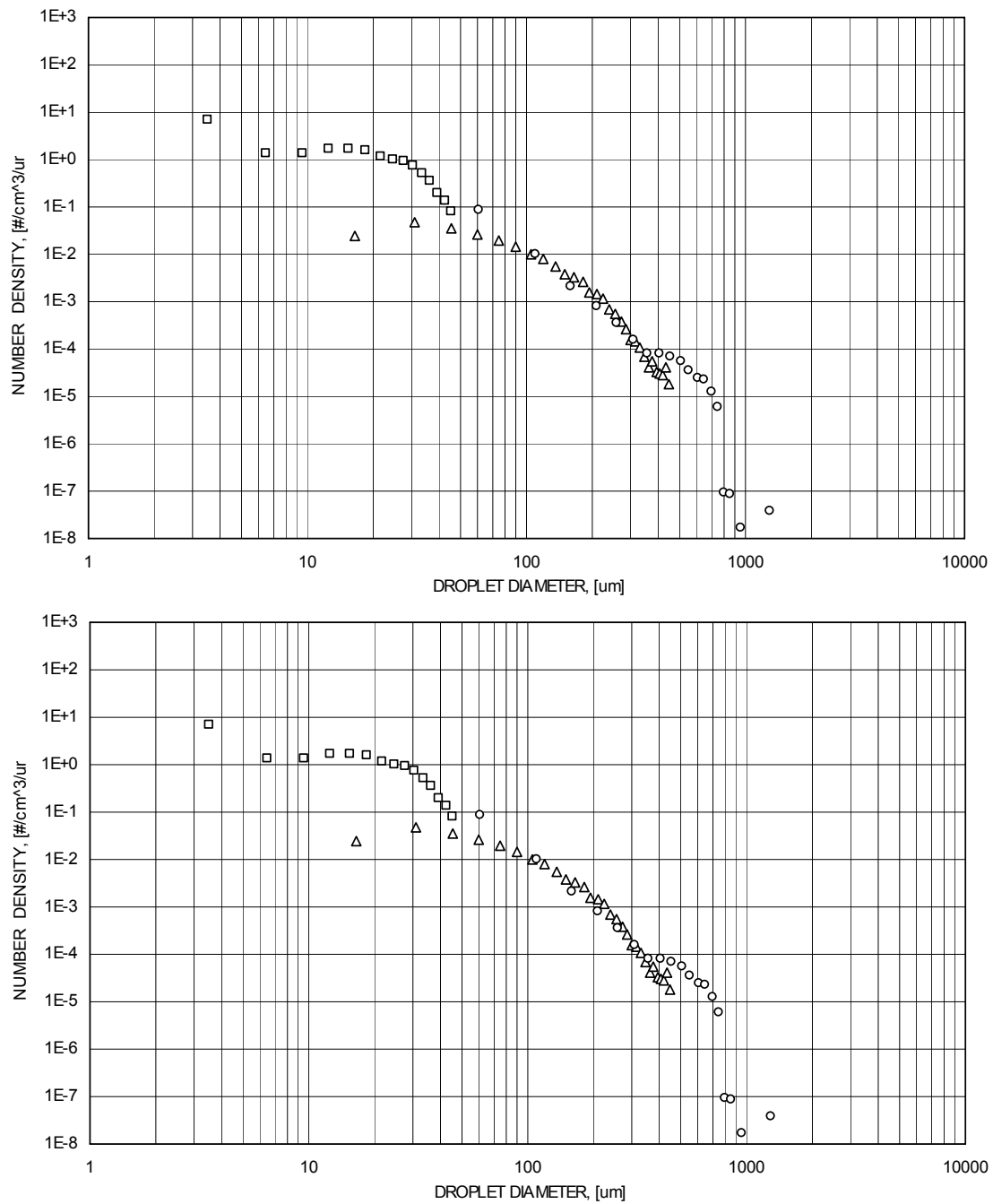


Figure 45.—Measured MVD and LWC distributions for 2003 IRT tests (MVD = 236  $\mu\text{m}$ ).



Figure 46a.—Reference collector mechanism blades.

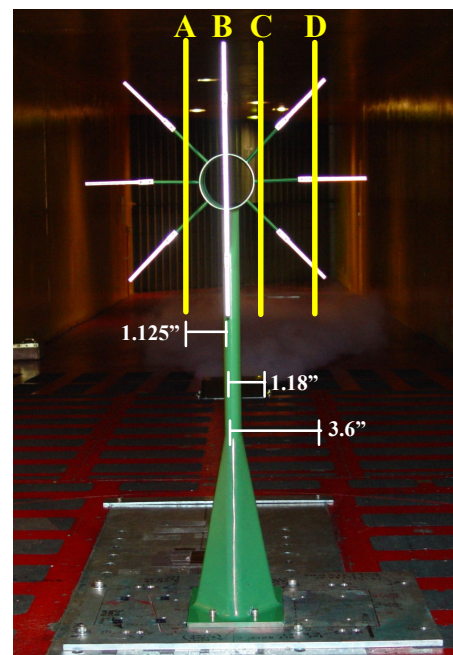
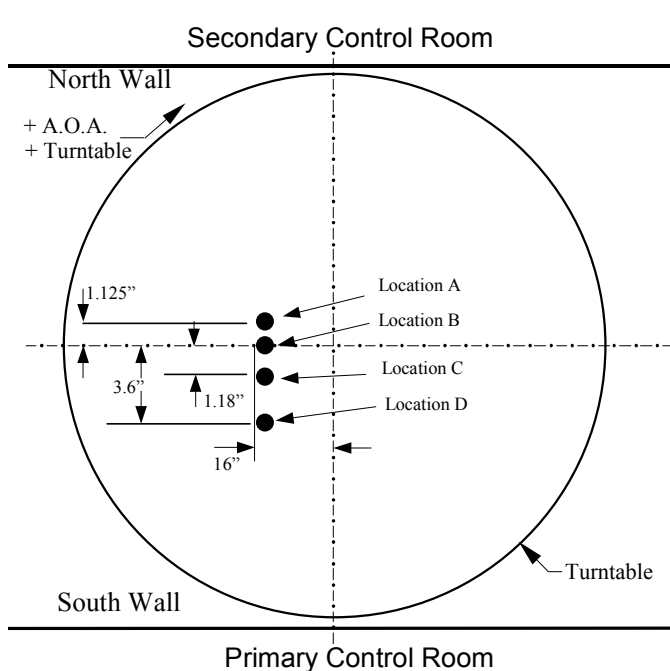


Figure 46b.—Collector vertical blade locations in the IRT test section.



Figure 47.—Spectrophotometry equipments used for colorimetric analysis.

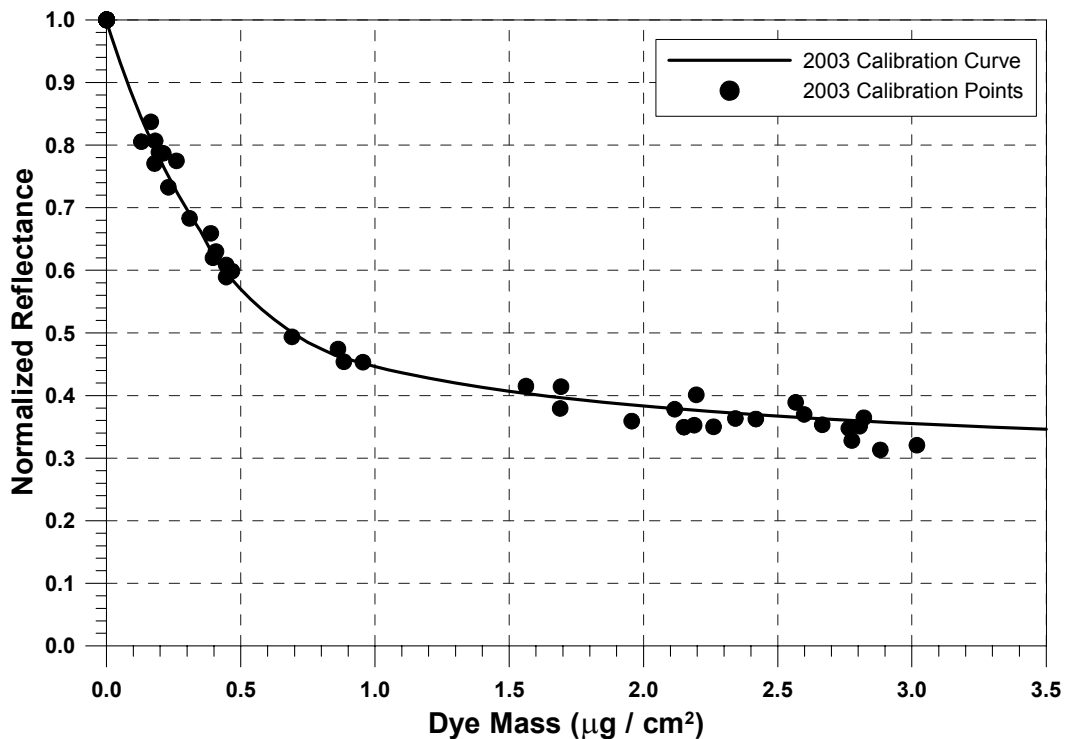


Figure 48.—Reflectometer calibration curve.

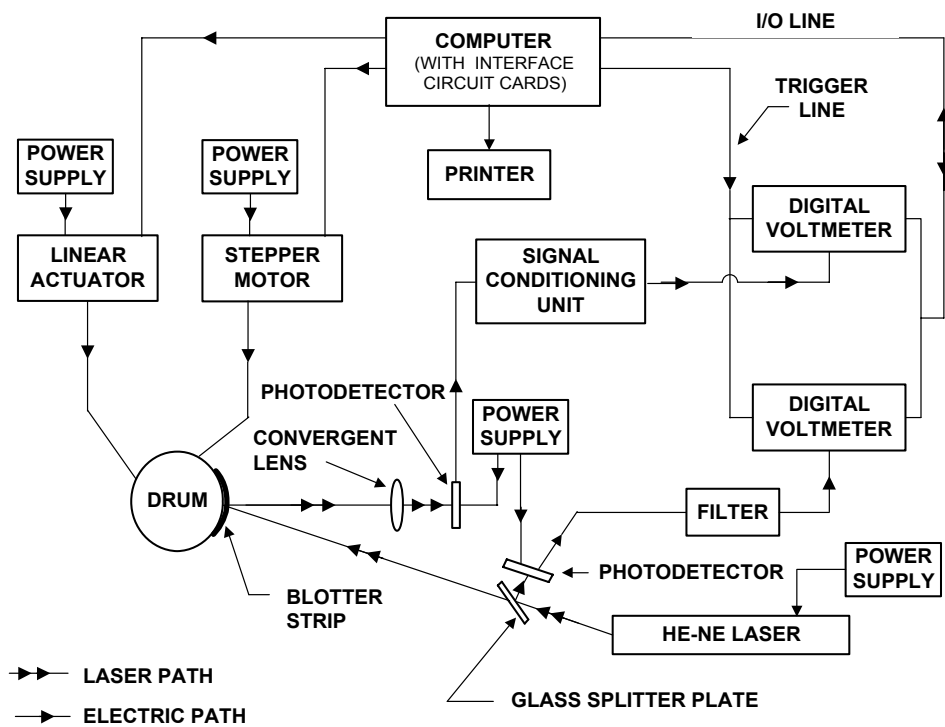


Figure 49a.—Schematic of automated laser reflectometer and digital data acquisition system.

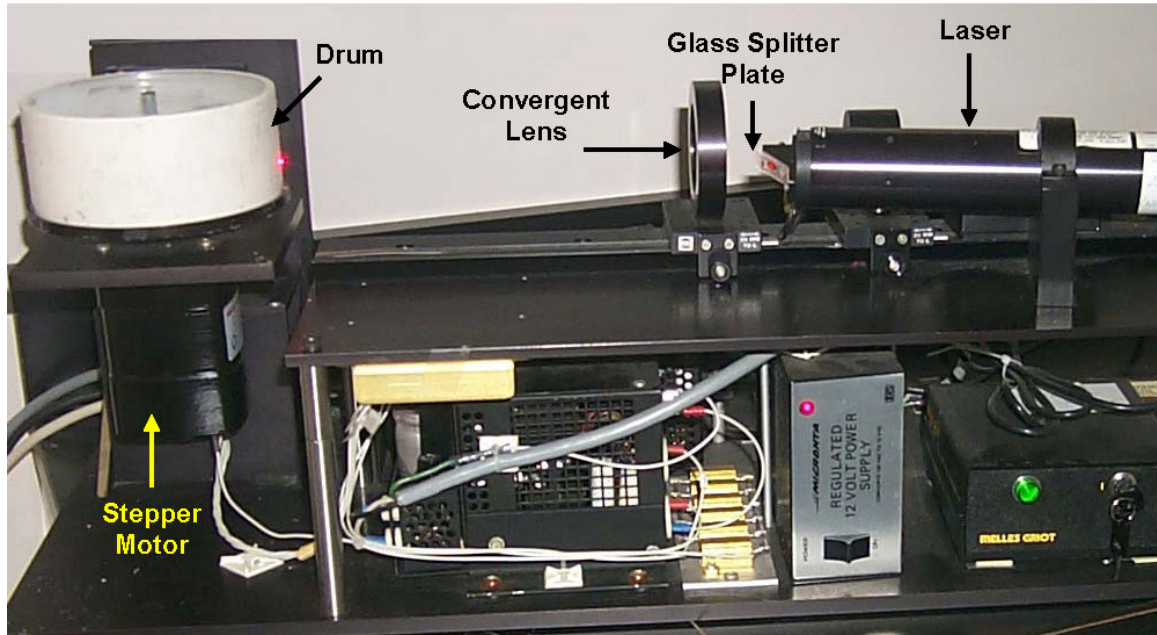


Figure 49b.—Laser reflectometer data reduction setup.

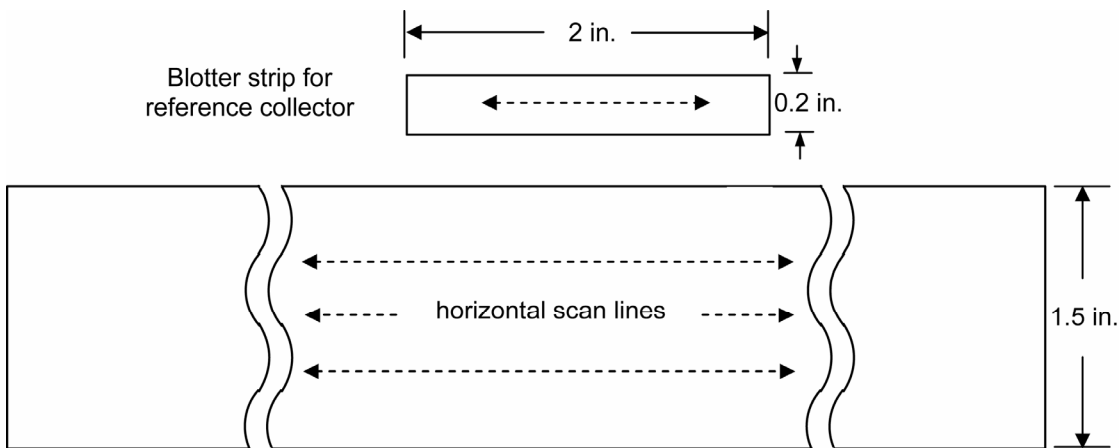


Figure 50a.—Scan locations for test model and reference collector strips.

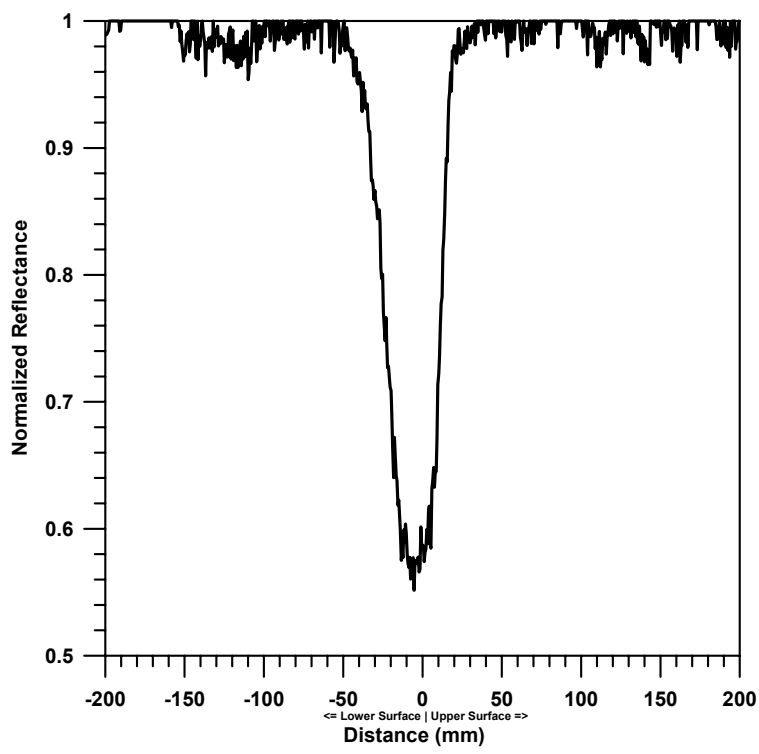


Figure 50b.—Typical normalized surface reflectance distribution for a dyed blotter strip using the laser data reduction system.

- (A) Computer
- (B) CCD Control Unit
- (C) CCD Camera
- (D) Light Control Unit
- (E) Light Units
- (F) Power Supply for Lights
- (G) Table
- (H) Portable Dark Room

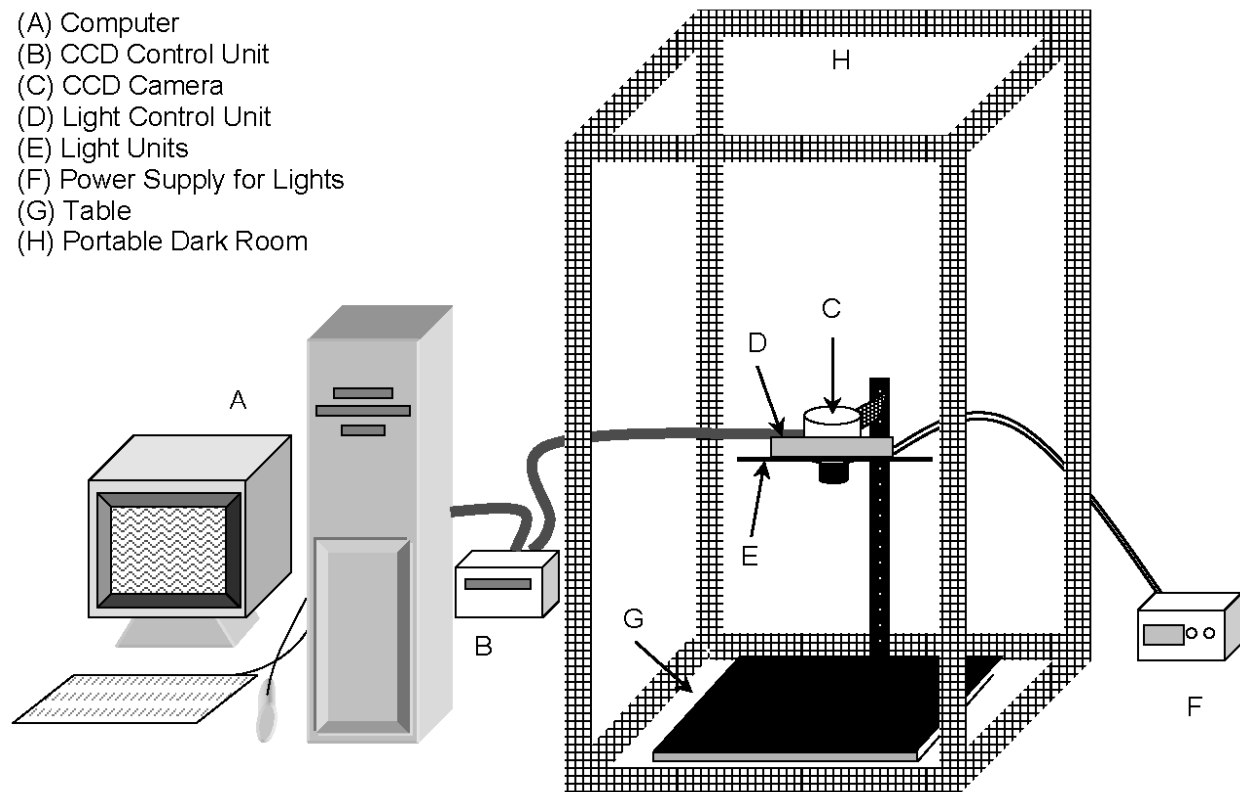


Figure 51a.—Schematic diagram of the CCD reflectometer.



Figure 51b.—CCD data reduction system setup.

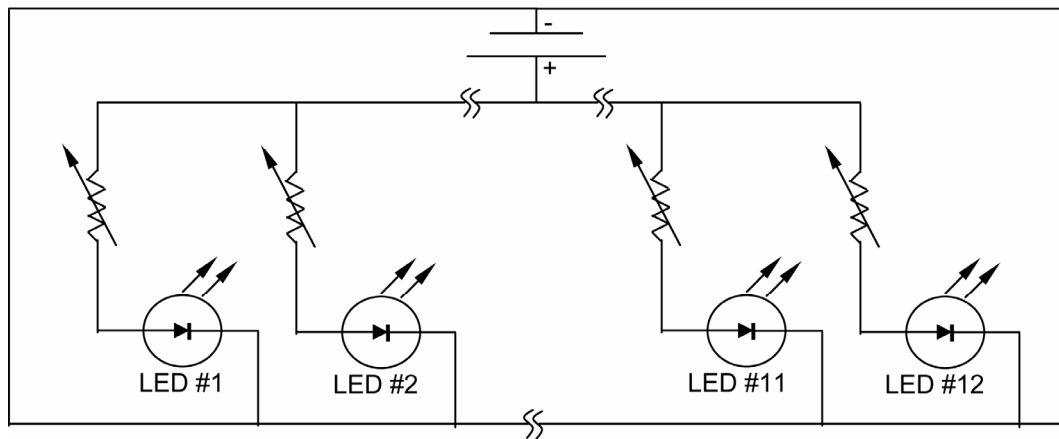


Figure 52a.—Schematic diagram of the CCD reflectometer lighting system.

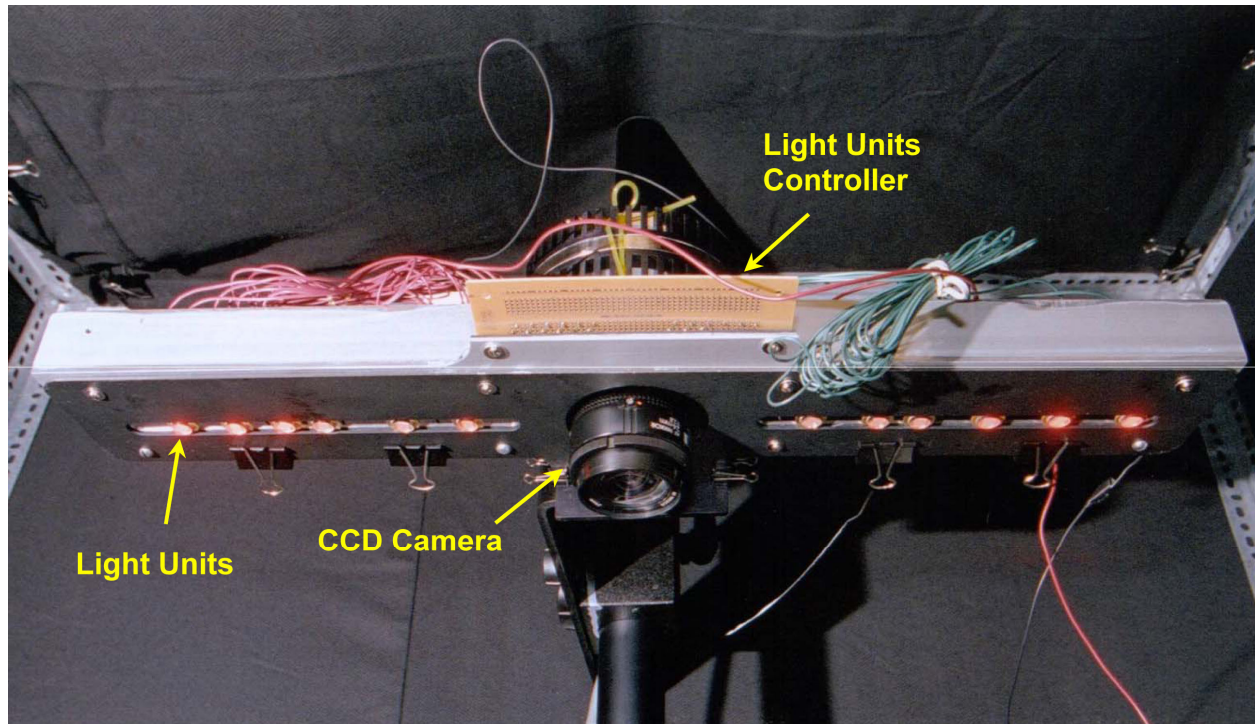


Figure 52b.—CCD reflectometer lighting setup.

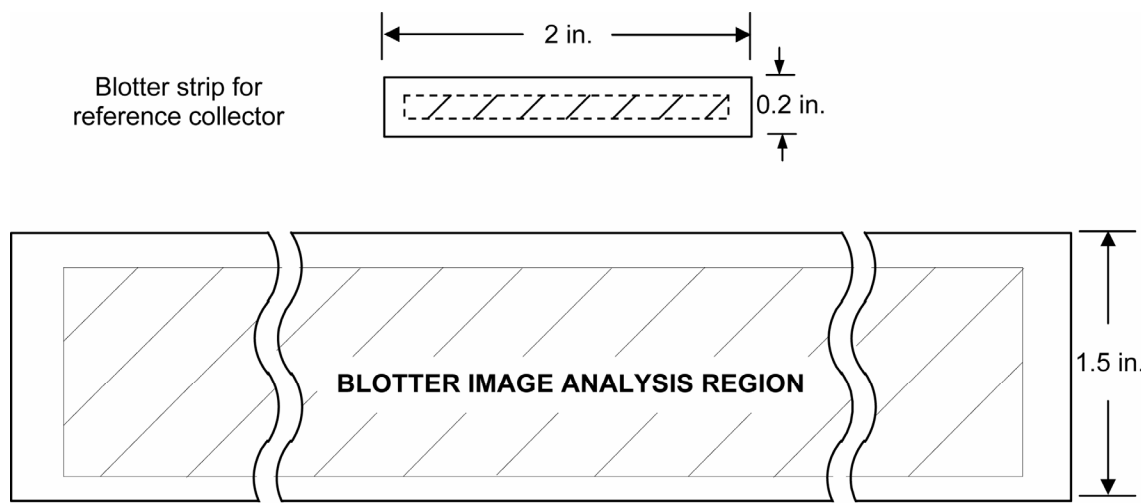


Figure 53.—Blotter strip image analysis region for CCD data reduction system.

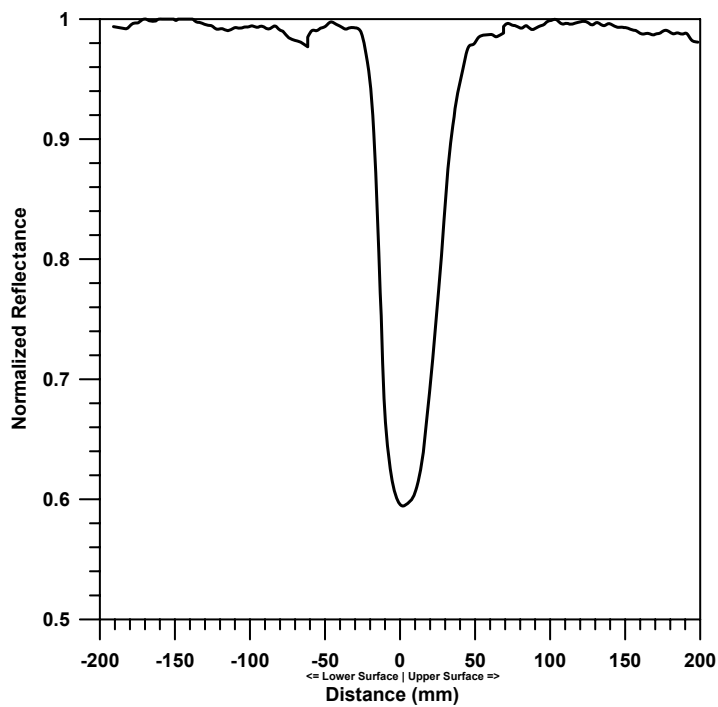


Figure 54.—Typical normalized surface reflectance distribution for a dyed blotter strip using CCD data reduction system.

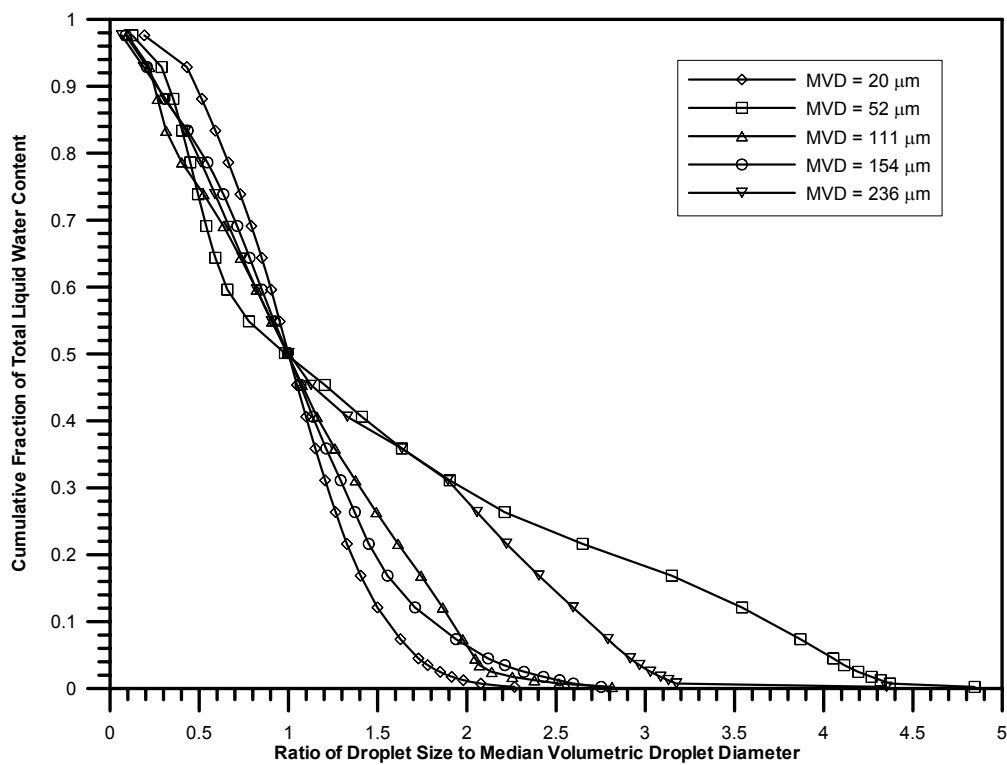


Figure 55.—27-bin droplet distributions.

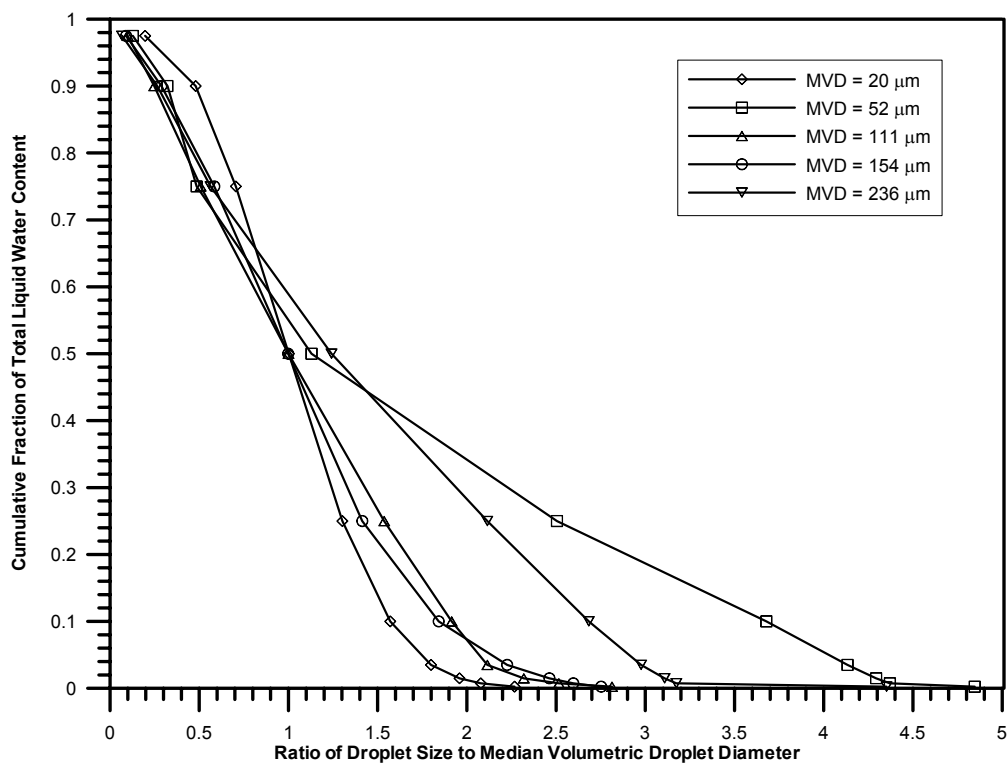


Figure 56.—10-bin droplet distributions.

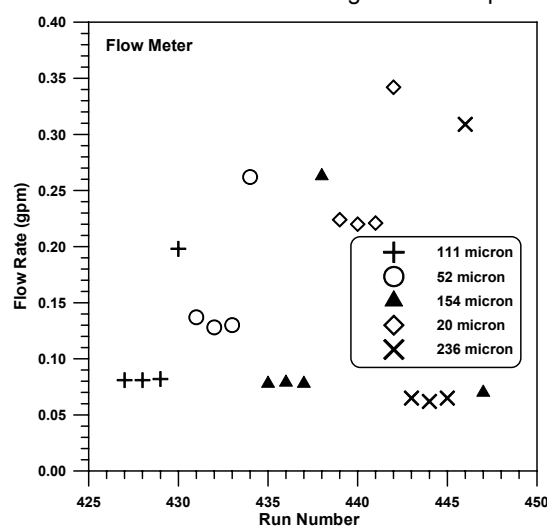
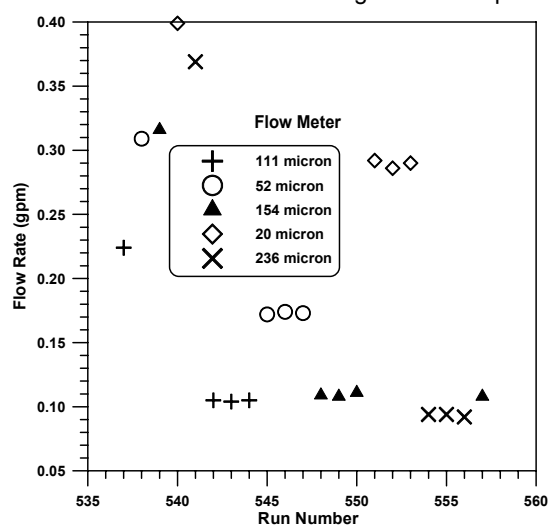
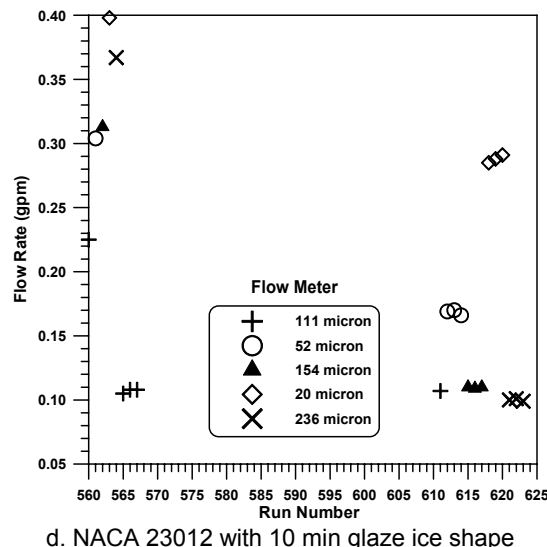
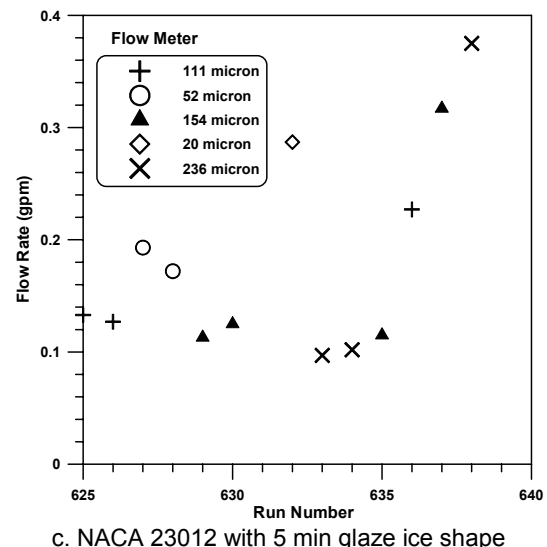
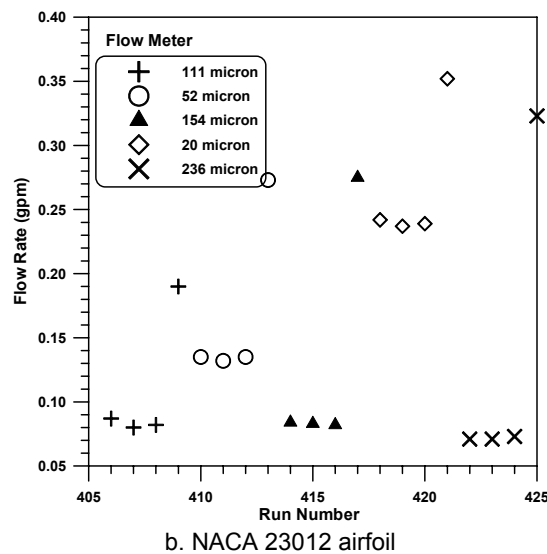
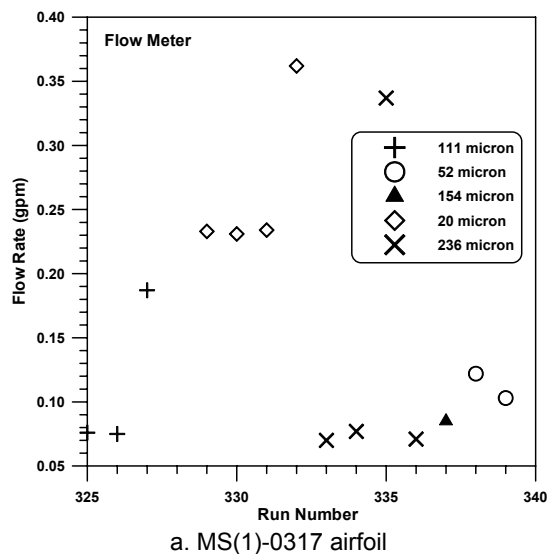
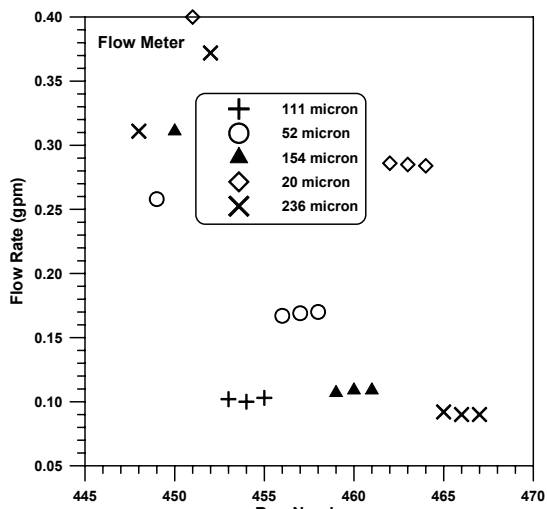
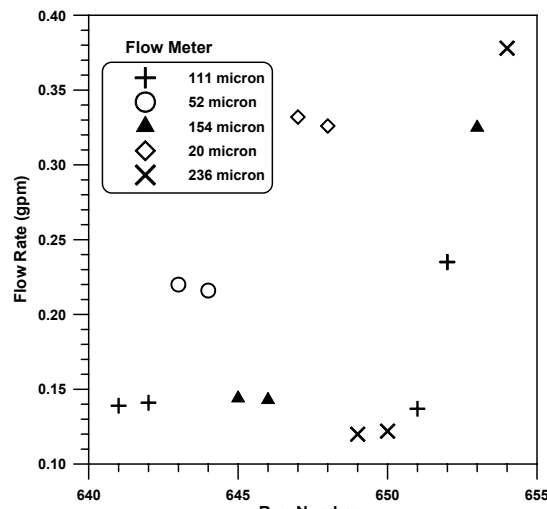


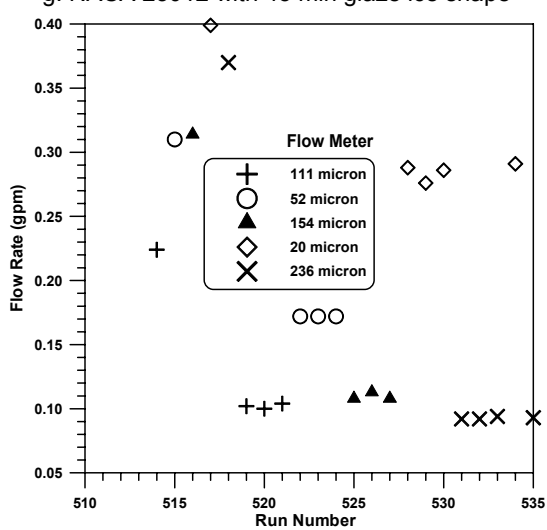
Figure 57.—Variation in WSU 16-nozzle spray system water flow rate (2003 tests).



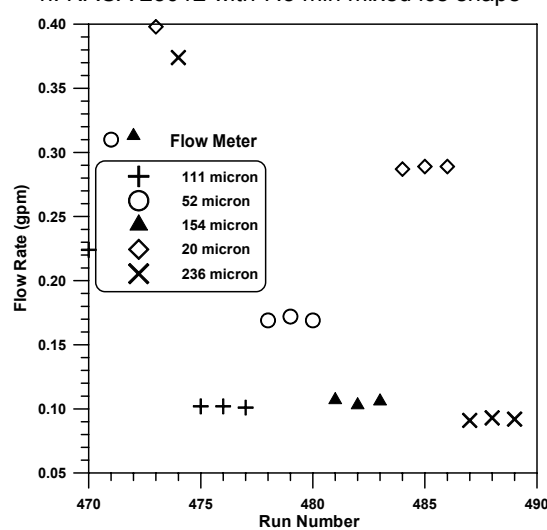
g. NACA 23012 with 45 min glaze ice shape



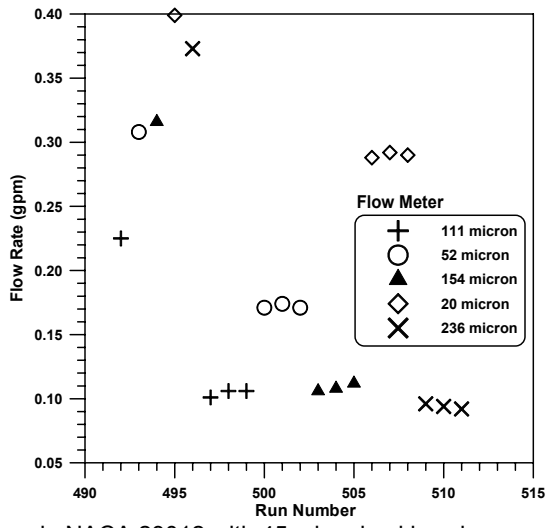
h. NACA 23012 with 7.5 min mixed ice shape



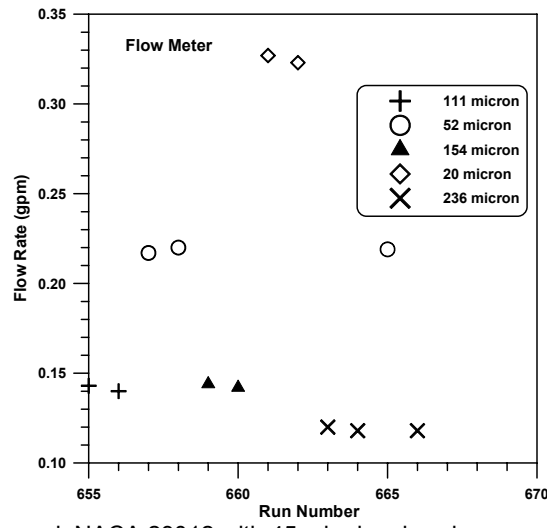
i. NACA 23012 with 15 min mixed ice shape



j. NACA 23012 with 22.5 min mixed ice shape



k. NACA 23012 with 45 min mixed ice shape



l. NACA 23012 with 45 min rime ice shape

Figure 57.—(Continued) Variation in WSU 16-nozzle spray system water flow rate (2003 tests).

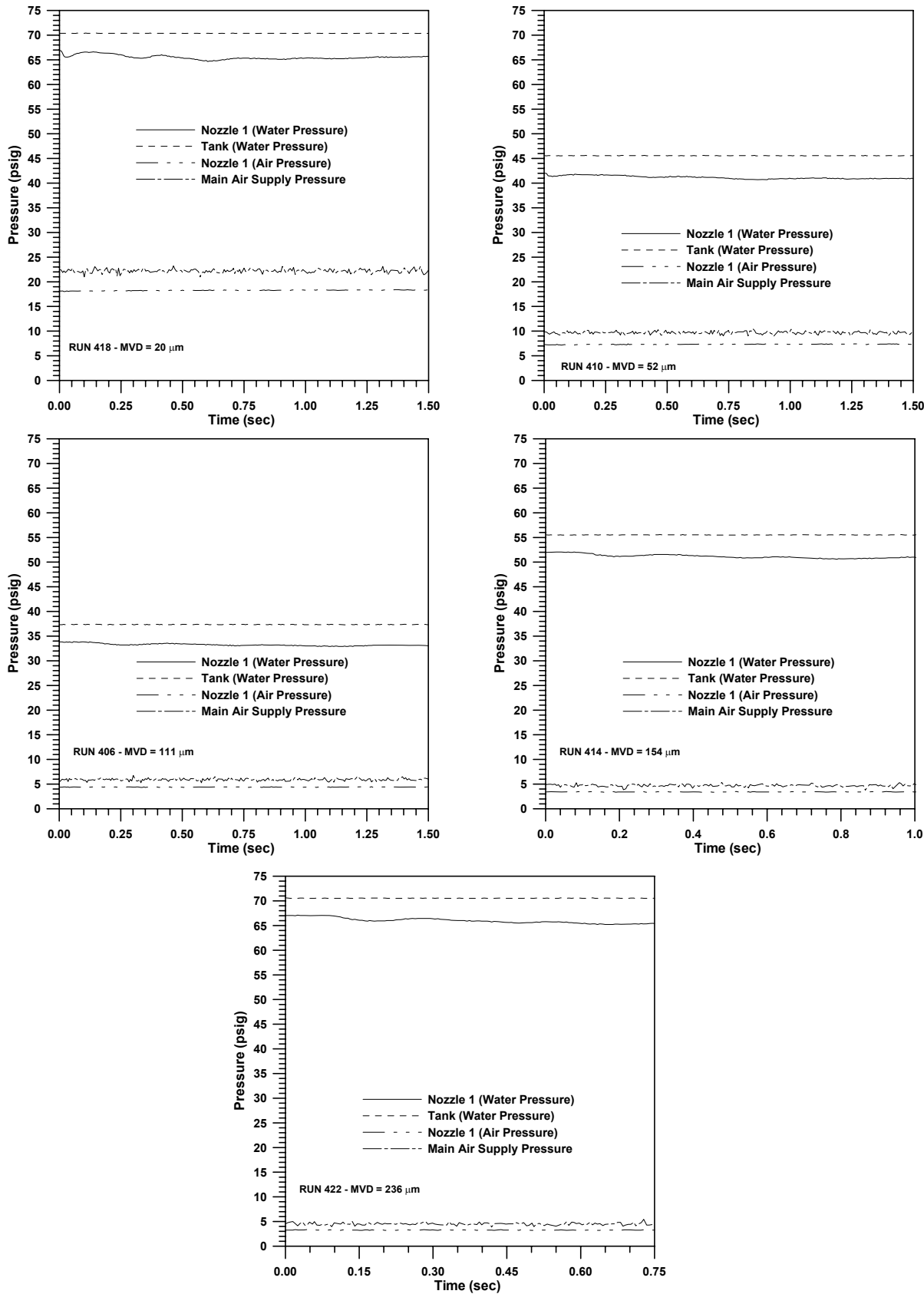


Figure 58.—Spray system pressures versus spray time for all MVD cases.

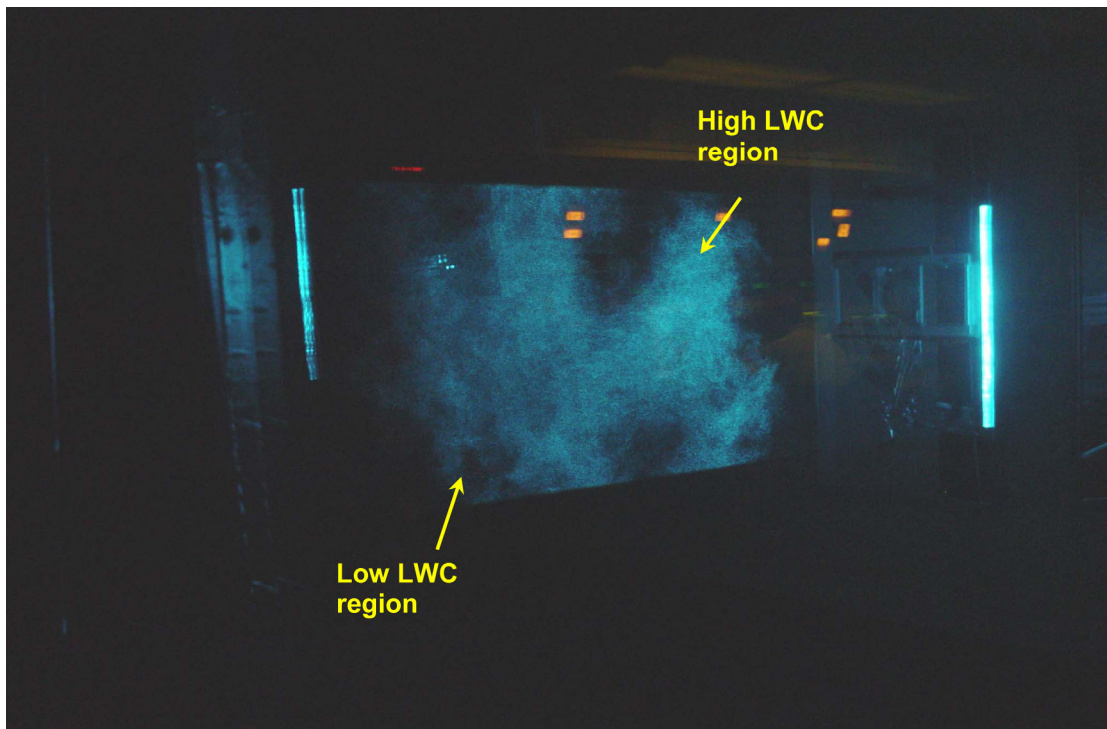


Figure 59a.—Typical laser sheet produced in the IRT test section.

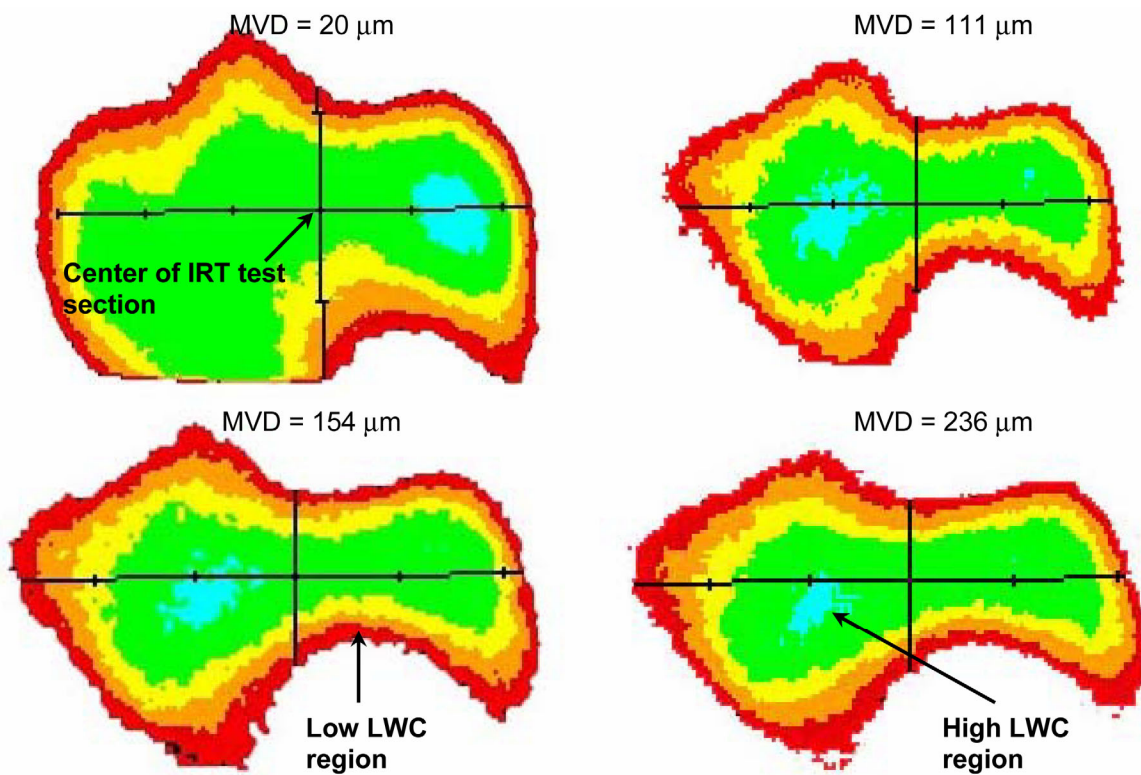


Figure 59b.—Sample of cloud uniformity images obtained using the laser sheet method.

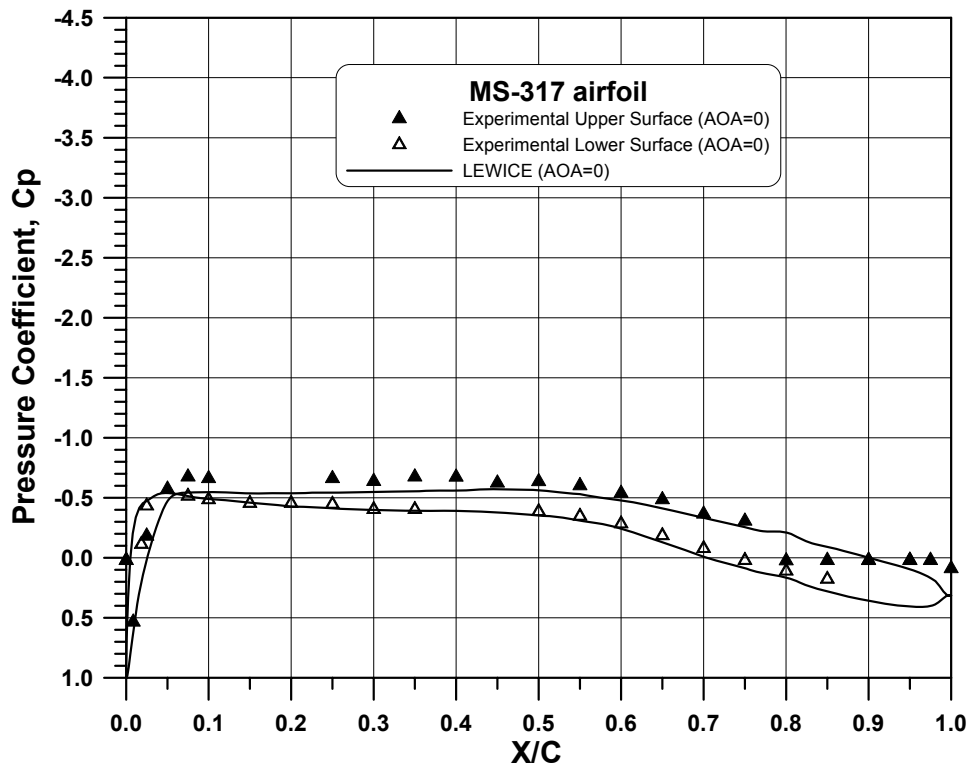


Figure 60.—Comparison of pressure distribution for MS-317 airfoil at  $\alpha = 0^\circ$ .

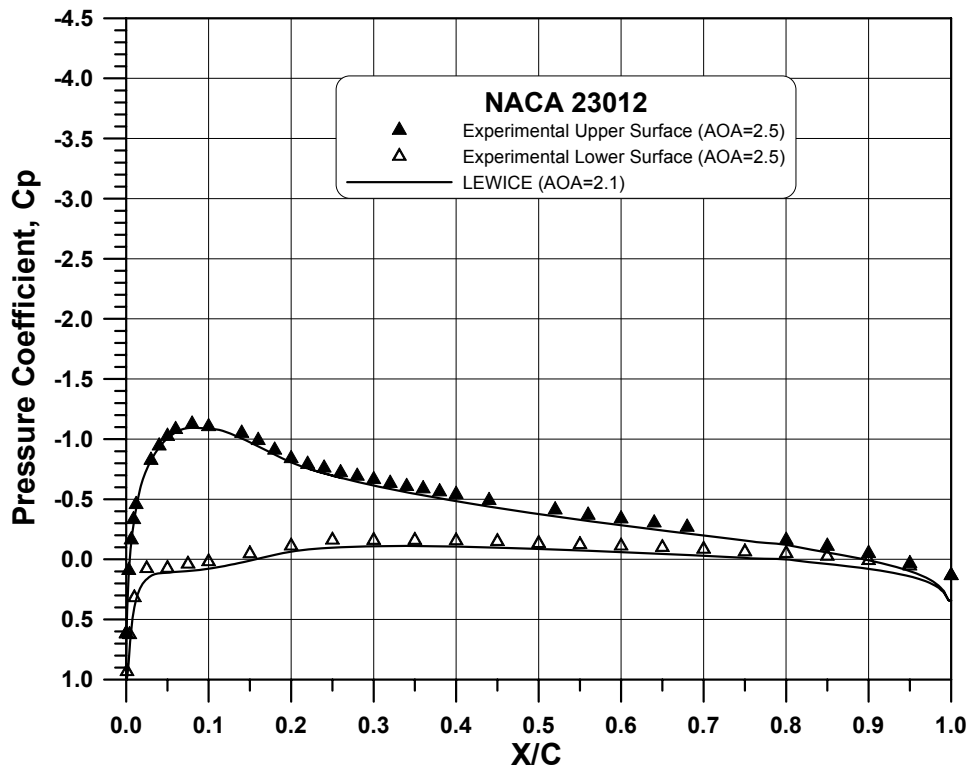


Figure 61.—Comparison of pressure distribution for NACA 23012 airfoil at  $\alpha = 2.5^\circ$ .

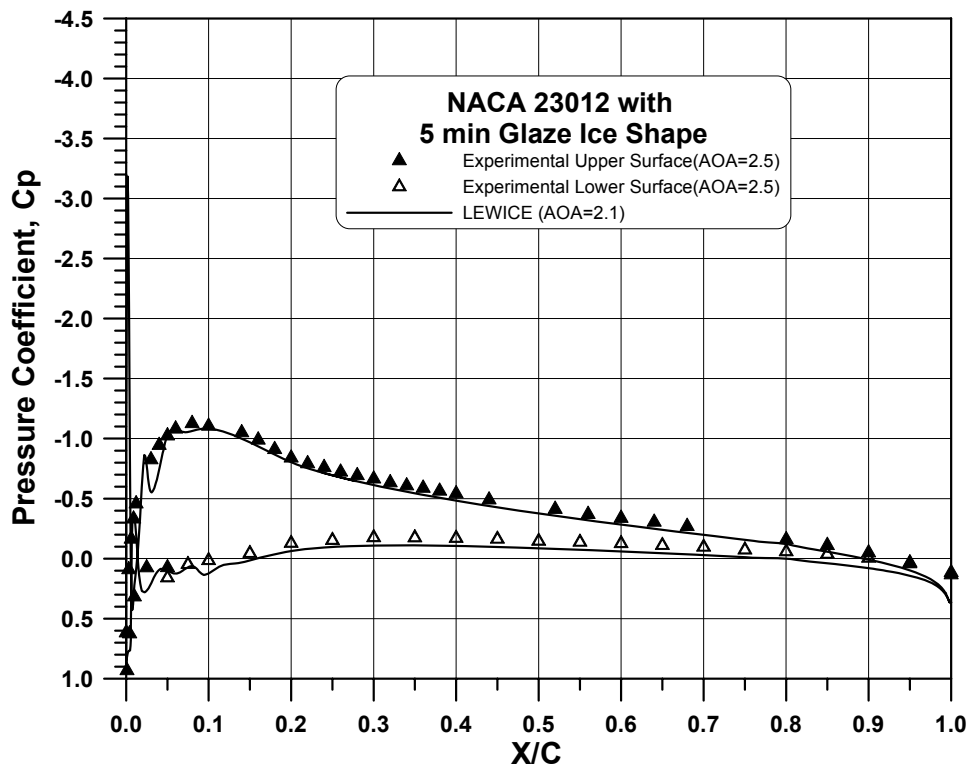


Figure 62.—Comparison of pressure distribution for NACA 23012 with 5-min glaze ice shape at  $\alpha = 2.5^\circ$ .

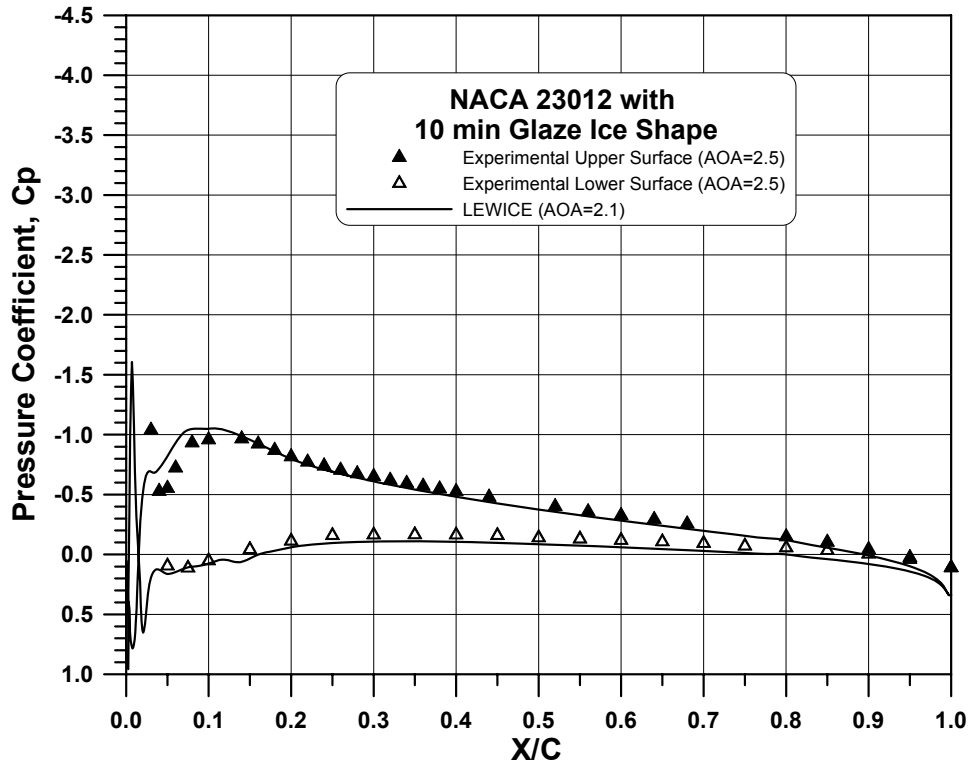


Figure 63.—Comparison of pressure distribution for NACA 23012 with 10-min glaze ice shape at  $\alpha = 2.5^\circ$ .

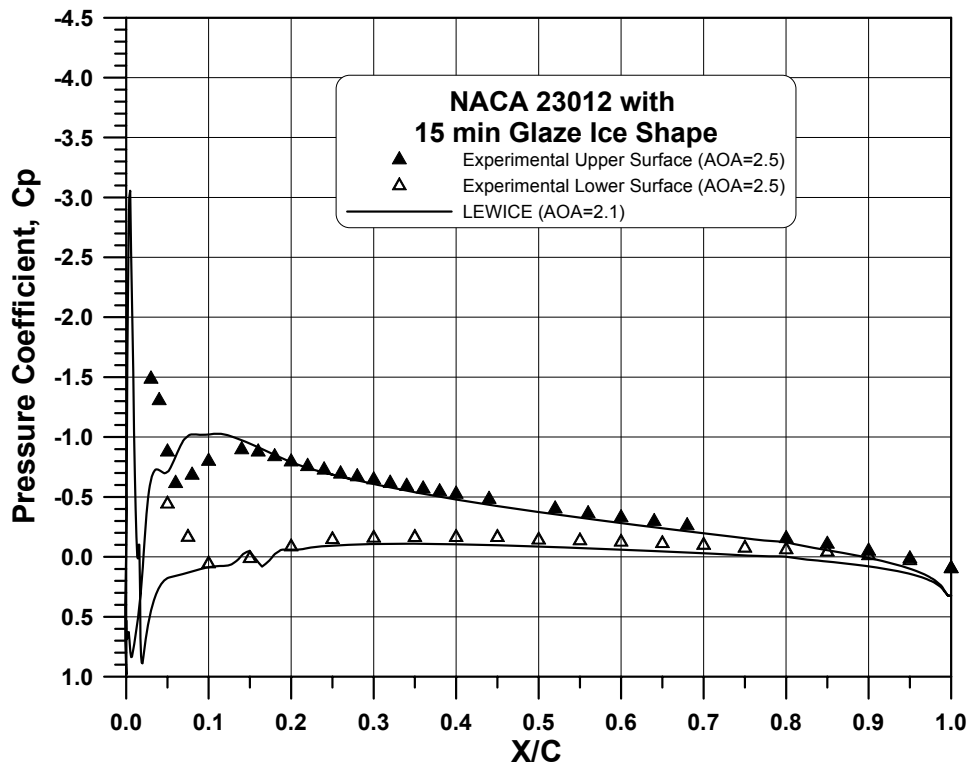


Figure 64.—Comparison of pressure distribution for NACA 23012 with 15-min glaze ice shape at  $\alpha = 2.5^\circ$ .

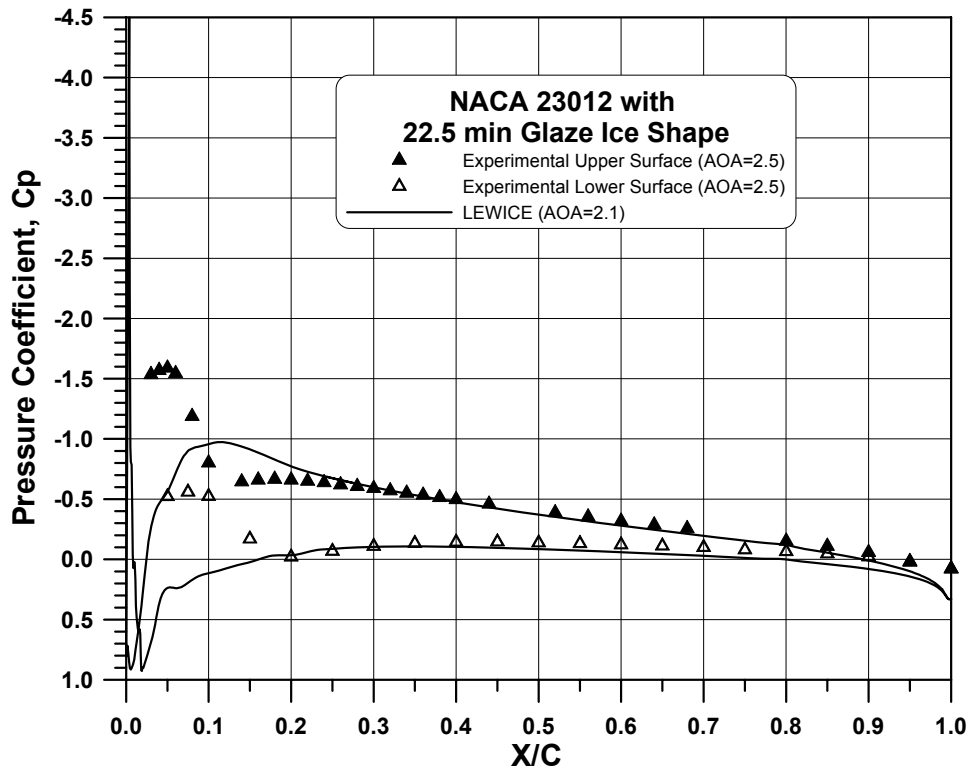


Figure 65.—Comparison of pressure distribution for NACA 23012 with 22.5-min glaze ice shape at  $\alpha = 2.5^\circ$ .

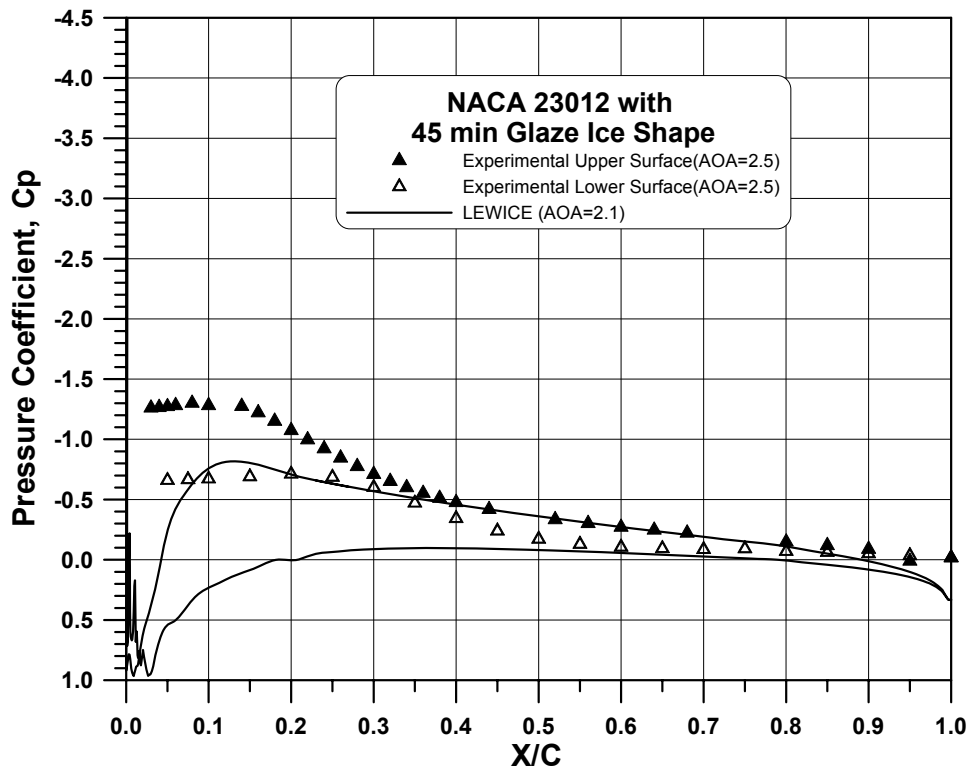


Figure 66.—Comparison of pressure distribution for NACA 23012 with 45-min glaze ice shape at  $\alpha = 2.5^\circ$ .

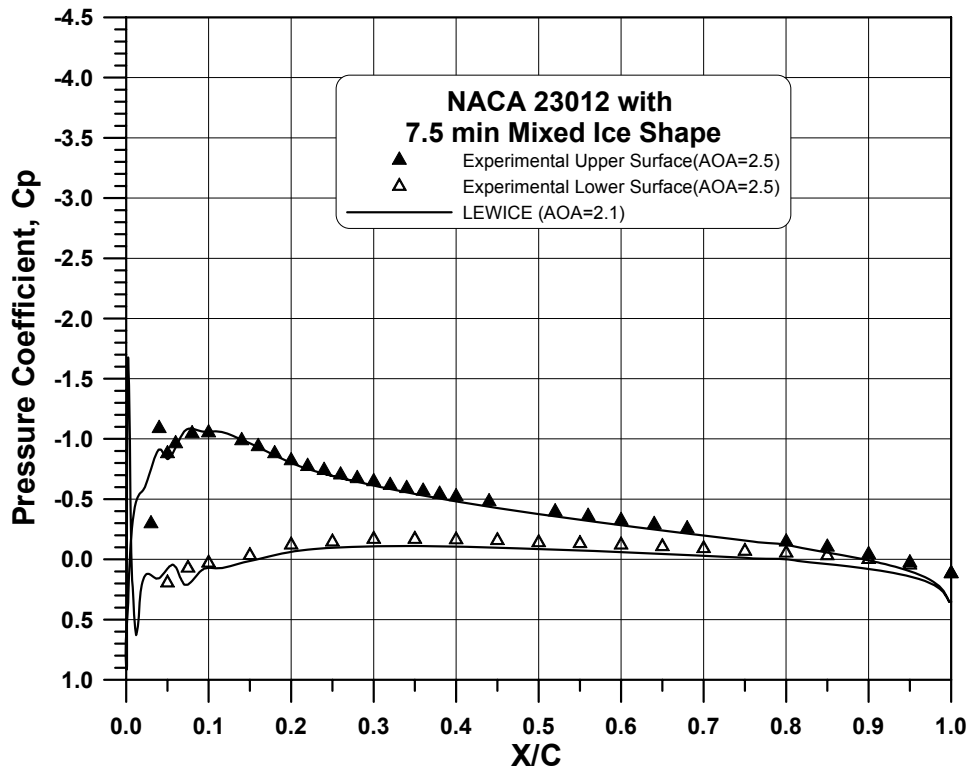


Figure 67.—Comparison of pressure distribution for NACA 23012 with 7.5-min mixed ice shape at  $\alpha = 2.5^\circ$ .

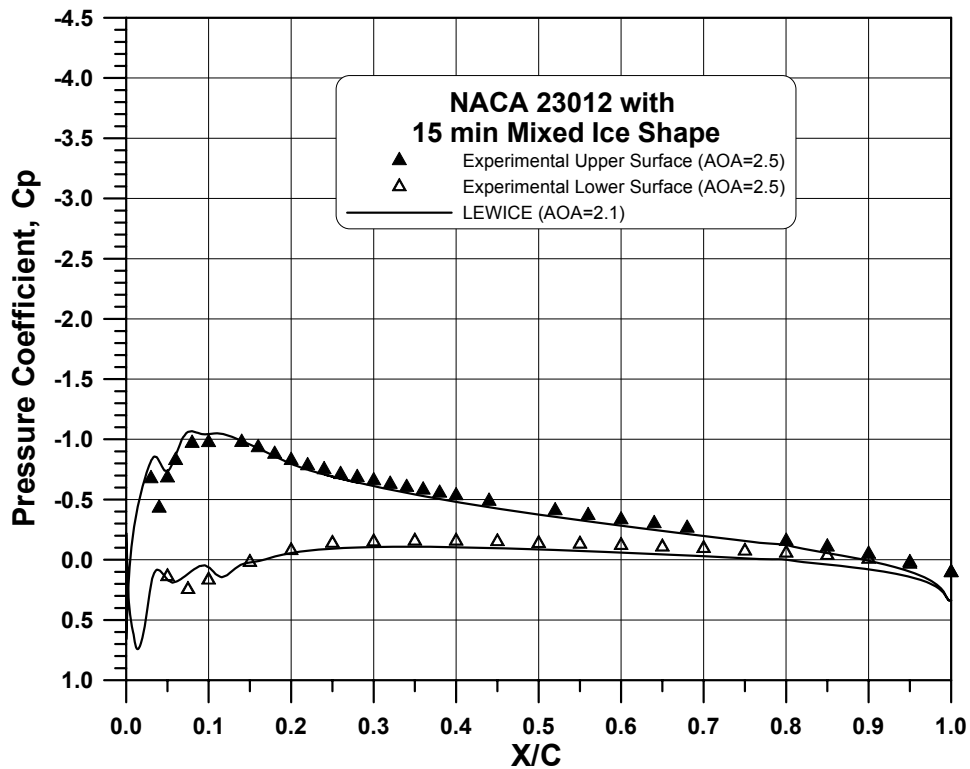


Figure 68.—Comparison of pressure distribution for NACA 23012 with 15-min mixed ice shape at  $\alpha = 2.5^\circ$ .

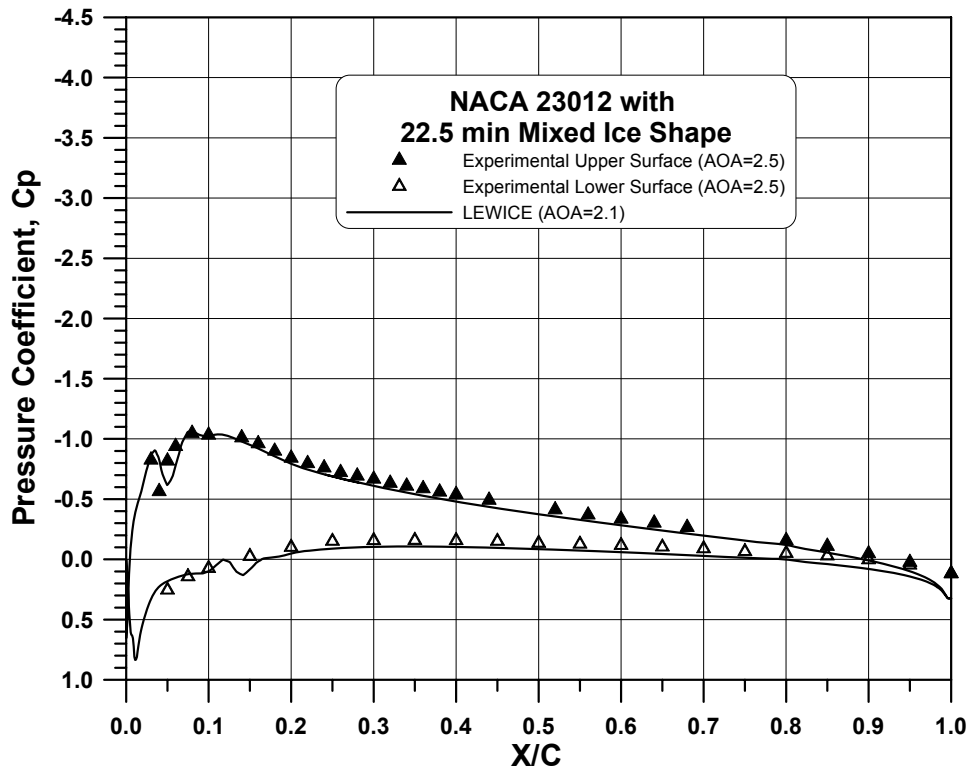


Figure 69.—Comparison of pressure distribution for NACA 23012 with 22.5-min mixed ice shape at  $\alpha = 2.5^\circ$ .

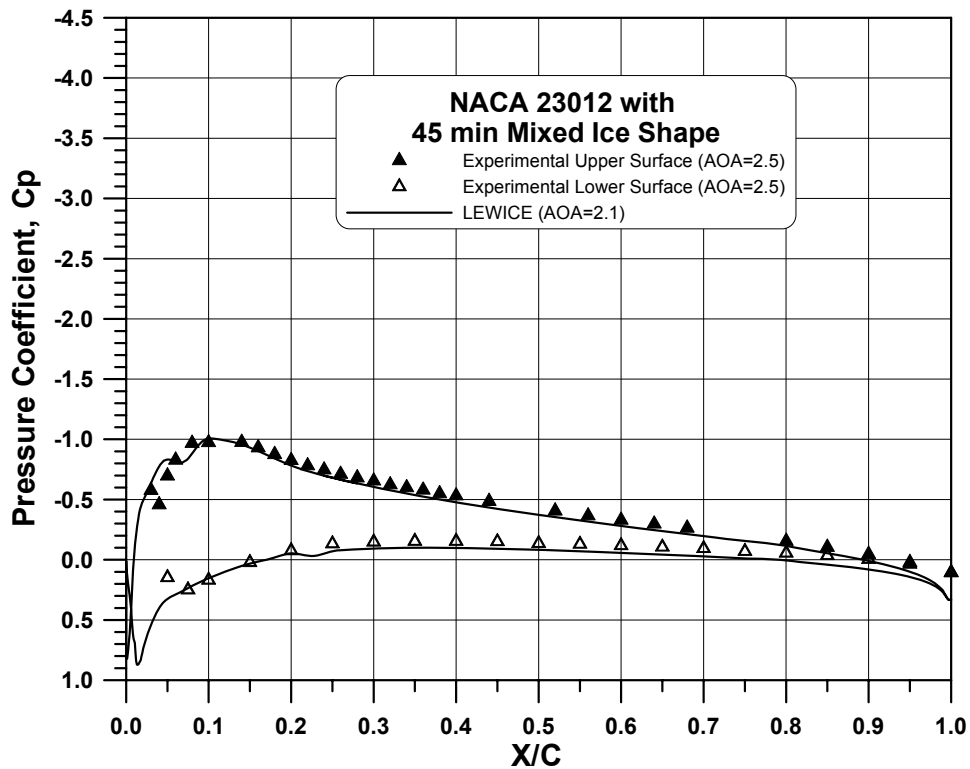


Figure 70.—Comparison of pressure distribution for NACA 23012 with 45-min mixed ice shape at  $\alpha = 2.5^\circ$ .

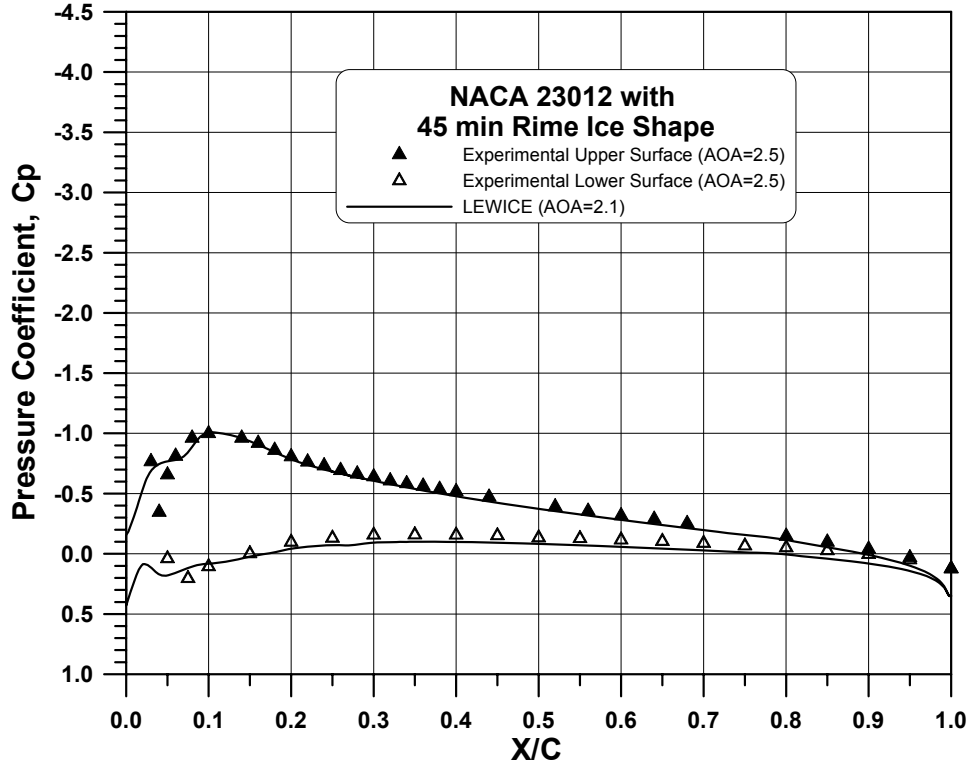


Figure 71.—Comparison of pressure distribution for NACA 23012 with 45-min rime ice shape at  $\alpha = 2.5^\circ$ .

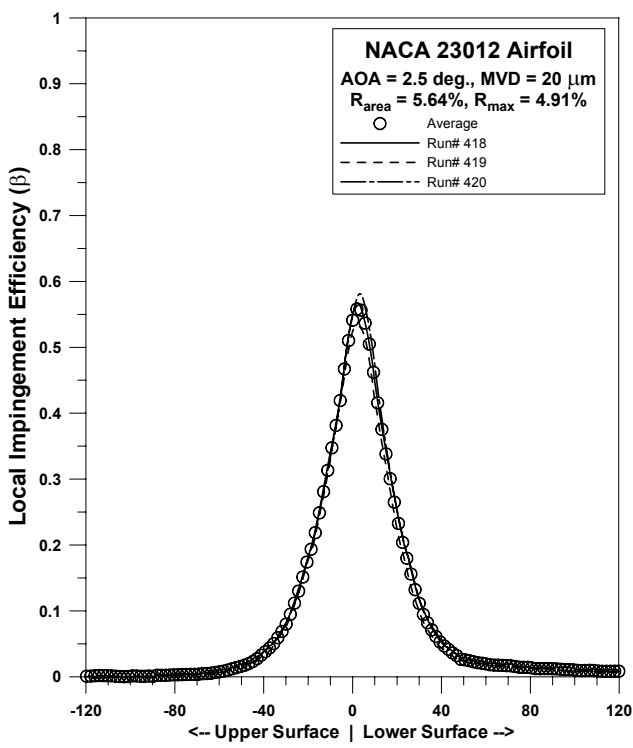


Figure 72a.—NACA 23012  
repeatability, MVD = 20  $\mu\text{m}$ .

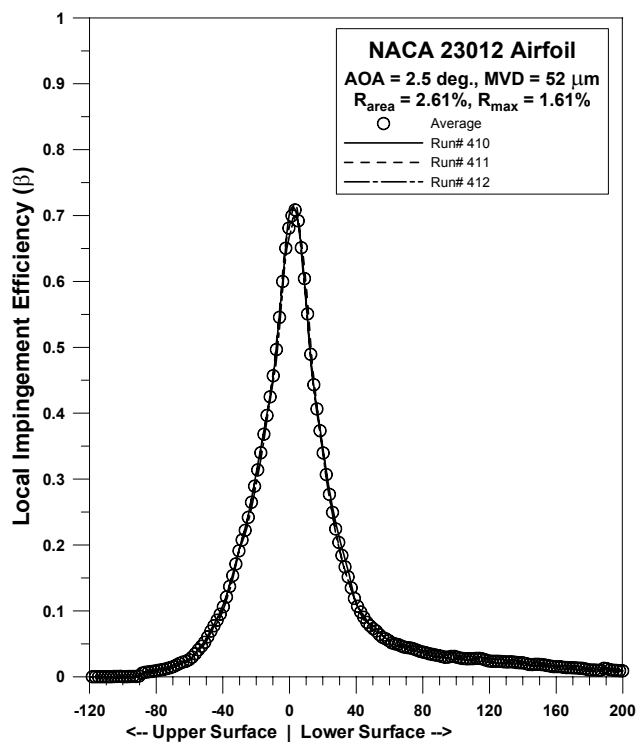


Figure 72b.—NACA 23012  
repeatability, MVD = 52  $\mu\text{m}$ .

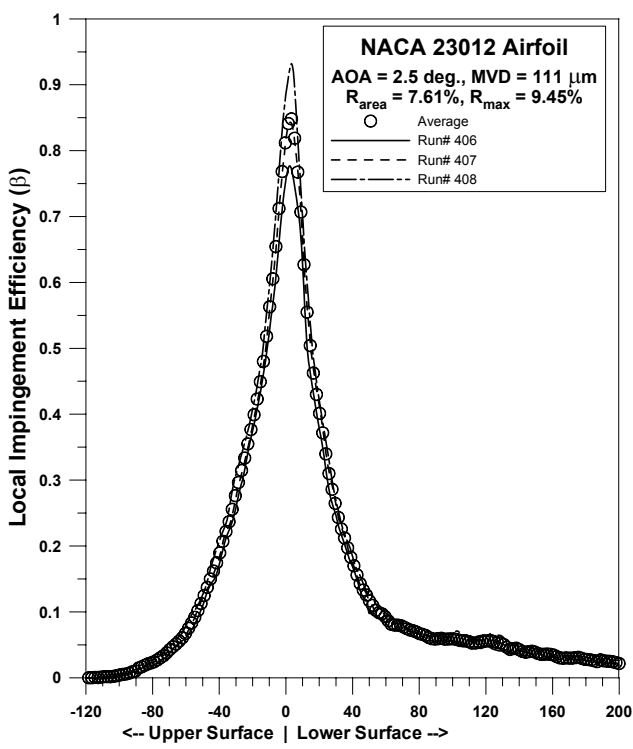


Figure 72c.—NACA 23012  
repeatability, MVD = 111  $\mu\text{m}$ .

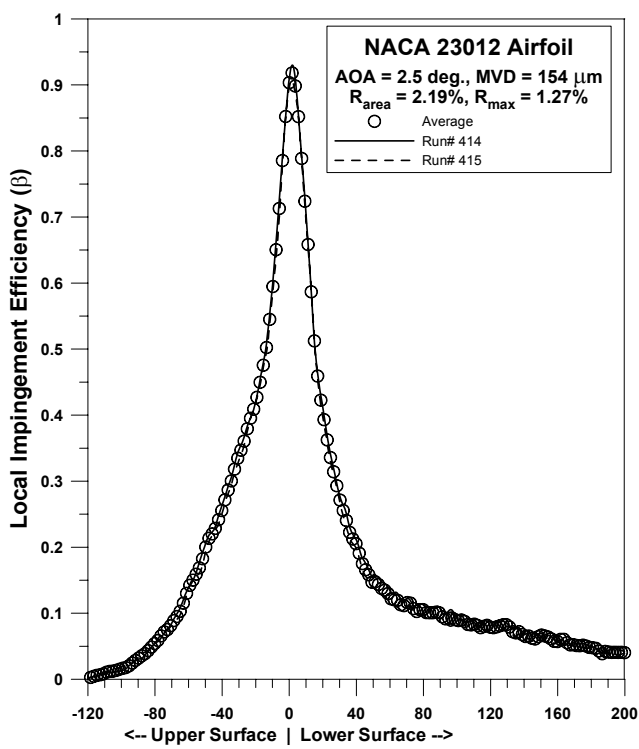


Figure 72d.—NACA 23012  
repeatability, MVD = 154  $\mu\text{m}$ .

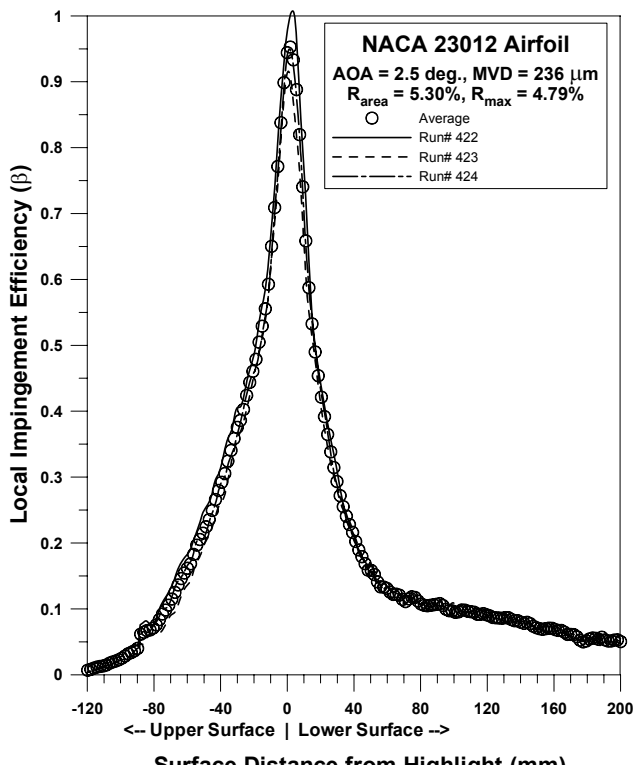


Figure 72e.—NACA 23012 repeatability, MVD = 236  $\mu\text{m}$ .

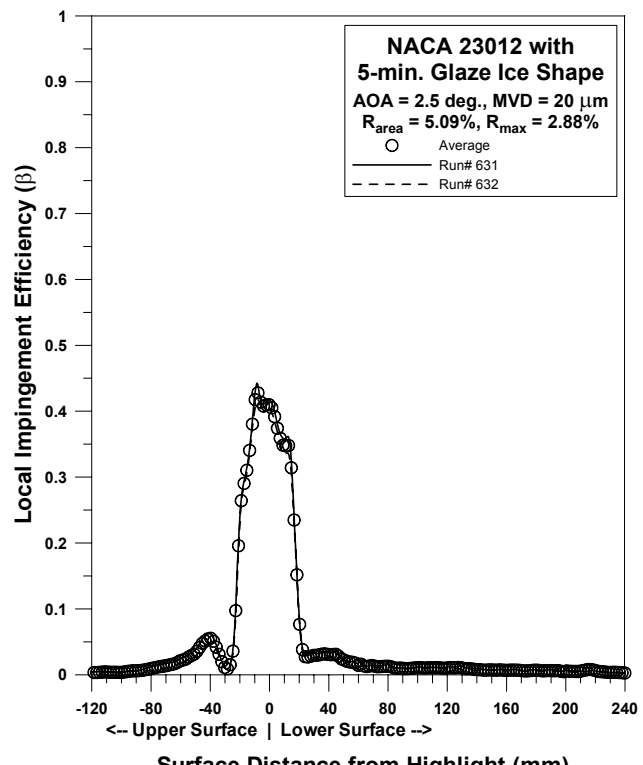


Figure 73a.—NACA 23012 with 5-min glaze ice repeatability, MVD = 20  $\mu\text{m}$ .

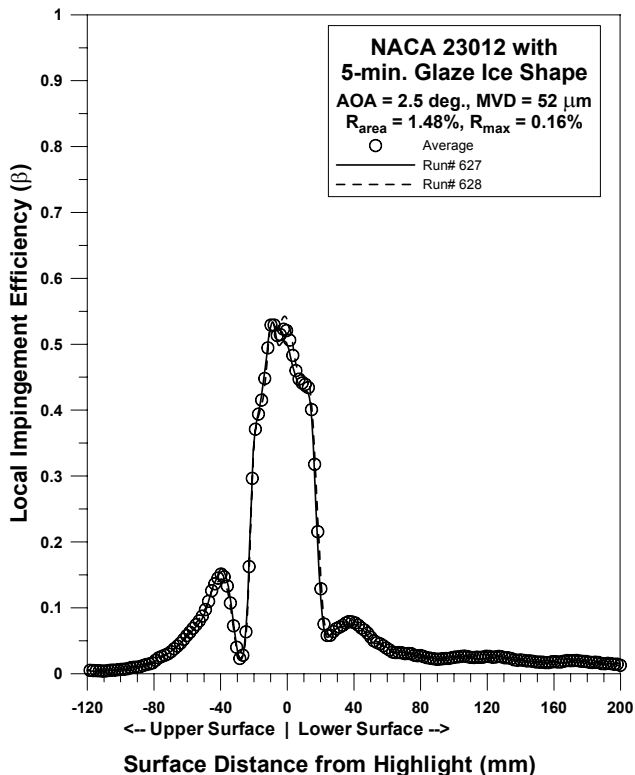


Figure 73b.—NACA 23012 with 5-min glaze ice repeatability, MVD = 52  $\mu\text{m}$ .

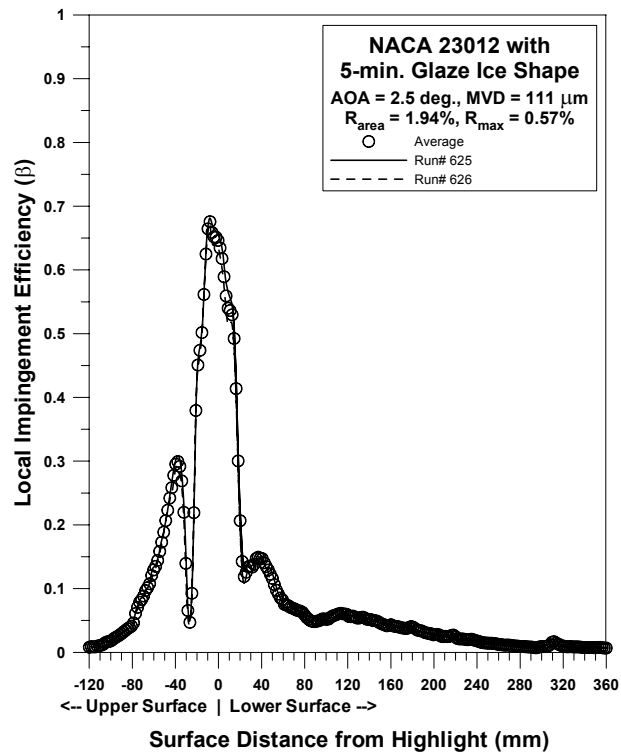


Figure 73c.—NACA 23012 with 5-min glaze ice repeatability, MVD = 111  $\mu\text{m}$ .

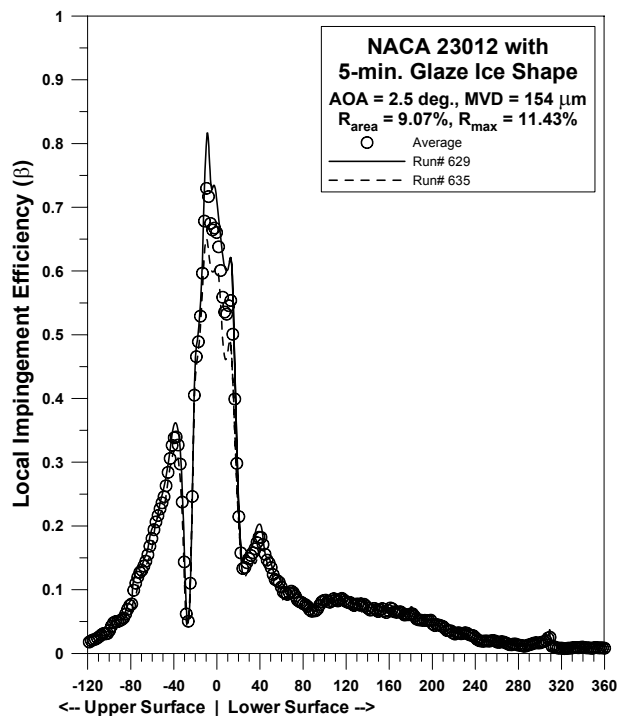


Figure 73d.—NACA 23012 with 5-min glaze ice repeatability, MVD = 154  $\mu\text{m}$ .

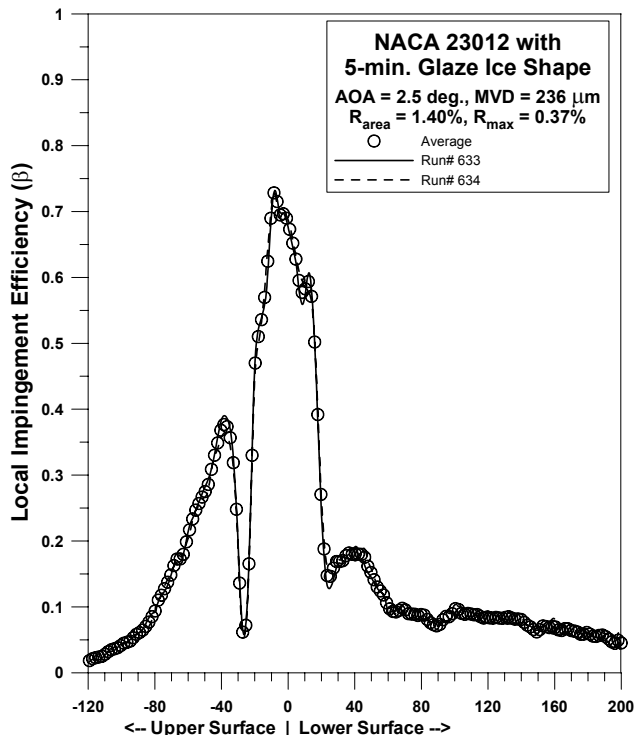


Figure 73e.—NACA 23012 with 5-min glaze ice repeatability, MVD = 236  $\mu\text{m}$ .

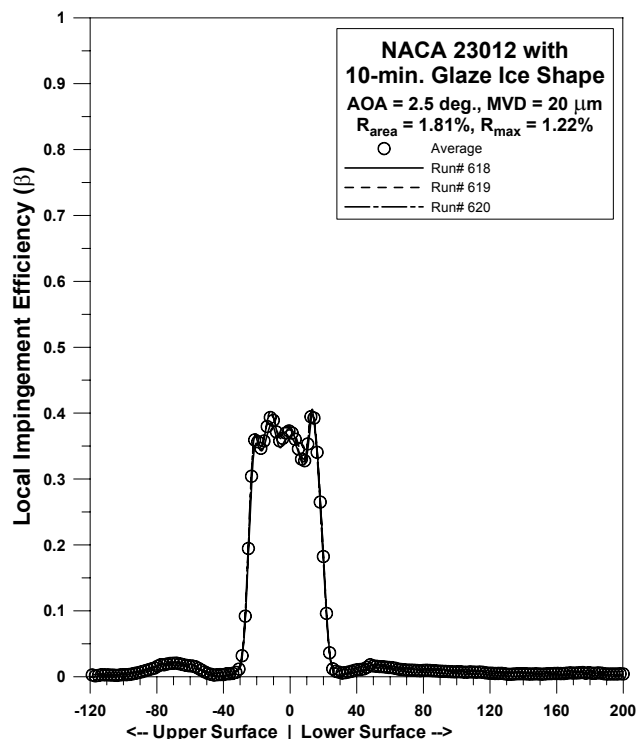


Figure 74a.—NACA 23012 with 10-min glaze ice repeatability, MVD = 20  $\mu\text{m}$ .

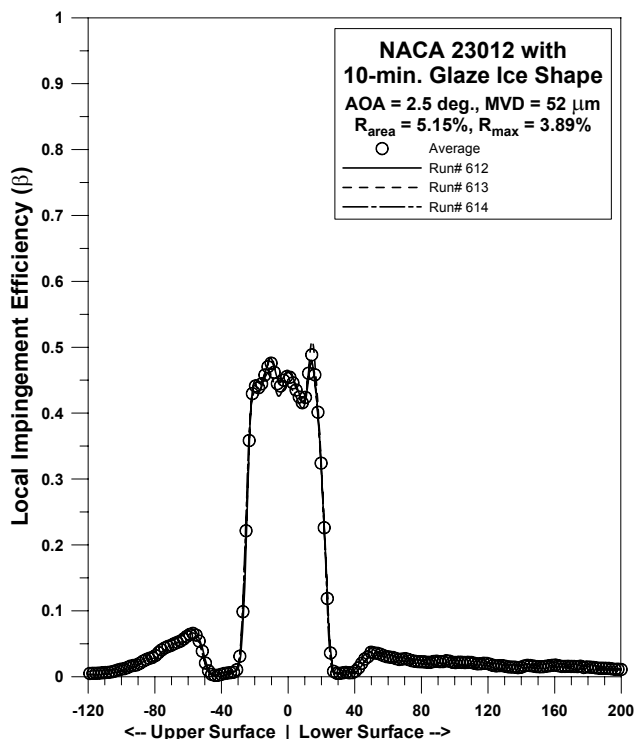


Figure 74b.—NACA 23012 with 10-min glaze ice repeatability, MVD = 52  $\mu\text{m}$ .

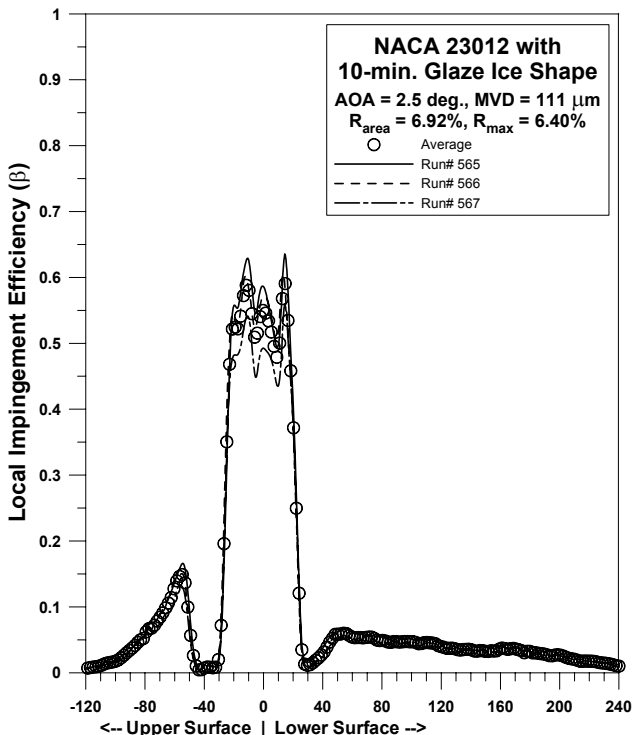


Figure 74c.—NACA 23012 with 10-min glaze ice repeatability, MVD = 111  $\mu\text{m}$ .

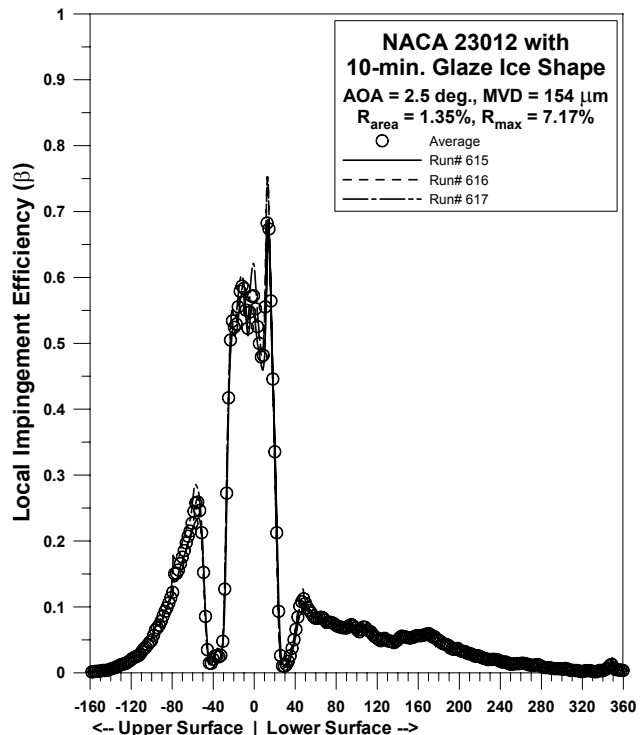


Figure 74d.—NACA 23012 with 10-min glaze ice repeatability, MVD = 154  $\mu\text{m}$ .

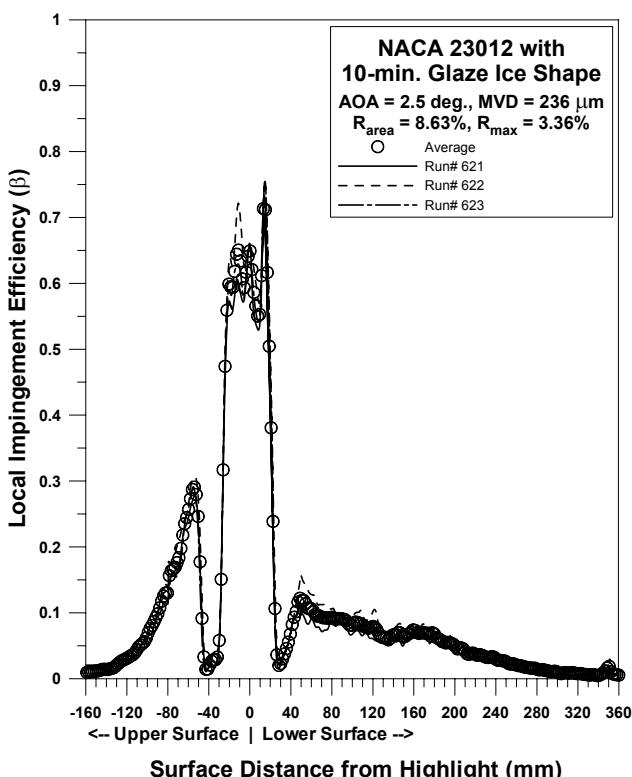


Figure 74e.—NACA 23012 with 10-min glaze ice repeatability, MVD = 236  $\mu\text{m}$ .

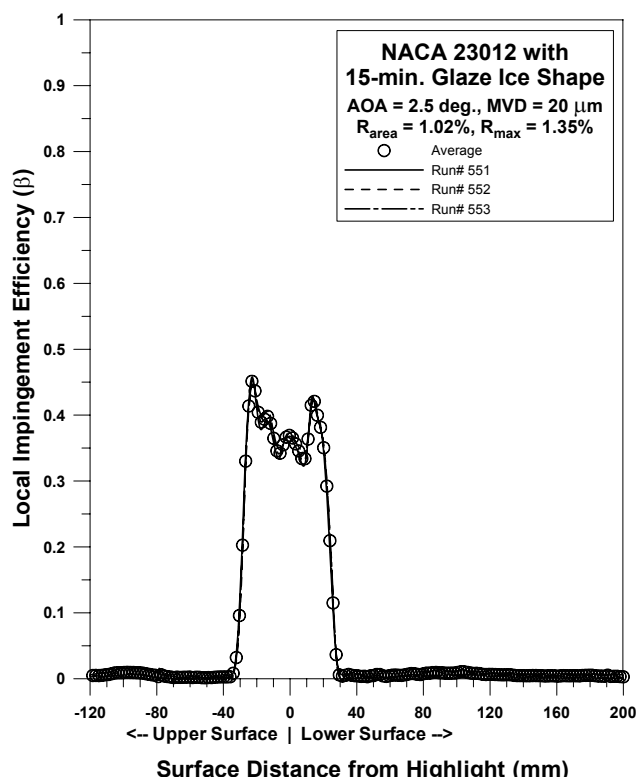


Figure 75a.—NACA 23012 with 15-min glaze ice repeatability, MVD = 20  $\mu\text{m}$ .

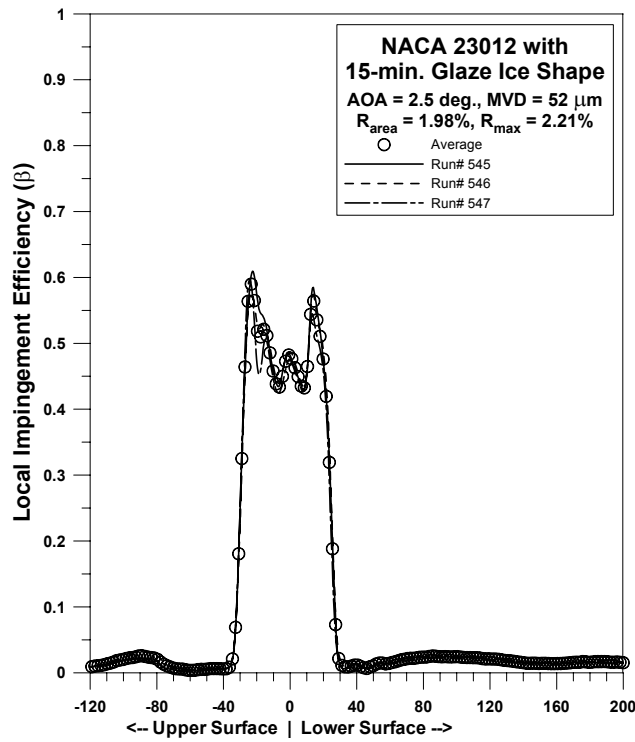


Figure 75b.—NACA 23012 with 15-min glaze ice repeatability, MVD = 52  $\mu\text{m}$ .

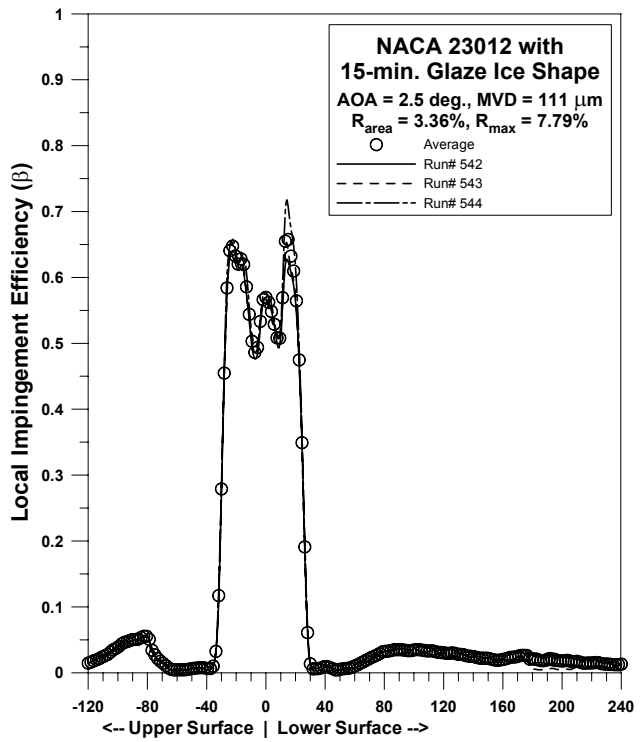


Figure 75c.—NACA 23012 with 15-min glaze ice repeatability, MVD = 111  $\mu\text{m}$ .

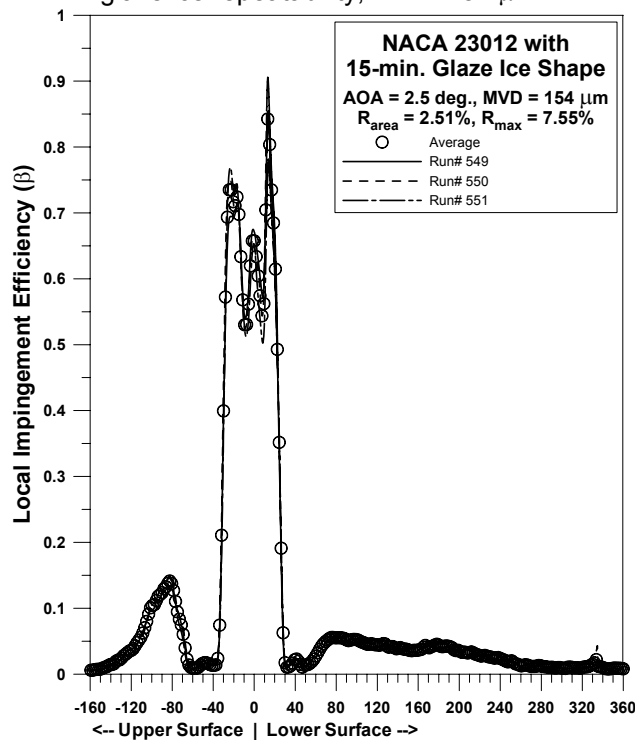


Figure 75d.—NACA 23012 with 15-min glaze ice repeatability, MVD = 154  $\mu\text{m}$ .

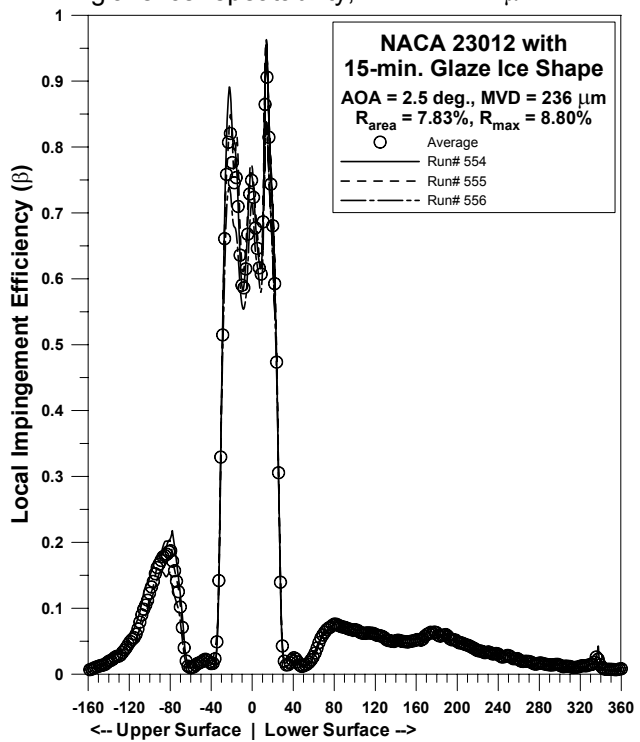
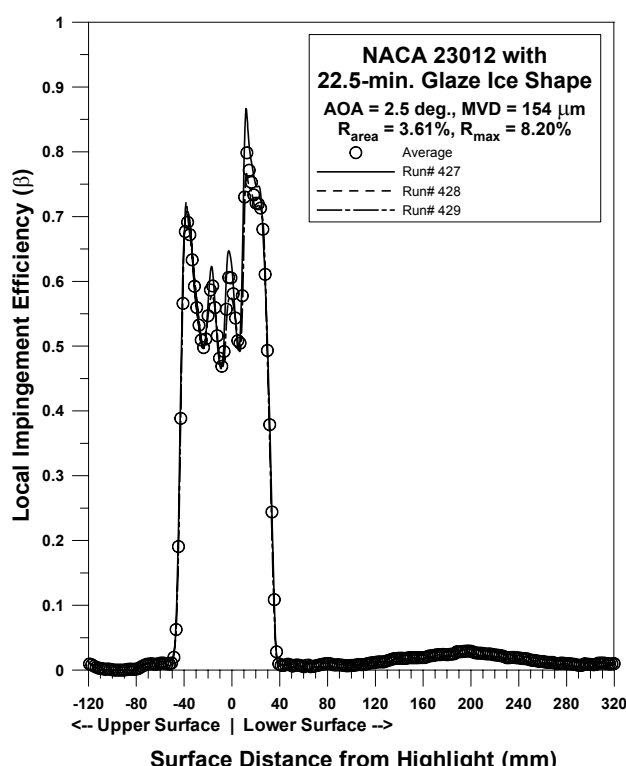
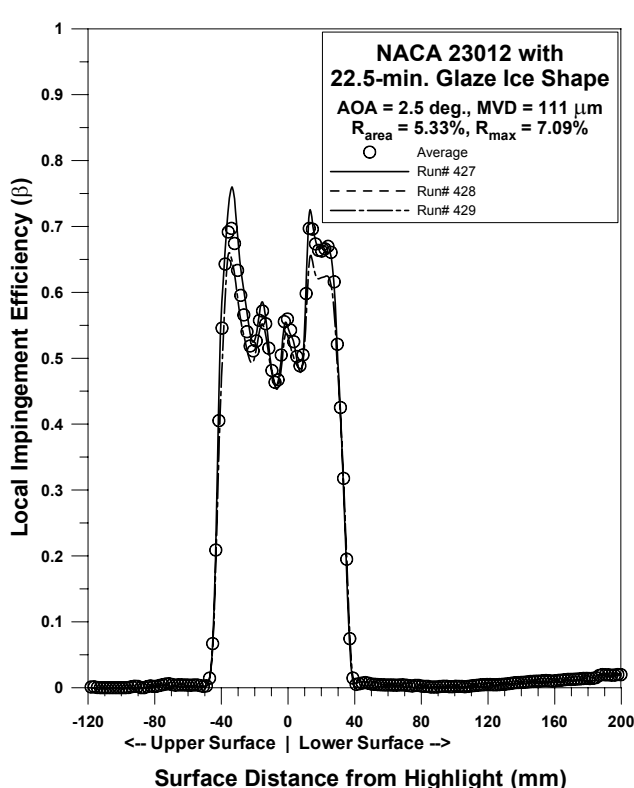
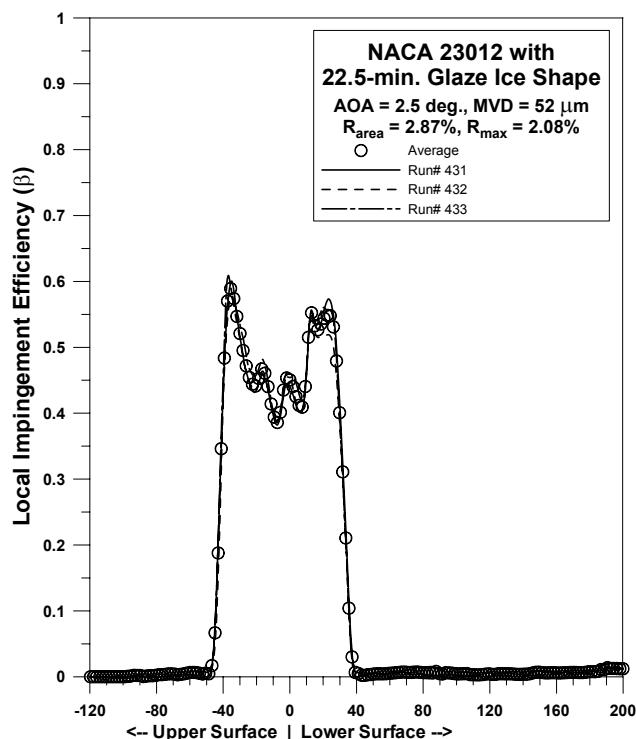
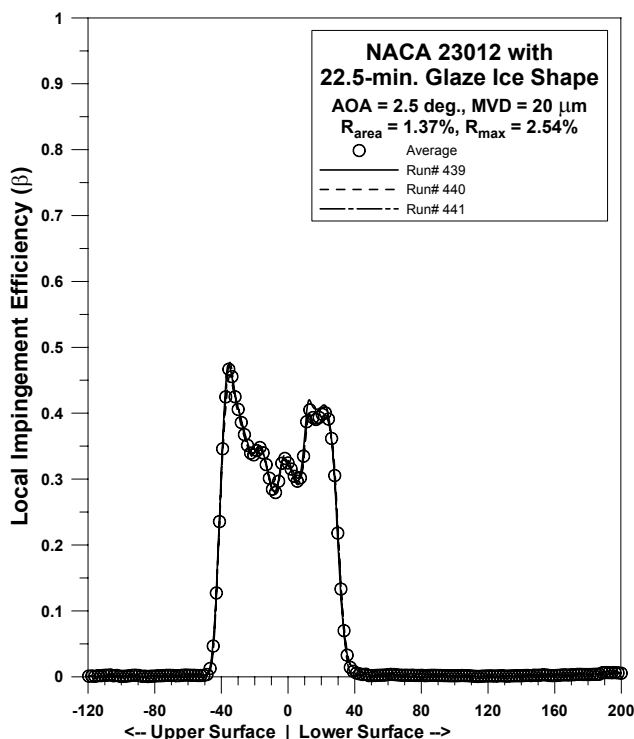


Figure 75e.—NACA 23012 with 15-min glaze ice repeatability, MVD = 236  $\mu\text{m}$ .



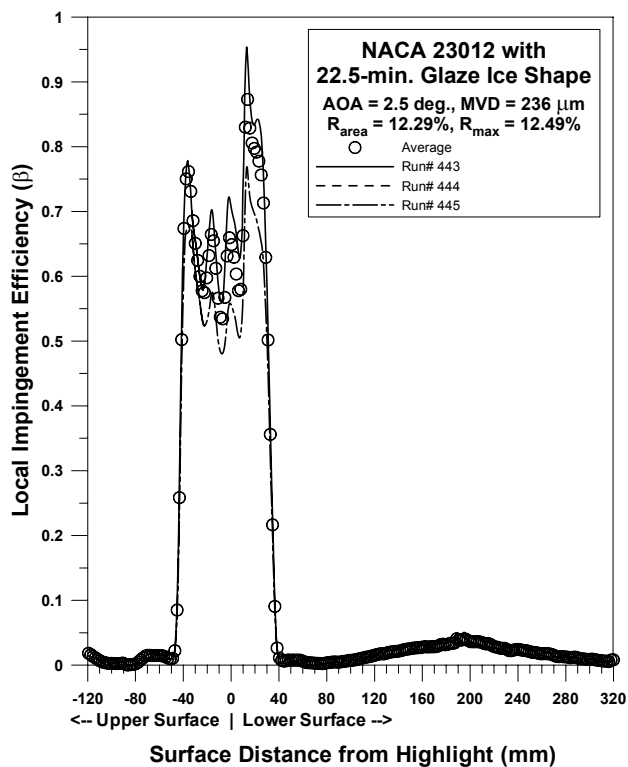


Figure 76e.—NACA 23012 with 22.5-min glaze ice repeatability, MVD = 236  $\mu\text{m}$ .

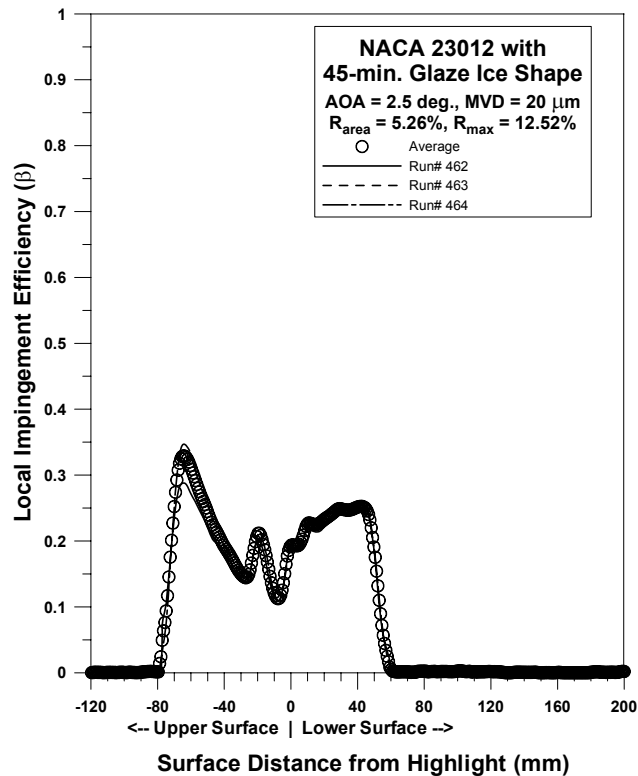


Figure 77a.—NACA 23012 with 45-min glaze ice repeatability, MVD = 20  $\mu\text{m}$ .

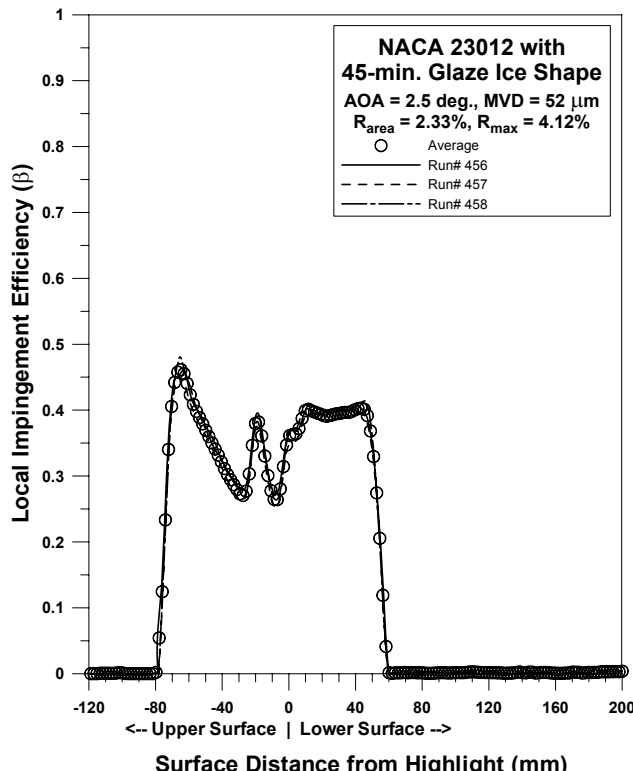


Figure 77b.—NACA 23012 with 45-min glaze ice repeatability, MVD = 52  $\mu\text{m}$ .

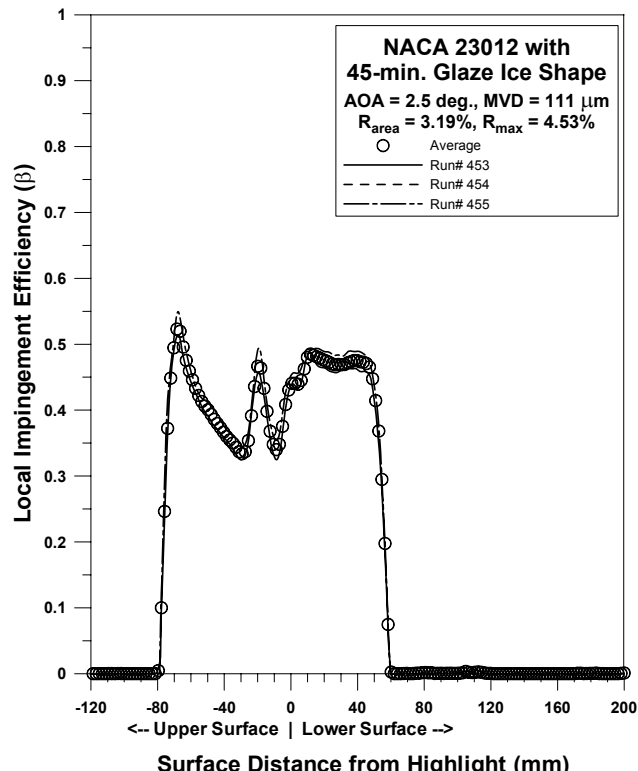


Figure 77c.—NACA 23012 with 45-min glaze ice repeatability, MVD = 111  $\mu\text{m}$ .

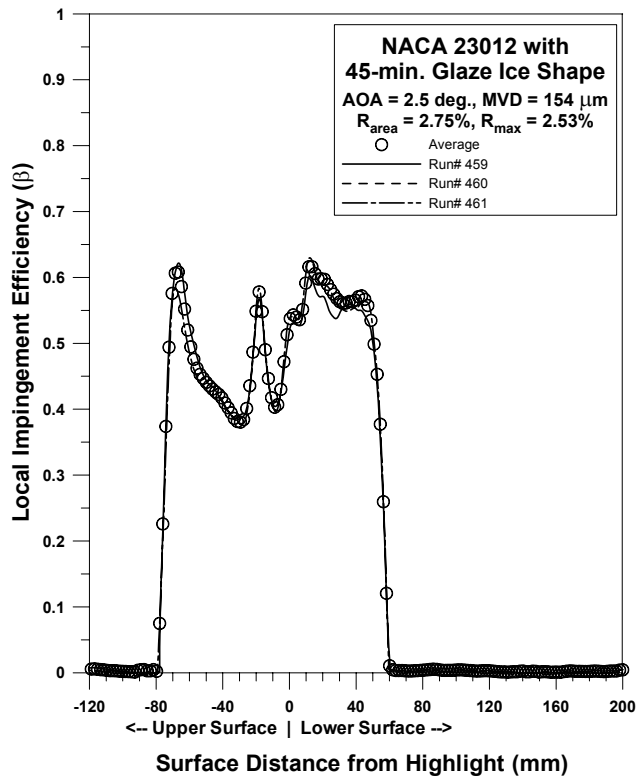


Figure 77d.—NACA 23012 with 45-min glaze ice repeatability, MVD = 154  $\mu\text{m}$ .

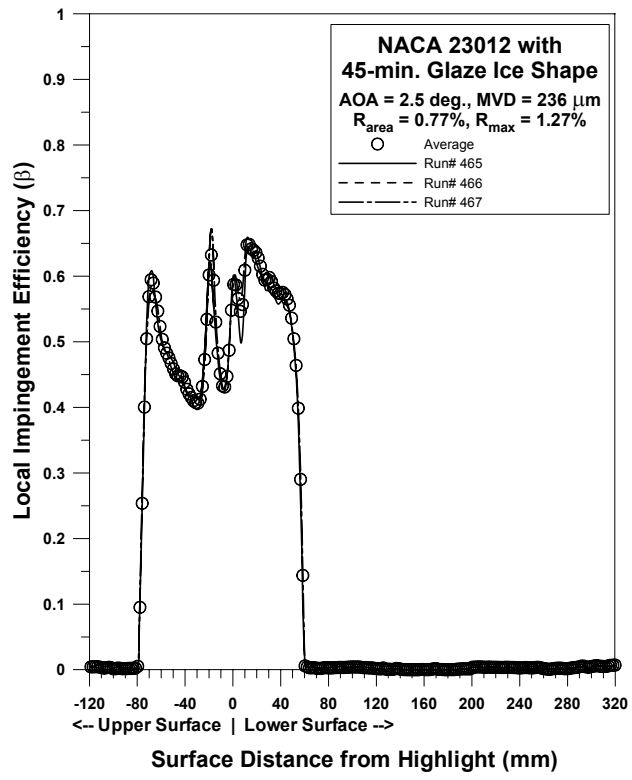


Figure 77e.—NACA 23012 with 45-min glaze ice repeatability, MVD = 236  $\mu\text{m}$ .

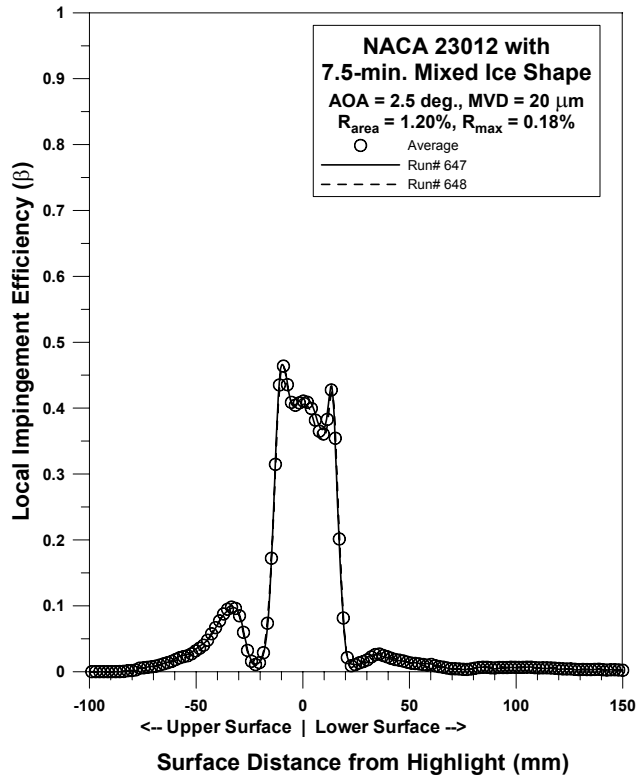


Figure 78a.—NACA 23012 with 7.5-min mixed ice repeatability, MVD = 20  $\mu\text{m}$ .

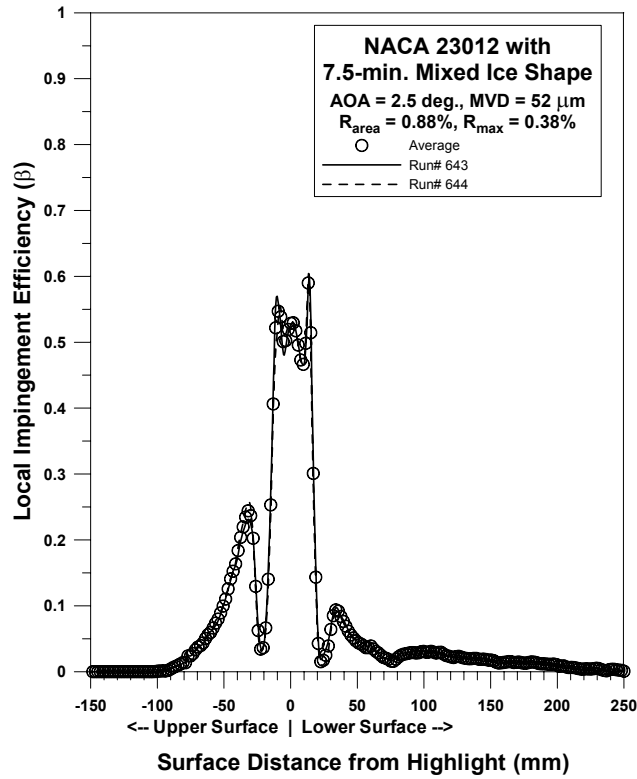


Figure 78b.—NACA 23012 with 7.5-min mixed ice repeatability, MVD = 52  $\mu\text{m}$ .

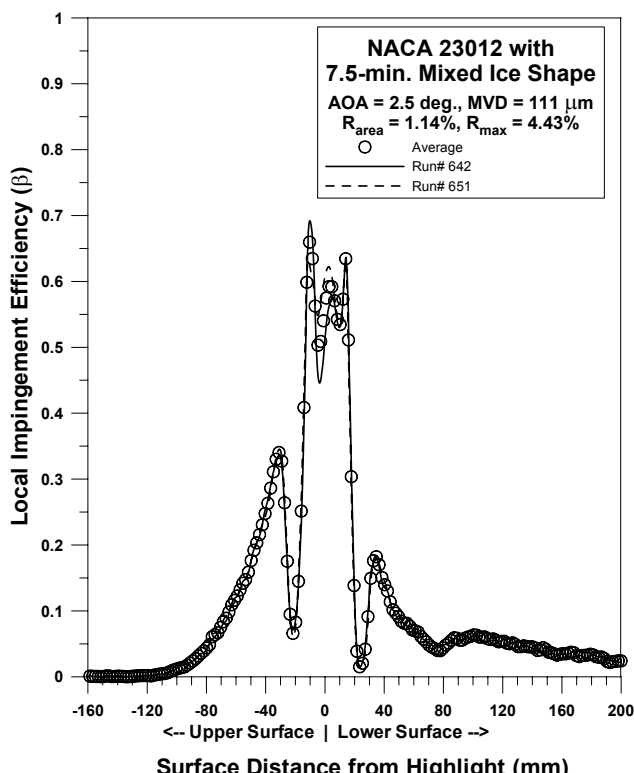


Figure 78c.—NACA 23012 with 7.5-min mixed ice repeatability, MVD = 111  $\mu\text{m}$ .

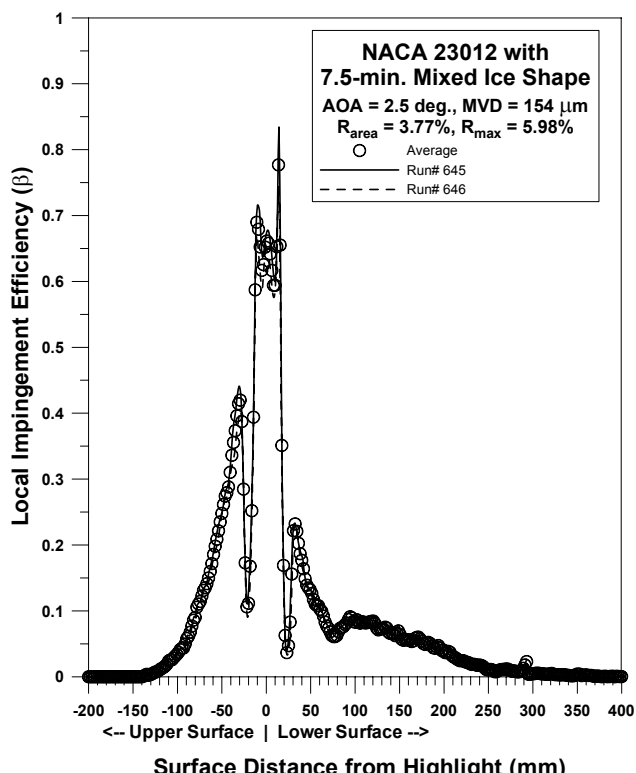


Figure 78d.—NACA 23012 with 7.5-min mixed ice repeatability, MVD = 154  $\mu\text{m}$ .

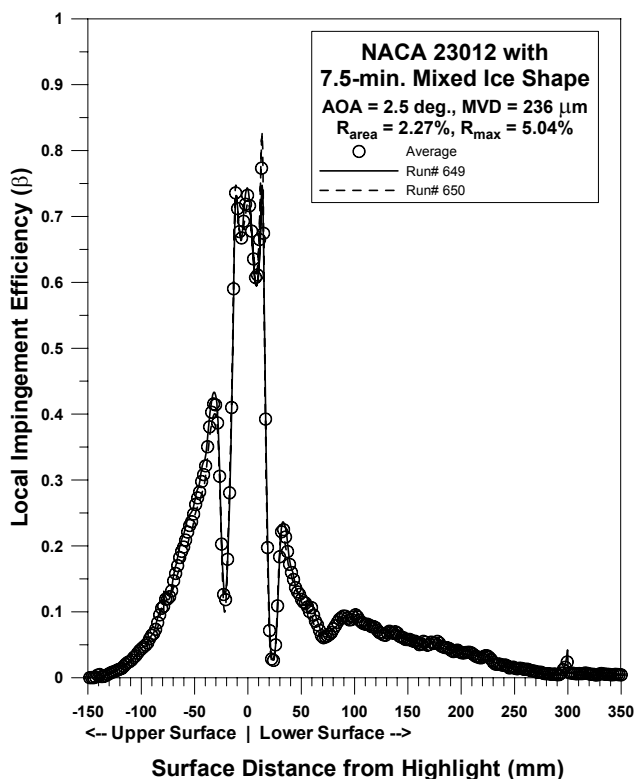


Figure 78e.—NACA 23012 with 7.5-min mixed ice repeatability, MVD = 236  $\mu\text{m}$ .

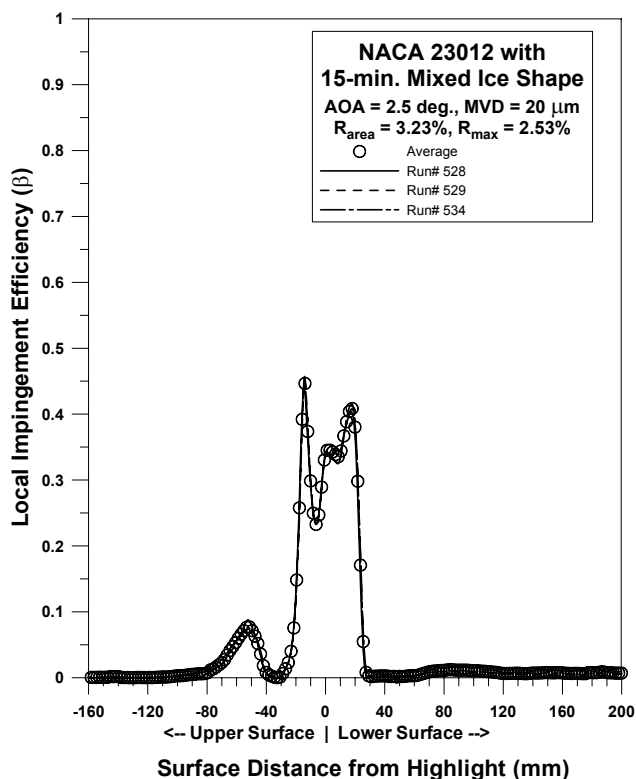


Figure 79a.—NACA 23012 with 15-min mixed ice repeatability, MVD = 20  $\mu\text{m}$ .

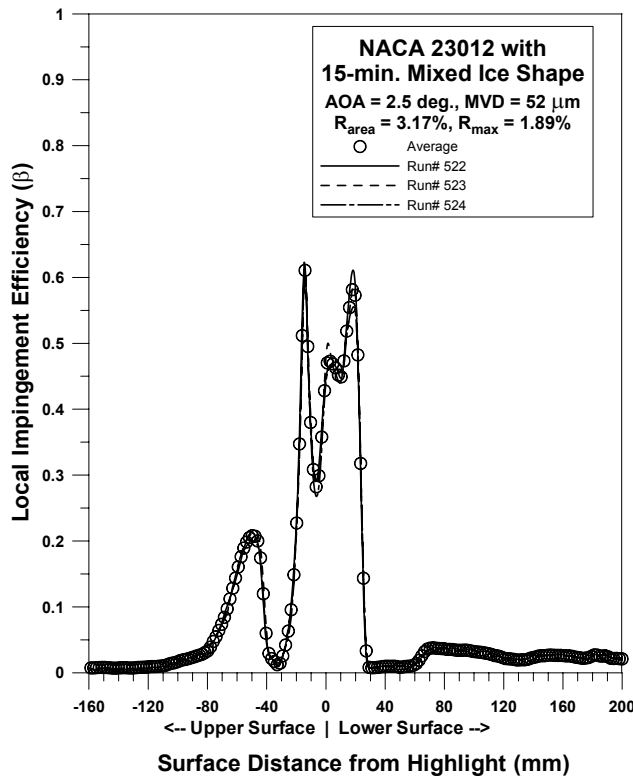


Figure 79b.—NACA 23012 with 15-min mixed ice repeatability, MVD = 52  $\mu\text{m}$ .

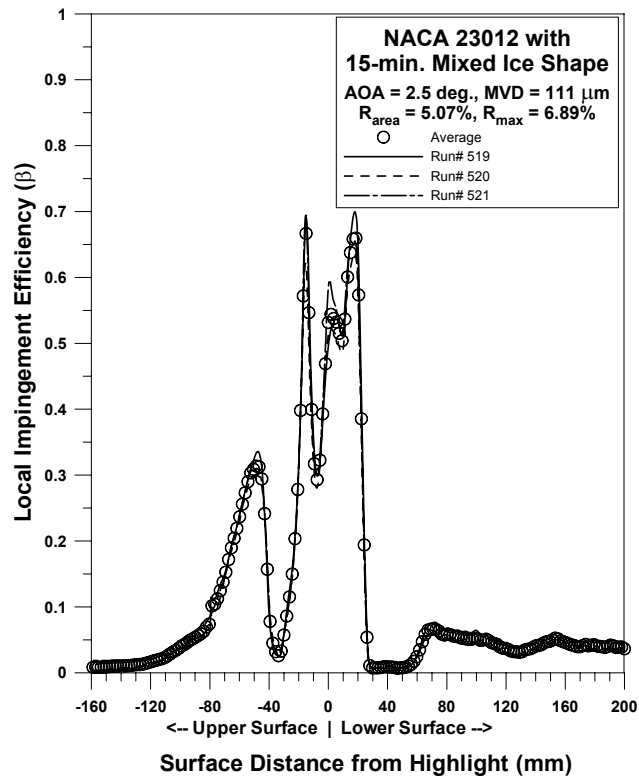


Figure 79c.—NACA 23012 with 15-min mixed ice repeatability, MVD = 111  $\mu\text{m}$ .

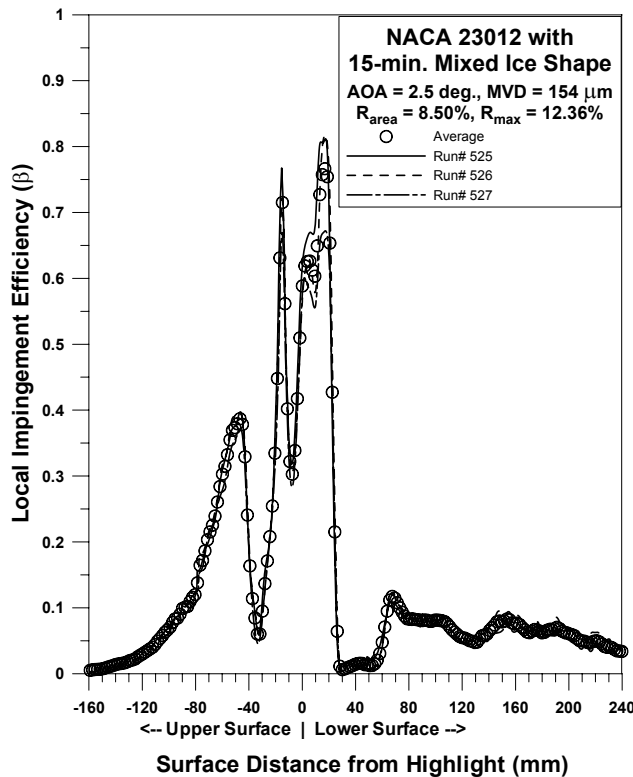


Figure 79d.—NACA 23012 with 15-min mixed ice repeatability, MVD = 154  $\mu\text{m}$ .

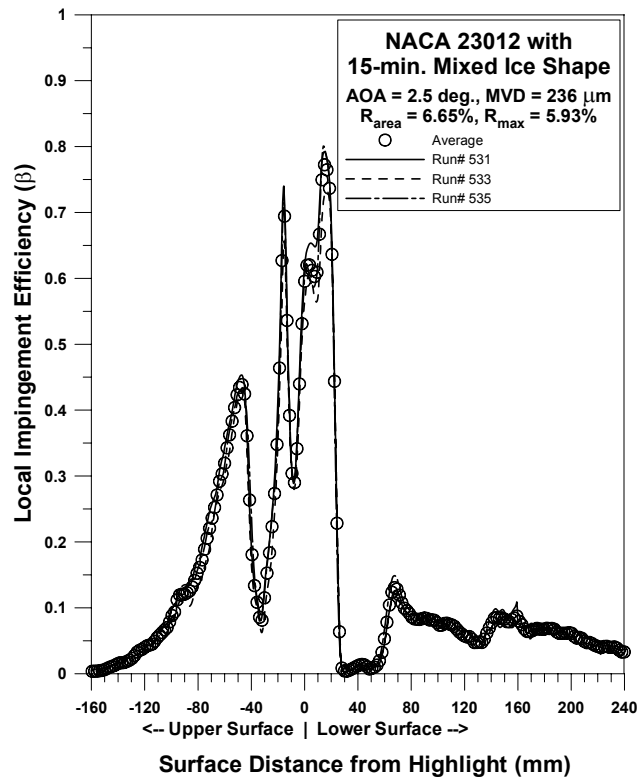


Figure 79e.—NACA 23012 with 15-min mixed ice repeatability, MVD = 236  $\mu\text{m}$ .

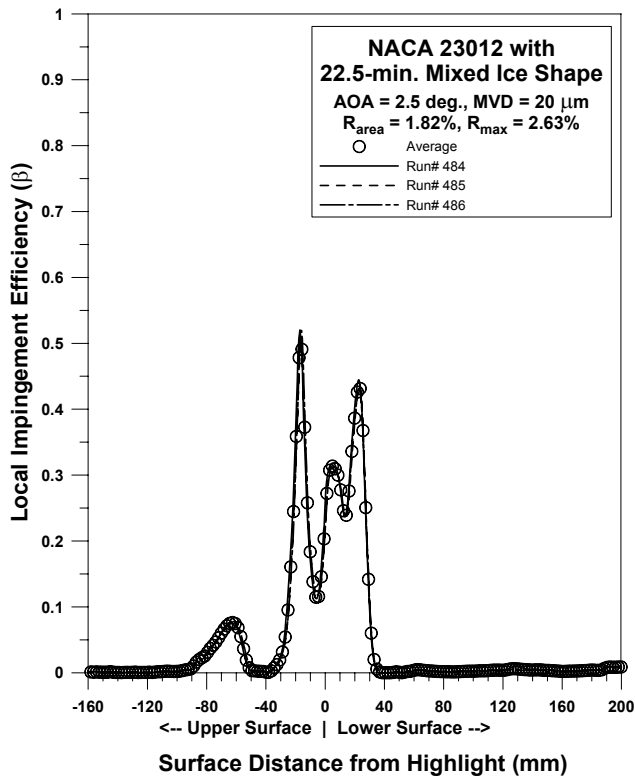


Figure 80a.—NACA 23012 with 22.5-min mixed ice repeatability, MVD = 20  $\mu\text{m}$ .

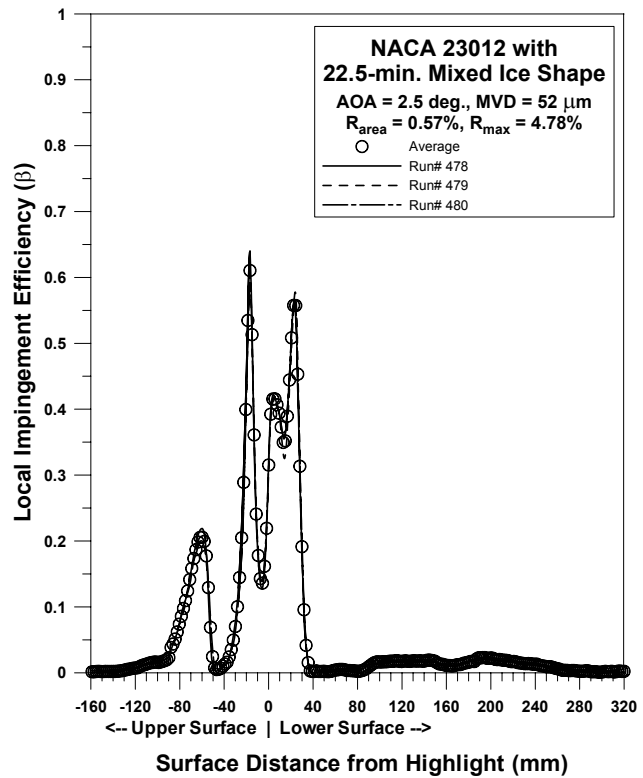


Figure 80b.—NACA 23012 with 22.5-min mixed ice repeatability, MVD = 52  $\mu\text{m}$ .

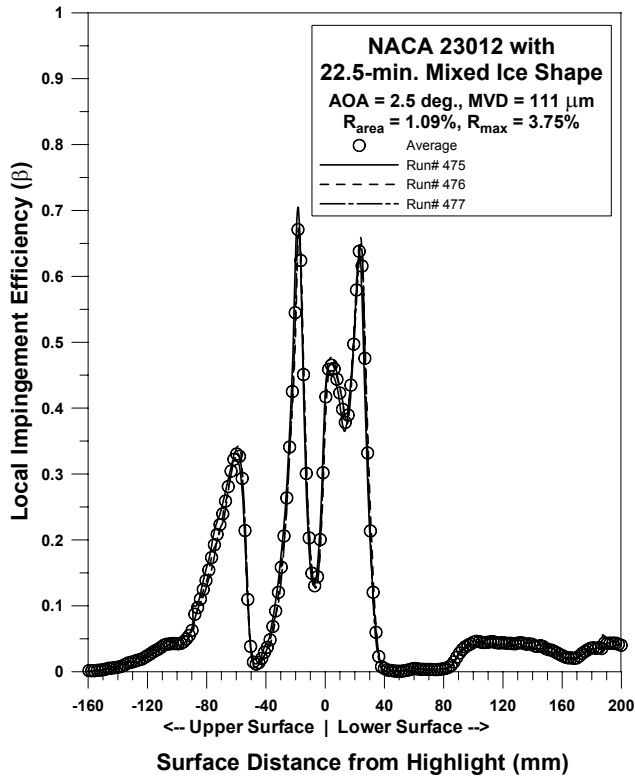


Figure 80c.—NACA 23012 with 22.5-min mixed ice repeatability, MVD = 111  $\mu\text{m}$ .

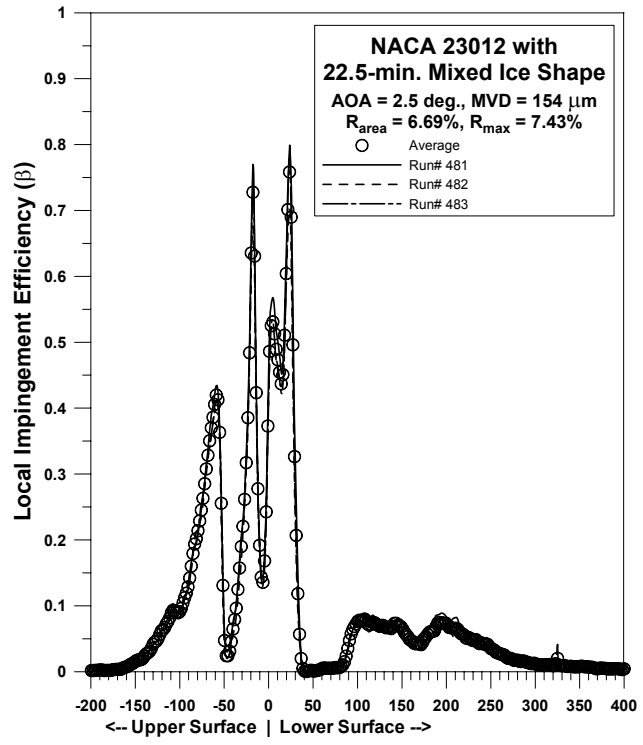


Figure 80d.—NACA 23012 with 22.5-min mixed ice repeatability, MVD = 154  $\mu\text{m}$ .

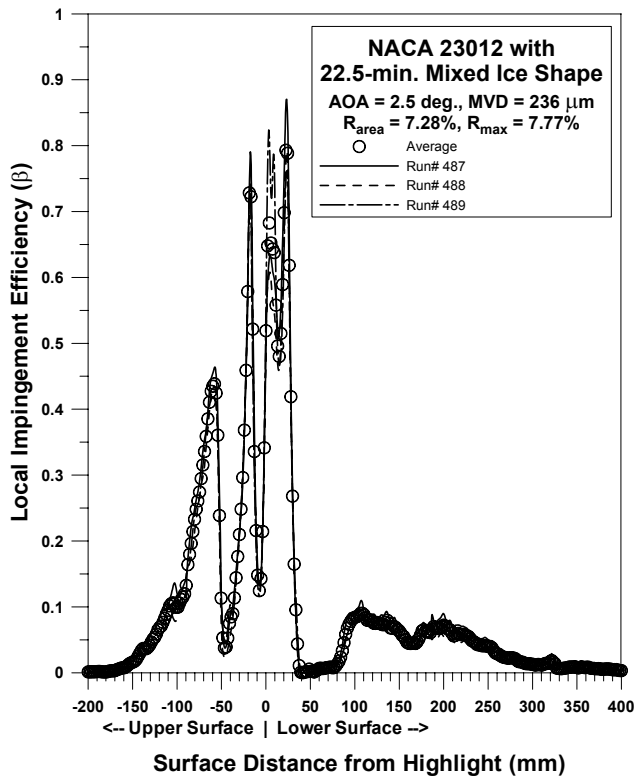


Figure 80e.—NACA 23012 with 22.5-min mixed ice repeatability, MVD = 236  $\mu\text{m}$ .

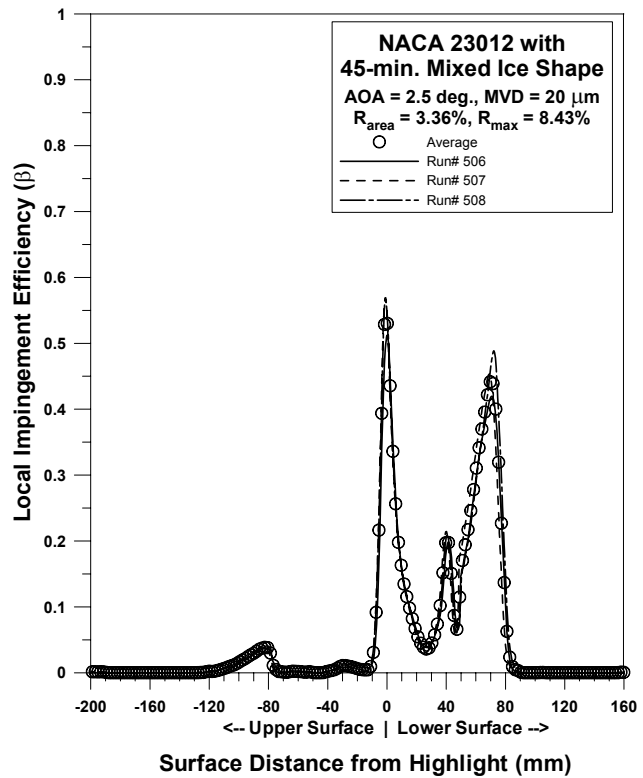


Figure 81a.—NACA 23012 with 45-min mixed ice repeatability, MVD = 20  $\mu\text{m}$ .

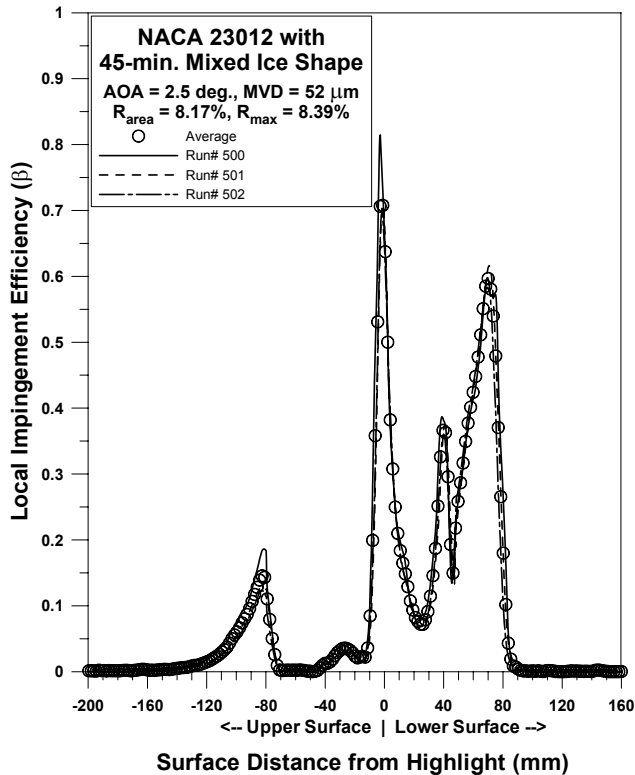


Figure 81b.—NACA 23012 with 45-min mixed ice repeatability, MVD = 52  $\mu\text{m}$ .

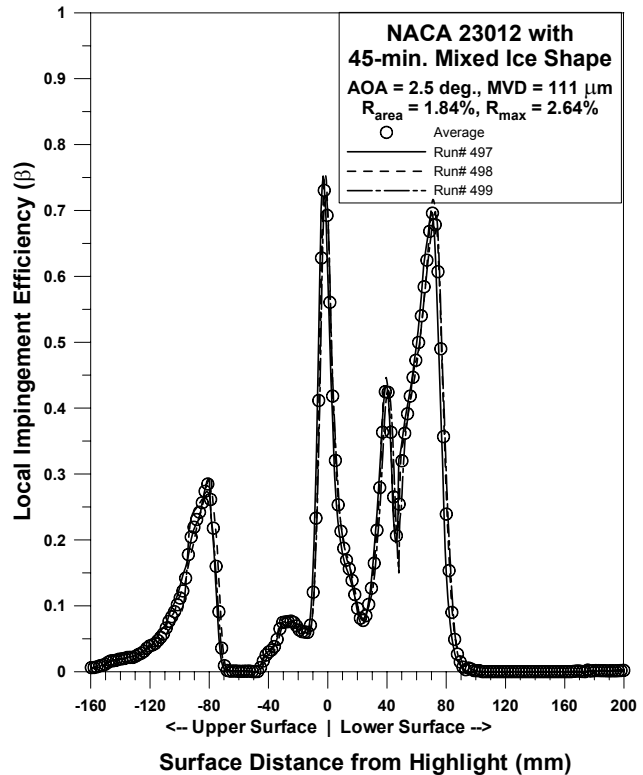


Figure 81c.—NACA 23012 with 45-min mixed ice repeatability, MVD = 111  $\mu\text{m}$ .

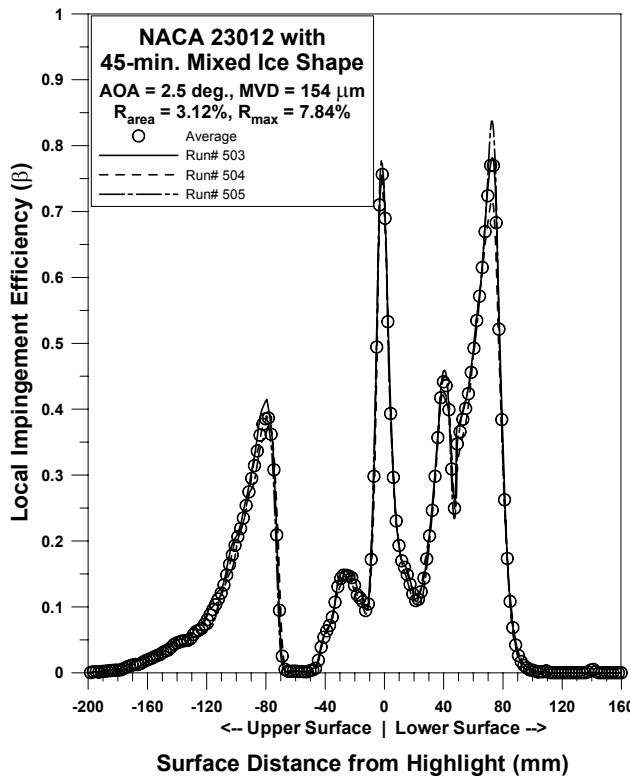


Figure 81d.—NACA 23012 with 45-min mixed ice repeatability, MVD = 154  $\mu\text{m}$ .

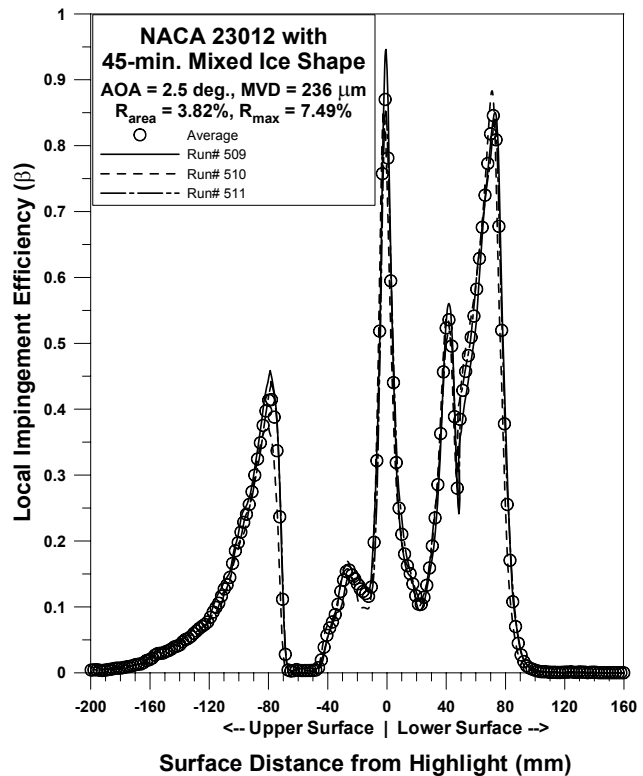


Figure 81e.—NACA 23012 with 45-min mixed ice repeatability, MVD = 236  $\mu\text{m}$ .

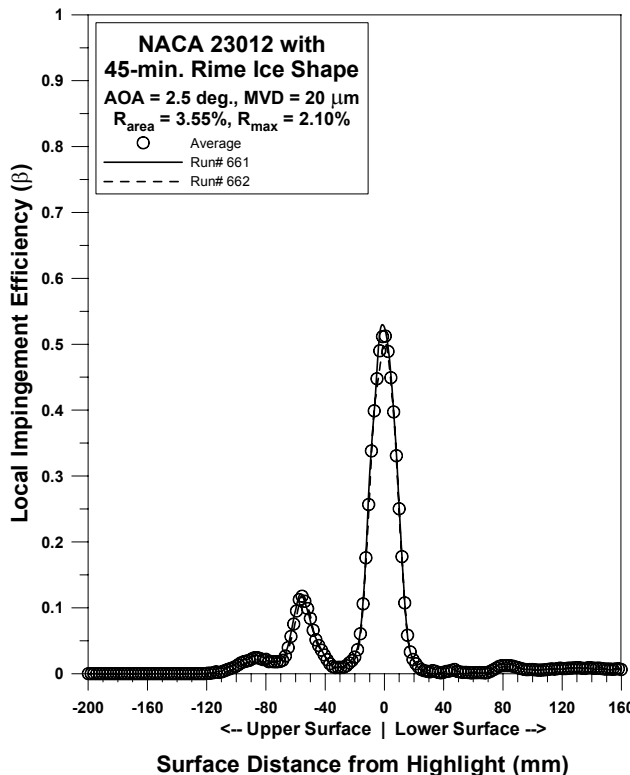


Figure 82a.—NACA 23012 with 45-min rime ice repeatability, MVD = 20  $\mu\text{m}$ .

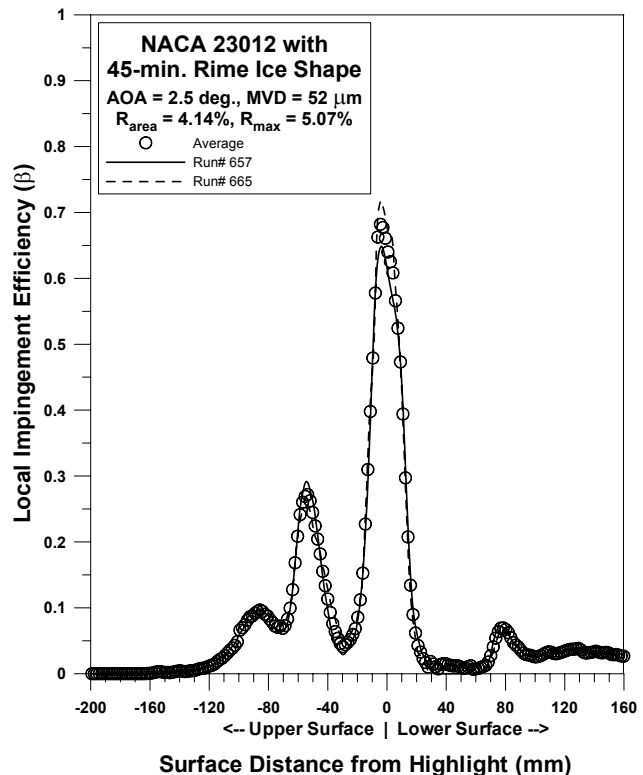


Figure 82b.—NACA 23012 with 45-min rime ice repeatability, MVD = 52  $\mu\text{m}$ .

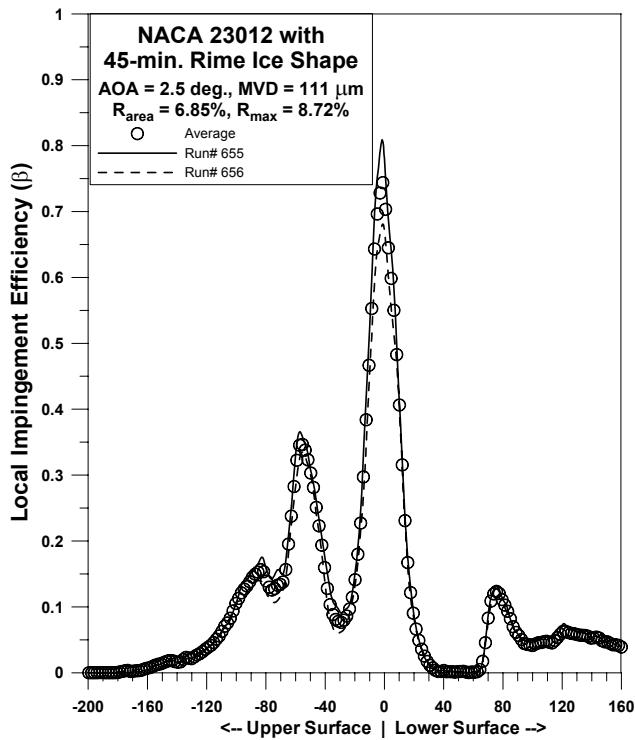


Figure 82c.—NACA 23012 with 45-min rime ice repeatability, MVD = 111  $\mu\text{m}$ .

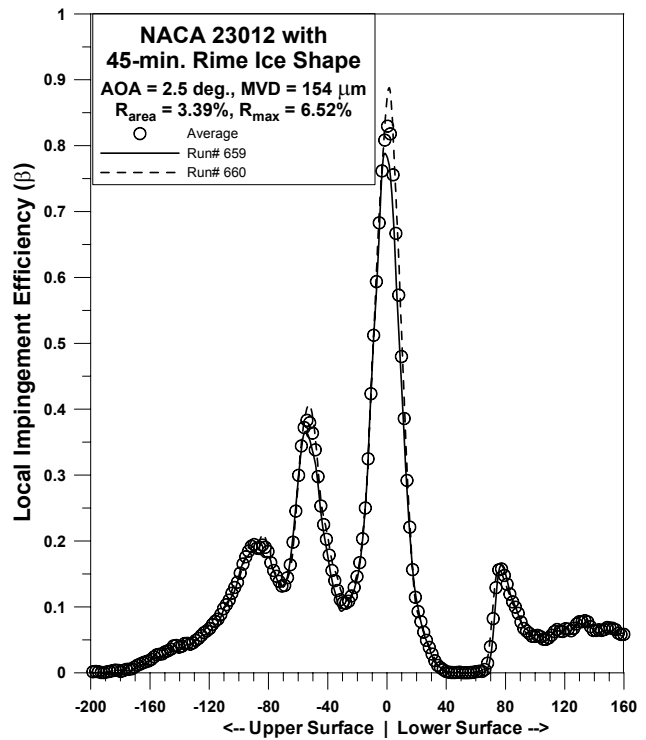


Figure 82d.—NACA 23012 with 45-min rime ice repeatability, MVD = 154  $\mu\text{m}$ .

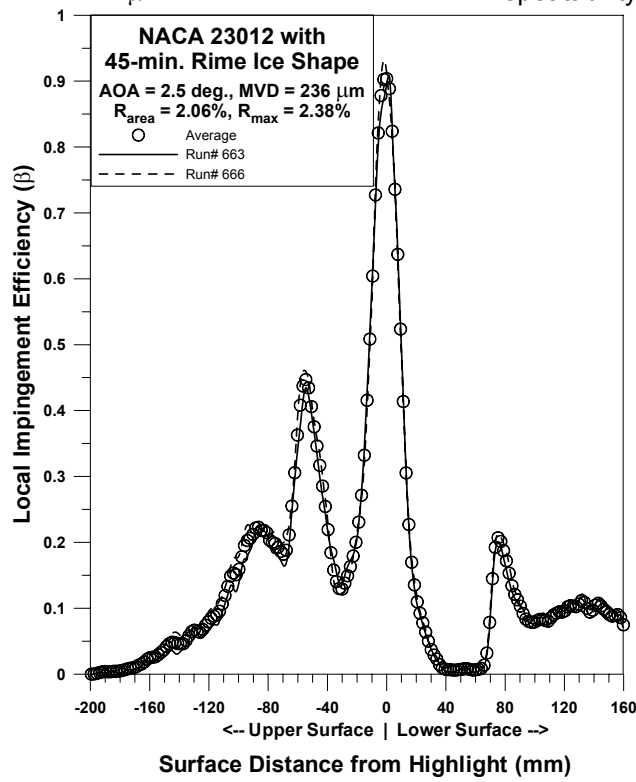


Figure 82e.—NACA 23012 with 45-min rime ice repeatability, MVD = 236  $\mu\text{m}$ .

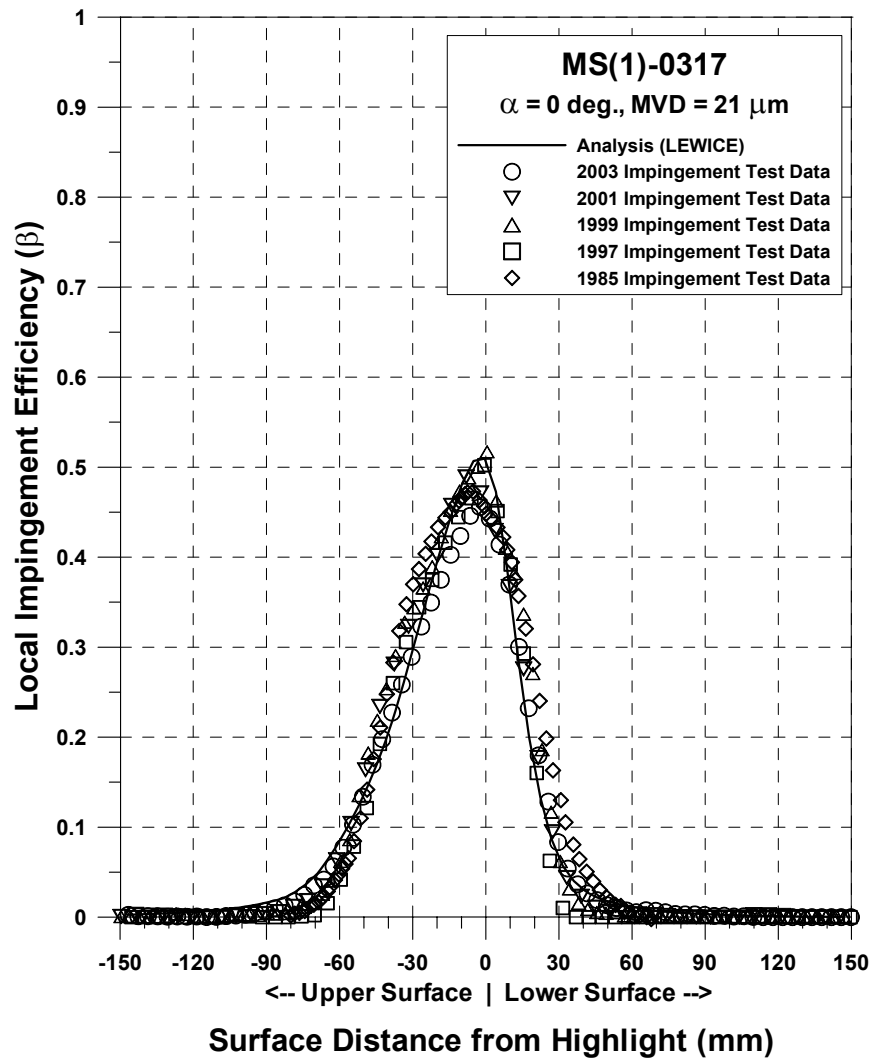


Figure 83.—Impingement efficiency distribution for MS-317 airfoil from 1985, 1997, 1999, 2001 and 2003 entries;  
 $c = 36\text{-in.}$ ,  $V_\infty = 175 \text{ mph}$ ,  $\text{AOA} = 0^\circ$ ,  $\text{MVD} = 20\text{--}21 \mu\text{m}$ .

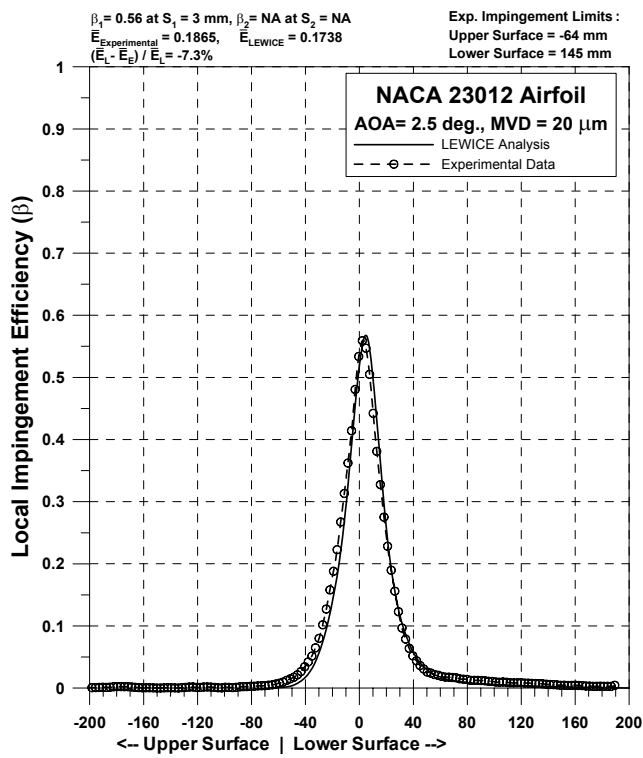


Figure 84a.—Impingement efficiency distribution for NACA 23012 airfoil;  
 $c = 36\text{-in.}$ ,  $V_\infty = 175$  mph, AOA =  $2.5^\circ$ , MVD = 20  $\mu\text{m}$ .

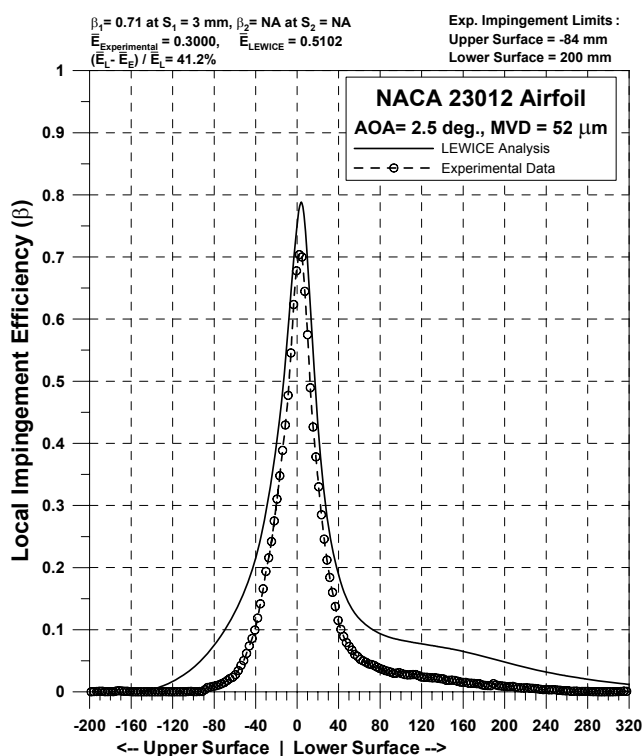


Figure 84b.—Impingement efficiency distribution for NACA 23012 airfoil;  
 $c = 36\text{-in.}$ ,  $V_\infty = 175$  mph, AOA =  $2.5^\circ$ , MVD = 52  $\mu\text{m}$ .

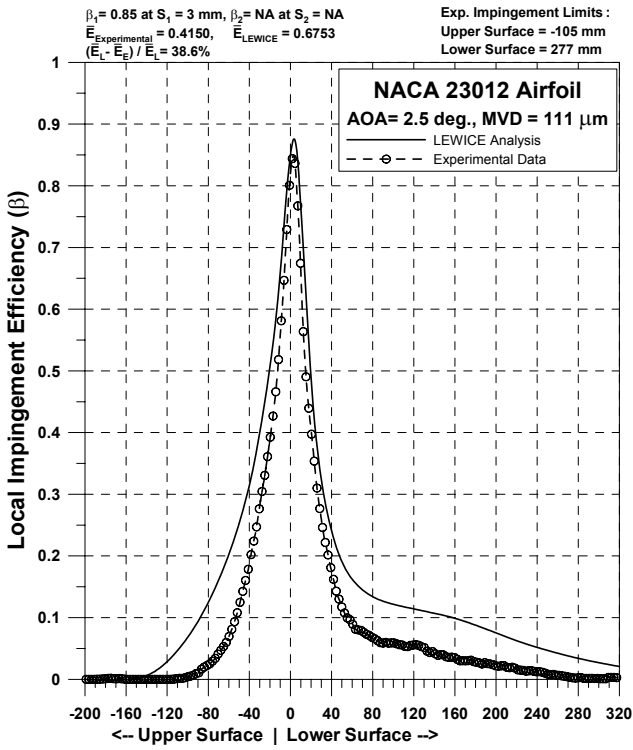


Figure 84c.—Impingement efficiency distribution for NACA 23012 airfoil;  
 $c = 36\text{-in.}$ ,  $V_\infty = 175$  mph, AOA =  $2.5^\circ$ , MVD = 111  $\mu\text{m}$ .

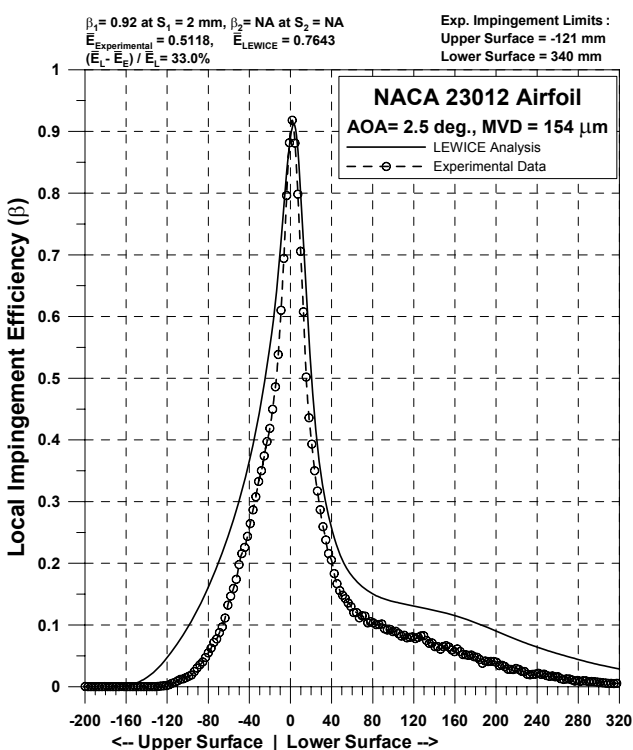


Figure 84d.—Impingement efficiency distribution for NACA 23012 airfoil;  
 $c = 36\text{-in.}$ ,  $V_\infty = 175$  mph, AOA =  $2.5^\circ$ , MVD = 154  $\mu\text{m}$ .

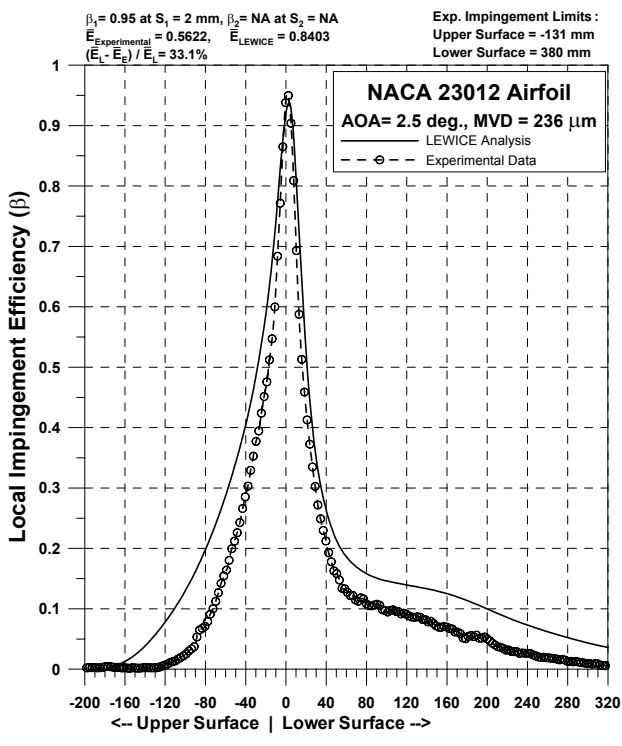


Figure 84e.—Impingement efficiency distribution for NACA 23012 airfoil;  
 $c = 36\text{-in.}$ ,  $V_\infty = 175$  mph, AOA =  $2.5^\circ$ , MVD =  $236 \mu\text{m}$ .

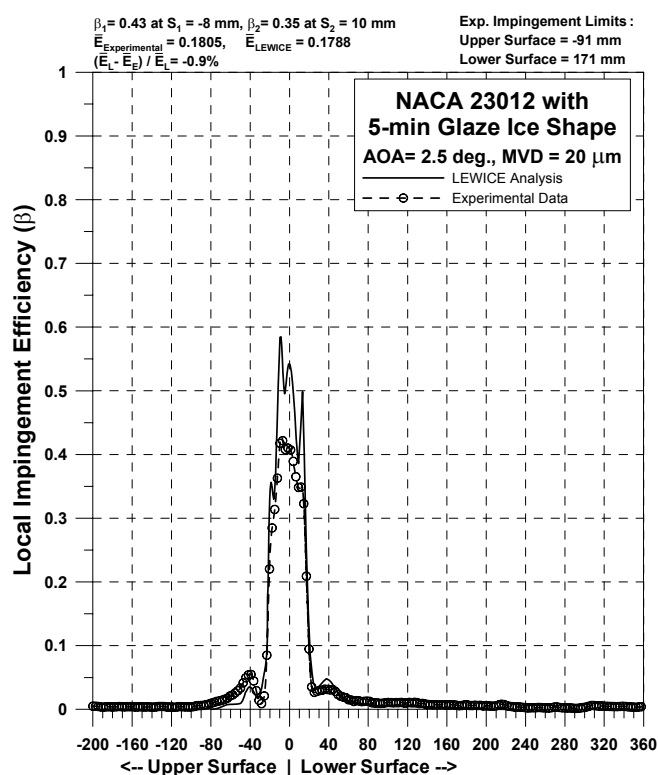


Figure 85a.—Impingement efficiency distribution for NACA 23012 airfoil with 5-min glaze ice shape;  $c = 36\text{-in.}$ ,  $V_\infty = 175$  mph, AOA =  $2.5^\circ$ , MVD =  $20 \mu\text{m}$ .

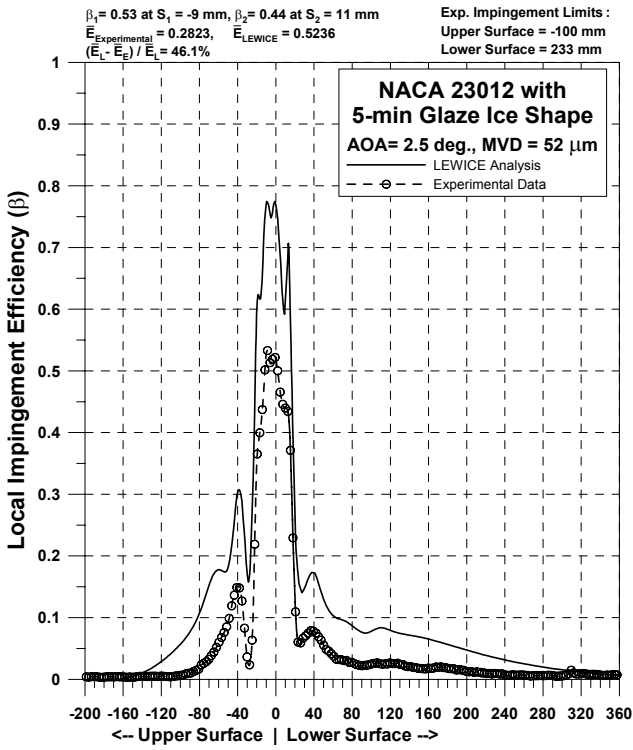


Figure 85b.—Impingement efficiency distribution for NACA 23012 airfoil with 5-min glaze ice shape;  $c = 36$ -in.,  $V_\infty = 175$  mph, AOA = 2.5°, MVD = 52  $\mu\text{m}$ .

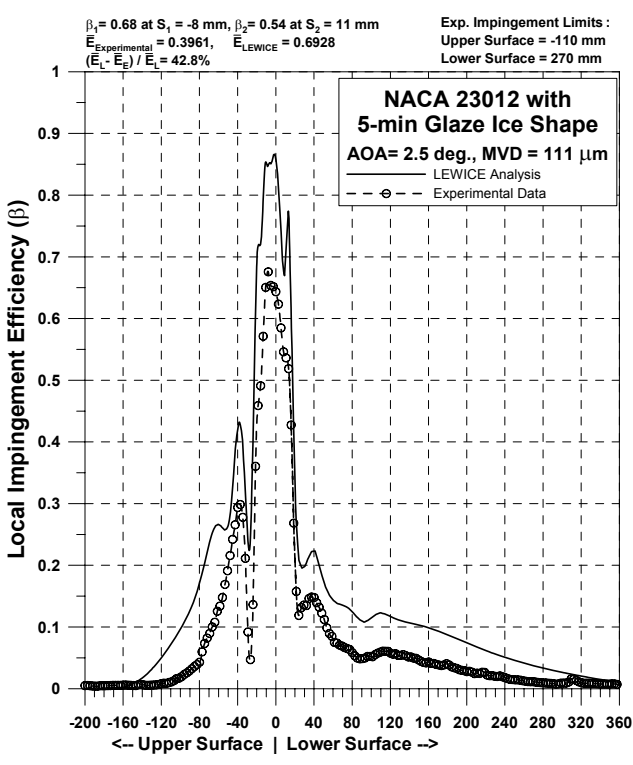


Figure 85c.—Impingement efficiency distribution for NACA 23012 airfoil with 5-min glaze ice shape;  $c = 36$ -in.,  $V_\infty = 175$  mph, AOA = 2.5°, MVD = 111  $\mu\text{m}$ .

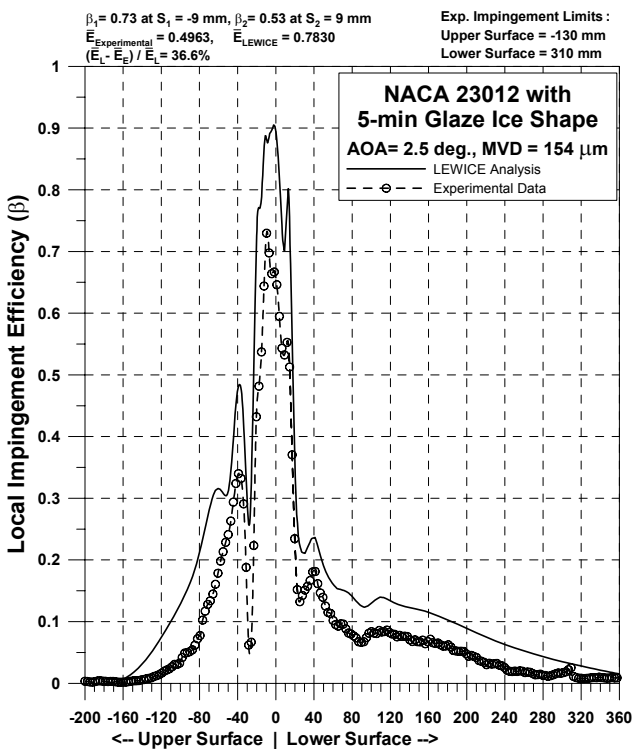


Figure 85d.—Impingement efficiency distribution for NACA 23012 airfoil with 5-min glaze ice shape;  $c = 36$ -in.,  $V_\infty = 175$  mph, AOA =  $2.5^\circ$ , MVD = 154  $\mu\text{m}$ .

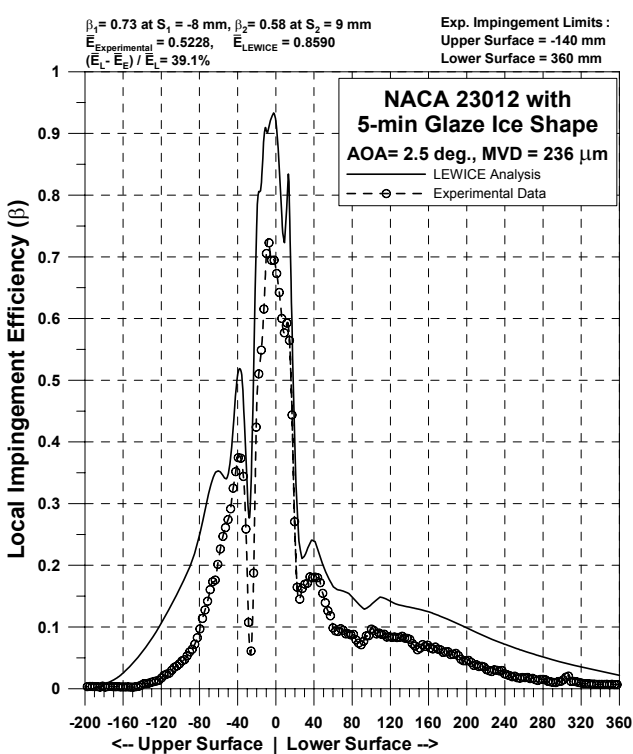


Figure 85e.—Impingement efficiency distribution for NACA 23012 airfoil with 5-min glaze ice shape;  $c = 36$ -in.,  $V_\infty = 175$  mph, AOA =  $2.5^\circ$ , MVD = 236  $\mu\text{m}$ .

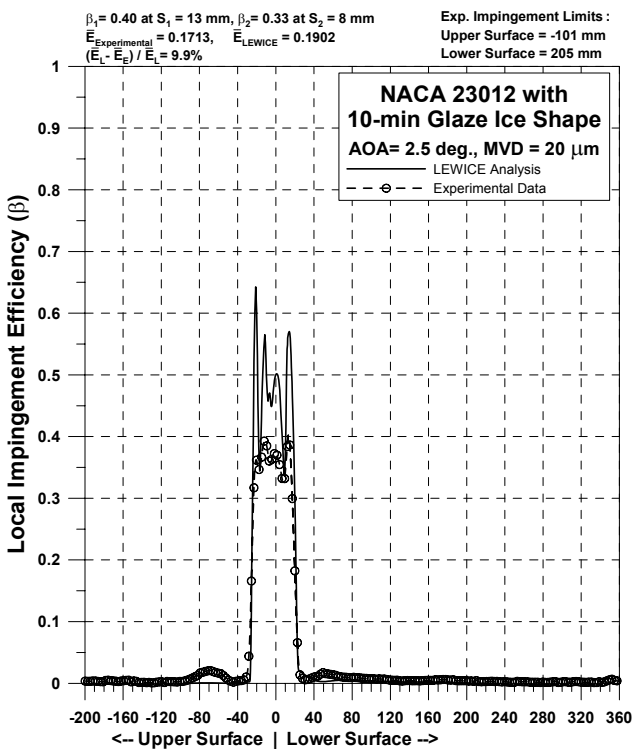


Figure 86a.—Impingement efficiency distribution for NACA 23012 airfoil with 10-min glaze ice shape;  $c = 36$ -in.,  $V_\infty = 175$  mph, AOA =  $2.5^\circ$ , MVD = 20  $\mu\text{m}$ .

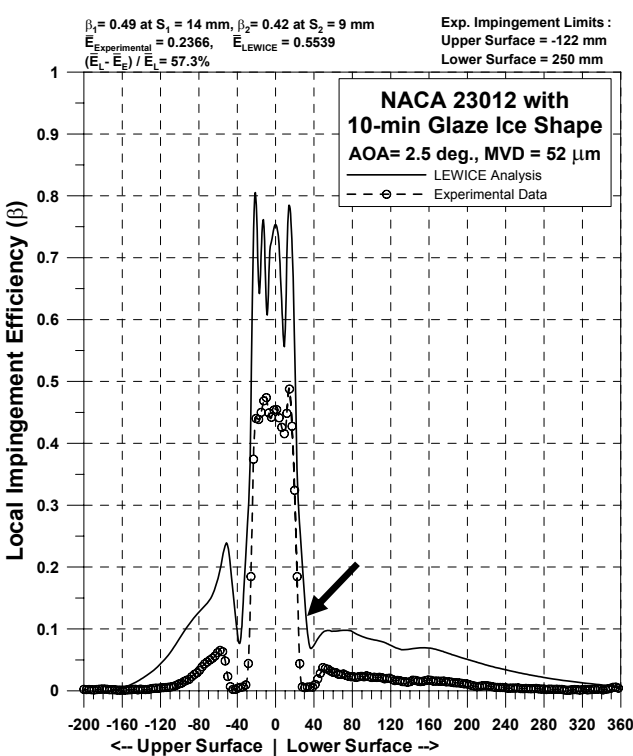


Figure 86b.—Impingement efficiency distribution for NACA 23012 airfoil with 10-min glaze ice shape;  $c = 36$ -in.,  $V_\infty = 175$  mph, AOA =  $2.5^\circ$ , MVD = 52  $\mu\text{m}$ .

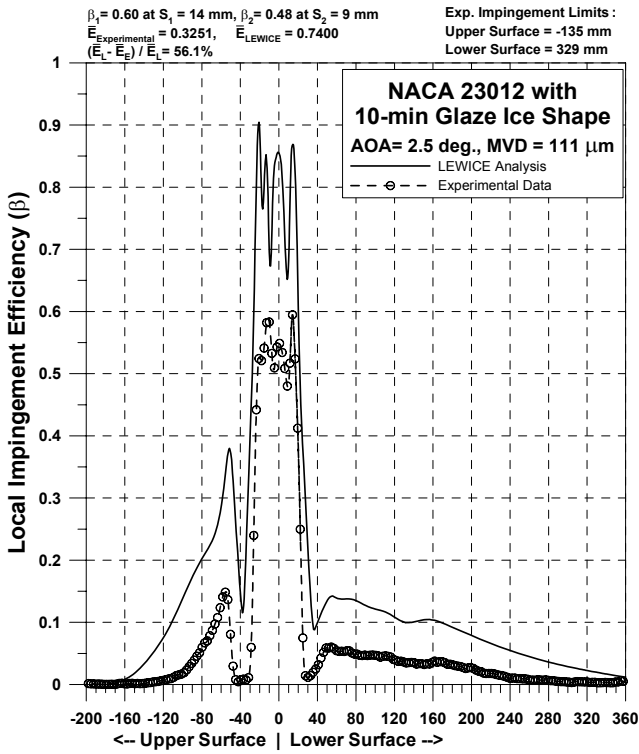


Figure 86c.—Impingement efficiency distribution for NACA 23012 airfoil with 10-min glaze ice shape;  $c = 36$ -in.,  $V_\infty = 175$  mph, AOA =  $2.5^\circ$ , MVD = 111  $\mu\text{m}$ .

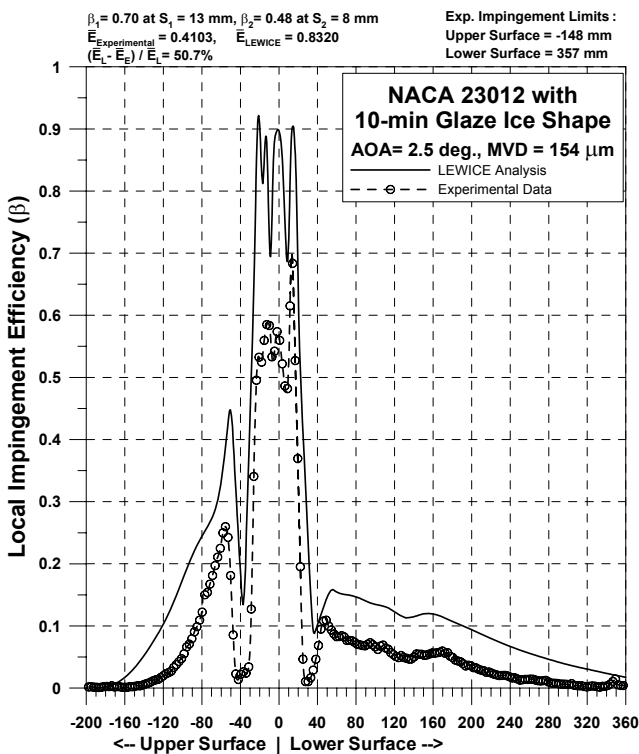


Figure 86d.—Impingement efficiency distribution for NACA 23012 airfoil with 10-min glaze ice shape;  $c = 36$ -in.,  $V_\infty = 175$  mph, AOA =  $2.5^\circ$ , MVD = 154  $\mu\text{m}$ .

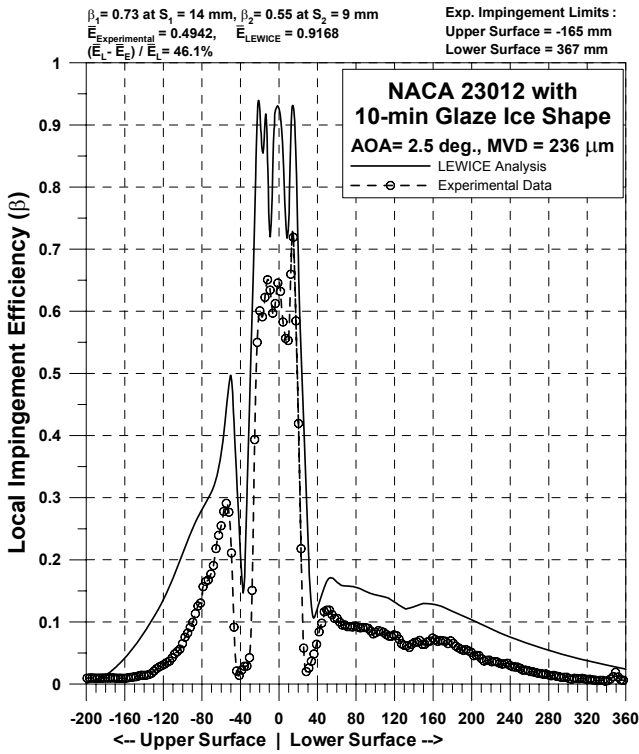


Figure 86e.—Impingement efficiency distribution for NACA 23012 airfoil with 10-min glaze ice shape;  $c = 36\text{-in.}$ ,  $V_\infty = 175 \text{ mph}$ ,  $\text{AOA} = 2.5^\circ$ ,  $\text{MVD} = 236 \mu\text{m}$ .

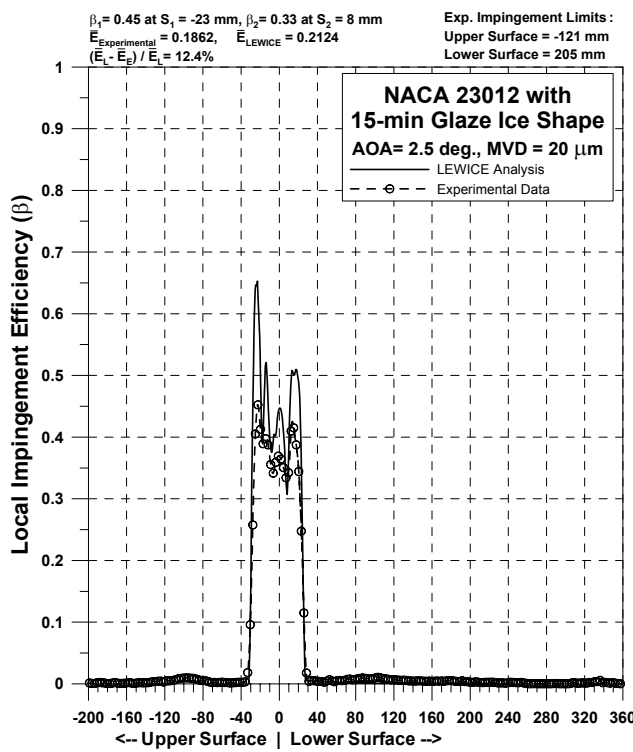


Figure 87a.—Impingement efficiency distribution for NACA 23012 airfoil with 15-min glaze ice shape;  $c = 36\text{-in.}$ ,  $V_\infty = 175 \text{ mph}$ ,  $\text{AOA} = 2.5^\circ$ ,  $\text{MVD} = 20 \mu\text{m}$ .

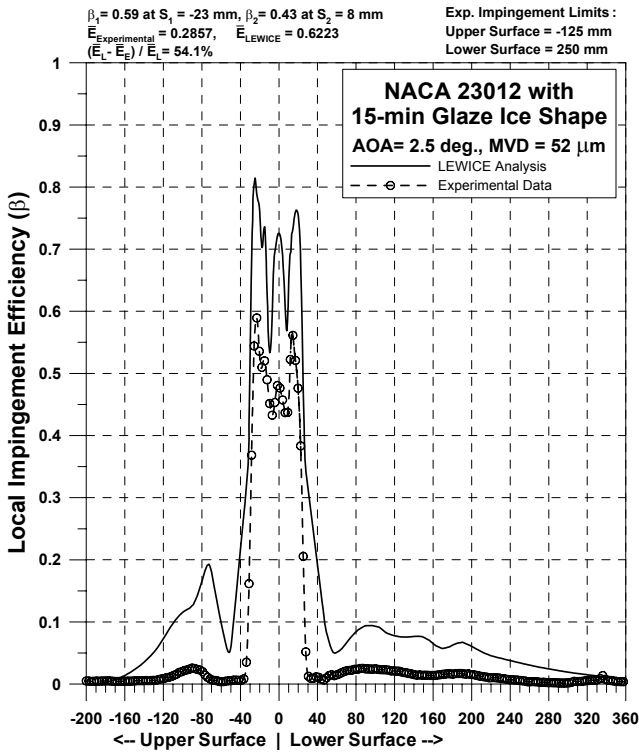


Figure 87b.—Impingement efficiency distribution for NACA 23012 airfoil with 15-min glaze ice shape;  $c = 36\text{-in.}$ ,  $V_\infty = 175 \text{ mph}$ ,  $\text{AOA} = 2.5^\circ$ ,  $\text{MVD} = 52 \mu\text{m}$ .

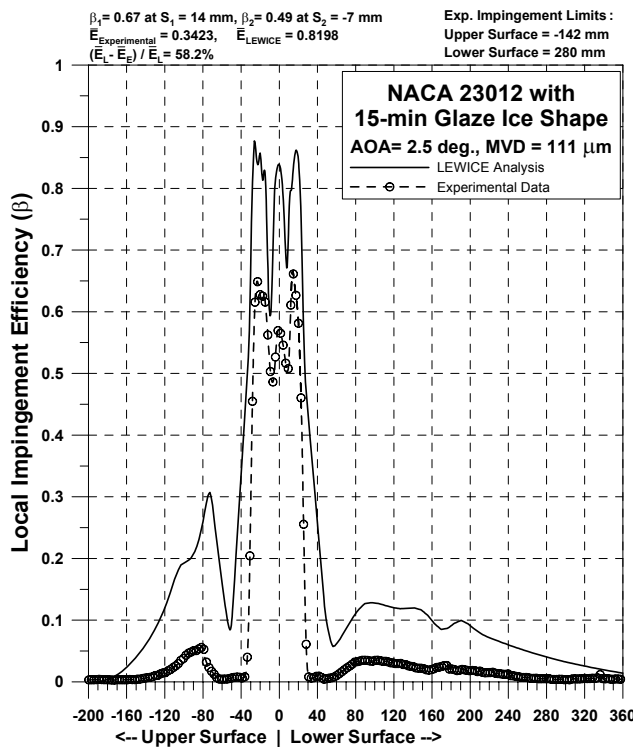


Figure 87c.—Impingement efficiency distribution for NACA 23012 airfoil with 15-min glaze ice shape;  $c = 36\text{-in.}$ ,  $V_\infty = 175 \text{ mph}$ ,  $\text{AOA} = 2.5^\circ$ ,  $\text{MVD} = 111 \mu\text{m}$ .

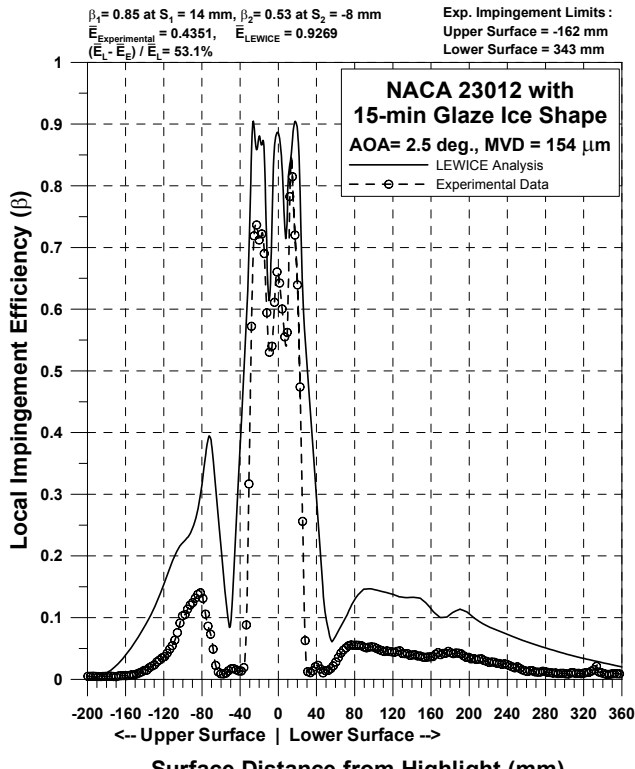


Figure 87d.—Impingement efficiency distribution for NACA 23012 airfoil with 15-min glaze ice shape;  $c = 36$ -in.,  $V_\infty = 175$  mph, AOA =  $2.5^\circ$ , MVD =  $154 \mu\text{m}$ .

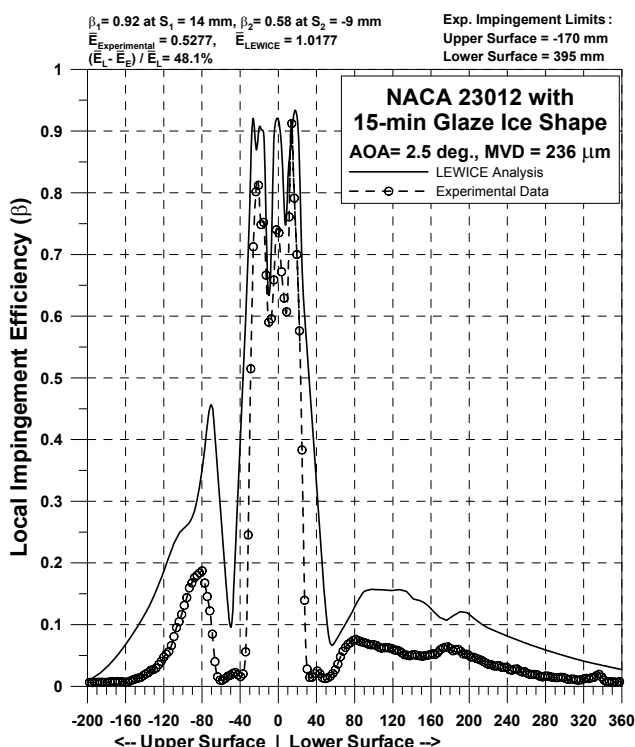


Figure 87e.—Impingement efficiency distribution for NACA 23012 airfoil with 15-min glaze ice shape;  $c = 36$ -in.,  $V_\infty = 175$  mph, AOA =  $2.5^\circ$ , MVD =  $236 \mu\text{m}$ .

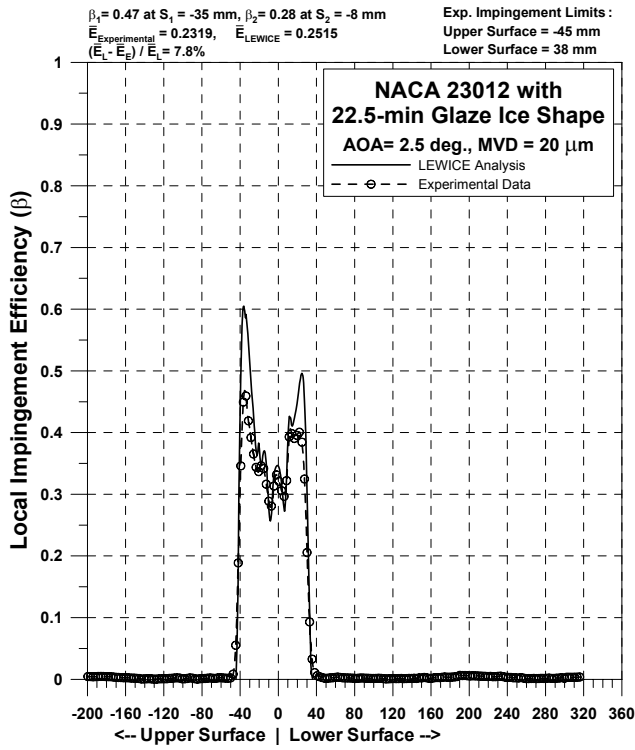


Figure 88a.—Impingement efficiency distribution for NACA 23012 airfoil with 22.5-min glaze ice shape;  $c = 36$ -in.,  $V_\infty = 175$  mph, AOA =  $2.5^\circ$ , MVD = 20  $\mu\text{m}$ .

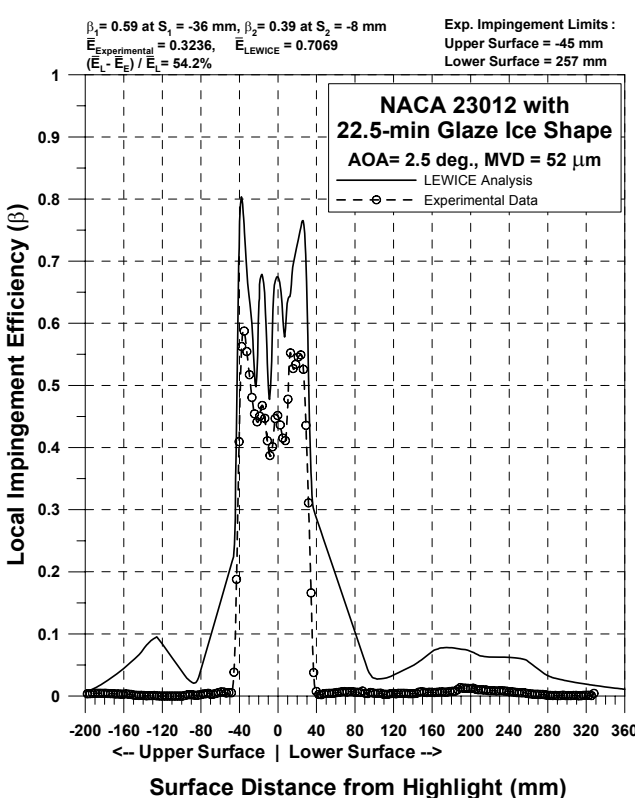


Figure 88b.—Impingement efficiency distribution for NACA 23012 airfoil with 22.5-min glaze ice shape;  $c = 36$ -in.,  $V_\infty = 175$  mph, AOA =  $2.5^\circ$ , MVD = 52  $\mu\text{m}$ .

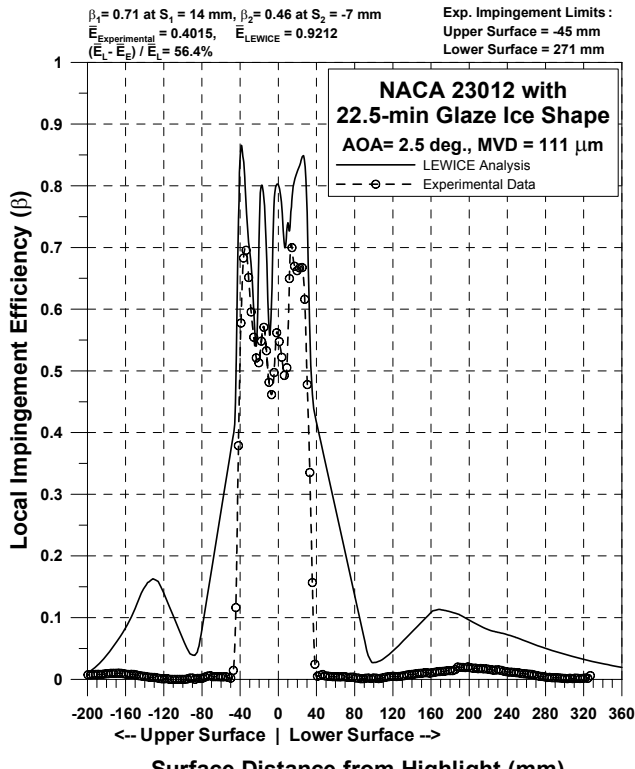


Figure 88c.—Impingement efficiency distribution for NACA 23012 airfoil with 22.5-min glaze ice shape;  $c = 36$ -in.,  $V_\infty = 175$  mph, AOA =  $2.5^\circ$ , MVD = 111  $\mu\text{m}$ .

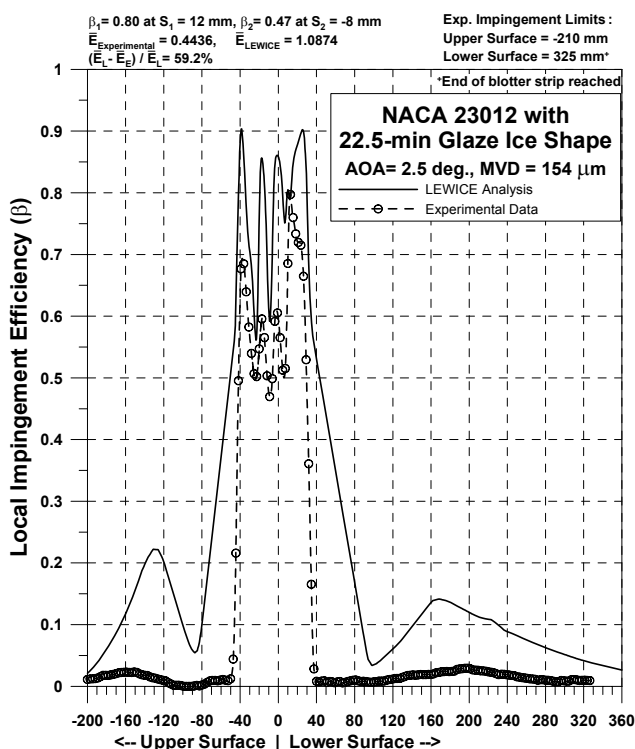


Figure 88d.—Impingement efficiency distribution for NACA 23012 airfoil with 22.5-min glaze ice shape;  $c = 36$ -in.,  $V_\infty = 175$  mph, AOA =  $2.5^\circ$ , MVD = 154  $\mu\text{m}$ .

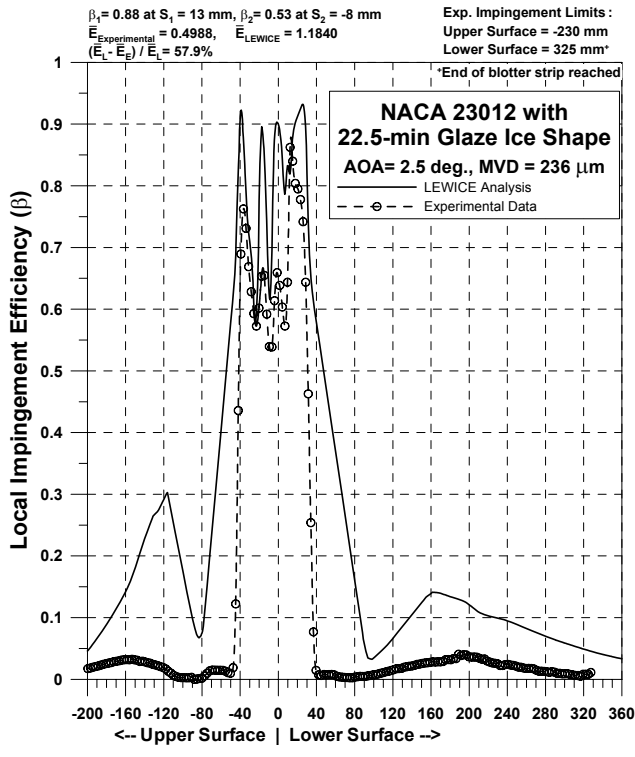


Figure 88e.—Impingement efficiency distribution for NACA 23012 airfoil with 22.5-min glaze ice shape;  $c = 36$ -in.,  $V_\infty = 175$  mph, AOA =  $2.5^\circ$ , MVD =  $236 \mu\text{m}$ .

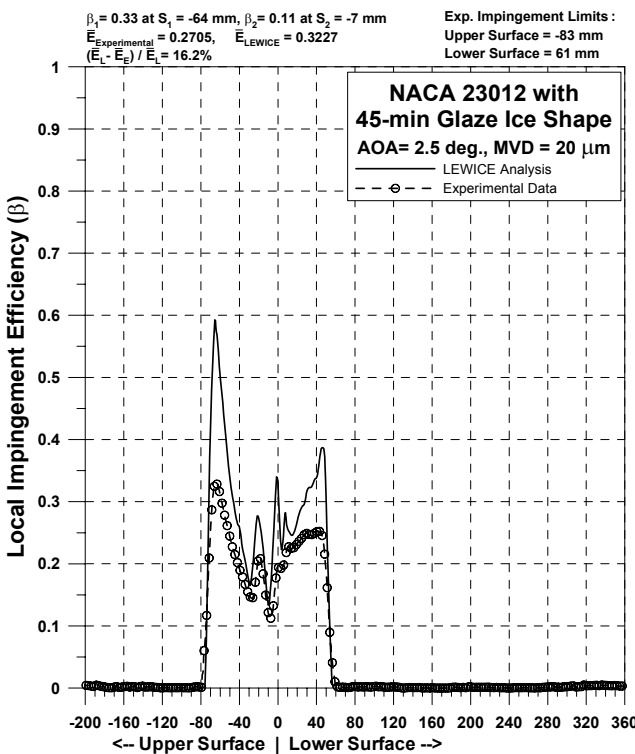


Figure 89a.—Impingement efficiency distribution for NACA 23012 airfoil with 45-min glaze ice shape;  $c = 36$ -in.,  $V_\infty = 175$  mph, AOA =  $2.5^\circ$ , MVD =  $20 \mu\text{m}$ .

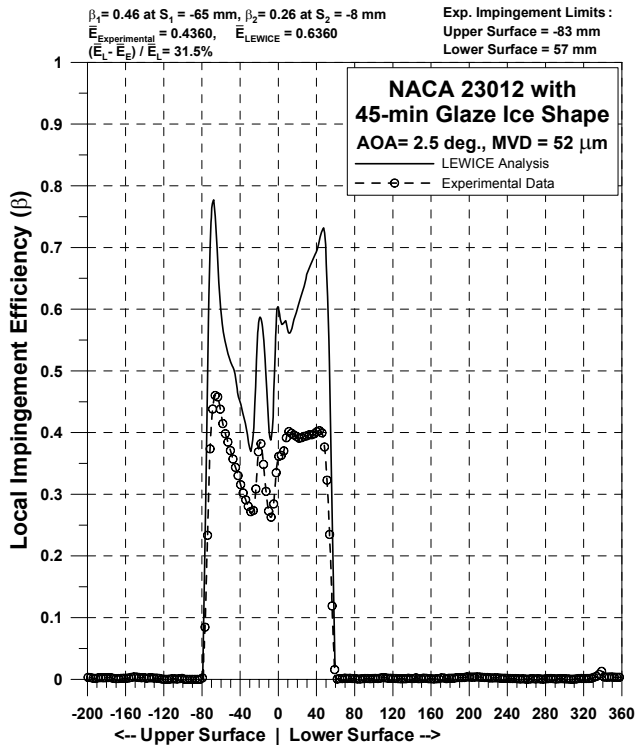


Figure 89b.—Impingement efficiency distribution for NACA 23012 airfoil with 45-min glaze ice shape;  $c = 36$ -in.,  $V_\infty = 175$  mph,  $\text{AOA} = 2.5^\circ$ ,  $\text{MVD} = 52 \mu\text{m}$ .

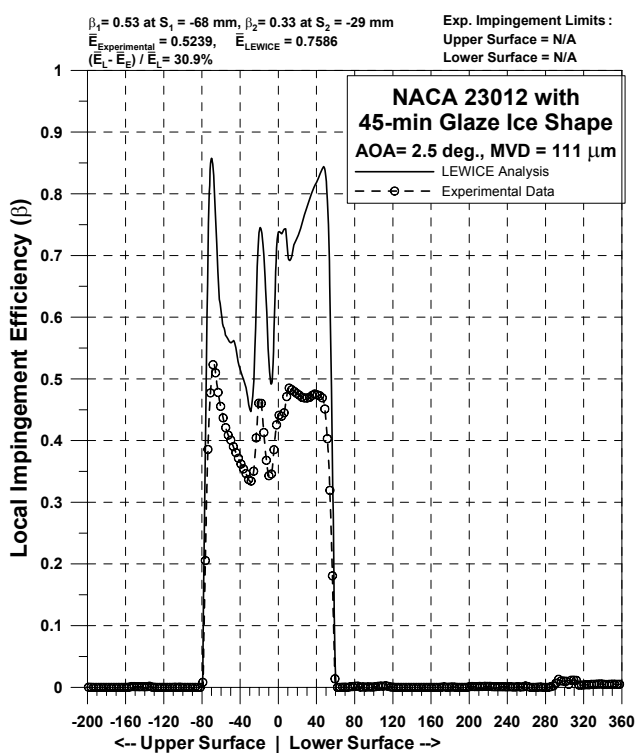


Figure 89c.—Impingement efficiency distribution for NACA 23012 airfoil with 45-min glaze ice shape;  $c = 36$ -in.,  $V_\infty = 175$  mph,  $\text{AOA} = 2.5^\circ$ ,  $\text{MVD} = 111 \mu\text{m}$ .

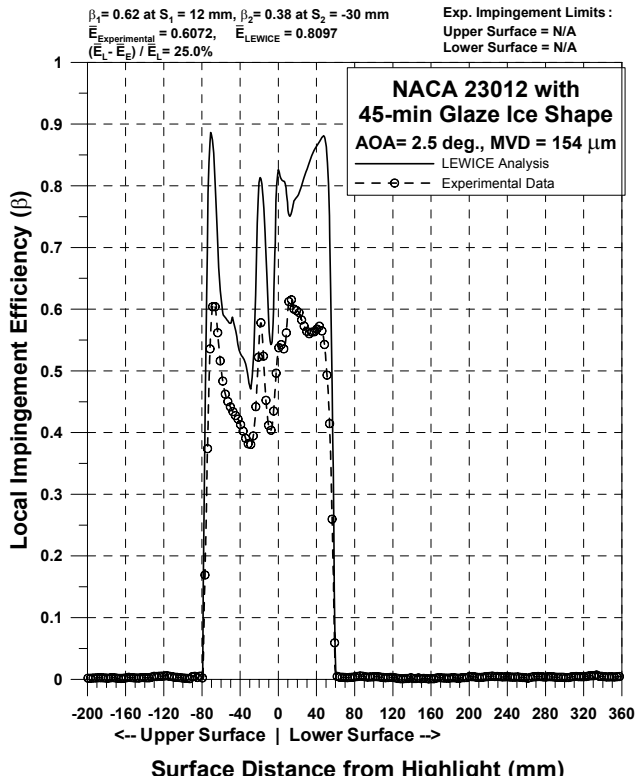


Figure 89d.—Impingement efficiency distribution for NACA 23012 airfoil with 45-min glaze ice shape;  $c = 36\text{-in.}$ ,  $V_\infty = 175 \text{ mph}$ , AOA =  $2.5^\circ$ , MVD =  $154 \mu\text{m}$ .

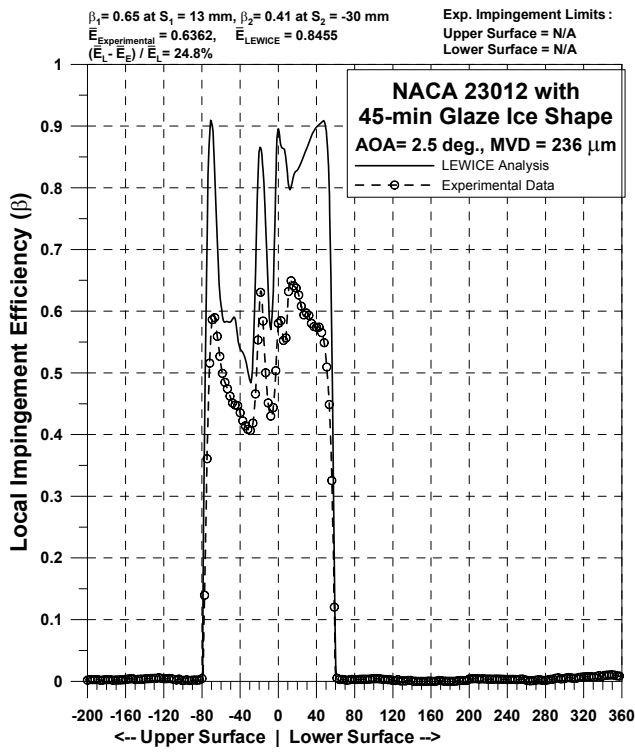


Figure 89e.—Impingement efficiency distribution for NACA 23012 airfoil with 45-min glaze ice shape;  $c = 36\text{-in.}$ ,  $V_\infty = 175 \text{ mph}$ , AOA =  $2.5^\circ$ , MVD =  $236 \mu\text{m}$ .

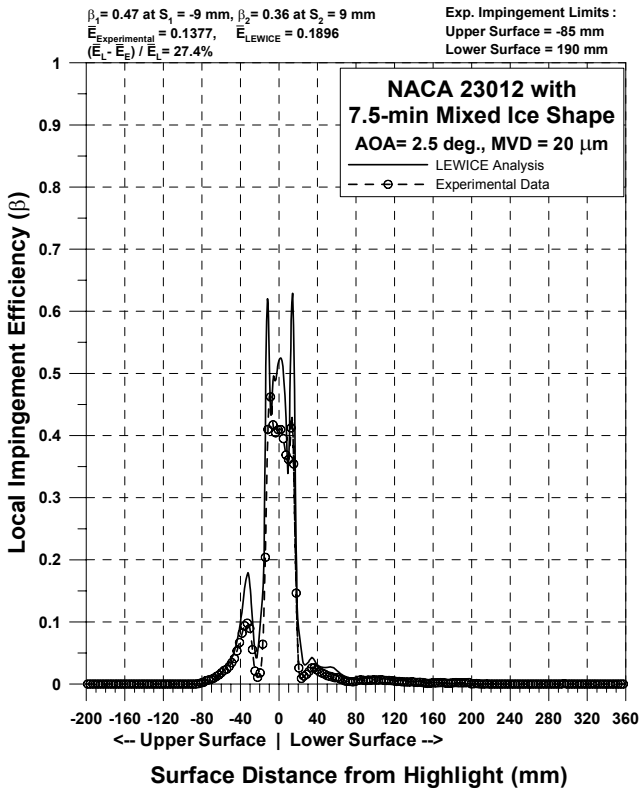


Figure 90a.—Impingement efficiency distribution for NACA 23012 airfoil with 7.5-min mixed ice shape;  $c = 36$ -in.,  $V_\infty = 175$  mph, AOA =  $2.5^\circ$ , MVD = 20  $\mu\text{m}$ .

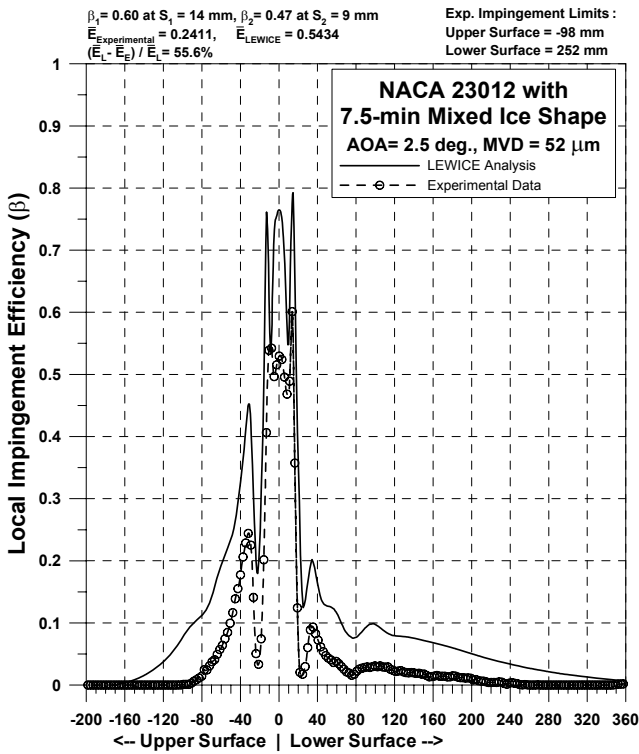


Figure 90b.—Impingement efficiency distribution for NACA 23012 airfoil with 7.5-min mixed ice shape;  $c = 36$ -in.,  $V_\infty = 175$  mph, AOA =  $2.5^\circ$ , MVD = 52  $\mu\text{m}$ .

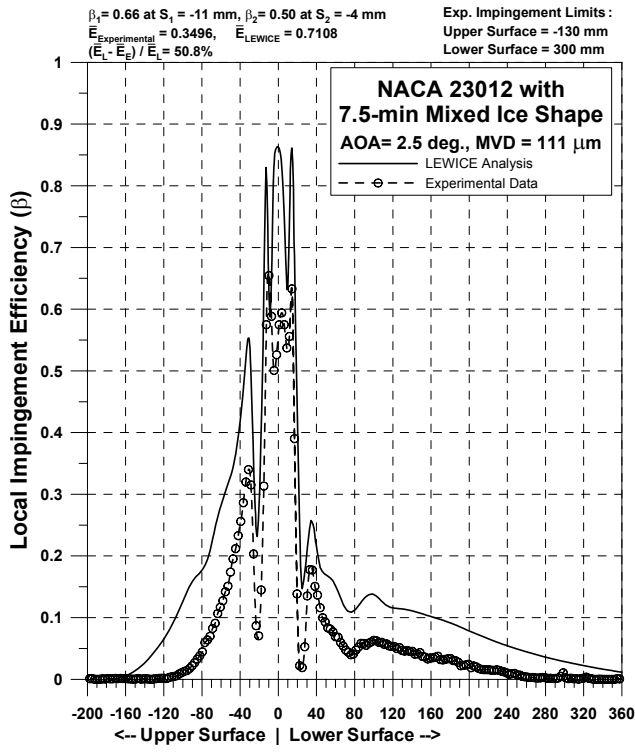


Figure 90c.—Impingement efficiency distribution for NACA 23012 airfoil with 7.5-min mixed ice shape;  $c = 36\text{-in.}$ ,  $V_\infty = 175 \text{ mph}$ ,  $\text{AOA} = 2.5^\circ$ ,  $\text{MVD} = 111 \mu\text{m}$ .

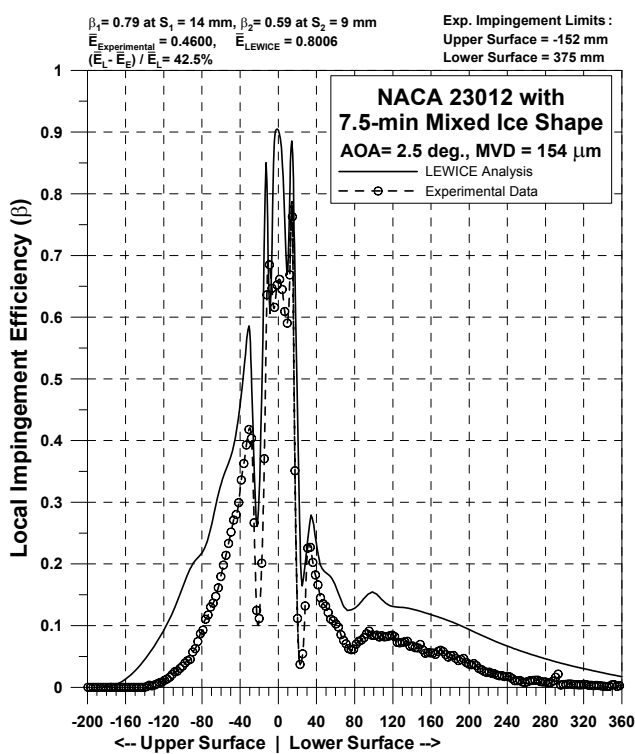


Figure 90d.—Impingement efficiency distribution for NACA 23012 airfoil with 7.5-min mixed ice shape;  $c = 36\text{-in.}$ ,  $V_\infty = 175 \text{ mph}$ ,  $\text{AOA} = 2.5^\circ$ ,  $\text{MVD} = 154 \mu\text{m}$ .

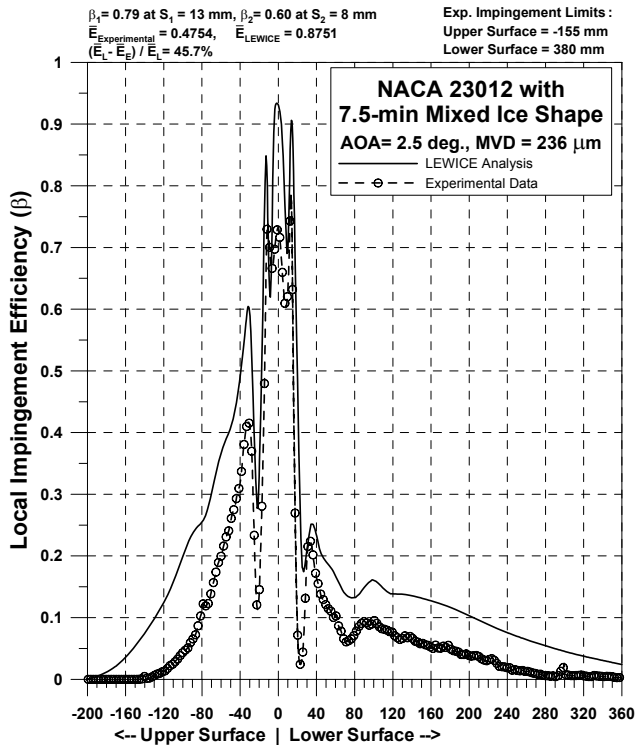


Figure 90e.—Impingement efficiency distribution for NACA 23012 airfoil with 7.5-min mixed ice shape;  $c = 36$ -in.,  $V_\infty = 175$  mph, AOA =  $2.5^\circ$ , MVD = 236  $\mu\text{m}$ .

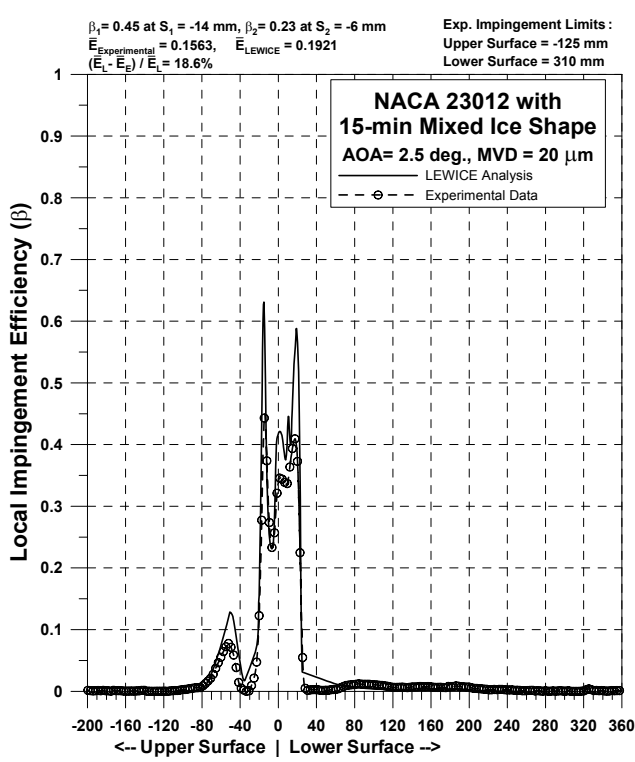


Figure 91a.—Impingement efficiency distribution for NACA 23012 airfoil with 15-min mixed ice shape;  $c = 36$ -in.,  $V_\infty = 175$  mph, AOA =  $2.5^\circ$ , MVD = 20  $\mu\text{m}$ .

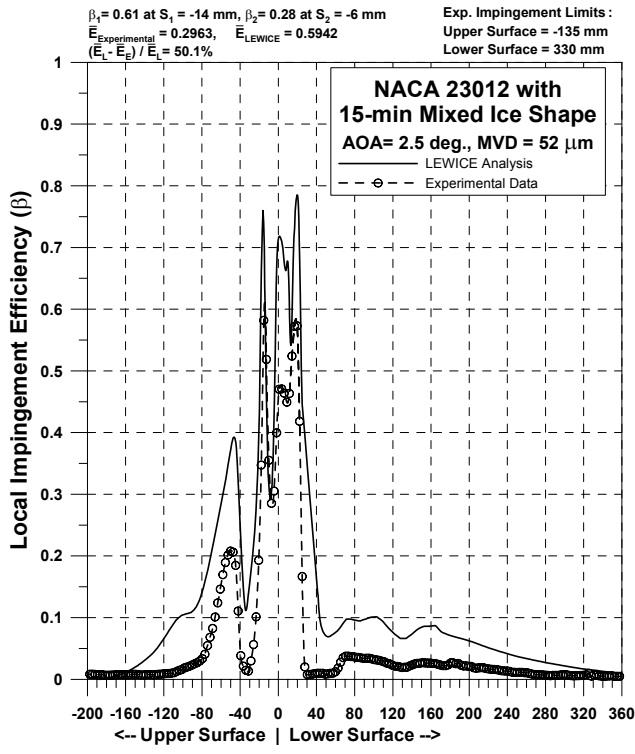


Figure 91b.—Impingement efficiency distribution for NACA 23012 airfoil with 15-min mixed ice shape;  $c = 36\text{-in.}$ ,  $V_\infty = 175 \text{ mph}$ ,  $\text{AOA} = 2.5^\circ$ ,  $\text{MVD} = 52 \mu\text{m}$ .

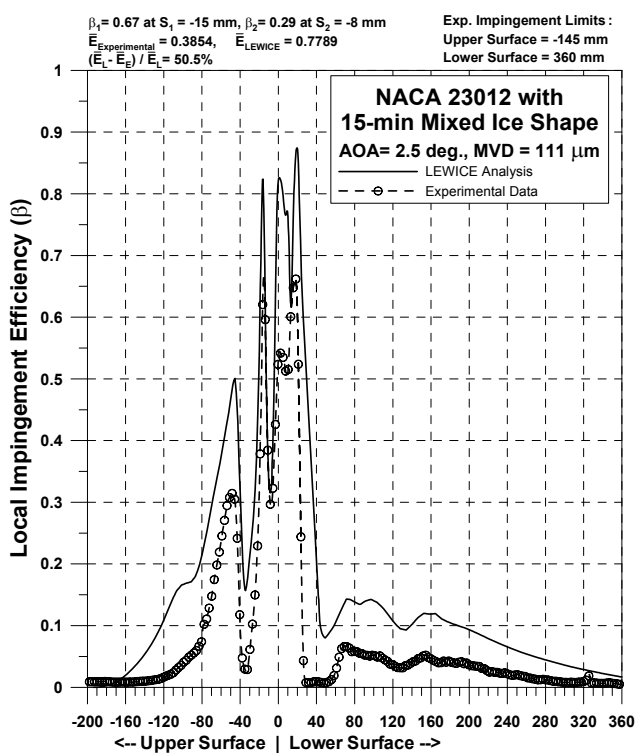


Figure 91c.—Impingement efficiency distribution for NACA 23012 airfoil with 15-min mixed ice shape;  $c = 36\text{-in.}$ ,  $V_\infty = 175 \text{ mph}$ ,  $\text{AOA} = 2.5^\circ$ ,  $\text{MVD} = 111 \mu\text{m}$ .

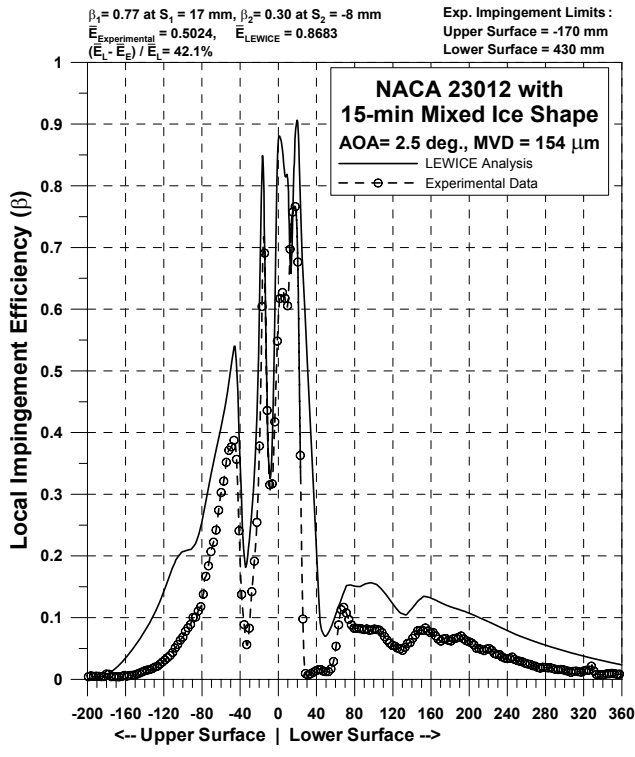


Figure 91d.—Impingement efficiency distribution for NACA 23012 airfoil with 15-min mixed ice shape;  $c = 36\text{-in.}$ ,  $V_\infty = 175 \text{ mph}$ ,  $\text{AOA} = 2.5^\circ$ ,  $\text{MVD} = 154 \mu\text{m}$ .

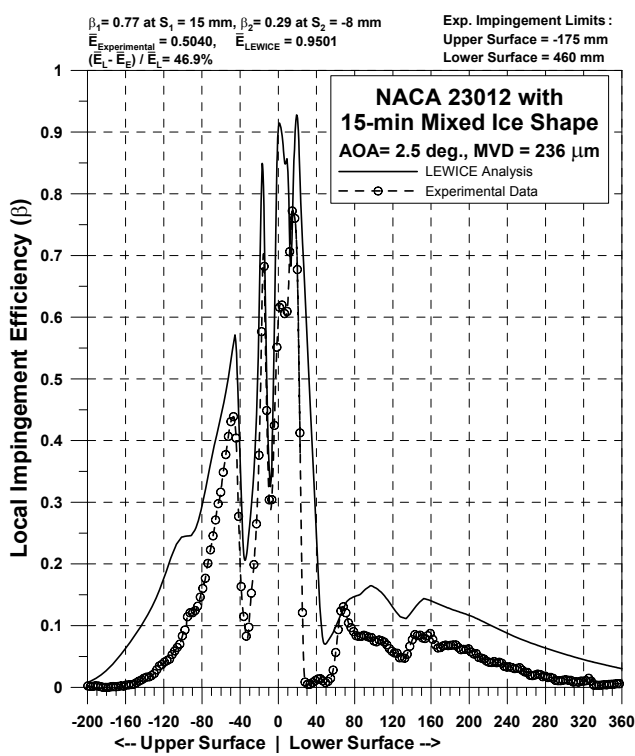


Figure 91e.—Impingement efficiency distribution for NACA 23012 airfoil with 15-min mixed ice shape;  $c = 36\text{-in.}$ ,  $V_\infty = 175 \text{ mph}$ ,  $\text{AOA} = 2.5^\circ$ ,  $\text{MVD} = 236 \mu\text{m}$ .

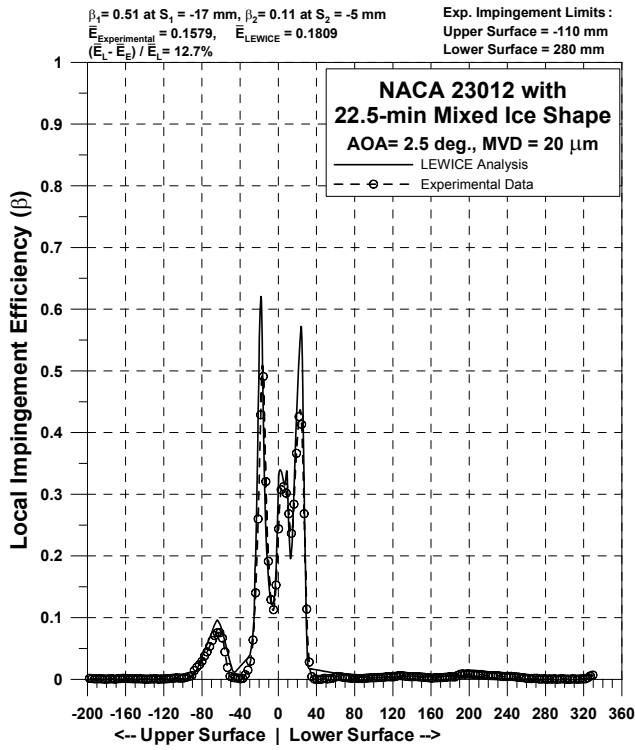


Figure 92a.—Impingement efficiency distribution for NACA 23012 airfoil with 22.5-min mixed ice shape;  $c = 36$ -in.,  $V_\infty = 175$  mph, AOA =  $2.5^\circ$ , MVD = 20  $\mu\text{m}$ .

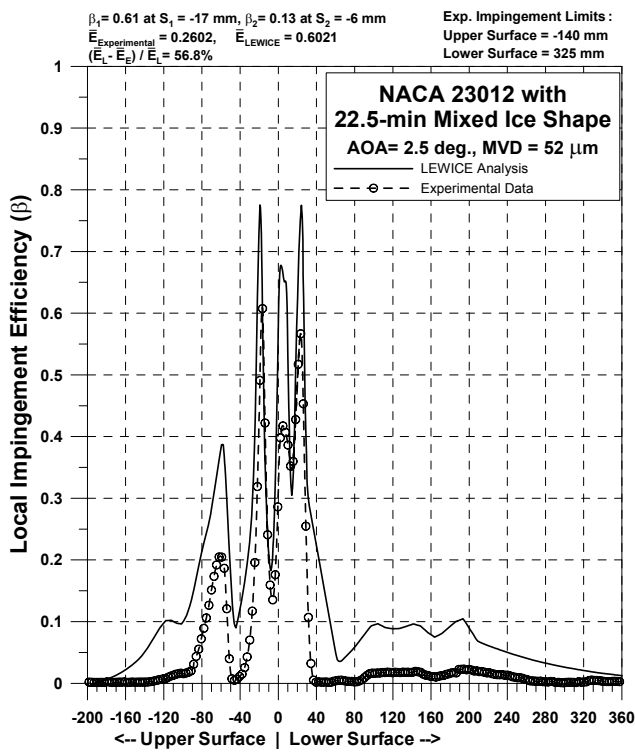


Figure 92b.—Impingement efficiency distribution for NACA 23012 airfoil with 22.5-min mixed ice shape;  $c = 36$ -in.,  $V_\infty = 175$  mph, AOA =  $2.5^\circ$ , MVD = 52  $\mu\text{m}$ .

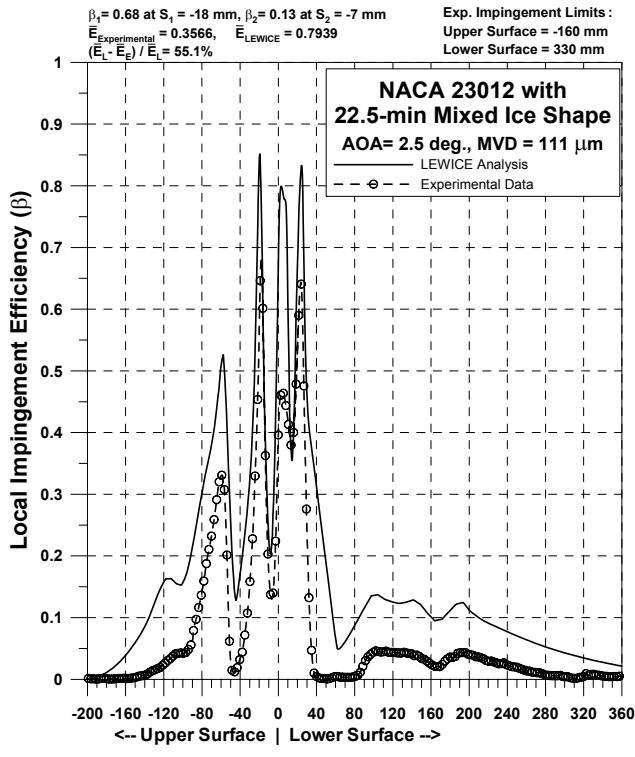


Figure 92c.—Impingement efficiency distribution for NACA 23012 airfoil with 22.5-min mixed ice shape;  $c = 36$ -in.,  $V_\infty = 175$  mph, AOA =  $2.5^\circ$ , MVD = 111  $\mu\text{m}$ .

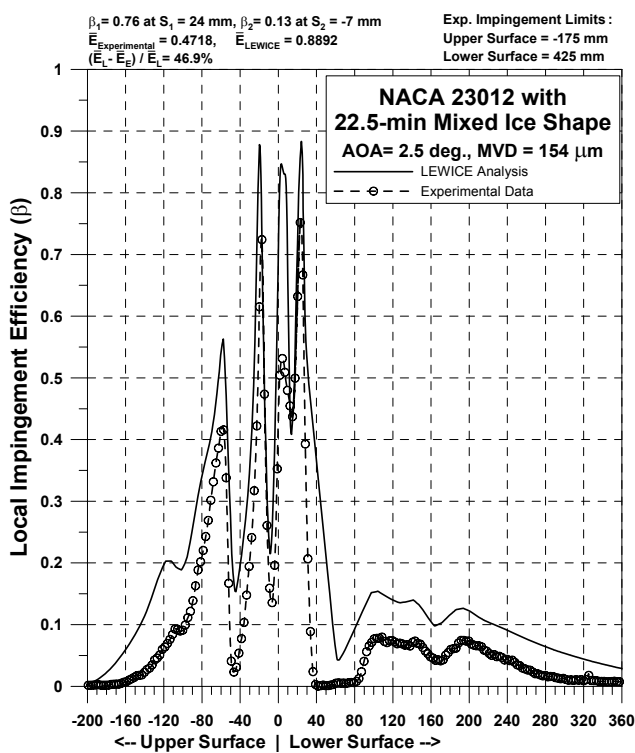


Figure 92d.—Impingement efficiency distribution for NACA 23012 airfoil with 22.5-min mixed ice shape;  $c = 36$ -in.,  $V_\infty = 175$  mph, AOA =  $2.5^\circ$ , MVD = 154  $\mu\text{m}$ .

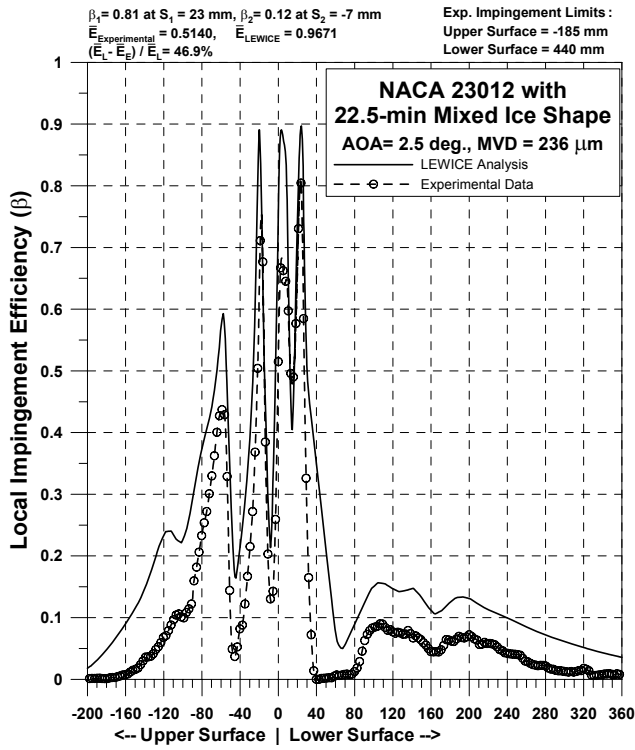


Figure 92e.—Impingement efficiency distribution for NACA 23012 airfoil with 22.5-min mixed ice shape;  $c = 36$ -in.,  $V_\infty = 175$  mph, AOA =  $2.5^\circ$ , MVD = 236  $\mu\text{m}$ .

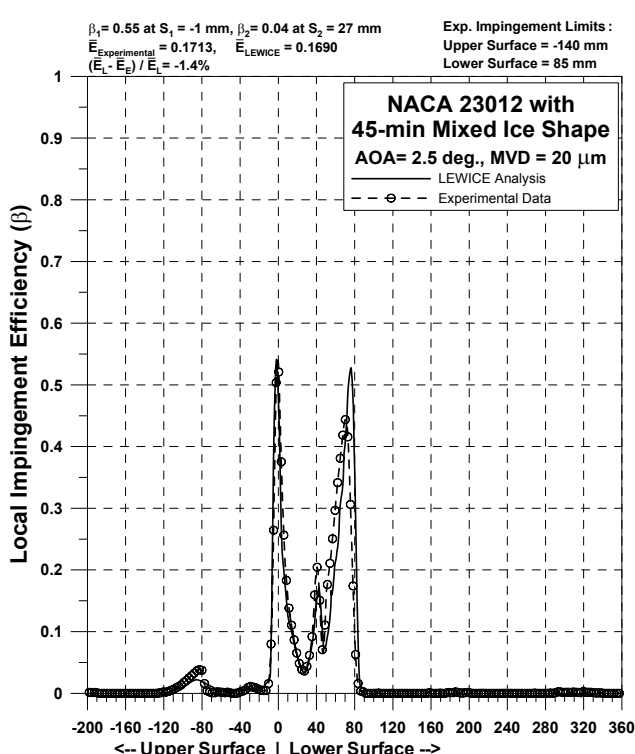


Figure 93a.—Impingement efficiency distribution for NACA 23012 airfoil with 45-min mixed ice shape;  $c = 36$ -in.,  $V_\infty = 175$  mph, AOA =  $2.5^\circ$ , MVD = 20  $\mu\text{m}$ .

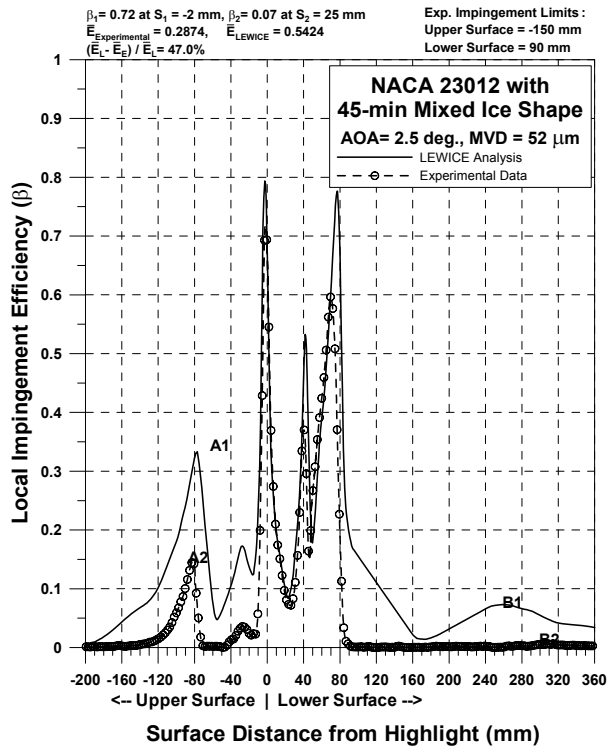


Figure 93b.—Impingement efficiency distribution for NACA 23012 airfoil with 45-min mixed ice shape;  $c = 36$ -in.,  $V_\infty = 175$  mph, AOA =  $2.5^\circ$ , MVD =  $52 \mu\text{m}$ .

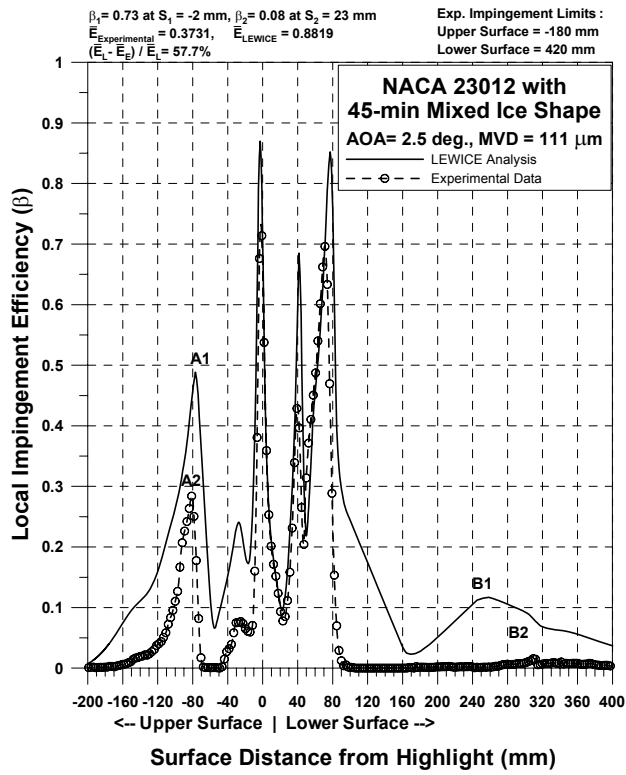


Figure 93c.—Impingement efficiency distribution for NACA 23012 airfoil with 45-min mixed ice shape;  $c = 36$ -in.,  $V_\infty = 175$  mph, AOA =  $2.5^\circ$ , MVD =  $111 \mu\text{m}$ .

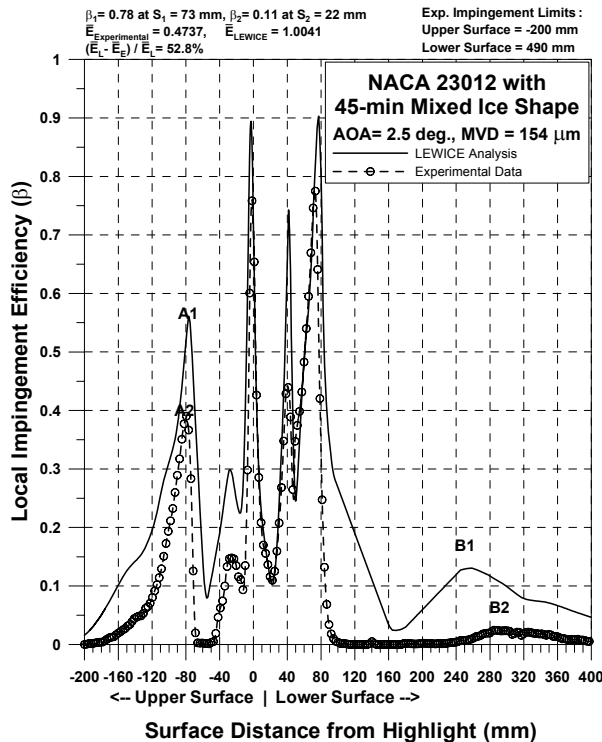


Figure 93d.—Impingement efficiency distribution for NACA 23012 airfoil with 45-min mixed ice shape;  $c = 36$ -in.,  $V_\infty = 175$  mph, AOA =  $2.5^\circ$ , MVD =  $154 \mu\text{m}$ .

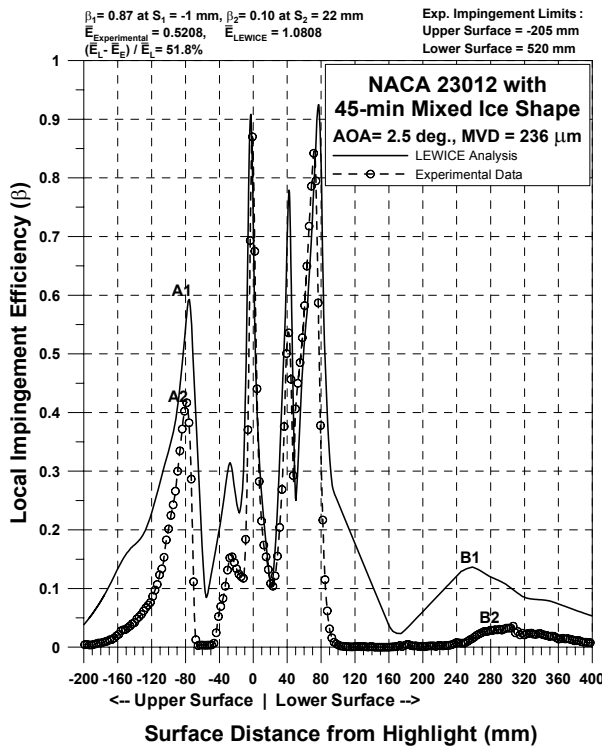


Figure 93e.—Impingement efficiency distribution for NACA 23012 airfoil with 45-min mixed ice shape;  $c = 36$ -in.,  $V_\infty = 175$  mph, AOA =  $2.5^\circ$ , MVD =  $236 \mu\text{m}$ .

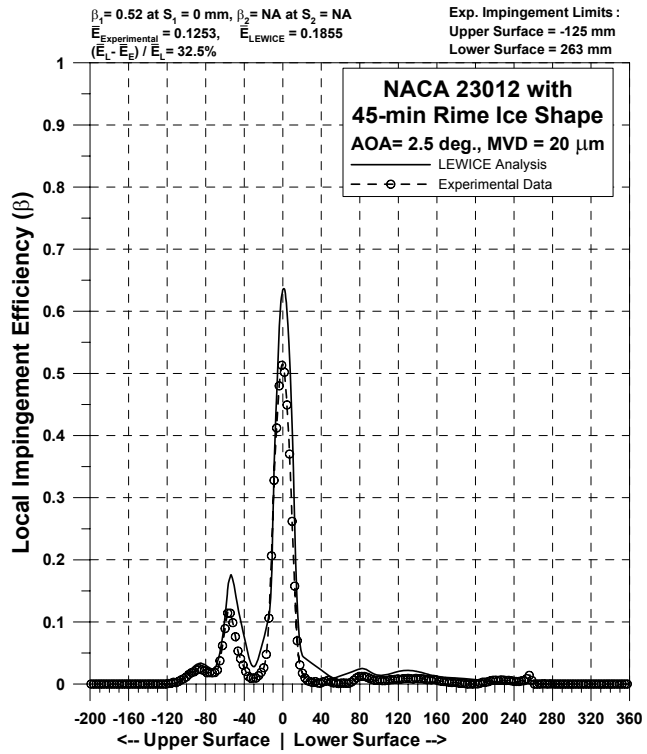


Figure 94a.—Impingement efficiency distribution for NACA 23012 airfoil with 45-min rime ice shape;  $c = 36$ -in.,  $V_\infty = 175$  mph, AOA =  $2.5^\circ$ , MVD = 20  $\mu\text{m}$ .

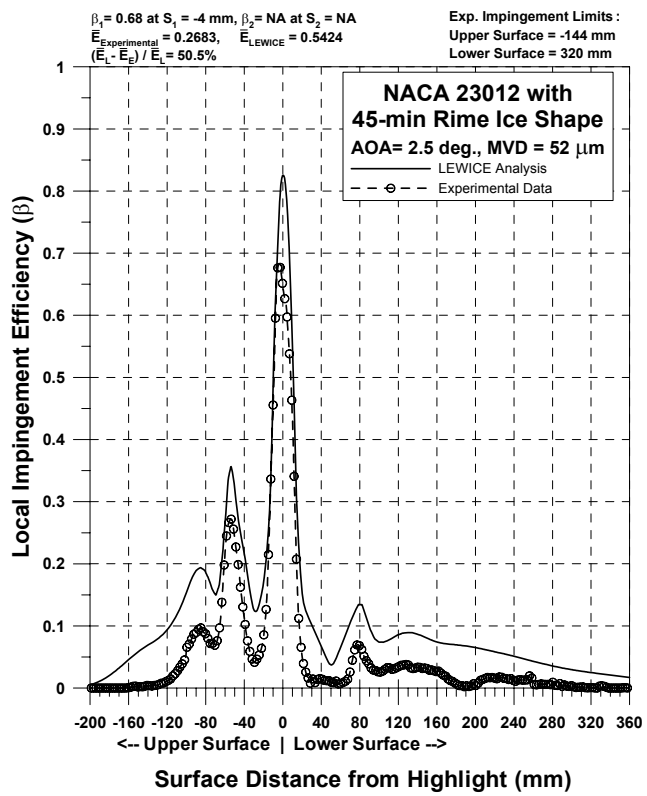


Figure 94b.—Impingement efficiency distribution for NACA 23012 airfoil with 45-min rime ice shape;  $c = 36$ -in.,  $V_\infty = 175$  mph, AOA =  $2.5^\circ$ , MVD = 52  $\mu\text{m}$ .

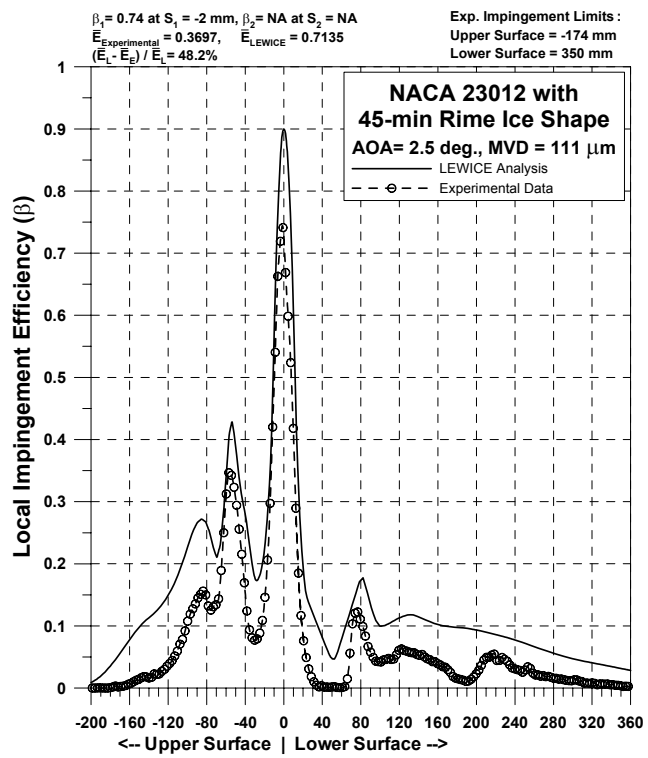


Figure 94c.—Impingement efficiency distribution for NACA 23012 airfoil with 45-min rime ice shape;  $c = 36\text{-in.}$ ,  $V_\infty = 175$  mph,  $\text{AOA} = 2.5^\circ$ ,  $\text{MVD} = 111 \mu\text{m}$ .

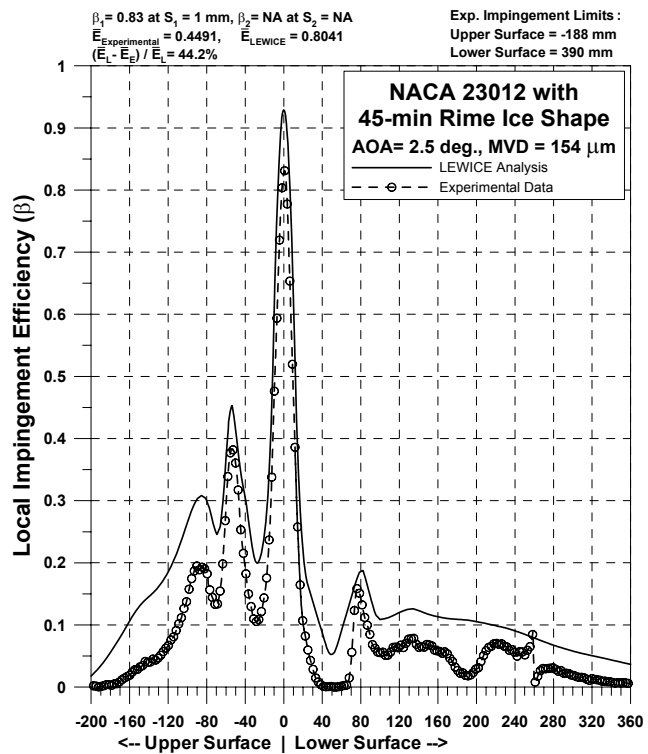


Figure 94d.—Impingement efficiency distribution for NACA 23012 airfoil with 45-min rime ice shape;  $c = 36\text{-in.}$ ,  $V_\infty = 175$  mph,  $\text{AOA} = 2.5^\circ$ ,  $\text{MVD} = 154 \mu\text{m}$ .

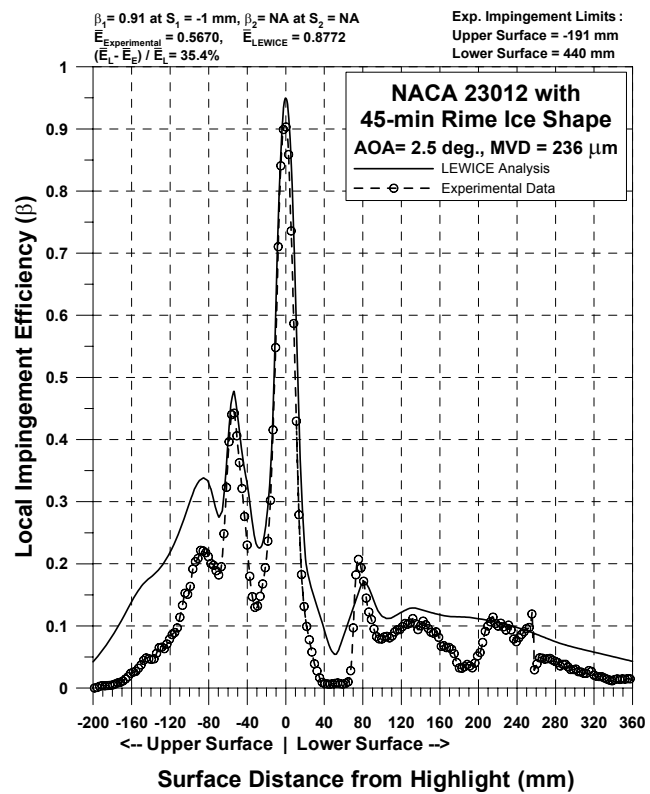
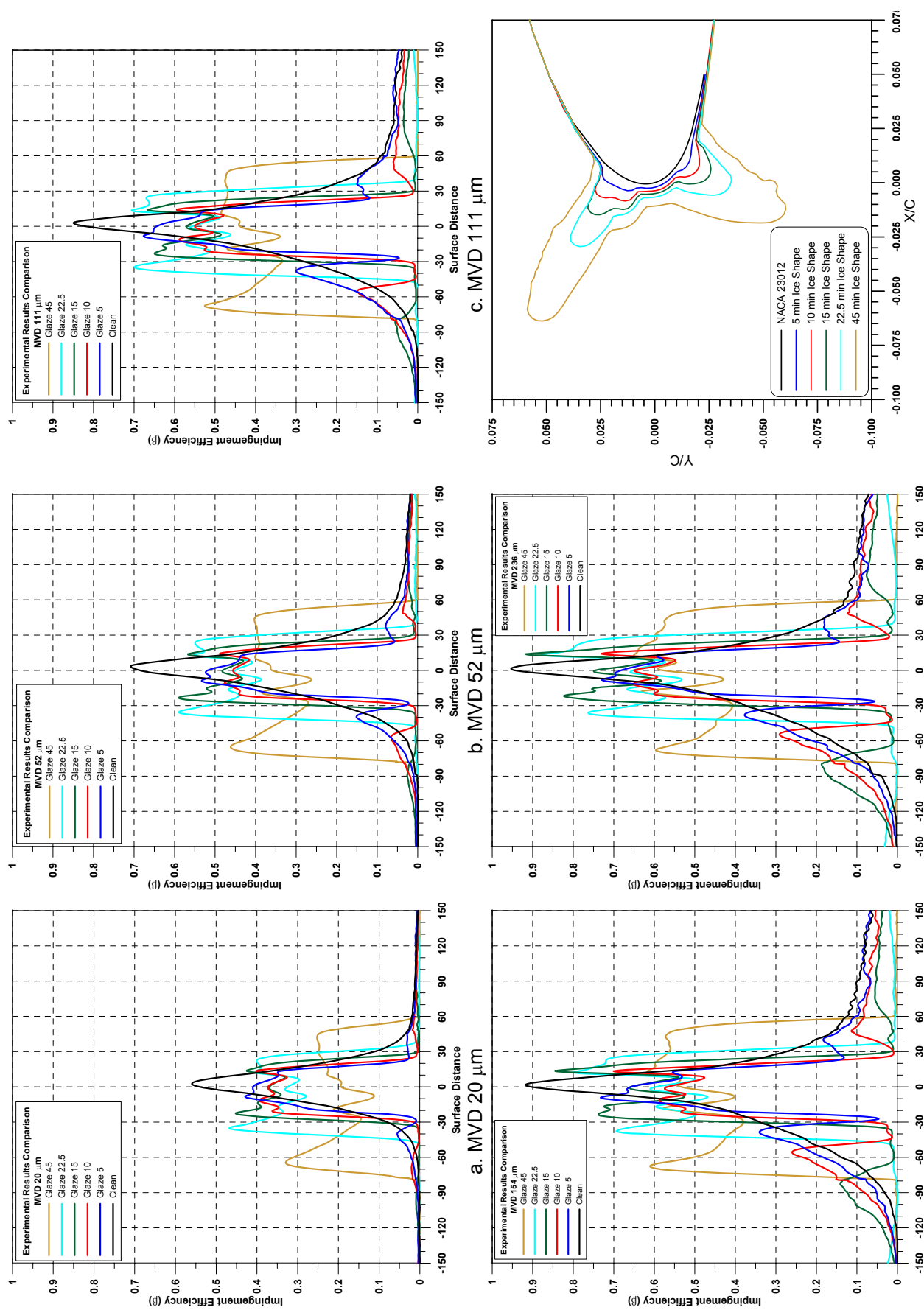
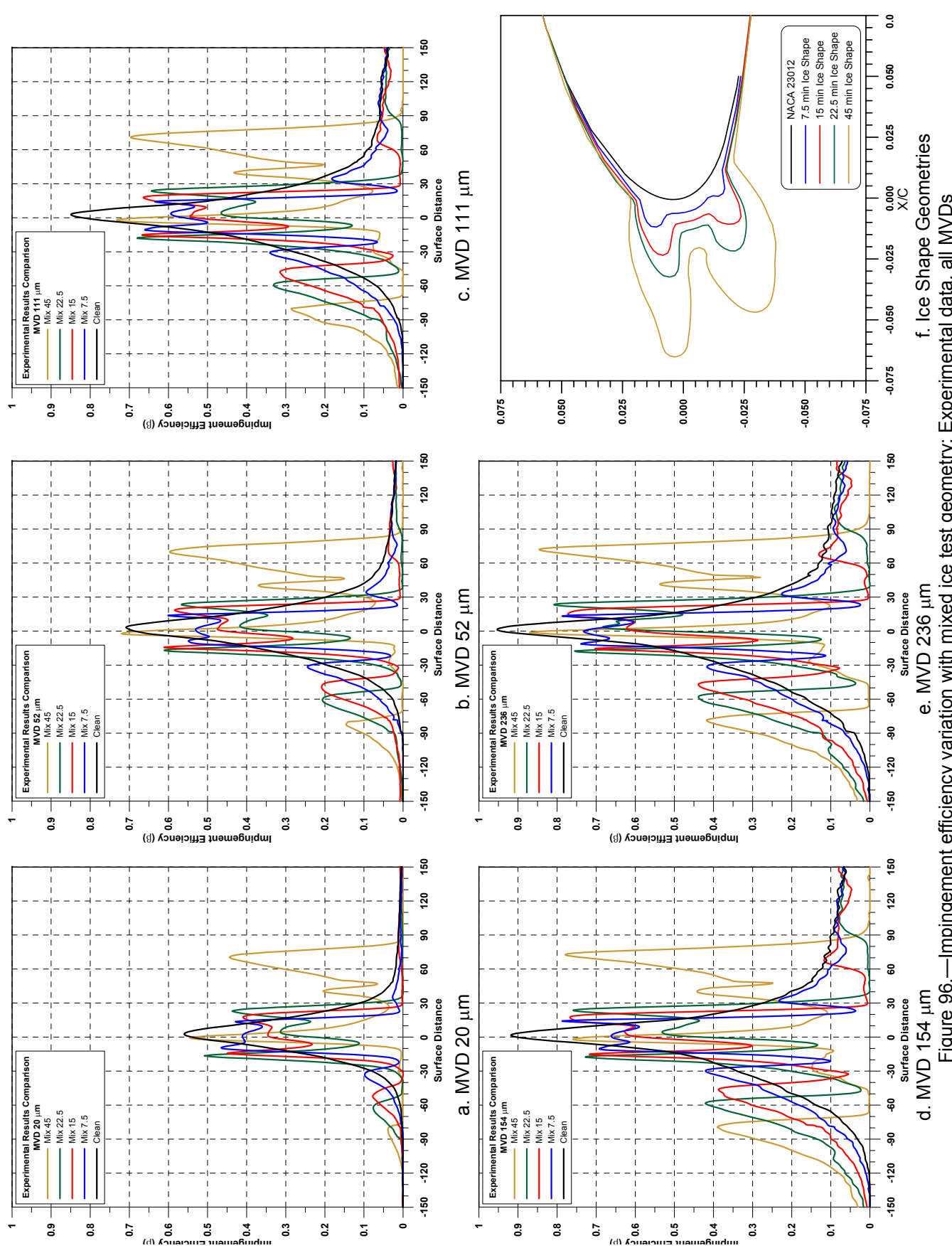


Figure 94e—Impingement efficiency distribution for NACA 23012 airfoil with 45-min rime ice shape;  $c = 36\text{-in.}$ ,  $V_\infty = 175$  mph,  $\text{AOA} = 2.5^\circ$ ,  $\text{MVD} = 236 \mu\text{m}$ .





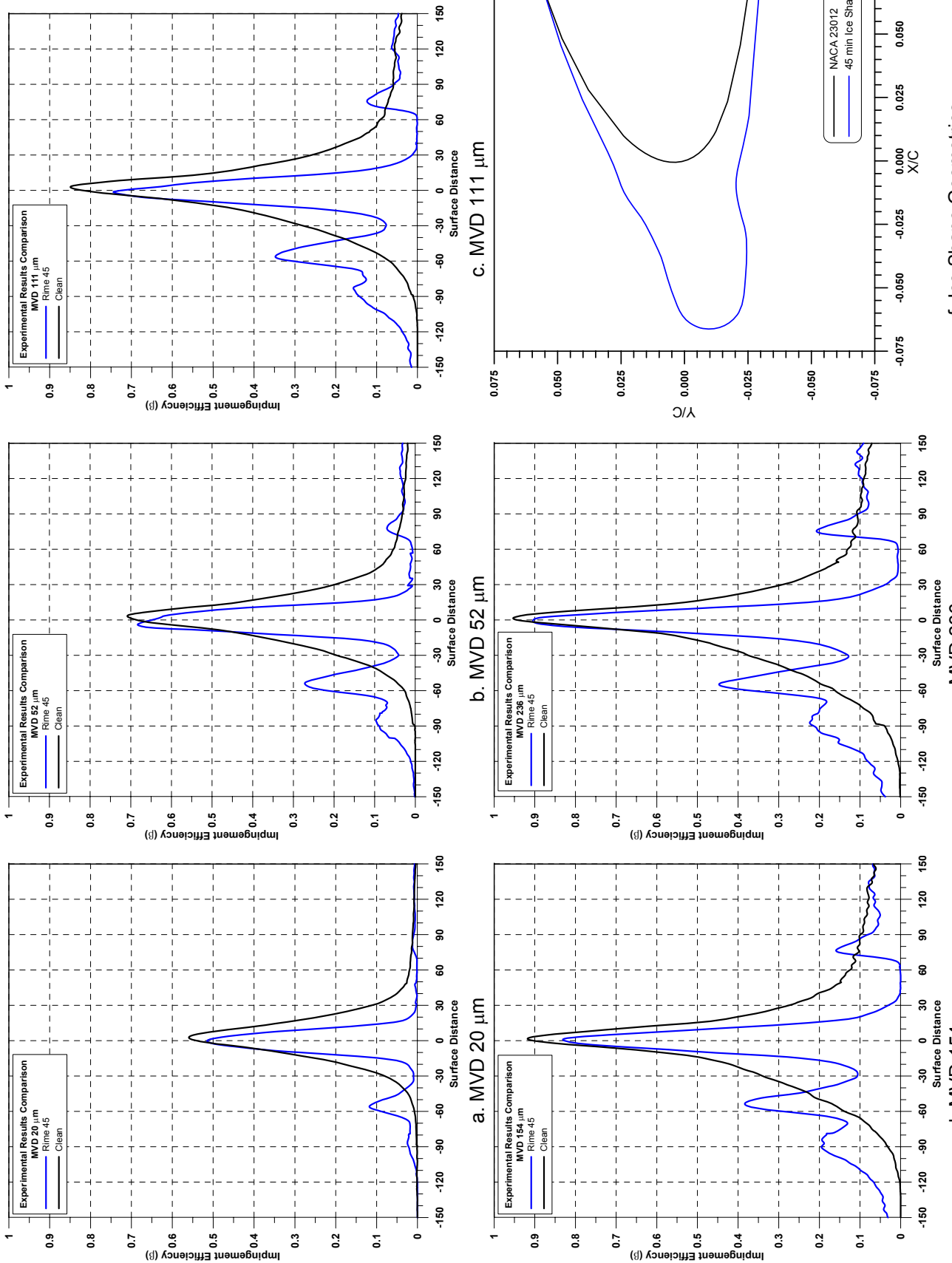


Figure 97.—Impingement efficiency variation with rime ice test geometry; experimental data, all MVDs.

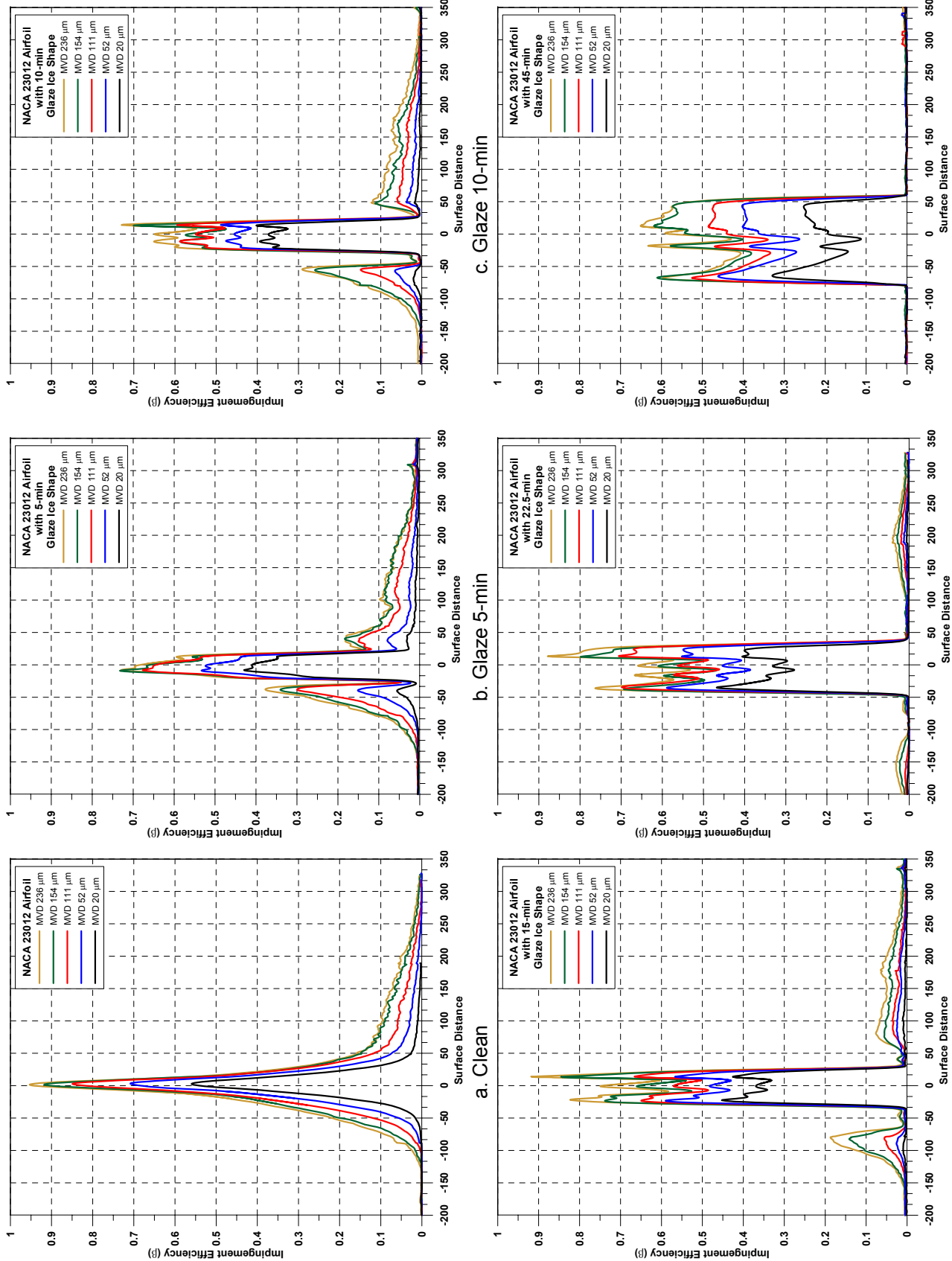


Figure 98.—Impingement efficiency variation with MVD; experimental data, clean and glaze ice geometries.

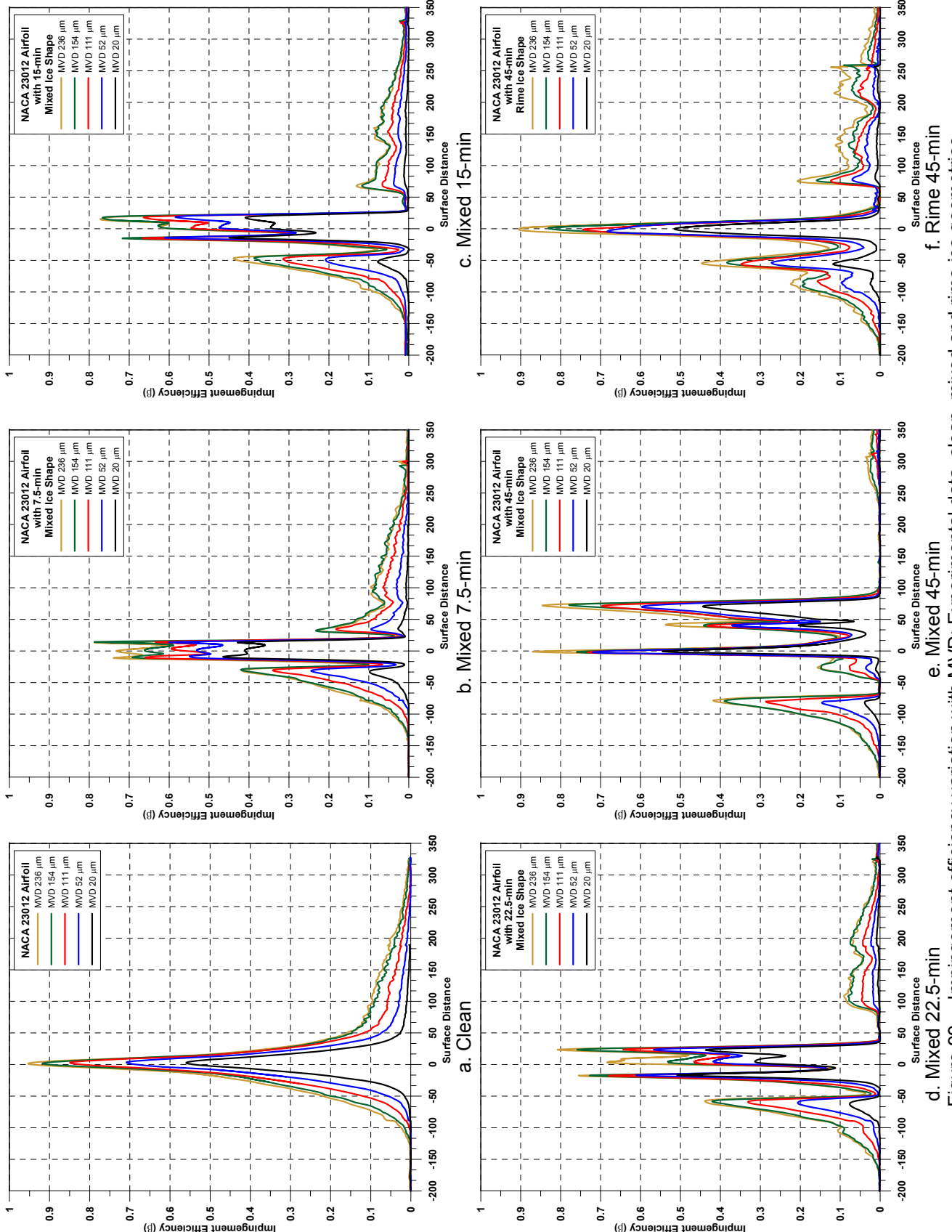


Figure 99.—Impingement efficiency variation with MVD; Experimental data, clean, mixed and rime ice geometries.

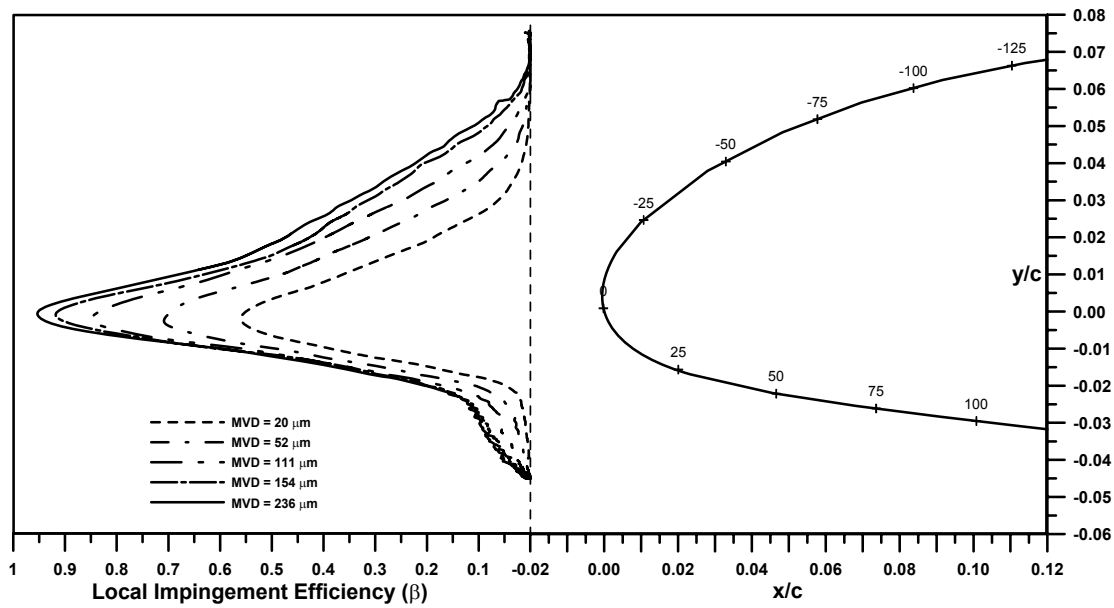


Figure 100.—Experimental Y/c vs Beta, NACA23012.

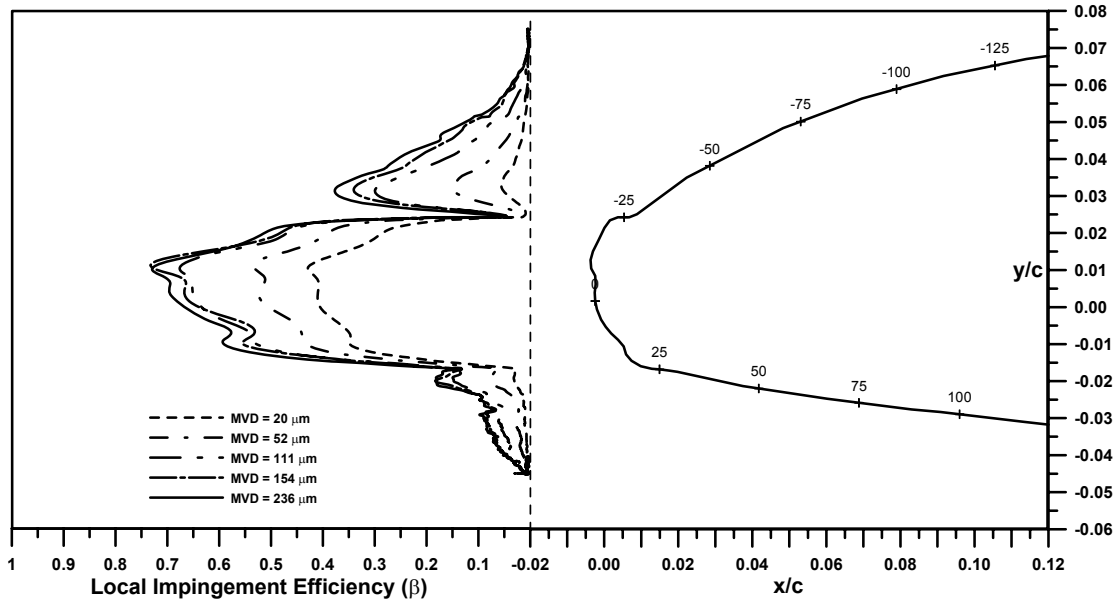


Figure 101.—Experimental Y/c vs Beta, NACA23012 with 5-min glaze ice shape.

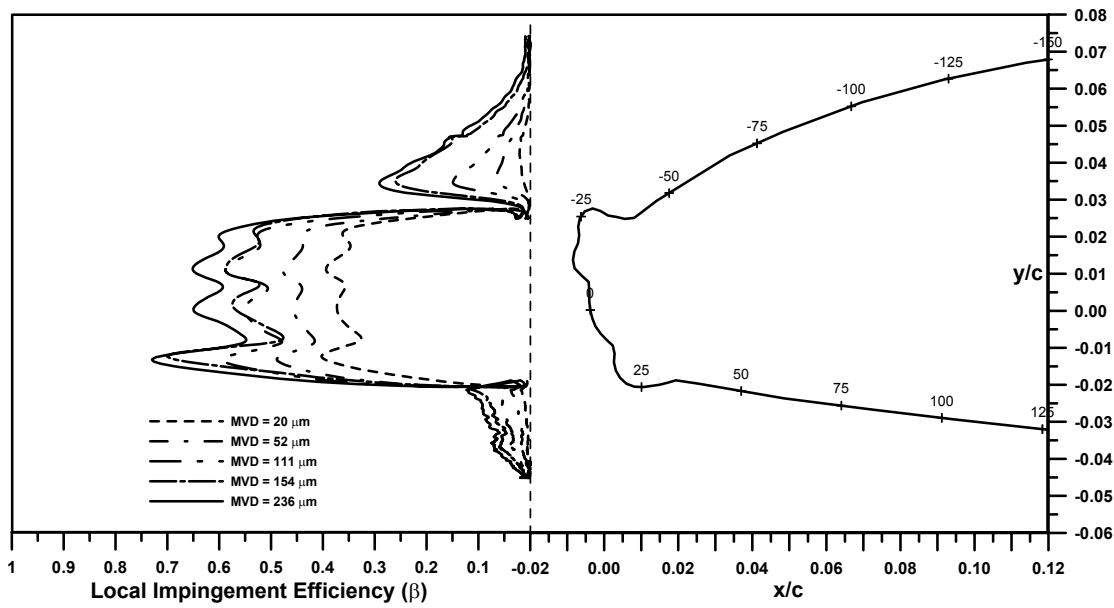


Figure 102.—Experimental  $Y/c$  vs Beta, NACA23012 with 10-min glaze ice shape.

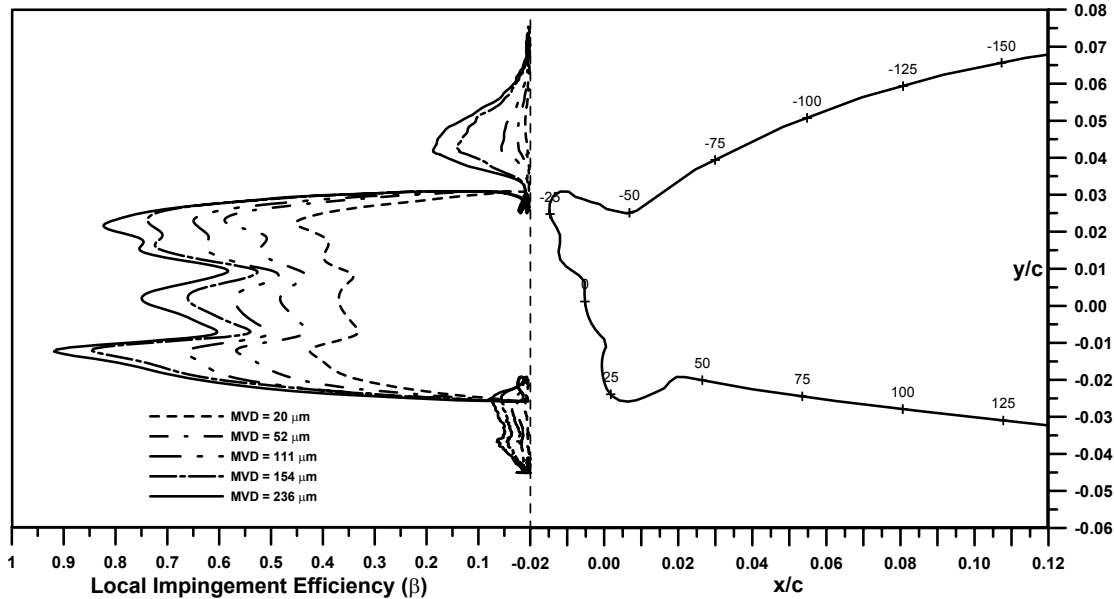


Figure 103.—Experimental  $Y/c$  vs Beta, NACA23012 with 15-min glaze ice shape.

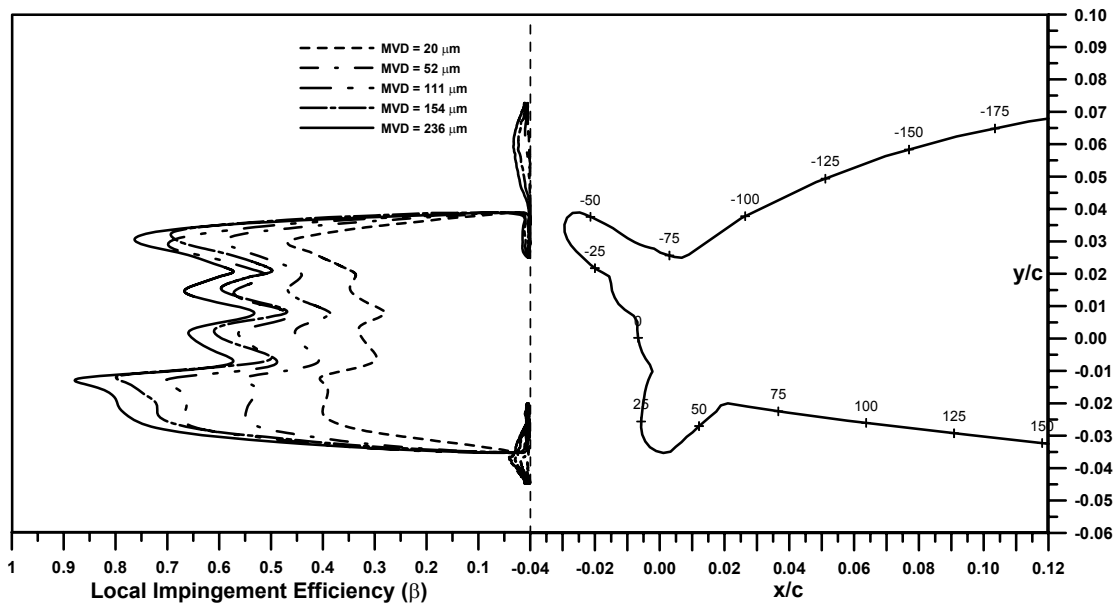


Figure 104.—Experimental  $Y/c$  vs Beta, NACA23012 with 22.5-min glaze ice shape.

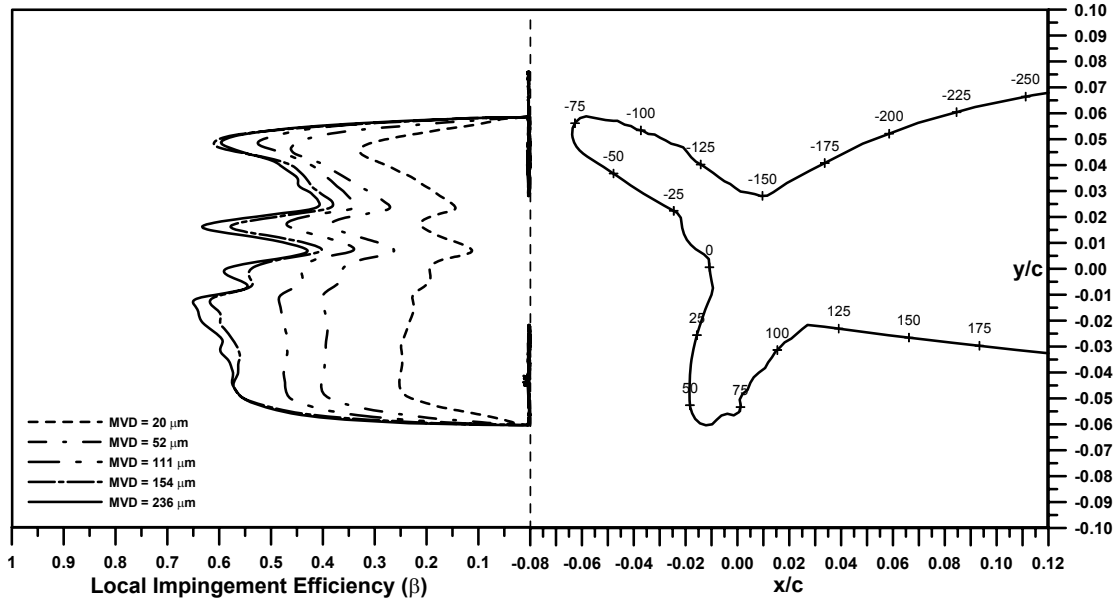


Figure 105.—Experimental  $Y/c$  vs Beta, NACA23012 with 45-min glaze ice shape.

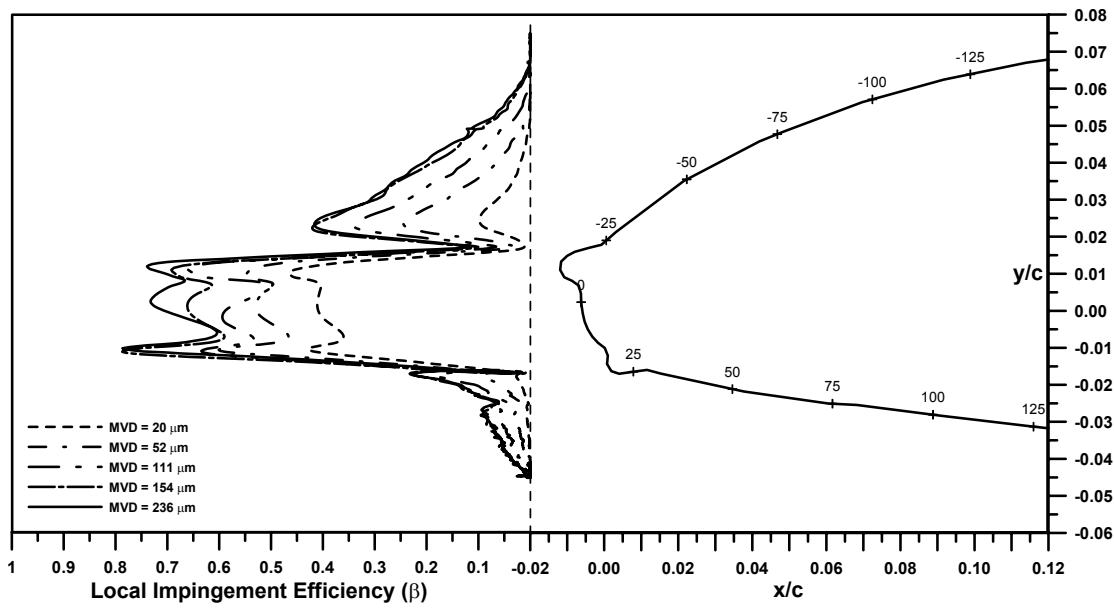


Figure 106.—Experimental Y/c vs Beta, NACA23012 with 7.5-min mixed ice shape.

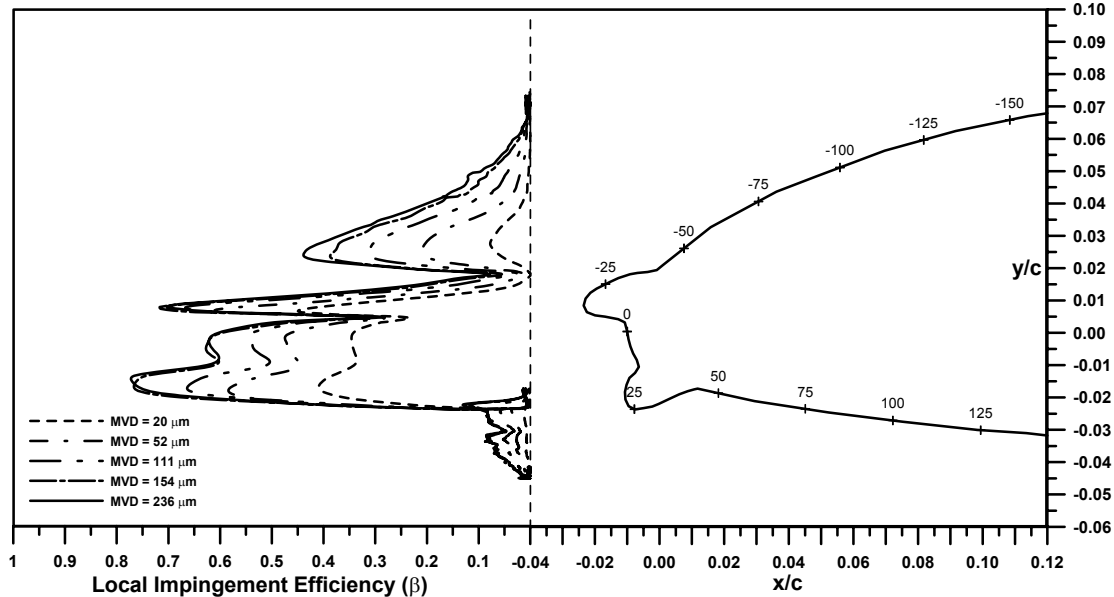


Figure 107.—Experimental Y/c vs Beta, NACA23012 with 15-min mixed ice shape.

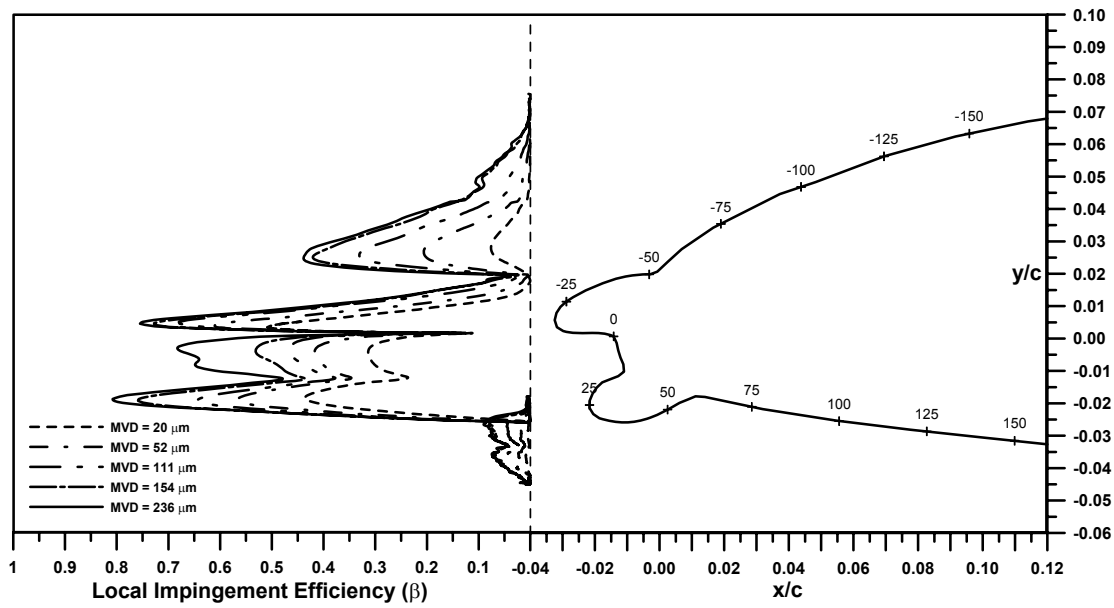


Figure 108.—Experimental  $Y/c$  vs Beta, NACA23012 with 22.5-min mixed ice shape.

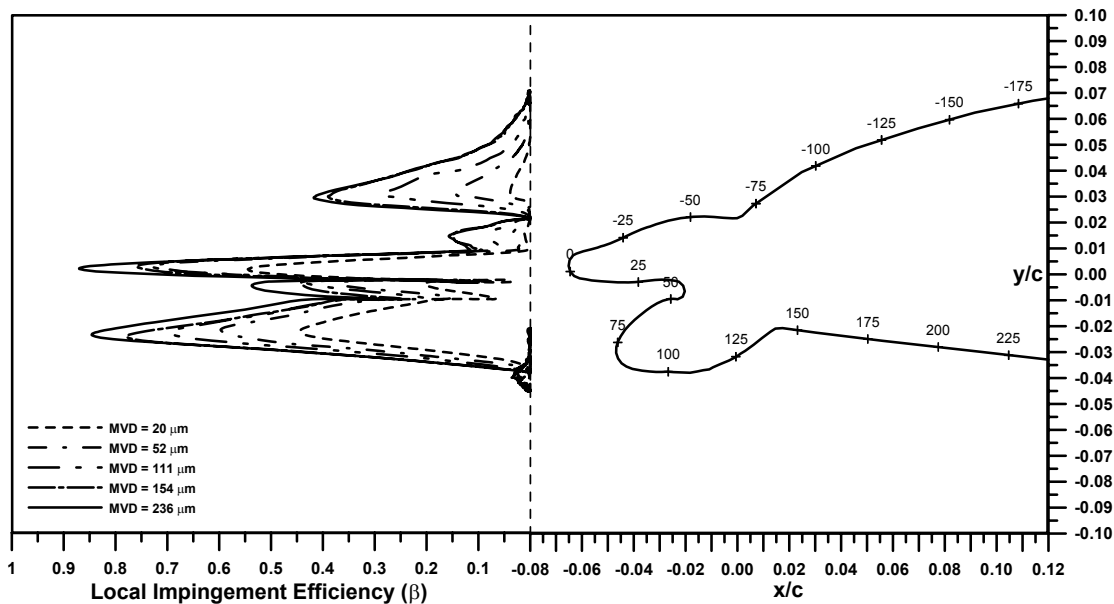


Figure 109.—Experimental  $Y/c$  vs Beta, NACA23012 with 45-min mixed ice shape.

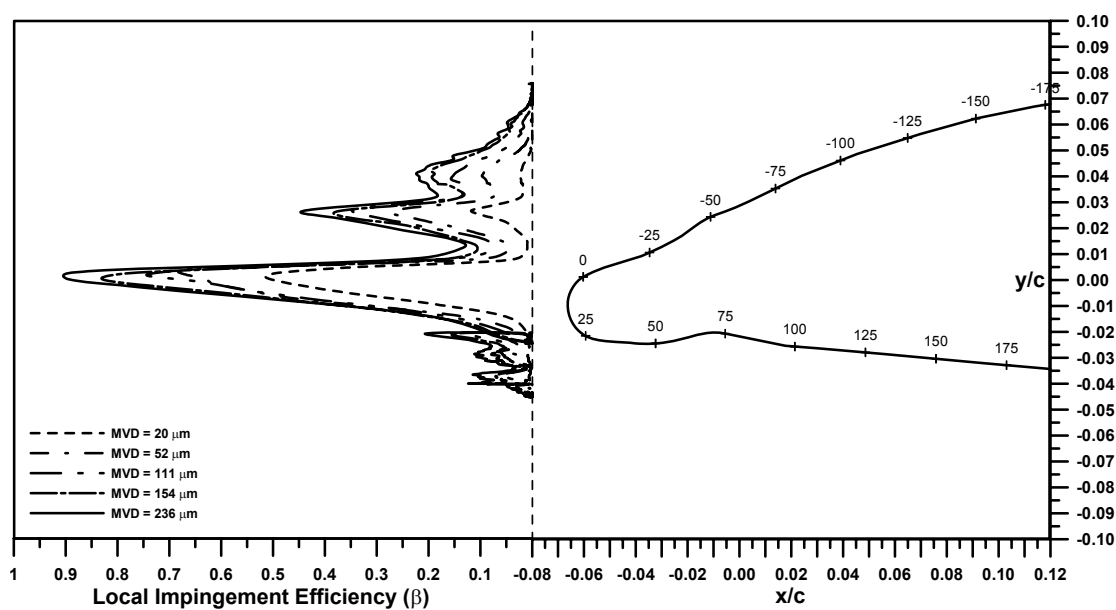
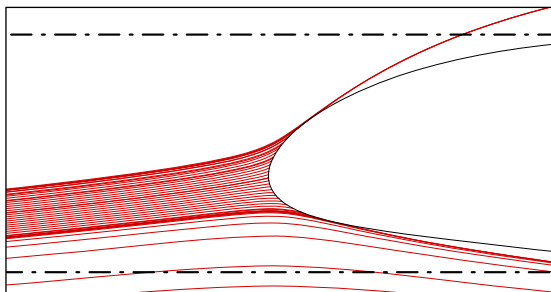
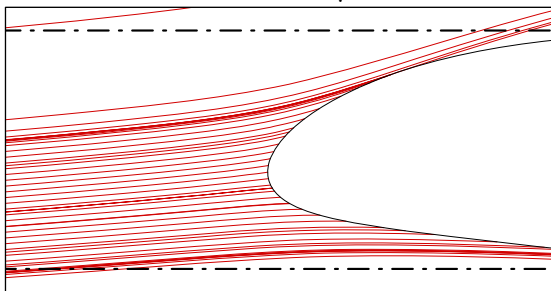


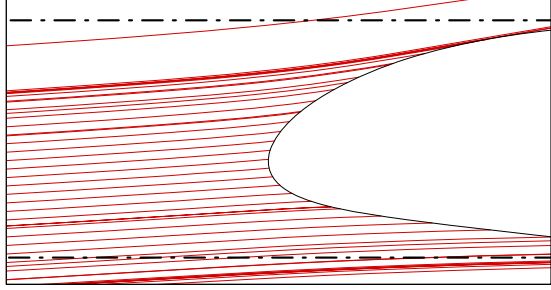
Figure 110.—Y/c vs Beta, NACA23012 with 45-min rime ice shape.



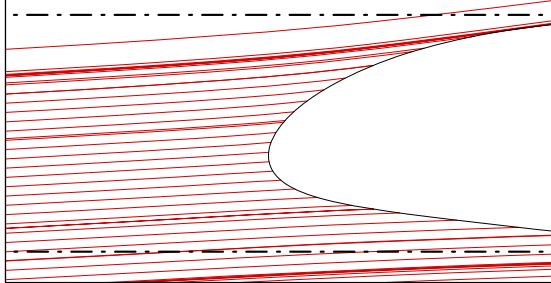
a. MVD = 20  $\mu\text{m}$



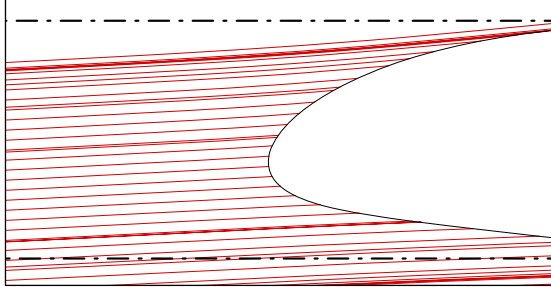
b. MVD = 52  $\mu\text{m}$



c. MVD = 111  $\mu\text{m}$

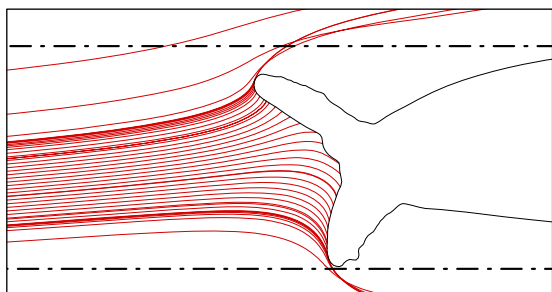


d. MVD = 154  $\mu\text{m}$

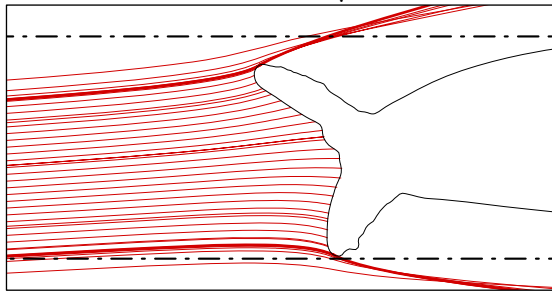


e. MVD = 236  $\mu\text{m}$

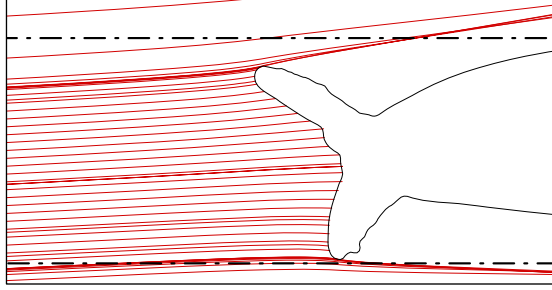
Figure 111.—Particles trajectories;  
NACA 23012 airfoil.



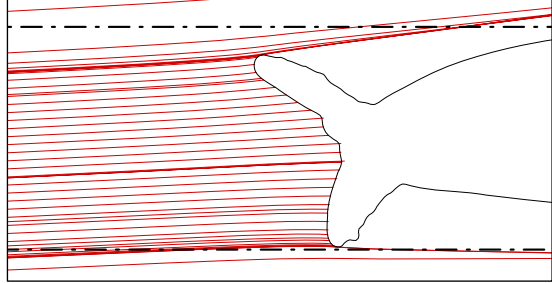
a. MVD = 20  $\mu\text{m}$



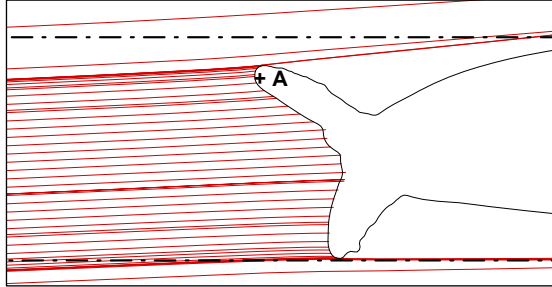
b. MVD = 52  $\mu\text{m}$



c. MVD = 111  $\mu\text{m}$

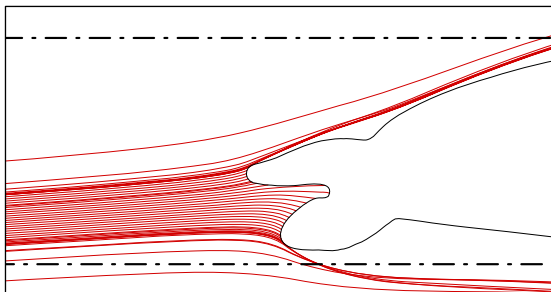


d. MVD = 154  $\mu\text{m}$

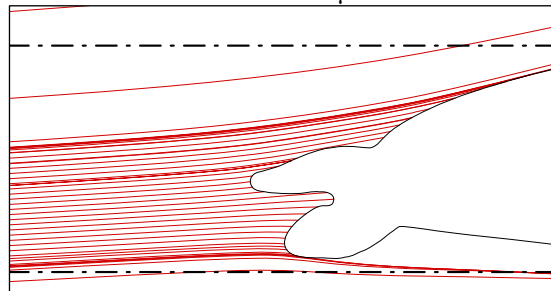


e. MVD = 236  $\mu\text{m}$

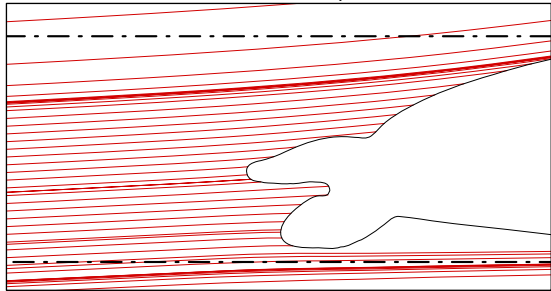
Figure 112.—Particles trajectories;  
NACA 23012 with 45-min glaze ice.



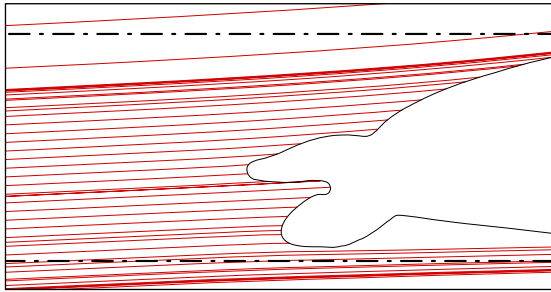
a. MVD = 20  $\mu\text{m}$



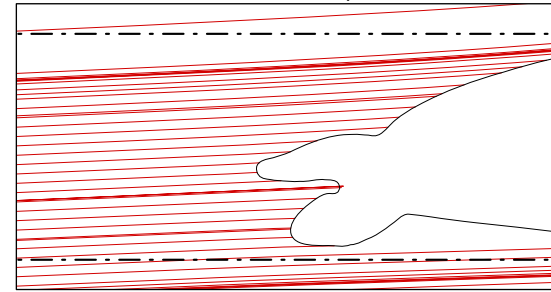
b. MVD = 52  $\mu\text{m}$



c. MVD = 111  $\mu\text{m}$

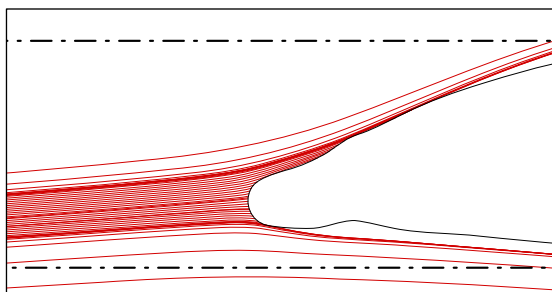


d. MVD = 154  $\mu\text{m}$

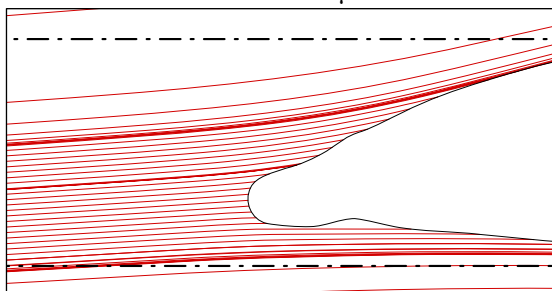


e. MVD = 236  $\mu\text{m}$

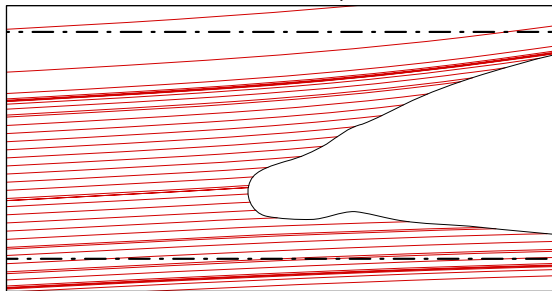
Figure 113.—Particles trajectories;  
NACA 23012 with 45-min mixed ice.



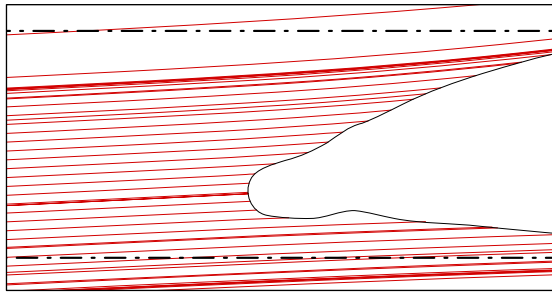
a. MVD = 20  $\mu\text{m}$



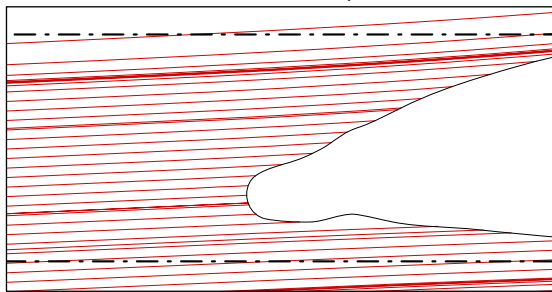
b. MVD = 52  $\mu\text{m}$



c. MVD = 111  $\mu\text{m}$



d. MVD = 154  $\mu\text{m}$



e. MVD = 236  $\mu\text{m}$

Figure 114.—Particles trajectories;  
NACA 23012 with 45-min rime ice.

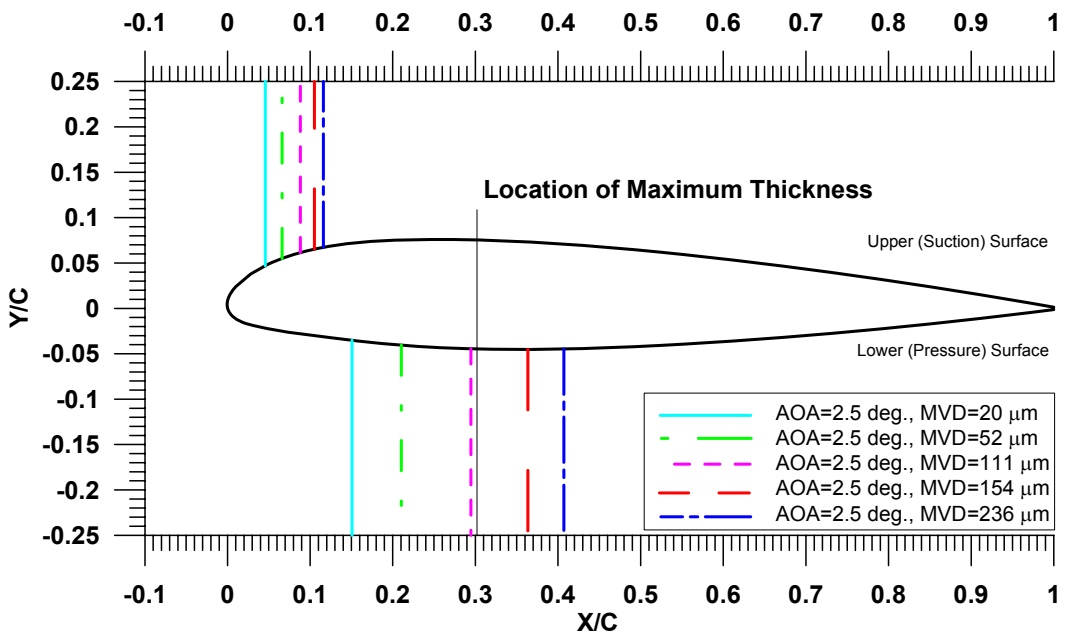


Figure 115.—Experimental impingement limits for NACA 23012 airfoil at AOA = 2.5°.

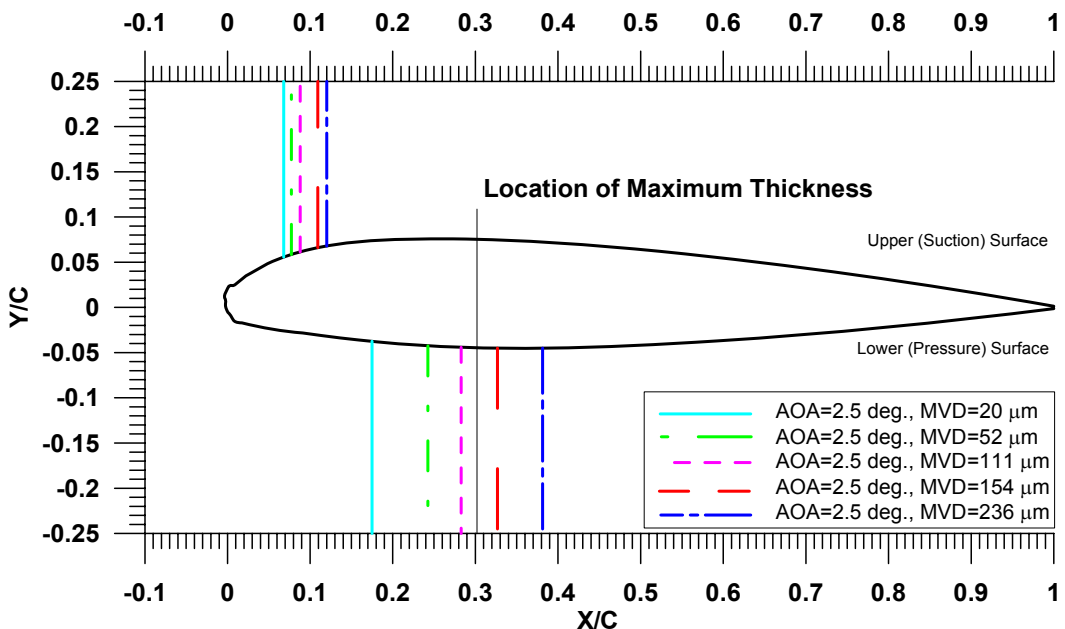


Figure 116.—Experimental impingement limits for NACA 23012 airfoil with 5-min glaze ice shape at AOA=2.5°.

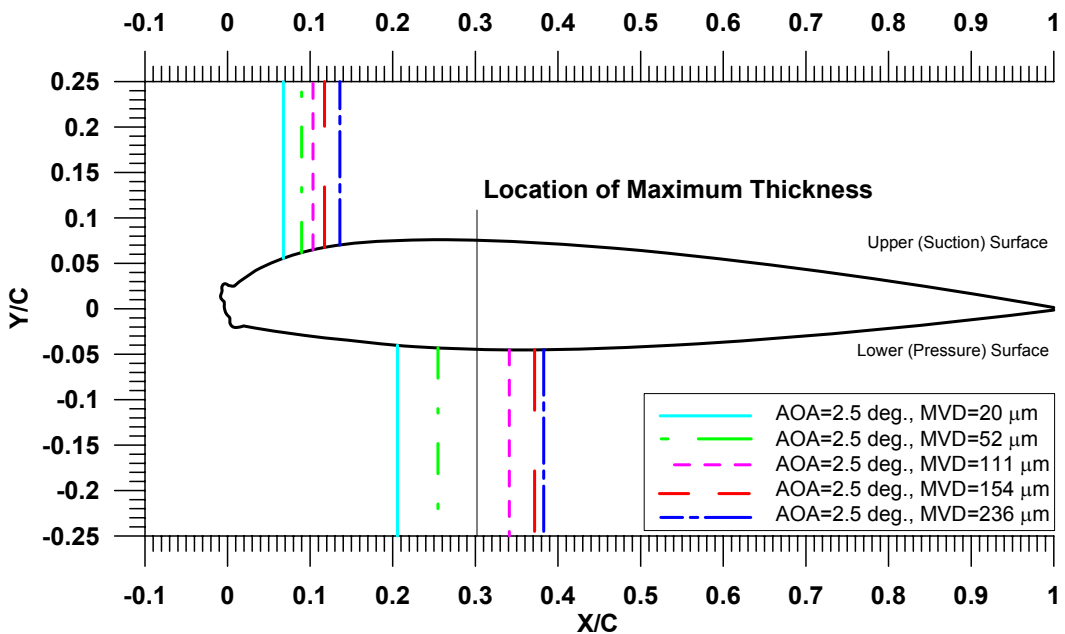


Figure 117.—Experimental impingement limits for NACA 23012 airfoil with 10-min glaze ice shape at AOA=2.5°.

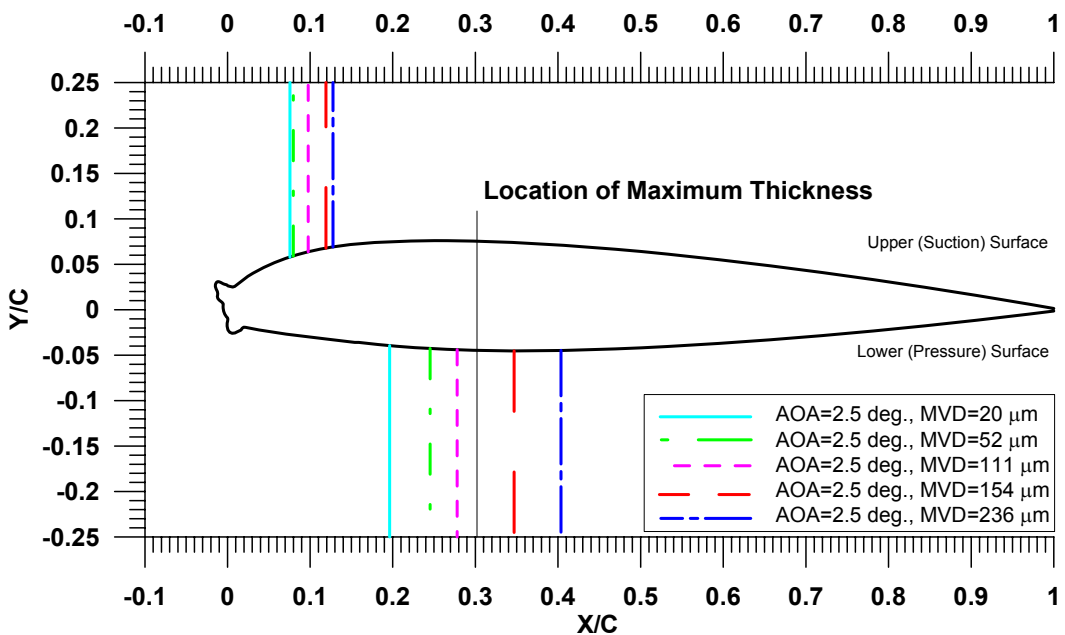


Figure 118.—Experimental impingement limits for NACA 23012 airfoil with 15-min glaze ice shape at AOA=2.5°.

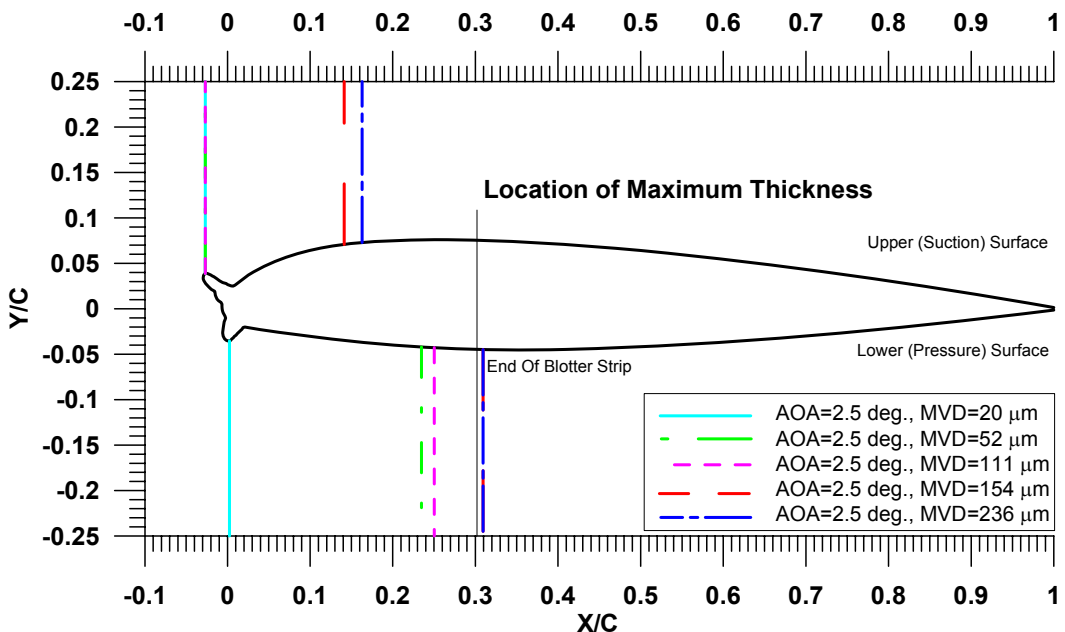


Figure 119.—Experimental impingement limits for NACA 23012 airfoil with 22.5-min glaze ice shape at AOA = 2.5°.

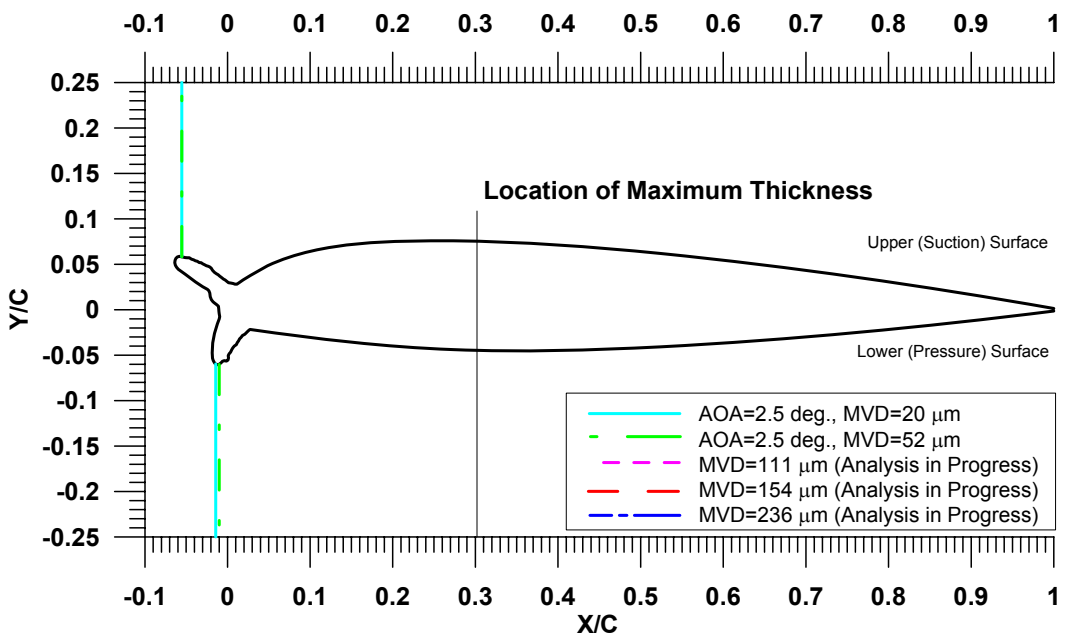


Figure 120.—Experimental impingement limits for NACA 23012 airfoil with 45-min glaze ice shape at AOA = 2.5°.

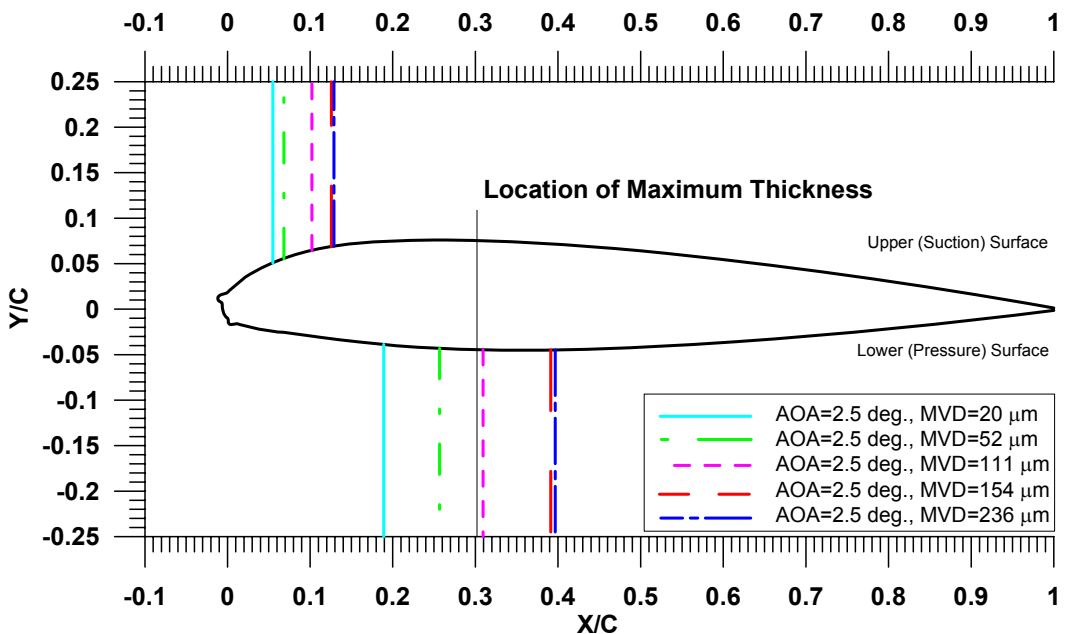


Figure 121.—Experimental impingement limits for NACA 23012 airfoil with 7.5-min mixed ice shape at AOA = 2.5°.

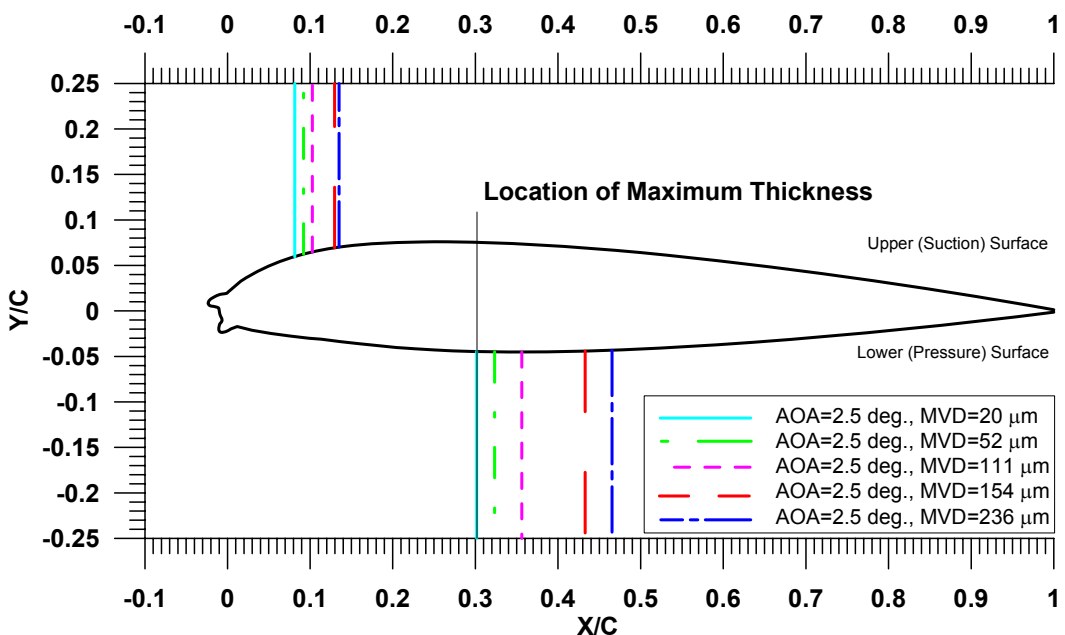


Figure 122.—Experimental impingement limits for NACA 23012 airfoil with 15-min mixed ice shape at AOA = 2.5°.

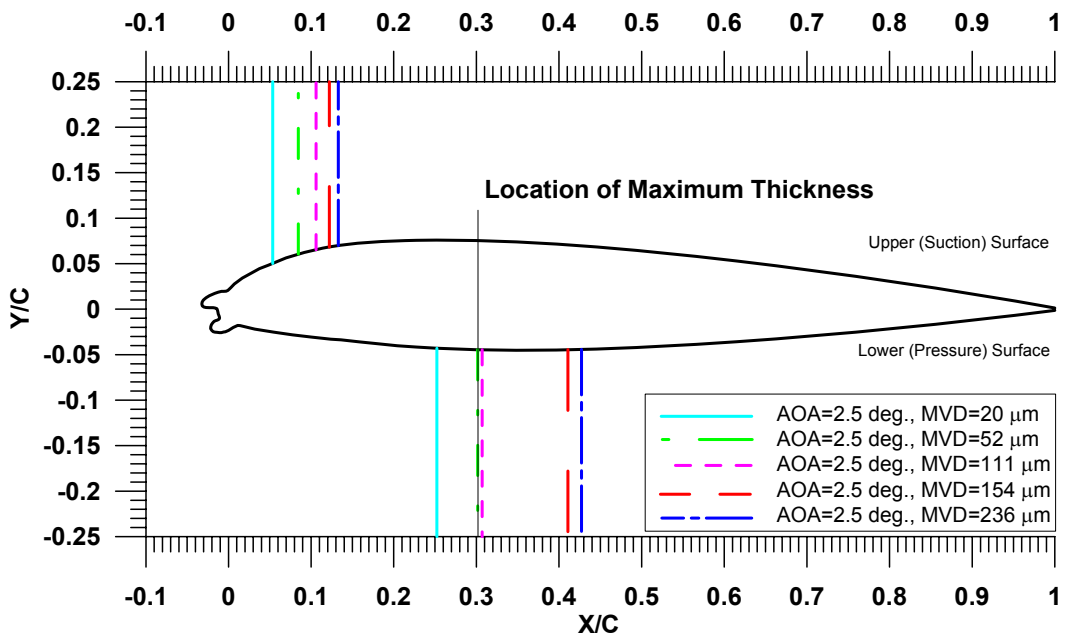


Figure 123.—Experimental impingement limits for NACA 23012 airfoil with 22.5-min mixed ice shape at AOA = 2.5°.

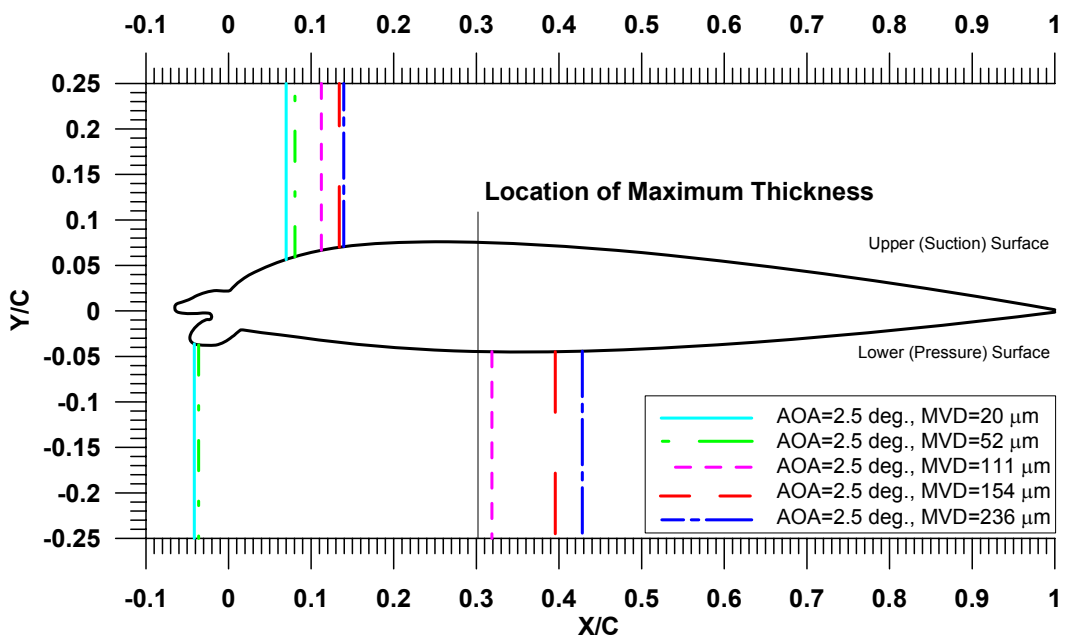


Figure 124.—Experimental impingement limits for NACA 23012 airfoil with 45-min mixed ice shape at AOA = 2.5°.

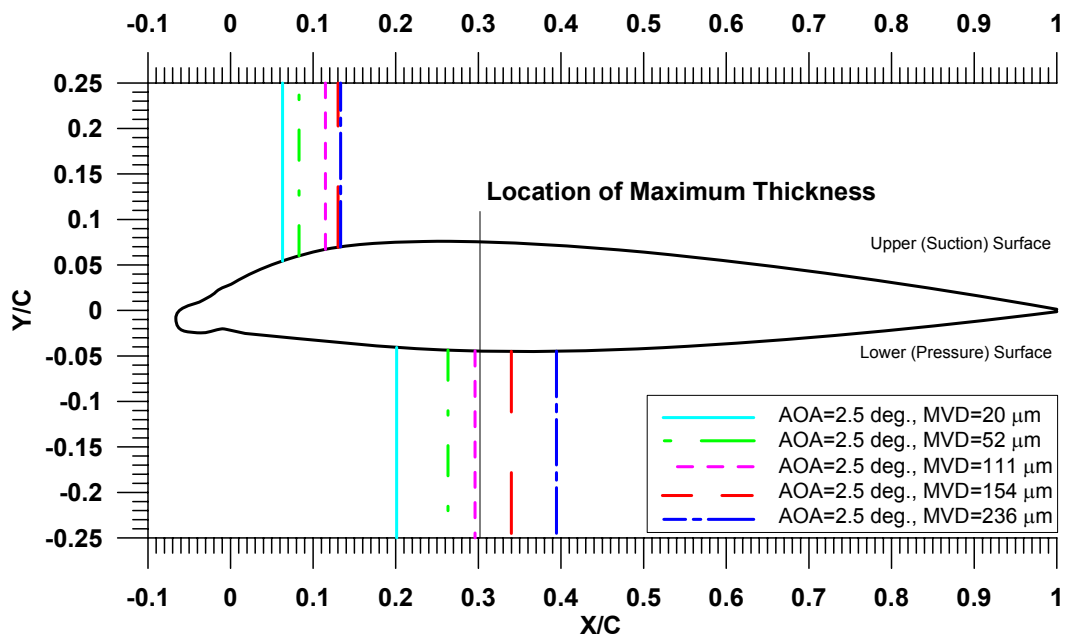


Figure 125.—Experimental impingement limits for NACA 23012 airfoil with 45-min rime ice shape at  $\text{AOA} = 2.5^\circ$ .

## Appendix A—Model Geometry and Pressure Port Coordinates

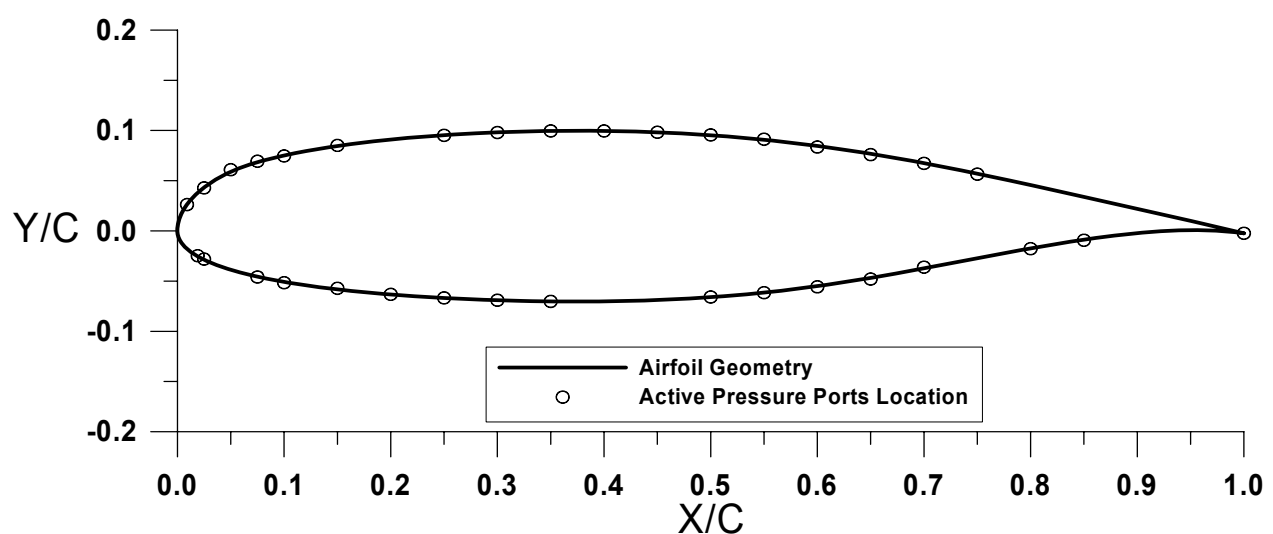


Figure A1.—MS(1)-0317 Airfoil.

TABLE A1.1.—COORDINATES OF MS(1)-0317 AIRFOIL

| Lower Surface |         |        |         | Upper Surface |        |        |        |
|---------------|---------|--------|---------|---------------|--------|--------|--------|
| x/c           | y/c     | x/c    | y/c     | x/c           | y/c    | x/c    | y/c    |
| 1             | -0.0024 | 0.3147 | -0.0695 | 0.0000        | 0.0022 | 0.2795 | 0.0972 |
| 0.9848        | -0.0007 | 0.2977 | -0.0690 | 0.0001        | 0.0042 | 0.2959 | 0.0980 |
| 0.9725        | 0.0002  | 0.2811 | -0.0684 | 0.0004        | 0.0062 | 0.3118 | 0.0986 |
| 0.9603        | 0.0007  | 0.2643 | -0.0676 | 0.0008        | 0.0081 | 0.3251 | 0.0990 |
| 0.9469        | 0.0007  | 0.2473 | -0.0667 | 0.0013        | 0.0101 | 0.3375 | 0.0993 |
| 0.9332        | 0.0002  | 0.2306 | -0.0657 | 0.0018        | 0.0120 | 0.3527 | 0.0996 |
| 0.9193        | -0.0006 | 0.2145 | -0.0645 | 0.0025        | 0.0139 | 0.3690 | 0.0997 |
| 0.9051        | -0.0017 | 0.1982 | -0.0631 | 0.0032        | 0.0157 | 0.3854 | 0.0997 |
| 0.8907        | -0.0032 | 0.1814 | -0.0616 | 0.0040        | 0.0176 | 0.4020 | 0.0995 |
| 0.8760        | -0.0050 | 0.1657 | -0.0600 | 0.0049        | 0.0193 | 0.4183 | 0.0992 |
| 0.8612        | -0.0070 | 0.1502 | -0.0582 | 0.0059        | 0.0211 | 0.4341 | 0.0988 |
| 0.8460        | -0.0093 | 0.1348 | -0.0562 | 0.0068        | 0.0229 | 0.4498 | 0.0983 |
| 0.8304        | -0.0119 | 0.1199 | -0.0540 | 0.0079        | 0.0246 | 0.4658 | 0.0975 |
| 0.8145        | -0.0147 | 0.1055 | -0.0516 | 0.0090        | 0.0262 | 0.4818 | 0.0966 |
| 0.7981        | -0.0177 | 0.0911 | -0.0489 | 0.0101        | 0.0279 | 0.4971 | 0.0956 |
| 0.7812        | -0.0210 | 0.0772 | -0.0459 | 0.0113        | 0.0295 | 0.5129 | 0.0943 |
| 0.7640        | -0.0244 | 0.0640 | -0.0427 | 0.0126        | 0.0311 | 0.5290 | 0.0929 |
| 0.7443        | -0.0283 | 0.0496 | -0.0385 | 0.0138        | 0.0326 | 0.5446 | 0.0913 |
| 0.7249        | -0.0323 | 0.0394 | -0.0350 | 0.0152        | 0.0341 | 0.5601 | 0.0896 |
| 0.7061        | -0.0361 | 0.0323 | -0.0321 | 0.0165        | 0.0355 | 0.5755 | 0.0877 |
| 0.6903        | -0.0392 | 0.0273 | -0.0298 | 0.0180        | 0.0370 | 0.5908 | 0.0857 |
| 0.6732        | -0.0425 | 0.0238 | -0.0280 | 0.0194        | 0.0383 | 0.6063 | 0.0836 |
| 0.6576        | -0.0454 | 0.0213 | -0.0267 | 0.0209        | 0.0397 | 0.6223 | 0.0812 |
| 0.6433        | -0.0479 | 0.0196 | -0.0257 | 0.0224        | 0.0410 | 0.6383 | 0.0787 |
| 0.6273        | -0.0507 | 0.0179 | -0.0247 | 0.0245        | 0.0428 | 0.6545 | 0.0760 |
| 0.6112        | -0.0533 | 0.0162 | -0.0236 | 0.0276        | 0.0453 | 0.6713 | 0.0730 |
| 0.5956        | -0.0557 | 0.0145 | -0.0225 | 0.0320        | 0.0485 | 0.6871 | 0.0701 |
| 0.5802        | -0.0578 | 0.0129 | -0.0213 | 0.0384        | 0.0527 | 0.7018 | 0.0673 |
| 0.5648        | -0.0597 | 0.0113 | -0.0201 | 0.0479        | 0.0579 | 0.7178 | 0.0639 |
| 0.5488        | -0.0615 | 0.0098 | -0.0188 | 0.0588        | 0.0628 | 0.7353 | 0.0602 |
| 0.5328        | -0.0632 | 0.0083 | -0.0175 | 0.0708        | 0.0671 | 0.7518 | 0.0565 |
| 0.5172        | -0.0646 | 0.0070 | -0.0160 | 0.0835        | 0.0709 | 0.7687 | 0.0528 |
| 0.5014        | -0.0658 | 0.0056 | -0.0145 | 0.0967        | 0.0743 | 0.7858 | 0.0489 |
| 0.4851        | -0.0669 | 0.0044 | -0.0129 | 0.1103        | 0.0774 | 0.8025 | 0.0451 |
| 0.4690        | -0.0679 | 0.0034 | -0.0112 | 0.1245        | 0.0802 | 0.8211 | 0.0407 |
| 0.4529        | -0.0687 | 0.0024 | -0.0095 | 0.1391        | 0.0828 | 0.8389 | 0.0365 |
| 0.4367        | -0.0693 | 0.0016 | -0.0076 | 0.1541        | 0.0852 | 0.8565 | 0.0324 |
| 0.4202        | -0.0698 | 0.0010 | -0.0057 | 0.1690        | 0.0873 | 0.8758 | 0.0278 |
| 0.4061        | -0.0701 | 0.0005 | -0.0038 | 0.1843        | 0.0892 | 0.8946 | 0.0233 |
| 0.3966        | -0.0702 | 0.0002 | -0.0018 | 0.2001        | 0.0910 | 0.9130 | 0.0189 |
| 0.3824        | -0.0703 | 0.0000 | 0.0002  | 0.2156        | 0.0925 | 0.9312 | 0.0145 |
| 0.3655        | -0.0703 |        |         | 0.2313        | 0.0939 | 0.9486 | 0.0103 |
| 0.3487        | -0.0702 |        |         | 0.2473        | 0.0952 | 0.9658 | 0.0062 |
| 0.3317        | -0.0699 |        |         | 0.2633        | 0.0962 | 0.9827 | 0.0020 |

TABLE A1.2.—COORDINATES OF ACTIVE  
PRESSURE PORTS OF MS(1)-0317 AIRFOIL

| <b>Lower Surface</b> |          | <b>Upper Surface</b> |         |
|----------------------|----------|----------------------|---------|
| x/c                  | y/c      | x/c                  | y/c     |
| 1.0000               | -0.00236 | 0.0090               | 0.02624 |
| 0.8500               | -0.00932 | 0.0250               | 0.04282 |
| 0.8000               | -0.01772 | 0.0500               | 0.06098 |
| 0.7000               | -0.03612 | 0.0750               | 0.06941 |
| 0.6500               | -0.04792 | 0.1000               | 0.07465 |
| 0.6000               | -0.05566 | 0.1500               | 0.08515 |
| 0.5500               | -0.06151 | 0.2500               | 0.09516 |
| 0.5000               | -0.06581 | 0.3000               | 0.09797 |
| 0.3500               | -0.07019 | 0.3500               | 0.09956 |
| 0.3000               | -0.06901 | 0.4000               | 0.09953 |
| 0.2500               | -0.06670 | 0.4500               | 0.09827 |
| 0.2000               | -0.06314 | 0.5000               | 0.09557 |
| 0.1500               | -0.05714 | 0.5500               | 0.09131 |
| 0.1000               | -0.05157 | 0.6000               | 0.08358 |
| 0.0750               | -0.04592 | 0.6500               | 0.07596 |
| 0.0250               | -0.02804 | 0.7000               | 0.06726 |
| 0.0190               | -0.02472 | 0.7500               | 0.05654 |

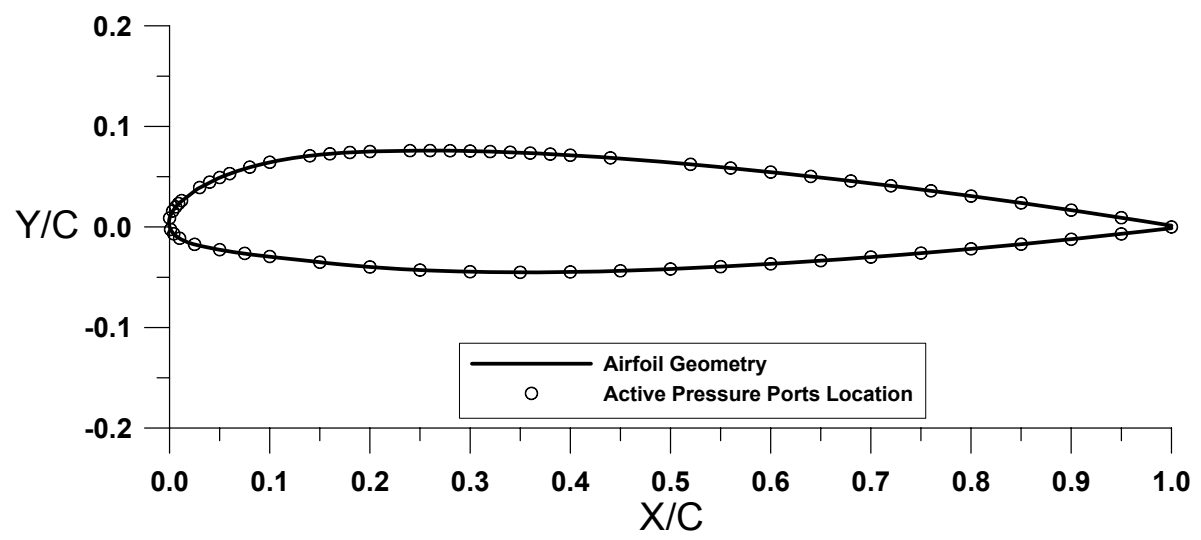


Figure A2.—NACA 23012 airfoil.

TABLE A2.1.—COORDINATES OF NACA 23012 AIRFOIL

| Lower Surface |         |        |         | Upper Surface |     |         |        |
|---------------|---------|--------|---------|---------------|-----|---------|--------|
| x/c           | y/c     | x/c    | y/c     | x/c           | y/c | x/c     | y/c    |
| 1.0000        | -0.0013 | 0.0234 | -0.0170 |               |     | -0.0002 | 0.0008 |
| 0.9783        | -0.0038 | 0.0118 | -0.0124 |               |     | -0.0005 | 0.0031 |
| 0.9556        | -0.0063 | 0.0096 | -0.0112 |               |     | -0.0005 | 0.0054 |
| 0.9330        | -0.0088 | 0.0077 | -0.0099 |               |     | -0.0001 | 0.0076 |
| 0.9103        | -0.0112 | 0.0059 | -0.0085 |               |     | 0.0004  | 0.0099 |
| 0.8876        | -0.0135 | 0.0043 | -0.0070 |               |     | 0.0012  | 0.0120 |
| 0.8649        | -0.0157 | 0.0028 | -0.0053 |               |     | 0.0022  | 0.0141 |
| 0.8421        | -0.0179 | 0.0015 | -0.0034 |               |     | 0.0034  | 0.0161 |
| 0.8194        | -0.0200 | 0.0005 | -0.0013 |               |     | 0.0099  | 0.0241 |
| 0.7967        | -0.0220 |        |         |               |     | 0.0280  | 0.0379 |
| 0.7740        | -0.0240 |        |         |               |     | 0.0483  | 0.0483 |
| 0.7512        | -0.0259 |        |         |               |     | 0.0696  | 0.0563 |
| 0.7285        | -0.0277 |        |         |               |     | 0.0916  | 0.0624 |
| 0.7057        | -0.0295 |        |         |               |     | 0.1140  | 0.0670 |
| 0.6830        | -0.0312 |        |         |               |     | 0.1365  | 0.0703 |
| 0.6602        | -0.0328 |        |         |               |     | 0.1592  | 0.0727 |
| 0.6375        | -0.0344 |        |         |               |     | 0.1820  | 0.0742 |
| 0.6147        | -0.0358 |        |         |               |     | 0.2048  | 0.0752 |
| 0.5919        | -0.0372 |        |         |               |     | 0.2276  | 0.0757 |
| 0.5691        | -0.0385 |        |         |               |     | 0.2504  | 0.0760 |
| 0.5463        | -0.0397 |        |         |               |     | 0.2732  | 0.0759 |
| 0.5236        | -0.0408 |        |         |               |     | 0.2961  | 0.0756 |
| 0.5008        | -0.0418 |        |         |               |     | 0.3189  | 0.0750 |
| 0.4780        | -0.0427 |        |         |               |     | 0.3417  | 0.0742 |
| 0.4552        | -0.0435 |        |         |               |     | 0.3645  | 0.0732 |
| 0.4323        | -0.0441 |        |         |               |     | 0.3873  | 0.0721 |
| 0.4095        | -0.0446 |        |         |               |     | 0.4100  | 0.0707 |
| 0.3867        | -0.0449 |        |         |               |     | 0.4328  | 0.0692 |
| 0.3639        | -0.0451 |        |         |               |     | 0.4556  | 0.0676 |
| 0.3411        | -0.0451 |        |         |               |     | 0.4783  | 0.0659 |
| 0.3183        | -0.0449 |        |         |               |     | 0.5011  | 0.0640 |
| 0.2954        | -0.0445 |        |         |               |     | 0.5238  | 0.0620 |
| 0.2726        | -0.0438 |        |         |               |     | 0.5465  | 0.0599 |
| 0.2498        | -0.0429 |        |         |               |     | 0.5692  | 0.0577 |
| 0.2271        | -0.0417 |        |         |               |     | 0.5919  | 0.0554 |
| 0.2043        | -0.0401 |        |         |               |     | 0.6146  | 0.0530 |
| 0.1816        | -0.0382 |        |         |               |     | 0.6373  | 0.0506 |
| 0.1588        | -0.0360 |        |         |               |     | 0.6600  | 0.0480 |
| 0.1362        | -0.0336 |        |         |               |     | 0.6826  | 0.0454 |
| 0.1135        | -0.0310 |        |         |               |     | 0.7053  | 0.0427 |
| 0.0908        | -0.0283 |        |         |               |     | 0.7280  | 0.0400 |
| 0.0682        | -0.0255 |        |         |               |     | 0.7506  | 0.0371 |
| 0.0456        | -0.0220 |        |         |               |     | 0.7732  | 0.0342 |

TABLE A2.2.—COORDINATES OF ACTIVE  
PRESSURE PORTS OF NACA 23012 AIRFOIL

| Lower Surface |          | Upper Surface |         |
|---------------|----------|---------------|---------|
| x/c           | y/c      | x/c           | y/c     |
| 1.0000        | 0.00000  | 0.0000        | 0.00886 |
| 0.9500        | -0.00693 | 0.0031        | 0.01589 |
| 0.9000        | -0.01223 | 0.0061        | 0.02001 |
| 0.8500        | -0.01716 | 0.0090        | 0.02329 |
| 0.8000        | -0.02175 | 0.0120        | 0.02623 |
| 0.7500        | -0.02601 | 0.0300        | 0.03921 |
| 0.7000        | -0.02994 | 0.0400        | 0.04456 |
| 0.6500        | -0.03352 | 0.0500        | 0.04915 |
| 0.6000        | -0.03673 | 0.0600        | 0.05306 |
| 0.5500        | -0.03951 | 0.0800        | 0.05949 |
| 0.5000        | -0.04183 | 0.1000        | 0.06435 |
| 0.4500        | -0.04360 | 0.1400        | 0.07075 |
| 0.4000        | -0.04474 | 0.1600        | 0.07272 |
| 0.3500        | -0.04512 | 0.1800        | 0.07408 |
| 0.3000        | -0.04456 | 0.2000        | 0.07497 |
| 0.2500        | -0.04289 | 0.2400        | 0.07589 |
| 0.2000        | -0.03979 | 0.2600        | 0.07596 |
| 0.1500        | -0.03506 | 0.2800        | 0.07583 |
| 0.1000        | -0.02938 | 0.3000        | 0.07548 |
| 0.0750        | -0.02626 | 0.3200        | 0.07496 |
| 0.0500        | -0.02261 | 0.3400        | 0.07428 |
| 0.0250        | -0.01728 | 0.3600        | 0.07343 |
| 0.0100        | -0.01121 | 0.3800        | 0.07245 |
| 0.0042        | -0.00681 | 0.4000        | 0.07134 |
| 0.0010        | -0.00245 | 0.4400        | 0.06874 |
|               |          | 0.5200        | 0.06232 |
|               |          | 0.5600        | 0.05859 |
|               |          | 0.6000        | 0.05456 |
|               |          | 0.6400        | 0.05026 |
|               |          | 0.6800        | 0.04571 |
|               |          | 0.7200        | 0.04093 |
|               |          | 0.7600        | 0.03593 |
|               |          | 0.8000        | 0.03071 |
|               |          | 0.8500        | 0.02389 |
|               |          | 0.9000        | 0.01673 |
|               |          | 0.9500        | 0.00919 |

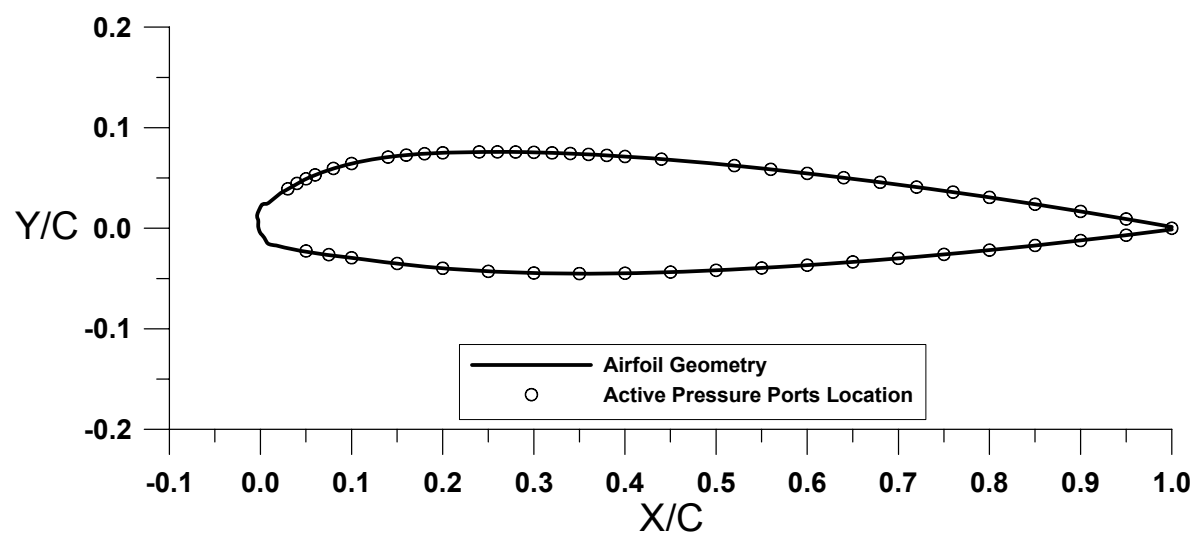


Figure A3.—NACA 23012 with 5-min glaze ice shape.

TABLE A3.1.—COORDINATES OF NACA 23012 WITH 5-MIN GLAZE ICE SHAPE

| Lower Surface |         |         |         | Upper Surface |        |        |        |
|---------------|---------|---------|---------|---------------|--------|--------|--------|
| x/c           | y/c     | x/c     | y/c     | x/c           | y/c    | x/c    | y/c    |
| 1.0000        | -0.0013 | 0.0375  | -0.0213 | -0.0025       | 0.0016 | 0.6826 | 0.0454 |
| 0.9783        | -0.0038 | 0.0197  | -0.0175 | -0.0026       | 0.0039 | 0.7053 | 0.0427 |
| 0.9556        | -0.0063 | 0.0174  | -0.0171 | -0.0023       | 0.0062 | 0.7280 | 0.0400 |
| 0.9330        | -0.0088 | 0.0152  | -0.0168 | -0.0024       | 0.0084 | 0.7506 | 0.0371 |
| 0.9103        | -0.0112 | 0.0129  | -0.0167 | -0.0035       | 0.0104 | 0.7732 | 0.0342 |
| 0.8876        | -0.0135 | 0.0099  | -0.0160 | -0.0037       | 0.0127 | 0.7958 | 0.0313 |
| 0.8649        | -0.0157 | 0.0074  | -0.0145 | -0.0030       | 0.0151 | 0.8185 | 0.0282 |
| 0.8421        | -0.0179 | 0.0059  | -0.0128 | -0.0016       | 0.0180 | 0.8411 | 0.0251 |
| 0.8194        | -0.0200 | 0.0052  | -0.0106 | 0.0001        | 0.0214 | 0.8637 | 0.0220 |
| 0.7967        | -0.0220 | 0.0037  | -0.0088 | 0.0016        | 0.0234 | 0.8863 | 0.0187 |
| 0.7740        | -0.0240 | 0.0019  | -0.0071 | 0.0037        | 0.0243 | 0.9088 | 0.0154 |
| 0.7512        | -0.0259 | 0.0004  | -0.0053 | 0.0068        | 0.0242 | 0.9314 | 0.0120 |
| 0.7285        | -0.0277 | -0.0008 | -0.0034 | 0.0088        | 0.0251 | 0.9540 | 0.0086 |
| 0.7057        | -0.0295 | -0.0020 | -0.0006 | 0.0223        | 0.0350 | 0.9765 | 0.0050 |
| 0.6830        | -0.0312 |         |         | 0.0280        | 0.0379 |        |        |
| 0.6602        | -0.0328 |         |         | 0.0483        | 0.0483 |        |        |
| 0.6375        | -0.0344 |         |         | 0.0696        | 0.0563 |        |        |
| 0.6147        | -0.0358 |         |         | 0.0916        | 0.0624 |        |        |
| 0.5919        | -0.0372 |         |         | 0.1140        | 0.0670 |        |        |
| 0.5691        | -0.0385 |         |         | 0.1365        | 0.0703 |        |        |
| 0.5463        | -0.0397 |         |         | 0.1592        | 0.0727 |        |        |
| 0.5236        | -0.0408 |         |         | 0.1820        | 0.0742 |        |        |
| 0.5008        | -0.0418 |         |         | 0.2048        | 0.0752 |        |        |
| 0.4780        | -0.0427 |         |         | 0.2276        | 0.0757 |        |        |
| 0.4552        | -0.0435 |         |         | 0.2504        | 0.0760 |        |        |
| 0.4323        | -0.0441 |         |         | 0.2732        | 0.0759 |        |        |
| 0.4095        | -0.0446 |         |         | 0.2961        | 0.0756 |        |        |
| 0.3867        | -0.0449 |         |         | 0.3189        | 0.0750 |        |        |
| 0.3639        | -0.0451 |         |         | 0.3417        | 0.0742 |        |        |
| 0.3411        | -0.0451 |         |         | 0.3645        | 0.0732 |        |        |
| 0.3183        | -0.0449 |         |         | 0.3873        | 0.0721 |        |        |
| 0.2954        | -0.0445 |         |         | 0.4100        | 0.0707 |        |        |
| 0.2726        | -0.0438 |         |         | 0.4328        | 0.0692 |        |        |
| 0.2498        | -0.0429 |         |         | 0.4556        | 0.0676 |        |        |
| 0.2271        | -0.0417 |         |         | 0.4783        | 0.0659 |        |        |
| 0.2043        | -0.0401 |         |         | 0.5011        | 0.0640 |        |        |
| 0.1816        | -0.0382 |         |         | 0.5238        | 0.0620 |        |        |
| 0.1588        | -0.0360 |         |         | 0.5465        | 0.0599 |        |        |
| 0.1362        | -0.0336 |         |         | 0.5692        | 0.0577 |        |        |
| 0.1135        | -0.0310 |         |         | 0.5919        | 0.0554 |        |        |
| 0.0908        | -0.0283 |         |         | 0.6146        | 0.0530 |        |        |
| 0.0830        | -0.0277 |         |         | 0.6373        | 0.0506 |        |        |
| 0.0602        | -0.0248 |         |         | 0.6600        | 0.0480 |        |        |

TABLE A3.2.—COORDINATES OF ACTIVE PRESSURE PORTS OF NACA 23012 WITH 5-MIN GLAZE ICE SHAPE

| Lower Surface |          | Upper Surface |         |
|---------------|----------|---------------|---------|
| x/c           | y/c      | x/c           | y/c     |
| 1.0000        | 0.00000  | 0.0300        | 0.03921 |
| 0.9500        | -0.00693 | 0.0400        | 0.04456 |
| 0.9000        | -0.01223 | 0.0500        | 0.04915 |
| 0.8500        | -0.01716 | 0.0600        | 0.05306 |
| 0.8000        | -0.02175 | 0.0800        | 0.05949 |
| 0.7500        | -0.02601 | 0.1000        | 0.06435 |
| 0.7000        | -0.02994 | 0.1400        | 0.07075 |
| 0.6500        | -0.03352 | 0.1600        | 0.07272 |
| 0.6000        | -0.03673 | 0.1800        | 0.07408 |
| 0.5500        | -0.03951 | 0.2000        | 0.07497 |
| 0.5000        | -0.04183 | 0.2400        | 0.07589 |
| 0.4500        | -0.04360 | 0.2600        | 0.07596 |
| 0.4000        | -0.04474 | 0.2800        | 0.07583 |
| 0.3500        | -0.04512 | 0.3000        | 0.07548 |
| 0.3000        | -0.04456 | 0.3200        | 0.07496 |
| 0.2500        | -0.04289 | 0.3400        | 0.07428 |
| 0.2000        | -0.03979 | 0.3600        | 0.07343 |
| 0.1500        | -0.03506 | 0.3800        | 0.07245 |
| 0.1000        | -0.02938 | 0.4000        | 0.07134 |
| 0.0750        | -0.02626 | 0.4400        | 0.06874 |
| 0.0500        | -0.02261 | 0.5200        | 0.06232 |
|               |          | 0.5600        | 0.05859 |
|               |          | 0.6000        | 0.05456 |
|               |          | 0.6400        | 0.05026 |
|               |          | 0.6800        | 0.04571 |
|               |          | 0.7200        | 0.04093 |
|               |          | 0.7600        | 0.03593 |
|               |          | 0.8000        | 0.03071 |
|               |          | 0.8500        | 0.02389 |
|               |          | 0.9000        | 0.01673 |
|               |          | 0.9500        | 0.00919 |

## **LEWICE 2.2 Input File for the NACA 23012 with 5-min Glaze Ice Shape**

```
Glaze 5-min Case
&LEW20
ITIMFL = 0
TSTOP  = 300.
IBOD   = 1
IFLO   = 4
DSMN   = 4.0D-4
NPL    = 24
&END
&DIST
FLWC  = 0.05, 0.1, 0.2, 0.3, 0.2, 0.1, 0.03, 0.01, 0.005, 0.005
DPD   = 4., 9.7, 14.2, 20.9, 28.2, 45.2, 70.1, 88.9, 103.4, 164.
&END
&ICE1
CHORD = 0.9144
AOA   = 2.5
VINF  = 78.2
LWC   = 0.50
TINF  = 267.87
PINF  = 94806.00
RH    = 100.0
&END
&LPRNT
FPRT  = 1
HPRT  = 1
BPRT  = 1
TPRT  = 0
&END
&RDATA
&END
```

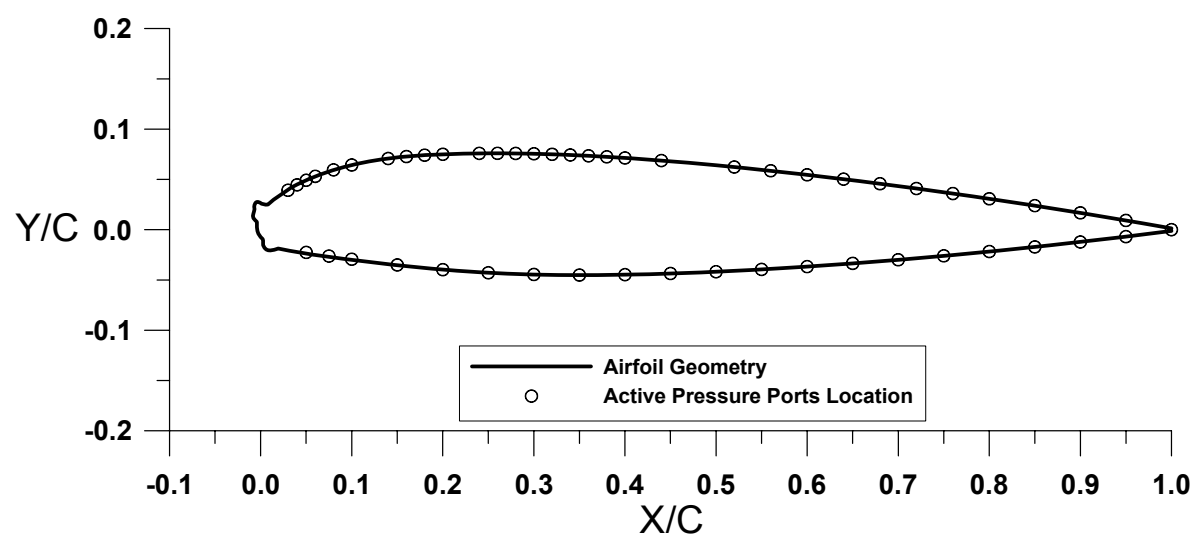


Figure A4.—NACA 23012 with 10-min glaze ice shape.

TABLE A4.1.—COORDINATES OF NACA 23012 WITH 10-MIN GLAZE ICE SHAPE

| <b>Lower Surface</b> |         |         |         | <b>Upper Surface</b> |         |        |        |        |
|----------------------|---------|---------|---------|----------------------|---------|--------|--------|--------|
| x/c                  | y/c     | x/c     | y/c     | x/c                  | y/c     | x/c    | y/c    |        |
| 1.0000               | -0.0013 | 0.0171  | -0.0194 |                      | -0.0038 | 0.0002 | 0.5919 | 0.0554 |
| 0.9783               | -0.0038 | 0.0149  | -0.0200 |                      | -0.0040 | 0.0025 | 0.6146 | 0.0530 |
| 0.9556               | -0.0063 | 0.0106  | -0.0206 |                      | -0.0040 | 0.0048 | 0.6373 | 0.0506 |
| 0.9330               | -0.0088 | 0.0081  | -0.0205 |                      | -0.0042 | 0.0078 | 0.6600 | 0.0480 |
| 0.9103               | -0.0112 | 0.0060  | -0.0197 |                      | -0.0060 | 0.0094 | 0.6826 | 0.0454 |
| 0.8876               | -0.0135 | 0.0043  | -0.0181 |                      | -0.0080 | 0.0115 | 0.7053 | 0.0427 |
| 0.8649               | -0.0157 | 0.0031  | -0.0161 |                      | -0.0084 | 0.0137 | 0.7280 | 0.0400 |
| 0.8421               | -0.0179 | 0.0026  | -0.0139 |                      | -0.0081 | 0.0160 | 0.7506 | 0.0371 |
| 0.8194               | -0.0200 | 0.0028  | -0.0116 |                      | -0.0071 | 0.0181 | 0.7732 | 0.0342 |
| 0.7967               | -0.0220 | 0.0023  | -0.0094 |                      | -0.0068 | 0.0204 | 0.7958 | 0.0313 |
| 0.7740               | -0.0240 | 0.0006  | -0.0078 |                      | -0.0070 | 0.0227 | 0.8185 | 0.0282 |
| 0.7512               | -0.0259 | -0.0010 | -0.0061 |                      | -0.0066 | 0.0250 | 0.8411 | 0.0251 |
| 0.7285               | -0.0277 | -0.0023 | -0.0042 |                      | -0.0053 | 0.0268 | 0.8637 | 0.0220 |
| 0.7057               | -0.0295 | -0.0032 | -0.0021 |                      | -0.0031 | 0.0276 | 0.8863 | 0.0187 |
| 0.6830               | -0.0312 |         |         |                      | -0.0010 | 0.0269 | 0.9088 | 0.0154 |
| 0.6602               | -0.0328 |         |         |                      | 0.0010  | 0.0257 | 0.9314 | 0.0120 |
| 0.6375               | -0.0344 |         |         |                      | 0.0033  | 0.0253 | 0.9540 | 0.0086 |
| 0.6147               | -0.0358 |         |         |                      | 0.0056  | 0.0249 | 0.9765 | 0.0050 |
| 0.5919               | -0.0372 |         |         |                      | 0.0081  | 0.0251 | 1.0000 | 0.0013 |
| 0.5691               | -0.0385 |         |         |                      | 0.0141  | 0.0297 |        |        |
| 0.5463               | -0.0397 |         |         |                      | 0.0339  | 0.0420 |        |        |
| 0.5236               | -0.0408 |         |         |                      | 0.0483  | 0.0483 |        |        |
| 0.5008               | -0.0418 |         |         |                      | 0.0696  | 0.0563 |        |        |
| 0.4780               | -0.0427 |         |         |                      | 0.0916  | 0.0624 |        |        |
| 0.4552               | -0.0435 |         |         |                      | 0.1140  | 0.0670 |        |        |
| 0.4323               | -0.0441 |         |         |                      | 0.1365  | 0.0703 |        |        |
| 0.4095               | -0.0446 |         |         |                      | 0.1592  | 0.0727 |        |        |
| 0.3867               | -0.0449 |         |         |                      | 0.1820  | 0.0742 |        |        |
| 0.3639               | -0.0451 |         |         |                      | 0.2048  | 0.0752 |        |        |
| 0.3411               | -0.0451 |         |         |                      | 0.2276  | 0.0757 |        |        |
| 0.3183               | -0.0449 |         |         |                      | 0.2504  | 0.0760 |        |        |
| 0.2954               | -0.0445 |         |         |                      | 0.2732  | 0.0759 |        |        |
| 0.2726               | -0.0438 |         |         |                      | 0.2961  | 0.0756 |        |        |
| 0.2498               | -0.0429 |         |         |                      | 0.3189  | 0.0750 |        |        |
| 0.2271               | -0.0417 |         |         |                      | 0.3417  | 0.0742 |        |        |
| 0.2043               | -0.0401 |         |         |                      | 0.3645  | 0.0732 |        |        |
| 0.1816               | -0.0382 |         |         |                      | 0.3873  | 0.0721 |        |        |
| 0.1588               | -0.0360 |         |         |                      | 0.4100  | 0.0707 |        |        |
| 0.1362               | -0.0336 |         |         |                      | 0.4328  | 0.0692 |        |        |
| 0.1179               | -0.0319 |         |         |                      | 0.4556  | 0.0676 |        |        |
| 0.0948               | -0.0294 |         |         |                      | 0.4783  | 0.0659 |        |        |
| 0.0717               | -0.0266 |         |         |                      | 0.5011  | 0.0640 |        |        |
| 0.0486               | -0.0236 |         |         |                      | 0.5238  | 0.0620 |        |        |
| 0.0257               | -0.0198 |         |         |                      | 0.5465  | 0.0599 |        |        |
| 0.0193               | -0.0188 |         |         |                      | 0.5692  | 0.0577 |        |        |

TABLE A4.2.—COORDINATES OF ACTIVE PRESSURE PORTS OF NACA 23012 WITH 10-MIN GLAZE ICE SHAPE

| Lower Surface |          | Upper Surface |         |
|---------------|----------|---------------|---------|
| x/c           | y/c      | x/c           | y/c     |
| 1.0000        | 0.00000  | 0.0300        | 0.03921 |
| 0.9500        | -0.00693 | 0.0400        | 0.04456 |
| 0.9000        | -0.01223 | 0.0500        | 0.04915 |
| 0.8500        | -0.01716 | 0.0600        | 0.05306 |
| 0.8000        | -0.02175 | 0.0800        | 0.05949 |
| 0.7500        | -0.02601 | 0.1000        | 0.06435 |
| 0.7000        | -0.02994 | 0.1400        | 0.07075 |
| 0.6500        | -0.03352 | 0.1600        | 0.07272 |
| 0.6000        | -0.03673 | 0.1800        | 0.07408 |
| 0.5500        | -0.03951 | 0.2000        | 0.07497 |
| 0.5000        | -0.04183 | 0.2400        | 0.07589 |
| 0.4500        | -0.04360 | 0.2600        | 0.07596 |
| 0.4000        | -0.04474 | 0.2800        | 0.07583 |
| 0.3500        | -0.04512 | 0.3000        | 0.07548 |
| 0.3000        | -0.04456 | 0.3200        | 0.07496 |
| 0.2500        | -0.04289 | 0.3400        | 0.07428 |
| 0.2000        | -0.03979 | 0.3600        | 0.07343 |
| 0.1500        | -0.03506 | 0.3800        | 0.07245 |
| 0.1000        | -0.02938 | 0.4000        | 0.07134 |
| 0.0750        | -0.02626 | 0.4400        | 0.06874 |
| 0.0500        | -0.02261 | 0.5200        | 0.06232 |
|               |          | 0.5600        | 0.05859 |
|               |          | 0.6000        | 0.05456 |
|               |          | 0.6400        | 0.05026 |
|               |          | 0.6800        | 0.04571 |
|               |          | 0.7200        | 0.04093 |
|               |          | 0.7600        | 0.03593 |
|               |          | 0.8000        | 0.03071 |
|               |          | 0.8500        | 0.02389 |
|               |          | 0.9000        | 0.01673 |
|               |          | 0.9500        | 0.00919 |

## **LEWICE 2.2 Input File for the NACA 23012 with 10-min Glaze Ice Shape**

Glaze 10-min Case

&LEW20

ITIMFL = 0

TSTOP = 600.

IBOD = 1

IFLO = 8

DSMN = 4.0D-4

NPL = 24

&END

&DIST

FLWC = 0.05, 0.1, 0.2, 0.3, 0.2, 0.1, 0.03, 0.01, 0.005, 0.005

DPD = 4., 9.7, 14.2, 20.9, 28.2, 45.2, 70.1, 88.9, 103.4, 164.

&END

&ICE1

CHORD = 0.9144

AOA = 2.5

VINF = 78.2

LWC = 0.50

TINF = 267.87

PINF = 94806.00

RH = 100.0

&END

&LPRNT

FPRT = 1

HPRT = 1

BPRT = 1

TPRT = 0

&END

&RDATA

&END

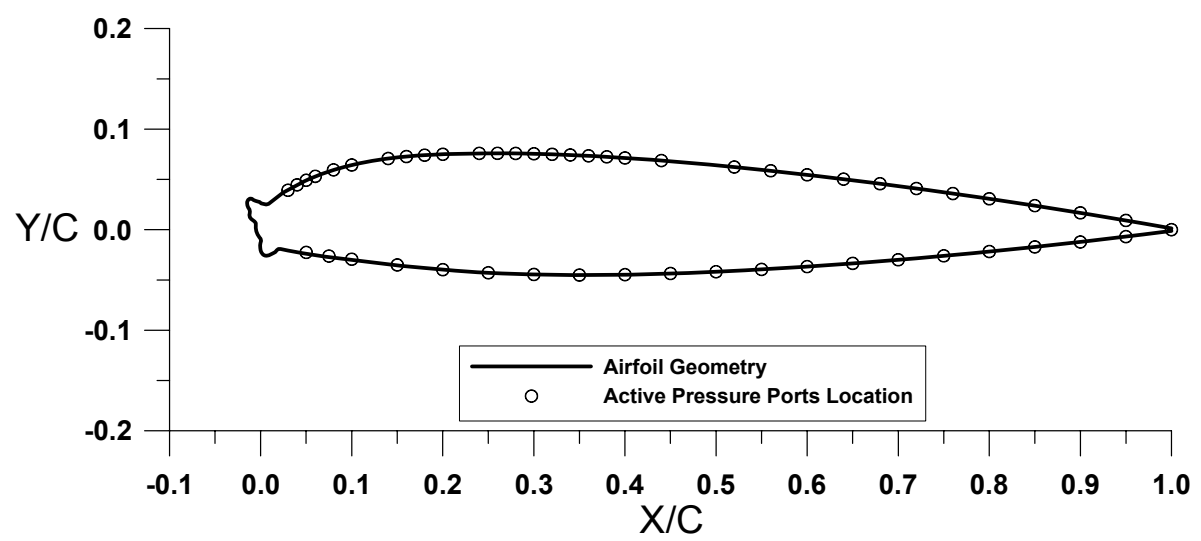


Figure A5.—NACA 23012 with 15-min glaze ice shape.

TABLE A5.1.—COORDINATES OF NACA 23012 WITH 15-MIN GLAZE ICE SHAPE

| Lower Surface |         |         | Upper Surface |         |        |
|---------------|---------|---------|---------------|---------|--------|
| x/c           | y/c     | x/c     | y/c           | x/c     | y/c    |
| 1.0000        | -0.0013 | 0.0195  | -0.0192       | -0.0052 | 0.0012 |
| 0.9783        | -0.0038 | 0.0177  | -0.0205       | -0.0053 | 0.0035 |
| 0.9556        | -0.0063 | 0.0162  | -0.0223       | -0.0053 | 0.0065 |
| 0.9330        | -0.0088 | 0.0142  | -0.0232       | -0.0067 | 0.0081 |
| 0.9103        | -0.0112 | 0.0110  | -0.0247       | -0.0103 | 0.0106 |
| 0.8876        | -0.0135 | 0.0086  | -0.0255       | -0.0118 | 0.0124 |
| 0.8649        | -0.0157 | 0.0064  | -0.0259       | -0.0124 | 0.0146 |
| 0.8421        | -0.0179 | 0.0041  | -0.0256       | -0.0119 | 0.0169 |
| 0.8194        | -0.0200 | 0.0022  | -0.0244       | -0.0119 | 0.0191 |
| 0.7967        | -0.0220 | 0.0008  | -0.0226       | -0.0129 | 0.0212 |
| 0.7740        | -0.0240 | 0.0000  | -0.0205       | -0.0141 | 0.0232 |
| 0.7512        | -0.0259 | -0.0005 | -0.0182       | -0.0148 | 0.0253 |
| 0.7285        | -0.0277 | -0.0006 | -0.0155       | -0.0147 | 0.0276 |
| 0.7057        | -0.0295 | -0.0003 | -0.0132       | -0.0137 | 0.0296 |
| 0.6830        | -0.0312 | 0.0005  | -0.0111       | -0.0119 | 0.0309 |
| 0.6602        | -0.0328 | 0.0000  | -0.0090       | -0.0096 | 0.0308 |
| 0.6375        | -0.0344 | -0.0017 | -0.0072       | -0.0078 | 0.0295 |
| 0.6147        | -0.0358 | -0.0031 | -0.0053       | -0.0056 | 0.0288 |
| 0.5919        | -0.0372 | -0.0041 | -0.0033       | -0.0035 | 0.0280 |
| 0.5691        | -0.0385 | -0.0048 | -0.0011       | -0.0013 | 0.0275 |
| 0.5463        | -0.0397 |         |               | 0.0006  | 0.0262 |
| 0.5236        | -0.0408 |         |               | 0.0029  | 0.0256 |
| 0.5008        | -0.0418 |         |               | 0.0061  | 0.0250 |
| 0.4780        | -0.0427 |         |               | 0.0087  | 0.0257 |
| 0.4552        | -0.0435 |         |               | 0.0246  | 0.0368 |
| 0.4323        | -0.0441 |         |               | 0.0483  | 0.0483 |
| 0.4095        | -0.0446 |         |               | 0.0696  | 0.0563 |
| 0.3867        | -0.0449 |         |               | 0.0916  | 0.0624 |
| 0.3639        | -0.0451 |         |               | 0.1140  | 0.0670 |
| 0.3411        | -0.0451 |         |               | 0.1365  | 0.0703 |
| 0.3183        | -0.0449 |         |               | 0.1592  | 0.0727 |
| 0.2954        | -0.0445 |         |               | 0.1820  | 0.0742 |
| 0.2726        | -0.0438 |         |               | 0.2048  | 0.0752 |
| 0.2498        | -0.0429 |         |               | 0.2276  | 0.0757 |
| 0.2271        | -0.0417 |         |               | 0.2504  | 0.0760 |
| 0.2043        | -0.0401 |         |               | 0.2732  | 0.0759 |
| 0.1816        | -0.0382 |         |               | 0.2961  | 0.0756 |
| 0.1588        | -0.0360 |         |               | 0.3189  | 0.0750 |
| 0.1539        | -0.0358 |         |               | 0.3417  | 0.0742 |
| 0.1310        | -0.0335 |         |               | 0.3645  | 0.0732 |
| 0.1083        | -0.0310 |         |               | 0.3873  | 0.0721 |
| 0.0855        | -0.0285 |         |               | 0.4100  | 0.0707 |
| 0.0627        | -0.0257 |         |               | 0.4328  | 0.0692 |
| 0.0400        | -0.0225 |         |               | 0.4556  | 0.0676 |
| 0.0219        | -0.0193 |         |               | 0.4783  | 0.0659 |

TABLE A5.2.—COORDINATES OF ACTIVE PRESSURE PORTS OF NACA 23012 WITH 15-MIN GLAZE ICE SHAPE

| Lower Surface |          | Upper Surface |         |
|---------------|----------|---------------|---------|
| x/c           | y/c      | x/c           | y/c     |
| 1.0000        | 0.00000  | 0.0300        | 0.03921 |
| 0.9500        | -0.00693 | 0.0400        | 0.04456 |
| 0.9000        | -0.01223 | 0.0500        | 0.04915 |
| 0.8500        | -0.01716 | 0.0600        | 0.05306 |
| 0.8000        | -0.02175 | 0.0800        | 0.05949 |
| 0.7500        | -0.02601 | 0.1000        | 0.06435 |
| 0.7000        | -0.02994 | 0.1400        | 0.07075 |
| 0.6500        | -0.03352 | 0.1600        | 0.07272 |
| 0.6000        | -0.03673 | 0.1800        | 0.07408 |
| 0.5500        | -0.03951 | 0.2000        | 0.07497 |
| 0.5000        | -0.04183 | 0.2400        | 0.07589 |
| 0.4500        | -0.04360 | 0.2600        | 0.07596 |
| 0.4000        | -0.04474 | 0.2800        | 0.07583 |
| 0.3500        | -0.04512 | 0.3000        | 0.07548 |
| 0.3000        | -0.04456 | 0.3200        | 0.07496 |
| 0.2500        | -0.04289 | 0.3400        | 0.07428 |
| 0.2000        | -0.03979 | 0.3600        | 0.07343 |
| 0.1500        | -0.03506 | 0.3800        | 0.07245 |
| 0.1000        | -0.02938 | 0.4000        | 0.07134 |
| 0.0750        | -0.02626 | 0.4400        | 0.06874 |
| 0.0500        | -0.02261 | 0.5200        | 0.06232 |
|               |          | 0.5600        | 0.05859 |
|               |          | 0.6000        | 0.05456 |
|               |          | 0.6400        | 0.05026 |
|               |          | 0.6800        | 0.04571 |
|               |          | 0.7200        | 0.04093 |
|               |          | 0.7600        | 0.03593 |
|               |          | 0.8000        | 0.03071 |
|               |          | 0.8500        | 0.02389 |
|               |          | 0.9000        | 0.01673 |
|               |          | 0.9500        | 0.00919 |

## **LEWICE 2.2 Input File for the NACA 23012 with 15-min Glaze Ice Shape**

```
Glaze 15-min Case
&LEW20
ITIMFL = 0
TSTOP  = 900.
IBOD   = 1
IFLO   = 12
DSMN   = 4.0D-4
NPL    = 24
&END
&DIST
FLWC  = 0.05, 0.1, 0.2, 0.3, 0.2, 0.1, 0.03, 0.01, 0.005, 0.005
DPD   = 4., 9.7, 14.2, 20.9, 28.2, 45.2, 70.1, 88.9, 103.4, 164.
&END
&ICE1
CHORD = 0.9144
AOA   = 2.5
VINF  = 78.2
LWC   = 0.50
TINF  = 267.87
PINF  = 94806.00
RH    = 100.0
&END
&LPRNT
FPRT  = 1
HPRT  = 1
BPRT  = 1
TPRT  = 0
&END
&RDATA
&END
```

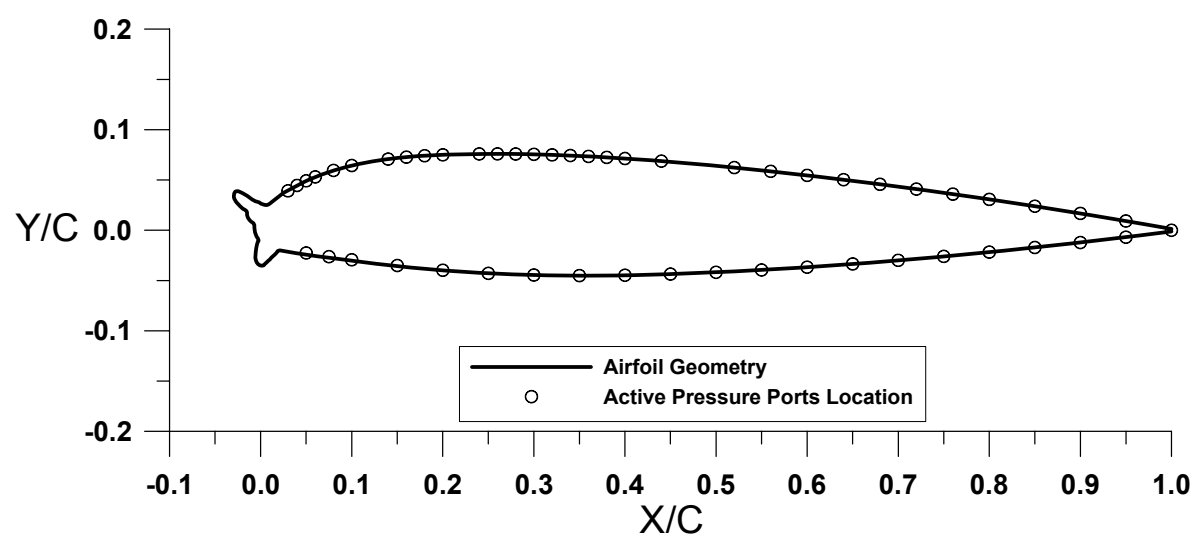


Figure A6.—NACA 23012 with 22.5-min ice shape.

TABLE A6.1.—COORDINATES OF NACA 23012 WITH 22.5-MIN GLAZE ICE SHAPE

| Lower Surface |         |         |         | Upper Surface |        |        |        |
|---------------|---------|---------|---------|---------------|--------|--------|--------|
| x/c           | y/c     | x/c     | y/c     | x/c           | y/c    | x/c    | y/c    |
| 1.0000        | -0.0013 | 0.0175  | -0.0225 | -0.0067       | 0.0002 | 0.1820 | 0.0742 |
| 0.9783        | -0.0038 | 0.0155  | -0.0242 | -0.0069       | 0.0027 | 0.2048 | 0.0752 |
| 0.9556        | -0.0063 | 0.0118  | -0.0273 | -0.0069       | 0.0051 | 0.2276 | 0.0757 |
| 0.9330        | -0.0088 | 0.0102  | -0.0289 | -0.0080       | 0.0070 | 0.2504 | 0.0760 |
| 0.9103        | -0.0112 | 0.0083  | -0.0303 | -0.0108       | 0.0089 | 0.2732 | 0.0759 |
| 0.8876        | -0.0135 | 0.0067  | -0.0320 | -0.0127       | 0.0107 | 0.2961 | 0.0756 |
| 0.8649        | -0.0157 | 0.0050  | -0.0334 | -0.0139       | 0.0126 | 0.3189 | 0.0750 |
| 0.8421        | -0.0179 | 0.0033  | -0.0349 | -0.0148       | 0.0148 | 0.3417 | 0.0742 |
| 0.8194        | -0.0200 | 0.0011  | -0.0353 | -0.0150       | 0.0170 | 0.3645 | 0.0732 |
| 0.7967        | -0.0220 | -0.0011 | -0.0348 | -0.0156       | 0.0192 | 0.3873 | 0.0721 |
| 0.7740        | -0.0240 | -0.0031 | -0.0335 | -0.0175       | 0.0203 | 0.4100 | 0.0707 |
| 0.7512        | -0.0259 | -0.0045 | -0.0318 | -0.0195       | 0.0214 | 0.4328 | 0.0692 |
| 0.7285        | -0.0277 | -0.0054 | -0.0297 | -0.0214       | 0.0228 | 0.4556 | 0.0676 |
| 0.7057        | -0.0295 | -0.0058 | -0.0274 | -0.0232       | 0.0245 | 0.4783 | 0.0659 |
| 0.6830        | -0.0312 | -0.0057 | -0.0251 | -0.0258       | 0.0270 | 0.5011 | 0.0640 |
| 0.6602        | -0.0328 | -0.0053 | -0.0211 | -0.0274       | 0.0288 | 0.5238 | 0.0620 |
| 0.6375        | -0.0344 | -0.0047 | -0.0176 | -0.0286       | 0.0307 | 0.5465 | 0.0599 |
| 0.6147        | -0.0358 | -0.0041 | -0.0144 | -0.0293       | 0.0329 | 0.5692 | 0.0577 |
| 0.5919        | -0.0372 | -0.0033 | -0.0122 | -0.0294       | 0.0351 | 0.5919 | 0.0554 |
| 0.5691        | -0.0385 | -0.0023 | -0.0102 | -0.0286       | 0.0373 | 0.6146 | 0.0530 |
| 0.5463        | -0.0397 | -0.0030 | -0.0081 | -0.0269       | 0.0387 | 0.6373 | 0.0506 |
| 0.5236        | -0.0408 | -0.0044 | -0.0062 | -0.0247       | 0.0389 | 0.6600 | 0.0480 |
| 0.5008        | -0.0418 | -0.0054 | -0.0042 | -0.0226       | 0.0381 | 0.6826 | 0.0454 |
| 0.4780        | -0.0427 | -0.0062 | -0.0020 | -0.0205       | 0.0372 | 0.7053 | 0.0427 |
| 0.4552        | -0.0435 |         |         | -0.0185       | 0.0362 | 0.7280 | 0.0400 |
| 0.4323        | -0.0441 |         |         | -0.0165       | 0.0351 | 0.7506 | 0.0371 |
| 0.4095        | -0.0446 |         |         | -0.0145       | 0.0340 | 0.7732 | 0.0342 |
| 0.3867        | -0.0449 |         |         | -0.0126       | 0.0327 | 0.7958 | 0.0313 |
| 0.3639        | -0.0451 |         |         | -0.0105       | 0.0314 | 0.8185 | 0.0282 |
| 0.3411        | -0.0451 |         |         | -0.0081       | 0.0299 | 0.8411 | 0.0251 |
| 0.3183        | -0.0449 |         |         | -0.0061       | 0.0290 | 0.8637 | 0.0220 |
| 0.2954        | -0.0445 |         |         | -0.0039       | 0.0283 | 0.8863 | 0.0187 |
| 0.2726        | -0.0438 |         |         | -0.0017       | 0.0278 | 0.9088 | 0.0154 |
| 0.2498        | -0.0429 |         |         | 0.0002        | 0.0265 | 0.9314 | 0.0120 |
| 0.2271        | -0.0417 |         |         | 0.0023        | 0.0258 | 0.9540 | 0.0086 |
| 0.2043        | -0.0401 |         |         | 0.0045        | 0.0252 | 0.9765 | 0.0050 |
| 0.1760        | -0.0381 |         |         | 0.0068        | 0.0249 | 1.0000 | 0.0013 |
| 0.1532        | -0.0359 |         |         | 0.0090        | 0.0259 |        |        |
| 0.1304        | -0.0336 |         |         | 0.0252        | 0.0372 |        |        |
| 0.1076        | -0.0311 |         |         | 0.0483        | 0.0483 |        |        |
| 0.0848        | -0.0286 |         |         | 0.0696        | 0.0563 |        |        |
| 0.0621        | -0.0258 |         |         | 0.0916        | 0.0624 |        |        |
| 0.0393        | -0.0229 |         |         | 0.1140        | 0.0670 |        |        |
| 0.0210        | -0.0200 |         |         | 0.1365        | 0.0703 |        |        |
| 0.0188        | -0.0207 |         |         | 0.1592        | 0.0727 |        |        |

TABLE A6.2.—COORDINATES OF ACTIVE PRESSURE  
PORTS OF NACA 23012 WITH 22.5-MIN GLAZE ICE SHAPE

| Lower Surface |          | Upper Surface |         |
|---------------|----------|---------------|---------|
| x/c           | y/c      | x/c           | y/c     |
| 1.0000        | 0.00000  | 0.0300        | 0.03921 |
| 0.9500        | -0.00693 | 0.0400        | 0.04456 |
| 0.9000        | -0.01223 | 0.0500        | 0.04915 |
| 0.8500        | -0.01716 | 0.0600        | 0.05306 |
| 0.8000        | -0.02175 | 0.0800        | 0.05949 |
| 0.7500        | -0.02601 | 0.1000        | 0.06435 |
| 0.7000        | -0.02994 | 0.1400        | 0.07075 |
| 0.6500        | -0.03352 | 0.1600        | 0.07272 |
| 0.6000        | -0.03673 | 0.1800        | 0.07408 |
| 0.5500        | -0.03951 | 0.2000        | 0.07497 |
| 0.5000        | -0.04183 | 0.2400        | 0.07589 |
| 0.4500        | -0.04360 | 0.2600        | 0.07596 |
| 0.4000        | -0.04474 | 0.2800        | 0.07583 |
| 0.3500        | -0.04512 | 0.3000        | 0.07548 |
| 0.3000        | -0.04456 | 0.3200        | 0.07496 |
| 0.2500        | -0.04289 | 0.3400        | 0.07428 |
| 0.2000        | -0.03979 | 0.3600        | 0.07343 |
| 0.1500        | -0.03506 | 0.3800        | 0.07245 |
| 0.1000        | -0.02938 | 0.4000        | 0.07134 |
| 0.0750        | -0.02626 | 0.4400        | 0.06874 |
| 0.0500        | -0.02261 | 0.5200        | 0.06232 |
|               |          | 0.5600        | 0.05859 |
|               |          | 0.6000        | 0.05456 |
|               |          | 0.6400        | 0.05026 |
|               |          | 0.6800        | 0.04571 |
|               |          | 0.7200        | 0.04093 |
|               |          | 0.7600        | 0.03593 |
|               |          | 0.8000        | 0.03071 |
|               |          | 0.8500        | 0.02389 |
|               |          | 0.9000        | 0.01673 |
|               |          | 0.9500        | 0.00919 |

## LEWICE 2.2 Input File for the NACA 23012 with 22.5-min Glaze Ice Shape

Glaze 22.5-min Case

&LEW20

ITIMFL = 0

TSTOP = 1350.

IBOD = 1

IFLO = 18

DSMN = 4.0D-4

NPL = 24

&END

&DIST

FLWC = 0.05, 0.1, 0.2, 0.3, 0.2, 0.1, 0.03, 0.01, 0.005, 0.005

DPD = 4., 9.7, 14.2, 20.9, 28.2, 45.2, 70.1, 88.9, 103.4, 164.

&END

&ICE1

CHORD = 0.9144

AOA = 2.5

VINF = 78.2

LWC = 0.50

TINF = 267.87

PINF = 94806.00

RH = 100.0

&END

&LPRNT

FPRT = 1

HPRT = 1

BPRT = 1

TPRT = 0

&END

&RDATA

&END

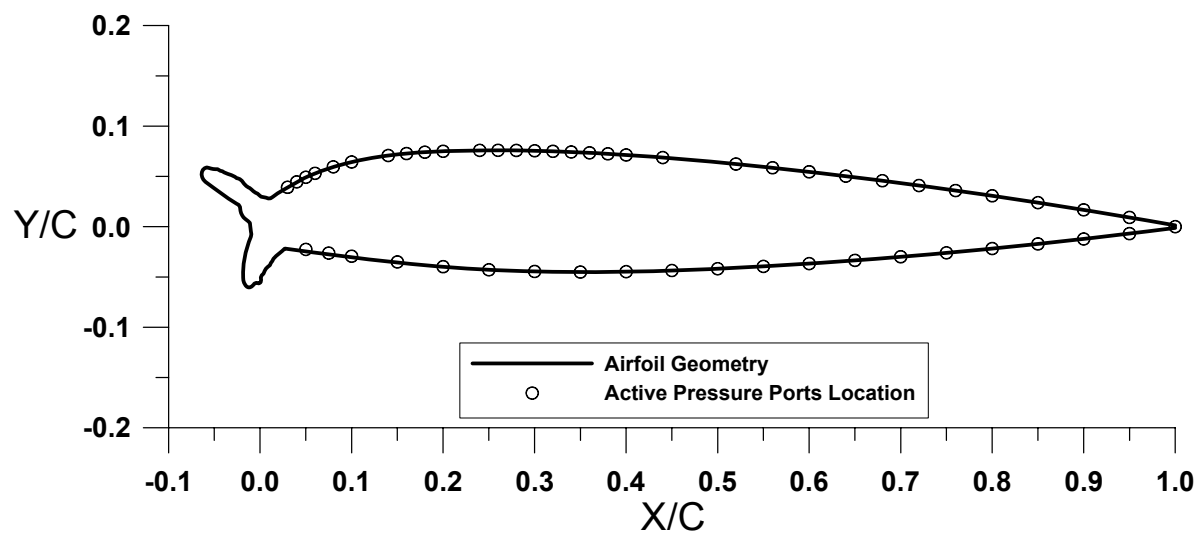


Figure A7.—NACA 23012 with 45-min glaze ice shape.

TABLE A7.1.—COORDINATES OF NACA 23012 WITH 45-MIN GLAZE ICE SHAPE

| Lower Surface |         |         |         | Upper Surface |        |         |        |
|---------------|---------|---------|---------|---------------|--------|---------|--------|
| x/c           | y/c     | x/c     | y/c     | x/c           | y/c    | x/c     | y/c    |
| 1.0000        | -0.0013 | 0.0232  | -0.0248 | -0.0108       | 0.0006 | -0.0233 | 0.0476 |
| 0.9783        | -0.0038 | 0.0208  | -0.0269 | -0.0111       | 0.0038 | -0.0210 | 0.0468 |
| 0.9556        | -0.0063 | 0.0181  | -0.0284 | -0.0130       | 0.0055 | -0.0194 | 0.0450 |
| 0.9330        | -0.0088 | 0.0164  | -0.0303 | -0.0161       | 0.0076 | -0.0179 | 0.0430 |
| 0.9103        | -0.0112 | 0.0146  | -0.0320 | -0.0180       | 0.0092 | -0.0160 | 0.0413 |
| 0.8876        | -0.0135 | 0.0133  | -0.0341 | -0.0196       | 0.0112 | -0.0134 | 0.0397 |
| 0.8649        | -0.0157 | 0.0118  | -0.0361 | -0.0207       | 0.0134 | -0.0114 | 0.0384 |
| 0.8421        | -0.0179 | 0.0106  | -0.0383 | -0.0213       | 0.0158 | -0.0094 | 0.0370 |
| 0.8194        | -0.0200 | 0.0082  | -0.0401 | -0.0219       | 0.0197 | -0.0072 | 0.0353 |
| 0.7967        | -0.0220 | 0.0063  | -0.0418 | -0.0233       | 0.0216 | -0.0050 | 0.0338 |
| 0.7740        | -0.0240 | 0.0050  | -0.0439 | -0.0256       | 0.0229 | -0.0028 | 0.0327 |
| 0.7512        | -0.0259 | 0.0038  | -0.0467 | -0.0279       | 0.0242 | -0.0009 | 0.0312 |
| 0.7285        | -0.0277 | 0.0019  | -0.0483 | -0.0309       | 0.0257 | 0.0012  | 0.0298 |
| 0.7057        | -0.0295 | 0.0009  | -0.0505 | -0.0330       | 0.0271 | 0.0039  | 0.0294 |
| 0.6830        | -0.0312 | 0.0013  | -0.0529 | -0.0351       | 0.0283 | 0.0066  | 0.0288 |
| 0.6602        | -0.0328 | 0.0006  | -0.0553 | -0.0383       | 0.0303 | 0.0090  | 0.0281 |
| 0.6375        | -0.0344 | -0.0014 | -0.0565 | -0.0408       | 0.0319 | 0.0114  | 0.0282 |
| 0.6147        | -0.0358 | -0.0039 | -0.0559 | -0.0437       | 0.0339 | 0.0139  | 0.0296 |
| 0.5919        | -0.0372 | -0.0062 | -0.0566 | -0.0464       | 0.0358 | 0.0191  | 0.0331 |
| 0.5691        | -0.0385 | -0.0081 | -0.0583 | -0.0484       | 0.0371 | 0.0280  | 0.0379 |
| 0.5463        | -0.0397 | -0.0098 | -0.0600 | -0.0517       | 0.0393 | 0.0483  | 0.0483 |
| 0.5236        | -0.0408 | -0.0122 | -0.0604 | -0.0538       | 0.0406 | 0.0696  | 0.0563 |
| 0.5008        | -0.0418 | -0.0145 | -0.0596 | -0.0568       | 0.0425 | 0.0916  | 0.0624 |
| 0.4780        | -0.0427 | -0.0163 | -0.0579 | -0.0597       | 0.0446 | 0.1140  | 0.0670 |
| 0.4552        | -0.0435 | -0.0175 | -0.0557 | -0.0619       | 0.0468 | 0.1365  | 0.0703 |
| 0.4323        | -0.0441 | -0.0183 | -0.0534 | -0.0631       | 0.0490 | 0.1592  | 0.0727 |
| 0.4095        | -0.0446 | -0.0185 | -0.0509 | -0.0638       | 0.0518 | 0.1820  | 0.0742 |
| 0.3867        | -0.0449 | -0.0185 | -0.0484 | -0.0636       | 0.0543 | 0.2048  | 0.0752 |
| 0.3639        | -0.0451 | -0.0185 | -0.0459 | -0.0626       | 0.0565 | 0.2276  | 0.0757 |
| 0.3411        | -0.0451 | -0.0184 | -0.0414 | -0.0607       | 0.0581 | 0.2504  | 0.0760 |
| 0.3183        | -0.0449 | -0.0181 | -0.0381 | -0.0584       | 0.0588 | 0.2732  | 0.0759 |
| 0.2954        | -0.0445 | -0.0178 | -0.0350 | -0.0560       | 0.0583 | 0.2961  | 0.0756 |
| 0.2726        | -0.0438 | -0.0170 | -0.0311 | -0.0536       | 0.0579 | 0.3189  | 0.0750 |
| 0.2498        | -0.0429 | -0.0163 | -0.0281 | -0.0512       | 0.0574 | 0.3417  | 0.0742 |
| 0.2271        | -0.0417 | -0.0154 | -0.0248 | -0.0488       | 0.0572 | 0.3645  | 0.0732 |
| 0.2043        | -0.0401 | -0.0146 | -0.0223 | -0.0463       | 0.0571 | 0.3873  | 0.0721 |
| 0.1816        | -0.0386 | -0.0133 | -0.0184 | -0.0435       | 0.0556 | 0.4100  | 0.0707 |
| 0.1569        | -0.0364 | -0.0124 | -0.0157 | -0.0411       | 0.0551 | 0.4328  | 0.0692 |
| 0.1322        | -0.0339 | -0.0115 | -0.0134 | -0.0390       | 0.0538 | 0.4556  | 0.0676 |
| 0.1074        | -0.0313 | -0.0100 | -0.0100 | -0.0366       | 0.0533 | 0.4783  | 0.0659 |
| 0.0827        | -0.0285 | -0.0095 | -0.0074 | -0.0344       | 0.0520 | 0.5011  | 0.0640 |
| 0.0581        | -0.0256 | -0.0100 | -0.0046 | -0.0320       | 0.0518 | 0.5238  | 0.0620 |
| 0.0334        | -0.0223 | -0.0106 | -0.0019 | -0.0299       | 0.0506 | 0.5465  | 0.0599 |
| 0.0270        | -0.0217 |         |         | -0.0277       | 0.0495 | 0.5692  | 0.0577 |
| 0.0251        | -0.0232 |         |         | -0.0256       | 0.0483 | 0.5919  | 0.0554 |

TABLE A7.2.—COORDINATES OF ACTIVE PRESSURE PORTS OF NACA 23012 WITH 45-MIN GLAZE ICE SHAPE

| <b>Lower Surface</b> |          | <b>Upper Surface</b> |         |
|----------------------|----------|----------------------|---------|
| x/c                  | y/c      | x/c                  | y/c     |
| 1.0000               | 0.00000  | 0.0300               | 0.03921 |
| 0.9500               | -0.00693 | 0.0400               | 0.04456 |
| 0.9000               | -0.01223 | 0.0500               | 0.04915 |
| 0.8500               | -0.01716 | 0.0600               | 0.05306 |
| 0.8000               | -0.02175 | 0.0800               | 0.05949 |
| 0.7500               | -0.02601 | 0.1000               | 0.06435 |
| 0.7000               | -0.02994 | 0.1400               | 0.07075 |
| 0.6500               | -0.03352 | 0.1600               | 0.07272 |
| 0.6000               | -0.03673 | 0.1800               | 0.07408 |
| 0.5500               | -0.03951 | 0.2000               | 0.07497 |
| 0.5000               | -0.04183 | 0.2400               | 0.07589 |
| 0.4500               | -0.04360 | 0.2600               | 0.07596 |
| 0.4000               | -0.04474 | 0.2800               | 0.07583 |
| 0.3500               | -0.04512 | 0.3000               | 0.07548 |
| 0.3000               | -0.04456 | 0.3200               | 0.07496 |
| 0.2500               | -0.04289 | 0.3400               | 0.07428 |
| 0.2000               | -0.03979 | 0.3600               | 0.07343 |
| 0.1500               | -0.03506 | 0.3800               | 0.07245 |
| 0.1000               | -0.02938 | 0.4000               | 0.07134 |
| 0.0750               | -0.02626 | 0.4400               | 0.06874 |
| 0.0500               | -0.02261 | 0.5200               | 0.06232 |
|                      |          | 0.5600               | 0.05859 |
|                      |          | 0.6000               | 0.05456 |
|                      |          | 0.6400               | 0.05026 |
|                      |          | 0.6800               | 0.04571 |
|                      |          | 0.7200               | 0.04093 |
|                      |          | 0.7600               | 0.03593 |
|                      |          | 0.8000               | 0.03071 |
|                      |          | 0.8500               | 0.02389 |
|                      |          | 0.9000               | 0.01673 |
|                      |          | 0.9500               | 0.00919 |

## **LEWICE 2.2 Input File for the NACA 23012 with 45-min Glaze Ice Shape**

```
Glaze 45-min Case
&LEW20
ITIMFL = 1
TSTOP  = 2700.
IBOD   = 1
IFLO   = 18
DSMN   = 4.0D-4
NPL    = 24
&END
&DIST
FLWC  = 0.05, 0.1, 0.2, 0.3, 0.2, 0.1, 0.03, 0.01, 0.005, 0.005
DPD   = 4., 9.7, 14.2, 20.9, 28.2, 45.2, 70.1, 88.9, 103.4, 164.
&END
&ICE1
CHORD = 0.9144
AOA   = 2.5
VINF  = 78.2
LWC   = 0.50
TINF  = 267.87
PINF  = 94806.00
RH    = 100.0
&END
&LPRNT
FPRT  = 1
HPRT  = 1
BPRT  = 1
TPRT  = 0
&END
&RDATA
&END
```

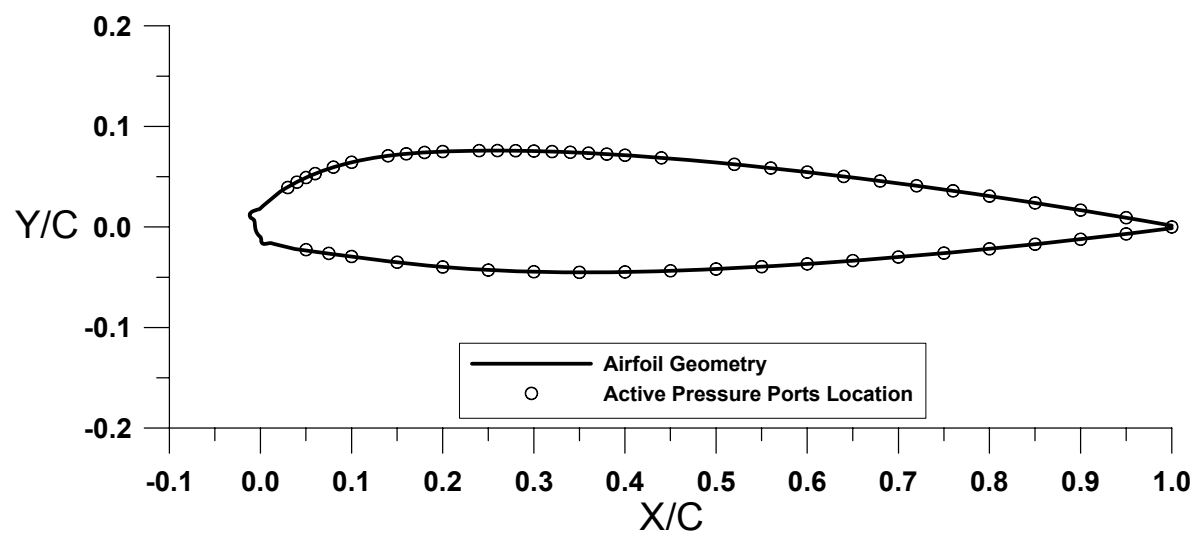


Figure A8.—NACA 23012 with 7.5-min mixed ice shape.

TABLE A8.1.—COORDINATES OF NACA 23012 WITH 7.5-MIN MIXED ICE SHAPE

| Lower Surface |         |         |         | Upper Surface |        |        |        |
|---------------|---------|---------|---------|---------------|--------|--------|--------|
| x/c           | y/c     | x/c     | y/c     | x/c           | y/c    | x/c    | y/c    |
| 1.0000        | -0.0013 | 0.0115  | -0.0160 | -0.0062       | 0.0023 | 0.7506 | 0.0371 |
| 0.9783        | -0.0038 | 0.0093  | -0.0163 | -0.0063       | 0.0046 | 0.7732 | 0.0342 |
| 0.9556        | -0.0063 | 0.0065  | -0.0167 | -0.0069       | 0.0068 | 0.7958 | 0.0313 |
| 0.9330        | -0.0088 | 0.0040  | -0.0170 | -0.0087       | 0.0081 | 0.8185 | 0.0282 |
| 0.9103        | -0.0112 | 0.0019  | -0.0163 | -0.0108       | 0.0091 | 0.8411 | 0.0251 |
| 0.8876        | -0.0135 | 0.0008  | -0.0144 | -0.0119       | 0.0110 | 0.8637 | 0.0220 |
| 0.8649        | -0.0157 | 0.0010  | -0.0121 | -0.0116       | 0.0133 | 0.8863 | 0.0187 |
| 0.8421        | -0.0179 | 0.0002  | -0.0101 | -0.0100       | 0.0148 | 0.9088 | 0.0154 |
| 0.8194        | -0.0200 | -0.0017 | -0.0087 | -0.0080       | 0.0159 | 0.9314 | 0.0120 |
| 0.7967        | -0.0220 | -0.0032 | -0.0070 | -0.0039       | 0.0170 | 0.9540 | 0.0086 |
| 0.7740        | -0.0240 | -0.0045 | -0.0050 | -0.0008       | 0.0178 | 0.9765 | 0.0050 |
| 0.7512        | -0.0259 | -0.0053 | -0.0029 | 0.0032        | 0.0213 | 1.0000 | 0.0013 |
| 0.7285        | -0.0277 | -0.0058 | -0.0007 | 0.0215        | 0.0351 |        |        |
| 0.7057        | -0.0295 |         |         | 0.0419        | 0.0457 |        |        |
| 0.6830        | -0.0312 |         |         | 0.0483        | 0.0483 |        |        |
| 0.6602        | -0.0328 |         |         | 0.0696        | 0.0563 |        |        |
| 0.6375        | -0.0344 |         |         | 0.0916        | 0.0624 |        |        |
| 0.6147        | -0.0358 |         |         | 0.1140        | 0.0670 |        |        |
| 0.5919        | -0.0372 |         |         | 0.1365        | 0.0703 |        |        |
| 0.5691        | -0.0385 |         |         | 0.1592        | 0.0727 |        |        |
| 0.5463        | -0.0397 |         |         | 0.1820        | 0.0742 |        |        |
| 0.5236        | -0.0408 |         |         | 0.2048        | 0.0752 |        |        |
| 0.5008        | -0.0418 |         |         | 0.2276        | 0.0757 |        |        |
| 0.4780        | -0.0427 |         |         | 0.2504        | 0.0760 |        |        |
| 0.4552        | -0.0435 |         |         | 0.2732        | 0.0759 |        |        |
| 0.4323        | -0.0441 |         |         | 0.2961        | 0.0756 |        |        |
| 0.4095        | -0.0446 |         |         | 0.3189        | 0.0750 |        |        |
| 0.3867        | -0.0449 |         |         | 0.3417        | 0.0742 |        |        |
| 0.3639        | -0.0451 |         |         | 0.3645        | 0.0732 |        |        |
| 0.3411        | -0.0451 |         |         | 0.3873        | 0.0721 |        |        |
| 0.3183        | -0.0449 |         |         | 0.4100        | 0.0707 |        |        |
| 0.2954        | -0.0445 |         |         | 0.4328        | 0.0692 |        |        |
| 0.2726        | -0.0438 |         |         | 0.4556        | 0.0676 |        |        |
| 0.2498        | -0.0429 |         |         | 0.4783        | 0.0659 |        |        |
| 0.2271        | -0.0417 |         |         | 0.5011        | 0.0640 |        |        |
| 0.2043        | -0.0401 |         |         | 0.5238        | 0.0620 |        |        |
| 0.1816        | -0.0382 |         |         | 0.5465        | 0.0599 |        |        |
| 0.1588        | -0.0360 |         |         | 0.5692        | 0.0577 |        |        |
| 0.1362        | -0.0336 |         |         | 0.5919        | 0.0554 |        |        |
| 0.1135        | -0.0310 |         |         | 0.6146        | 0.0530 |        |        |
| 0.0908        | -0.0283 |         |         | 0.6373        | 0.0506 |        |        |
| 0.0682        | -0.0255 |         |         | 0.6600        | 0.0480 |        |        |
| 0.0605        | -0.0250 |         |         | 0.6826        | 0.0454 |        |        |
| 0.0377        | -0.0218 |         |         | 0.7053        | 0.0427 |        |        |
| 0.0153        | -0.0170 |         |         | 0.7280        | 0.0400 |        |        |

TABLE A8.2.—COORDINATES OF ACTIVE PRESSURE PORTS OF NACA 23012 WITH 7.5-MIN MIXED ICE SHAPE

| <b>Lower Surface</b> |          | <b>Upper Surface</b> |         |
|----------------------|----------|----------------------|---------|
| x/c                  | y/c      | x/c                  | y/c     |
| 1.0000               | 0.00000  | 0.0300               | 0.03921 |
| 0.9500               | -0.00693 | 0.0400               | 0.04456 |
| 0.9000               | -0.01223 | 0.0500               | 0.04915 |
| 0.8500               | -0.01716 | 0.0600               | 0.05306 |
| 0.8000               | -0.02175 | 0.0800               | 0.05949 |
| 0.7500               | -0.02601 | 0.1000               | 0.06435 |
| 0.7000               | -0.02994 | 0.1400               | 0.07075 |
| 0.6500               | -0.03352 | 0.1600               | 0.07272 |
| 0.6000               | -0.03673 | 0.1800               | 0.07408 |
| 0.5500               | -0.03951 | 0.2000               | 0.07497 |
| 0.5000               | -0.04183 | 0.2400               | 0.07589 |
| 0.4500               | -0.04360 | 0.2600               | 0.07596 |
| 0.4000               | -0.04474 | 0.2800               | 0.07583 |
| 0.3500               | -0.04512 | 0.3000               | 0.07548 |
| 0.3000               | -0.04456 | 0.3200               | 0.07496 |
| 0.2500               | -0.04289 | 0.3400               | 0.07428 |
| 0.2000               | -0.03979 | 0.3600               | 0.07343 |
| 0.1500               | -0.03506 | 0.3800               | 0.07245 |
| 0.1000               | -0.02938 | 0.4000               | 0.07134 |
| 0.0750               | -0.02626 | 0.4400               | 0.06874 |
| 0.0500               | -0.02261 | 0.5200               | 0.06232 |
|                      |          | 0.5600               | 0.05859 |
|                      |          | 0.6000               | 0.05456 |
|                      |          | 0.6400               | 0.05026 |
|                      |          | 0.6800               | 0.04571 |
|                      |          | 0.7200               | 0.04093 |
|                      |          | 0.7600               | 0.03593 |
|                      |          | 0.8000               | 0.03071 |
|                      |          | 0.8500               | 0.02389 |
|                      |          | 0.9000               | 0.01673 |
|                      |          | 0.9500               | 0.00919 |

## **LEWICE 2.2 Input File for the NACA 23012 with 7.5-min Mixed Ice Shape**

```
Mixed 7.5-min Case
&LEW20
ITIMFL = 0
TSTOP = 450.
IBOD = 1
IFLO = 6
DSMN = 4.0D-4
NPL = 24
&END
&DIST
FLWC = 0.05, 0.1, 0.2, 0.3, 0.2, 0.1, 0.03, 0.01, 0.005, 0.005
DPD = 4., 9.7, 14.2, 20.9, 28.2, 45.2, 70.1, 88.9, 103.4, 164.
&END
&ICE1
CHORD = 0.9144
AOA = 2.5
VINF = 78.2
LWC = 0.50
TINF = 264.
PINF = 94806.00
RH = 100.0
&END
&LPRNT
```

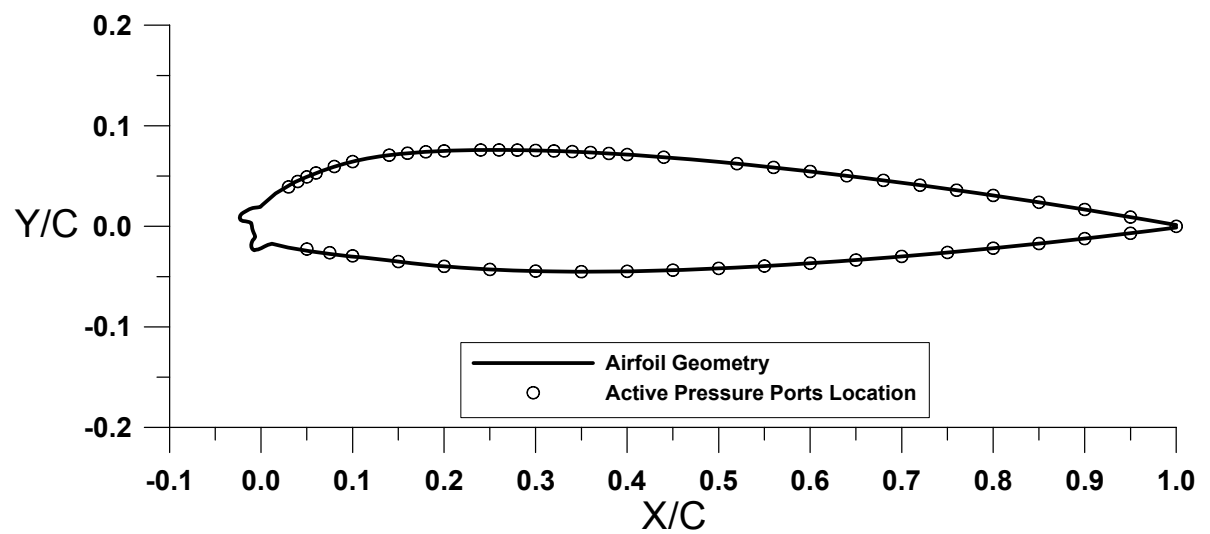


Figure A9.—NACA 23012 with 15-min mixed ice shape.

TABLE A9.1.—COORDINATES OF NACA 23012 WITH 15-MIN MIXED ICE SHAPE

| Lower Surface |         |         | Upper Surface |         |        |
|---------------|---------|---------|---------------|---------|--------|
| x/c           | y/c     | x/c     | y/c           | x/c     | y/c    |
| 1.0000        | -0.0013 | 0.0095  | -0.0178       | -0.0100 | 0.0004 |
| 0.9783        | -0.0038 | 0.0069  | -0.0187       | -0.0108 | 0.0032 |
| 0.9556        | -0.0063 | 0.0044  | -0.0197       | -0.0128 | 0.0042 |
| 0.9330        | -0.0088 | 0.0012  | -0.0213       | -0.0169 | 0.0050 |
| 0.9103        | -0.0112 | -0.0023 | -0.0228       | -0.0200 | 0.0054 |
| 0.8876        | -0.0135 | -0.0050 | -0.0233       | -0.0225 | 0.0064 |
| 0.8649        | -0.0157 | -0.0076 | -0.0237       | -0.0235 | 0.0084 |
| 0.8421        | -0.0179 | -0.0096 | -0.0227       | -0.0229 | 0.0106 |
| 0.8194        | -0.0200 | -0.0106 | -0.0206       | -0.0214 | 0.0124 |
| 0.7967        | -0.0220 | -0.0107 | -0.0183       | -0.0195 | 0.0137 |
| 0.7740        | -0.0240 | -0.0102 | -0.0161       | -0.0155 | 0.0157 |
| 0.7512        | -0.0259 | -0.0093 | -0.0140       | -0.0127 | 0.0169 |
| 0.7285        | -0.0277 | -0.0076 | -0.0124       | -0.0091 | 0.0181 |
| 0.7057        | -0.0295 | -0.0064 | -0.0106       | -0.0069 | 0.0185 |
| 0.6830        | -0.0312 | -0.0071 | -0.0084       | -0.0037 | 0.0188 |
| 0.6602        | -0.0328 | -0.0082 | -0.0064       | -0.0009 | 0.0194 |
| 0.6375        | -0.0344 | -0.0090 | -0.0042       | 0.0010  | 0.0210 |
| 0.6147        | -0.0358 | -0.0096 | -0.0020       | 0.0158  | 0.0326 |
| 0.5919        | -0.0372 |         |               | 0.0362  | 0.0436 |
| 0.5691        | -0.0385 |         |               | 0.0483  | 0.0483 |
| 0.5463        | -0.0397 |         |               | 0.0696  | 0.0563 |
| 0.5236        | -0.0408 |         |               | 0.0916  | 0.0624 |
| 0.5008        | -0.0418 |         |               | 0.1140  | 0.0670 |
| 0.4780        | -0.0427 |         |               | 0.1365  | 0.0703 |
| 0.4552        | -0.0435 |         |               | 0.1592  | 0.0727 |
| 0.4323        | -0.0441 |         |               | 0.1820  | 0.0742 |
| 0.4095        | -0.0446 |         |               | 0.2048  | 0.0752 |
| 0.3867        | -0.0449 |         |               | 0.2276  | 0.0757 |
| 0.3639        | -0.0451 |         |               | 0.2504  | 0.0760 |
| 0.3411        | -0.0451 |         |               | 0.2732  | 0.0759 |
| 0.3183        | -0.0449 |         |               | 0.2961  | 0.0756 |
| 0.2954        | -0.0445 |         |               | 0.3189  | 0.0750 |
| 0.2726        | -0.0438 |         |               | 0.3417  | 0.0742 |
| 0.2498        | -0.0429 |         |               | 0.3645  | 0.0732 |
| 0.2271        | -0.0417 |         |               | 0.3873  | 0.0721 |
| 0.2043        | -0.0401 |         |               | 0.4100  | 0.0707 |
| 0.1816        | -0.0382 |         |               | 0.4328  | 0.0692 |
| 0.1588        | -0.0360 |         |               | 0.4556  | 0.0676 |
| 0.1362        | -0.0336 |         |               | 0.4783  | 0.0659 |
| 0.1135        | -0.0310 |         |               | 0.5011  | 0.0640 |
| 0.0983        | -0.0300 |         |               | 0.5238  | 0.0620 |
| 0.0753        | -0.0275 |         |               | 0.5465  | 0.0599 |
| 0.0523        | -0.0246 |         |               | 0.5692  | 0.0577 |
| 0.0294        | -0.0211 |         |               | 0.5919  | 0.0554 |
| 0.0118        | -0.0172 |         |               | 0.6146  | 0.0530 |

TABLE A9.2.—COORDINATES OF ACTIVE PRESSURE PORTS OF NACA 23012 WITH 15-MIN MIXED ICE SHAPE

| Lower Surface |          | Upper Surface |         |
|---------------|----------|---------------|---------|
| x/c           | y/c      | x/c           | y/c     |
| 1.0000        | 0.00000  | 0.0300        | 0.03921 |
| 0.9500        | -0.00693 | 0.0400        | 0.04456 |
| 0.9000        | -0.01223 | 0.0500        | 0.04915 |
| 0.8500        | -0.01716 | 0.0600        | 0.05306 |
| 0.8000        | -0.02175 | 0.0800        | 0.05949 |
| 0.7500        | -0.02601 | 0.1000        | 0.06435 |
| 0.7000        | -0.02994 | 0.1400        | 0.07075 |
| 0.6500        | -0.03352 | 0.1600        | 0.07272 |
| 0.6000        | -0.03673 | 0.1800        | 0.07408 |
| 0.5500        | -0.03951 | 0.2000        | 0.07497 |
| 0.5000        | -0.04183 | 0.2400        | 0.07589 |
| 0.4500        | -0.04360 | 0.2600        | 0.07596 |
| 0.4000        | -0.04474 | 0.2800        | 0.07583 |
| 0.3500        | -0.04512 | 0.3000        | 0.07548 |
| 0.3000        | -0.04456 | 0.3200        | 0.07496 |
| 0.2500        | -0.04289 | 0.3400        | 0.07428 |
| 0.2000        | -0.03979 | 0.3600        | 0.07343 |
| 0.1500        | -0.03506 | 0.3800        | 0.07245 |
| 0.1000        | -0.02938 | 0.4000        | 0.07134 |
| 0.0750        | -0.02626 | 0.4400        | 0.06874 |
| 0.0500        | -0.02261 | 0.5200        | 0.06232 |
|               |          | 0.5600        | 0.05859 |
|               |          | 0.6000        | 0.05456 |
|               |          | 0.6400        | 0.05026 |
|               |          | 0.6800        | 0.04571 |
|               |          | 0.7200        | 0.04093 |
|               |          | 0.7600        | 0.03593 |
|               |          | 0.8000        | 0.03071 |
|               |          | 0.8500        | 0.02389 |
|               |          | 0.9000        | 0.01673 |
|               |          | 0.9500        | 0.00919 |

## **LEWICE 2.2 Input File for the NACA 23012 with 15-min Mixed Ice Shape**

```
Mixed 15-min Case
&LEW20
ITIMFL = 0
TSTOP = 900.
IBOD = 1
IFLO = 12
DSMN = 4.0D-4
NPL = 24
&END
&DIST
FLWC = 0.05, 0.1, 0.2, 0.3, 0.2, 0.1, 0.03, 0.01, 0.005, 0.005
DPD = 4., 9.7, 14.2, 20.9, 28.2, 45.2, 70.1, 88.9, 103.4, 164.
&END
&ICE1
CHORD = 0.9144
AOA = 2.5
VINF = 78.2
LWC = 0.50
TINF = 264.
PINF = 94806.00
RH = 100.0
&END
&LPRNT
```

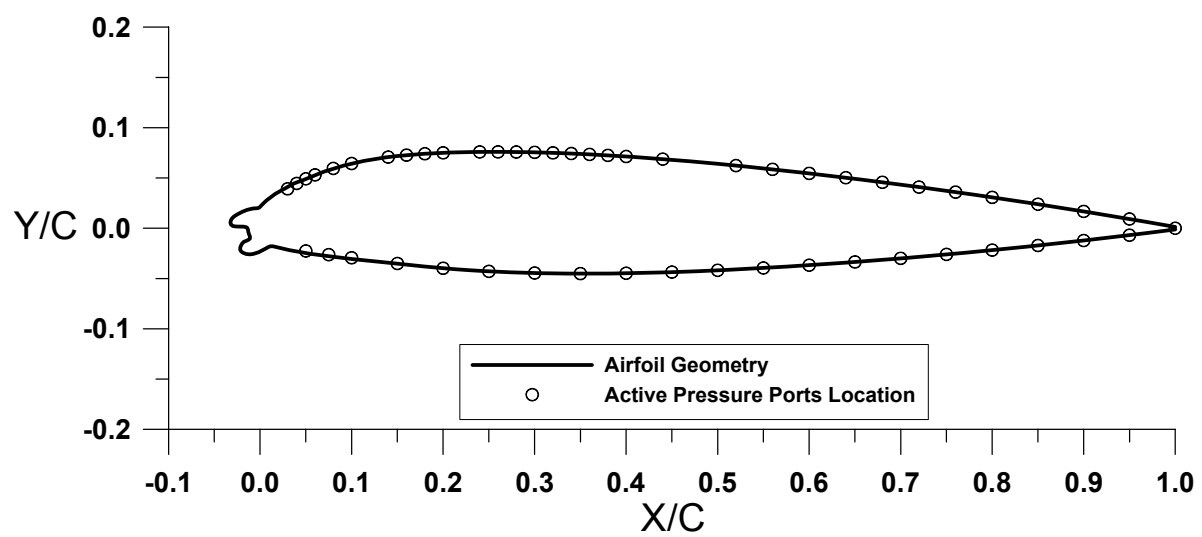


Figure A10.—NACA 23012 with 22.5-min mixed ice shape.

TABLE A10.1.—COORDINATES OF NACA 23012 WITH 22.5-MIN MIXED ICE SHAPE

| Lower Surface |         |         |         | Upper Surface |        |        |        |
|---------------|---------|---------|---------|---------------|--------|--------|--------|
| x/c           | y/c     | x/c     | y/c     | x/c           | y/c    | x/c    | y/c    |
| 1.0000        | -0.0013 | 0.0111  | -0.0178 | -0.0142       | 0.0007 | 0.5238 | 0.0620 |
| 0.9783        | -0.0038 | 0.0090  | -0.0187 | -0.0164       | 0.0014 | 0.5465 | 0.0599 |
| 0.9556        | -0.0063 | 0.0062  | -0.0199 | -0.0187       | 0.0017 | 0.5692 | 0.0577 |
| 0.9330        | -0.0088 | 0.0030  | -0.0217 | -0.0230       | 0.0016 | 0.5919 | 0.0554 |
| 0.9103        | -0.0112 | -0.0007 | -0.0236 | -0.0272       | 0.0018 | 0.6146 | 0.0530 |
| 0.8876        | -0.0135 | -0.0028 | -0.0244 | -0.0298       | 0.0023 | 0.6373 | 0.0506 |
| 0.8649        | -0.0157 | -0.0058 | -0.0252 | -0.0317       | 0.0035 | 0.6600 | 0.0480 |
| 0.8421        | -0.0179 | -0.0087 | -0.0258 | -0.0324       | 0.0056 | 0.6826 | 0.0454 |
| 0.8194        | -0.0200 | -0.0110 | -0.0259 | -0.0319       | 0.0079 | 0.7053 | 0.0427 |
| 0.7967        | -0.0220 | -0.0141 | -0.0256 | -0.0306       | 0.0098 | 0.7280 | 0.0400 |
| 0.7740        | -0.0240 | -0.0164 | -0.0253 | -0.0289       | 0.0113 | 0.7506 | 0.0371 |
| 0.7512        | -0.0259 | -0.0186 | -0.0246 | -0.0267       | 0.0128 | 0.7732 | 0.0342 |
| 0.7285        | -0.0277 | -0.0205 | -0.0233 | -0.0228       | 0.0148 | 0.7958 | 0.0313 |
| 0.7057        | -0.0295 | -0.0217 | -0.0214 | -0.0198       | 0.0162 | 0.8185 | 0.0282 |
| 0.6830        | -0.0312 | -0.0216 | -0.0191 | -0.0151       | 0.0179 | 0.8411 | 0.0251 |
| 0.6602        | -0.0328 | -0.0207 | -0.0170 | -0.0124       | 0.0187 | 0.8637 | 0.0220 |
| 0.6375        | -0.0344 | -0.0194 | -0.0151 | -0.0084       | 0.0195 | 0.8863 | 0.0187 |
| 0.6147        | -0.0358 | -0.0177 | -0.0135 | -0.0058       | 0.0197 | 0.9088 | 0.0154 |
| 0.5919        | -0.0372 | -0.0156 | -0.0127 | -0.0028       | 0.0198 | 0.9314 | 0.0120 |
| 0.5691        | -0.0385 | -0.0128 | -0.0116 | -0.0007       | 0.0207 | 0.9540 | 0.0086 |
| 0.5463        | -0.0397 | -0.0110 | -0.0102 | 0.0026        | 0.0237 | 0.9765 | 0.0050 |
| 0.5236        | -0.0408 | -0.0112 | -0.0080 | 0.0069        | 0.0276 | 1.0000 | 0.0013 |
| 0.5008        | -0.0418 | -0.0121 | -0.0059 | 0.0166        | 0.0342 |        |        |
| 0.4780        | -0.0427 | -0.0128 | -0.0036 | 0.0372        | 0.0446 |        |        |
| 0.4552        | -0.0435 | -0.0133 | -0.0014 | 0.0483        | 0.0483 |        |        |
| 0.4323        | -0.0441 |         |         | 0.0696        | 0.0563 |        |        |
| 0.4095        | -0.0446 |         |         | 0.0916        | 0.0624 |        |        |
| 0.3867        | -0.0449 |         |         | 0.1140        | 0.0670 |        |        |
| 0.3639        | -0.0451 |         |         | 0.1365        | 0.0703 |        |        |
| 0.3411        | -0.0451 |         |         | 0.1592        | 0.0727 |        |        |
| 0.3183        | -0.0449 |         |         | 0.1820        | 0.0742 |        |        |
| 0.2954        | -0.0445 |         |         | 0.2048        | 0.0752 |        |        |
| 0.2726        | -0.0438 |         |         | 0.2276        | 0.0757 |        |        |
| 0.2498        | -0.0429 |         |         | 0.2504        | 0.0760 |        |        |
| 0.2271        | -0.0417 |         |         | 0.2732        | 0.0759 |        |        |
| 0.2043        | -0.0401 |         |         | 0.2961        | 0.0756 |        |        |
| 0.1816        | -0.0382 |         |         | 0.3189        | 0.0750 |        |        |
| 0.1588        | -0.0360 |         |         | 0.3417        | 0.0742 |        |        |
| 0.1362        | -0.0336 |         |         | 0.3645        | 0.0732 |        |        |
| 0.1237        | -0.0330 |         |         | 0.3873        | 0.0721 |        |        |
| 0.1007        | -0.0306 |         |         | 0.4100        | 0.0707 |        |        |
| 0.0777        | -0.0281 |         |         | 0.4328        | 0.0692 |        |        |
| 0.0547        | -0.0254 |         |         | 0.4556        | 0.0676 |        |        |
| 0.0319        | -0.0218 |         |         | 0.4783        | 0.0659 |        |        |
| 0.0140        | -0.0180 |         |         | 0.5011        | 0.0640 |        |        |

TABLE A10.2.—COORDINATES OF ACTIVE PRESSURE PORTS OF NACA 23012 WITH 22.5-MIN MIXED ICE SHAPE

| <b>Lower Surface</b> |          | <b>Upper Surface</b> |         |
|----------------------|----------|----------------------|---------|
| x/c                  | y/c      | x/c                  | y/c     |
| 1.0000               | 0.00000  | 0.0300               | 0.03921 |
| 0.9500               | -0.00693 | 0.0400               | 0.04456 |
| 0.9000               | -0.01223 | 0.0500               | 0.04915 |
| 0.8500               | -0.01716 | 0.0600               | 0.05306 |
| 0.8000               | -0.02175 | 0.0800               | 0.05949 |
| 0.7500               | -0.02601 | 0.1000               | 0.06435 |
| 0.7000               | -0.02994 | 0.1400               | 0.07075 |
| 0.6500               | -0.03352 | 0.1600               | 0.07272 |
| 0.6000               | -0.03673 | 0.1800               | 0.07408 |
| 0.5500               | -0.03951 | 0.2000               | 0.07497 |
| 0.5000               | -0.04183 | 0.2400               | 0.07589 |
| 0.4500               | -0.04360 | 0.2600               | 0.07596 |
| 0.4000               | -0.04474 | 0.2800               | 0.07583 |
| 0.3500               | -0.04512 | 0.3000               | 0.07548 |
| 0.3000               | -0.04456 | 0.3200               | 0.07496 |
| 0.2500               | -0.04289 | 0.3400               | 0.07428 |
| 0.2000               | -0.03979 | 0.3600               | 0.07343 |
| 0.1500               | -0.03506 | 0.3800               | 0.07245 |
| 0.1000               | -0.02938 | 0.4000               | 0.07134 |
| 0.0750               | -0.02626 | 0.4400               | 0.06874 |
| 0.0500               | -0.02261 | 0.5200               | 0.06232 |
|                      |          | 0.5600               | 0.05859 |
|                      |          | 0.6000               | 0.05456 |
|                      |          | 0.6400               | 0.05026 |
|                      |          | 0.6800               | 0.04571 |
|                      |          | 0.7200               | 0.04093 |
|                      |          | 0.7600               | 0.03593 |
|                      |          | 0.8000               | 0.03071 |
|                      |          | 0.8500               | 0.02389 |
|                      |          | 0.9000               | 0.01673 |
|                      |          | 0.9500               | 0.00919 |

## **LEWICE 2.2 Input File for the NACA 23012 with 22.5-min Mixed Ice Shape**

Mixed 22.5-min Case  
&LEW20  
ITIMFL = 0  
TSTOP = 1350.  
IBOD = 1  
IFLO = 18  
DSMN = 4.0D-4  
NPL = 24  
&END  
&DIST  
FLWC = 0.05, 0.1, 0.2, 0.3, 0.2, 0.1, 0.03, 0.01, 0.005, 0.005  
DPD = 4., 9.7, 14.2, 20.9, 28.2, 45.2, 70.1, 88.9, 103.4, 164.  
&END  
&ICE1  
CHORD = 0.9144  
AOA = 2.5  
VINF = 78.2  
LWC = 0.50  
TINF = 264.  
PINF = 94806.00  
RH = 100.0  
&END  
&LPRNT

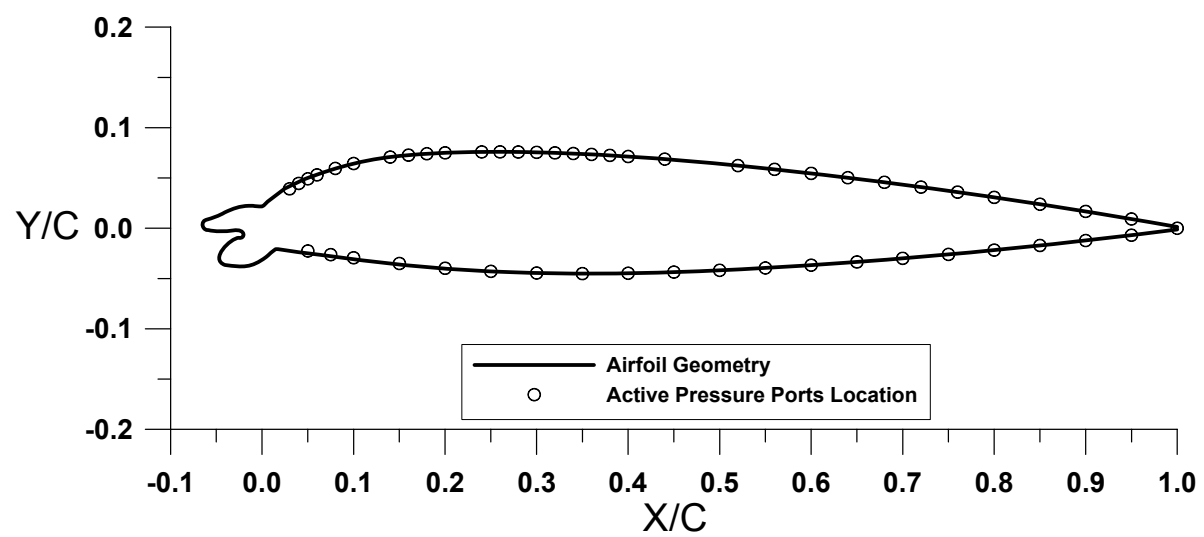


Figure A11.—NACA 23012 with 45-min mixed ice shape.

TABLE A11.1.—COORDINATES OF NACA 23012 WITH 45-MIN MIXED ICE SHAPE

| Lower Surface |         |         |         | Upper Surface |         |         |        |
|---------------|---------|---------|---------|---------------|---------|---------|--------|
| x/c           | y/c     | x/c     | y/c     | x/c           | y/c     | x/c     | y/c    |
| 1.0000        | -0.0013 | 0.0126  | -0.0223 | -0.0342       | -0.0024 | -0.0646 | 0.0011 |
| 0.9783        | -0.0038 | 0.0095  | -0.0245 | -0.0374       | -0.0029 | -0.0652 | 0.0033 |
| 0.9556        | -0.0063 | 0.0065  | -0.0269 | -0.0402       | -0.0030 | -0.0648 | 0.0055 |
| 0.9330        | -0.0088 | 0.0043  | -0.0286 | -0.0435       | -0.0031 | -0.0635 | 0.0073 |
| 0.9103        | -0.0112 | 0.0011  | -0.0306 | -0.0462       | -0.0031 | -0.0614 | 0.0083 |
| 0.8876        | -0.0135 | -0.0013 | -0.0322 | -0.0500       | -0.0028 | -0.0592 | 0.0090 |
| 0.8649        | -0.0157 | -0.0033 | -0.0333 | -0.0527       | -0.0026 | -0.0570 | 0.0094 |
| 0.8421        | -0.0179 | -0.0057 | -0.0343 | -0.0562       | -0.0023 | -0.0548 | 0.0101 |
| 0.8194        | -0.0200 | -0.0087 | -0.0355 | -0.0585       | -0.0019 | -0.0527 | 0.0108 |
| 0.7967        | -0.0220 | -0.0109 | -0.0367 | -0.0609       | -0.0016 | -0.0502 | 0.0116 |
| 0.7740        | -0.0240 | -0.0132 | -0.0370 | -0.0630       | -0.0006 | -0.0474 | 0.0127 |
| 0.7512        | -0.0259 | -0.0155 | -0.0375 |               |         | -0.0452 | 0.0137 |
| 0.7285        | -0.0277 | -0.0183 | -0.0380 |               |         | -0.0405 | 0.0158 |
| 0.7057        | -0.0295 | -0.0215 | -0.0379 |               |         | -0.0365 | 0.0176 |
| 0.6830        | -0.0312 | -0.0246 | -0.0377 |               |         | -0.0337 | 0.0184 |
| 0.6602        | -0.0328 | -0.0269 | -0.0376 |               |         | -0.0295 | 0.0199 |
| 0.6375        | -0.0344 | -0.0292 | -0.0377 |               |         | -0.0258 | 0.0210 |
| 0.6147        | -0.0358 | -0.0315 | -0.0377 |               |         | -0.0228 | 0.0215 |
| 0.5919        | -0.0372 | -0.0339 | -0.0375 |               |         | -0.0196 | 0.0219 |
| 0.5691        | -0.0385 | -0.0368 | -0.0372 |               |         | -0.0169 | 0.0223 |
| 0.5463        | -0.0397 | -0.0405 | -0.0365 |               |         | -0.0146 | 0.0223 |
| 0.5236        | -0.0408 | -0.0429 | -0.0356 |               |         | -0.0123 | 0.0223 |
| 0.5008        | -0.0418 | -0.0447 | -0.0343 |               |         | -0.0100 | 0.0222 |
| 0.4780        | -0.0427 | -0.0461 | -0.0325 |               |         | -0.0078 | 0.0220 |
| 0.4552        | -0.0435 | -0.0468 | -0.0303 |               |         | -0.0055 | 0.0219 |
| 0.4323        | -0.0441 | -0.0467 | -0.0280 |               |         | -0.0032 | 0.0216 |
| 0.4095        | -0.0446 | -0.0461 | -0.0259 |               |         | -0.0002 | 0.0217 |
| 0.3867        | -0.0449 | -0.0451 | -0.0238 |               |         | 0.0019  | 0.0226 |
| 0.3639        | -0.0451 | -0.0434 | -0.0213 |               |         | 0.0060  | 0.0265 |
| 0.3411        | -0.0451 | -0.0417 | -0.0195 |               |         | 0.0248  | 0.0394 |
| 0.3183        | -0.0449 | -0.0397 | -0.0175 |               |         | 0.0457  | 0.0487 |
| 0.2954        | -0.0445 | -0.0376 | -0.0158 |               |         | 0.0696  | 0.0563 |
| 0.2726        | -0.0438 | -0.0347 | -0.0135 |               |         | 0.0916  | 0.0624 |
| 0.2498        | -0.0429 | -0.0319 | -0.0117 |               |         | 0.1140  | 0.0670 |
| 0.2271        | -0.0417 | -0.0299 | -0.0106 |               |         | 0.1365  | 0.0703 |
| 0.1995        | -0.0403 | -0.0277 | -0.0098 |               |         | 0.1592  | 0.0727 |
| 0.1766        | -0.0385 | -0.0255 | -0.0095 |               |         | 0.1820  | 0.0742 |
| 0.1538        | -0.0365 | -0.0232 | -0.0096 |               |         | 0.2048  | 0.0752 |
| 0.1310        | -0.0342 | -0.0212 | -0.0086 |               |         | 0.2276  | 0.0757 |
| 0.1083        | -0.0316 | -0.0203 | -0.0066 |               |         | 0.2504  | 0.0760 |
| 0.0855        | -0.0290 | -0.0210 | -0.0044 |               |         | 0.2732  | 0.0759 |
| 0.0627        | -0.0263 | -0.0226 | -0.0029 |               |         | 0.2961  | 0.0756 |
| 0.0400        | -0.0238 | -0.0249 | -0.0024 |               |         | 0.3189  | 0.0750 |
| 0.0174        | -0.0208 | -0.0282 | -0.0021 |               |         | 0.3417  | 0.0742 |
| 0.0146        | -0.0209 | -0.0315 | -0.0021 |               |         | 0.3645  | 0.0732 |

TABLE A11.2.—COORDINATES OF ACTIVE PRESSURE PORTS OF NACA 23012 WITH 45-MIN MIXED ICE SHAPE

| <b>Lower Surface</b> |          | <b>Upper Surface</b> |         |
|----------------------|----------|----------------------|---------|
| x/c                  | y/c      | x/c                  | y/c     |
| 1.0000               | 0.00000  | 0.0300               | 0.03921 |
| 0.9500               | -0.00693 | 0.0400               | 0.04456 |
| 0.9000               | -0.01223 | 0.0500               | 0.04915 |
| 0.8500               | -0.01716 | 0.0600               | 0.05306 |
| 0.8000               | -0.02175 | 0.0800               | 0.05949 |
| 0.7500               | -0.02601 | 0.1000               | 0.06435 |
| 0.7000               | -0.02994 | 0.1400               | 0.07075 |
| 0.6500               | -0.03352 | 0.1600               | 0.07272 |
| 0.6000               | -0.03673 | 0.1800               | 0.07408 |
| 0.5500               | -0.03951 | 0.2000               | 0.07497 |
| 0.5000               | -0.04183 | 0.2400               | 0.07589 |
| 0.4500               | -0.04360 | 0.2600               | 0.07596 |
| 0.4000               | -0.04474 | 0.2800               | 0.07583 |
| 0.3500               | -0.04512 | 0.3000               | 0.07548 |
| 0.3000               | -0.04456 | 0.3200               | 0.07496 |
| 0.2500               | -0.04289 | 0.3400               | 0.07428 |
| 0.2000               | -0.03979 | 0.3600               | 0.07343 |
| 0.1500               | -0.03506 | 0.3800               | 0.07245 |
| 0.1000               | -0.02938 | 0.4000               | 0.07134 |
| 0.0750               | -0.02626 | 0.4400               | 0.06874 |
| 0.0500               | -0.02261 | 0.5200               | 0.06232 |
|                      |          | 0.5600               | 0.05859 |
|                      |          | 0.6000               | 0.05456 |
|                      |          | 0.6400               | 0.05026 |
|                      |          | 0.6800               | 0.04571 |
|                      |          | 0.7200               | 0.04093 |
|                      |          | 0.7600               | 0.03593 |
|                      |          | 0.8000               | 0.03071 |
|                      |          | 0.8500               | 0.02389 |
|                      |          | 0.9000               | 0.01673 |
|                      |          | 0.9500               | 0.00919 |

## **LEWICE 2.2 Input File for the NACA 23012 with 45-min Mixed Ice Shape**

```
Mixed 45-min Case
&LEW20
ITIMFL = 1
TSTOP  = 2700.
IBOD   = 1
IFLO   = 18
DSMN   = 4.0D-4
NPL    = 24
&END
&DIST
FLWC  = 0.05, 0.1, 0.2, 0.3, 0.2, 0.1, 0.03, 0.01, 0.005, 0.005
DPD   = 4., 9.7, 14.2, 20.9, 28.2, 45.2, 70.1, 88.9, 103.4, 164.
&END
&ICE1
CHORD = 0.9144
AOA   = 2.5
VINF  = 78.2
LWC   = 0.50
TINF  = 264.
PINF  = 94806.00
RH    = 100.0
&END
&LPRNT
FPRT  = 1
HPRT  = 1
BPRT  = 1
TPRT  = 0
&END
&RDATA
&END
```

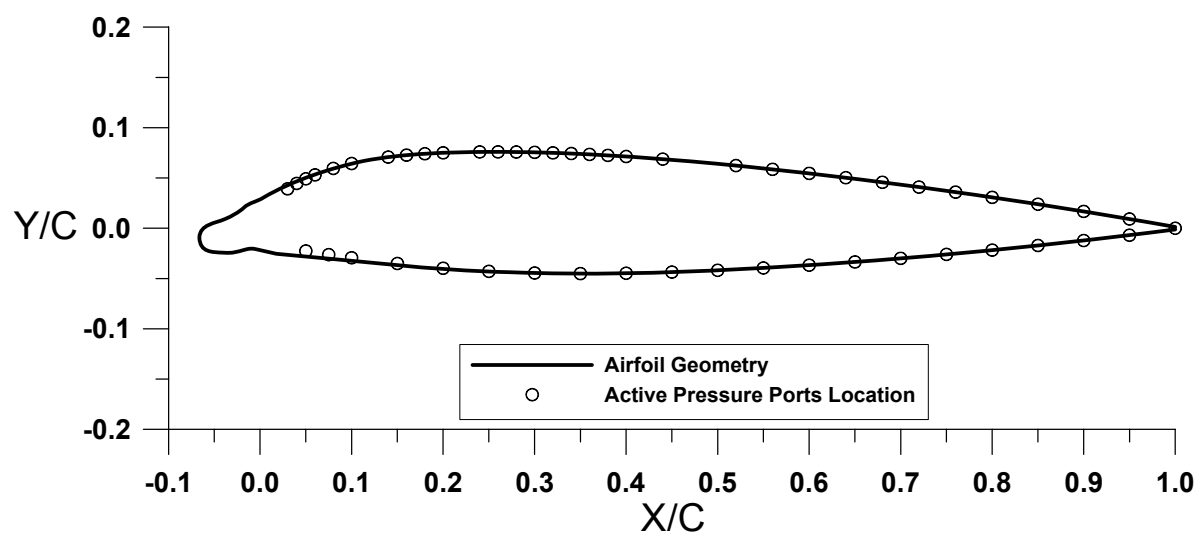


Figure A12.—NACA 23012 with 45-min rime ice shape.

TABLE A12.1.—COORDINATES OF NACA 23012 WITH 45-MIN RIME ICE SHAPE

| Lower Surface |         |         | Upper Surface |         |        |
|---------------|---------|---------|---------------|---------|--------|
| x/c           | y/c     | x/c     | y/c           | x/c     | y/c    |
| 1.0000        | -0.0013 | -0.0076 | -0.0203       | -0.0603 | 0.0012 |
| 0.9783        | -0.0038 | -0.0102 | -0.0202       | -0.0576 | 0.0027 |
| 0.9556        | -0.0063 | -0.0125 | -0.0205       | -0.0550 | 0.0037 |
| 0.9330        | -0.0088 | -0.0164 | -0.0212       | -0.0511 | 0.0051 |
| 0.9103        | -0.0112 | -0.0206 | -0.0222       | -0.0464 | 0.0067 |
| 0.8876        | -0.0135 | -0.0260 | -0.0237       | -0.0409 | 0.0083 |
| 0.8649        | -0.0157 | -0.0286 | -0.0241       | -0.0379 | 0.0092 |
| 0.8421        | -0.0179 | -0.0310 | -0.0244       | -0.0352 | 0.0104 |
| 0.8194        | -0.0200 | -0.0359 | -0.0245       | -0.0301 | 0.0128 |
| 0.7967        | -0.0220 | -0.0402 | -0.0244       | -0.0252 | 0.0153 |
| 0.7740        | -0.0240 | -0.0457 | -0.0240       | -0.0223 | 0.0171 |
| 0.7512        | -0.0259 | -0.0498 | -0.0237       | -0.0177 | 0.0204 |
| 0.7285        | -0.0277 | -0.0531 | -0.0234       | -0.0151 | 0.0222 |
| 0.7057        | -0.0295 | -0.0567 | -0.0226       | -0.0123 | 0.0238 |
| 0.6830        | -0.0312 | -0.0598 | -0.0214       | -0.0098 | 0.0250 |
| 0.6602        | -0.0328 | -0.0617 | -0.0199       | -0.0053 | 0.0266 |
| 0.6375        | -0.0344 | -0.0637 | -0.0177       | -0.0016 | 0.0280 |
| 0.6147        | -0.0358 | -0.0649 | -0.0158       | 0.0036  | 0.0303 |
| 0.5919        | -0.0372 | -0.0657 | -0.0136       | 0.0241  | 0.0403 |
| 0.5691        | -0.0385 | -0.0661 | -0.0114       | 0.0454  | 0.0487 |
| 0.5463        | -0.0397 | -0.0663 | -0.0091       | 0.0696  | 0.0563 |
| 0.5236        | -0.0408 | -0.0658 | -0.0062       | 0.0916  | 0.0624 |
| 0.5008        | -0.0418 | -0.0650 | -0.0040       | 0.1140  | 0.0670 |
| 0.4780        | -0.0427 | -0.0638 | -0.0021       | 0.1365  | 0.0703 |
| 0.4552        | -0.0435 | -0.0624 | -0.0003       | 0.1592  | 0.0727 |
| 0.4323        | -0.0441 |         |               | 0.1820  | 0.0742 |
| 0.4095        | -0.0446 |         |               | 0.2048  | 0.0752 |
| 0.3867        | -0.0449 |         |               | 0.2276  | 0.0757 |
| 0.3639        | -0.0451 |         |               | 0.2504  | 0.0760 |
| 0.3411        | -0.0451 |         |               | 0.2732  | 0.0759 |
| 0.3183        | -0.0449 |         |               | 0.2961  | 0.0756 |
| 0.2954        | -0.0445 |         |               | 0.3189  | 0.0750 |
| 0.2726        | -0.0438 |         |               | 0.3417  | 0.0742 |
| 0.2460        | -0.0429 |         |               | 0.3645  | 0.0732 |
| 0.2232        | -0.0419 |         |               | 0.3873  | 0.0721 |
| 0.2003        | -0.0406 |         |               | 0.4100  | 0.0707 |
| 0.1775        | -0.0390 |         |               | 0.4328  | 0.0692 |
| 0.1546        | -0.0372 |         |               | 0.4556  | 0.0676 |
| 0.1318        | -0.0353 |         |               | 0.4783  | 0.0659 |
| 0.1090        | -0.0334 |         |               | 0.5011  | 0.0640 |
| 0.0862        | -0.0314 |         |               | 0.5238  | 0.0620 |
| 0.0634        | -0.0292 |         |               | 0.5465  | 0.0599 |
| 0.0405        | -0.0273 |         |               | 0.5692  | 0.0577 |
| 0.0177        | -0.0254 |         |               | 0.5919  | 0.0554 |
| -0.0047       | -0.0208 |         |               | 0.6146  | 0.0530 |

TABLE A12.2.—COORDINATES OF ACTIVE PRESSURE PORTS OF NACA 23012 WITH 45-MIN RIME ICE SHAPE

| Lower Surface |          | Upper Surface |         |
|---------------|----------|---------------|---------|
| x/c           | y/c      | x/c           | y/c     |
| 1.0000        | 0.00000  | 0.0300        | 0.03921 |
| 0.9500        | -0.00693 | 0.0400        | 0.04456 |
| 0.9000        | -0.01223 | 0.0500        | 0.04915 |
| 0.8500        | -0.01716 | 0.0600        | 0.05306 |
| 0.8000        | -0.02175 | 0.0800        | 0.05949 |
| 0.7500        | -0.02601 | 0.1000        | 0.06435 |
| 0.7000        | -0.02994 | 0.1400        | 0.07075 |
| 0.6500        | -0.03352 | 0.1600        | 0.07272 |
| 0.6000        | -0.03673 | 0.1800        | 0.07408 |
| 0.5500        | -0.03951 | 0.2000        | 0.07497 |
| 0.5000        | -0.04183 | 0.2400        | 0.07589 |
| 0.4500        | -0.04360 | 0.2600        | 0.07596 |
| 0.4000        | -0.04474 | 0.2800        | 0.07583 |
| 0.3500        | -0.04512 | 0.3000        | 0.07548 |
| 0.3000        | -0.04456 | 0.3200        | 0.07496 |
| 0.2500        | -0.04289 | 0.3400        | 0.07428 |
| 0.2000        | -0.03979 | 0.3600        | 0.07343 |
| 0.1500        | -0.03506 | 0.3800        | 0.07245 |
| 0.1000        | -0.02938 | 0.4000        | 0.07134 |
| 0.0750        | -0.02626 | 0.4400        | 0.06874 |
| 0.0500        | -0.02261 | 0.5200        | 0.06232 |
|               |          | 0.5600        | 0.05859 |
|               |          | 0.6000        | 0.05456 |
|               |          | 0.6400        | 0.05026 |
|               |          | 0.6800        | 0.04571 |
|               |          | 0.7200        | 0.04093 |
|               |          | 0.7600        | 0.03593 |
|               |          | 0.8000        | 0.03071 |
|               |          | 0.8500        | 0.02389 |
|               |          | 0.9000        | 0.01673 |
|               |          | 0.9500        | 0.00919 |

## **LEWICE 2.2 Input File for the NACA 23012 with 45-min Rime Ice Shape**

```
Rime 45-min Case
&LEW20
ITIMFL = 1
TSTOP  = 2700.
IBOD   = 1
IFLO   = 18
DSMN   = 4.0D-4
NPL    = 24
&END
&DIST
FLWC  = 0.05, 0.1, 0.2, 0.3, 0.2, 0.1, 0.03, 0.01, 0.005, 0.005
DPD   = 4., 9.7, 14.2, 20.9, 28.2, 45.2, 70.1, 88.9, 103.4, 164.
&END
&ICE1
CHORD = 0.9144
AOA   = 2.5
VINF  = 78.2
LWC   = 0.50
TINF  = 252.32
PINF  = 94806.00
RH    = 100.0
&END
&LPRNT
FPRT  = 1
HPRT  = 1
BPRT  = 1
TPRT  = 0
&END
&RDATA
&END
```

## **Appendix B—Run Log for 2003 Impingement Tests**

Date: 04/07/2003 Monday  
 Concentration: 0.0003 grams/cc  
 Average  $P_{\text{static}} = 13.821$  psi, Average  $P_{\text{total}} = 14.364$  psi  
 Geometry: MS-317 airfoil

| Run I.D. | TAS (mph) | AOA (deg.) | TOTAL TEMP. (°F) | STATIC TEMP. (°F) | R.H. (%) | $P_{\text{air}}$ (psi) | $P_{\text{water}}$ (psi) | MVD (μm) | Spray Time (sec) | Clock Time (EST) | IRT Air (psi) | Remark                                   |
|----------|-----------|------------|------------------|-------------------|----------|------------------------|--------------------------|----------|------------------|------------------|---------------|--|
| 325      | 175       | 0          | 40.4             | 34.9              | 69.8     | 6                      | 37                       | 111      | 1.5              | 19:57            | 40            | ALL minus N1, N6 and N7, steam on, doors |
| 326      | 175       | 0          | 40.4             | 35.0              | 70.0     | 6                      | 37                       | 111      | 1.5              | 20:12            | 40            | ALL minus N1, N6 and N7, steam on, doors |
| 327      | 175       | 0          | 40.6             | 35.1              | 69.0     | 6                      | 37                       | 111      | 4                | 20:21            | 40            | ALL minus N1, N6 and N7, steam on, doors |
| 328      | 175       | 0          | 40.8             | 35.2              | 69.9     | 6                      | 37                       | 111      | 1.5              | 20:44            | 60            | ALL minus N1, N6 and N7, steam on, doors |
| 329      | 175       | 0          | 39.3             | 33.9              | 71.3     | 22                     | 70                       | 20       | 1.5              | 21:22            | 40            | ALL, steam on, doors                     |
| 330      | 175       | 0          | 39.6             | 34.1              | 70.4     | 22                     | 70                       | 20       | 1.5              | 21:27            | 40            | ALL, steam on, doors                     |
| 331      | 175       | 0          | 40.9             | 35.4              | 70.0     | 22                     | 70                       | 20       | 1.5              | 21:34            | 40            | ALL, steam on, doors                     |
| 332      | 175       | 0          | 39.9             | 34.4              | 68.1     | 22                     | 70                       | 20       | 4                | 21:45            | 40            | ALL, steam on, doors                     |
| 333      | 175       | 0          | 39.5             | 34.1              | 67.4     | 5                      | 70                       | 236      | 0.75             | 21:55            | 40            | ALL minus N1, N6 and N7, steam on, doors |
| 334      | 175       | 0          | 39.3             | 33.9              | 68.7     | 5                      | 70                       | 236      | 0.75             | 22:07            | 40            | ALL minus N1, N6 and N7, steam on, doors |
| 335      | 175       | 0          | 40.3             | 34.8              | 74.5     | 5                      | 70                       | 236      | 4                | 22:24            | 40            | ALL minus N1, N6 and N7, steam on, doors |
| 336      | 175       | 0          | 41.0             | 35.5              | 70.7     | 5                      | 70                       | 236      | 0.75             | 22:30            | 40            | ALL minus N1, N6 and N7, steam on, doors |
| 337      | 175       | 0          | 40.4             | 34.9              | 70.8     | 5                      | 55                       | 154      | 1                | 22:39            | 40            | ALL minus N1, N6 and N7, steam on, doors |
| 338      | 175       | 0          | 41.5             | 36.0              | 70.8     | 10                     | 45                       | 52       | 1.5              | 22:44            | 40            | ALL, steam on, doors                     |
| 339      | 175       | 0          | 39.6             | 34.1              | 68.5     | 10                     | 45                       | 52       | 1.5              | 22:52            | 40            | ALL minus N1, N6 and N7, steam on, doors |

(AOA)<sub>IRT</sub> = (AOA)<sub>MS-317</sub>, The bottom edge of the blotter strip is placed 37" above the floor.

Date: 04/10/2003 Thursday  
 Concentration: 0.0003 grams/cc  
 Average  $P_{\text{static}} = 13.807 \text{ psi}$ , Average  $P_{\text{total}} = 14.321 \text{ psi}$   
 Geometry: NACA 23012 airfoil

| Run I.D. | TAS (mph) | AOA (deg.) | TOTAL TEMP. (°F) | STATIC TEMP. (°F) | R.H. (%) | $P_{\text{air}}$ (psi) | $P_{\text{water}}$ (psi) | MVD ( $\mu\text{m}$ ) | Spray Time (sec) | Clock Time (EST) | IRT Air (psi) | Remark                            |
|----------|-----------|------------|------------------|-------------------|----------|------------------------|--------------------------|-----------------------|------------------|------------------|---------------|-----------------------------------|
| 406      | 175       | 2.5        | 69.7             | 64.2              | 71.1     | 6                      | 37                       | 111                   | 1.5              | 19:30            | 40            | ALL minus N1, N6 and N7, steam on |
| 407      | 175       | 2.5        | 68.9             | 63.4              | 70.9     | 6                      | 37                       | 111                   | 1.5              | 19:42            | 40            | ALL minus N1, N6 and N7, steam on |
| 408      | 175       | 2.5        | 68.4             | 62.9              | 71.8     | 6                      | 37                       | 111                   | 1.5              | 19:54            | 40            | ALL minus N1, N6 and N7, steam on |
| 409      | 175       | 2.5        | 68.2             | 62.6              | 71.7     | 6                      | 37                       | 111                   | 4                | 20:06            | 40            | ALL minus N1, N6 and N7, steam on |
| 410      | 175       | 2.5        | 67.9             | 62.4              | 71.8     | 10                     | 45                       | 52                    | 1.5              | 20:18            | 40            | ALL, steam on                     |
| 411      | 175       | 2.5        | 67.6             | 62.1              | 71.8     | 10                     | 45                       | 52                    | 1.5              | 20:30            | 40            | ALL, steam on                     |
| 412      | 175       | 2.5        | 67.6             | 62.2              | 71.8     | 10                     | 45                       | 52                    | 1.5              | 20:41            | 40            | ALL, steam on                     |
| 413      | 175       | 2.5        | 67.6             | 62.1              | 71.7     | 10                     | 45                       | 52                    | 4                | 20:53            | 40            | ALL, steam on                     |
| 414      | 175       | 2.5        | 67.5             | 61.9              | 71.7     | 5                      | 55                       | 154                   | 1                | 21:02            | 40            | ALL minus N1, N6 and N7, steam on |
| 415      | 175       | 2.5        | 67.5             | 62.0              | 71.6     | 5                      | 55                       | 154                   | 1                | 21:13            | 40            | ALL minus N1, N6 and N7, steam on |
| 416      | 175       | 2.5        | 67.4             | 61.9              | 72.0     | 5                      | 55                       | 154                   | 1                | 21:23            | 40            | ALL minus N1, N6 and N7, steam on |
| 417      | 175       | 2.5        | 67.4             | 61.9              | 71.7     | 5                      | 55                       | 154                   | 4                | 21:33            | 40            | ALL minus N1, N6 and N7, steam on |
| 418      | 175       | 2.5        | 67.4             | 62.2              | 71.2     | 22                     | 70                       | 20                    | 1.5              | 21:44            | 40            | ALL, steam on                     |
| 419      | 175       | 2.5        | 67.3             | 61.9              | 71.7     | 22                     | 70                       | 20                    | 1.5              | 21:53            | 40            | ALL, steam on                     |
| 420      | 175       | 2.5        | 67.2             | 71.5              | 71.5     | 22                     | 70                       | 20                    | 1.5              | 22:02            | 40            | ALL, steam on                     |
| 421      | 175       | 2.5        | 67.1             | 61.7              | 72.0     | 22                     | 70                       | 20                    | 4                | 22:13            | 40            | ALL, steam on                     |
| 422      | 175       | 2.5        | 67.1             | 61.7              | 71.8     | 5                      | 70                       | 236                   | 0.75             | 22:20            | 40            | ALL minus N1, N6 and N7, steam on |
| 423      | 175       | 2.5        | 66.9             | 61.4              | 71.8     | 5                      | 70                       | 236                   | 0.75             | 22:33            | 40            | ALL minus N1, N6 and N7, steam on |
| 424      | 175       | 2.5        | 67.0             | 61.5              | 71.9     | 5                      | 70                       | 236                   | 0.75             | 22:41            | 40            | ALL minus N1, N6 and N7, steam on |
| 425      | 175       | 2.5        | 66.8             | 61.3              | 71.9     | 5                      | 70                       | 236                   | 4                | 22:53            | 40            | ALL minus N1, N6 and N7, steam on |

AOA's tabulated are respect to geometry. They are negative to IRT turnable AOAs. i.e.,  $(AOA)_{\text{NACA}} = -(AOA)_{\text{IRT}}$

Date: 04/11/2003 Friday  
 Concentration: 0.0003 grams/cc  
 Average  $P_{\text{static}} = 13.731 \text{ psi}$ , Average  $P_{\text{total}} = 14.240 \text{ psi}$   
 Geometry: NACA 23012 airfoil + 22.5 min glaze ice

| Run I.D. | TAS (mph) | AOA (deg.) | TOTAL TEMP. (°F) | STATIC TEMP. (°F) | R.H. (%) | $P_{\text{air}}$ (psi) | $P_{\text{water}}$ (psi) | MVD (μm) | Spray Time (sec) | Clock Time (EST) | IRT Air (psi) | Remark                            |
|----------|-----------|------------|------------------|-------------------|----------|------------------------|--------------------------|----------|------------------|------------------|---------------|-----------------------------------|
| 427      | 175       | 2.5        | 69.6             | 64.2              | 68.5     | 6                      | 37                       | 111      | 1.5              | 19:00            | 40            | ALL minus N1, N6 and N7, steam on |
| 428      | 175       | 2.5        | 69.0             | 63.6              | 69.0     | 6                      | 37                       | 111      | 1.5              | 19:27            | 40            | ALL minus N1, N6 and N7, steam on |
| 429      | 175       | 2.5        | 68.6             | 63.1              | 71.7     | 6                      | 37                       | 111      | 1.5              | 19:51            | 40            | ALL minus N1, N6 and N7, steam on |
| 430      | 175       | 2.5        | 68.5             | 63.0              | 71.4     | 6                      | 37                       | 111      | 4                | 20:13            | 40            | ALL minus N1, N6 and N7, steam on |
| 431      | 175       | 2.5        | 68.2             | 62.8              | 72.0     | 10                     | 45                       | 52       | 1.5              | 20:33            | 40            | ALL, steam on                     |
| 432      | 175       | 2.5        | 67.7             | 62.4              | 71.1     | 10                     | 45                       | 52       | 1.5              | 20:56            | 40            | ALL, steam on                     |
| 433      | 175       | 2.5        | 67.3             | 61.8              | 71.8     | 10                     | 45                       | 52       | 1.5              | 21:21            | 40            | ALL, steam on                     |
| 434      | 175       | 2.5        | 67.4             | 61.9              | 71.3     | 10                     | 45                       | 52       | 4                | 21:43            | 40            | ALL, steam on                     |
| 435      | 175       | 2.5        | 67.3             | 61.9              | 72.0     | 5                      | 55                       | 154      | 1                | 22:03            | 40            | ALL minus N1, N6 and N7, steam on |
| 436      | 175       | 2.5        | 67.0             | 61.5              | 71.9     | 5                      | 55                       | 154      | 1                | 22:26            | 40            | ALL minus N1, N6 and N7, steam on |
| 437      | 175       | 2.5        | 66.9             | 61.5              | 71.6     | 5                      | 55                       | 154      | 1                | 22:45            | 40            | ALL minus N1, N6 and N7, steam on |

Date: 04/12/2003 Saturday  
 Concentration: 0.0003 grams/cc  
 Average  $P_{\text{static}} = 13.780 \text{ psi}$ , Average  $P_{\text{total}} = 14.290 \text{ psi}$   
 Geometry: NACA 23012 airfoil + 22.5 min glaze ice (R438-R447) / 45 min glaze ice (R448-R449)

| Run I.D. | TAS (mph) | AOA (deg.) | TOTAL TEMP. (°F) | STATIC TEMP. (°F) | R.H. (%) | $P_{\text{air}}$ (psi) | $P_{\text{water}}$ (psi) | MVD (μm) | Spray Time (sec) | Clock Time (EST) | IRT Air (psi) | Remark                                 |
|----------|-----------|------------|------------------|-------------------|----------|------------------------|--------------------------|----------|------------------|------------------|---------------|--|
| 438      | 175       | 2.5        | 72.2             | 66.6              | 71.7     | 5                      | 55                       | 154      | 4                | 09:24            | 40            | ALL minus N1, N6 and N7, steam on      |
| 439      | 175       | 2.5        | 71.3             | 65.9              | 72.1     | 22                     | 70                       | 20       | 1.5              | 09:47            | 40            | ALL, steam on                          |
| 440      | 175       | 2.5        | 71.0             | 65.5              | 71.7     | 22                     | 70                       | 20       | 1.5              | 10:11            | 40            | ALL, steam on                          |
| 441      | 175       | 2.5        | 70.6             | 65.2              | 71.7     | 22                     | 70                       | 20       | 1.5              | 10:32            | 40            | ALL, steam on                          |
| 442      | 175       | 2.5        | 70.3             | 64.8              | 72.1     | 22                     | 70                       | 20       | 4                | 10:51            | 40            | ALL, steam on                          |
| 443      | 175       | 2.5        | 70.0             | 64.6              | 71.5     | 5                      | 70                       | 236      | 0.75             | 11:14            | 40            | ALL minus N1, N6 and N7, steam on      |
| 444      | 175       | 2.5        | 70.0             | 64.6              | 71.9     | 5                      | 70                       | 236      | 0.75             | 11:33            | 40            | ALL minus N1, N6 and N7, steam on      |
| 445      | 175       | 2.5        | 69.8             | 64.3              | 71.6     | 5                      | 70                       | 236      | 0.75             | 11:53            | 40            | ALL minus N1, N6 and N7, steam on      |
| 446      | 175       | 2.5        | 69.6             | 64.2              | 72.2     | 5                      | 70                       | 236      | 4                | 12:13            | 40            | ALL minus N1, N6 and N7, steam on      |
| 447      | 175       | 2.5        | 69.3             | 63.9              | 71.9     | 5                      | 55                       | 154      | 1                | 12:34            | 40            | ALL minus N1, N6 and N7, <b>Repeat</b> |
| 448      | 175       | 2.5        | 68.0             | 62.6              | 71.8     | 6                      | 37                       | 111      | 4                | 14:26            | 40            | ALL minus N1, N6 and N7, steam on      |
| 449      | 175       | 2.5        | 67.7             | 62.3              | 71.5     | 10                     | 45                       | 52       | 4                | 15:03            | 40            | ALL, steam on                          |

Date: 04/14/2003 Monday  
 Concentration: 0.0003 grams/cc  
 $P_{\text{static}} = 13.867 \text{ psi}$ , Average  $P_{\text{total}} = 14.379 \text{ psi}$   
 Geometry: NACA 23012 airfoil +45 min glaze ice

| Run I.D. | TAS (mph) | AOA (deg.) | TOTAL TEMP. (°F) | STATIC TEMP. (°F) | R.H. (%) | P <sub>air</sub> (psi) | P <sub>water</sub> (psi) | MVD (μm) | Spray Time (sec) | Clock Time (EST) | IRT Air (psi) | Remark                            |
|----------|-----------|------------|------------------|-------------------|----------|------------------------|--------------------------|----------|------------------|------------------|---------------|-----------------------------------|
| 450      | 175       | 2.5        | 68.7             | 63.4              | 71.4     | 5                      | 55                       | 154      | 4                | 15:17            | 40            | ALL minus N1, N6 and N7, steam on |
| 451      | 175       | 2.5        | 68.2             | 62.7              | 71.6     | 22                     | 70                       | 20       | 4                | 15:35            | 40            | ALL, steam on                     |
| 452      | 175       | 2.5        | 67.6             | 62.2              | 71.8     | 5                      | 70                       | 236      | 4                | 15:57            | 40            | ALL minus N1, N6 and N7, steam on |
| 452A     | 175       | 2.5        | 67.7             | 62.3              | 70.1     | 5                      | 70                       | 236      | 30               | 15:19            | 40            | ALL minus N1, N6 and N7, steam on |
| 453      | 175       | 2.5        | 69.0             | 63.5              | 71.9     | 6                      | 37                       | 111      | 1.5              | 16:41            | 40            | ALL minus N1, N6 and N7, steam on |
| 454      | 175       | 2.5        | 70.0             | 64.5              | 71.5     | 6                      | 37                       | 111      | 1.5              | 17:04            | 40            | ALL minus N1, N6 and N7, steam on |
| 455      | 175       | 2.5        | 70.7             | 65.3              | 71.6     | 6                      | 37                       | 111      | 1.5              | 17:21            | 40            | ALL minus N1, N6 and N7, steam on |
| 456      | 175       | 2.5        | 71.1             | 65.6              | 71.7     | 10                     | 45                       | 52       | 1.5              | 17:39            | 40            | ALL, steam on                     |
| 457      | 175       | 2.5        | 71.3             | 65.9              | 71.7     | 10                     | 45                       | 52       | 1.5              | 17:57            | 40            | ALL, steam on                     |
| 458      | 175       | 2.5        | 71.5             | 66.0              | 71.7     | 10                     | 45                       | 52       | 1.5              | 18:17            | 40            | ALL, steam on                     |
| 459      | 175       | 2.5        | 71.7             | 66.3              | 71.9     | 5                      | 55                       | 154      | 1                | 18:35            | 40            | ALL minus N1, N6 and N7, steam on |
| 460      | 175       | 2.5        | 71.9             | 66.5              | 71.7     | 5                      | 55                       | 154      | 1                | 18:53            | 40            | ALL minus N1, N6 and N7, steam on |
| 461      | 175       | 2.5        | 72.1             | 66.7              | 71.6     | 5                      | 55                       | 154      | 1                | 19:11            | 40            | ALL minus N1, N6 and N7, steam on |
| 462      | 175       | 2.5        | 72.4             | 66.9              | 71.4     | 22                     | 70                       | 20       | 1.5              | 19:32            | 40            | ALL, steam on                     |
| 463      | 175       | 2.5        | 72.8             | 67.3              | 71.9     | 22                     | 70                       | 20       | 1.5              | 19:48            | 40            | ALL, steam on                     |
| 464      | 175       | 2.5        | 72.7             | 67.3              | 71.9     | 22                     | 70                       | 20       | 1.5              | 20:06            | 40            | ALL, steam on                     |
| 465      | 175       | 2.5        | 73.1             | 67.6              | 72.1     | 5                      | 70                       | 236      | 0.75             | 20:24            | 40            | ALL minus N1, N6 and N7, steam on |
| 466      | 175       | 2.5        | 73.1             | 67.7              | 71.3     | 5                      | 70                       | 236      | 0.75             | 20:40            | 40            | ALL minus N1, N6 and N7, steam on |
| 467      | 175       | 2.5        | 73.2             | 67.7              | 71.9     | 5                      | 70                       | 236      | 0.75             | 20:55            | 40            | ALL minus N1, N6 and N7, steam on |

Date: 04/15/2003 Tuesday  
 Concentration: 0.0003 grams/cc  
 Average  $P_{\text{static}} = 13.756 \text{ psi}$ , Average  $P_{\text{total}} = 14.260 \text{ psi}$   
 Geometry: NACA 23012 airfoil +22.5 min mixed ice

| Run I.D. | TAS (mph) | AOA (deg.) | TOTAL TEMP. (°F) | STATIC TEMP. (°F) | R.H. (%) | $P_{\text{air}}$ (psi) | $P_{\text{water}}$ (psi) | MVD (μm) | Spray Time (sec) | Clock Time (EST) | IRT Air (psi) | Remark                            |
|----------|-----------|------------|------------------|-------------------|----------|------------------------|--------------------------|----------|------------------|------------------|---------------|-----------------------------------|
| 470      | 175       | 2.5        | 76.1             | 70.7              | 66.7     | 6                      | 37                       | 111      | 4                | 15:15            | 40            | ALL minus N1, N6 and N7, steam on |
| 471      | 175       | 2.5        | 75.2             | 69.7              | 72.1     | 10                     | 45                       | 52       | 4                | 15:41            | 40            | ALL, steam on                     |
| 472      | 175       | 2.5        | 75.4             | 70.0              | 71.4     | 5                      | 55                       | 154      | 4                | 16:04            | 40            | ALL minus N1, N6 and N7, steam on |
| 473      | 175       | 2.5        | 75.6             | 70.2              | 71.6     | 22                     | 70                       | 20       | 4                | 16:26            | 40            | ALL, steam on                     |
| 474      | 175       | 2.5        | 75.8             | 70.3              | 71.7     | 5                      | 70                       | 236      | 4                | 16:47            | 40            | ALL minus N1, N6 and N7, steam on |
| 475      | 175       | 2.5        | 76.1             | 70.6              | 71.8     | 6                      | 37                       | 111      | 1.5              | 17:07            | 40            | ALL minus N1, N6 and N7, steam on |
| 476      | 175       | 2.5        | 76.4             | 70.9              | 71.4     | 6                      | 37                       | 111      | 1.5              | 17:27            | 40            | ALL minus N1, N6 and N7, steam on |
| 477      | 175       | 2.5        | 76.6             | 71.1              | 71.4     | 6                      | 37                       | 111      | 1.5              | 17:47            | 40            | ALL minus N1, N6 and N7, steam on |
| 478      | 175       | 2.5        | 76.6             | 71.1              | 71.9     | 10                     | 45                       | 52       | 1.5              | 18:06            | 40            | ALL, steam on                     |
| 479      | 175       | 2.5        | 76.8             | 71.3              | 71.7     | 10                     | 45                       | 52       | 1.5              | 18:26            | 40            | ALL, steam on                     |
| 480      | 175       | 2.5        | 76.9             | 71.4              | 71.9     | 10                     | 45                       | 52       | 1.5              | 18:46            | 40            | ALL, steam on                     |
| 481      | 175       | 2.5        | 77.1             | 71.6              | 70.3     | 5                      | 55                       | 154      | 1                | 19:04            | 40            | ALL minus N1, N6 and N7, steam on |
| 482      | 175       | 2.5        | 77.5             | 71.9              | 72.0     | 5                      | 55                       | 154      | 1                | 19:24            | 40            | ALL minus N1, N6 and N7, steam on |
| 483      | 175       | 2.5        | 77.6             | 72.2              | 71.8     | 5                      | 55                       | 154      | 1                | 19:40            | 40            | ALL minus N1, N6 and N7, steam on |
| 484      | 175       | 2.5        | 77.4             | 72.0              | 71.8     | 22                     | 70                       | 20       | 1.5              | 19:58            | 40            | ALL, steam on                     |
| 485      | 175       | 2.5        | 77.4             | 71.9              | 71.9     | 22                     | 70                       | 20       | 1.5              | 20:17            | 40            | ALL, steam on                     |
| 486      | 175       | 2.5        | 77.4             | 71.9              | 71.9     | 22                     | 70                       | 20       | 1.5              | 20:35            | 40            | ALL, steam on                     |
| 487      | 175       | 2.5        | 77.2             | 71.8              | 72.0     | 5                      | 70                       | 236      | 0.75             | 20:53            | 40            | ALL minus N1, N6 and N7, steam on |
| 488      | 175       | 2.5        | 77.1             | 71.6              | 71.7     | 5                      | 70                       | 236      | 0.75             | 21:12            | 40            | ALL minus N1, N6 and N7, steam on |
| 489      | 175       | 2.5        | 77.0             | 71.5              | 71.9     | 5                      | 70                       | 236      | 0.75             | 21:30            | 40            | ALL minus N1, N6 and N7, steam on |

Date: 04/16/2003 Wednesday  
 Concentration: 0.0003 grams/cc  
 Average  $P_{\text{static}} = 13.772 \text{ psi}$ , Average  $P_{\text{total}} = 14.277 \text{ psi}$   
 Geometry: NACA 23012 airfoil +45 min mixed ice

| Run I.D. | TAS (mph) | AOA (deg.) | TOTAL TEMP. (°F) | STATIC TEMP. (°F) | R.H. (%) | $P_{\text{air}}$ (psi) | $P_{\text{water}}$ (psi) | MVD ( $\mu\text{m}$ ) | Spray Time (sec) | Clock Time (EST) | IRT Air (psi) | Remark                            |
|----------|-----------|------------|------------------|-------------------|----------|------------------------|--------------------------|-----------------------|------------------|------------------|---------------|-----------------------------------|
| 492      | 175       | 2.5        | 77.3             | 71.8              | 71.9     | 10                     | 45                       | 52                    | 4                | 15:07            | 40            | ALL minus N1, N6 and N7, steam on |
| 493      | 175       | 2.5        | 76.8             | 71.3              | 71.9     | 5                      | 55                       | 154                   | 4                | 15:27            | 40            | ALL, steam on                     |
| 494      | 175       | 2.5        | 76.7             | 71.2              | 71.9     | 22                     | 70                       | 20                    | 4                | 15:45            | 40            | ALL minus N1, N6 and N7, steam on |
| 495      | 175       | 2.5        | 76.6             | 71.1              | 72.0     | 5                      | 70                       | 236                   | 4                | 16:04            | 40            | ALL, steam on                     |
| 496      | 175       | 2.5        | 76.6             | 71.2              | 71.7     | 6                      | 37                       | 111                   | 1.5              | 16:23            | 40            | ALL minus N1, N6 and N7, steam on |
| 497      | 175       | 2.5        | 76.7             | 71.2              | 71.7     | 6                      | 37                       | 111                   | 1.5              | 16:41            | 40            | ALL minus N1, N6 and N7, steam on |
| 498      | 175       | 2.5        | 76.7             | 71.3              | 71.5     | 6                      | 37                       | 111                   | 1.5              | 16:59            | 40            | ALL minus N1, N6 and N7, steam on |
| 499      | 175       | 2.5        | 76.5             | 71.0              | 72.2     | 6                      | 37                       | 111                   | 1.5              | 17:16            | 40            | ALL minus N1, N6 and N7, steam on |
| 500      | 175       | 2.5        | 76.3             | 70.9              | 71.8     | 10                     | 45                       | 52                    | 1.5              | 17:33            | 40            | ALL, steam on                     |
| 501      | 175       | 2.5        | 76.1             | 70.7              | 72.0     | 10                     | 45                       | 52                    | 1.5              | 17:50            | 40            | ALL, steam on                     |
| 502      | 175       | 2.5        | 75.8             | 70.4              | 71.9     | 10                     | 45                       | 52                    | 1.5              | 18:09            | 40            | ALL, steam on                     |
| 503      | 175       | 2.5        | 75.4             | 69.9              | 72.1     | 5                      | 55                       | 154                   | 1                | 18:28            | 40            | ALL minus N1, N6 and N7, steam on |
| 504      | 175       | 2.5        | 74.4             | 68.9              | 71.5     | 5                      | 55                       | 154                   | 1                | 18:54            | 40            | ALL minus N1, N6 and N7, steam on |
| 505      | 175       | 2.5        | 74.6             | 69.2              | 72.2     | 5                      | 55                       | 154                   | 1                | 19:11            | 40            | ALL minus N1, N6 and N7, steam on |
| 506      | 175       | 2.5        | 74.5             | 69.0              | 72.0     | 22                     | 70                       | 20                    | 1.5              | 19:28            | 40            | ALL, steam on                     |
| 507      | 175       | 2.5        | 74.3             | 68.9              | 71.8     | 22                     | 70                       | 20                    | 1.5              | 19:44            | 40            | ALL, steam on                     |
| 508      | 175       | 2.5        | 74.1             | 68.6              | 71.8     | 22                     | 70                       | 20                    | 1.5              | 20:02            | 40            | ALL, steam on                     |
| 509      | 175       | 2.5        | 73.9             | 68.4              | 71.5     | 5                      | 70                       | 236                   | 0.75             | 20:20            | 40            | ALL minus N1, N6 and N7, steam on |
| 510      | 175       | 2.5        | 73.7             | 68.3              | 71.6     | 5                      | 70                       | 236                   | 0.75             | 20:37            | 40            | ALL minus N1, N6 and N7, steam on |
| 511      | 175       | 2.5        | 73.6             | 68.1              | 71.9     | 5                      | 70                       | 236                   | 0.75             | 20:53            | 40            | ALL minus N1, N6 and N7, steam on |

Date: 04/17/2003 Thursday

Concentration: 0.0003 grams/cc

Average  $P_{\text{static}}$  = 13,770 psi, Average  $P_{\text{total}}$  = 14,280 psi

Geometry: NACA 23012 airfoil + 15 min mixed ice (R514-535) / 15 min glaze ice (R537-541)

| Run I.D. | TAS (mph) | AOA (deg.) | TOTAL TEMP. (°F) | STATIC TEMP. (°F) | R.H. (%) | $P_{\text{air}}$ (psi) | $P_{\text{water}}$ (psi) | MVD (μm) | Spray Time (sec) | Clock Time (EST) | IRT Air (psi) | Remark                            |
|----------|-----------|------------|------------------|-------------------|----------|------------------------|--------------------------|----------|------------------|------------------|---------------|-----------------------------------|
| 514      | 175       | 2.5        | 69.2             | 63.7              | 72.2     | 6                      | 37                       | 111      | 4                | 15:03            | 40            | ALL minus N1, N6 and N7, steam on |
| 515      | 175       | 2.5        | 69.8             | 64.4              | 72.1     | 10                     | 45                       | 52       | 4                | 15:20            | 40            | ALL, steam on                     |
| 516      | 175       | 2.5        | 70.3             | 64.8              | 71.9     | 5                      | 55                       | 154      | 4                | 15:38            | 40            | ALL minus N1, N6 and N7, steam on |
| 517      | 175       | 2.5        | 70.6             | 65.1              | 72.0     | 22                     | 70                       | 20       | 4                | 15:56            | 40            | ALL, steam on                     |
| 518      | 175       | 2.5        | 70.8             | 65.3              | 71.8     | 5                      | 70                       | 236      | 4                | 16:12            | 40            | ALL minus N1, N6 and N7, steam on |
| 519      | 175       | 2.5        | 70.7             | 65.2              | 72.0     | 6                      | 37                       | 111      | 1.5              | 16:27            | 40            | ALL minus N1, N6 and N7, steam on |
| 520      | 175       | 2.5        | 70.8             | 65.3              | 71.7     | 6                      | 37                       | 111      | 1.5              | 16:42            | 40            | ALL minus N1, N6 and N7, steam on |
| 521      | 175       | 2.5        | 70.9             | 65.4              | 71.9     | 6                      | 37                       | 111      | 1.5              | 16:55            | 40            | ALL minus N1, N6 and N7, steam on |
| 522      | 175       | 2.5        | 71.0             | 65.5              | 71.9     | 10                     | 45                       | 52       | 1.5              | 17:08            | 40            | ALL, steam on                     |
| 523      | 175       | 2.5        | 71.1             | 65.7              | 71.7     | 10                     | 45                       | 52       | 1.5              | 17:21            | 40            | ALL, steam on                     |
| 524      | 175       | 2.5        | 71.3             | 65.7              | 71.9     | 10                     | 45                       | 52       | 1.5              | 17:34            | 40            | ALL, steam on                     |
| 525      | 175       | 2.5        | 71.4             | 65.9              | 71.1     | 5                      | 55                       | 154      | 1                | 17:48            | 40            | ALL minus N1, N6 and N7, steam on |
| 526      | 175       | 2.5        | 71.4             | 66.0              | 71.9     | 5                      | 55                       | 154      | 1                | 18:03            | 40            | ALL minus N1, N6 and N7, steam on |
| 527      | 175       | 2.5        | 71.5             | 66.0              | 71.8     | 5                      | 55                       | 154      | 1                | 18:16            | 40            | ALL minus N1, N6 and N7, steam on |
| 528      | 175       | 2.5        | 72.3             | 66.8              | 69.0     | 22                     | 70                       | 20       | 1.5              | 18:31            | 40            | ALL, steam on                     |
| 529      | 175       | 2.5        | 72.2             | 66.8              | 71.9     | 22                     | 70                       | 20       | 1.5              | 18:46            | 40            | ALL, steam on                     |
| 530      | 175       | 2.5        | 72.2             | 66.7              | 71.9     | 22                     | 70                       | 20       | 1.5              | 18:59            | 40            | ALL, steam on                     |
| 531      | 175       | 2.5        | 72.3             | 66.9              | 71.8     | 5                      | 70                       | 236      | 0.75             | 19:13            | 40            | ALL minus N1, N6 and N7, steam on |
| 532      | 175       | 2.5        | 72.7             | 67.2              | 71.9     | 5                      | 70                       | 236      | 0.75             | 19:26            | 40            | ALL minus N1, N6 and N7, steam on |
| 533      | 175       | 2.5        | 72.8             | 67.3              | 71.8     | 5                      | 70                       | 236      | 0.75             | 19:40            | 40            | ALL minus N1, N6 and N7, steam on |
| 534      | 175       | 2.5        | 72.9             | 67.4              | 71.9     | 22                     | 70                       | 20       | 1.5              | 19:53            | 40            | ALL, steam on, REPEAT             |
| 535      | 175       | 2.5        | 73.0             | 67.5              | 72.0     | 5                      | 70                       | 236      | 0.75             | 20:09            | 40            | ALL minus N1, N6 and N7, REPEAT   |
| 537      | 175       | 2.5        | 73.6             | 68.2              | 71.7     | 6                      | 37                       | 111      | 4                | 21:36            | 40            | ALL minus N1, N6 and N7, steam on |
| 538      | 175       | 2.5        | 73.6             | 68.1              | 71.8     | 10                     | 45                       | 52       | 4                | 21:51            | 40            | ALL, steam on                     |
| 539      | 175       | 2.5        | 73.4             | 67.9              | 71.9     | 5                      | 55                       | 154      | 4                | 22:05            | 40            | ALL minus N1, N6 and N7, steam on |
| 540      | 175       | 2.5        | 73.2             | 67.7              | 71.9     | 22                     | 70                       | 20       | 4                | 22:20            | 40            | ALL, steam on                     |
| 541      | 175       | 2.5        | 73.2             | 67.8              | 71.4     | 5                      | 70                       | 236      | 4                | 22:33            | 40            | ALL minus N1, N6 and N7, steam on |

Date: 04/18/2003 Friday

Concentration: 0.0003 grams/cc

Average  $P_{\text{static}}$  = 13.866 psi, Average  $P_{\text{total}}$  = 14.376 psi

Geometry: NACA 23012 airfoil + 15 min glaze ice (R542-557) / 10 min glaze ice (R560-R567)

| Run I.D. | TAS (mph) | AOA (deg.) | TOTAL TEMP. (°F) | STATIC TEMP. (°F) | R.H. (%) | $P_{\text{air}}$ (psi) | $P_{\text{water}}$ (psi) | MVD (μm) | Spray Time (sec) | Clock Time (EST) | IRT Air (psi) | Remark                            |
|----------|-----------|------------|------------------|-------------------|----------|------------------------|--------------------------|----------|------------------|------------------|---------------|-----------------------------------|
| 542      | 175       | 2.5        | 72.4             | 67.1              | 72.1     | 6                      | 37                       | 111      | 1.5              | 15:08            | 40            | ALL minus N1, N6 and N7, steam on |
| 543      | 175       | 2.5        | 72.5             | 67.0              | 72.1     | 6                      | 37                       | 111      | 1.5              | 15:23            | 40            | ALL minus N1, N6 and N7, steam on |
| 544      | 175       | 2.5        | 72.6             | 67.2              | 72.1     | 6                      | 37                       | 111      | 1.5              | 15:38            | 40            | ALL minus N1, N6 and N7, steam on |
| 545      | 175       | 2.5        | 72.9             | 67.4              | 72.0     | 10                     | 45                       | 52       | 1.5              | 15:50            | 40            | ALL, steam on                     |
| 546      | 175       | 2.5        | 72.9             | 67.4              | 72.0     | 10                     | 45                       | 52       | 1.5              | 16:05            | 40            | ALL, steam on                     |
| 547      | 175       | 2.5        | 73.3             | 67.8              | 71.9     | 10                     | 45                       | 52       | 1.5              | 16:23            | 40            | ALL, steam on                     |
| 548      | 175       | 2.5        | 73.7             | 68.2              | 71.9     | 5                      | 55                       | 154      | 1                | 16:36            | 40            | ALL minus N1, N6 and N7, steam on |
| 549      | 175       | 2.5        | 74.0             | 68.5              | 72.0     | 5                      | 55                       | 154      | 1                | 16:46            | 40            | ALL minus N1, N6 and N7, steam on |
| 550      | 175       | 2.5        | 73.9             | 68.4              | 72.0     | 5                      | 55                       | 154      | 1                | 16:58            | 40            | ALL minus N1, N6 and N7, steam on |
| 551      | 175       | 2.5        | 73.9             | 68.5              | 71.7     | 22                     | 70                       | 20       | 1.5              | 17:11            | 40            | ALL, steam on                     |
| 552      | 175       | 2.5        | 74.1             | 68.6              | 71.7     | 22                     | 70                       | 20       | 1.5              | 17:23            | 40            | ALL, steam on                     |
| 553      | 175       | 2.5        | 74.3             | 68.8              | 71.9     | 22                     | 70                       | 20       | 1.5              | 17:34            | 40            | ALL, steam on                     |
| 554      | 175       | 2.5        | 74.2             | 68.8              | 71.8     | 5                      | 70                       | 236      | 0.75             | 17:47            | 40            | ALL minus N1, N6 and N7, steam on |
| 555      | 175       | 2.5        | 74.4             | 68.9              | 71.9     | 5                      | 70                       | 236      | 0.75             | 17:59            | 40            | ALL minus N1, N6 and N7, steam on |
| 556      | 175       | 2.5        | 74.5             | 69.0              | 72.1     | 5                      | 70                       | 236      | 0.75             | 18:12            | 40            | ALL minus N1, N6 and N7, steam on |
| 557      | 175       | 2.5        | 74.6             | 69.1              | 71.9     | 5                      | 55                       | 154      | 1                | 18:24            | 40            | ALL minus N1, N6 and N7, steam on |
| 560      | 175       | 2.5        | 75.8             | 70.4              | 71.9     | 6                      | 37                       | 111      | 4                | 21:14            | 40            | ALL minus N1, N6 and N7, steam on |
| 561      | 175       | 2.5        | 76.2             | 70.6              | 71.7     | 10                     | 45                       | 52       | 4                | 21:27            | 40            | ALL, steam on                     |
| 562      | 175       | 2.5        | 75.9             | 70.4              | 71.9     | 5                      | 55                       | 154      | 4                | 21:38            | 40            | ALL minus N1, N6 and N7, steam on |
| 563      | 175       | 2.5        | 75.8             | 70.3              | 71.8     | 22                     | 70                       | 20       | 4                | 21:52            | 40            | ALL, steam on                     |
| 564      | 175       | 2.5        | 75.7             | 70.2              | 72.1     | 5                      | 70                       | 236      | 4                | 22:04            | 40            | ALL minus N1, N6 and N7, steam on |
| 565      | 175       | 2.5        | 75.6             | 70.1              | 72.0     | 6                      | 37                       | 111      | 1.5              | 22:17            | 40            | ALL minus N1, N6 and N7, steam on |
| 566      | 175       | 2.5        | 75.4             | 69.9              | 71.6     | 6                      | 37                       | 111      | 1.5              | 22:29            | 40            | ALL minus N1, N6 and N7, steam on |
| 567      | 175       | 2.5        | 75.5             | 70.0              | 71.8     | 6                      | 37                       | 111      | 1.5              | 22:40            | 40            | ALL minus N1, N6 and N7, steam on |

Date: 04/22/2003 Tuesday

Concentration: 0.0003 grams/cc

Average  $P_{\text{static}}$  = 13.794 psi, Average  $P_{\text{total}}$  = 14.315 psi

Geometry: NACA 23012 airfoil + 10-min glaze ice

| Run I.D. | TAS (mph) | AOA (deg.) | TOTAL TEMP. (°F) | STATIC TEMP. (°F) | R.H. (%) | $P_{\text{air}}$ (psi) | $P_{\text{water}}$ (psi) | MVD (μm) | Spray Time (sec) | Clock Time (EST) | IRT Air (psi) | Remark                            |
|----------|-----------|------------|------------------|-------------------|----------|------------------------|--------------------------|----------|------------------|------------------|---------------|-----------------------------------|
| 611      | 175       | 2.5        | 66.9             | 61.4              | 72.1     | 6                      | 37                       | 111      | 1.5              | 19:19            | 40            | ALL minus N1, N6 and N7, steam on |
| 612A     | 175       | 2.5        | 67.2             | 61.7              | 71.2     | 10                     | 45                       | 52       | 1.5              | 19:33            | 40            | ALL, steam on                     |
| 612B     | 175       | 2.5        | 65.4             | 59.9              | 71.9     | 10                     | 45                       | 52       | 1.5              | 20:07            | 40            | ALL, steam on                     |
| 613      | 175       | 2.5        | 66.1             | 60.5              | 71.9     | 10                     | 45                       | 52       | 1.5              | 20:19            | 40            | ALL, steam on                     |
| 614      | 175       | 2.5        | 66.7             | 61.1              | 71.8     | 10                     | 45                       | 52       | 1.5              | 20:33            | 40            | ALL, steam on                     |
| 615      | 175       | 2.5        | 67.1             | 61.1              | 72.1     | 5                      | 55                       | 154      | 1                | 20:45            | 40            | ALL minus N1, N6 and N7, steam on |
| 616      | 175       | 2.5        | 67.4             | 61.9              | 72.1     | 5                      | 55                       | 154      | 1                | 20:58            | 40            | ALL minus N1, N6 and N7, steam on |
| 617      | 175       | 2.5        | 67.2             | 62.1              | 72.5     | 5                      | 55                       | 154      | 1                | 20:10            | 40            | ALL minus N1, N6 and N7, steam on |
| 618      | 175       | 2.5        | 67.9             | 62.4              | 72.1     | 22                     | 70                       | 20       | 1.5              | 20:24            | 40            | ALL, steam on                     |
| 619      | 175       | 2.5        | 68.1             | 62.5              | 72.2     | 22                     | 70                       | 20       | 1.5              | 20:35            | 40            | ALL, steam on                     |
| 620      | 175       | 2.5        | 68.1             | 62.6              | 72.2     | 22                     | 70                       | 20       | 1.5              | 20:46            | 40            | ALL, steam on                     |
| 621      | 175       | 2.5        | 68.2             | 62.7              | 72.1     | 5                      | 70                       | 236      | 0.75             | 20:58            | 40            | ALL minus N1, N6 and N7, steam on |
| 622      | 175       | 2.5        | 68.3             | 62.7              | 72.2     | 5                      | 70                       | 236      | 0.75             | 21:09            | 40            | ALL minus N1, N6 and N7, steam on |
| 623      | 175       | 2.5        | 68.3             | 62.8              | 72.1     | 5                      | 70                       | 236      | 0.75             | 21:21            | 40            | ALL minus N1, N6 and N7, steam on |

Date: 04/23/2003 Wednesday

Concentration: 0.0003 grams/cc

Average  $P_{\text{static}}$  = 13.868 psi, Average  $P_{\text{total}}$  = 14.387 psi

Geometry: NACA 23012 airfoil + 5-min glaze ice

| Run I.D. | TAS (mph) | AOA (deg.) | TOTAL TEMP. (°F) | STATIC TEMP. (°F) | R.H. (%) | $P_{\text{air}}$ (psi) | $P_{\text{water}}$ (psi) | MVD (μm) | Spray Time (sec) | Clock Time (EST) | IRT Air (psi) | Remark                            |
|----------|-----------|------------|------------------|-------------------|----------|------------------------|--------------------------|----------|------------------|------------------|---------------|-----------------------------------|
| 625A     | 175       | 2.5        | 64.3             | 58.9              | 71.5     | 6                      | 37                       | 111      | 1.5              | 17:00            | 40            | ALL minus N1, N6 and N7, steam on |
| 626A     | 175       | 2.5        | 64.2             | 58.7              | 70.3     | 6                      | 37                       | 111      | 1.5              | 17:20            | 40            | ALL minus N1, N6 and N7, steam on |
| 625B     | 175       | 2.5        | 69.0             | 63.4              | 68.2     | 6                      | 37                       | 111      | 1.5              | 19:35            | 40            | ALL minus N1, N6 and N7, steam on |
| 626B     | 175       | 2.5        | 68.4             | 62.8              | 71.6     | 6                      | 37                       | 111      | 1.5              | 19:50            | 40            | ALL minus N1, N6 and N7, steam on |
| 627      | 175       | 2.5        | 68.0             | 62.5              | 71.2     | 10                     | 45                       | 52       | 1.5              | 20:04            | 40            | ALL, steam on                     |
| 628      | 175       | 2.5        | 67.8             | 62.3              | 72.1     | 10                     | 45                       | 52       | 1.5              | 20:17            | 40            | ALL, steam on                     |
| 629      | 175       | 2.5        | 67.6             | 62.1              | 72.1     | 5                      | 55                       | 154      | 1                | 20:32            | 40            | ALL minus N1, N6 and N7, steam on |
| 630      | 175       | 2.5        | 67.6             | 62.1              | 72.1     | 5                      | 55                       | 154      | 1                | 20:44            | 40            | ALL minus N1, N6 and N7, steam on |
| 631      | 175       | 2.5        | 67.4             | 61.9              | 72.1     | 22                     | 70                       | 20       | 1.5              | 20:57            | 40            | ALL, steam on                     |
| 632      | 175       | 2.5        | 67.5             | 61.9              | 72.0     | 22                     | 70                       | 20       | 1.5              | 21:08            | 40            | ALL, steam on                     |
| 633      | 175       | 2.5        | 67.3             | 61.8              | 72.2     | 5                      | 70                       | 236      | 0.75             | 21:22            | 40            | ALL minus N1, N6 and N7, steam on |
| 634      | 175       | 2.5        | 67.2             | 61.6              | 71.9     | 5                      | 70                       | 236      | 0.75             | 21:34            | 40            | ALL minus N1, N6 and N7, steam on |
| 635      | 175       | 2.5        | 67.0             | 61.5              | 72.3     | 5                      | 55                       | 154      | 1                | 21:47            | 40            | ALL minus N1, N6 and N7, steam on |
| 636      | 175       | 2.5        | 66.8             | 61.3              | 72.0     | 6                      | 37                       | 111      | 4                | 22:00            | 40            | ALL minus N1, N6 and N7, steam on |
| 637      | 175       | 2.5        | 66.5             | 61.1              | 72.1     | 5                      | 55                       | 154      | 4                | 22:15            | 40            | ALL minus N1, N6 and N7, steam on |
| 638      | 175       | 2.5        | 66.5             | 61.0              | 71.9     | 5                      | 70                       | 236      | 4                | 22:28            | 40            | ALL minus N1, N6 and N7, steam on |

Date: 04/24/2003 Thursday

Concentration: 0.0003 grams/cc

Average  $P_{\text{static}} = 13.794 \text{ psi}$ , Average  $P_{\text{total}} = 14.306 \text{ psi}$

Geometry: NACA 23012 airfoil + 7.5-min mixed ice (R641-R654) / 45-min rime ice (R655-R666)

| Run I.D. | TAS (mph) | AOA (deg.) | TOTAL TEMP. (°F) | STATIC TEMP. (°F) | R.H. (%) | $P_{\text{air}}$ (psi) | $MVD$ (μm) | Spray Time (sec) | Clock Time (EST) | IRT Air (psi) | Remark |
|----------|-----------|------------|------------------|-------------------|----------|------------------------|------------|------------------|------------------|---------------|--------|
| 641      | 175       | 2.5        | 71.4             | 65.9              | 71.8     | 6                      | 37         | 111              | 1.5              | 16:21         | 40     |
| 642      | 175       | 2.5        | 71.4             | 66.0              | 72.1     | 6                      | 37         | 111              | 1.5              | 16:36         | 40     |
| 643      | 175       | 2.5        | 71.3             | 65.8              | 72.1     | 10                     | 45         | 52               | 1.5              | 16:49         | 40     |
| 644      | 175       | 2.5        | 71.2             | 65.8              | 72.1     | 10                     | 45         | 52               | 1.5              | 17:03         | 40     |
| 645      | 175       | 2.5        | 71.2             | 65.7              | 71.9     | 5                      | 55         | 154              | 1                | 17:16         | 40     |
| 646      | 175       | 2.5        | 70.9             | 65.5              | 72.0     | 5                      | 55         | 154              | 1                | 17:30         | 40     |
| 647      | 175       | 2.5        | 70.9             | 65.4              | 72.0     | 22                     | 70         | 20               | 1.5              | 17:44         | 40     |
| 648      | 175       | 2.5        | 71.0             | 65.4              | 72.0     | 22                     | 70         | 20               | 1.5              | 17:57         | 40     |
| 649      | 175       | 2.5        | 70.8             | 65.3              | 71.7     | 5                      | 70         | 236              | 0.75             | 18:12         | 40     |
| 650      | 175       | 2.5        | 70.8             | 65.3              | 72.0     | 5                      | 70         | 236              | 0.75             | 18:25         | 40     |
| 651      | 175       | 2.5        | 70.6             | 65.1              | 72.0     | 6                      | 37         | 111              | 1.5              | 18:39         | 40     |
| 652      | 175       | 2.5        | 70.4             | 65.0              | 71.6     | 6                      | 37         | 111              | 4                | 18:54         | 40     |
| 653      | 175       | 2.5        | 70.3             | 64.8              | 72.1     | 5                      | 55         | 154              | 4                | 19:08         | 40     |
| 654      | 175       | 2.5        | 70.1             | 64.7              | 72.8     | 5                      | 70         | 236              | 4                | 19:23         | 40     |
| 655      | 175       | 2.5        | 69.2             | 63.9              | 71.9     | 6                      | 37         | 111              | 1.5              | 20:18         | 40     |
| 656      | 175       | 2.5        | 69.4             | 63.9              | 71.2     | 6                      | 37         | 111              | 1.5              | 20:30         | 40     |
| 657      | 175       | 2.5        | 69.5             | 64.0              | 72.0     | 10                     | 45         | 52               | 1.5              | 20:42         | 40     |
| 658      | 175       | 2.5        | 69.5             | 64.0              | 72.1     | 10                     | 45         | 52               | 1.5              | 20:55         | 40     |
| 659      | 175       | 2.5        | 69.7             | 64.2              | 71.4     | 5                      | 55         | 154              | 1                | 21:07         | 40     |
| 660      | 175       | 2.5        | 69.7             | 64.2              | 71.0     | 5                      | 55         | 154              | 1                | 21:22         | 40     |
| 661      | 175       | 2.5        | 69.6             | 64.2              | 72.0     | 22                     | 70         | 20               | 1.5              | 21:35         | 40     |
| 662      | 175       | 2.5        | 69.8             | 64.3              | 71.9     | 22                     | 70         | 20               | 1.5              | 21:47         | 40     |
| 663      | 175       | 2.5        | 69.6             | 64.2              | 72.1     | 5                      | 70         | 236              | 0.75             | 22:01         | 40     |
| 664      | 175       | 2.5        | 69.7             | 64.2              | 72.0     | 5                      | 70         | 236              | 0.75             | 22:14         | 40     |
| 665      | 175       | 2.5        | 69.7             | 64.2              | 72.0     | 10                     | 45         | 52               | 1.5              | 22:25         | 40     |
| 666      | 175       | 2.5        | 69.6             | 64.1              | 72.0     | 5                      | 70         | 236              | 0.75             | 22:40         | 40     |



## **Appendix C—Summary of Experimental and LEWICE Impingement Data—All Test Geometries and MVDs**

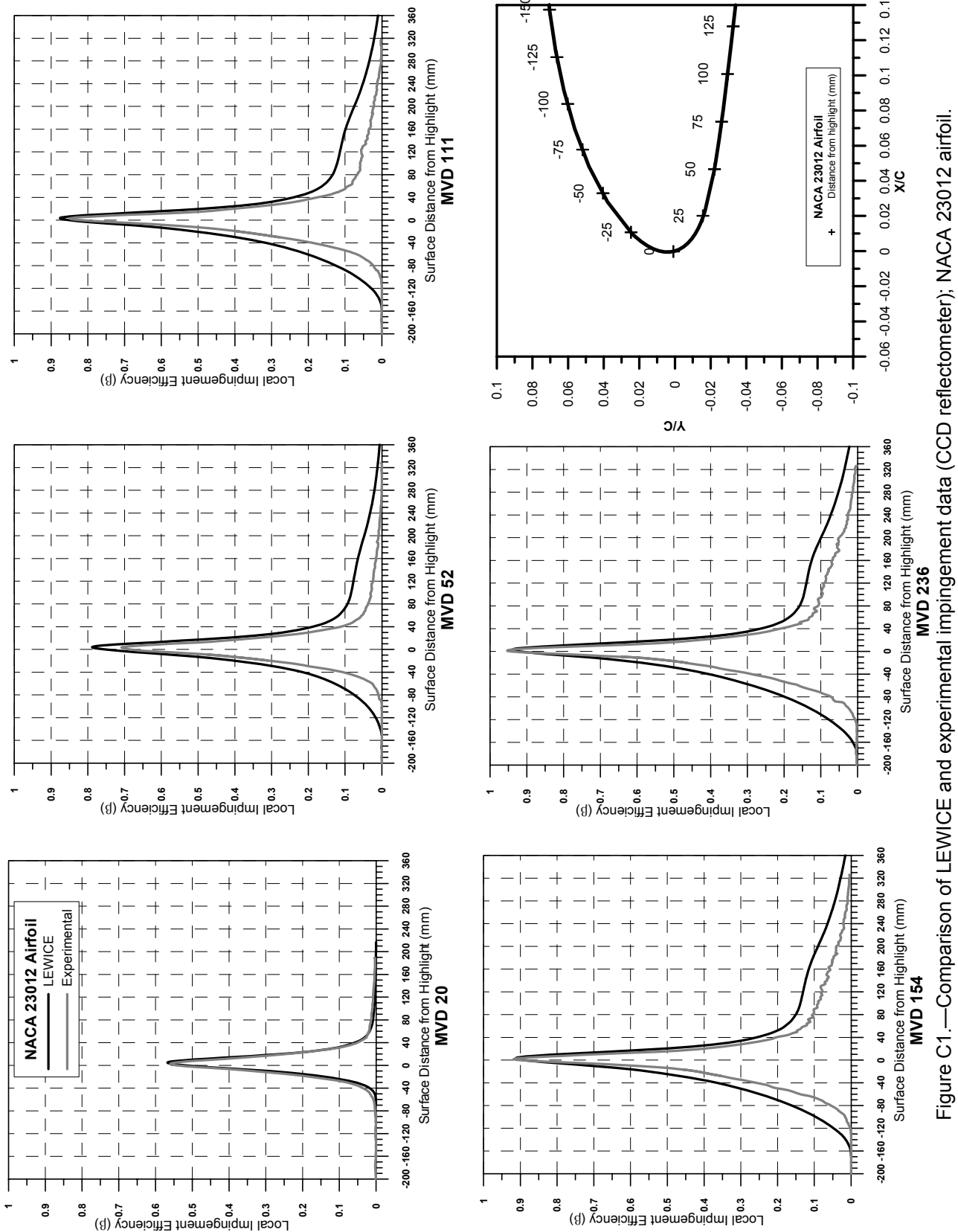


Figure C1.—Comparison of LEWICE and experimental impingement data (CCD reflectometer); NACA 23012 airfoil.

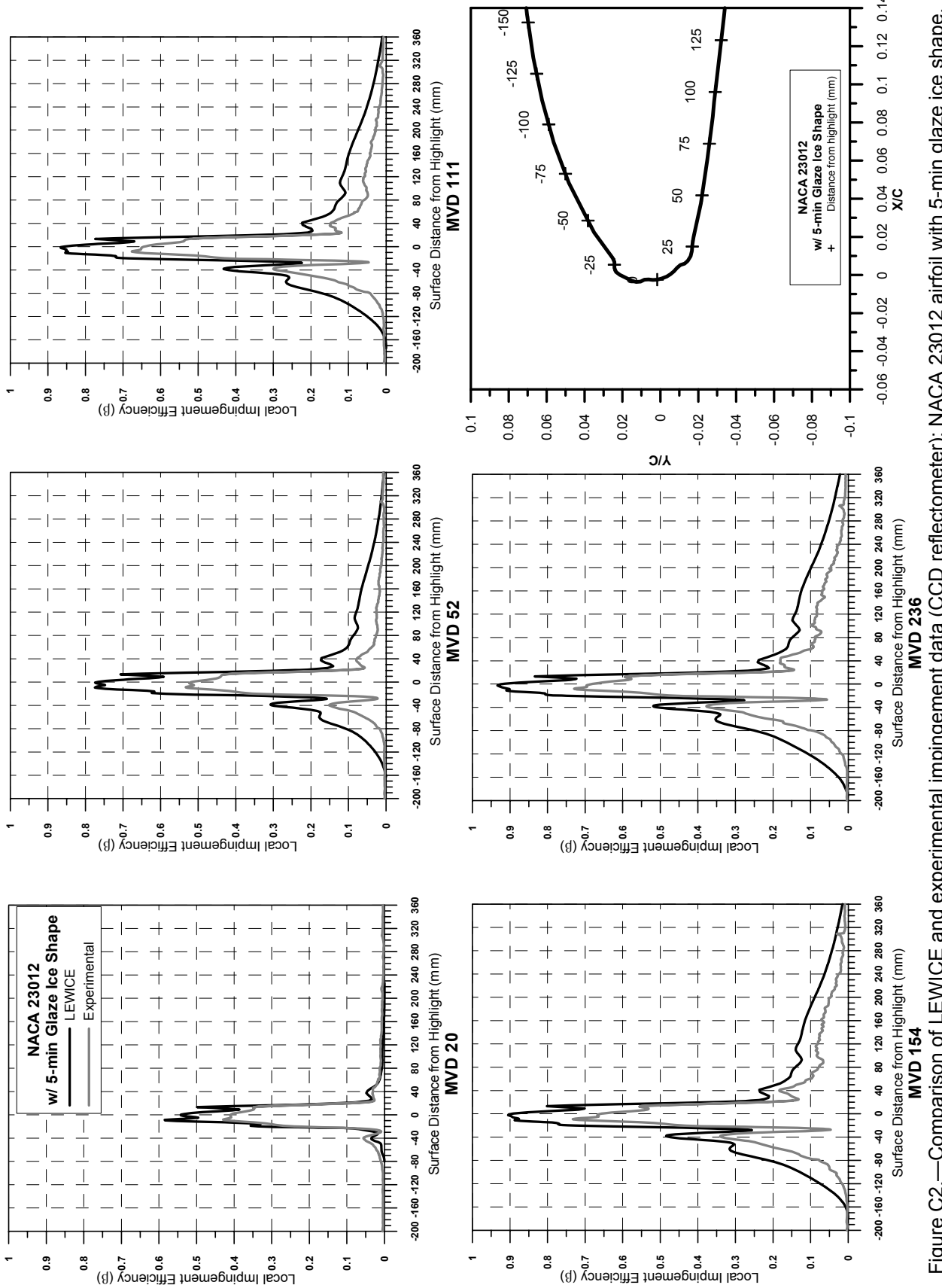


Figure C2.—Comparison of LEWICE and experimental impingement data (CCD reflectometer); NACA 23012 airfoil with 5-min glaze ice shape.

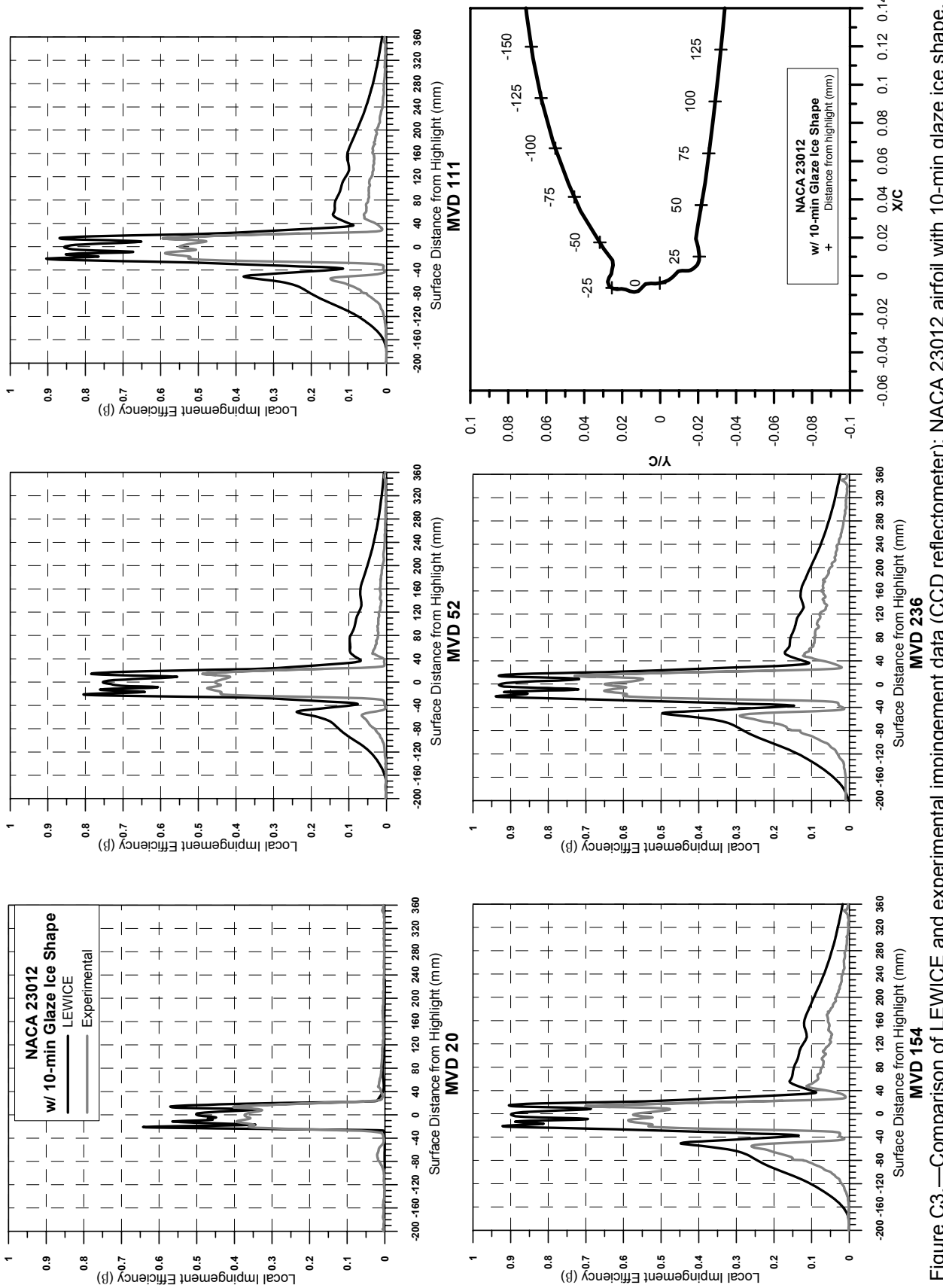


Figure C3.—Comparison of LEWICE and experimental impingement data (CCD reflectometer); NACA 23012 airfoil with 10-min glaze ice shape.

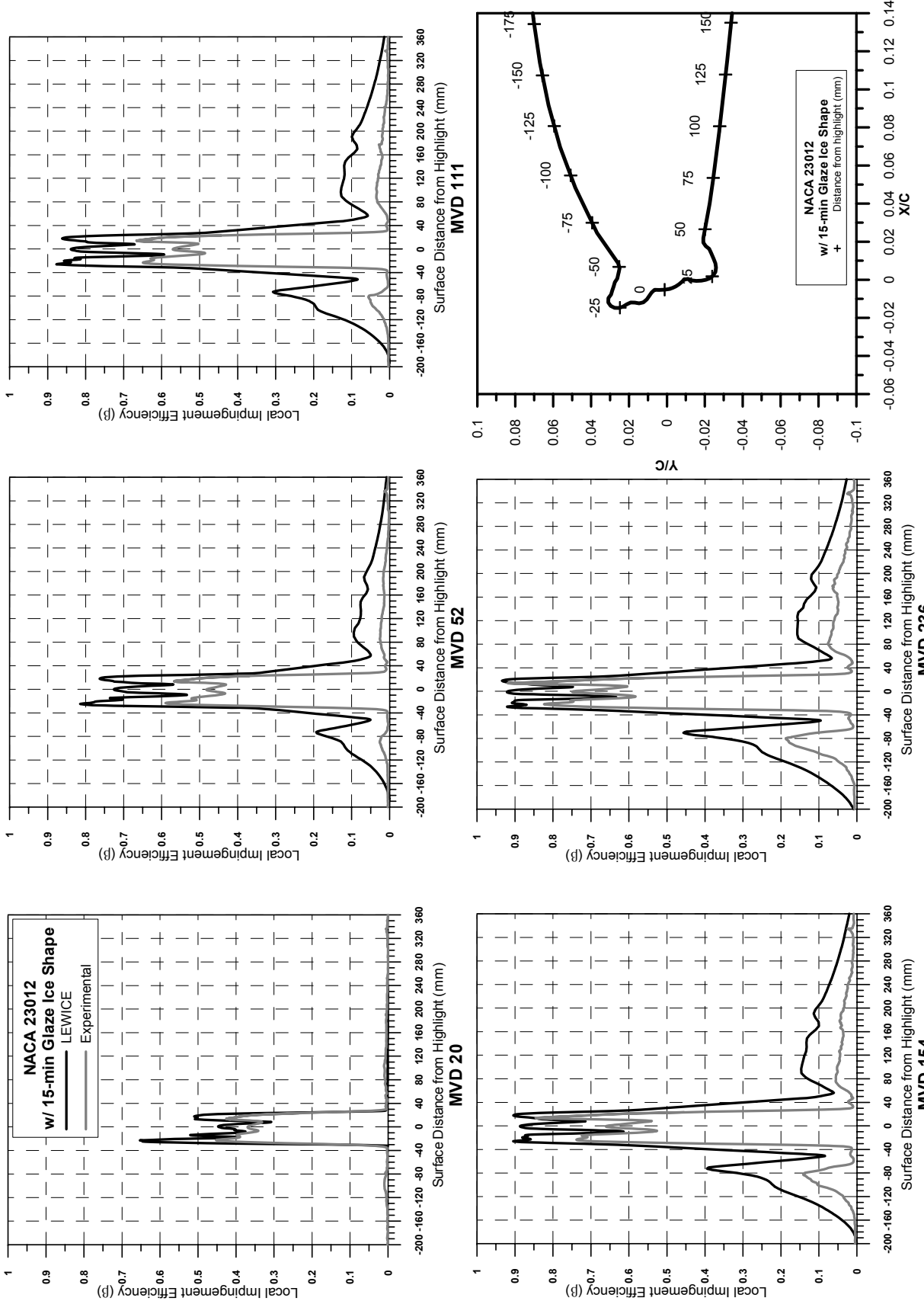


Figure C4.—Comparison of LEWICE and experimental impingement data (CCD reflectometer); NACA 23012 airfoil with 15-min glaze ice shape.

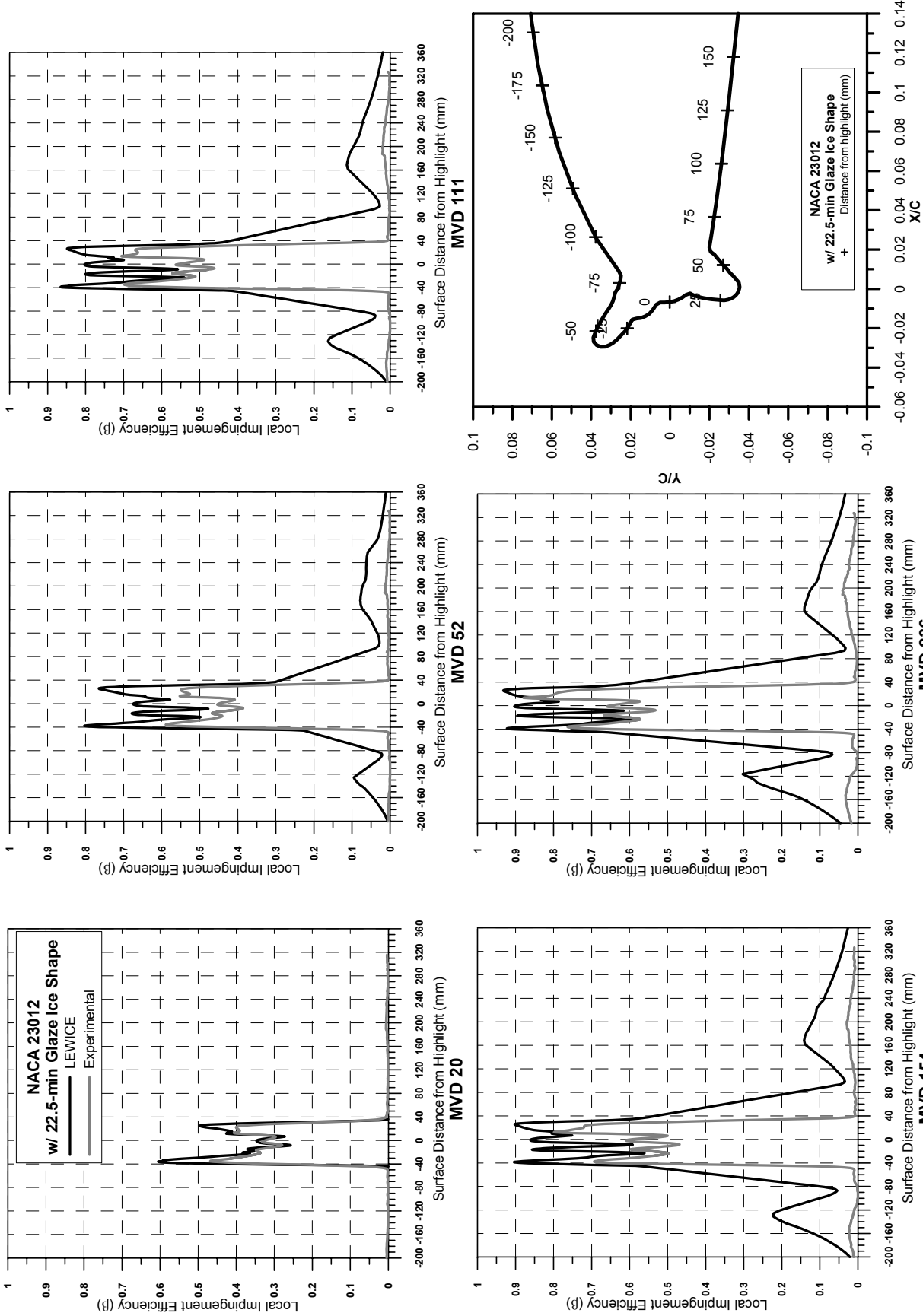


Figure C5.—Comparison of LEWICE and experimental impingement data (CCD reflectometer); NACA 23012 airfoil with 22.5-min glaze ice shape.

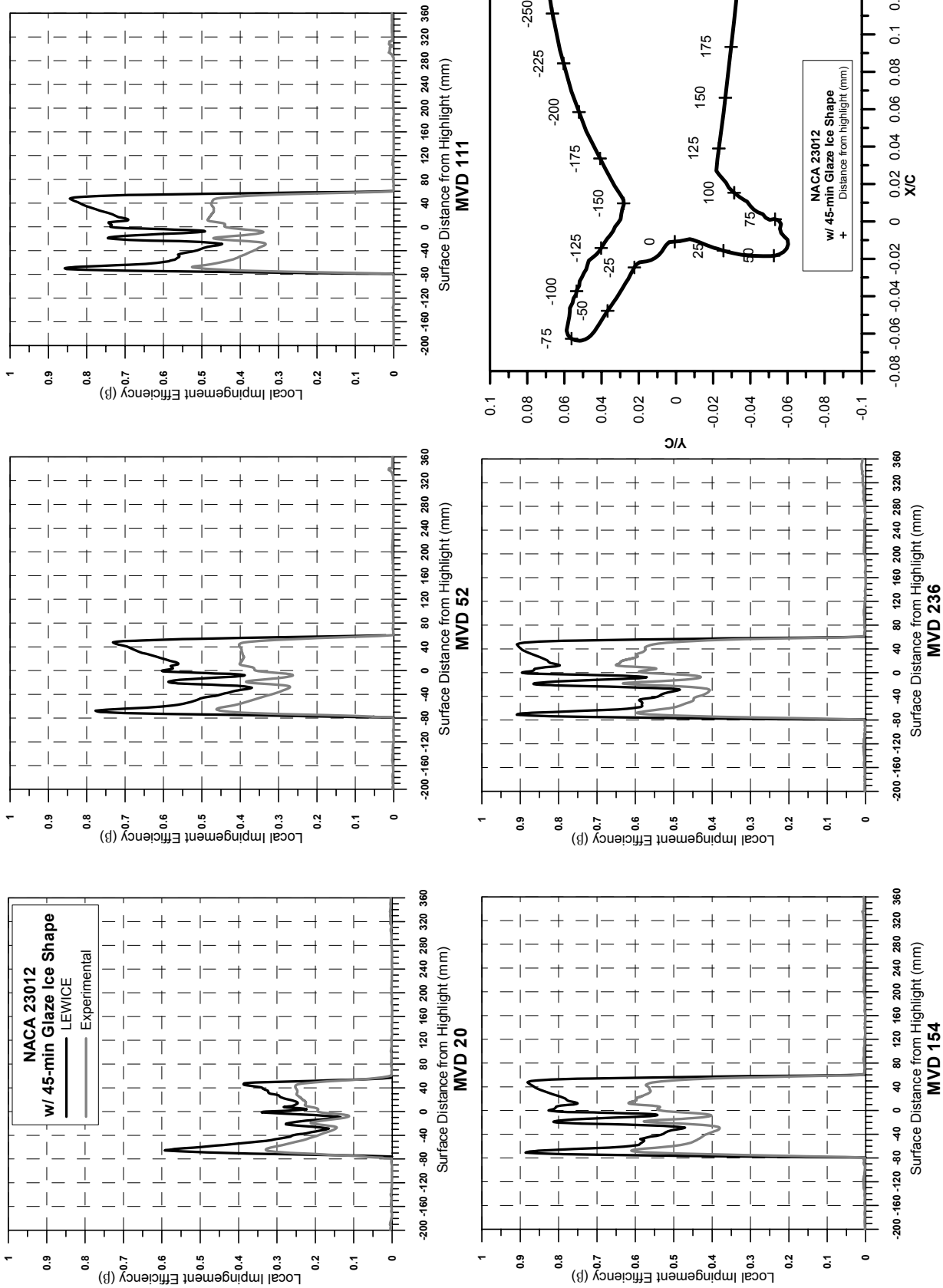


Figure C6.—Comparison of LEWICE and experimental impingement data (CCD reflectometer); NACA 23012 airfoil with 45-min glaze ice shape.

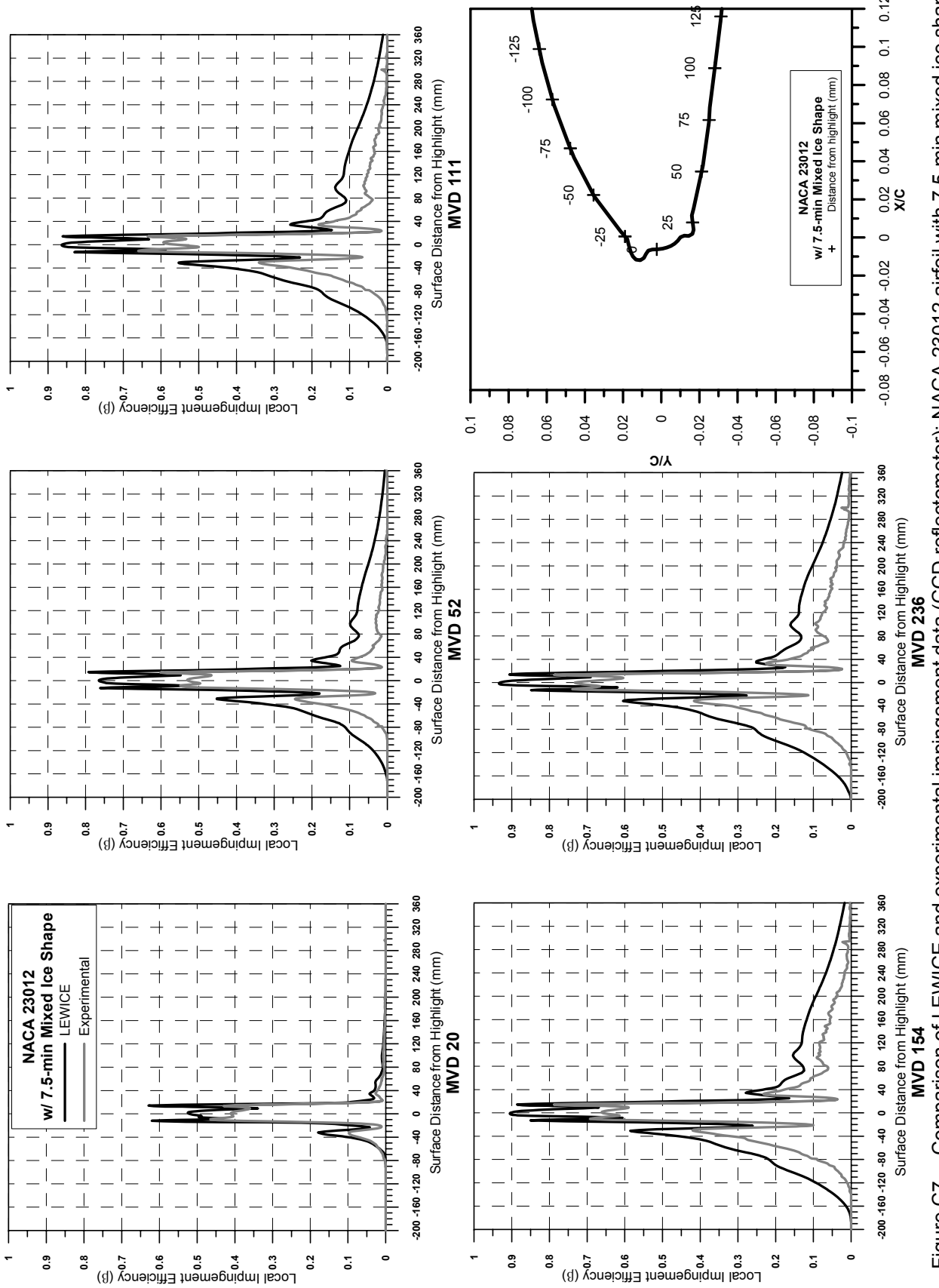


Figure C7.—Comparison of LEWICE and experimental impingement data (CCD reflectometer); NACA 23012 airfoil with 7.5-min mixed ice shape.

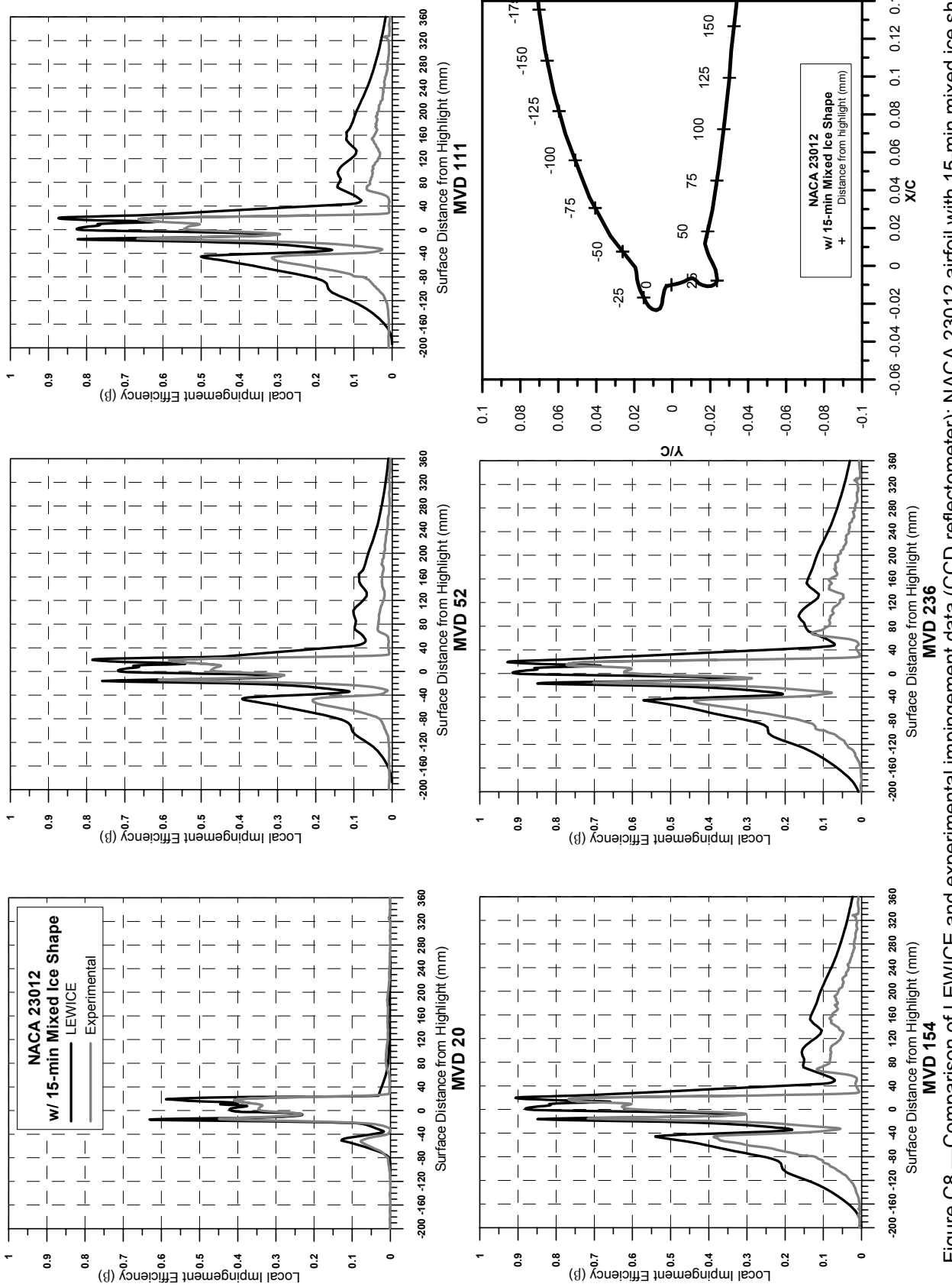


Figure C8.—Comparison of LEWICE and experimental impingement data (CCD reflectometer); NACA 23012 airfoil with 15-min mixed ice shape.

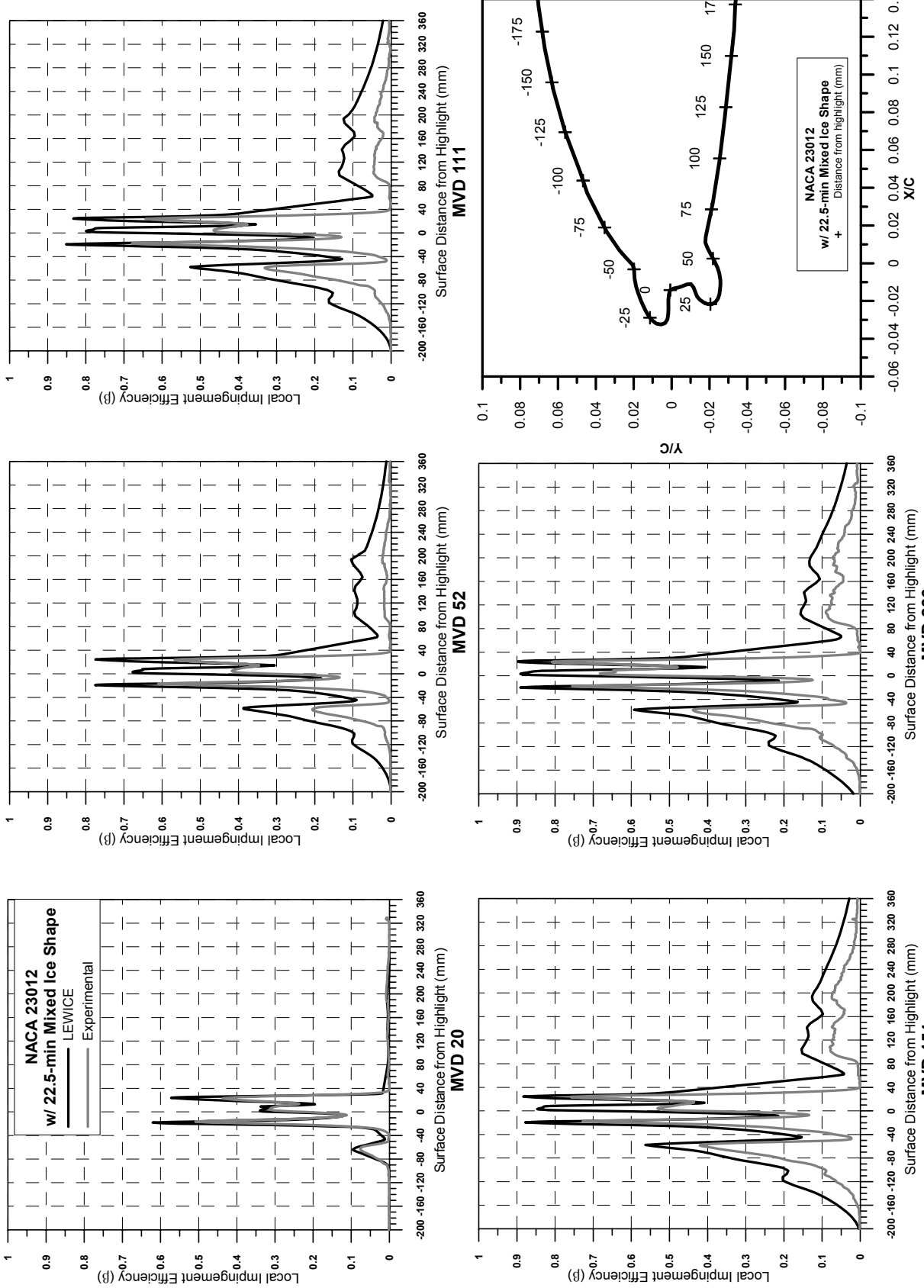


Figure C9.—Comparison of LEWICE and experimental impingement data (CCD reflectometer); NACA 23012 airfoil with 22.5-min mixed ice shape.

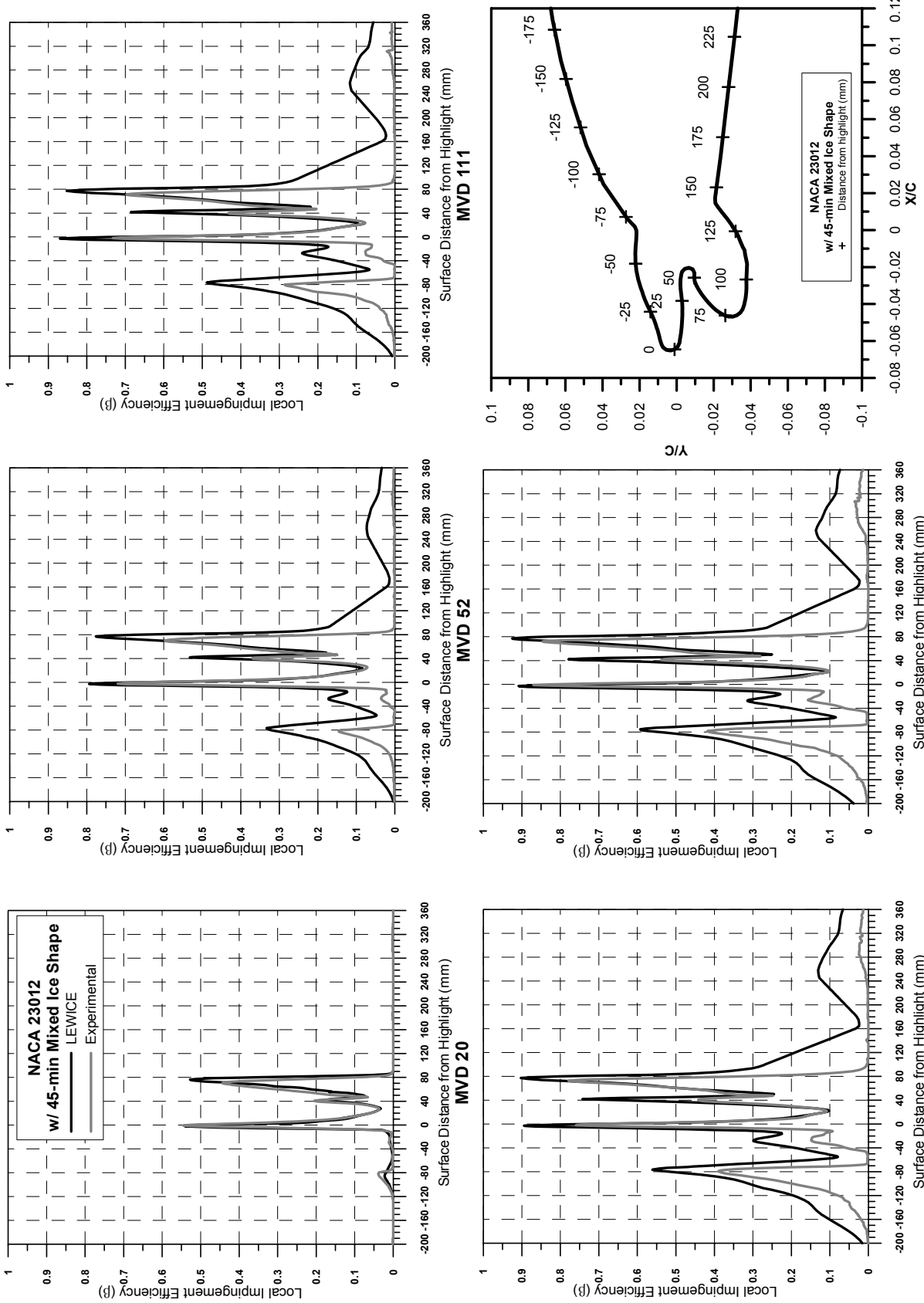


Figure C10.—Comparison of LEWICE and experimental impingement data (CCD reflectometer); NACA 23012 airfoil with 45-min mixed ice shape.

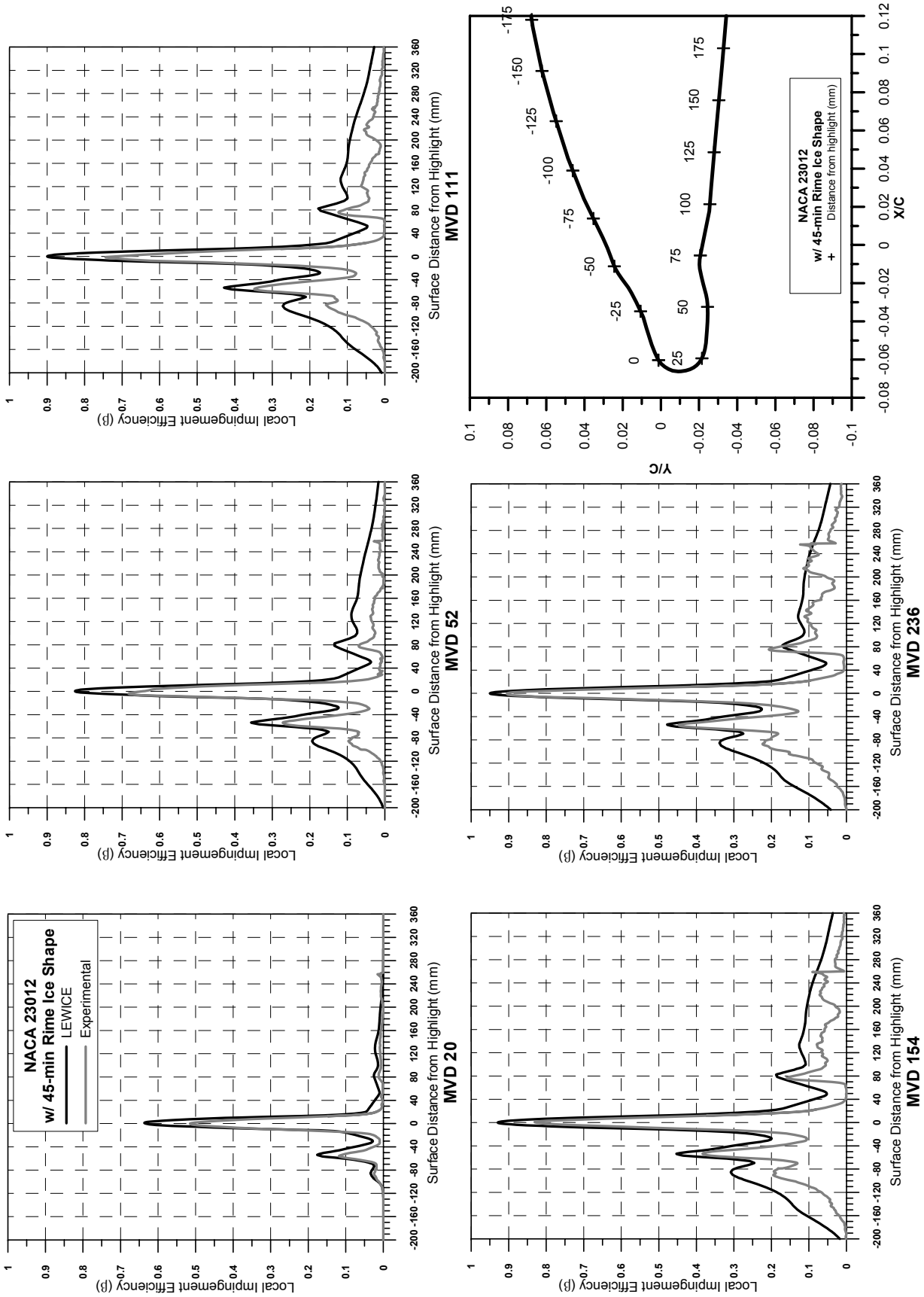


Figure C11.—Comparison of LEWICE and experimental impingement data (CCD reflectometer); NACA 23012 airfoil with 45-min rime ice shape.

## Appendix D—Droplet Trajectories

The trajectories presented in this appendix were computed using the LEWICE 1.7 code and the 10-point discrete approximations (table 5) of the measured droplet distributions. Figures D1 to D8 consist of 10 trajectory plots each, one plot for each droplet size in the measured droplet distributions. Each of the ten plots in the figures was obtained with the LEWICE code using a single drop size. Note that the LEWICE code does not simulate large droplet splashing, thus, the trajectory simulations for the large MVD cases do not include droplet splashing effects. Furthermore, for some cases such as the 45-min glaze ice shape the flowfield predicted by LEWICE was not in good agreement with the experimental pressure data as shown in figure 66. This was due to the inability of the potential flow method used in LEWICE to simulate flow separation and viscous effects such as the ones associated with large glaze ice accretions. In spite of these limitations, however, the computed trajectories provide insight into the contributions made by the individual droplet sizes in the spray clouds used in the experiments. Consider, for example, the computed trajectories for the 45-min glaze ice shape presented in figure D4. For the large MVD of 236  $\mu\text{m}$  the smallest droplet in the 10-point distribution was 16.3  $\mu\text{m}$ . For this droplet size the trajectories experienced considerable deflection near the 45-min ice shapes. The remaining nine droplet sizes in the distribution ranged from 63.7 to 1046.8  $\mu\text{m}$ . For these droplet sizes the deflection of the trajectories became progressively smaller until about 508.5  $\mu\text{m}$ . For droplets larger than 508.5  $\mu\text{m}$  the trajectories were practically straight. Thus, for the angle of attack of 2.5° used in the experiments, the small droplets in the distribution contributed more to the impingement in the upper horn area while the impingement due to the large droplets in the distribution was more even across the region between the two horns.

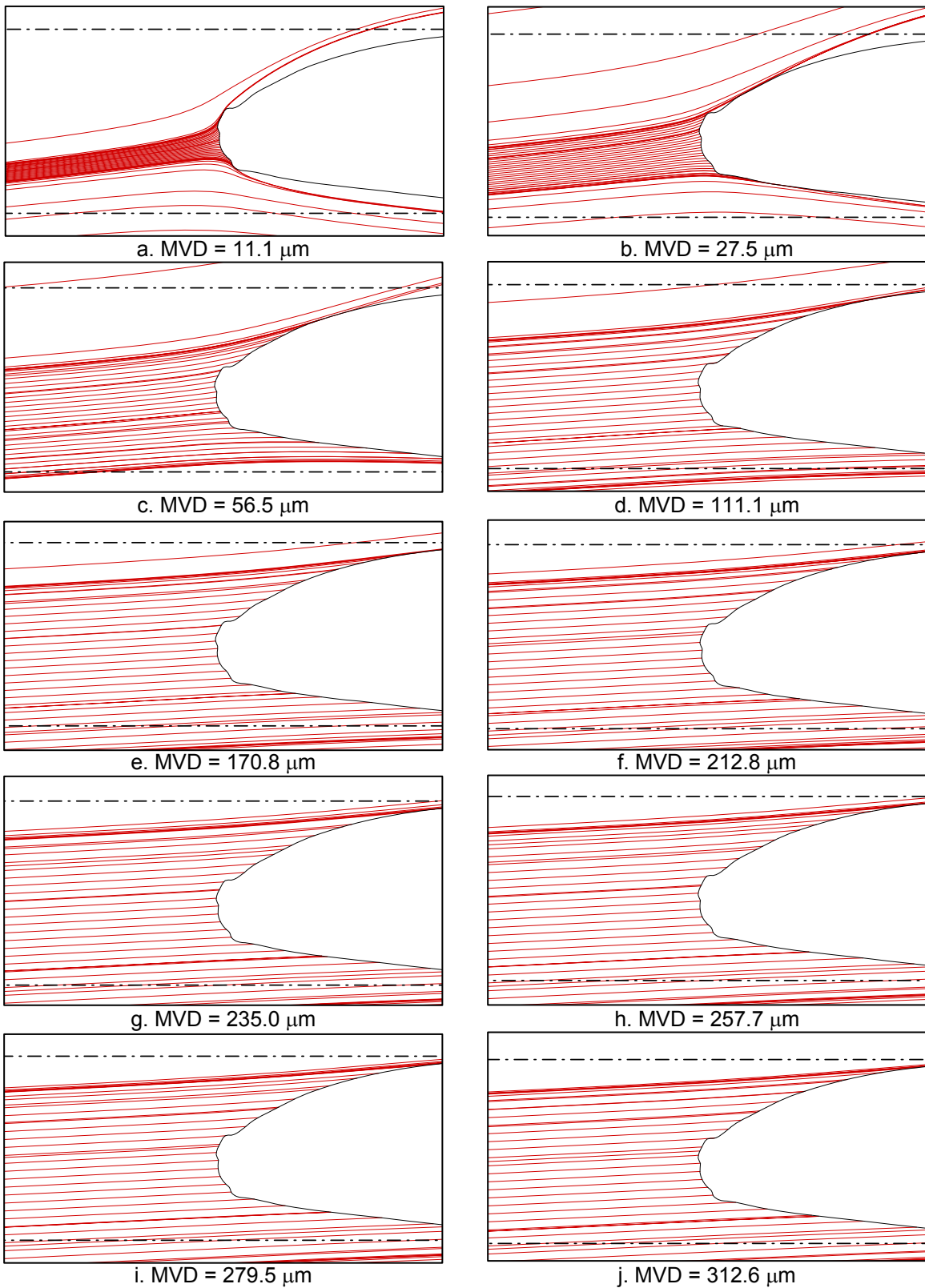


Figure D1.—Computed droplet trajectories with LEWICE code;  
NACA 23012 with 5-min glaze ice, 111  $\mu\text{m}$  spray cloud.

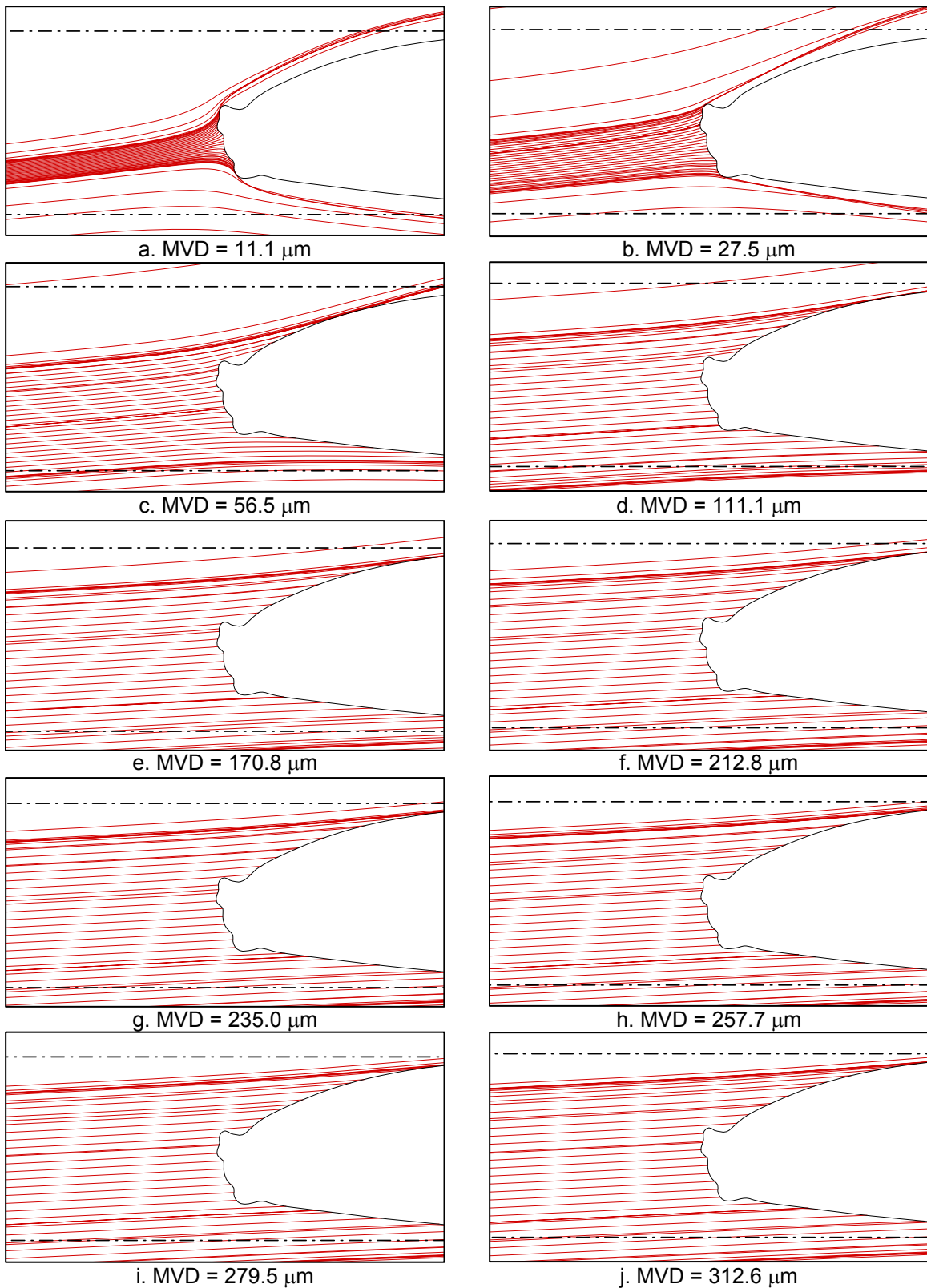


Figure D2.—Computed droplet trajectories with LEWICE code;  
NACA 23012 with 10-min glaze ice, 111  $\mu\text{m}$  spray cloud.

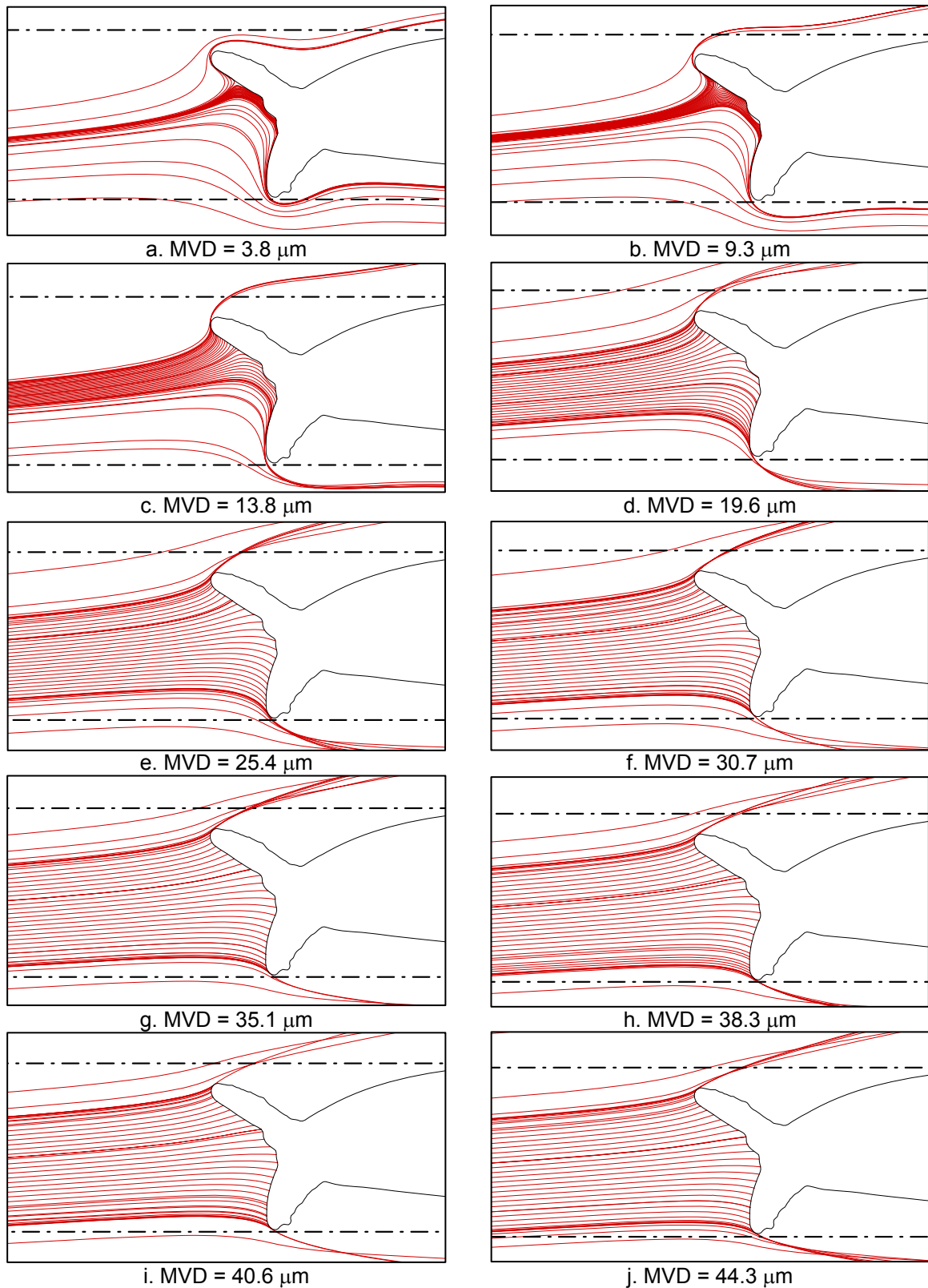


Figure D3.—Computed droplet trajectories with LEWICE code;  
NACA 23012 with 45-min glaze ice, 20  $\mu\text{m}$  spray cloud.

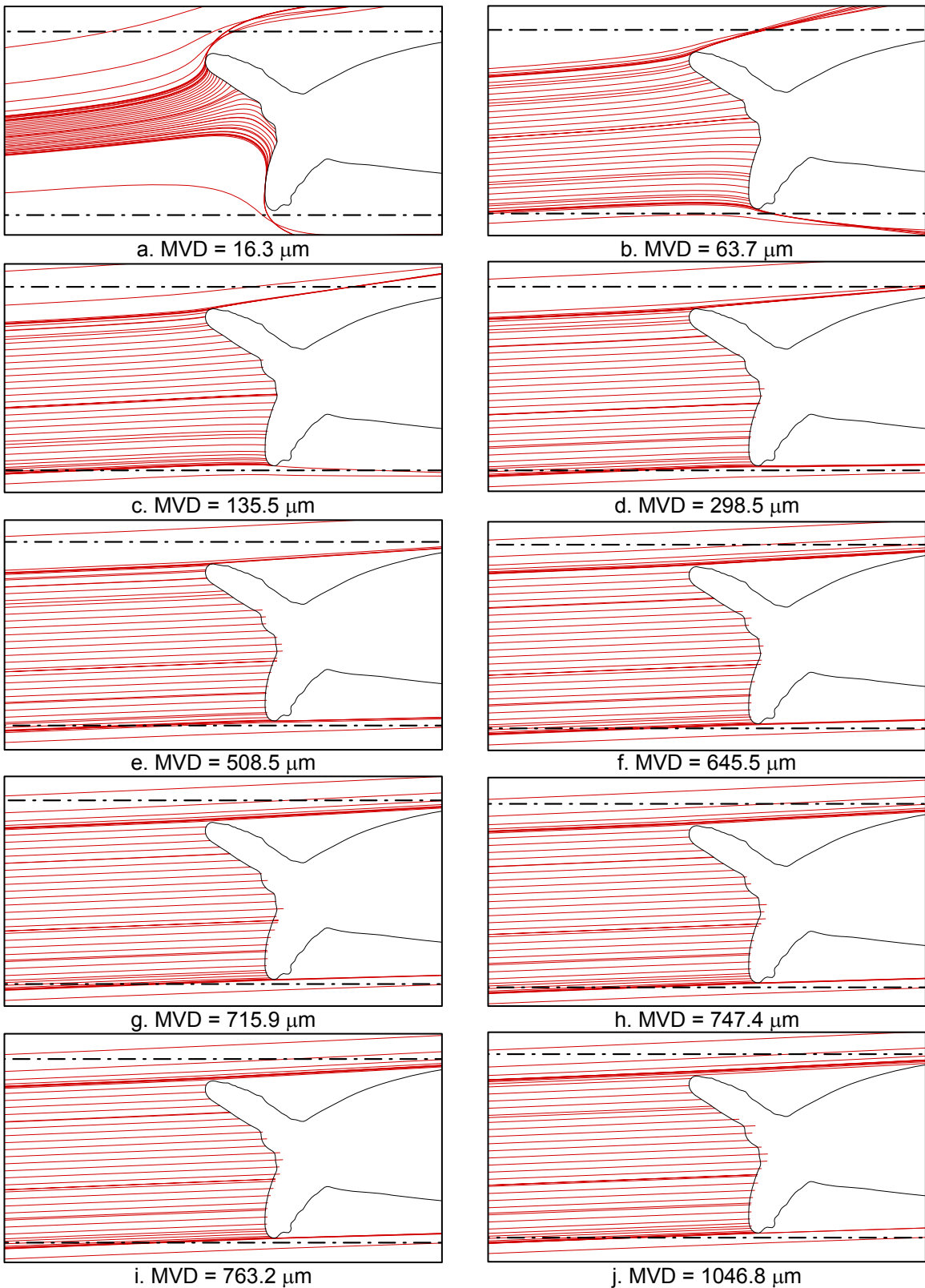


Figure D4.—Computed droplet trajectories with LEWICE code;  
NACA 23012 with 45-min glaze ice, 236  $\mu\text{m}$  spray cloud.

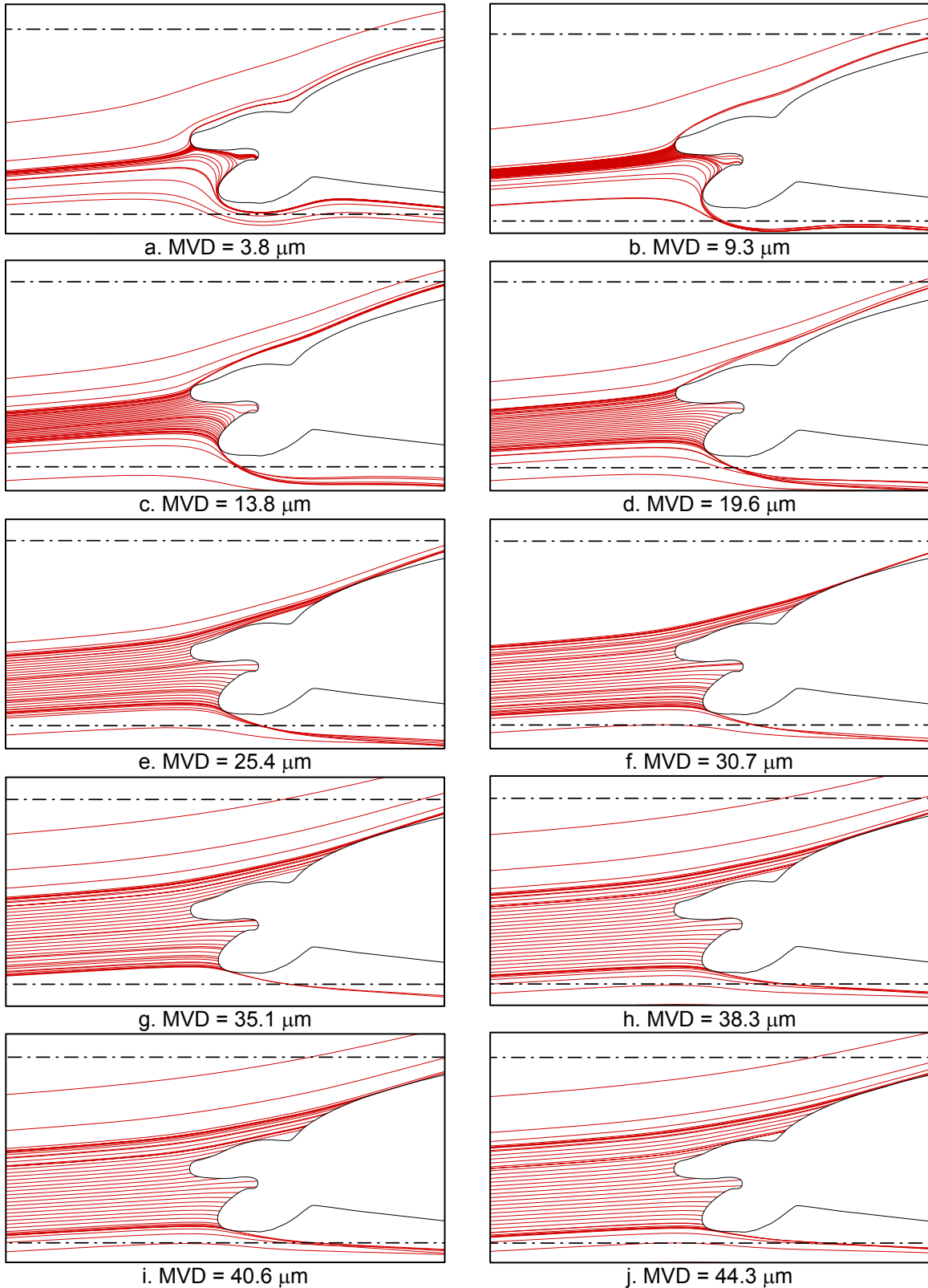


Figure D5.—Computed droplet trajectories with LEWICE code;  
NACA 23012 with 45-min mixed ice, 20  $\mu\text{m}$  spray cloud.

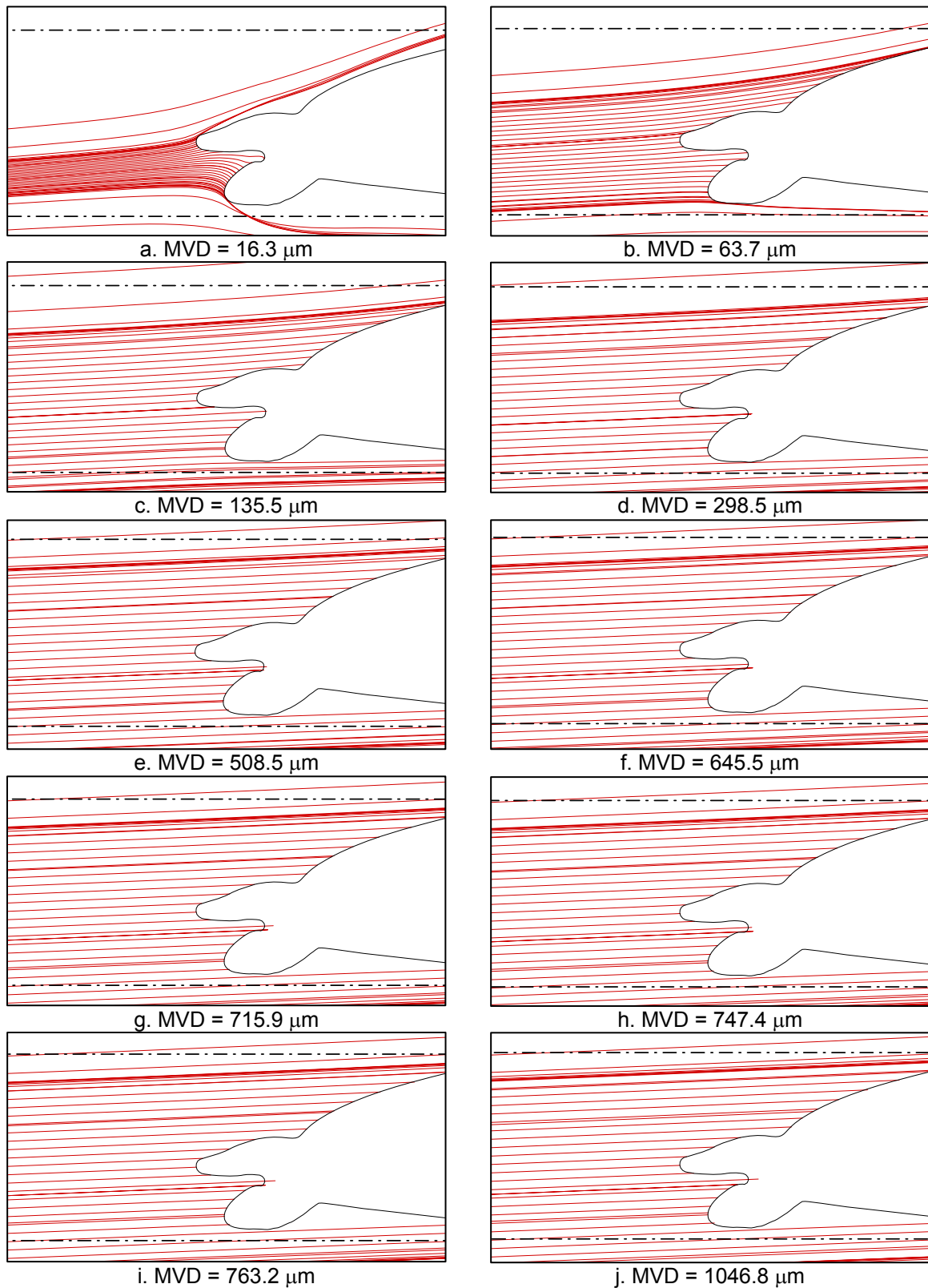


Figure D6.—Computed droplet trajectories with LEWICE code;  
NACA 23012 with 45-min mixed ice, 236  $\mu\text{m}$  spray cloud.

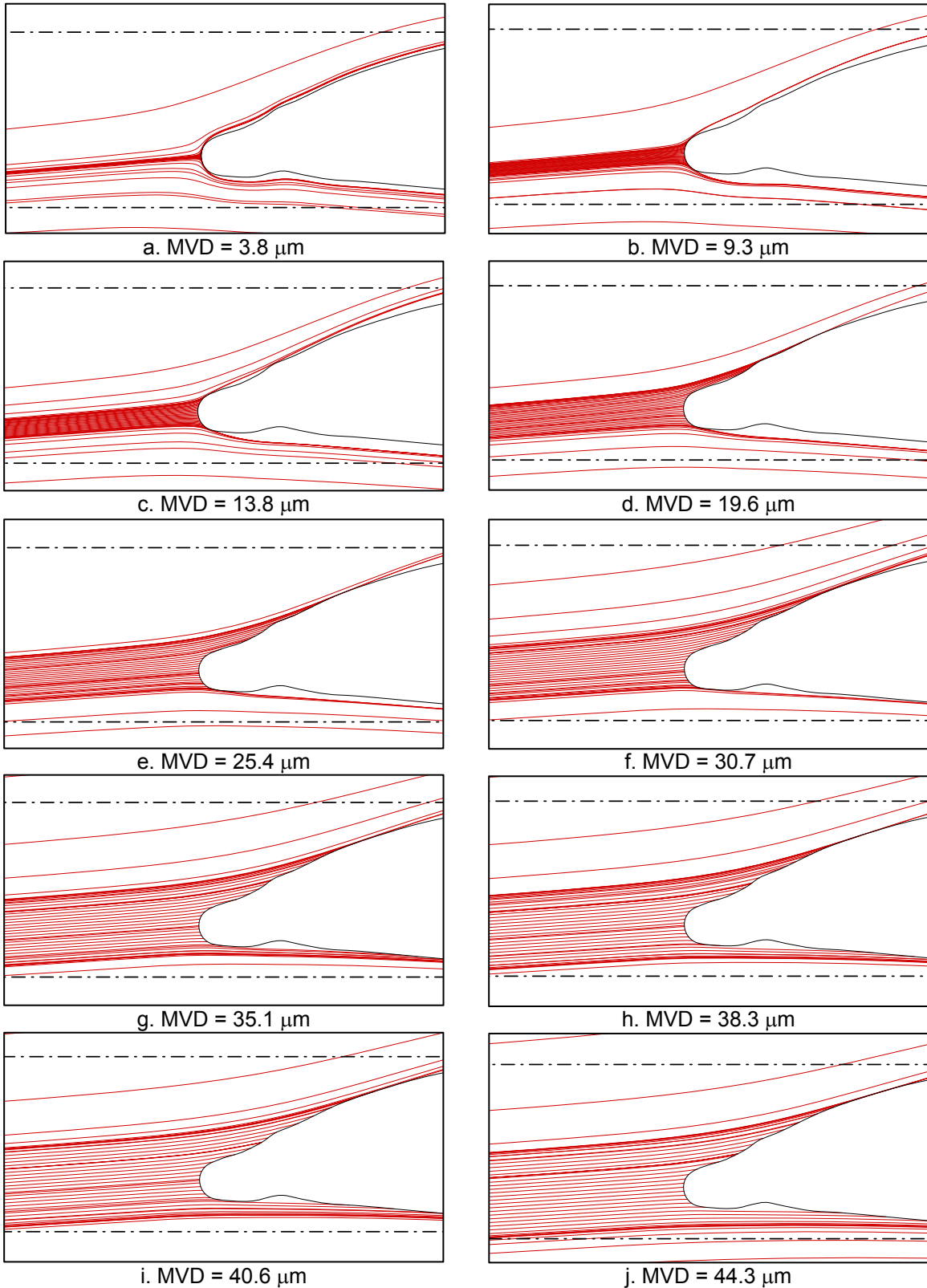


Figure D7.—Computed droplet trajectories with LEWICE code;  
NACA 23012 with 45-min rime ice, 20  $\mu\text{m}$  spray cloud.

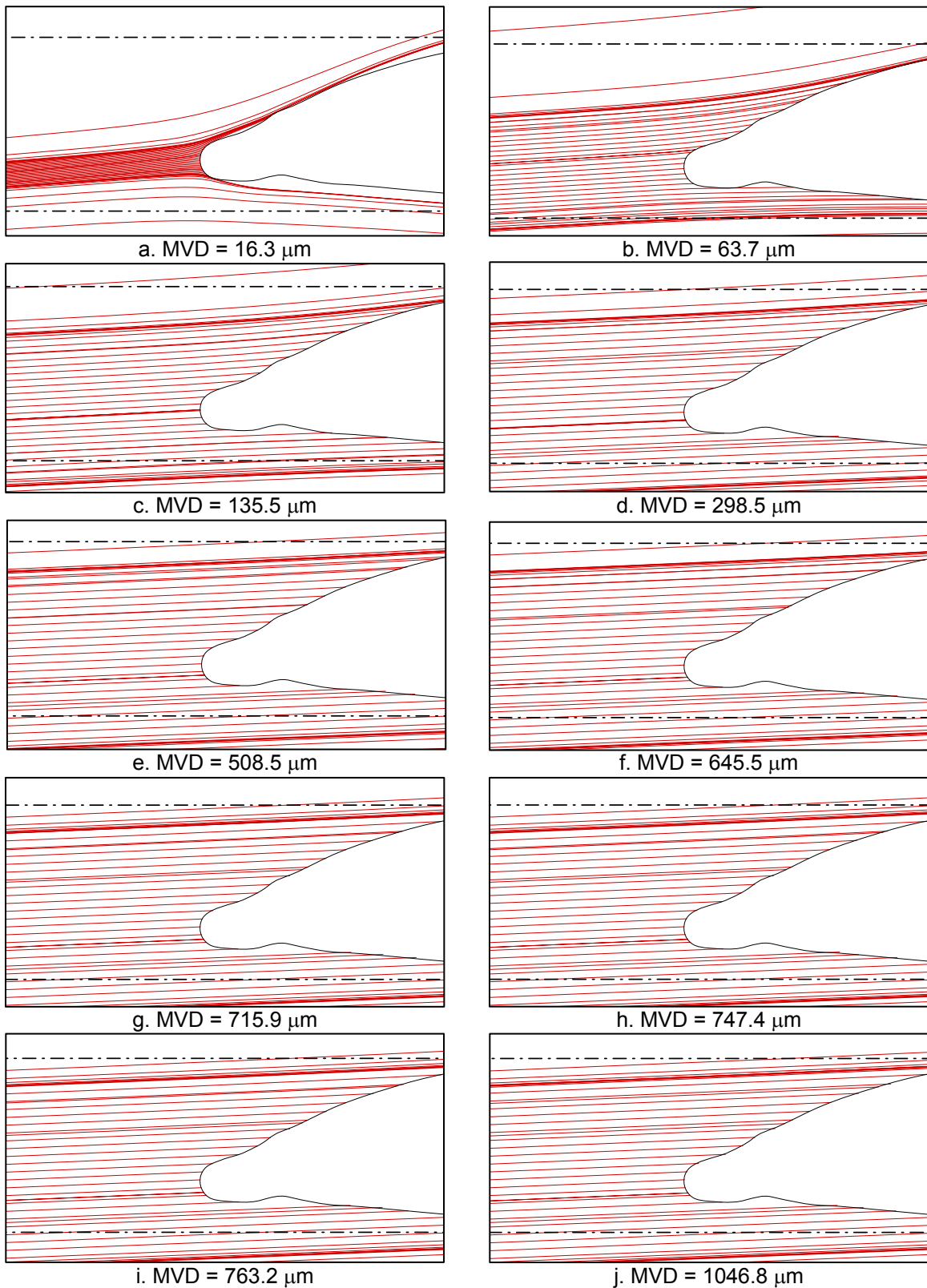


Figure D8.—Computed droplet trajectories with LEWICE code;  
NACA 23012 with 45-min rime ice, 236  $\mu\text{m}$  spray cloud.



## Appendix E—Analysis Impingement Data Computed with a Modified LEWICE Code Using the Monte-Carlo Method

Computations of collection efficiency were conducted with a modified LEWICE program capable of performing droplet trajectory analysis using the Monte-Carlo method. The Monte-Carlo method was developed to allow the incorporation of more sophisticated droplet splashing and droplet breakup models. The method also overcomes some of interpolation difficulties found in the public version of the LEWICE code which affect the computation of collection efficiency in shadow impingement regions downstream of ice shapes with large horns.

The Monte-Carlo collection efficiency method involves the tracking of individual particles to and about a body. The method has the capability to recursively track the resulting particles from a droplet breakup (due to excessive acceleration or deceleration) or splash (due to impact with the surface). The method stores the amount of mass collected at each surface panel from the impacting droplets. From this mass the local collection efficiency is calculated. The following equations are used to calculate the collection efficiency at each panel due to a droplet distribution which can breakup due to splashing or excessive acceleration.

$$\tilde{\beta}_m = 1 / \omega_\tau \sum_{i=1}^{ndis} \beta_{im} \Delta \omega_i \quad (E-1)$$

$$\beta_{im} = D_i^3 A_i / (N_i A_m) \sum_{j=1}^{nimp_{im}} d_{imj}^{-3} \quad (E-2)$$

where,

|                   |   |  |
|-------------------|---|--|
| $\beta_m$         | = | collection efficiency at panel m   |
| $\omega_\tau$     | = | total normalized liquid water content  |
| $\Delta \omega_i$ | = | fraction of total liquid contained in droplet i in distribution              |
| $\beta_{im}$      | = | collection efficiency at panel m due to droplet i in distribution            |
| $A_i$             | = | Free-stream release area of impacting particles of droplet i in distribution |
| $A_m$             | = | Area of panel m  |
| $D_i$             | = | Diameter of droplet i in distribution  |
| $d_{imj}$         | = | Diameter of droplet j impacting panel m from droplet i in distribution       |
| $ndis$            | = | number of droplets defining distribution                                     |
| $nimp_{im}$       | = | number of particles impacting panel m from droplet i in distribution         |
| $N_i$             | = | number of particles released from free-stream for particle size i            |

In the Monte-Carlo collection efficiency method the impact droplets are totaled to compute the correct collection efficiency at the surface. The term “Monte-Carlo” does not necessarily suggest randomization employed in release of particles from a distribution. For the computations presented in this appendix, an evenly distributed set of particles for each of the 27 bins (on the order of a thousand) were released from the freestream position. The number of particles which hit each surface panel along with the panel area was used to calculate the collection efficiency. Figures E1 through E50 compare experimental impingement data for the 10 ice shapes and the five MVDs tested with LEWICE data obtained with the standard version of the LEWICE 1.6 code (in-house 27-bin) and the LEWICE Monte-Carlo version. Consider, for example the figures E7, E12, E17, E18, E43, etc., the artificial impingement tails produced by the interpolation method in the standard LEWICE version are absent in the results obtained with the Monte-Carlo version of LEWICE. Note that no attempt was made to model droplet splashing

and breakup with the LEWICE Monte-Carlo version. In Figs E53 to E60, the total impingement efficiency distributions obtained with the two LEWICE methods for a given geometry are compared to the experimental data as a function of MVD size. Figures E61 and E62 summarize the total impingement efficiency distributions as function of geometry and MVD size from the experimental and LEWICE Monte-Carlo results respectively. The percentage differences in total impingement efficiency between LEWICE 1.6 and experimental data for all geometries and MVDs are presented in figure E63, whereas the percentage differences in total impingement efficiency between LEWICE Monte-Carlo and experimental data are presented in figure E64.

TABLE E1.—SUMMARY OF IMPINGEMENT EFFICIENCY DATA FOR 2003 IRT TESTS

| Model   | Test Conditions |     | $\bar{E}_L$ | $\bar{E}_E$ | $\bar{E}_{LMC}$ | $(\bar{E}_L - \bar{E}_E) / \bar{E}_E (\%)$ | $(\bar{E}_{LMC} - \bar{E}_E) / \bar{E}_E (\%)$ | $(\bar{E}_L - \bar{E}_E) / \bar{E}_{LMC} (\%)$ | $(\bar{E}_{LMC} - \bar{E}_E) / \bar{E}_{LMC} (\%)$ |
|---|-----------------|-----|-------------|-------------|-----------------|--|--|--|--|
|   | AOA             | MVD |             |             |                 |  |  |  |  |
| NACA 23012<br>with 5-min<br>Glaze ice<br>shape    | 2.5             | 20  | 0.1788      | 0.1805      | 0.1714          | -0.9                                       | -5.0   | -1.0   | -5.3   |
|   |                 | 52  | 0.5236      | 0.2823      | 0.5061          | 85.5                                       | 79.3   | 47.7   | 44.2   |
|   |                 | 111 | 0.6928      | 0.3961      | 0.6719          | 74.9                                       | 69.6   | 44.2   | 41.0   |
|   |                 | 154 | 0.7830      | 0.4963      | 0.7619          | 57.8                                       | 53.5   | 37.6   | 34.9   |
|   |                 | 236 | 0.8590      | 0.5228      | 0.8369          | 64.3                                       | 60.1   | 40.2   | 37.5   |
| NACA 23012<br>with 10-min<br>Glaze ice<br>shape   | 2.5             | 20  | 0.1902      | 0.1713      | 0.1859          | 11.0                                       | 8.5  | 10.2   | 7.9  |
|   |                 | 52  | 0.5539      | 0.2366      | 0.5066          | 134.1                                      | 114.1  | 62.6   | 53.3   |
|   |                 | 111 | 0.7400      | 0.3251      | 0.6708          | 127.6                                      | 106.3  | 61.9   | 51.5   |
|   |                 | 154 | 0.8320      | 0.4103      | 0.7597          | 102.8                                      | 85.2   | 55.5   | 46.0   |
|   |                 | 236 | 0.9168      | 0.4942      | 0.8372          | 85.5                                       | 69.4   | 50.5   | 41.0   |
| NACA 23012<br>with 15-min<br>Glaze ice<br>shape   | 2.5             | 20  | 0.2124      | 0.1862      | 0.2104          | 14.1                                       | 13.0   | 12.5   | 11.5   |
|   |                 | 52  | 0.6223      | 0.2857      | 0.5146          | 117.8                                      | 80.1   | 65.4   | 44.5   |
|   |                 | 111 | 0.8198      | 0.3423      | 0.6713          | 139.5                                      | 96.1   | 71.1   | 49.0   |
|   |                 | 154 | 0.9269      | 0.4351      | 0.7607          | 113.0                                      | 74.8   | 64.7   | 42.8   |
|   |                 | 236 | 1.0177      | 0.5277      | 0.8372          | 92.9                                       | 58.7   | 58.5   | 37.0   |
| NACA 23012<br>with 22.5-min<br>Glaze ice<br>shape | 2.5             | 20  | 0.2515      | 0.2319      | 0.2501          | 8.5  | 7.9  | 7.8  | 7.3  |
|   |                 | 52  | 0.7069      | 0.3236      | 0.4977          | 118.4                                      | 53.8   | 77.0   | 35.0   |
|   |                 | 111 | 0.9212      | 0.4015      | 0.6615          | 129.4                                      | 64.8   | 78.6   | 39.3   |
|   |                 | 154 | 1.0874      | 0.4436      | 0.7493          | 145.1                                      | 68.9   | 85.9   | 40.8   |
|   |                 | 236 | 1.1840      | 0.4988      | 0.8291          | 137.4                                      | 66.2   | 82.6   | 39.8   |
| NACA 23012<br>with 45-min<br>Glaze ice<br>shape   | 2.5             | 20  | 0.3227      | 0.2705      | 0.3077          | 19.3                                       | 13.7   | 17.0   | 12.1   |
|   |                 | 52  | 0.6360      | 0.4360      | 0.6356          | 45.9                                       | 45.8   | 31.5   | 31.4   |
|   |                 | 111 | 0.7586      | 0.5239      | 0.7605          | 44.8                                       | 45.2   | 30.9   | 31.1   |
|   |                 | 154 | 0.8097      | 0.6072      | 0.8122          | 33.3                                       | 33.8   | 24.9   | 25.2   |
|   |                 | 236 | 0.8455      | 0.6362      | 0.8469          | 32.9                                       | 33.1   | 24.7   | 24.9   |
| NACA 23012<br>with 7.5-min<br>Mixed ice<br>shape  | 2.5             | 20  | 0.1896      | 0.1377      | 0.1688          | 37.7                                       | 22.6   | 30.7   | 18.4   |
|   |                 | 52  | 0.5434      | 0.2411      | 0.5063          | 125.4                                      | 110.0  | 59.7   | 52.4   |
|   |                 | 111 | 0.7108      | 0.3496      | 0.6737          | 103.3                                      | 92.7   | 53.6   | 48.1   |
|   |                 | 154 | 0.8006      | 0.4600      | 0.7627          | 74.0                                       | 65.8   | 44.7   | 39.7   |
|   |                 | 236 | 0.8751      | 0.4754      | 0.8368          | 84.1                                       | 76.0   | 47.8   | 43.2   |
| NACA 23012<br>with 15-min<br>Mixed ice<br>shape   | 2.5             | 20  | 0.1921      | 0.1563      | 0.1700          | 22.9                                       | 8.8  | 21.1   | 8.1  |
|   |                 | 52  | 0.5942      | 0.2963      | 0.5059          | 100.5                                      | 70.7   | 58.9   | 41.4   |
|   |                 | 111 | 0.7789      | 0.3854      | 0.6738          | 102.1                                      | 74.8   | 58.4   | 42.8   |
|   |                 | 154 | 0.8683      | 0.5024      | 0.7619          | 72.8                                       | 51.7   | 48.0   | 34.1   |
|   |                 | 236 | 0.9501      | 0.5040      | 0.8379          | 88.5                                       | 66.2   | 53.2   | 39.8   |
| NACA 23012<br>with 22.5-min<br>Mixed ice<br>shape | 2.5             | 20  | 0.1809      | 0.1579      | 0.1603          | 14.6                                       | 1.5  | 14.3   | 1.5  |
|   |                 | 52  | 0.6021      | 0.2602      | 0.5021          | 131.4                                      | 93.0   | 68.1   | 48.2   |
|   |                 | 111 | 0.7939      | 0.3566      | 0.6701          | 122.6                                      | 87.9   | 65.3   | 46.8   |
|   |                 | 154 | 0.8892      | 0.4718      | 0.7612          | 88.5                                       | 61.3   | 54.8   | 38.0   |
|   |                 | 236 | 0.9671      | 0.5140      | 0.8374          | 88.2                                       | 62.9   | 54.1   | 38.6   |
| NACA 23012<br>with 45-min<br>Mixed ice<br>shape   | 2.5             | 20  | 0.1690      | 0.1713      | 0.1564          | -1.3                                       | -8.7   | -1.5   | -9.5   |
|   |                 | 52  | 0.5424      | 0.2874      | 0.4903          | 88.7                                       | 70.6   | 52.0   | 41.4   |
|   |                 | 111 | 0.8819      | 0.3731      | 0.6548          | 136.4                                      | 75.5   | 77.7   | 43.0   |
|   |                 | 154 | 1.0041      | 0.4737      | 0.7494          | 112.0                                      | 58.2   | 70.8   | 36.8   |
|   |                 | 236 | 1.0808      | 0.5208      | 0.8299          | 107.5                                      | 59.3   | 67.5   | 37.2   |
| NACA 23012<br>with 45-min<br>Rime ice<br>shape    | 2.5             | 20  | 0.1855      | 0.1253      | 0.1541          | 48.0                                       | 23.0   | 39.1   | 18.7   |
|   |                 | 52  | 0.5424      | 0.2683      | 0.5013          | 102.2                                      | 86.9   | 54.7   | 46.5   |
|   |                 | 111 | 0.7135      | 0.3697      | 0.6726          | 93.0                                       | 81.9   | 51.1   | 45.0   |
|   |                 | 154 | 0.8041      | 0.4491      | 0.7616          | 79.0                                       | 69.6   | 46.6   | 41.1   |
|   |                 | 236 | 0.8772      | 0.5670      | 0.8355          | 54.7                                       | 47.4   | 37.1   | 32.1   |

$\bar{E}$  represents the total impingement efficiency, which is defined as  $\bar{E} = \frac{A_p}{A_f}$ , where  $A_f$  represents the projected frontal area of the airfoil.  $\bar{E}_E$  is the experimental total impingement efficiency.  $\bar{E}_L$  is computational total impingement efficiency using LEWICE 1.6. Note that few  $\bar{E}_L$  exceeded 1.0 due to presence of artificial impingement tails.  $\bar{E}_{LMC}$  is computational total impingement efficiency using LEWICE Monte-Carlo.

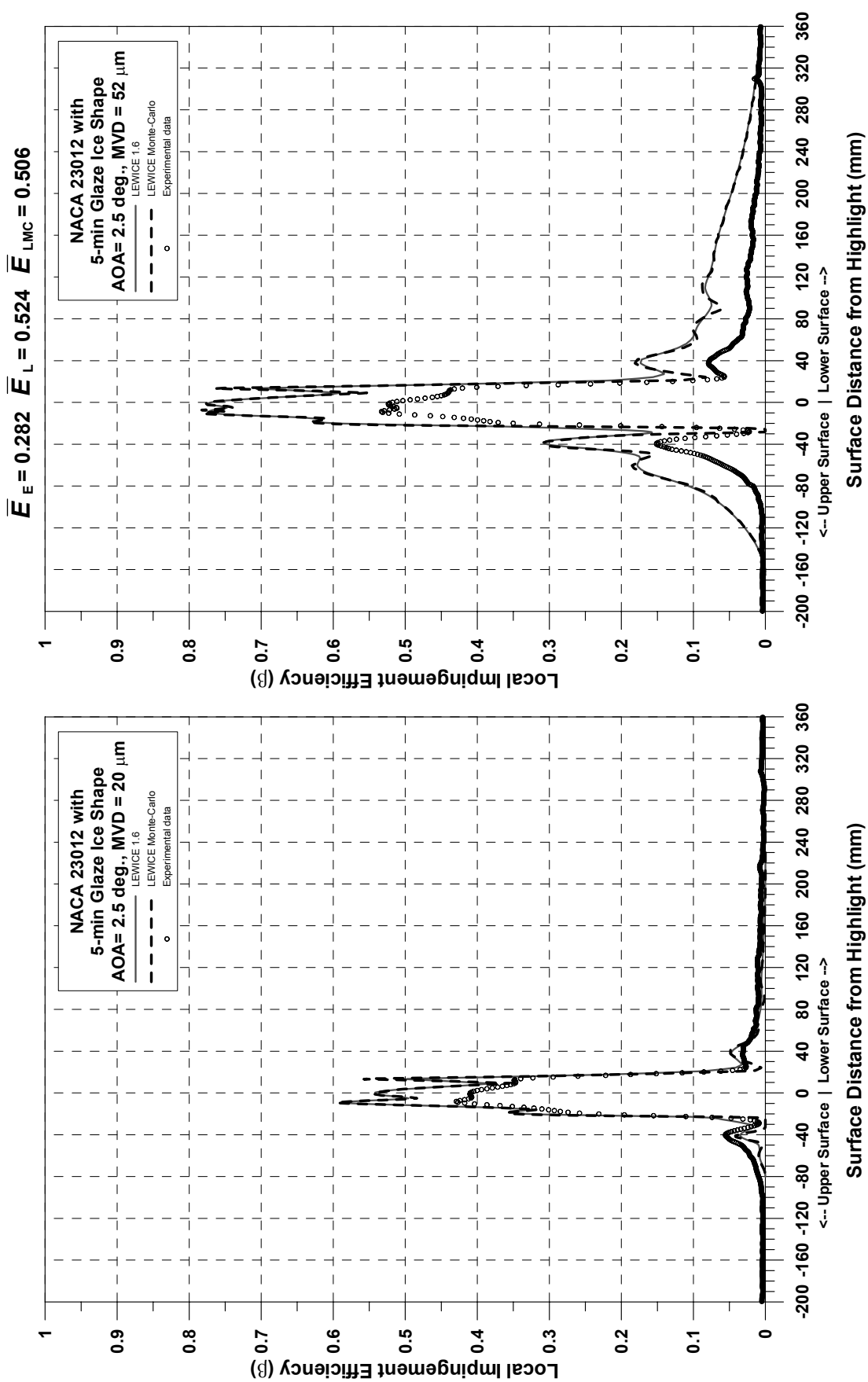
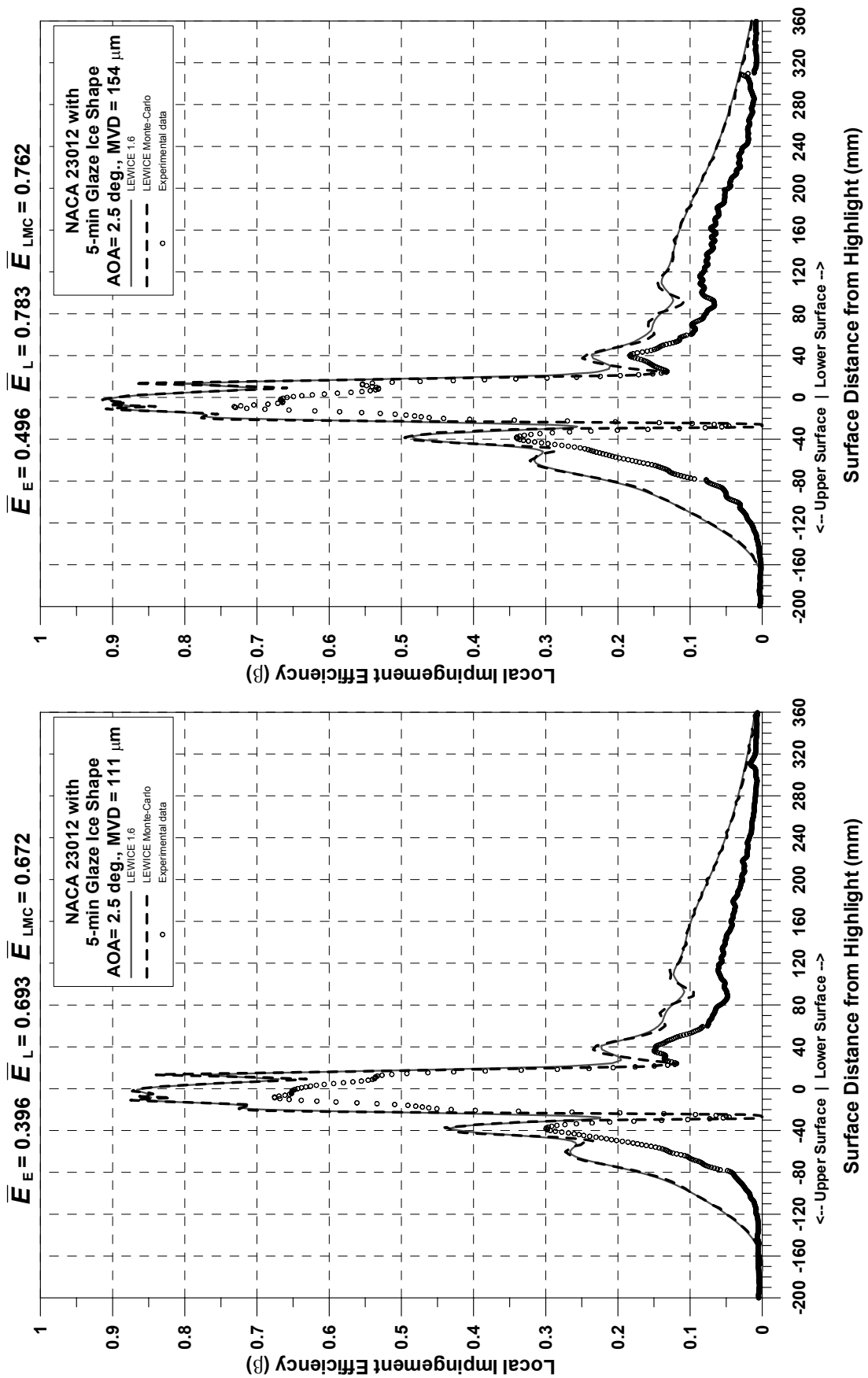


Figure E1.—Impingement efficiency distribution for NACA 23012 airfoil with 5-min glaze ice shape;  $c = 36\text{-in.}$ ,  $V_\infty = 175 \text{ mph}$ ,  $\text{AOA} = 2.5^\circ$ ,  $\text{MVD} = 20 \mu\text{m}$ .

Figure E2.—Impingement efficiency distribution for NACA 23012 airfoil with 5-min glaze ice shape;  $c = 36\text{-in.}$ ,  $V_\infty = 175 \text{ mph}$ ,  $\text{AOA} = 2.5^\circ$ ,  $\text{MVD} = 52 \mu\text{m}$ .



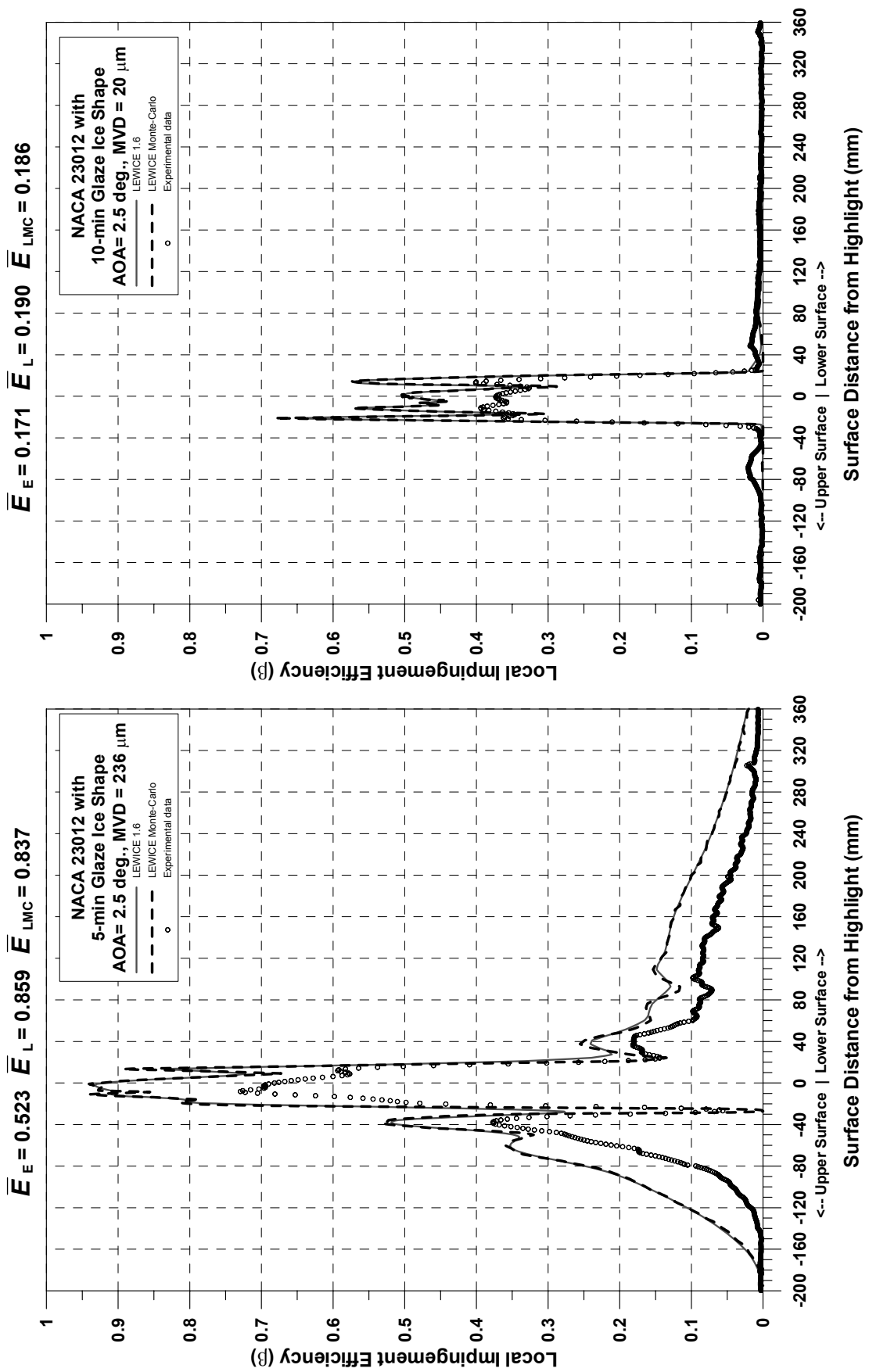


Figure E5.—Impingement efficiency distribution for NACA 23012 airfoil with 5-min glaze ice shape;  $c = 36\text{-in.}$ ,  $V_\infty = 175 \text{ mph}$ ,  $\text{AOA} = 2.5^\circ$ ,  $\text{MVD} = 236 \mu\text{m}$

Figure E6.—Impingement efficiency distribution for NACA 23012 airfoil with 10-min glaze ice shape;  $c = 36\text{-in.}$ ,  $V_\infty = 175 \text{ mph}$ ,  $\text{AOA} = 2.5^\circ$ ,  $\text{MVD} = 20 \mu\text{m}$ .

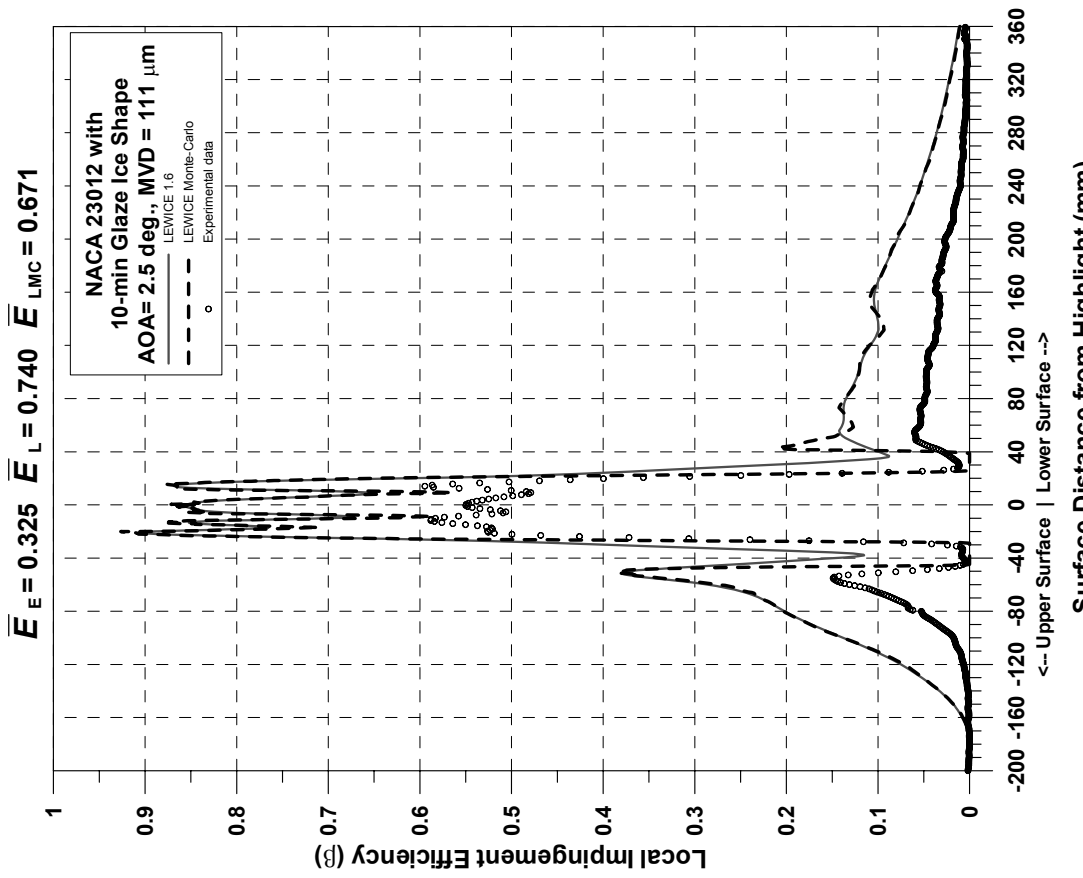
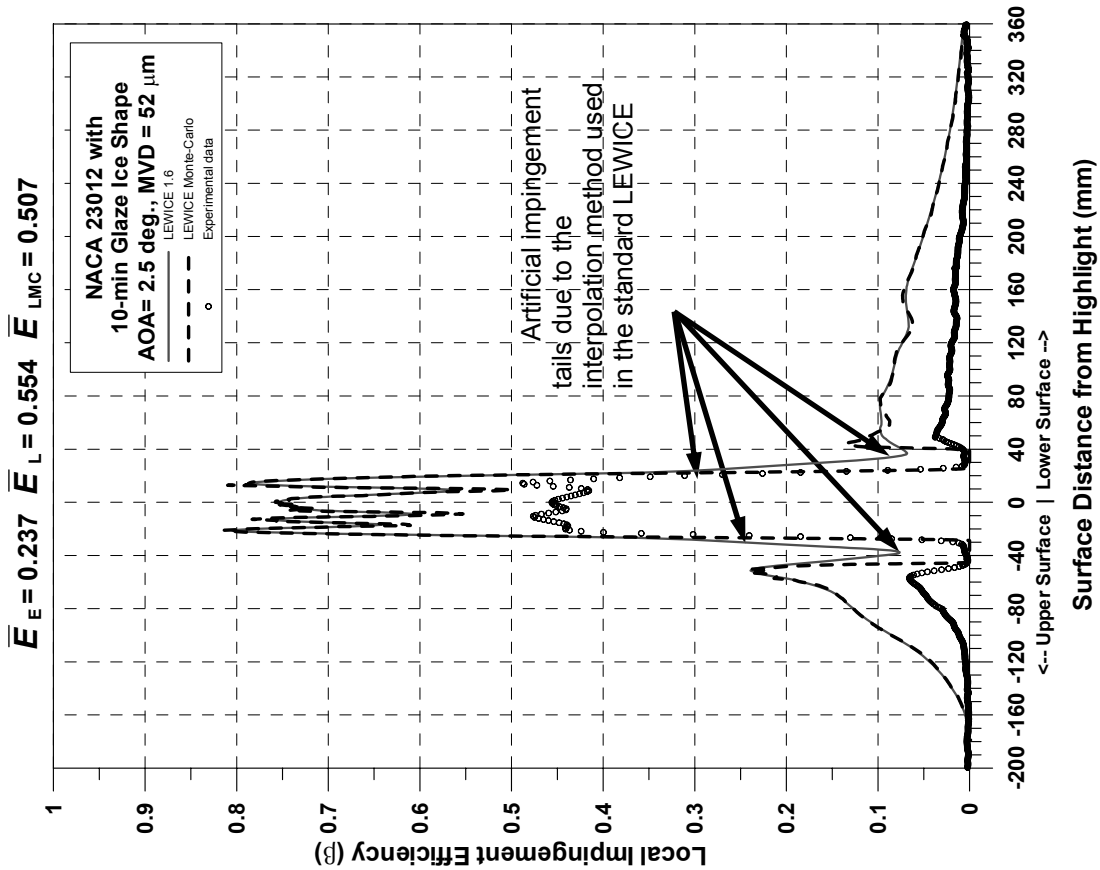


Figure E7.—Impingement efficiency distribution for NACA 23012 airfoil with 10-min glaze ice shape;  $c = 36\text{-in.}$ ,  $V_\infty = 175 \text{ mph}$ , AOA =  $2.5^\circ$ , MVD =  $52 \mu\text{m}$ .

Figure E8.—Impingement efficiency distribution for NACA 23012 airfoil with 10-min glaze ice shape;  $c = 36\text{-in.}$ ,  $V_\infty = 175 \text{ mph}$ , AOA =  $2.5^\circ$ , MVD =  $111 \mu\text{m}$ .

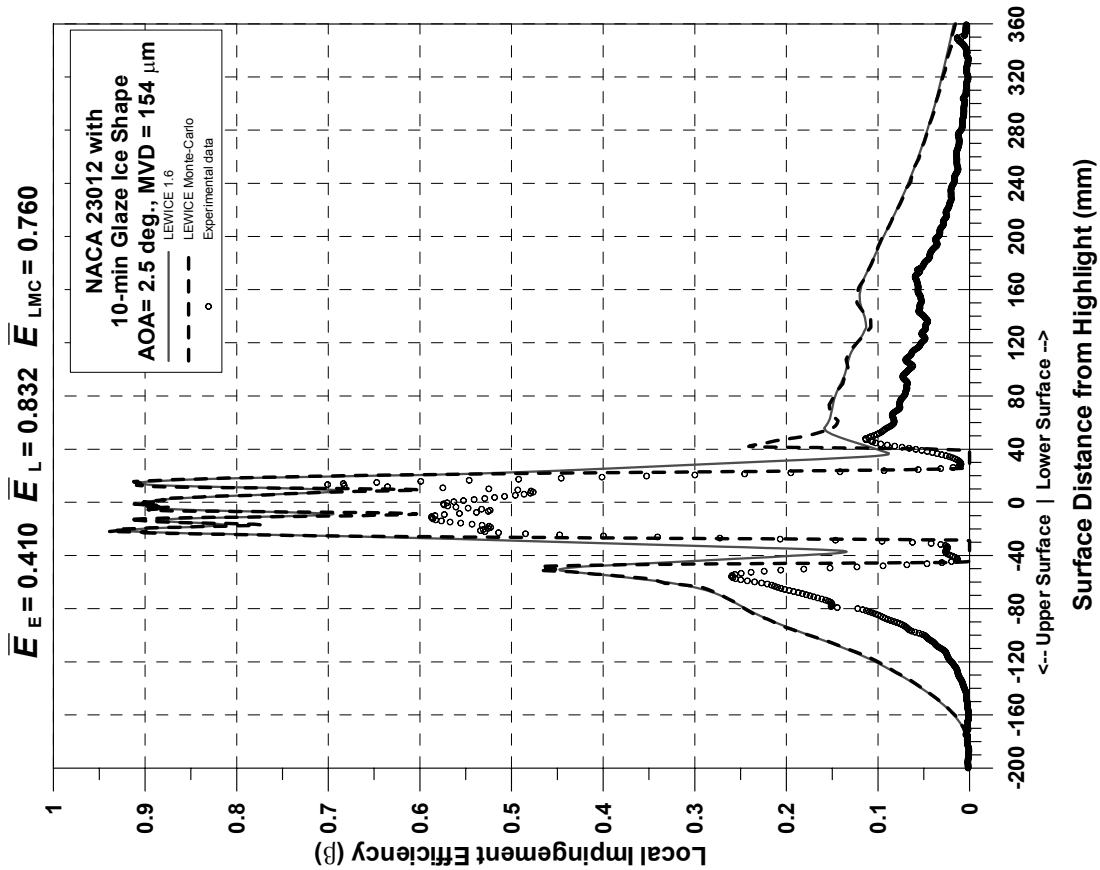


Figure E9.—Impingement efficiency distribution for NACA 23012 airfoil with 10-min glaze ice shape;  $c = 36\text{-in.}$ ,  $V_\infty = 175 \text{ mph}$ ,  $\text{AOA} = 2.5^\circ$ ,  $\text{MVD} = 154 \mu\text{m}$ .

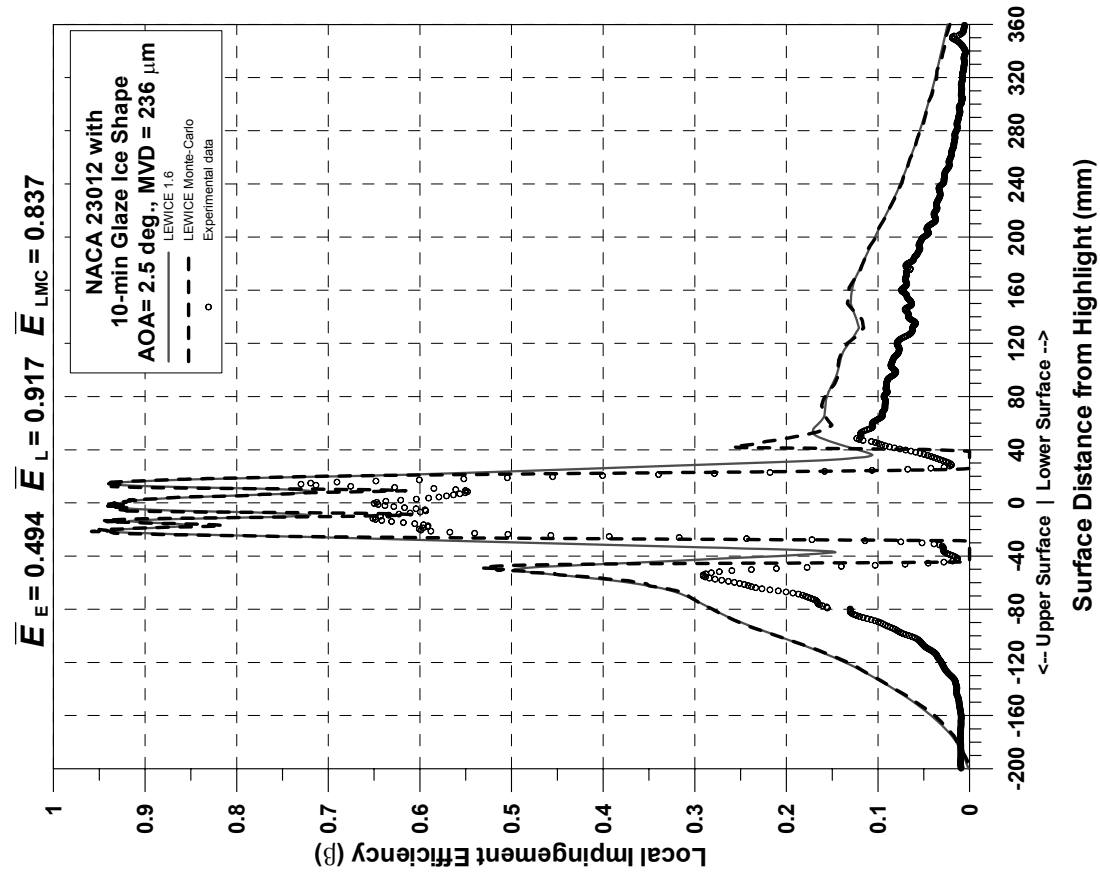


Figure E10.—Impingement efficiency distribution for NACA 23012 airfoil with 10-min glaze ice shape;  $c = 36\text{-in.}$ ,  $V_\infty = 175 \text{ mph}$ ,  $\text{AOA} = 2.5^\circ$ ,  $\text{MVD} = 236 \mu\text{m}$ .

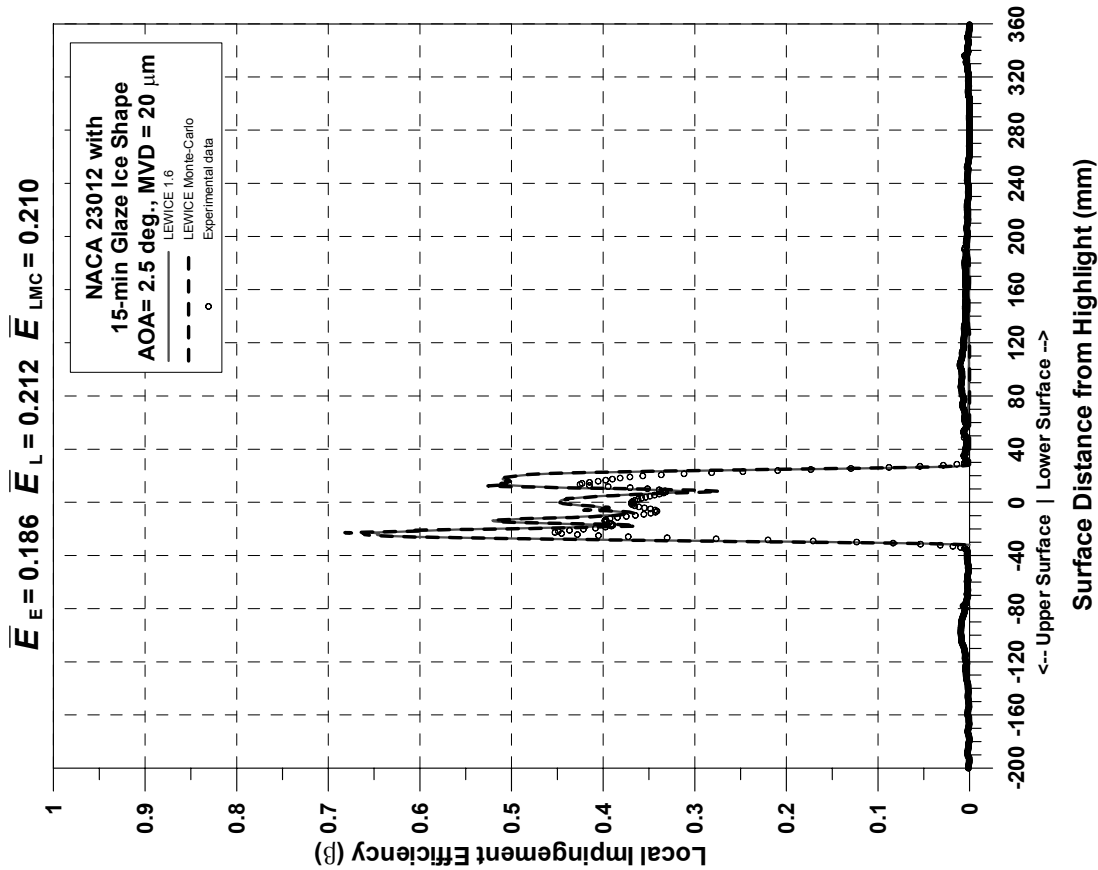


Figure E11.—Impingement efficiency distribution for NACA 23012 airfoil with 15-min glaze ice shape;  $c = 36\text{-in.}$ ,  $V_\infty = 175 \text{ mph}$ ,  $\text{AOA} = 2.5^\circ$ ,  $\text{MVD} = 20 \mu\text{m}$ .

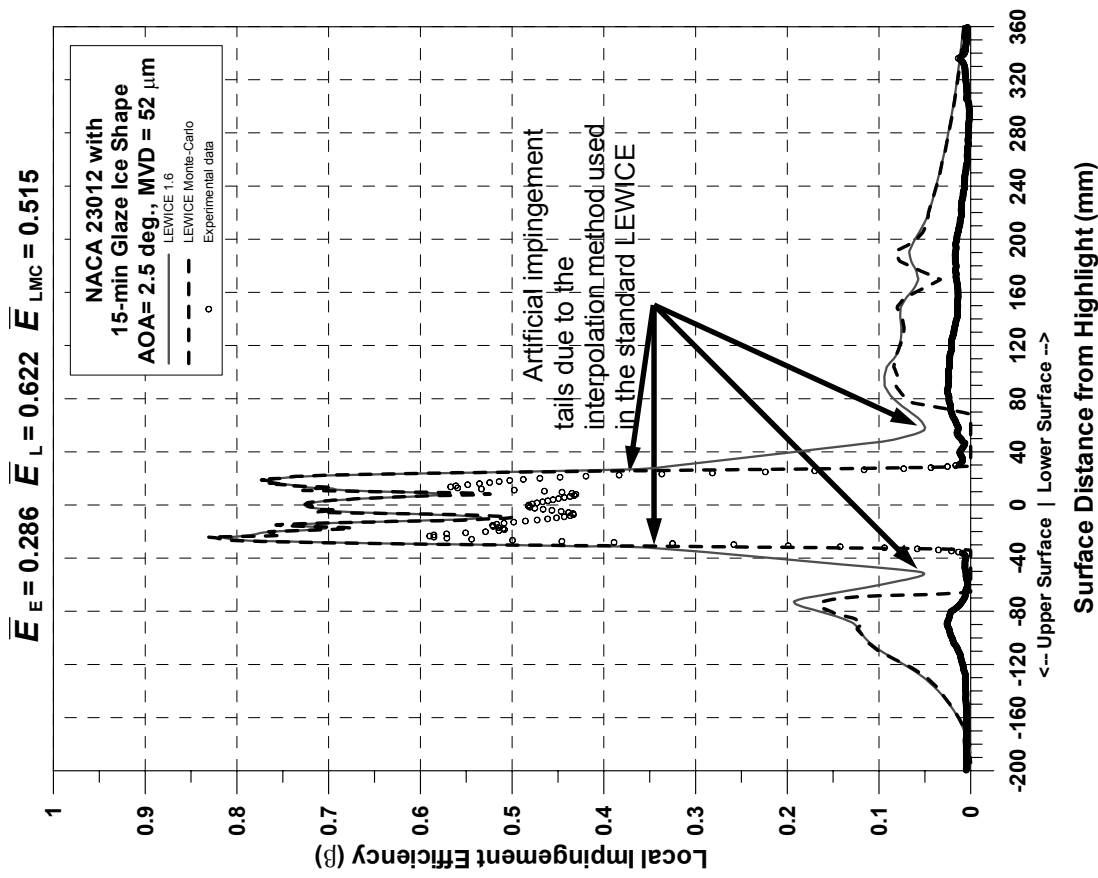


Figure E12.—Impingement efficiency distribution for NACA 23012 airfoil with 15-min glaze ice shape;  $c = 36\text{-in.}$ ,  $V_\infty = 175 \text{ mph}$ ,  $\text{AOA} = 2.5^\circ$ ,  $\text{MVD} = 52 \mu\text{m}$ .

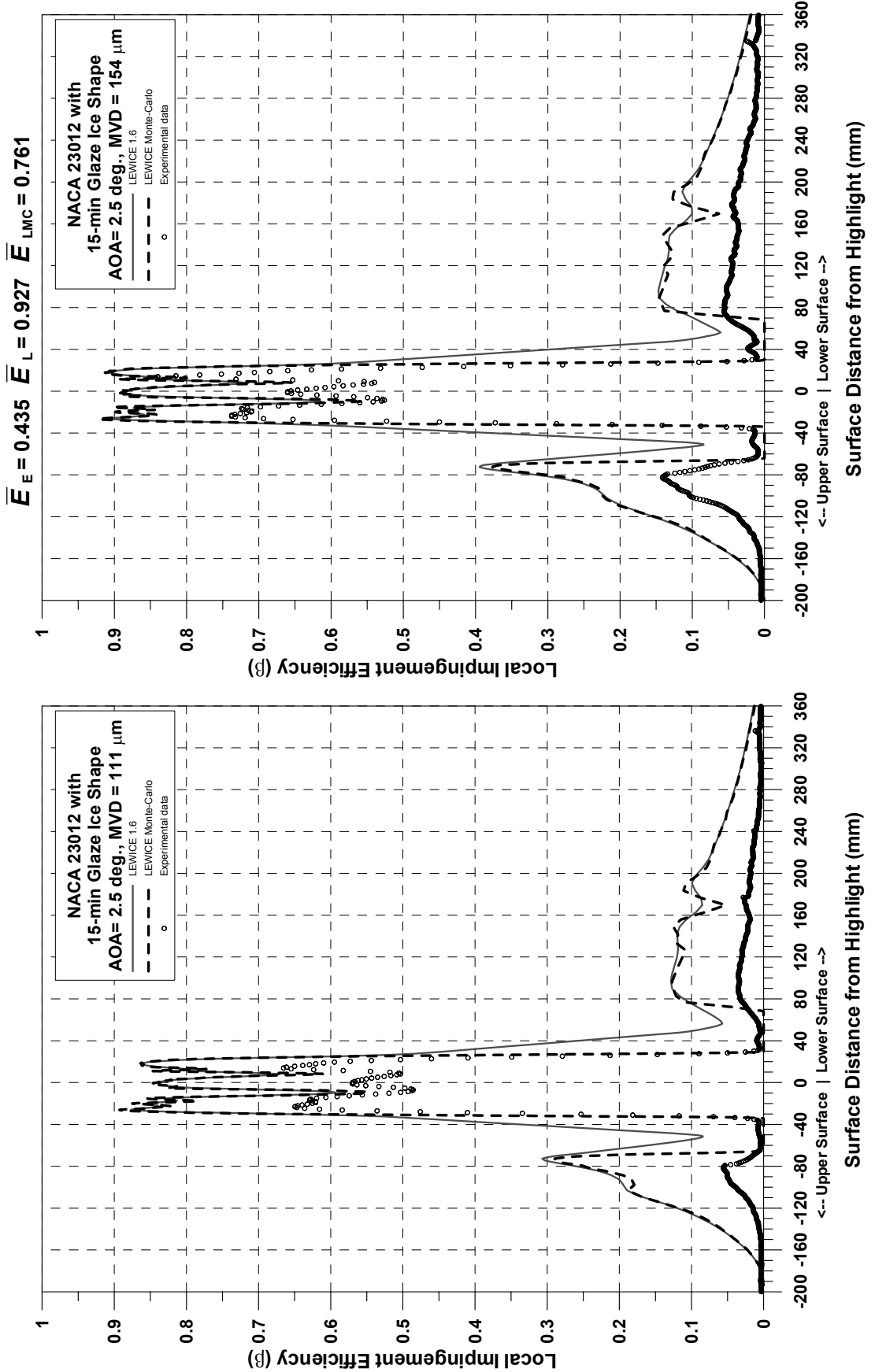


Figure E13.—Impingement efficiency distribution for NACA 23012 airfoil with 15-min glaze ice shape;  $c = 36\text{-in.}$ ,  $V_\infty = 175 \text{ mph}$ ,  $\text{AOA} = 2.5^\circ$ ,  $MVD = 111 \mu\text{m}$ .

Figure E14.—Impingement efficiency distribution for NACA 23012 airfoil with 15-min glaze ice shape;  $c = 36\text{-in.}$ ,  $V_\infty = 175 \text{ mph}$ ,  $\text{AOA} = 2.5^\circ$ ,  $MVD = 154 \mu\text{m}$ .

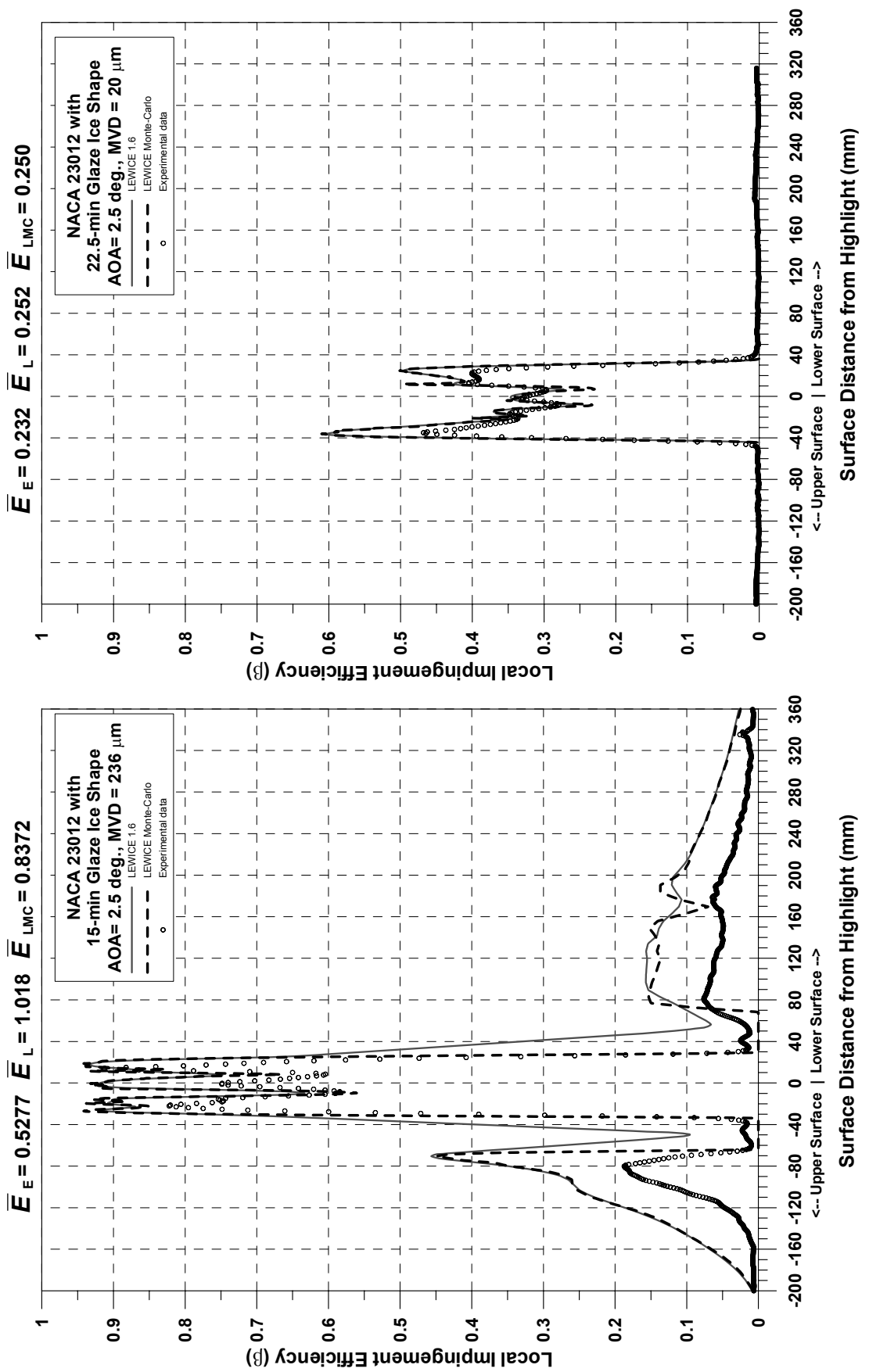


Figure E15.—Impingement efficiency distribution for NACA 23012 airfoil with 15-min glaze ice shape;  $c = 36\text{-in.}$ ,  $V_\infty = 175 \text{ mph}$ ,  $\text{AOA} = 2.5^\circ$ ,  $\text{MVD} = 236 \mu\text{m}$ .

Figure E16.—Impingement efficiency distribution for NACA 23012 airfoil with 22.5-min glaze ice shape;  $c = 36\text{-in.}$ ,  $V_\infty = 175 \text{ mph}$ ,  $\text{AOA} = 2.5^\circ$ ,  $\text{MVD} = 20 \mu\text{m}$ .

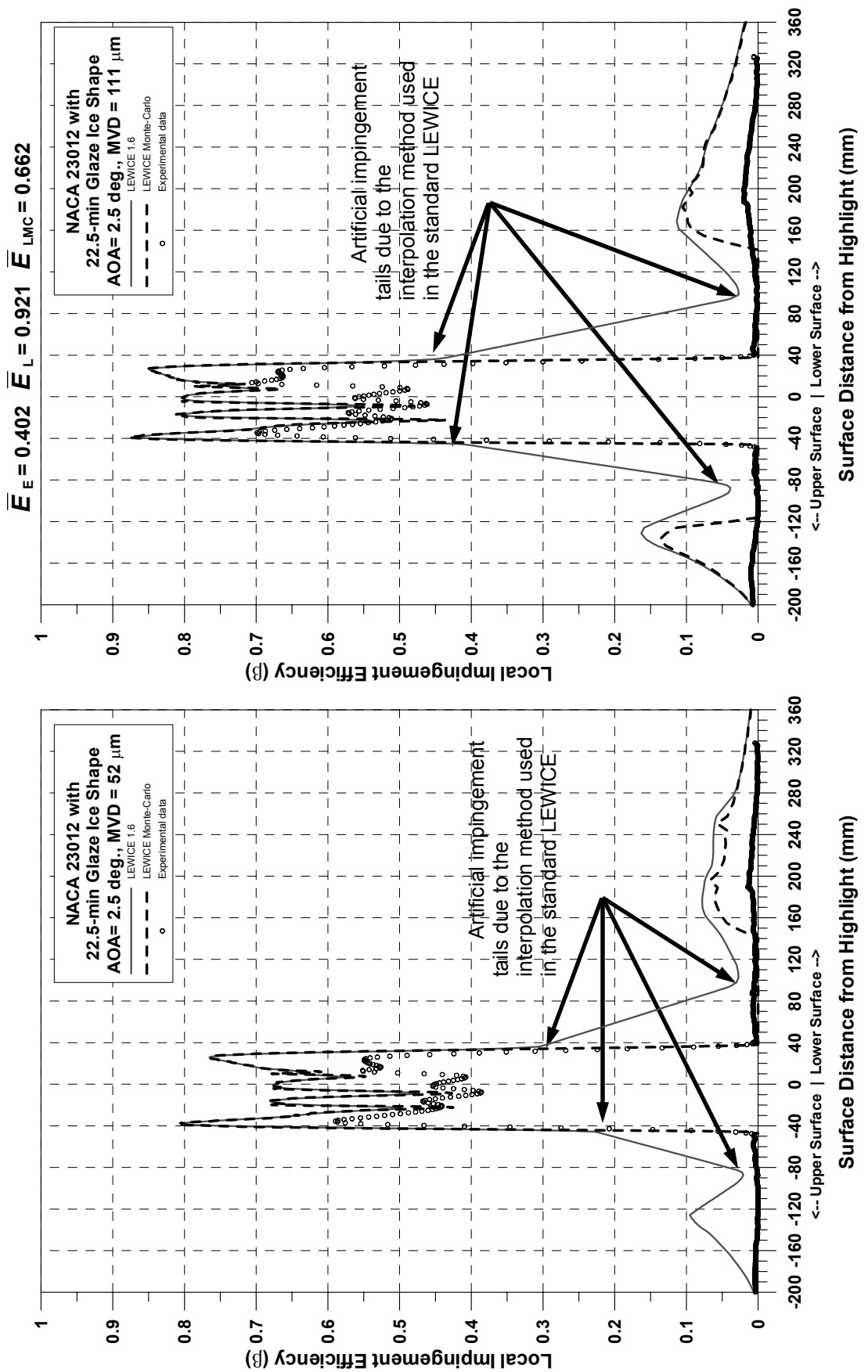


Figure E17.—Impingement efficiency distribution for NACA 23012 airfoil with 22.5-min glaze ice shape;  $c = 36\text{-in.}$ ,  $V_\infty = 175 \text{ mph}$ ,  $\text{AOA} = 2.5^\circ$ ,  $\text{MVD} = 52 \mu\text{m}$ .

Figure E18.—Impingement efficiency distribution for NACA 23012 airfoil with 22.5-min glaze ice shape;  $c = 36\text{-in.}$ ,  $V_\infty = 175 \text{ mph}$ ,  $\text{AOA} = 2.5^\circ$ ,  $\text{MVD} = 111 \mu\text{m}$ .

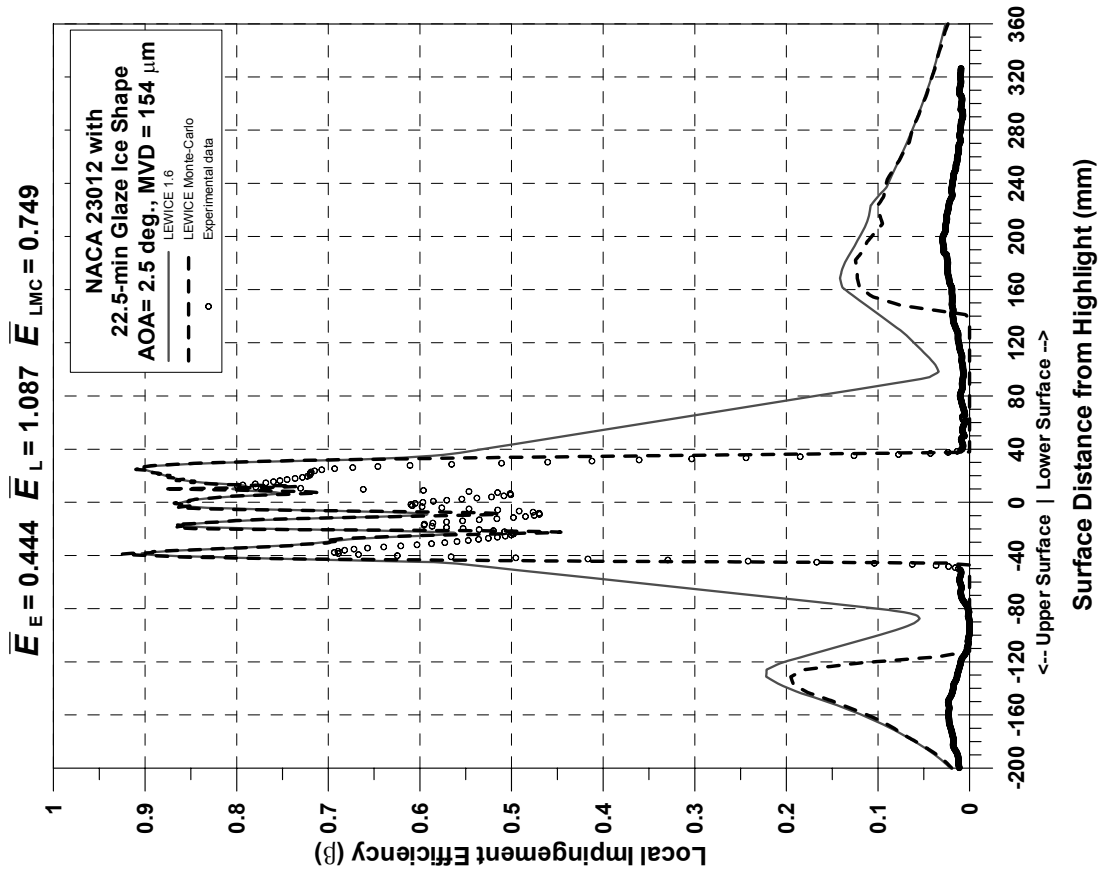


Figure E19.—Impingement efficiency distribution for NACA 23012 airfoil with 22.5-min glaze ice shape;  $c = 36\text{-in.}$ ,  $V_\infty = 175 \text{ mph}$ ,  $\text{AOA} = 2.5^\circ$ ,  $MVD = 154 \mu\text{m}$ .

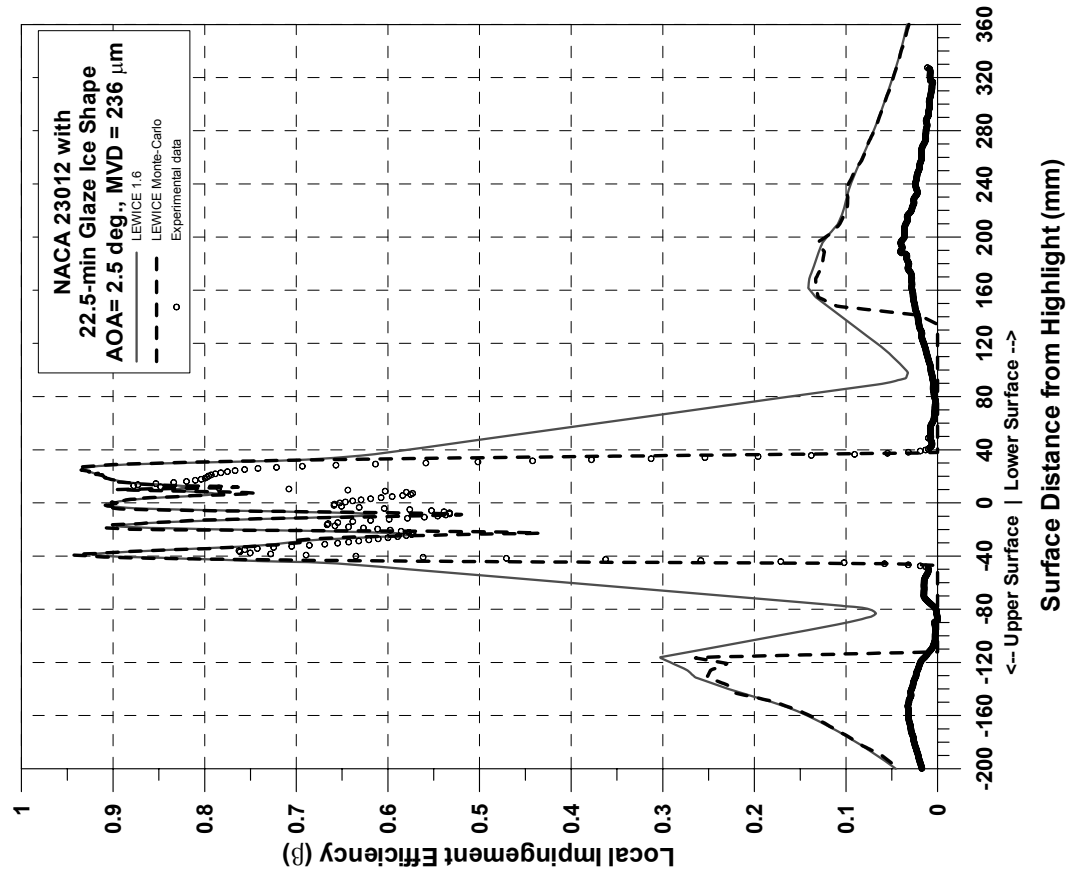


Figure E20.—Impingement efficiency distribution for NACA 23012 airfoil with 22.5-min glaze ice shape;  $c = 36\text{-in.}$ ,  $V_\infty = 175 \text{ mph}$ ,  $\text{AOA} = 2.5^\circ$ ,  $MVD = 236 \mu\text{m}$ .

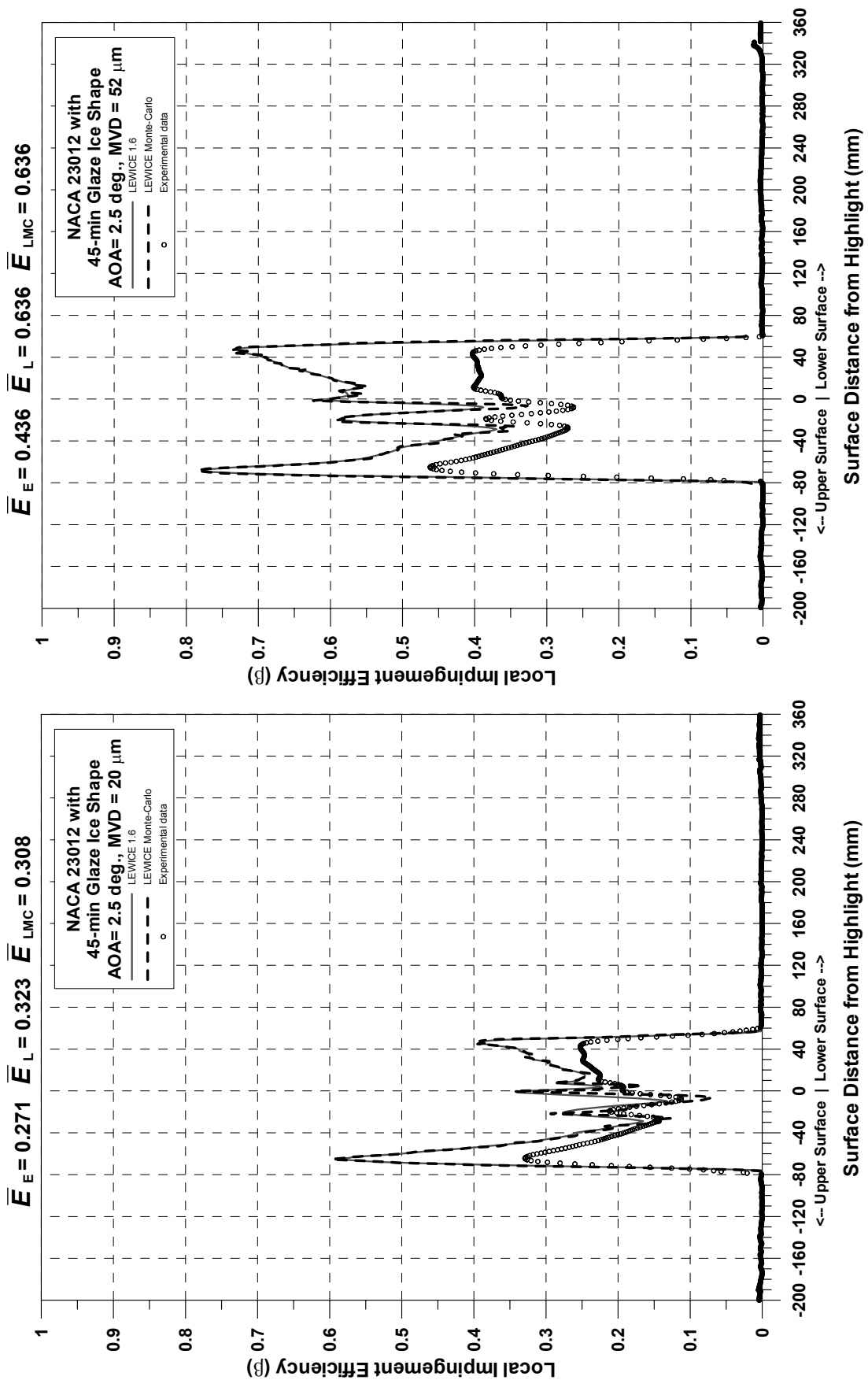
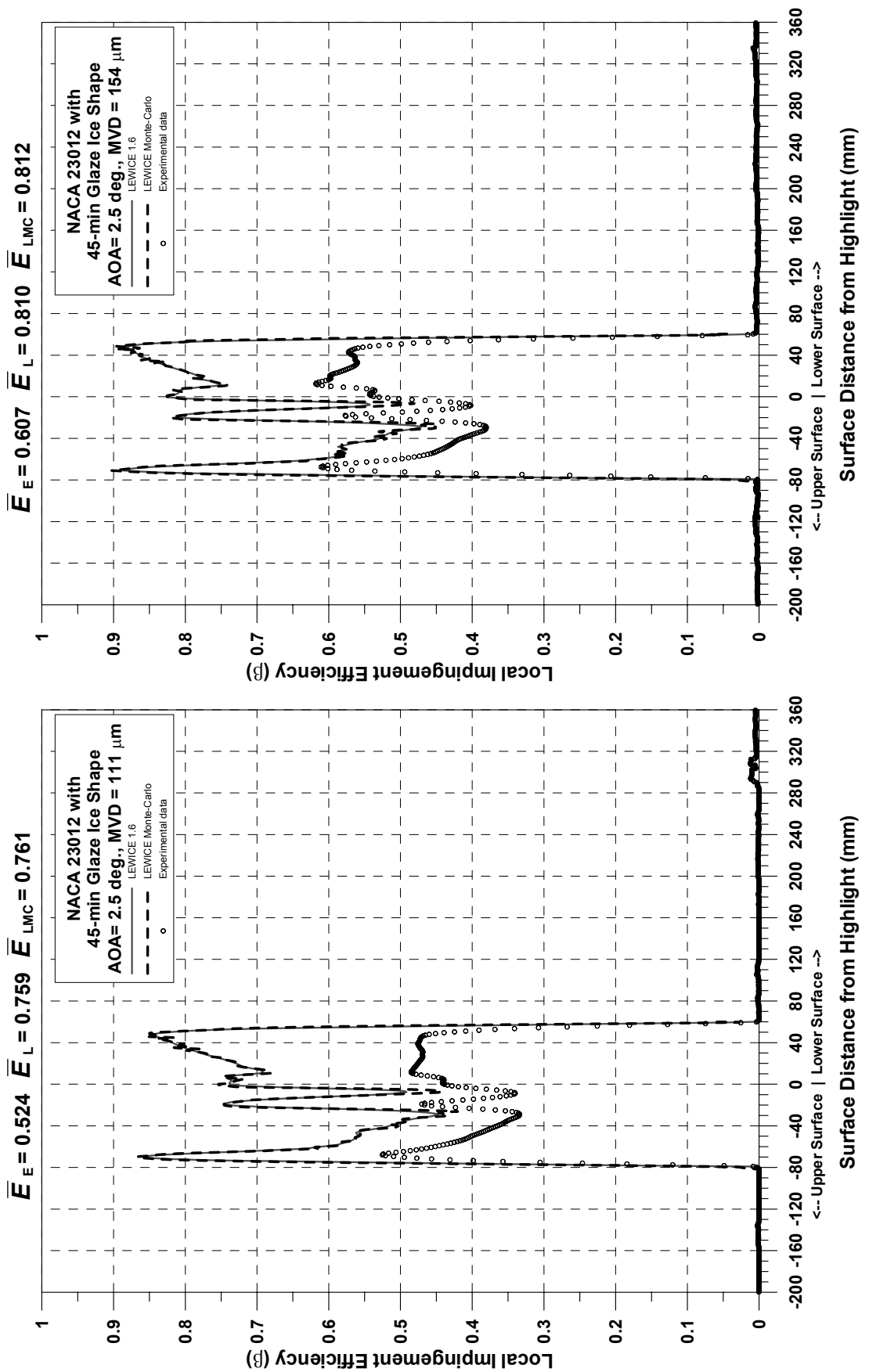
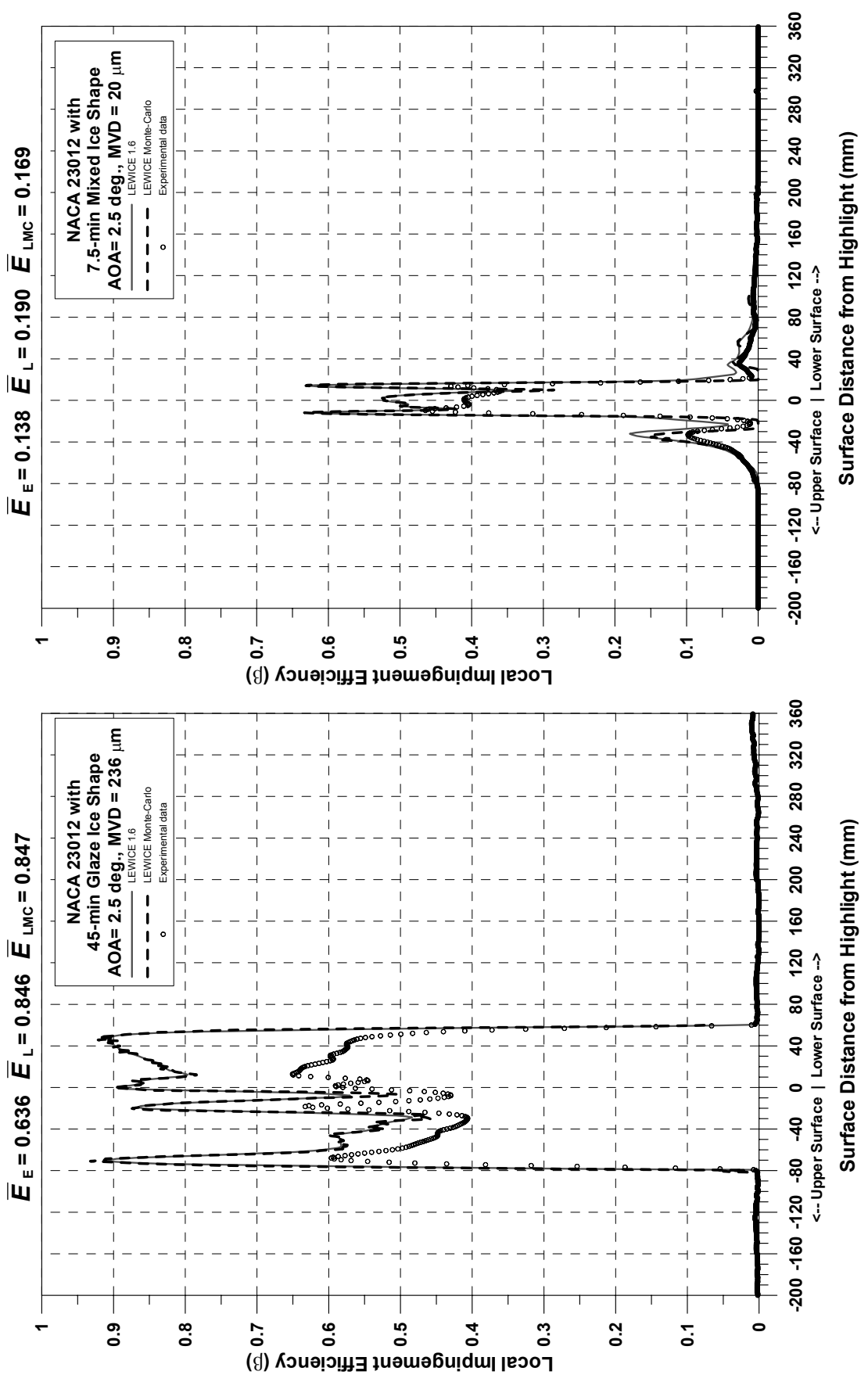


Figure E21.—Impingement efficiency distribution for NACA 23012 airfoil with 45-min glaze ice shape;  $c = 36\text{-in.}$ ,  $V_\infty = 175 \text{ mph}$ ,  $\text{AOA} = 2.5^\circ$ ,  $MVD = 20 \mu\text{m}$ .

Figure E22.—Impingement efficiency distribution for NACA 23012 airfoil with 45-min glaze ice shape;  $c = 36\text{-in.}$ ,  $V_\infty = 175 \text{ mph}$ ,  $\text{AOA} = 2.5^\circ$ ,  $MVD = 52 \mu\text{m}$ .





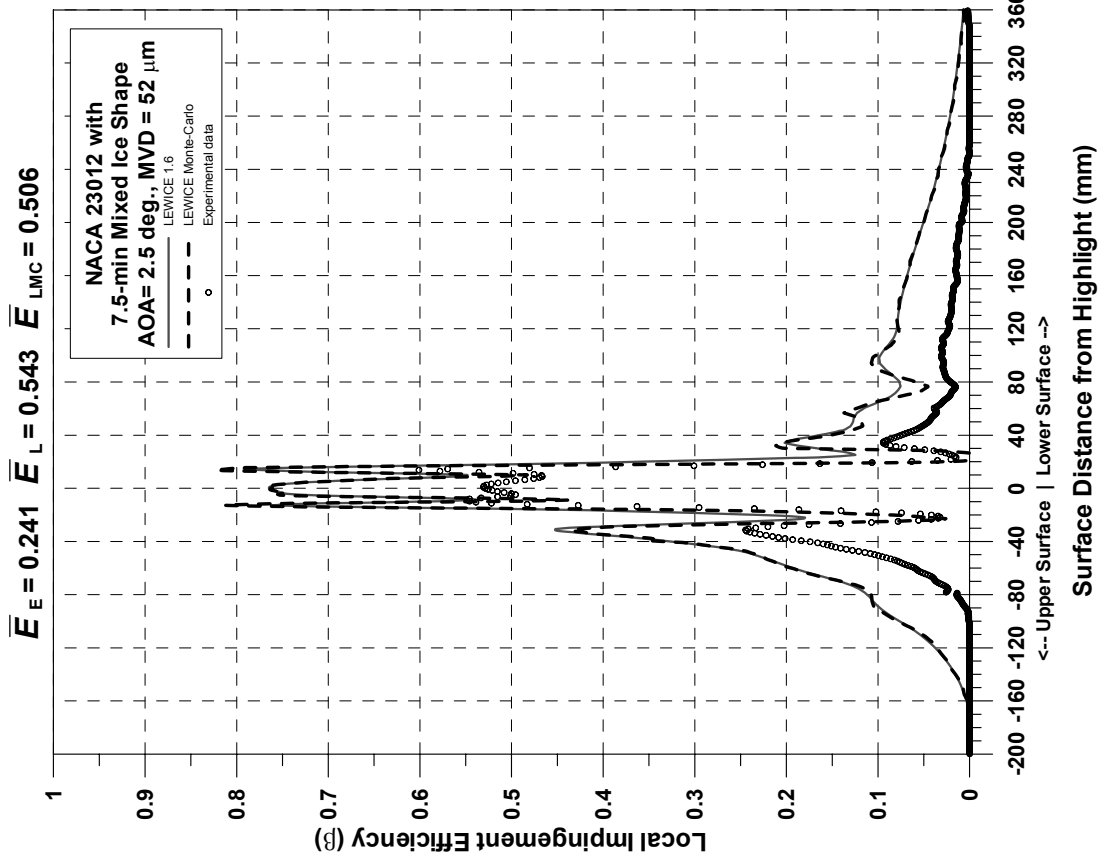


Figure E27.—Impingement efficiency distribution for NACA 23012 airfoil with 7.5-min mixed ice shape;  $c = 36\text{-in.}$ ,  $V_\infty = 175 \text{ mph}$ ,  $AOA = 2.5^\circ$ ,  $MVD = 52 \mu\text{m}$ .

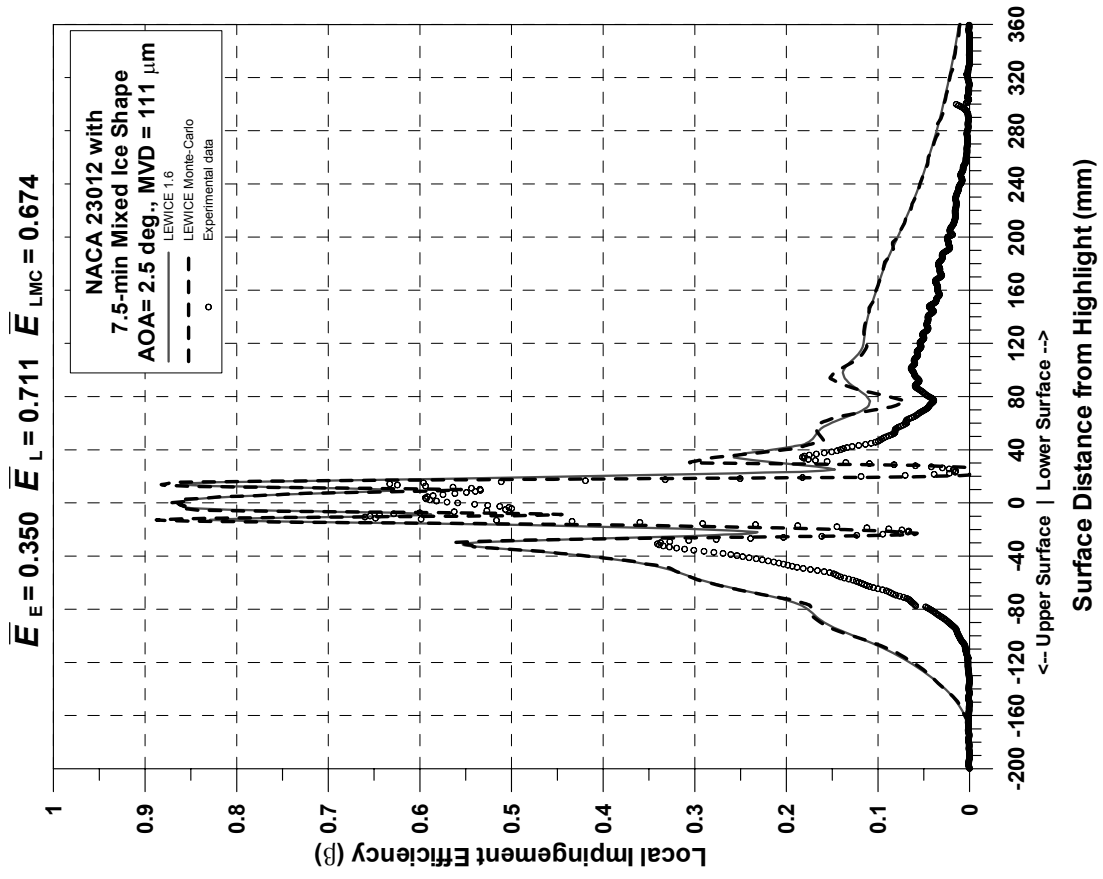
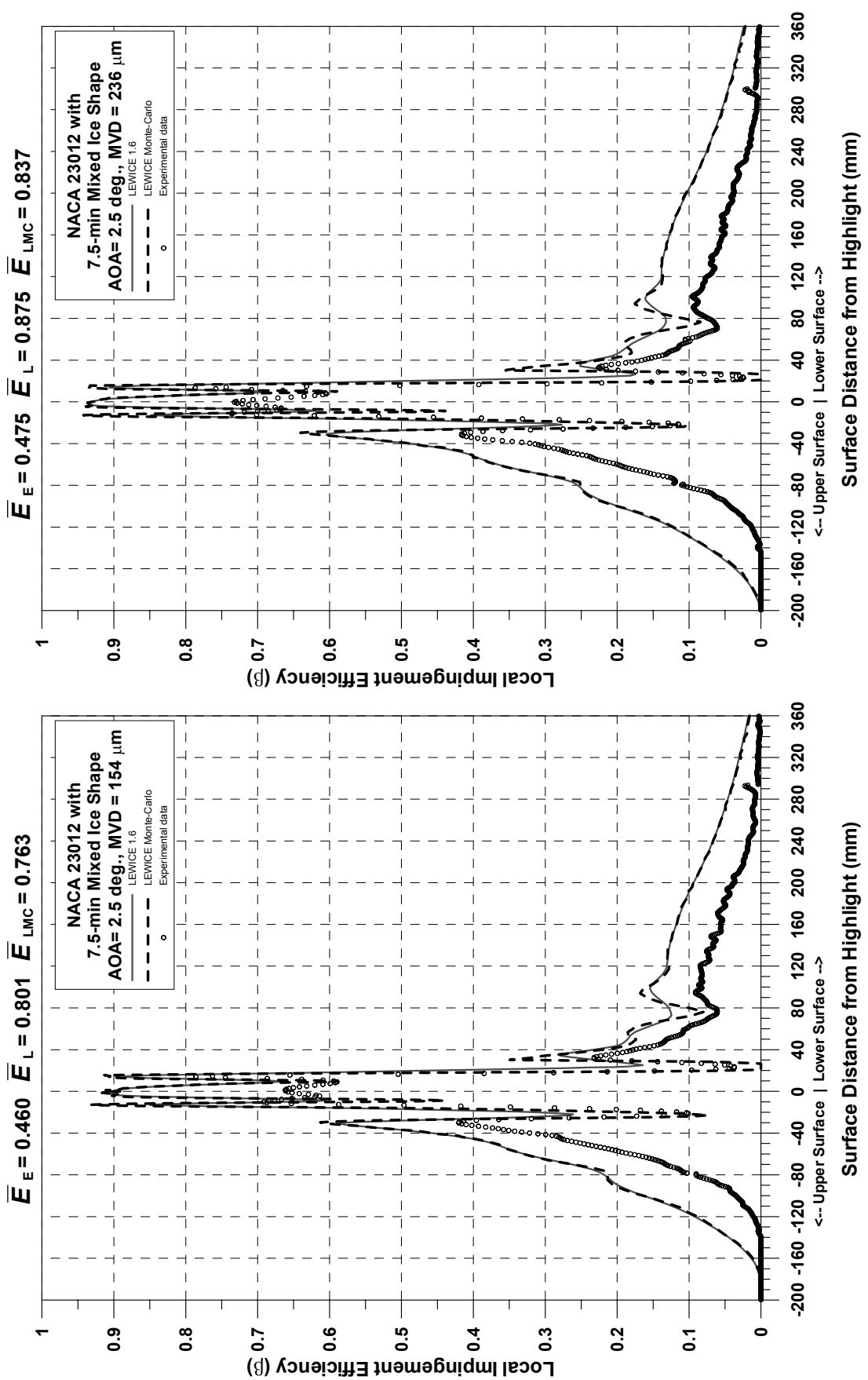


Figure E28.—Impingement efficiency distribution for NACA 23012 airfoil with 7.5-min mixed ice shape;  $c = 36\text{-in.}$ ,  $V_\infty = 175 \text{ mph}$ ,  $AOA = 2.5^\circ$ ,  $MVD = 111 \mu\text{m}$ .



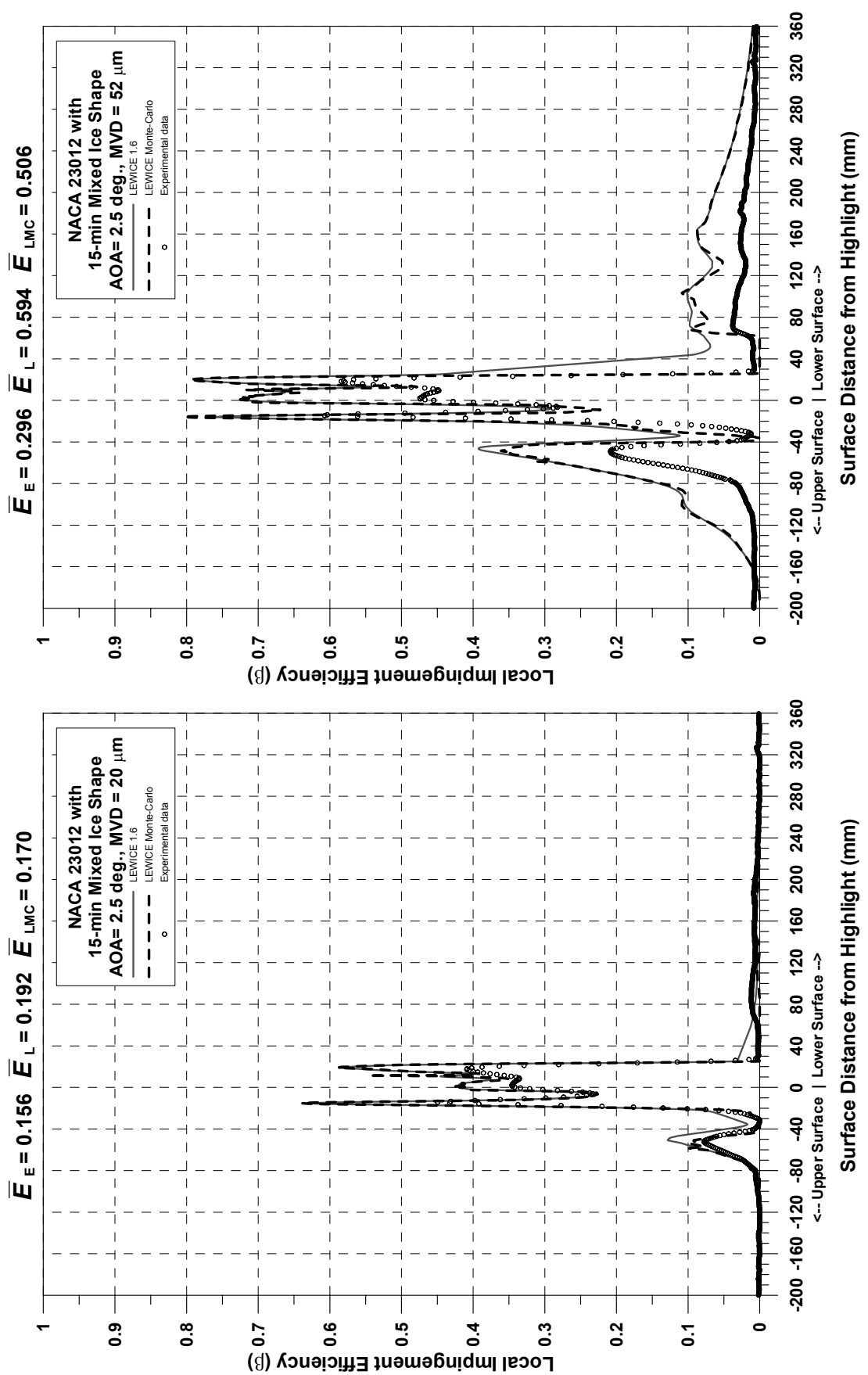
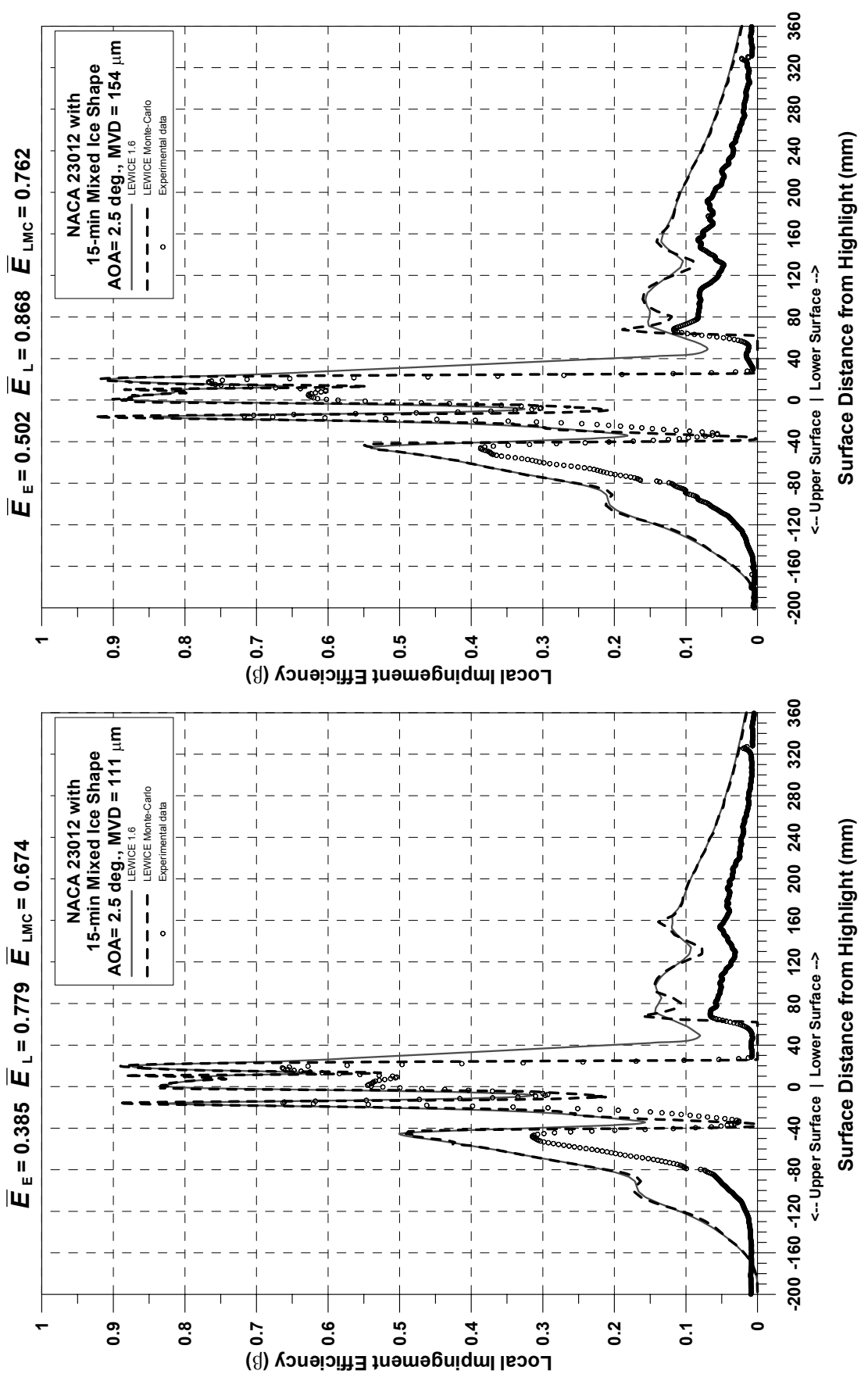
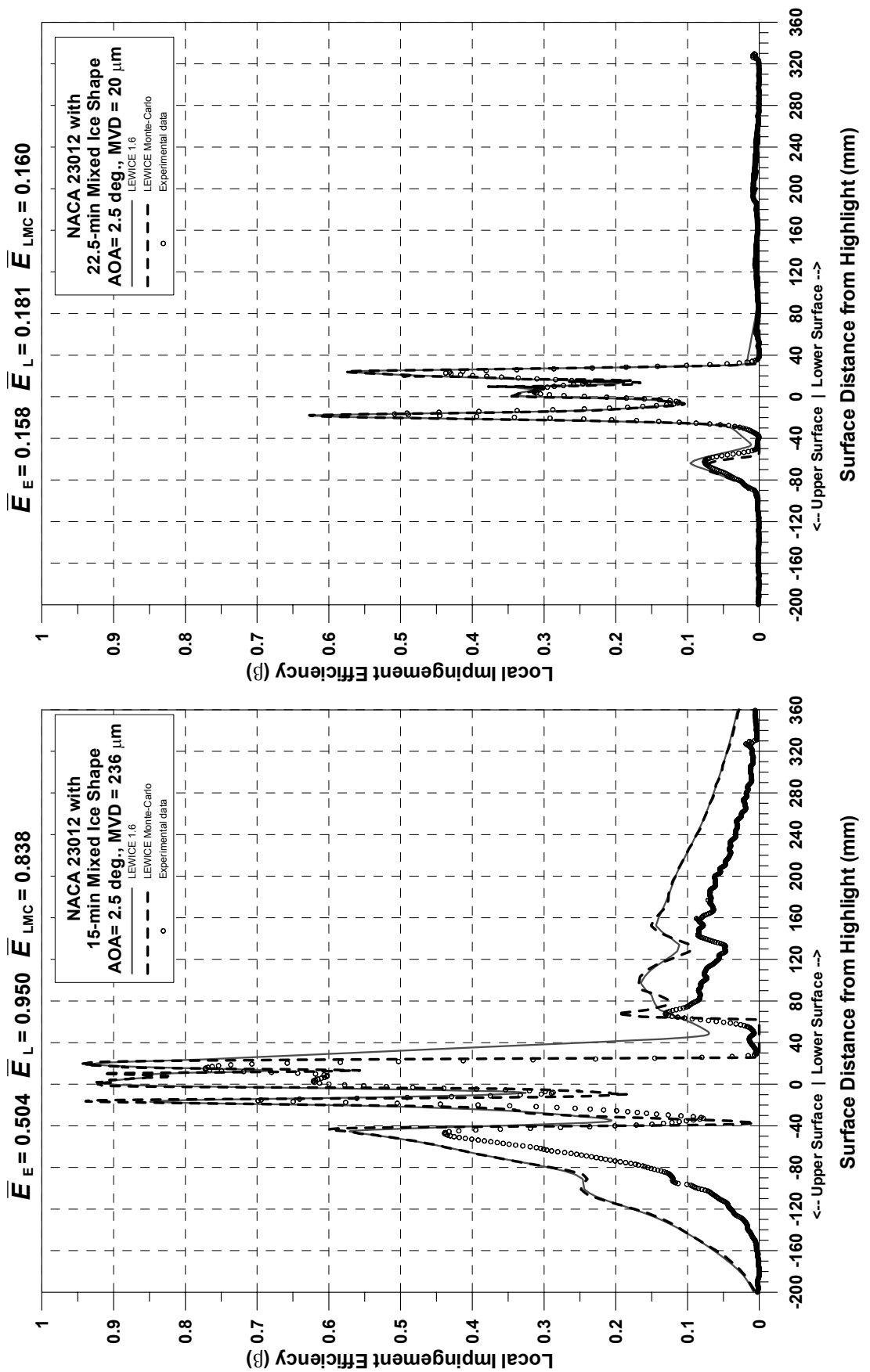
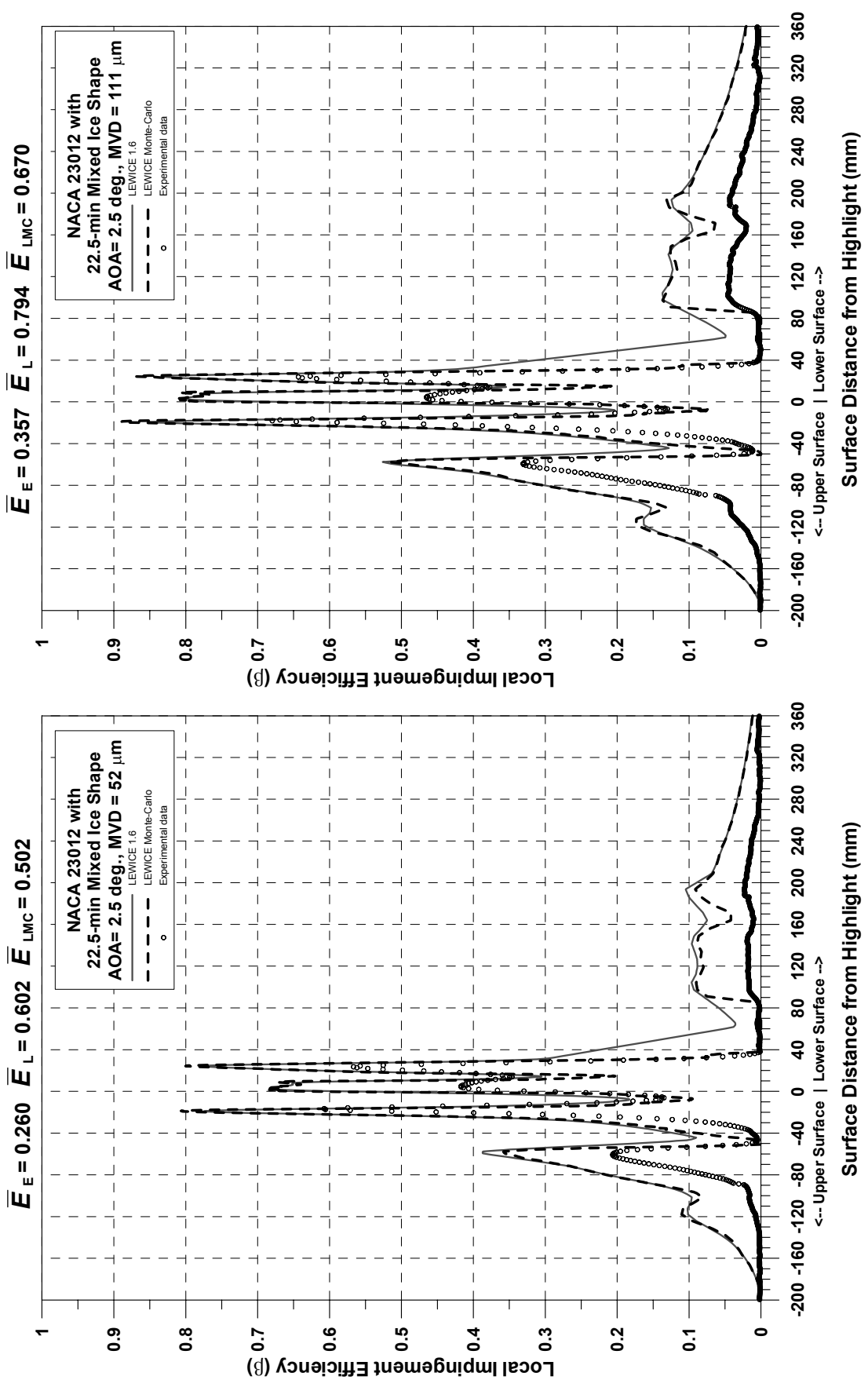


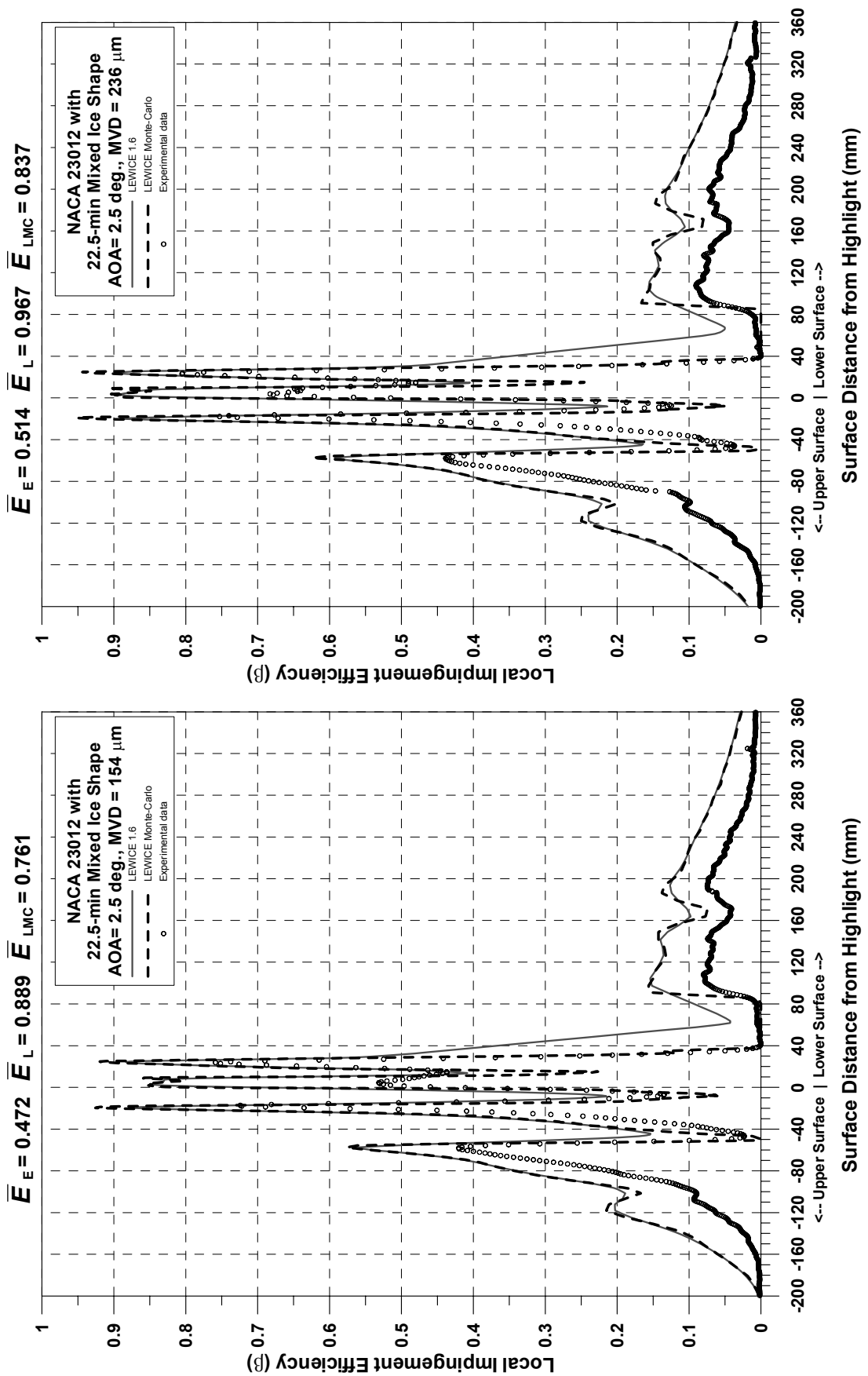
Figure E31.—Impingement efficiency distribution for NACA 23012 airfoil with 15-min mixed ice shape;  $c = 36\text{-in.}$ ,  $V_\infty = 175 \text{ mph}$ ,  $\text{AOA} = 2.5^\circ$ ,  $\text{MVD} = 20 \mu\text{m}$ .

Figure E32.—Impingement efficiency distribution for NACA 23012 airfoil with 15-min mixed ice shape;  $c = 36\text{-in.}$ ,  $V_\infty = 175 \text{ mph}$ ,  $\text{AOA} = 2.5^\circ$ ,  $\text{MVD} = 52 \mu\text{m}$ .









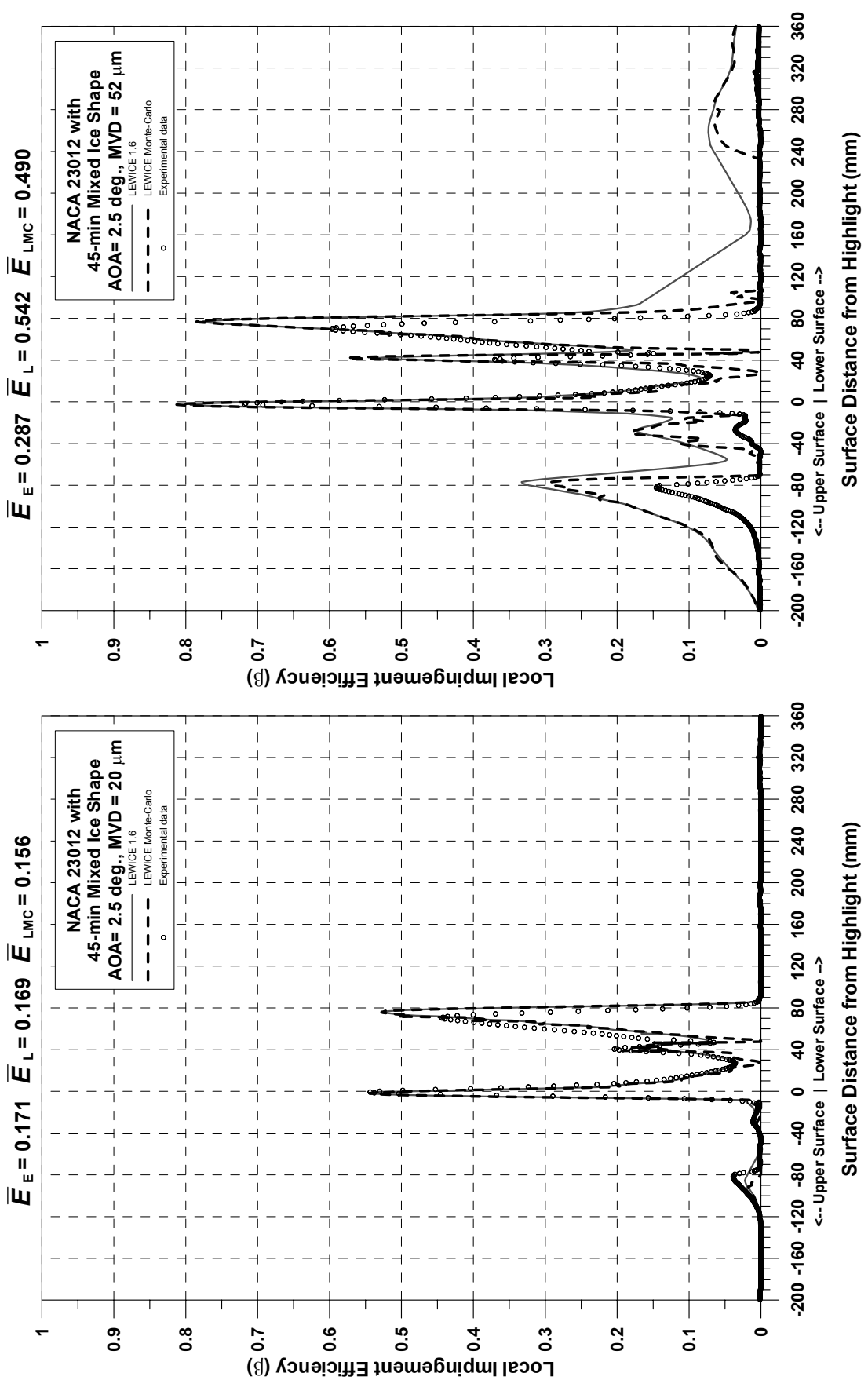
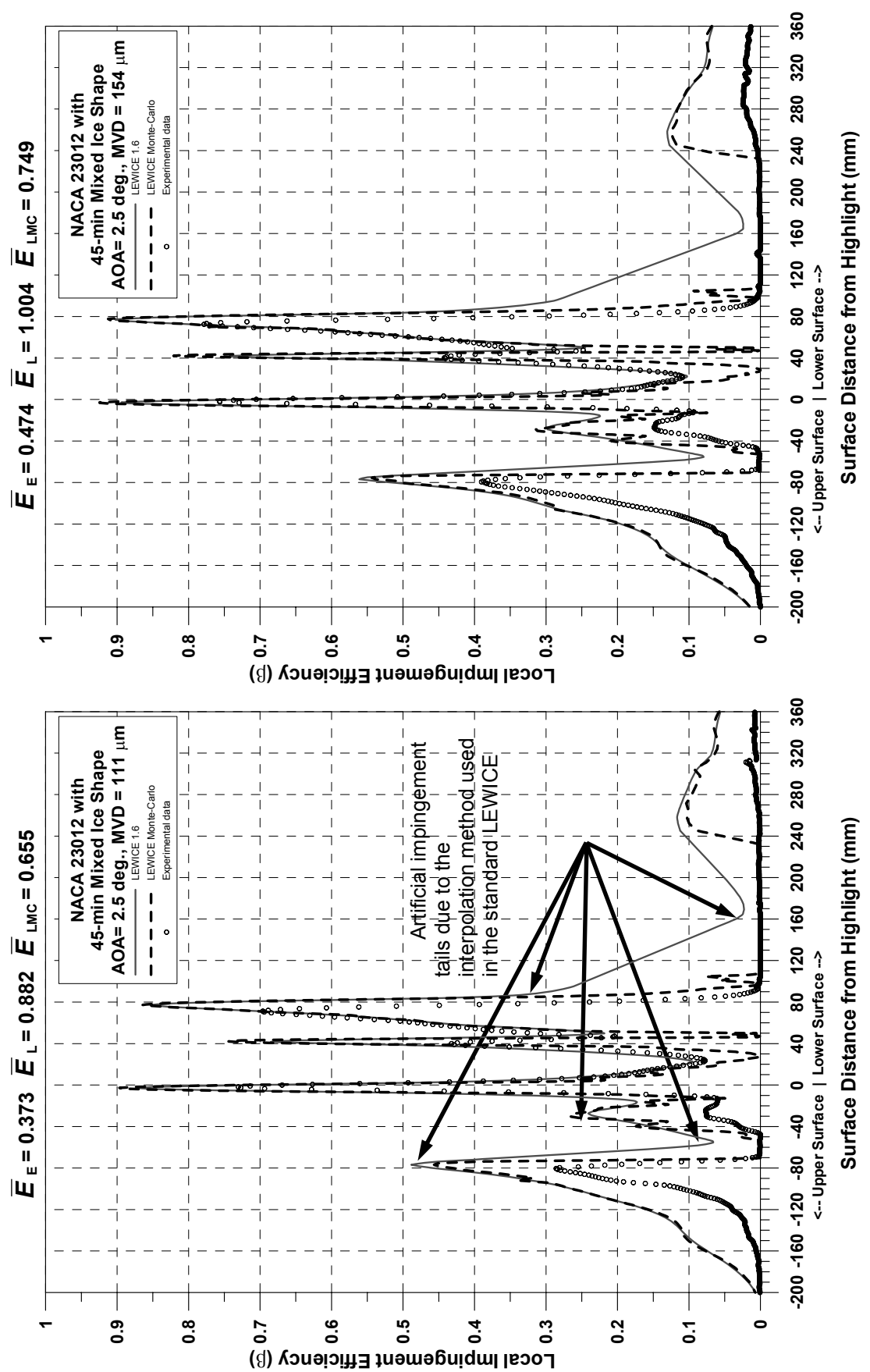
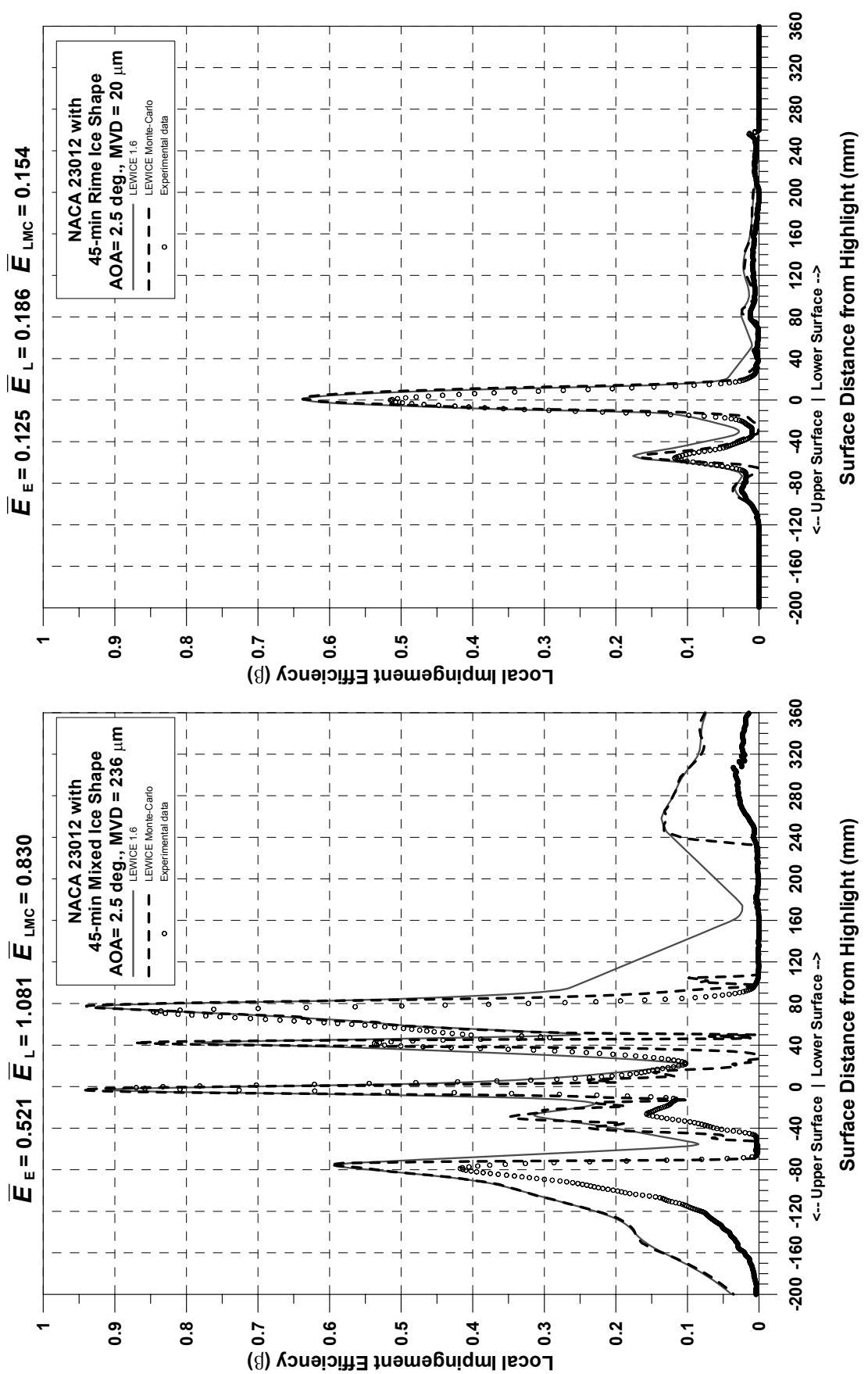
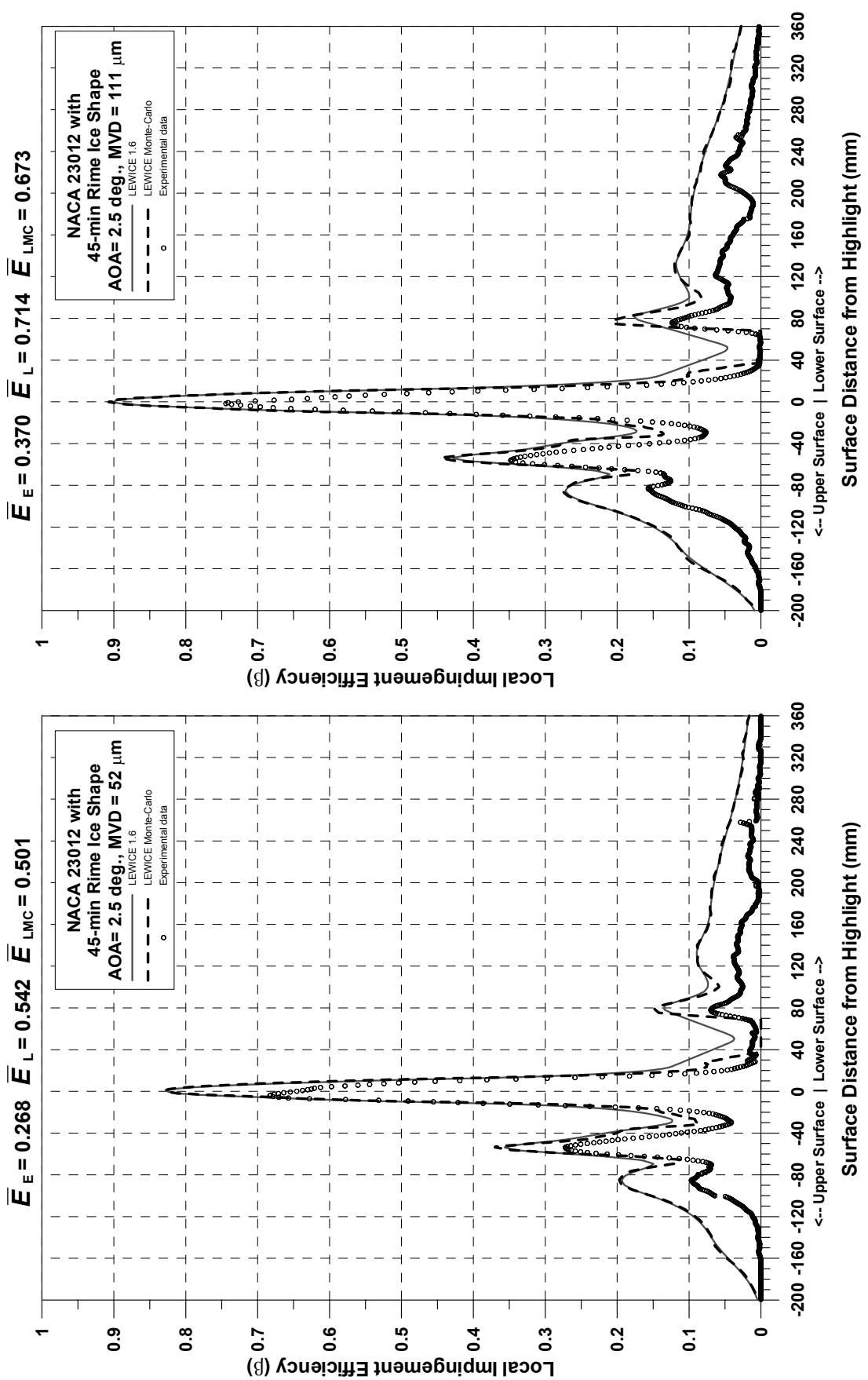


Figure E41.—Impingement efficiency distribution for NACA 23012 airfoil with 45-min mixed ice shape;  $c = 36$ -in.,  $V_\infty = 175$  mph,  $\text{AOA} = 2.5^\circ$ ,  $\text{MVD} = 20 \mu\text{m}$ .

Figure E42.—Impingement efficiency distribution for NACA 23012 airfoil with 45-min Mixed Ice Shape  $\text{AOA}=2.5 \deg$ ,  $\text{MVD} = 52 \mu\text{m}$ .







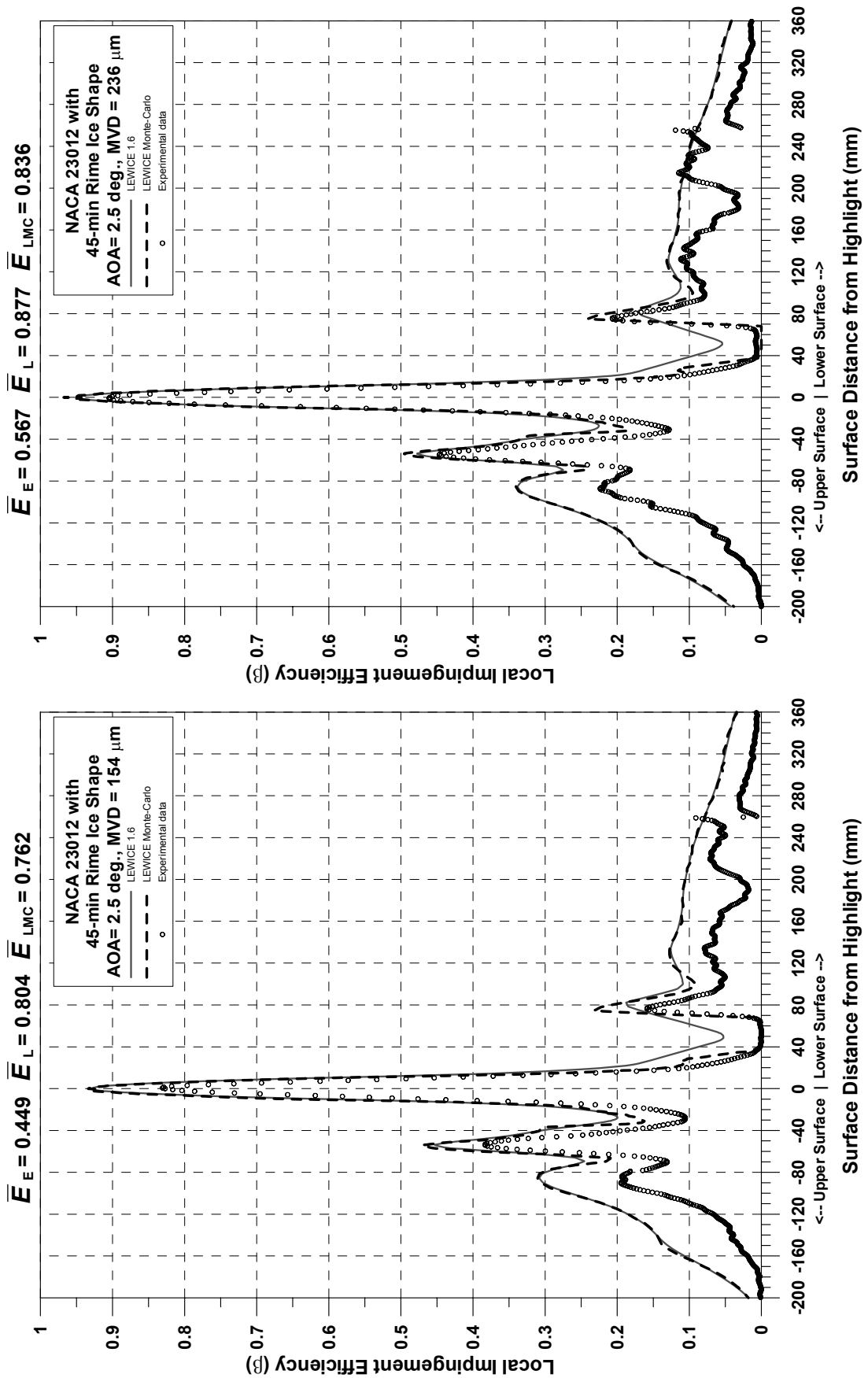


Figure E49—Impingement efficiency distribution for NACA 23012 airfoil with 45-min rime ice shape;  $C = 36$ -in.,  $V_\infty = 175$  mph,  $AOA = 2.5^\circ$ ,  $MVD = 154 \mu\text{m}$ .

Figure E50—Impingement efficiency distribution for NACA 23012 with 45-min Rime Ice Shape;  $AOA = 2.5$  deg,  $MVD = 236 \mu\text{m}$ .

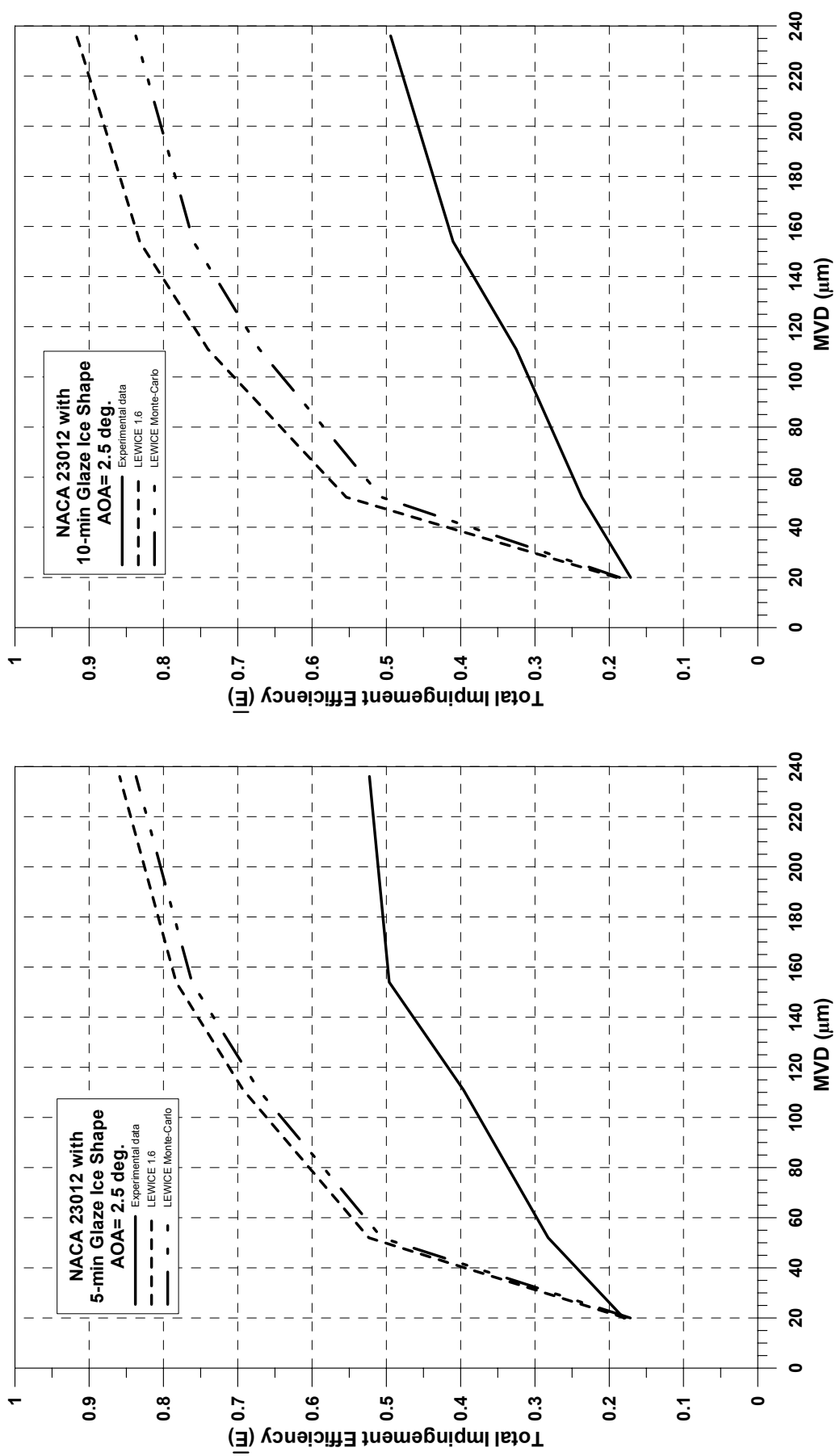
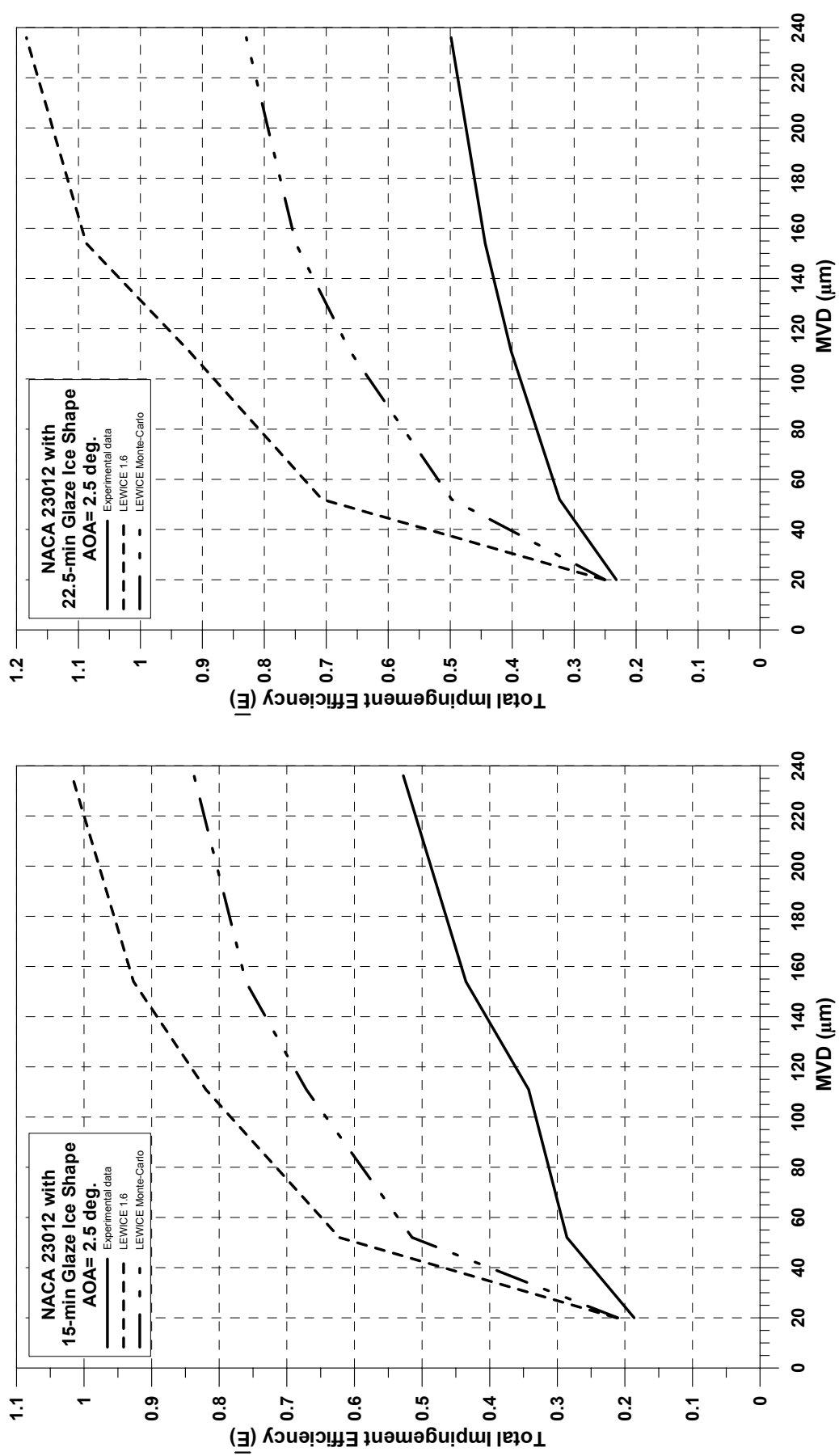


Figure E51.—Total Impingement efficiency distribution for NACA 23012 airfoil with 5-min glaze ice shape;  $c = 36\text{-in.}$ ,  $V_\infty = 175 \text{ mph}$ ,  $\text{AOA} = 2.5^\circ$ .

Figure E52.—Total Impingement efficiency distribution for NACA 23012 airfoil with 10-min glaze ice shape;  $c = 36\text{-in.}$ ,  $V_\infty = 175 \text{ mph}$ ,  $\text{AOA} = 2.5^\circ$ .



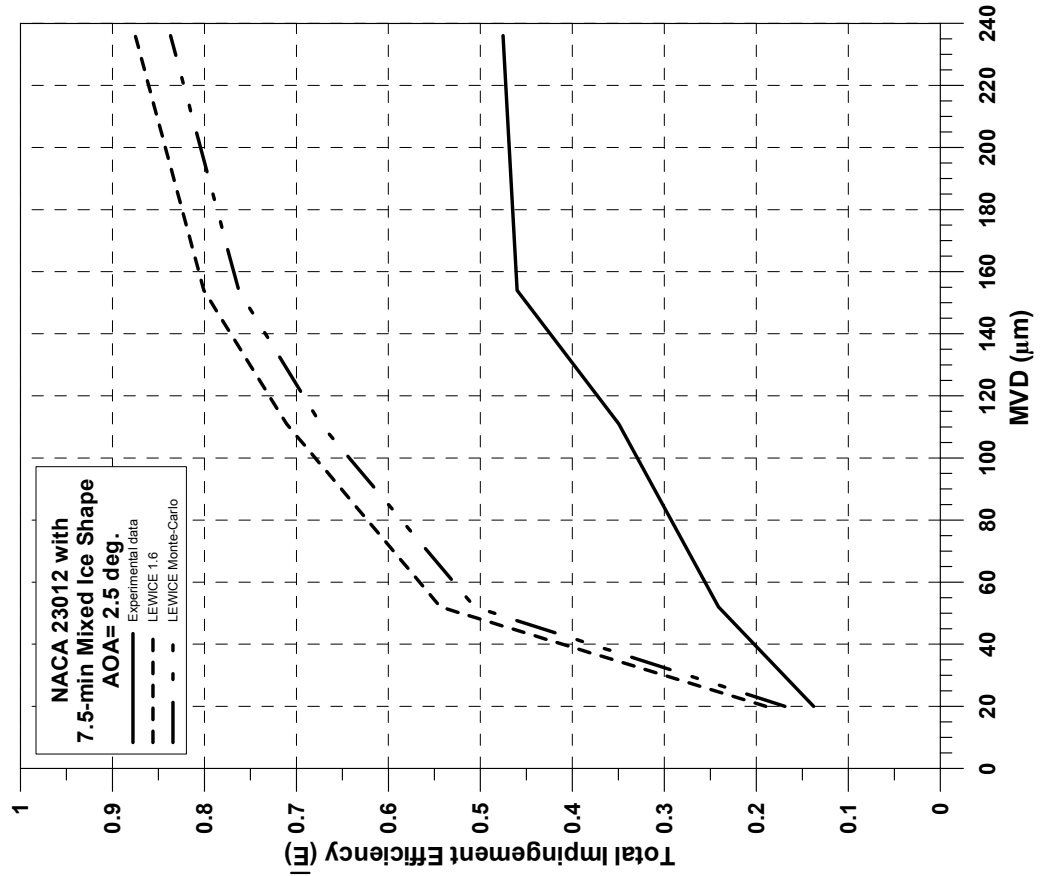


Figure E56—Total Impingement efficiency distribution for NACA 23012 airfoil with 7.5-min mixed ice shape;  
 $C = 36\text{-in.}$ ,  $V_\infty = 175 \text{ mph}$ ,  $\text{AOA} = 2.5^\circ$ .

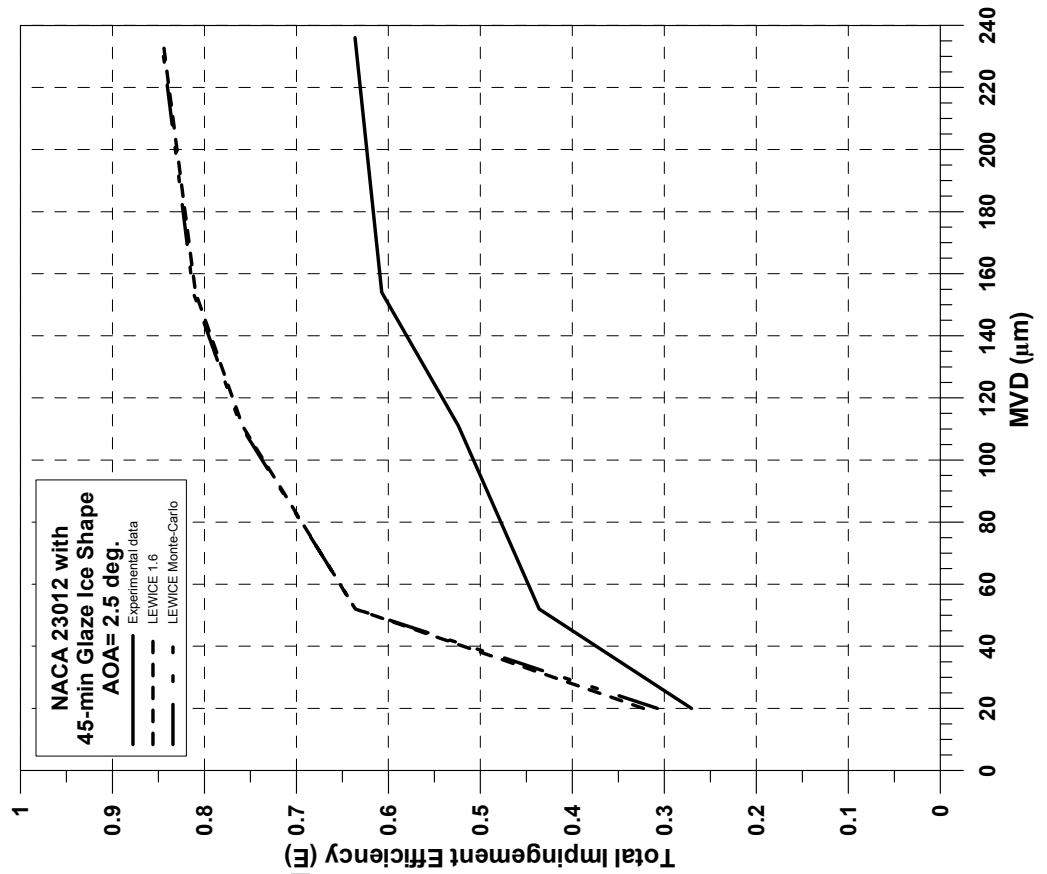
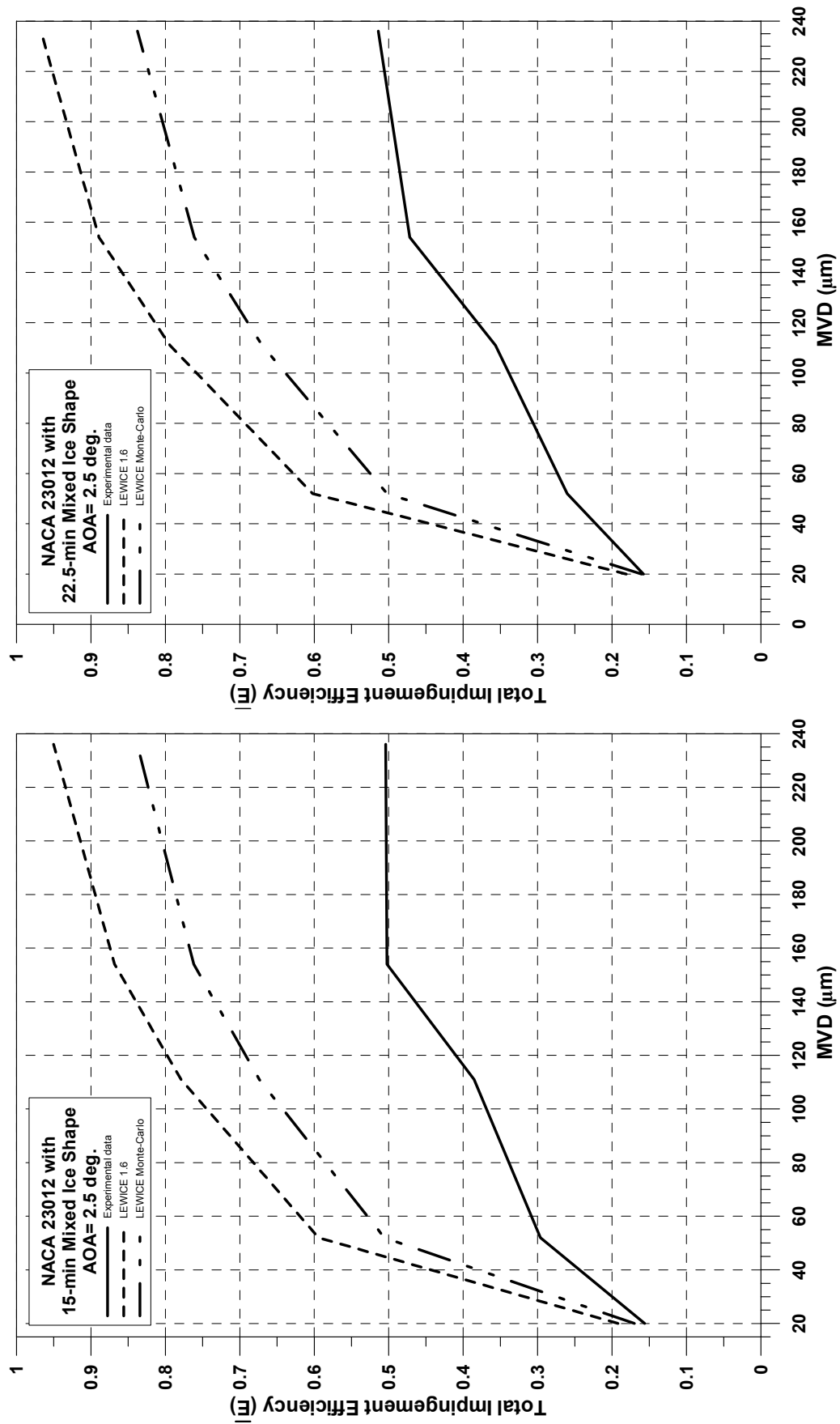
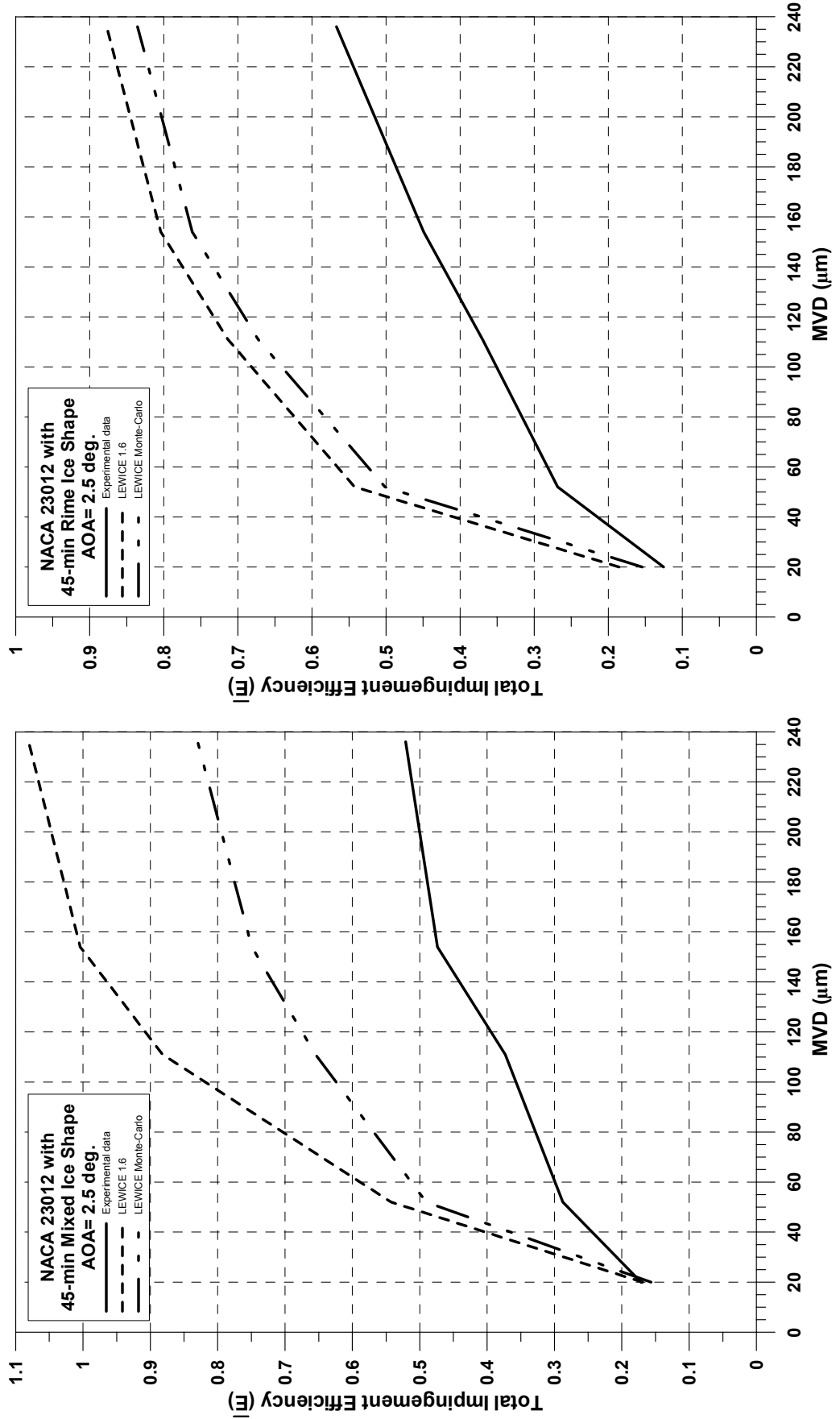


Figure E55—Total Impingement efficiency distribution for NACA 23012 airfoil with 45-min glaze ice shape;  
 $C = 36\text{-in.}$ ,  $V_\infty = 175 \text{ mph}$ ,  $\text{AOA} = 2.5^\circ$ .





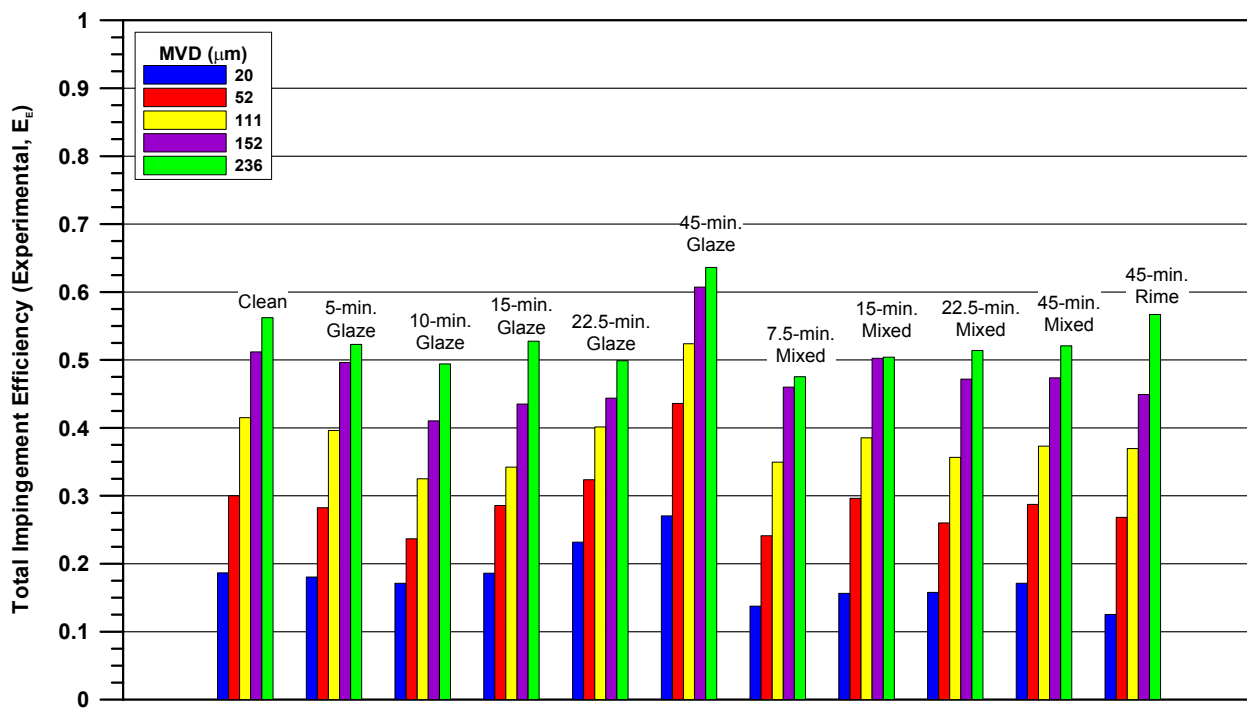


Figure E61.—Summary of experimental total impingement efficiency distributions.

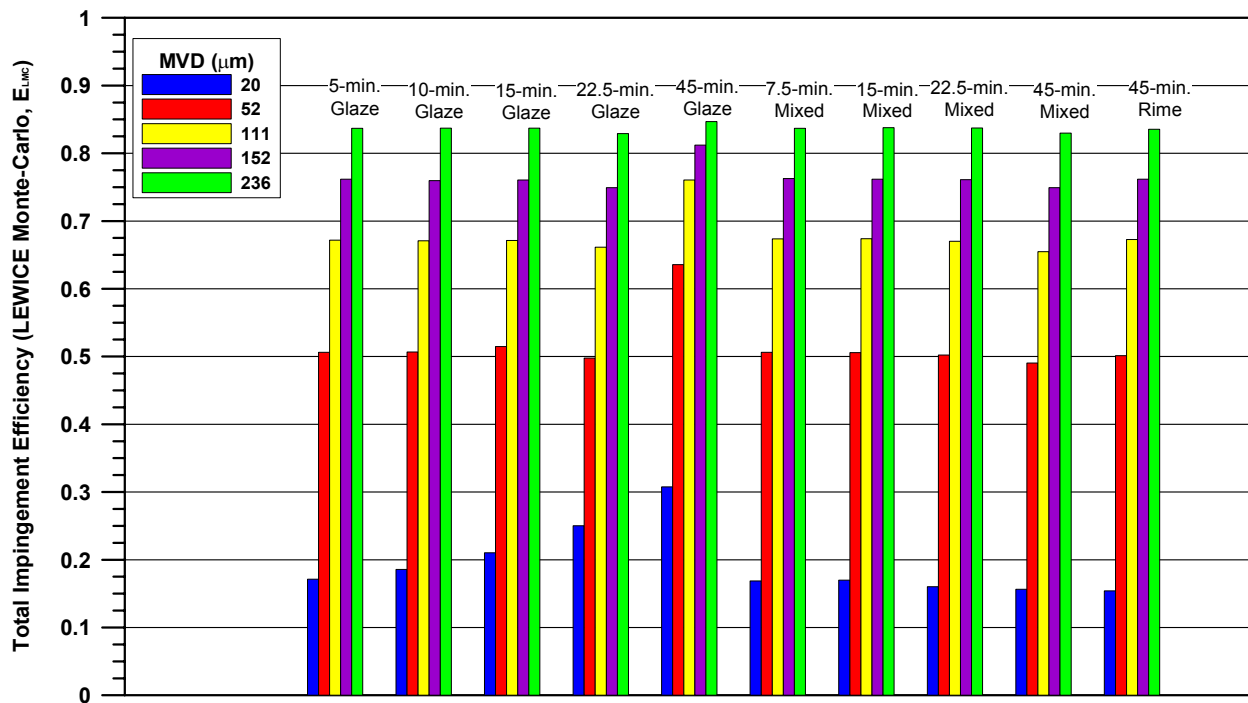


Figure E62.—Summary of LEWICE Monte-Carlo total impingement efficiency distributions.

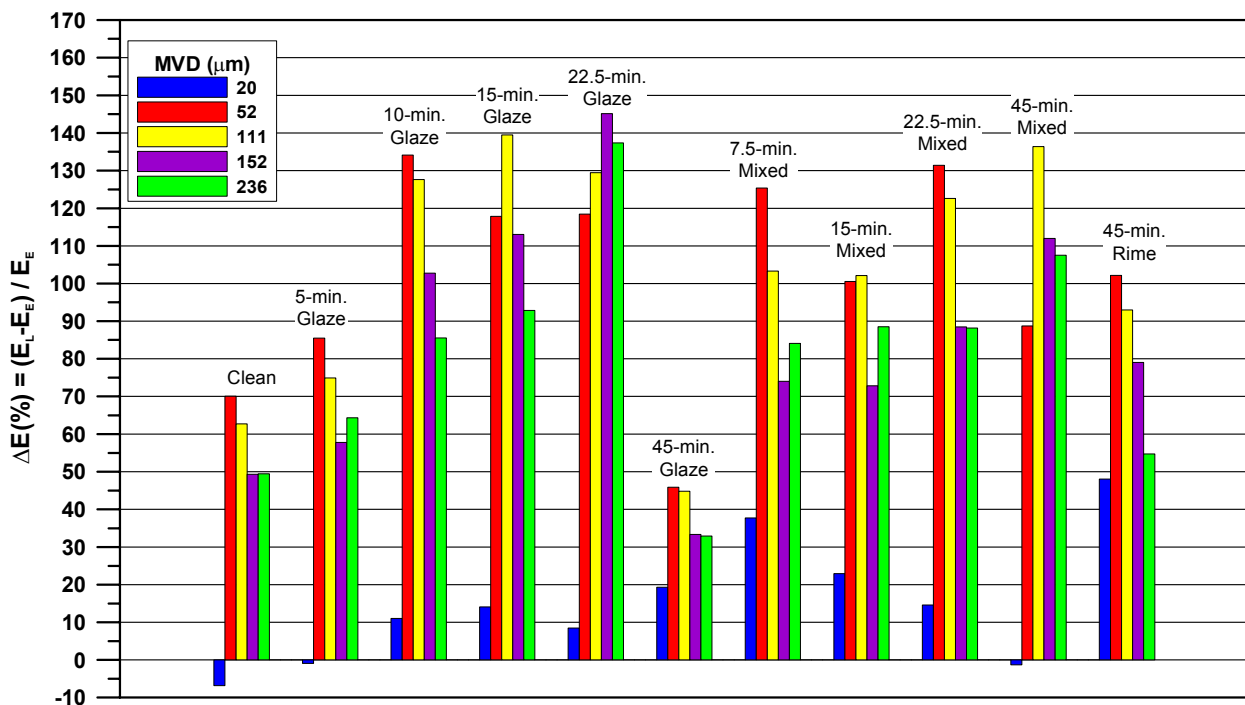


Figure E63.—Percentage difference in total impingement efficiency between LEWICE 1.6 and experimental data.

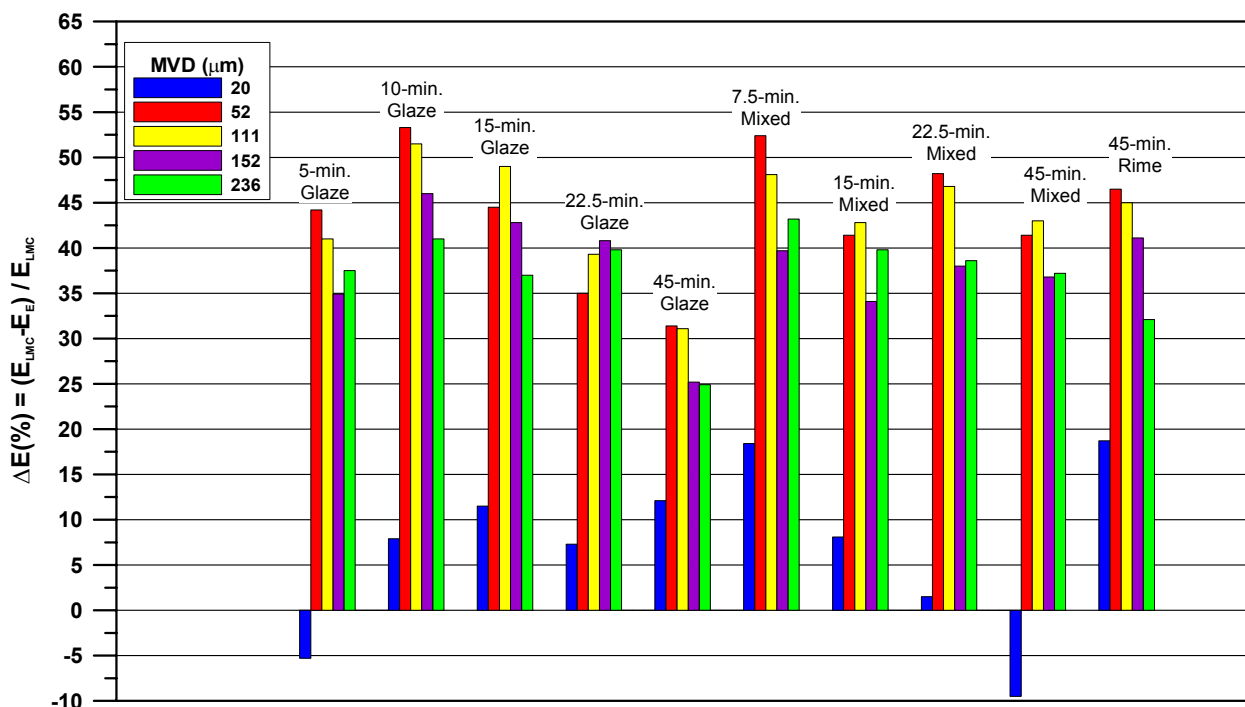


Figure E64.—Percentage difference in total impingement efficiency between LEWICE Monte-Carlo and experimental data.

## References

1. Wolfe, H.E. and Andersen, W.H., "Kinetics, Mechanism, and Resultant Droplet Sizes of the Aerodynamic Breakup of Liquid Drops," Aerojet-General Corporation research and engineering Division Report no. 0395-04 (18) SP, 1964.
2. Hinze, J.O., "Fundamentals of the Hydrodynamic Mechanism of Splitting in Dispersion Processes," A.I.Ch.E. Journal, vol. 1, no. 3, 289–295, 1955.
3. Mundo, Chr., Sommerfeld, M., and Tropea, C., "Droplet-wall collisions: Experimental studies of the deformation and Breakup process," Int. J. Multiphase Flow, vol. 21, no. 2, pp. 151–173, 1995.
4. Tan, S.C., and Papadakis, M., "General Effects of Large Droplet Dynamics on Ice Accretion Modeling," AIAA Paper 2003-0392, January 2003.
5. Tan, S.C., Papadakis, M., and Sampath, M.K., "Computational Study of Large Droplet Breakup in the Vicinity of an Airfoil," FAA report to be published.
6. Papadakis, M., Rachman, A., Wong, S.C., Hung, K.E., Vu, G.T., and Bidwell, C.S., "Experimental Study of SLD Impingement Effects," DOT/FAA/AR-03/59, September 2003.
7. Papadakis, M., and Bidwell, C.S., "An Experimental Investigation of SLD Impingement on Airfoils and Simulated Ice Shapes," Proceeding of the FAA In-flight Icing/Ground De-icing International Conference, Chicago, Illinois, June 2003.
8. Von Glahn, U., Gelder, T.F., and Smyers, W.H. Jr., "A Dye Tracer Technique for Experimentally Obtaining Impingement Characteristics of Arbitrary Bodies and a Method for Determining Droplet Size Distribution," NACA TN 3338, March 1955.
9. Gelder, T.F., Smyers, W.H. Jr, and Von Glahn, U., "Experimental Droplet Impingement on Several Two-Dimensional Airfoils with Thickness Ratios of 6 to 16 percent," NACA TN 3839, December 1956.
10. Lewis, J.O. and Ruggeri, R.S., "Experimental Droplet Impingement on Four Bodies of Revolution," NACA TN 3587, 1957.
11. Lewis, James O. and Ruggeri, Robert S., "Experimental Droplet Impingement on four bodies of revolution," NACA TN 4092, December 1955.
12. Gelder, T.F., "Droplet Impingement and Ingestion by Supersonic Nose Inlet in Subsonic Tunnel Conditions," NACA TN 4268, May 1958.
13. Papadakis, M., Elangovan, R., Freund, G.A., Jr., Breer, M., Zumwalt, G.W. and Whitmer, L., "An Experimental Method for Measuring Water Droplet Impingement Efficiency on Two- and Three-Dimensional Bodies," NASA CR 4257, DOT/FAA/CT-87/22, November 1989.
14. Papadakis, M., Breer, M.D., Craig, N., and Liu, X., "Experimental Water Droplet Impingement Data on Airfoils, Simulated Ice Shapes, an Engine Inlet and a Finite Wing," NASA CR 4636, DOT/FAA/CT-TN93/18, December 1994.
15. Phillips, E.H., "ATR42/72 Review Focuses on Icing," Aviation Week and Space Technology, November 14, 1994.
16. Phillips, E.H. "FAA Lifts Icing Ban on ATR Flights," Aviation Week and Space Technology, June 5, 1995.
17. Papadakis, M., Hung, K.E., Vu, G.T., Yeong, H.W., Bidwell, C., Breer, M.D., Bencic, T., "Experimental Investigation of Water Droplet Impingement on Airfoils, Finite Wings, and an S-Duct Engine Inlet," NASA/TM—2002-211700, September 2001.
18. FAA FAR PART 25: Airworthiness standards: Transport category airplanes, Title 14 CFR part 25 including Amendment 25-101 as published in the Federal Register on December 19, 2000.
19. Langmuir, I. And Blodgett, K.B., "A mathematical Investigation of Water Droplet Trajectories," Army Air Forces Technical Report No. 5418, 1946.

20. Wright, W.B. and Potapczuk, M.G., "Semi-empirical Modeling of SLD Physics," AIAA 2004-0412, 42nd AIAA Aerospace Sciences Meeting and Exhibit, 2004.
21. Beard K.V. and Pruppacher, H.R., "A Determination of the Terminal Velocity and Drag of Small Water Drops by Means of a Wind Tunnel," *Journal of Atmospheric Science*, vol. 26, no. 26, pp. 1066–1072, 1969.
22. Pilch, M., and Erdman, C.A., "Use of Breakup Time Data and Velocity History data to Predict the Maximum Size of Stable Fragments for Acceleration-Induced Breakup of a Liquid Drop," *International Journal of Multiphase Flow*, vol. 13, no. 6, pp. 741–757, 1987.
23. Rutkowsky, A., Wright, W.B., and Potapczuk, M., "Numerical Study of Droplet Splashing and Re-impingement," AIAA 2003-388, 41st AIAA Aerospace Sciences Meeting and Exhibit, 2003.
24. Soeder, R.H., Sheldon, D.W., Ide, R.F., Spera, D.A., and Andracchio, C.R., "NASA Glenn Icing Research Tunnel User Manual," National Aeronautics and Space Administration, Glenn Research Center, NASA/TM—2003-212004, September 2003.
25. McGhee, R.J., and Beasley, W.D., "Low-Speed Aerodynamic Characteristics of a 17-Percent-Thick Medium-Speed Airfoil Designed for General Application," NASA TP-1786, 1980.
26. Wright, W.B., "User Manual for the NASA Glenn Ice Accretion Code LEWICE, 2.2.2 Final Report," NASA/CR—2002-211793, August 2002.
27. Oldenburg, J.R. and Ide, R.F., "Comparison of Drop Size Distributions from Two Droplet Sizing Systems," NASA TM 102520, March 1990.
28. "CSIRO-KING Liquid Water Content Probe PMS Model KLWC-5—Operating and Servicing Manual," Particle Measuring Systems, Inc, Boulder, Colorado.
29. Papadakis, M., Vu, G.T., Hung, E.K., Bidwell, C.S., Bencic, T., and Breer, M.D., "Progress in Measuring Water Impingement Characteristics on Aircraft Surfaces," AIAA Paper 98-0488, January 1988.
30. Wright, W.B., "Users Manual for the Improved NASA Lewis Ice Accretion Code LEWICE 1.6," NASA CR 198355, June 1995.

## REPORT DOCUMENTATION PAGE

Form Approved  
OMB No. 0704-0188

The public reporting burden for this collection of information is estimated to average 1 hour per response, including the time for reviewing instructions, searching existing data sources, gathering and maintaining the data needed, and completing and reviewing the collection of information. Send comments regarding this burden estimate or any other aspect of this collection of information, including suggestions for reducing this burden, to Department of Defense, Washington Headquarters Services, Directorate for Information Operations and Reports (0704-0188), 1215 Jefferson Davis Highway, Suite 1204, Arlington, VA 22202-4302. Respondents should be aware that notwithstanding any other provision of law, no person shall be subject to any penalty for failing to comply with a collection of information if it does not display a currently valid OMB control number.

PLEASE DO NOT RETURN YOUR FORM TO THE ABOVE ADDRESS.

|   |                         |   |  |  |  |
|---|-------------------------|---|--|--|--|
| <b>1. REPORT DATE (DD-MM-YYYY)</b><br>01-10-2007  |                         |   | <b>2. REPORT TYPE</b><br>Technical Memorandum  |  | <b>3. DATES COVERED (From - To)</b>                              |
| <b>4. TITLE AND SUBTITLE</b><br>Water Droplet Impingement on Simulated Glaze, Mixed, and Rime Ice Accretions  |                         |   | <b>5a. CONTRACT NUMBER</b><br><br><b>5b. GRANT NUMBER</b><br><br><b>5c. PROGRAM ELEMENT NUMBER</b>                             |  |  |
| <b>6. AUTHOR(S)</b><br>Papadakis, Michael; Rachman, Arief; Wong, See-Cheuk; Yeong, Hsiung-Wei; Hung, Kuohsing, E.; Vu, Giao, T.; Bidwell, Colin, S.   |                         |   | <b>5d. PROJECT NUMBER</b><br><br><b>5e. TASK NUMBER</b><br><br><b>5f. WORK UNIT NUMBER</b><br>WBS-22-077-41-08                 |  |  |
| <b>7. PERFORMING ORGANIZATION NAME(S) AND ADDRESS(ES)</b><br>National Aeronautics and Space Administration<br>John H. Glenn Research Center at Lewis Field<br>Cleveland, Ohio 44135-3191  |                         |   | <b>8. PERFORMING ORGANIZATION REPORT NUMBER</b><br>E-15277   |  |  |
| <b>9. SPONSORING/MONITORING AGENCY NAME(S) AND ADDRESS(ES)</b><br>National Aeronautics and Space Administration<br>Washington, DC 20546-0001  |                         |   | <b>10. SPONSORING/MONITORS ACRONYM(S)</b><br>NASA<br><br><b>11. SPONSORING/MONITORING REPORT NUMBER</b><br>NASA/TM-2007-213961 |  |  |
| <b>12. DISTRIBUTION/AVAILABILITY STATEMENT</b><br>Unclassified-Unlimited<br>Subject Categories: 02, 03, and 34<br>Available electronically at <a href="http://gltrs.grc.nasa.gov">http://gltrs.grc.nasa.gov</a><br>This publication is available from the NASA Center for AeroSpace Information, 301-621-0390   |                         |   |  |  |  |
| <b>13. SUPPLEMENTARY NOTES</b>  |                         |   |  |  |  |
| <b>14. ABSTRACT</b><br>Water droplet impingement data were obtained at the NASA Glenn Icing Research Tunnel (IRT) for a 36-in. chord NACA 23012 airfoil with and without simulated ice using a dye-tracer method. The simulated ice shapes were defined with the NASA Glenn LEWICE 2.2 ice accretion program and including one rime, four mixed and five glaze ice shapes. The impingement experiments were performed with spray clouds having median volumetric diameters of 20, 52, 111, 154, and 236 µm. Comparisons to the experimental data were generated which showed good agreement for the rime and mixed shapes at lower drop sizes. For larger drops sizes LEWICE 2.2 over predicted the collection efficiencies due to droplet splashing effects which were not modeled in the program. Also for the more complex glaze ice shapes interpolation errors resulted in the over prediction of collection efficiencies in cove or shadow regions of ice shapes. |                         |   |  |  |  |
| <b>15. SUBJECT TERMS</b><br>Trajectory analysis; Validation; Aircraft icing; Ice formation; Impingement; Deicing; Airfoils; Wings; Swept wings  |                         |   |  |  |  |
| <b>16. SECURITY CLASSIFICATION OF:</b>  |                         | <b>17. LIMITATION OF ABSTRACT</b><br>UU | <b>18. NUMBER OF PAGES</b><br>301  | <b>19a. NAME OF RESPONSIBLE PERSON</b><br>STI Help Desk (email: <a href="mailto:help@sti.nasa.gov">help@sti.nasa.gov</a> ) |  |
| <b>a. REPORT</b><br>U   | <b>b. ABSTRACT</b><br>U |   |  | <b>c. THIS PAGE</b><br>U   | <b>19b. TELEPHONE NUMBER (include area code)</b><br>301-621-0390 |



